

# **Lysine-Targeting Covalent Inhibitors**

**James Knox**

Medicinal Chemistry, Centre for Cancer Drug Discovery

The Institute of Cancer Research

University of London

This thesis is submitted as partial fulfilment of the requirements for the degree of Doctor of Philosophy.

September 2023



## **Declaration**

I, James Knox, confirm that the work presented in this thesis is my own. Where information has been derived from other sources, I confirm that this has been indicated in the thesis.

James Knox

September 2023

## Acknowledgements

Firstly, I would like to thank my supervisors Matt, Gary, Ian and Tom for all of their guidance and support throughout my PhD. Matt, none of this work would have been possible without your knowledge and passion for science, so I'm extremely grateful for your mentorship over these past four years. I would also like to thank the MRC and AstraZeneca for funding my research.

I would also like to thank all of the past and present members of MedChem 3: Andy, Nicola, Lindsay, Jack, Nada, Tom, Tatiana, Gemma, Carmen, Adam, Alex and Brian. You all made the lab a much more enjoyable place to work in, and made the various trips to the California livelier than they would have otherwise been.

Thanks also to the rest of the chemistry department for making the ICR such a great place to work, and I would especially like to thank Amin, Maggie, Meirion, Joe, Lauren, Taleen, and Beth for all of their structural chemistry support and assistance. John, thank you for always being there to help me brainstorm my way through any synthesis challenges, you would always have a piece of useful advice on hand. I am also very grateful to my HDSO colleagues Olivier and Mark for their help in showing a lowly chemist how to prepare an assay plate and operate a plate reader.

No acknowledgements section would be complete without mentioning the student squad aka SCNSSFCFVCD: Iona, Charles, Will, Chaz, Beth, Dani, Gitu, Katie, Imogen, and Chloe in addition to those I have already mentioned. The themed nights out, pub crawls, bonkers conversations and general chaotic antics have been the highlight of my time in London, and I am going to miss spending time with you all. To Ali, Adam and Harriet; needless to say that without you three I would be much worse off, so thank you for keeping me grounded especially after some of the tougher days.

Mam, Dad, thanks for all of your love and support throughout my PhD, I promise that one day I will work out how to explain my research to you.

Finally, I would like to thank Miina. Your love, encouragement and belief in me have been constant and I truly couldn't have done it without you.

## Abstract

Targeted Covalent Inhibitors (TCIs) represent an increasingly important strategy in modern drug discovery. TCIs exploit high affinity, reversible ligands which are then modified with modestly-reactive electrophilic warheads to covalently modify active site, nucleophilic residues within the target enzyme to inhibit their function. Irreversible covalent enzyme inhibition can overcome competition with high abundance, high affinity substrates and low affinity, shallow binding sites. The nucleophilic amino acid cysteine is the most common residue targeted in TCI discovery efforts, but the low abundance of this residue in the proteome limits the scope of cysteine-TCIs. Lysine is a potentially attractive alternative residue to target for TCIs, owing to its nucleophilic amino group and greater natural abundance. The aim of my thesis is to investigate the potential of lysine-TCIs to modulate the function of difficult-to-drug targets.

The stress-inducible molecular chaperone, HSP72, is a well-validated oncology target and is considered difficult-to-drug owing to its high affinity for the abundant endogenous ligands ATP and ADP. Previously within our group, nucleoside-derived lysine-TCIs had been developed to target the non-catalytic Lys-56 of the HSP72 nucleotide binding domain. However, we estimated that the potencies of these TCIs, measured through the covalent kinetic parameter  $k_{\text{inact}}/K_{\text{I}}$ , were at least an order of magnitude too weak to attenuate HSP72 function in a cellular context, so required further optimisation.

Herein, I detail the design, synthesis and optimisation of a series of high affinity HSP72 lysine-TCIs. This required the development of a novel protecting group strategy to modify the densely-functionalised adenosine core in the presence of the covalent warhead. Extensive characterisation revealed exquisite biochemical potency, but despite substantial improvements in compound stability, the rate of electrophilic warhead hydrolysis under the cell assay conditions unfortunately remained too high to effect downregulation of HSP70 clients at  $<20 \mu\text{M}$  total concentration. However, by employing a hydrolytically stable lysine-reactive warhead, I discovered the lysine-TCI CCT400591, the state-of-the-art tool compound for investigating HSP70 inhibition *in vitro*.

Using our strategy, I then designed lysine-TCIs to overcome tertiary resistance mutations in the key oncogenic protein EGFR, leading to the discovery of a series of lysine-TCIs which covalently label the catalytic lysine within the EGFR tyrosine kinase domain.

## Statement of Independent Work

All work in this thesis was carried out by myself, other than the following:

- Cellular assays (Section 5.4.2 and 6.4) were performed by Marissa Powers of the CCDD RBMT team.
- Cell free fraction data (Section 6.4) were acquired by Pharmidex UK.
- EGFR activity assays (Section 7.2.4) were performed by Omar Alkhatib of AstraZeneca.
- EGFR intact protein mass spectrometry (Section 7.3.3) was performed by Marcus Ladds of AstraZeneca.

Additionally, the HSP72 intact protein mass spectrometry (Section 4.3.2, 4.4.3 and 6.3.2) and hydrolytic stability assay (5.3.2) were performed by myself with assistance from Amin Mirza of the CCDD Structural Chemistry department.

**Abbreviations**

°C	Degrees Celsius
Å	Angstrom
A	Active affinity label
ABPP	Activity-based protein profiling
Ac	Acetyl
ADP	Adenosine diphosphate
AISF	[4-(acetylamino)phenyl]imidodisulfuryl difluoride
atm	Atmospheres
ATP	Adenosine triphosphate
AUC	Area under the curve
AURKA	Aurora kinase A
BAG1	BCL2 associated athanogene 1
BD	Bürgi-Dunitz
Boc	<i>tert</i> -butyloxycarbonyl
BTK	Bruton's tyrosine kinase
CDK	Cyclin-dependent kinase
CE	Covalent efficiency
CHAPS	3-[(3-cholamidopropyl)dimethylammonio]-1-propanesulfonate
CLL	Chronic lymphocytic leukaemia
CML	Chronic myelogenous leukaemia
C <sub>u</sub>	Unbound concentration
CuAAC	Cu(I)-catalysed azide–alkyne cycloaddition
Da	Dalton
DABSO	1,4-diazabicyclo[2.2.2]octane bis(sulfur dioxide) adduct
DBU	1,8-diazabicyclo(5.4.0)undec-7-ene

DCE	1,2-dichloroethane
DIPEA	<i>N,N</i> -diisopropylethylamine
DMA	Dimethylacetamide
DMAP	4-dimethylaminopyridine
DMEM	Dulbecco's modified eagle's medium
DMF	Dimethylformamide
DMSO	Dimethyl sulfoxide
DNA	Deoxyribonucleic acid
dUMP	Deoxyuridine monophosphate
E	Enzyme
EGF	Epidermal growth factor
EGFR	Epidermal growth factor receptor
eIF4E	Eukaryotic translation initiation factor 4E
<i>ent</i>	Enantiomer
ERBB2	Avian erythroblastosis oncogene B-2
ESI	Electrospray ionisation
Et	Ethyl
EtOH	Ethanol
F <sub>b</sub>	Bound fraction
FBS	Foetal bovine serum
FDA	Food and Drug Administration
5-FdUMP	5-Fluorodeoxyuridine monophosphate
FL	Flippin-Lodge
FP	Fluorescence polarisation
FSBA	5'-(4-Fluorosulfonylbenzoyl)adenosine
g	Gram
GDP	Guanosine diphosphate

GI <sub>50</sub>	Half maximal growth inhibition concentration
GIST	Gastrointestinal stromal tumour
GRP78	78 kDa glucose-regulated protein
GSH	Glutathione
GTP	Guanosine triphosphate
h	Hour
HBD	Hydrogen bond donor
H-bonding	Hydrogen bonding
HbS	Sickle haemoglobin
HMBC	Heteronuclear multiple bond correlation
hmCK	Human muscle creatine kinase
HMDS	Hexamethyldisilazane
HRMS	High resolution mass spectrometry
HSC70	Heat shock cognate 71 kDa protein
HSP	Heat shock protein
HSP72	Heat shock 70 kDa protein 1
HSQC	Heteronuclear single quantum correlation
HSR	Heat shock response
I	Inhibitor
IAM	Iodoacetamide
<sup>i</sup> Bu	Isobutyl
IC <sub>50</sub>	Half maximal inhibitory concentration
IPMS	Intact protein mass spectrometry
<sup>i</sup> Pr	Isopropyl
IR	Infrared
IRE1 $\alpha$	Endoribonuclease inositol-requiring enzyme 1 $\alpha$
isoTOP	Isotopic tandem orthogonal proteolysis



JDP	J-domain protein
$k_{\text{cat}}$	Rate constant for maximal rate of enzymatic reaction
$K_{\text{d}}$	Dissociation constant
$k_{\text{hyd}}$	Rate constant for hydrolysis
$K_{\text{i}}$	Inhibition constant
$K_{\text{i}}^*$	Steady state inhibition constant
$K_{\text{I}}$	Half maximal rate of inactivation constant
$k_{\text{inact}}$	Rate constant for the maximal rate of inactivation
$K_{\text{M}}$	Michaelis constant
$k_{\text{obs}}$	Observed rate constant
KRAS	Kirsten rat sarcoma virus
LC	Liquid chromatography
LDA	Lithium diisopropylamide
LiHMDS	Lithium hexamethyldisilazane
Lysine-TCI	Lysine-targeting covalent inhibitor
M	Molar
$m$	Meta
MCL	Mantle cell lymphoma
Mcl-1	Myeloid leukaemia cell differentiation protein
Me	Methyl
MeOH	Methanol
min	Minute
MM	Michaelis-Menten
MMP	Molecular match pairs
MoA	Mechanism of action
mP	Millipolarisation
MS	Mass spectrometry

$\mu$ wave	Microwave
MW	Molecular weight
m/z	Mass-to-charge ratio
NBD	Nucleotide binding domain
NBS	<i>N</i> -bromosuccinimide
n-Bu	n-butyl
NEF	Nucleotide exchange factor
NFSI	<i>N</i> -fluorobenzenesulfonimide
NHS	<i>N</i> -hydroxysuccinimide
NME1	Nucleoside diphosphate kinase A
NMP	<i>N</i> -methylpyrrolidone
NMR	Nuclear magnetic resonance
NSCLC	Non-small cell lung cancer
<i>o</i>	Ortho
<i>p</i>	Para
PBS	Phosphate-buffered saline
PD	Pharmacodynamics
PDB	Protein data bank
PG	Protecting group
Ph	Phenyl
P <sub>i</sub>	Inorganic phosphate
PI3K $\delta$	Phosphoinositide 3-kinase delta
PK	Pharmacokinetics
P-loop	Phosphate binding loop
PLP	Pyridoxal 5'-phosphate
POI	Protein-of-interest
PTSA	<i>p</i> -toluenesulfonic acid

RNA	Ribonucleic acid
rpm	Revolutions per minute
rt	Room temperature
RTK	Receptor tyrosine kinase
SAR	Structure-activity relationship
SBD	Substrate binding domain
SEM	Trimethylsilylethoxymethyl
±SEM	Standard error of the mean
sHSP	Small heat shock protein
SILAC	Stable-isotope labelling by amino acids in cell culture
siRNA	Small interfering ribonucleic acid
S <sub>N</sub> Ar	Nucleophilic aromatic substitution
SPR	Surface plasmon resonance
SrtA	Sortase A
t	Time
t <sub>1/2</sub>	Half-life
TBAB	Tetrabutylammonium bromide
TBAF	Tetrabutylammonium fluoride
TBS	<i>tert</i> -butyldimethylsilyl
<sup>t</sup> Bu	<i>tert</i> -butyl
TCI	Targeted covalent inhibitor
TDFP	Time-dependent fluorescence polarisation
TEV	Tobacco etch virus
Tf	Triflate
TFA	Trifluoroacetic acid
THF	Tetrahydrofuran
TIPS	Triisopropylsilyl

TKD	Tyrosine kinase domain
TKI	Tyrosine kinase inhibitor
TLC	Thin-layer chromatography
TM	Triple mutant
TMS	Trimethylsilane
TMSI	Iodotrimethylsilane
TO	Total occupancy
ToF	Time-of-flight
TRIS	Tris(hydroxymethyl)aminomethane
TS	Thymidylate synthase
TTR	Transthyretin
VdW	Van der Waals
v/v	Volume-by-volume
WT	Wild type
w/v	Weight-by-volume

## Contents

<b>1</b>	<b>Introduction</b> .....	<b>1</b>
1.1	Small Molecule Drugs in Oncology .....	1
1.2	Irreversible Inhibition .....	3
1.2.1	Approaches to Irreversible Inhibition .....	3
1.2.2	Kinetics of Irreversible Targeted Covalent Inhibitors .....	7
1.2.3	Advantages of Targeted Covalent Inhibition .....	11
1.2.4	Design of Targeted Covalent Inhibitors .....	14
1.2.5	Activity-based Protein Profiling .....	16
1.2.6	Cysteine-Targeting Covalent Inhibitors .....	19
1.2.7	Lysine-Targeting Covalent Inhibitors .....	20
1.2.8	Design of Irreversible Lysine-Targeting Covalent Inhibitors .....	21
1.3	HSP70.....	26
1.3.1	Heat Shock Proteins .....	26
1.3.2	HSP70 protein family.....	26
1.3.3	HSP70 and Cancer .....	30
1.3.4	Targeting HSP70.....	30
1.3.5	HSP70 is Difficult-To-Drug.....	33
1.3.6	Lysine-Targeting Covalent Inhibitors of HSP72 .....	37
<b>2</b>	<b>Project Aims</b> .....	<b>42</b>
<b>3</b>	<b>Synthesis of HSP72 5'-Ether-Lysine-TCIs</b> .....	<b>45</b>
3.1	Introduction .....	45
3.1.1	Design of 3 <sup>rd</sup> Generation HSP72 Lysine-TCIs.....	45
3.1.2	Previous Work Towards the Synthesis of Adenosine-Derived 5'-Ethers.....	47
3.2	Optimisation of Synthetic Route to Access 5'-Ether .....	53
3.2.1	TBS Protecting Group Strategy .....	53

3.2.2	Protecting Group Strategy .....	56
3.3	Incorporating the Covalent Warhead .....	62
3.3.1	Accessing 8- <i>H</i> adenosine-derived TCI <b>101</b> .....	62
3.3.2	Accessing 8- <i>N</i> -benzyl adenosine-derived TCI <b>43</b> .....	66
3.4	Conclusions .....	67
<b>4</b>	<b>Characterisation of 5'-Ether-Linked HSP72 Lysine-TCIs .....</b>	<b>69</b>
4.1	Introduction .....	69
4.2	Time-Dependent Fluorescent Polarisation Assay .....	70
4.2.1	Introduction to Fluorescence Polarisation.....	70
4.2.2	Interpretation of Fluorescence Polarisation Assays .....	73
4.2.3	Limit of Detection for Fluorescence Polarisation Assays.....	77
4.2.4	Quantification of Covalent Kinetics.....	81
4.2.5	Synthesis of 5'-Ether-Linked TCI Analogues.....	86
4.2.6	Synthesis of 5'-Ether-Linked TCI Controls.....	92
4.2.7	Characterisation of New Analogues in the TDFP Assay .....	97
4.2.8	Characterisation with Higher Affinity Fluorescent Probe .....	100
4.3	Intact Protein Mass Spectrometry .....	107
4.3.1	Introduction to Intact Protein Mass Spectrometry .....	107
4.3.2	Profiling 5'-Ether-Linked TCIs by Intact Protein Mass Spectrometry ...	108
4.4	Development of Probe for Activity-Based Protein Profiling .....	112
4.4.1	Design Hypothesis of Probe for Activity-Based Protein Profiling .....	112
4.4.2	Synthesis of Probe for Activity-Based Protein Profiling .....	114
4.4.3	Characterisation of Probe for Activity-Based Protein Profiling .....	122
4.5	Conclusions .....	126
<b>5</b>	<b>Reactivity-Based Profiling of HSP72 Lysine-TCIs .....</b>	<b>128</b>
5.1	Introduction .....	128
5.2	Moderate Reversible Affinity 5'-Ether-Linked HSP72 Lysine-TCIs .....	130

5.2.1	Design of Moderate Reversible Affinity Compounds .....	130
5.2.2	Synthesis of Moderate Reversible Affinity Compounds .....	135
5.2.3	Characterisation of Moderate Reversible Affinity Compounds.....	138
5.3	Quantification of Intrinsic Reactivity .....	143
5.3.1	Introduction .....	143
5.3.2	Quantifying Hydrolytic Stability by Mass Spectrometry.....	145
5.3.3	Covalent Efficiency .....	149
5.4	Cellular Activity of HSP72 Lysine-Targeting Covalent Inhibitors.....	151
5.4.1	Stability in Cell Media .....	151
5.4.2	Biomarkers of HSP70 Inhibition.....	153
5.5	Conclusions .....	156
<b>6</b>	<b>Reversible HSP72 Lysine-TCIs.....</b>	<b>158</b>
6.1	Introduction .....	158
6.1.1	Alternative Lysine-Reactive Warheads.....	158
6.1.2	Reversible Targeted Covalent Inhibitors .....	160
6.1.3	Lysine-Targeting Reversible Covalent Inhibition.....	162
6.1.4	Stabilisation of the Lysine-Aldehyde Adduct .....	164
6.2	Design and Synthesis of HSP72 Reversible Lysine-TCI <b>232</b> .....	170
6.2.1	Design of HSP72 Reversible Lysine-TCI <b>232</b> .....	170
6.2.2	Synthesis of HSP72 Reversible Lysine-TCI <b>232</b> .....	171
6.3	Characterisation of Reversible Lysine-TCI <b>232</b> .....	175
6.3.1	Characterising Reversible Lysine-TCI <b>232</b> in the TDFP Assay .....	175
6.3.2	Characterising Reversible Lysine-TCI <b>232</b> by Intact Protein-MS .....	180
6.4	Biological Profiling of Reversible TCI <b>232</b> .....	183
6.5	Conclusions and Future Work .....	185
<b>7</b>	<b>Lysine-Targeting Covalent Inhibitors of EGFR .....</b>	<b>189</b>
7.1	Introduction .....	189

7.1.1	Epidermal Growth Factor Receptor .....	189
7.1.2	Small Molecule Inhibitors of the EGFR Tyrosine Kinase Domain .....	192
7.1.3	Targeting the Catalytic Lysine of EGFR .....	195
7.2	Design and Synthesis of 1 <sup>st</sup> Generation Lysine-TCIs of EGFR .....	196
7.2.1	Design of 1 <sup>st</sup> Generation EGFR Lysine-TCIs .....	196
7.2.2	Synthesis of 1 <sup>st</sup> Generation EGFR Lysine-TCIs .....	198
7.2.3	Synthesis of 1 <sup>st</sup> Generation EGFR Lysine-TCI Controls .....	203
7.2.4	Characterisation of 1 <sup>st</sup> Generation EGFR Lysine-TCIs .....	206
7.3	Design and Synthesis of 2 <sup>nd</sup> Generation EGFR Lysine-TCIs .....	209
7.3.1	Design of 2 <sup>nd</sup> Generation EGFR Lysine-TCIs .....	209
7.3.2	Synthesis of 2 <sup>nd</sup> Generation EGFR Lysine-TCIs .....	210
7.3.3	Characterisation of 2 <sup>nd</sup> Generation EGFR Lysine-TCIs .....	216
7.4	Conclusions and Future Work .....	219
<b>8</b>	<b>Experimental .....</b>	<b>222</b>
8.1	Chemical Synthesis .....	222
8.1.1	General Information .....	222
8.1.2	Chemistry Experimental Procedures .....	223
8.2	Biochemical Assays .....	398
8.2.1	Fluorescence Polarisation .....	398
8.2.2	Mass Spectrometry .....	399
8.2.3	EGFR Activity Assay .....	402
8.3	Assay Free Fraction .....	402
8.4	Biology Experimental .....	403
8.4.1	General Information .....	403
8.4.2	HCT116 Western Blot Analysis .....	404
<b>9</b>	<b>Appendix .....</b>	<b>406</b>
9.1	NMR Spectra of Key Compounds .....	406



9.2	HPLC Traces and Mass Spectra of Key Compounds.....	408
9.3	Chiral HPLC of Key Compounds .....	409
9.4	Western Blot Data .....	413
9.4.1	Figure 5.25 .....	413
9.4.2	Figure 6.25 .....	416
9.4.3	Figure 6.26 .....	418
<b>10</b>	<b>References .....</b>	<b>421</b>

# 1 Introduction

# 1 Introduction

## 1.1 Small Molecule Drugs in Oncology

Historically, the treatment of cancer has been accomplished using small molecule cytotoxic chemotherapeutic agents.<sup>1</sup> Chemotherapy drugs can be broadly classified into four main categories; antimicrotubule agents, which can bind to and depolymerise microtubules; topoisomerase inhibitors, which bind to topoisomerase and cause DNA double strand breaks; antimetabolites, which mimic regular nucleotides and inhibit DNA synthesis; and alkylating agents, which covalently label DNA inhibiting its replication.<sup>2</sup> Chemotherapeutics are characterised by their broad spectrum cytotoxicity, resulting in limited discrimination between normal and cancer tissue.<sup>3</sup>

The need for selective agents with improved safety profiles has been somewhat satisfied with the advent of small molecule targeted therapies,<sup>4</sup> pioneered with the approval of imatinib in 2001 for the treatment of chronic myelogenous leukaemia (CML), that target critical oncoproteins.<sup>5</sup> Tumour proliferation and survival hinges on function-altering mutations in oncogenes and tumour-suppressor genes,<sup>6</sup> termed “oncogene addiction”, in addition to non-mutated genes, which alleviate cellular stress and are otherwise essential for tumour survival,<sup>7</sup> termed “non-oncogene addiction”. Small molecules can bind to these proteins and inhibit their function, leading to tumour cell growth inhibition and/or cell death.

As of 2020, there were 43 small molecule targeted therapies approved by the US Food and Drug Administration (FDA) for oncology indications,<sup>4</sup> 84% of which reversibly inhibit their target enzyme. Reversible inhibitors bind to their target enzyme in an equilibrium process in which free enzyme (E) and inhibitor (I) bind to form an enzyme-inhibitor complex (E·I) (Figure 1.1 A).<sup>8</sup>

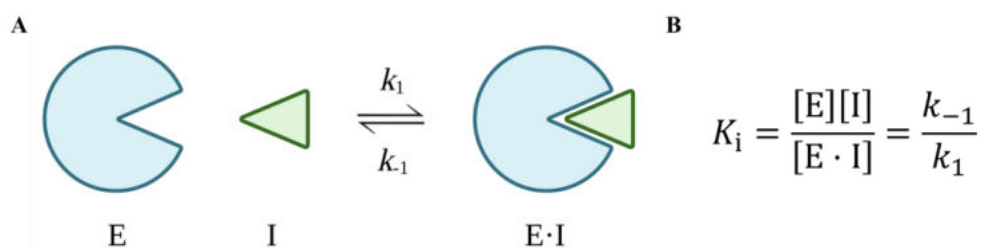


**Figure 1.1** **A** One step mechanism of targeted reversible inhibitors. **B** Inhibition dissociation constant,  $K_i$ , is governed by the forward rate constant  $k_1$ , and the reverse rate constant,  $k_{-1}$ .

Inhibition is quantified by the inhibition dissociation constant,  $K_i$  (Figure 1.1 B). The magnitude of the binding affinity  $K_i$ , which is a function of the on rate ( $k_1$ ) and the off-rate ( $k_{-1}$ ), is dependent on the non-covalent interaction forces between the protein and ligand, as well as protein-ligand shape complementarity and the hydrophobic effect.<sup>9</sup> Decreasing the  $K_i$  increases the extent of fractional target binding at equilibrium for a given free concentration. Occupancy of the target is what drives the efficacy of small molecule inhibitors,<sup>10</sup> therefore decreasing  $K_i$  will lead to an enhanced pharmacological effect.

*In vivo*, the efficacy of an inhibitor is determined by the free concentration at the site of action.<sup>11</sup> The free drug hypothesis states that, in the absence of active transport, a passively permeable compound at equilibrium will have the same free drug concentration on both sides of a biological membrane. Therefore, the pharmacological effect exerted by a reversible inhibitor is dependent on the unbound concentration ( $C_u$ ) of the drug at the site of action, which itself is dependent on its pharmacokinetic (PK) profile (Figure 1.2).

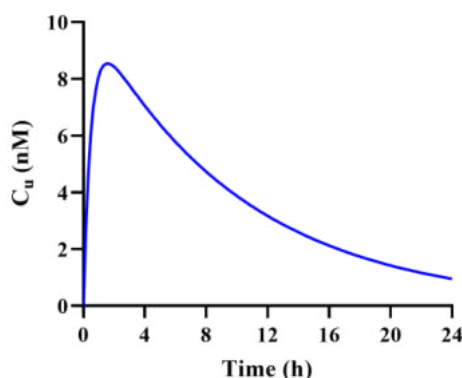


**Figure 1.2** Typical pharmacokinetic profile of a drug, following administration of a single oral dose at  $t = 0$ , showing how  $C_u$  varies over time.

To obtain the desired pharmacological effect for a small molecule reversible inhibitor through target occupancy,<sup>12</sup> the binding affinity for the target can be improved to decrease the required free concentration (decreasing  $K_i$ ), and/or by improving the PK properties of the drug to increase the unbound exposure.

Despite the prevalence of small molecule targeted therapies with a reversible mechanism of action (MoA) in oncology, competition with high affinity, high abundance endogenous substrates,<sup>13</sup> shallow or polar binding sites,<sup>14</sup> and therapy-induced resistance mechanisms<sup>15</sup> can limit their application against these difficult-to-drug enzymatic targets. Consequently, there is a need for alternative modalities to be explored.

## 1.2 Irreversible Inhibition

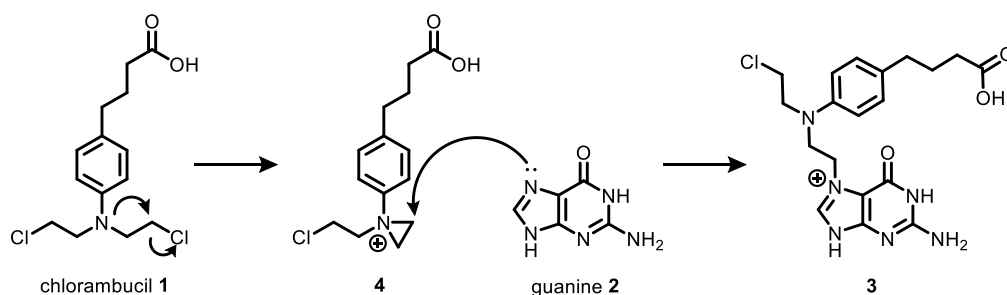
### 1.2.1 Approaches to Irreversible Inhibition

Irreversible inhibitors represent an attractive alternative paradigm to reversible inhibition. With an irreversible inhibitor, the small molecule reversible ligand is modified with an electrophilic group or warhead to form a covalent bond with the target.<sup>16</sup> ~30% of currently marketed drugs are reported to have a covalent MoA,<sup>17</sup> many of which were discovered serendipitously, with their mechanism only elucidated years after their approval. For example, discovered in 1890s by Bayer, the mechanism of the pain and inflammation medication aspirin was first elucidated in the 1970s,<sup>18</sup> where it was found to acetylate an active site serine residue of cyclooxygenase-1 and -2.<sup>19</sup>

Compounds containing electrophilic moieties are often excluded from drug discovery campaigns, owing to concerns over idiosyncratic toxicity arising from non-specific covalent labelling of anti-targets.<sup>20</sup> In 1973, a chemically reactive metabolite of paracetamol was discovered to induce hepatic necrosis in mice through covalent binding to liver macromolecules.<sup>21</sup> In addition to concerns of broad spectrum cytotoxicity, the risk of immune system activation as a result of protein conjugation with reactive metabolites resulting in haptensisation, has led to anxiety over the application of chemically reactive functionalities in biological systems.<sup>22</sup>

Despite these risks, non-targeted covalent drugs, such as alkylating agents, have found extensive use in traditional chemotherapy.<sup>23</sup> The most commonly applied alkylating agents are the nitrogen mustards, exemplified by chlorambucil **1**, which reacts with the

7-*N* of guanine **2** in DNA, forming alkyl-guanidine **3** *via* aziridinium ion **4**<sup>24</sup> leading to DNA breakdown and apoptosis of tumour cells (Scheme 1.1).<sup>25</sup>



**Scheme 1.1** Mechanism of chemotherapeutic chlorambucil **1** in the 7-*N*-alkylation of DNA base guanine **2**.

Alkylating agents such as nitrogen mustards are an example of non-specific affinity labels, which irreversibly covalently modify suitable nucleophiles both internal and external to the target binding site.<sup>8</sup> For an enzymatic reaction, non-specific affinity labels operate *via* a one-step mechanism in which free enzyme (E) and inhibitor (I) react to form the enzyme-inhibitor covalent complex (E-I), as described by the first order rate constant for inactivation,  $k_{\text{inact}}$  (Figure 1.3).

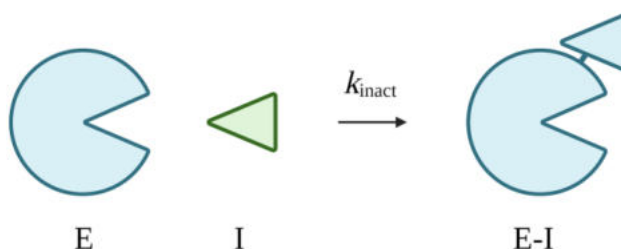


**Figure 1.3** Mechanism of non-specific affinity labels.

Non-specific affinity labels are typically only applied in cancer chemotherapy, as their lack of selectivity can lead to considerable toxicity and potential carcinogenicity.<sup>26</sup>

The second historical class of covalent drugs are the natural product-derived inhibitors,<sup>27</sup> which include Salinosporamide A **5**, TNP-470 **6**, wortmannin **7** and 5-fluorouracil **8** (Figure 1.4).

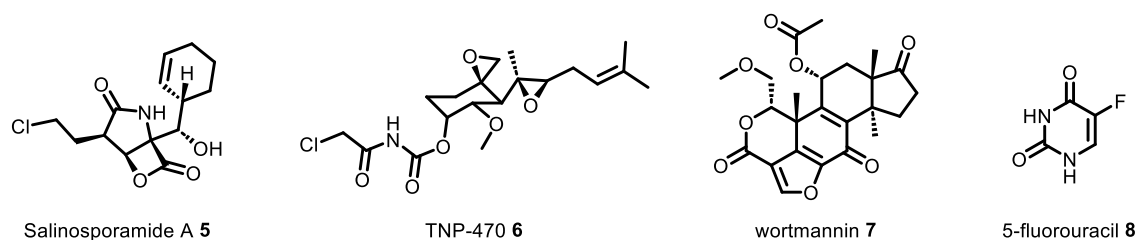


**Figure 1.4** Examples of natural product-derived inhibitors that have been applied in oncology.

Some natural product-derived covalent inhibitors, including 5-fluorouracil **8** and the antibiotic penicillin, are termed as mechanism-based inactivators, as they are recognised as alternative substrates by their enzymatic target, and participation in the catalytic reaction of the enzyme is required for covalent inactivation.<sup>28</sup> For mechanism-based inactivators, initial reversible binding of enzyme (E) and inhibitor (I) to form the enzyme-inhibitor complex (E·I) is followed by transformation of the inhibitor to the active affinity label (A) by the catalytic machinery of the enzyme, forming the E·A complex (Figure 1.5).

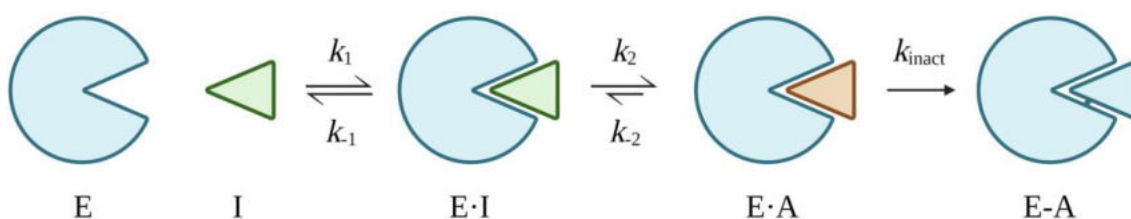
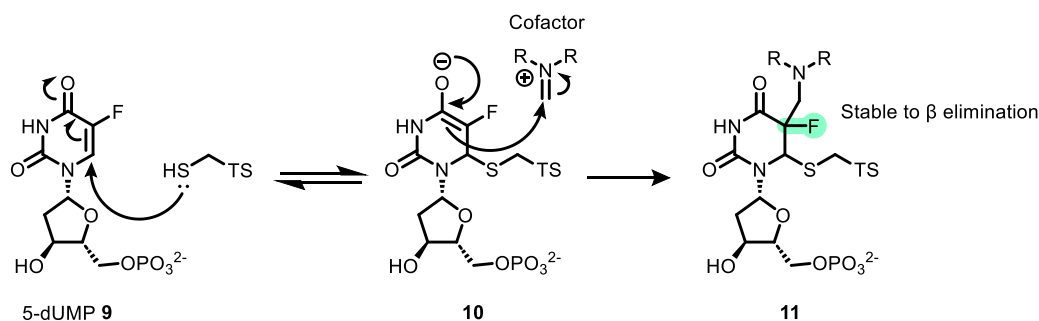


**Figure 1.5** Mechanism of mechanism-based inactivators. Formation of reversible E·I complex is followed by conversion of inhibitor I to an affinity label A by the enzyme, which forms an irreversible adduct E·A.

Finally, the affinity label undergoes adduct formation within the enzyme active site to form the inactivated enzyme (E·A).<sup>8</sup> The mechanism-based inactivator 5-fluorouracil **8** is a fluorinated derivative of the nucleobase uracil, which is converted to 5-fluorodeoxyuridine monophosphate (5-FdUMP) **9**, intracellularly. By mimicking native substrate, deoxyuridine monophosphate (dUMP), 5-FdUMP **9** reacts with the catalytic cysteine of thymidylate synthase (TS) to give covalent complex **10** (Scheme 1.2).<sup>29</sup> Alkylation by a cofactor leads to enzyme inactivation as the 5-fluorine atom prevents elimination, resulting in an irreversible adduct **11**.



**Scheme 1.2** Mechanism of inactivation of TS by 5-FdUMP **9**. Catalytic cysteine attacks Michael acceptor in 5-fluoruracil ring, and the resulting enolate **10** attacks a methylating cofactor giving stable adduct **11**.

Whilst natural product derived irreversible inhibitors can potentially function as potent and selective therapies, they are often hindered by limited target selectivity and poor physicochemical properties.<sup>30</sup> Additionally, the high structural complexity of some natural products can make analogue synthesis impractical for a drug discovery campaign.<sup>31</sup>

The third class of irreversible inhibitor are targeted covalent inhibitors (TCIs). TCIs are discovered through rational ligand design, typically by incorporating a modestly reactive covalent warhead into the scaffold of a reversible inhibitor.<sup>32</sup> Strategies to develop TCIs through structure-guided design originated in the 1990s in the development of compounds targeting the Epidermal Growth Factor Receptor (EGFR) and avian erythroblastosis oncogene B-2 (ERBB2).<sup>33</sup> Application of the TCI-strategy in oncology has led to the FDA approval of numerous targeted therapies employing this modality, including EGFR inhibitor osimertinib **12**,<sup>34</sup> Kirsten rat sarcoma virus (KRAS) G12C inhibitor sotorasib **13**,<sup>35</sup> and Bruton's tyrosine kinase (BTK) inhibitor acalabrutinib **14**<sup>36</sup> (Figure 1.6).



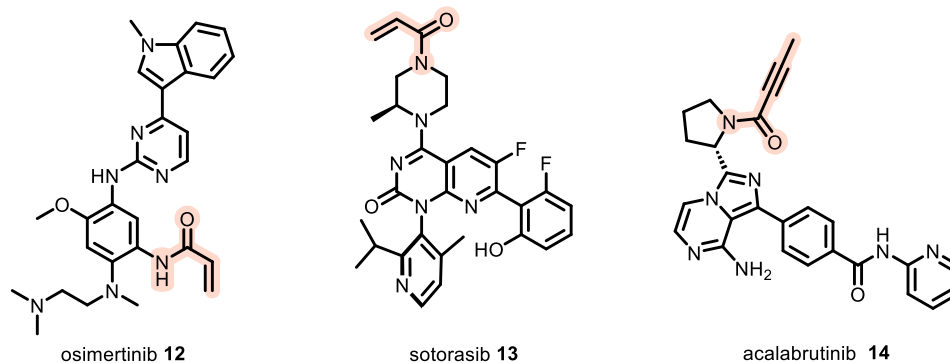


**Figure 1.6** Examples of approved targeted covalent inhibitors for oncology with covalent warhead highlighted.

### 1.2.2 Kinetics of Irreversible Targeted Covalent Inhibitors

Irreversible TCIs are defined by a two-step mechanism of inhibition.<sup>37</sup> Firstly, the inhibitor binds reversibly to form the enzyme-inhibitor complex (E·I), which is under equilibrium and can freely dissociate (Figure 1.7 A). The second step is the reaction of the covalent warhead with a nucleophilic amino acid in the binding site to form the inactivated enzyme (E-I), which only occurs at a significant rate within the enzyme inhibitor complex. This allows electrophiles with limited intrinsic reactivity to be employed as warheads in the TCI approach.

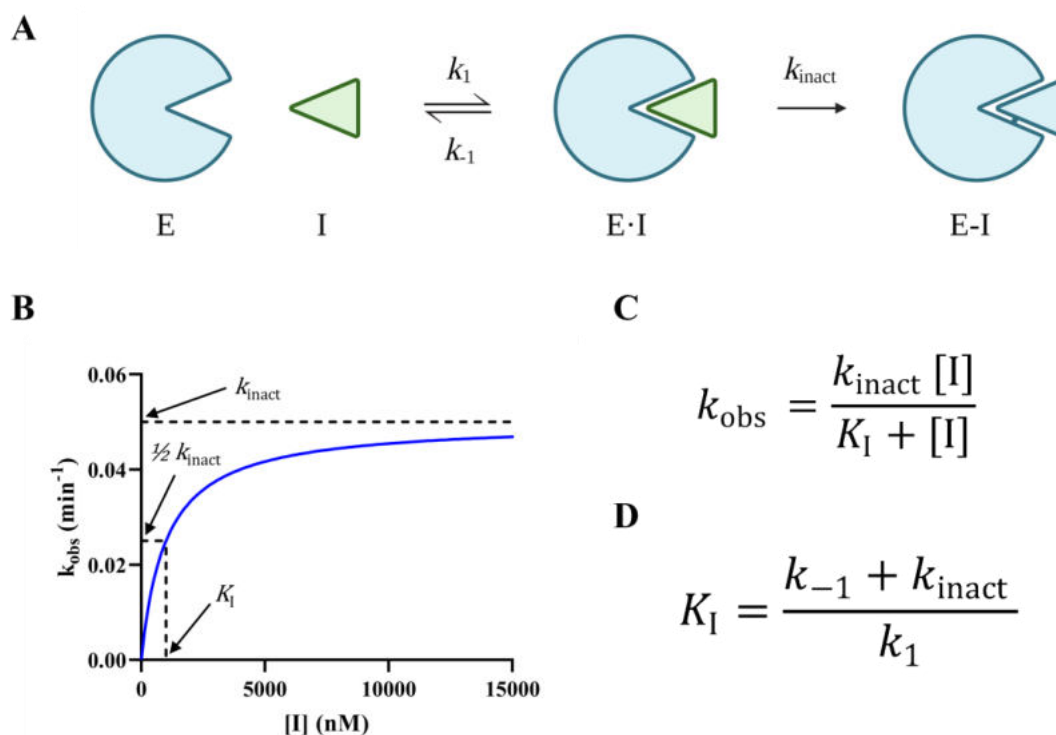


**Figure 1.7** **A** Mechanism of irreversible targeted covalent inhibitors, where complex E·I forms from reversible binding of the inhibitor, followed by reaction of the covalent warhead with a proximal residue within the binding site to form the inactivated enzyme E-I. **B** Simulated plot of the observed pseudo-first order rate constant  $k_{\text{obs}}$  against time,  $K_{\text{I}} = 1000$  nM,  $k_{\text{inact}} = 0.05$  min<sup>-1</sup>. Plotted in GraphPad Prism 9. **C** Relationship between observed rate constant  $k_{\text{obs}}$  and [I], which is also a function of the observed rate of inactivation  $k_{\text{inact}}$  and the inhibitor concentration equal to the half maximal rate of inactivation,  $K_{\text{I}}$ . **D** Relationship between  $K_{\text{I}}$ ,  $k_{\text{inact}}$  and the microscopic reversible rate constants  $k_1$  and  $k_{-1}$ .

Plotting  $k_{\text{obs}}$ , the observed pseudo-first order rate constant for the TCI reaction at a particular inhibitor concentration, against [I] illustrates that the  $k_{\text{obs}}$  eventually plateaus at high inhibitor concentrations (Figure 1.7 B). The relationship between  $k_{\text{obs}}$  and [I] is also dependent on  $k_{\text{inact}}$  and  $K_{\text{I}}$  (Figure 1.7 C). At high inhibitor concentrations ( $[\text{I}] \gg K_{\text{I}}$ ), the enzyme becomes reversibly saturated and therefore the observed rate constant,  $k_{\text{obs}}$ , is approximately equal to  $k_{\text{inact}}$ .  $k_{\text{inact}}$  therefore describes the maximal rate of inactivation at a theoretically infinite inhibitor concentration, which is analogous to  $k_{\text{cat}}$  in Michaelis-Menten (MM) enzyme kinetics. Alternatively, it can be expressed as the half-life of inactivation at infinite inhibitor concentration,  $t_{1/2}^{\infty} = \ln(2)/k_{\text{inact}}$ .

The term  $K_I$  is defined as the inhibitor concentration at half maximal rate of inactivation ( $k_{\text{obs}} = \frac{1}{2} k_{\text{inact}}$ ), which is analogous to the  $K_M$  of MM kinetics.  $K_I$  is distinct from  $K_i$ , the inhibition dissociation constant for reversible inhibitors, as it depends on  $k_{\text{inact}}$  in addition to the microscopic reversible rate constants  $k_1$  and  $k_{-1}$  (Figure 1.7 D).<sup>8</sup> However, when the dissociation from the reversible complex is much faster than the covalent bond formation step ( $k_{-1} \gg k_{\text{inact}}$ , rapid equilibrium), then  $K_I \approx K_i$  and the reversible affinities of TCIs and reversible inhibitors can be compared *via* their respective  $K_i$  values.

At low inhibitor concentrations ( $[I] \ll K_I$ ), the relationship between  $k_{\text{obs}}$  and  $[I]$  can be simplified further to a first order approximation (Figure 1.8 A). Plotting  $k_{\text{obs}}$  against  $[I]$  at low inhibitor concentrations is therefore linear with the pseudo-second order rate constant,  $k_{\text{inact}}/K_I$ , as the gradient (Figure 1.8 B).

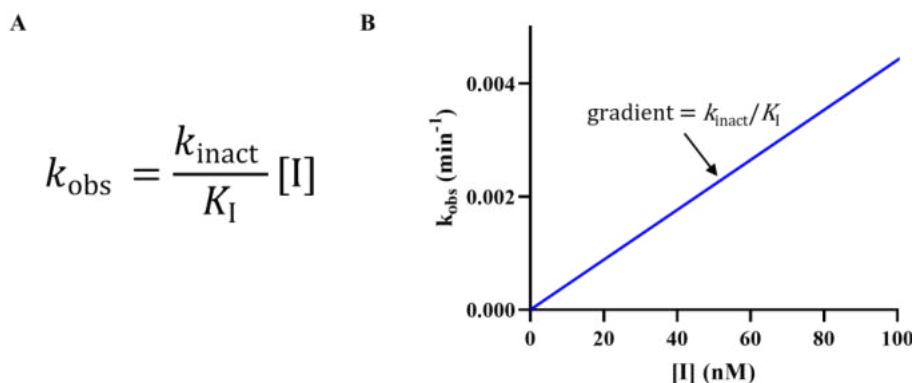


**Figure 1.8** **A** Relationship between  $k_{\text{obs}}$  and  $[I]$  when  $[I] \ll K_I$ . **B** Simulated plot of  $k_{\text{obs}}$  against  $[I]$  focussed on linear region,  $K_I = 1000$  nM,  $k_{\text{inact}} = 0.05$  min<sup>-1</sup>.

$k_{\text{inact}}/K_I$  is the principal metric through which the potency of a TCI is optimised, as it is a time-independent parameter which encapsulates the reversible affinity of the TCI, through  $K_I$ , and efficiency of the covalent bond formation step, through  $k_{\text{inact}}$ .<sup>37</sup> Whilst the assessment of  $k_{\text{inact}}/K_I$  is well-established as a strategy to quantify the potency of a TCI, it is often underutilised, owing to the challenges in measuring the individual kinetic parameters  $k_{\text{inact}}$  and  $K_I$ . This has resulted in an overreliance on half maximal inhibitory concentration ( $IC_{50}$ ) values to drive the optimisation of TCIs in drug discovery campaigns.  $IC_{50}$  values cannot furnish an estimate of the  $k_{\text{inact}}/K_I$ , as they are time-dependent, which can confound analysis.<sup>37</sup> As the enzyme is irreversibly inactivated over the course of an incubation, this leads to a time-dependent decrease in the free protein concentration, resulting in a decrease in the apparent  $IC_{50}$  value over time (Figure 1.9 A).

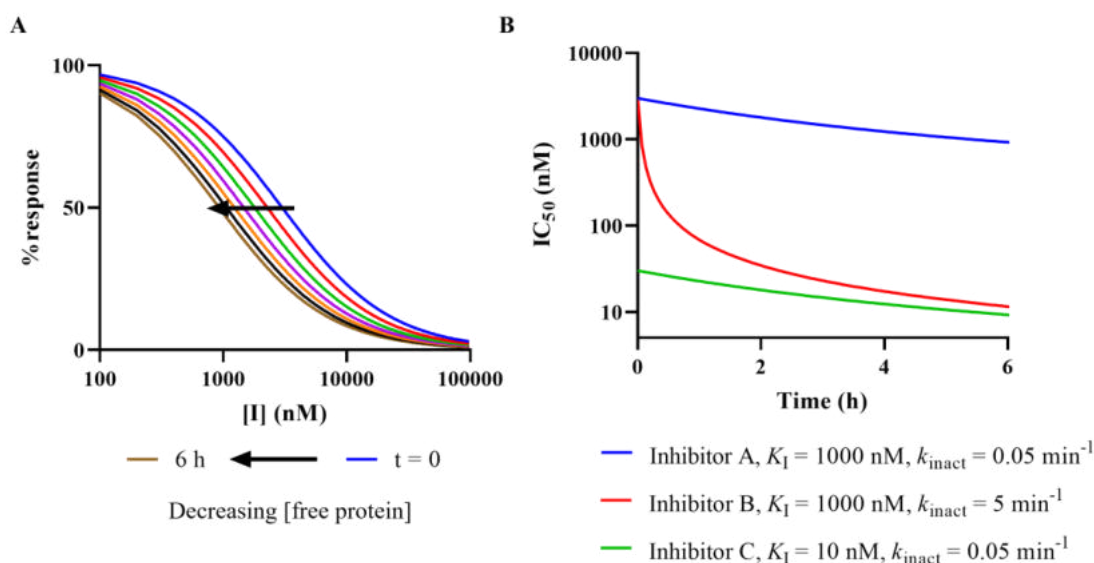


**Figure 1.9** **A** Simulated data showing time-dependent shift of  $IC_{50}$  values with an irreversible TCI. **B** Simulated plot of  $IC_{50}$  against time for an irreversible TCI using equation derived by Maurer et al.<sup>38</sup>

Relying on  $IC_{50}$  values in TCI optimisation can be unsuitable for understanding inhibitor potency, as the  $IC_{50}$  value fails to capture the contribution of each of the kinetic parameters  $k_{\text{inact}}$  and  $K_I$  to the affinity. To illustrate this, the time-dependent  $IC_{50}$  values were modelled for three hypothetical inhibitors A, B and C (Figure 1.9 B). Inhibitors A and B exhibit identical reversible affinities ( $K_I = 1000$  nM) but inhibitor B has a 100-fold greater  $k_{\text{inact}}$ . Analysis of the  $IC_{50}$  values for these two compounds at  $t = 0$  would suggest they are equipotent; however, over the course of an incubation, the greater  $k_{\text{inact}}$  of inhibitor B leads to a greater time-dependent shift in the  $IC_{50}$  resulting in an apparent 100-fold potency difference at  $t = 6$  h compared to inhibitor A.

Inhibitors B and C have identical  $k_{\text{inact}}/K_I$  values, and thus have almost equipotent  $IC_{50}$  values at longer incubations ( $t > 2$  h). However, inhibitor B possesses a relatively modest reversible affinity ( $K_I = 1000$  nM) and potent  $k_{\text{inact}}$  ( $k_{\text{inact}} = 5$  min<sup>-1</sup>) which suggests that further optimisation of this compound would likely involve improvements in its non-covalent interactions. In contrast, inhibitor C possesses a high reversibly affinity ( $K_I = 10$  nM) but a comparatively modest  $k_{\text{inact}}$  (0.05 min<sup>-1</sup>), which implies that improvements in its  $k_{\text{inact}}$  would be the most effective way to increase the second-order rate constant  $k_{\text{inact}}/K_I$ . It is important to note that the  $k_{\text{inact}}$  is not only dependent on the intrinsic reactivity of the warhead, which is the innate capacity of the electrophilic warhead to react with a

nucleophile in the absence of an initial reversible binding event, but crucially the positioning of the warhead within the binding pocket and the specific angles and distances to the reacting residue. Therefore, optimisation of the pre-covalent binding mode can lead to substantial improvements in  $k_{\text{inact}}$ , without modifying the intrinsic reactivity of the electrophile. The importance of optimising the  $k_{\text{inact}}$  in addition to the  $K_{\text{I}}$  will be illustrated in the following sections.

To summarise, the following points are key to the understanding and interpretation of the kinetics of targeted covalent inhibitors:

- $K_{\text{I}}$  is the inhibitor concentration at half maximal rate of inactivation.  $K_{\text{I}} = K_{\text{i}}$ , the inhibitor dissociation constant for reversible inhibitors, when  $k_{-1} \gg k_{\text{inact}}$ , and therefore  $K_{\text{I}}$  quantifies the reversible affinity of the TCI.
- $k_{\text{inact}}$  is the maximal rate of inactivation at infinite inhibitor concentration, which quantifies the rate of covalent bond formation within the reversible enzyme-inhibitor complex. Crucially it is distinct from the intrinsic reactivity of the electrophile, as it also depends on the orientation and positioning of the warhead within the reversible complex.
- $k_{\text{inact}}/K_{\text{I}}$  is the key pseudo-second order rate constant which denotes the overall biochemical potency of a TCI. Unlike the  $\text{IC}_{50}$  value, it is a time-independent parameter which quantifies both the reversible affinity and the rate of covalent bond formation.

### 1.2.3 Advantages of Targeted Covalent Inhibition

The typical two-step mechanism of a TCI furnishes several advantages over standard reversible inhibition, especially when attempting to overcome difficult-to-drug targets. Many enzymatic targets possess high affinity, high abundance endogenous substrates which can outcompete reversible inhibitors, reducing efficacy.<sup>13</sup> Also, proteins can possess shallow, solvent exposed binding sites that make it challenging to improve affinity by introducing non-covalent interactions.<sup>14</sup> As the efficacy of a small molecule inhibitor is dependent on target occupancy, modulating the function of difficult-to-drug targets is thus a key challenge for small molecule targeted therapies.<sup>39</sup> Irreversible TCIs, however, can successfully overcome this challenge as the total occupancy continuously increases in a time-dependent manner as a result of covalent bond formation.

Consequently, TCIs can achieve a pharmacological effect despite modest reversible affinity and/or competition with high affinity/high abundance substrates.

Simulating the %total occupancy (%TO)<sup>37</sup> against time for four inhibitors with identical  $k_{\text{inact}}$  values but varying  $K_{\text{I}}$  values illustrates how even a modest reversible affinity TCI ( $K_{\text{I}} = 1000 \text{ nM}$ ,  $K_{\text{I}} \gg [\text{I}]$ ) can demonstrate a time-dependent increase in target occupancy (Figure 1.10).

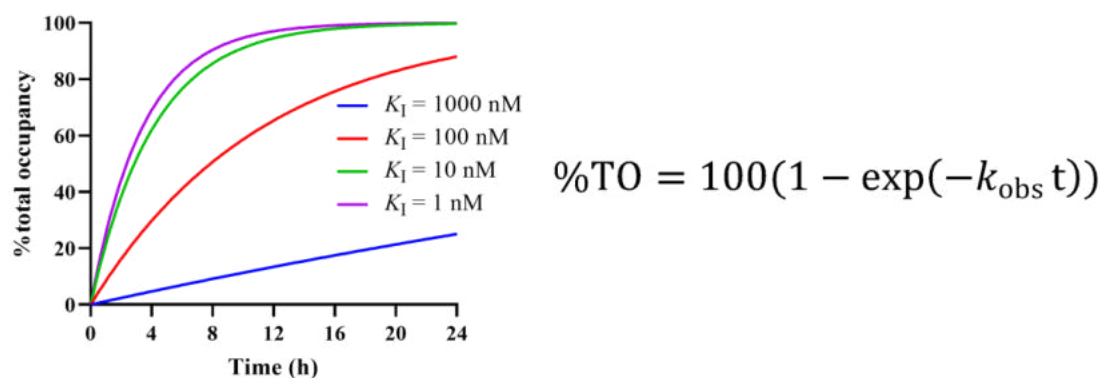


**Figure 1.10** Simulated plot of %total occupancy against time for four inhibitors with  $K_{\text{I}} = 1 - 1000 \text{ nM}$ , using %TO equation detailed by Strelow.<sup>37</sup>  $k_{\text{inact}} = 0.05 \text{ min}^{-1}$ ,  $[\text{I}] = 42 \text{ nM}$ .

A second advantage for irreversible TCIs is that they can potentially display an extended pharmacodynamic (PD) effect that is disconnected from the free concentration at the site of action, as determined by the PK profile of the compound.<sup>37</sup> When a reversible inhibitor is eliminated from the body, the decrease in unbound concentration leads to a reduced target occupancy at distribution equilibrium, and therefore a reduced PD effect, consistent with the free drug hypothesis. However, in addition to irreversible TCIs exhibiting a time-dependent increase in occupancy, the resulting covalent adduct is also unable to dissociate from the target. Therefore, despite the drug being eliminated from the body over time, there is no corresponding decrease in the occupancy of the target, and its functional activity can only be restored through protein resynthesis. Modelling the PK profile and %total occupancy illustrates how the occupancy of a protein target can remain at 100% after most of the TCI has been eliminated from the body (Figure 1.11). This PK/PD decoupling effect suggests that TCIs may be effectively exploited to target proteins which exhibit resynthesis rates beyond the PK profile of the compound. However, this feature may not be desirable for enzymatic targets where short residence times and partial inhibition are optimal.<sup>40</sup> Memantine, an NMDA receptor antagonist, exhibits modest

affinity and a fast off rate which enables it to block excessive activity of the receptor whilst sparing the normal function, minimising on-target toxicity and leading to an acceptable safety profile.<sup>41</sup>

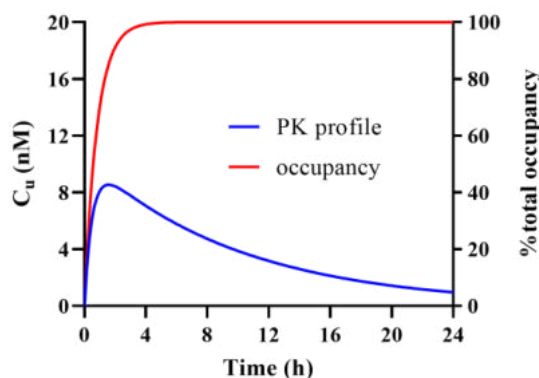


**Figure 1.11** Simulated PK profile and %total occupancy of a TCI.

Finally, an advantage of the two-step TCI mechanism is that it can potentially offer enhanced selectivity between two closely related protein targets. Protein kinases are a >500 member family of proteins which transfer the terminal phosphate group of ATP to a hydroxyl-containing amino acid residue of its protein substrate.<sup>42</sup> Despite the majority of FDA approved small molecule targeted therapies for oncology indications being kinase inhibitors,<sup>4</sup> achieving selectivity between different protein kinases remains a key challenge, owing to their structurally similar ATP binding pockets.<sup>43</sup> The resulting off-target toxicity is an important cause of failures of putative kinase-targeting small molecules in clinical trials.<sup>44</sup> Whilst obtaining selectivity through optimisation of the reversible affinity remains a challenge, inclusion of a covalent warhead has led to the discovery of selective, FDA approved TCIs of EGFR and BTK by targeting a non-catalytic cysteine that is only present in 2% of protein kinases.<sup>33</sup> The addition of a covalent MoA can thus be exploited to target poorly-conserved nucleophilic residues, enabling a  $k_{\text{inact}}$ -based selectivity. However, targeting non-catalytic, poorly conserved nucleophilic residues represents a potential liability of the TCI approach, as secondary resistance mutations can result in the loss of a covalent MoA and consequently a loss of efficacy.<sup>45,46</sup>

### 1.2.4 Design of Targeted Covalent Inhibitors

There are two principal approaches to discover TCIs: through incorporation of a modest intrinsic reactivity electrophilic functionality into an existing reversible ligand; or through a warhead-first approach where a covalent hit is optimised from the inception of the drug discovery process.<sup>20</sup> The discovery of the BTK inhibitor ibrutinib **15**, a transformative therapy for patients with chronic lymphocytic leukaemia (CLL) and mantle cell lymphoma (MCL),<sup>47</sup> is an example of the former. Starting from reversible ligand **16**, the scaffold was strategically modified with an aliphatic acrylamide warhead to covalently engage the non-catalytic, non-conserved Cys-481 of BTK in an effort to obtain pan-kinase selectivity (Figure 1.12 A).<sup>47</sup> A single crystal x-ray structure of ibrutinib **15** bound to BTK was obtained to confirm the binding mode of the compound, which shows the covalent adduct at Cys-481 (Figure 1.12 B).<sup>48</sup>

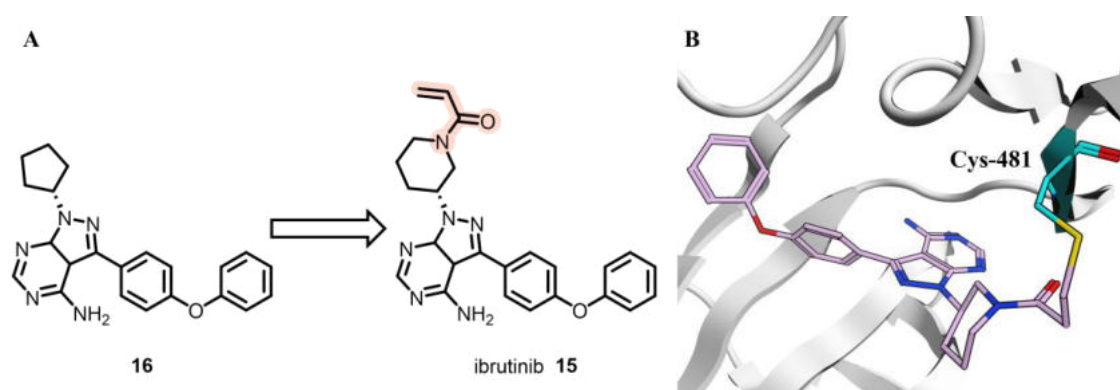


**Figure 1.12** **A** Design of BTK TCI ibrutinib **15**, incorporating acrylamide warhead (highlighted) into reversible scaffold of **16**. **B** Single crystal x-ray structure of ibrutinib **15** covalently bond to Cys-481 BTK (PDB: 5P9J).<sup>48</sup>

Conversely, the discovery of KRAS<sup>G12C</sup> inhibitor sotorasib **13** employed a warhead-first approach. In brief, KRAS is a GTPase and an oncogene which is mutated in 25% of all human cancers.<sup>49</sup> KRAS is difficult-to-drug target owing to picomolar affinities for its endogenous substrates, GTP and GDP, as well as shallow and inaccessible binding pockets.<sup>50</sup> In 2013, Ostrem et al. detailed the discovery of small molecule **17**, which irreversibly binds to Cys-12 in a shallow allosteric pocket of the KRAS<sup>G12C</sup> mutant, *via* a covalent fragment screen.<sup>51</sup> Optimisation of this early hit **17** involved modification of the warhead-containing linker to give ARS-853 **18**, which drove improvements in  $k_{\text{inact}}$  through a more favourable orientation of the warhead towards Cys-12 (Figure 1.13).<sup>52</sup>



Scaffold-hopping to a quinazoline core furnished more potent ARS-1620 **19**, with an atropisomeric fluorophenol moiety, which aimed to rigidify the conformation favouring the covalent reaction.<sup>53</sup> Amgen hybridised compounds from their own in-house KRAS<sup>G12C</sup> program with ARS-1620 **19**, which exploited an additional atropisomeric pyridinyl group to further rigidify the pre-covalent binding mode *via* binding to a cryptic pocket, giving the highly potent sotorasib **13** as the first clinically approved mutant KRAS small molecule inhibitor.<sup>54</sup>

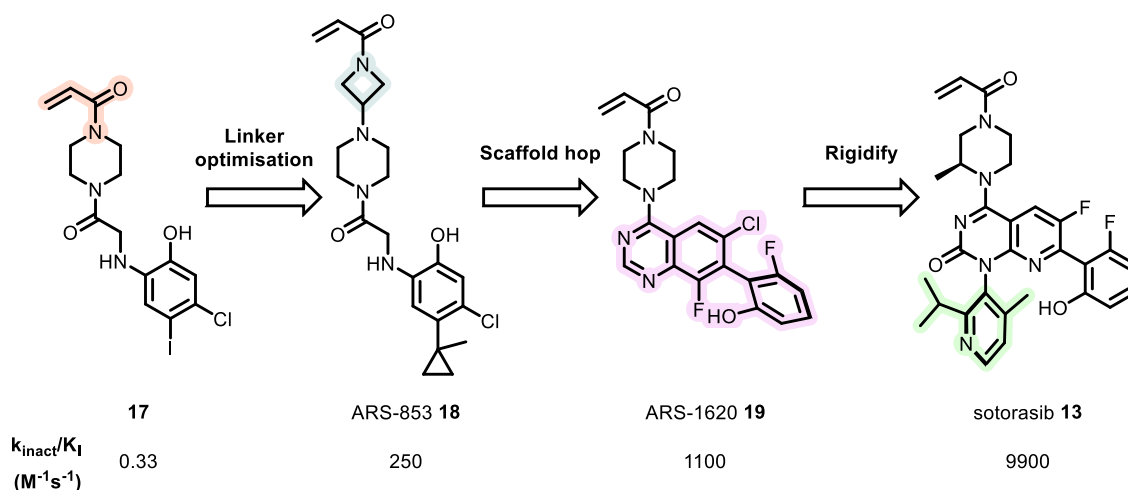


**Figure 1.13** Design of KRAS<sup>G12C</sup> TCI sotorasib **13** from initial covalent fragment hit **17**, with corresponding  $k_{\text{inact}}/K_{\text{I}}$  values reported in the literature.<sup>54,55</sup>

Intriguingly, despite the 30,000-fold improvement in the  $k_{\text{inact}}/K_{\text{I}}$  going from covalent hit **17** to approved drug sotorasib **13**, kinetic analysis of this series indicated that ARS-853 **18**, ARS-1620 **19** and sotorasib **13** all exhibit extremely weak reversible affinities ( $K_{\text{i}} > 100 \mu\text{M}$ ), suggesting that the potency increase is predominately  $k_{\text{inact}}$ -driven.<sup>55,56</sup> Quantitation of the intrinsic reactivity of **17**, **18** and **19**, through incubation of the compounds with cysteine-containing model peptides, showed that the compounds exhibit low non-specific reactivity, indicating that the improvements in  $k_{\text{inact}}$  result from an optimised orientation of the acrylamide relative to Cys-12.<sup>55</sup> This demonstrates that high reversible affinity is not necessarily a requirement for potency in a TCI; instead, strategic modification of the ligand core, to optimise the orientation of the covalent warhead within the pre-covalent binding mode, can be applied to facilitate target-specific acceleration of covalent bond formation.

### 1.2.5 Activity-based Protein Profiling

TCIs have successfully been applied in the development of chemical probes for activity-based protein profiling (ABPP).<sup>57</sup> Briefly, ABPP uses site-directed covalent probes to investigate enzyme function in biological systems.<sup>58</sup> ABPP probes typically consist of an irreversible inhibitor, which is designed to label a subset of the proteome, and a reporter group, such as a biotin, fluorophore or alkyne, for subsequent detection and enrichment of probe-labelled proteins (Figure 1.14).

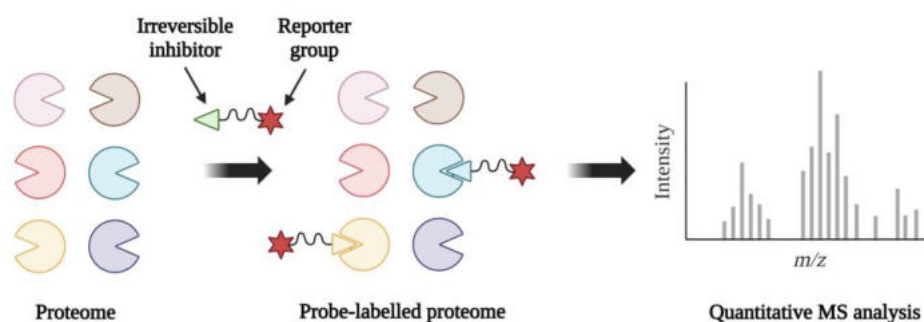


**Figure 1.14** Basic principle of an ABPP experiment, where a small subset of the proteome is covalently labelled by an ABPP probe, enriched and then quantitatively analysed.

First developed by Cravatt et al. in 1999 to profile the activity of serine hydrolases with biotinylated fluorophosphonate probes,<sup>59</sup> the ABPP strategy has since been applied to profile proteome-wide selectivity of covalent kinase inhibitors, including osimertinib **12** and ibrutinib **15**.<sup>60</sup> Firstly, the authors incorporated an alkyne moiety, which can be conjugated with a biotin or fluorescent group-containing azide *via* Cu(I)-catalysed azide-alkyne cycloaddition (CuAAC),<sup>61</sup> into the scaffold of ibrutinib **15** to yield ABPP probe **20** (Figure 1.15 A). Stable-isotope labelling by amino acids in cell culture (SILAC) technology was employed to quantify the proteomics. SILAC involves growing two cell populations; one grown in a medium containing “light” amino acids, and the other is grown in a medium containing “heavy” amino acids, with  $^{13}\text{C}$  instead of  $^{12}\text{C}$  and  $^{15}\text{N}$  instead of  $^{14}\text{N}$ .<sup>61</sup> The heavy cells were treated with probe **20** and the light cells with DMSO, and the cells were collected, lysed and their proteomes mixed (Figure 1.15 B). A biotinylated tag was conjugated to the labelled heavy proteins *via* CuAAC, which were enriched through loading onto streptavidin beads, followed by on-bead digestion with trypsin to yield a mixture of peptides. This peptide mixture was then analysed by mass spectrometry (MS) to identify the proteins that had been pulled down. The incorporation

of the heavy amino acids results in a known mass shift in the peptide containing the heavy tag, therefore, the ratio of light to heavy ion intensity quantifies the extent of enrichment arising from covalent labelling of the parent protein.

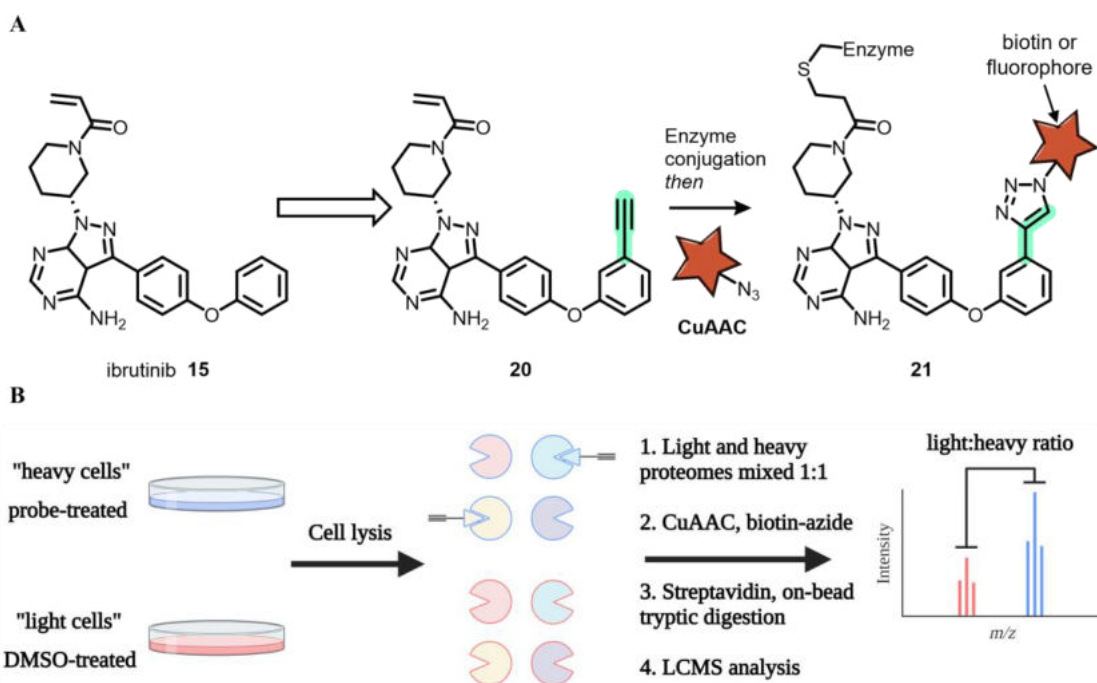


**Figure 1.15** ABPP applied to probe proteome-wide selectivity of kinase inhibitors. **A** BTK TCI ibrutinib **15** was modified with alkyne moiety to give ABPP probe **20**, and after conjugation with an enzyme the resulting adduct can be reacted with a suitable reporter group-containing azide to give adduct **21** for subsequent enrichment. **B** Workflow of ABPP employing SILAC technology. Cell cultures grown with isotopically heavy and light amino acids are treated with probe **20** and DMSO, respectively, and are then lysed and mixed in a 1:1 ratio. Copper catalysed click chemistry appends a biotin group to the labelled proteins, followed by streptavidin bead enrichment and trypsin digest to the constituent peptides. Finally, analysis by MS affords the light:heavy ratio of the peptides, which indicates the amount of enrichment. Figure adapted from Cravatt et al.<sup>60</sup>

Defining a successfully-labelled protein as a light:heavy ratio  $>5$ , the authors discovered 29 off-target proteins which they were able to characterise and investigate further.<sup>60</sup> Identifying and characterising off-targets is important for understanding the toxicity<sup>62</sup> and polypharmacology<sup>63</sup> of drugs and drug candidates, so by enabling the proteome-wide evaluation of inhibitor selectivity, ABPP is consequently a valuable tool in drug discovery.

Cravatt et al. have also applied ABPP strategy to investigate the global reactivity of cysteine residues in the proteome.<sup>64</sup> The authors apply isotopic tandem orthogonal proteolysis–activity-based protein profiling (isoTOP-ABPP), which utilises an alkyne-modified covalent probe **22**, derived from broad-spectrum cysteine reactive irreversible inhibitor iodoacetamide (IAM) **23**,<sup>65</sup> to label the proteome (Figure 1.16).

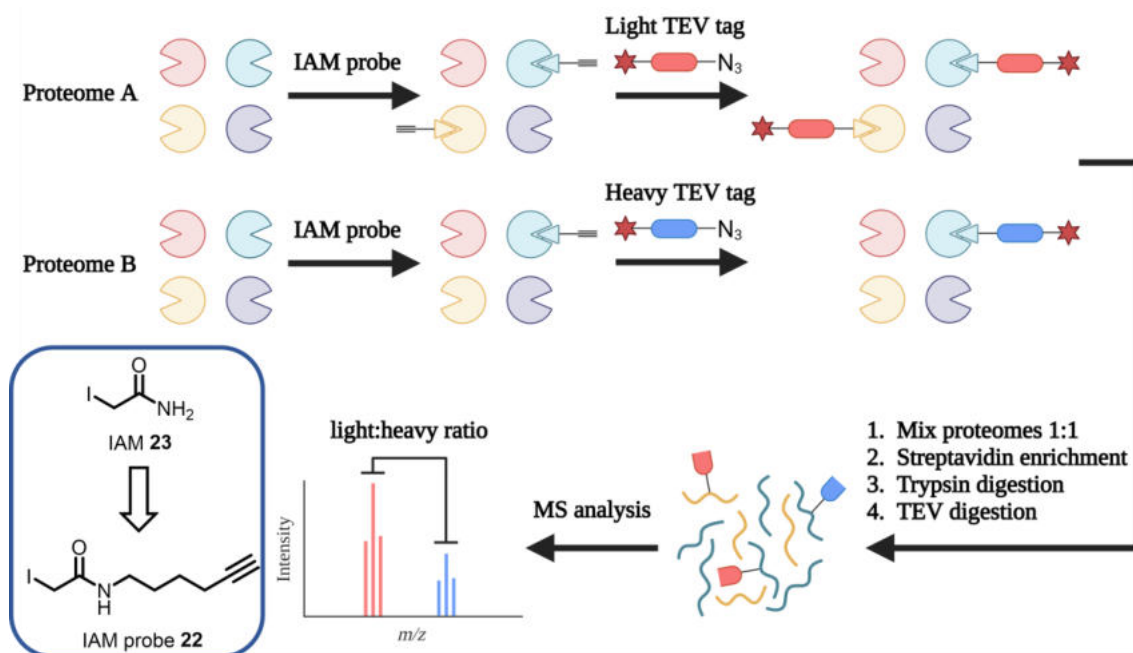


**Figure 1.16** Workflow of isoTOP-ABPP to profile global cysteine reactivity. Two proteomes, A and B, were incubated with different concentrations of cysteine-reactive IAM probe **22**, then conjugated with TEV tags containing an either light or heavy valine group and a biotin group. Mixing of the two proteomes was followed by streptavidin enrichment and sequential proteolytic digestion with trypsin and TEV protease. MS analysis of the resulting peptides enables quantification of the concentration-dependent cysteine modification through the light:heavy ion intensity ratio.

The alkyne-containing IAM probe **22** was incubated at varying concentrations with two proteomes, and the resulting labelled proteins were then conjugated *via* CuAAC with a tag-containing a biotin group, an isotopically light or heavy valine group, a cleavable tobacco etch virus (TEV) protease recognition peptide, and an azide moiety. The two proteomes were then mixed, enriched, subjected to a proteolytic digestion with trypsin and TEV protease, and then the constituent peptides were analysed by MS to identify the proteins that had been pulled down. A small subset of labelled cysteines (<10%) were designated as hyperreactive, owing to significant labelling being observed at the lowest

concentrations tested. Intriguingly, cysteines important for the catalytic reaction of the enzyme and those that function as sites of post-translational modification were more likely to exhibit hyperreactivity,<sup>64</sup> and would therefore likely be more suitable for targeting with the TCI approach.

### 1.2.6 Cysteine-Targeting Covalent Inhibitors

Neutral cysteine residues are the most nucleophilic of the 20 canonical amino acids within proteins, and the majority of TCIs, including every FDA approved TCI for oncology indications,<sup>32</sup> are designed to target cysteine.<sup>66</sup> The hyperreactivity of certain cysteine residues can be explained through the concept of  $pK_a$  perturbation. Free cysteine in aqueous solution has a  $pK_a$  value of  $\sim 8.6$ ,<sup>67</sup> which represents the equilibrium between neutral cysteine and the highly nucleophilic thiolate conjugate base (Figure 1.17).

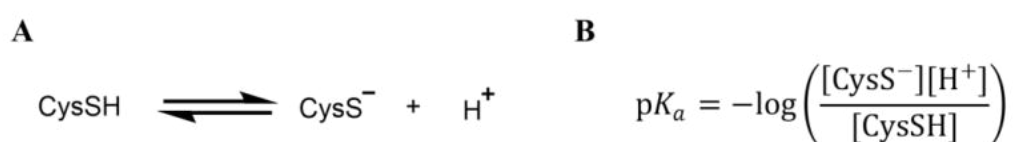


**Figure 1.17** **A** Cysteine thiol-thiolate equilibrium. **B** Definition of cysteine  $pK_a$ .

However, when amino acid residues are buried within the enzyme folded state, their intrinsic  $pK_a$  value can potentially be perturbed by interactions with neighbouring amino acids.<sup>68</sup> For example, a proximal histidine residue in cysteine proteases perturbs the  $pK_a$  of the catalytic cysteine residue to as low as 2.5, through stabilisation of the thiolate conjugate acid *via* the formation of a close-contact ion pair.<sup>69</sup> The  $pK_a$  of Cys-282 in human muscle creatine kinase (hmCK) was measured as 5.6, partially as a result of hydrogen bonding to a proximal serine residue.<sup>70</sup> Stabilisation of the thiolate negative charge, through an electrostatic charge-helix dipole interaction and hydrogen bonding, results in a  $pK_a$  perturbation of up to 5 units in the thioredoxin family of enzymes.<sup>71</sup> Therefore, the protein microenvironment can considerably affect the apparent  $pK_a$ , and thus the reactivity, of nucleophilic amino acid residues.

The high nucleophilicity of cysteine is advantageous as it permits the use of weakly reactive electrophiles, which reduces the risk of idiopathic and idiosyncratic toxicity arising from non-specific tagging of off-targets.<sup>72</sup> The low abundance of cysteine in the proteome (3.3%)<sup>73</sup> potentially facilitates the development of selective TCIs, but limits the

broader application of the TCI strategy when a suitable targetable cysteine is not available. Also, many cysteine residues are structural, either present in disulfide bridges or buried within non-solvent accessible lipophilic regions, so are unavailable for covalent adduct formation.<sup>74</sup> Additionally, the emergence of cysteine-to-serine secondary resistance mutations has become apparent as a considerable liability for cysteine-targeting covalent inhibitors (cysteine-TCIs),<sup>45,46</sup> as the decreased nucleophilicity of serine results in severely diminished efficacy through a loss of the irreversible MoA. Consequently, there is a need to explore alternative nucleophilic residues beyond cysteine.<sup>75</sup>

In recent years, residues including lysine, tyrosine, histidine, serine, threonine, glutamate, aspartate and methionine have been increasingly investigated to expand the scope of nucleophilic residues for the TCI strategy.<sup>66</sup>

### 1.2.7 Lysine-Targeting Covalent Inhibitors

The  $\epsilon$ -amino group of lysine has a  $pK_a$  of 10.4,<sup>76</sup> and consequently when exposed to bulk solvent on the surface of the protein lysine residues are very highly (>99%) protonated. (Figure 1.18).

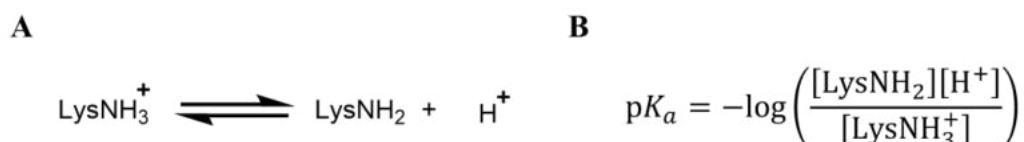


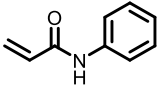
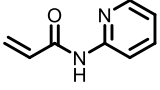
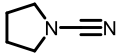
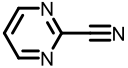
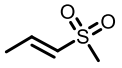
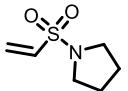
**Figure 1.18** **A** Equilibrium between non-nucleophilic ammonium and nucleophilic amine forms of lysine. **B** Definition of lysine  $pK_a$ .

Protonation of an amine masks the lone pair, making the group non-nucleophilic. Whereas the highly polar aqueous environment at the protein surface favours the charged form of the residue, transferring lysine residue to the hydrophobic protein interior disfavours ionisation, shifting the equilibrium to the neutral, nucleophilic form.<sup>77</sup> This desolvation effect can result in considerable  $pK_a$  perturbation for many internal lysine residues, with shifts of up to 5 units reported.<sup>78</sup>  $pK_a$  perturbation is highly advantageous for TCI design, as the protonated lysine residues on the protein surface are essentially non-nucleophilic, which minimises the risk of non-specific tagging. In contrast, internal lysine residues in a hydrophobic environment often display enhanced reactivity and can therefore be selectively targeted with a covalent inhibitor. As lysine is also one of the

most abundant amino acid residues in the proteome (7.2%),<sup>73</sup> targeting lysine has the potential to expand the versatility of the TCI approach.

### 1.2.8 Design of Irreversible Lysine-Targeting Covalent Inhibitors

The majority of reported cysteine-TCIs incorporate acrylamide or acrylamide-derived Michael acceptor motifs as covalent warheads.<sup>20</sup> However, the  $\epsilon$ -amino group of lysine possesses more weakly polarisable electron density compared to cysteine,<sup>79</sup> making it a harder nucleophile according to the Hard and Soft, Acids and Bases Theory (HSAB) so should react more quickly with a harder electrophile.<sup>80</sup> Dahal et al. attempted to quantify the intrinsic reactivity of a series of electrophiles with a lysine and cysteine model system.<sup>81</sup> Each electrophile was incubated with either *N*- $\alpha$ -acetyl-lysine at pH 10.2, to enable sufficient free concentration of the neutral, nucleophilic species, or glutathione (GSH) at pH 7.4, yielding a half-life ( $t_{1/2}$ ) for the reaction with the model nucleophiles (Table 1.1).

Entry	Structure	<i>N</i> - $\alpha$ -acetyl-lysine $t_{1/2}$ (h)	GSH $t_{1/2}^{int}$ (h)
1		2.06	0.66
2		0.67	0.13
3		7.70	2.91
4		4.78	0.5
5		3.08	28.0
6		0.33	0.53

**Table 1.1** Intrinsic reactivities of various electrophiles with *N*- $\alpha$ -acetyl-lysine and glutathione (Dahal et al).<sup>81</sup>

The softer GSH nucleophile exhibited increased reactivity with *N*-aryl acrylamides relative to *N*- $\alpha$ -acetyl-lysine (Table 1.1, Entries 1 and 2), and a similar reactivity trend was observed for the nitriles (Table 1.1, Entries 3 and 4). Conversely, the vinyl sulfone and sulfonamide electrophiles (Table 1.1, Entries 5 and 6) showed greater reactivity with

*N*- $\alpha$ -acetyl-lysine compared to GSH, which the authors speculate results from the highly electron-withdrawing sulfone moiety decreasing the electron density in the vinyl group and increasing its hardness.

Exploiting its apparent selectivity, Anscombe et al. modified reversible inhibitor NU6102 **24** with a vinyl sulfone moiety in an effort to develop an irreversible inhibitor of CDK2.<sup>82</sup> Having demonstrated a covalent MoA for the resulting inhibitor NU6300 **25**, further characterisation identified the non-catalytic Lys-89 as the modified residue (Figure 1.19). NU6300 **25** exhibited improved cellular activity relative to reversible analogue NU6102 **24**.

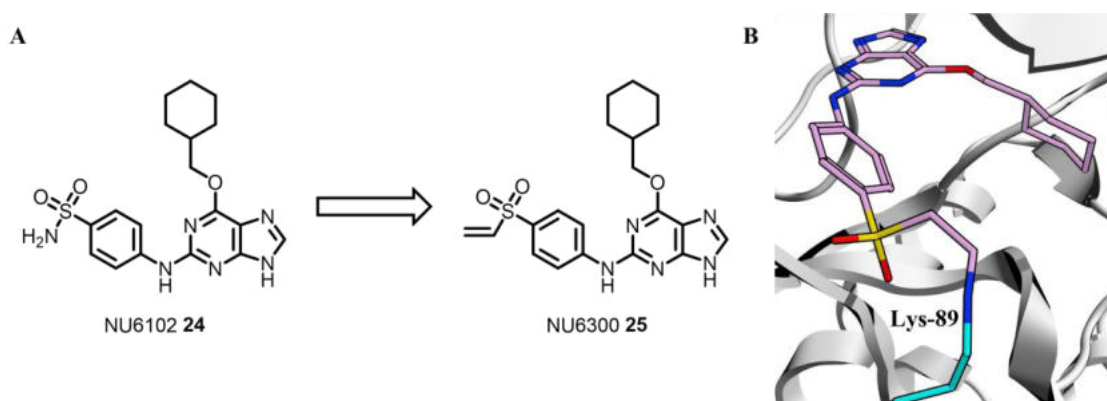


**Figure 1.19** A Design of CDK2 TCI NU6300 **25** from reversible inhibitor NU6102 **24**. B Single crystal x-ray structure of NU6300 **25** covalently bound to non-catalytic Lys-89 of CDK2 (PDB: 5CYI).<sup>82</sup>

Activated esters have also been applied as hard electrophiles in lysine-targeting agents. First detailed in the discovery of a covalent inhibitor targeting a non-catalytic lysine of the plasma protein transthyretin (TTR).<sup>83</sup> This approach was expanded by Dalton et al. to modify reversible inhibitor **26** with an activated ester to give TCI **27**, targeting the catalytic lysine of PI3K $\delta$  (Figure 1.20).<sup>84</sup> The lead compound **27** demonstrated high inactivation efficiency ( $k_{\text{inact}}/K_{\text{I}} = 2.1 \times 10^4 \text{ M}^{-1}\text{s}^{-1}$ ), and despite the catalytic lysine being conserved across the kinome,<sup>85</sup> it showed >20-fold selectivity for PI3K $\delta$  over other isoforms and related kinases *in vitro*.



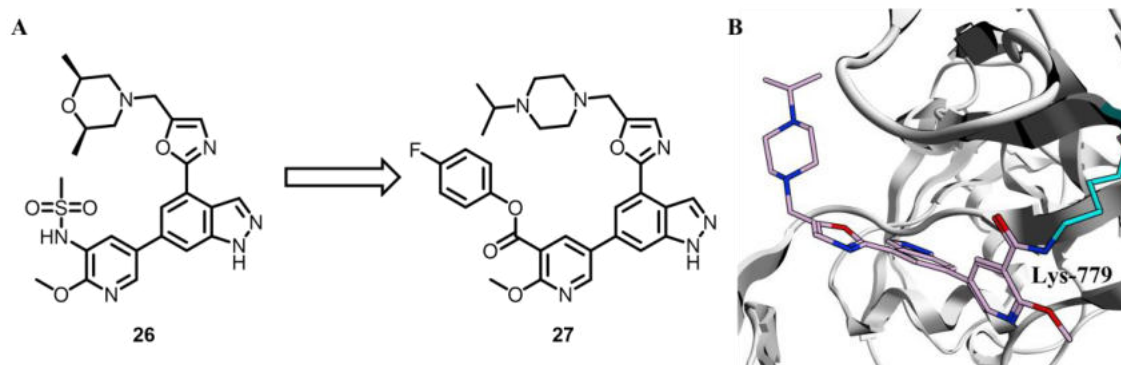
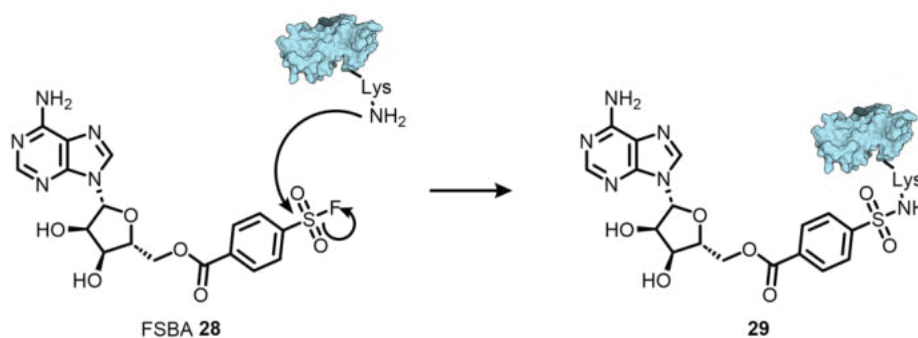


**Figure 1.20** Design of PI3K $\delta$  TCI **27** from reversible inhibitor **26**. **B** Single crystal x-ray structure of TCI **27** covalently bound to catalytic Lys-779 of PI3K $\delta$  (PDB: 6EYZ).<sup>84</sup>

Sulfur(VI)-fluoride electrophiles, including aryl sulfonyl fluorides and fluorosulfonates, have been extensively applied as agents targeting serine, tyrosine and lysine.<sup>86</sup> Sulfonyl fluoride groups are hard electrophiles, with moderate intrinsic reactivity, and exhibit sufficient aqueous stability to make them suitable for application in the design of lysine-TCIs.<sup>87</sup> Beginning with the discovery that sulfonyl fluorides covalently label the catalytic serine of serine proteases,<sup>88</sup> the warhead was subsequently used in the design of ATP analogue FSBA **28**,<sup>89</sup> a promiscuous inhibitor of protein kinases which covalently labels the catalytic lysine residue (Scheme 1.3).<sup>90</sup>



**Scheme 1.3** Mechanism of reaction of promiscuous kinase probe FSBA **28** with catalytic lysine of protein kinases to give sulfonamide adduct **29**.

Taunton et al. modified FSBA **28** with a *p*-tolyl group to improve selectivity for Src family kinases, and included a clickable alkyne group to develop probe **30** for application in ABPP (Figure 1.21).<sup>91</sup>

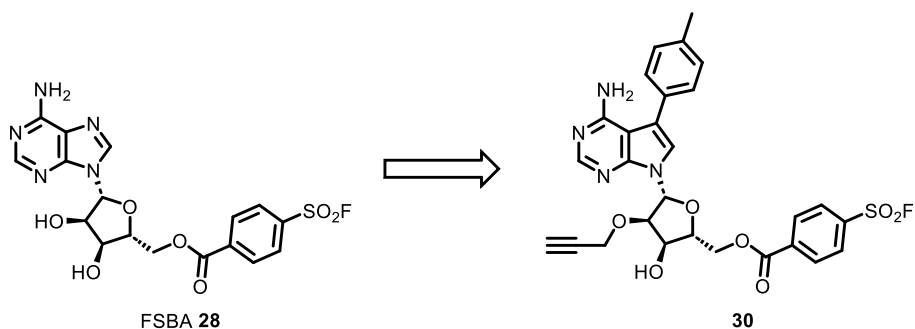


**Figure 1.21** Design of sulfonyl-fluoride based Src family kinase probe **30** from promiscuous kinase probe FSBA **28**.

Additional applications of sulfonyl fluoride warheads in the design of lysine-TCIs include TCI **31** targeting the non-catalytic Lys-15 of TTR (Figure 1.22).<sup>92</sup> Structural characterisation of ligand binding suggested that the warhead may be activated within the reversible binding mode through hydrogen bonding (H-bonding) interaction of the Lys-15 – Glu-54 salt bridge proton with the fluoride leaving group.

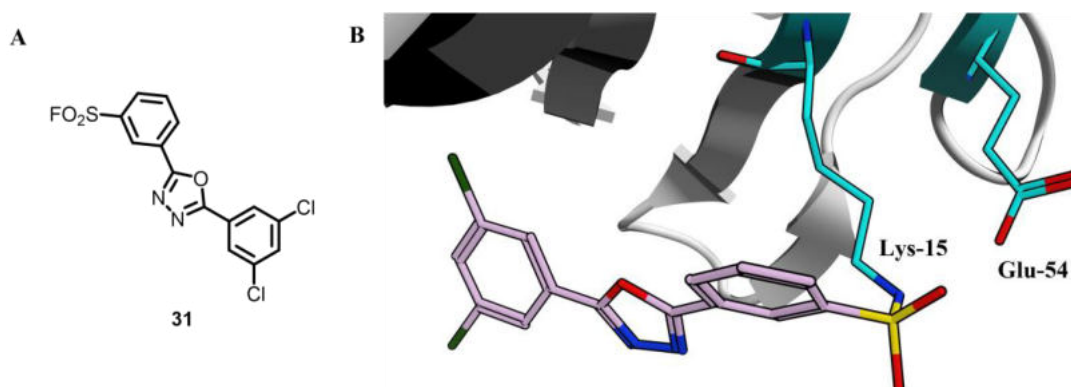


**Figure 1.22** A Structure of TCI **31**. B Single crystal x-ray structure of TCI **31** covalently bound to non-catalytic Lys-15 of TTR (PDB: 4FI6).<sup>92</sup>

Taunton et al. also developed TCI **32**, targeting Lys-162 of eIF4E, from covalent fragment **33** identified from a virtual library (Figure 1.23).<sup>93</sup> Characterisation of lysine-TCI **32** revealed potent reaction kinetics ( $k_{\text{inact}}/K_{\text{I}} = 5.5 \times 10^3 \text{ M}^{-1}\text{s}^{-1}$ ), and subsequent profiling in cells revealed it as the first example of a covalent eIF4E inhibitor with cellular activity.

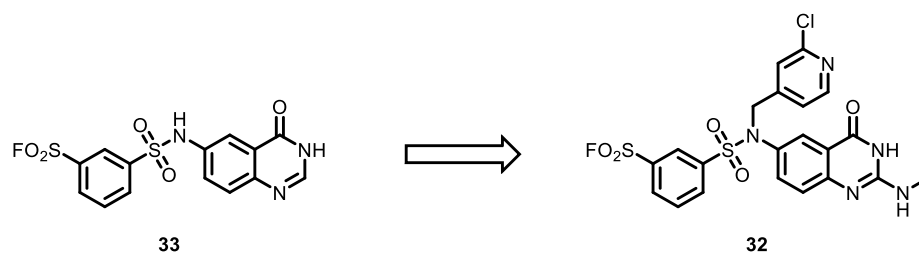


**Figure 1.23** Design of eIF4E lysine-TCI **32** from covalent fragment **33** identified from a virtual fragment library.

Aryl fluorosulfonates are closely related to sulfonyl fluorides, but typically exhibit attenuated intrinsic reactivity owing to oxygen-mediated resonance stabilisation.<sup>94</sup> Fluorosulfonate probes with a moderately complex organic scaffold, and containing a clickable alkyne linker, have recently been applied to profile reactive lysine residues across the proteome.<sup>95</sup> The approach, termed by the authors as “inverse drug discovery”, successfully demonstrated covalent labelling of a number of therapeutically relevant targets. Probe **34** was demonstrated to label Lys-12 of NME1, a promising kinase target for the treatment of multiple cancers,<sup>96,97</sup> which was speculated to have a decreased  $pK_a$  from interaction with the proximal basic Arg-105 (Figure 1.24).

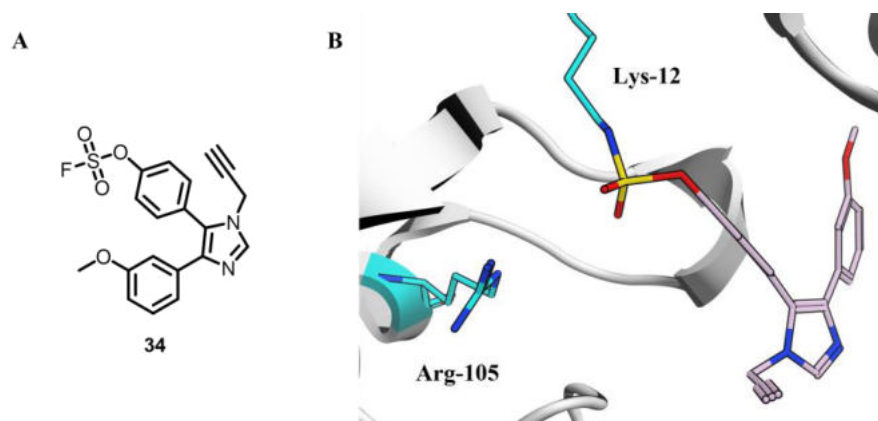


**Figure 1.24** **A** Structure of fluorosulfonate **34**. **B** Single crystal x-ray structure of fluorosulfonate **34** covalently bound to non-catalytic Lys-12 of NME1 (PDB: 5UI4).<sup>95</sup>

Despite an increasing interest in the development of lysine-TCIs as alternative approach to the dominant cysteine-targeting strategy, the field still remains in its infancy.<sup>98</sup> In the absence of any clinically approved lysine-TCIs, additional validation of the lysine-TCI approach is required. The aim of my project will be to further validate lysine-targeting covalent inhibition as a strategy to develop small molecule targeted therapies for

oncology, particularly with respect to overcoming one of the key challenges in oncology: difficult-to-drug targets.<sup>99</sup>

### 1.3 HSP70

#### 1.3.1 Heat Shock Proteins

Disruption of cellular homeostasis, such as through exposure to elevated temperatures, oxidative stress, heavy metals and chemicals, induces the heat shock response (HSR).<sup>100</sup> These external stresses lead to the destabilisation, unfolding and aggregation of proteins which can result in cell death.<sup>101</sup> The HSR counters cellular stress through the synthesis of the heat shock proteins (HSPs), a class of molecular chaperones that interact with and stabilise misfolded proteins to enable them to reacquire their functional conformation or be selected for degradation.<sup>102</sup> The HSPs are categorised according to their molecular weight, with the major families including HSP100, HSP90, HSP70, HSP60, HSP40 and the small heat shock proteins (sHSPs).

#### 1.3.2 HSP70 protein family

The HSP70 proteins are a 13-member isoform family of ATP-dependent molecular chaperones, which control protein refolding, translocation into organelles and disaggregation.<sup>103</sup> The HSP70 family are highly abundant, representing 1–2% of all cellular proteins,<sup>104</sup> and also highly conserved, with *Drosophila* and *E. coli* HSP70 possessing 72% and 50% sequence identity, respectively, with the corresponding human homolog.<sup>105</sup> Of the 13 HSP70 isoforms, the four most well characterised are the stress-induced HSP72 (*HSPA1A*),<sup>106</sup> the constitutively expressed HSC70 (*HSPA8*),<sup>107</sup> the endoplasmic reticulum form GRP78 (*HSPA5*),<sup>108</sup> and the mitochondrial HSPA9 (*HSPA9*).<sup>109</sup>

HSP70 proteins are ATPases, which use the energy from ATP hydrolysis to ADP and inorganic phosphate (P<sub>i</sub>) to enable their function.<sup>110</sup> The structure of the HSP70s is conserved across the family, and is exemplified by the bacterial homolog, DnaK: an N-terminal, 45 kDa nucleotide binding domain (NBD) is followed by an interdomain linker, connecting the NBD to a 15 kDa substrate binding domain (SBD $\beta$ ), 10 kDa lid domain (SBD $\alpha$ ) and a disordered C-terminal tail (Figure 1.25 A).<sup>110</sup>

The full length structure of human HSP70 has never been fully elucidated, but the structure of full length DnaK has been determined through x-ray crystallographic and solution phase NMR studies.<sup>111,112</sup> The solution phase structure shows how the NBD and SBD are connected *via* a flexible linker, and that the NBD is comprised of two lobes, domains I and II, which are both subdivided into A and B subdomains (Figure 1.25 B).

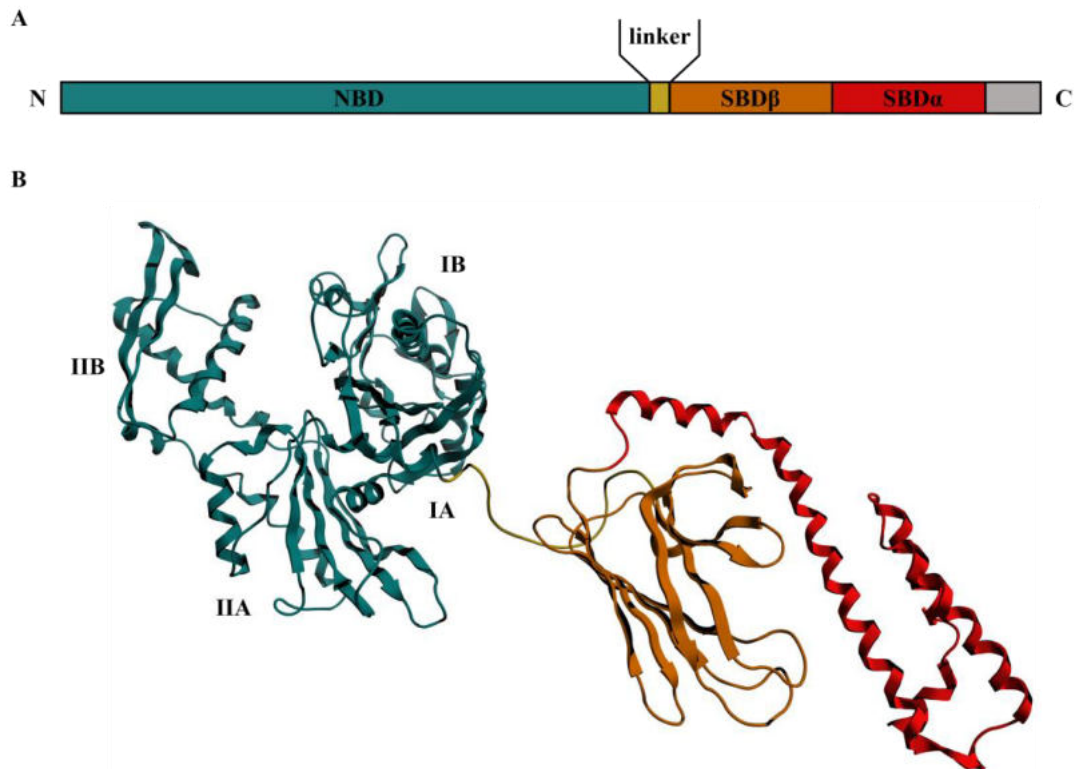


**Figure 1.25** **A** Domain organisation of HSP70 chaperones. **B** Full length structure of bacterial HSP70, DnaK (PDB: 2KHO).

The ATP binding site is located at the base of the cleft separating the two lobes of the NBD, coordinating all four subdomains and controlling the movement of each lobe.<sup>113</sup> Within the binding mode, the  $\beta$  and  $\gamma$  phosphates of ATP/ADP coordinate a divalent metal ion, such as  $Mg^{2+}$  or  $Ca^{2+}$ ,<sup>114</sup> which forms a water-mediated network important for the overall binding affinity of the nucleotide.<sup>115</sup> Moreover, the phosphate groups also make key interactions with polar residues within the NBD binding cleft, such as H-bonding of the  $\alpha$  phosphate with a conserved glycine, in addition to multiple H-bonding interactions with threonine residues within the phosphate binding loop (Figure 1.26).<sup>116</sup> The adenine ring is sandwiched between two hydrophobic segments containing two arginine residues, with the 6-*N* amino group positioned towards solvent. Overall, the binding of ATP/ADP

is critically dependent on interactions of the phosphate groups and the highly polar binding site occupied by the nucleotide.<sup>116</sup>

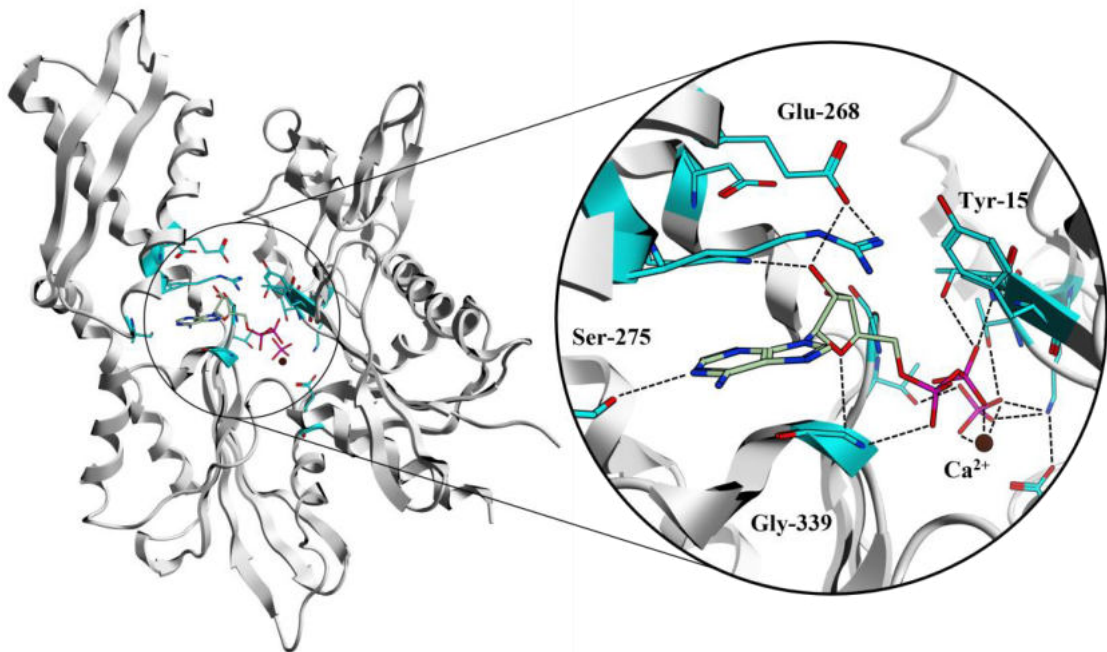


**Figure 1.26** Single crystal x-ray structure of human HSP72-NBD bound to ADP and  $P_i$ , showing key interactions of the nucleotide with the protein (PDB: 1S3X).

The SBD promiscuously binds to a broad range of substrates, including misfolded proteins, protein aggregates, and unfolded polypeptides from the ribosomal machinery.<sup>110</sup> DnaK was determined to preferentially bind to peptides with a five-residue hydrophobic sequence with a positively charged residue either side,<sup>117</sup> a motif which is common within the folded state of native proteins. Thus, when proteins unfold from a disruption to cellular homeostasis, this motif is exposed enabling binding of the HSP70 SBD.

The association and dissociation of substrates from HSP70 is governed by a complex allosteric mechanism, wherein ATP hydrolysis within the NBD regulates the binding of substrates within the SBD.<sup>118</sup> The binding of ATP to the NBD opens a cleft for the binding of the interdomain linker, resulting in the association of the  $\beta$ SBD and the NBD and consequently a perturbation of the NBD catalytic residues into an unfavourable conformation for ATP hydrolysis.<sup>119</sup> Binding of a substrate and a co-chaperone, such as a J-domain protein (JDP), synergistically induces dissociation of the NBD and SBD $\beta$ , a transition to an ATP hydrolysis-competent state and consequently stimulates the basal ATPase activity by >1000-fold.<sup>120</sup>

ATP hydrolysis to ADP/P<sub>i</sub> triggers the lid or SBD $\alpha$  to flip down onto the SBD $\beta$ , decreasing the rate of substrate dissociation and inducing a net 10-fold decrease in  $K_d$  of the SBD for the substrate (Figure 1.27).<sup>110</sup>

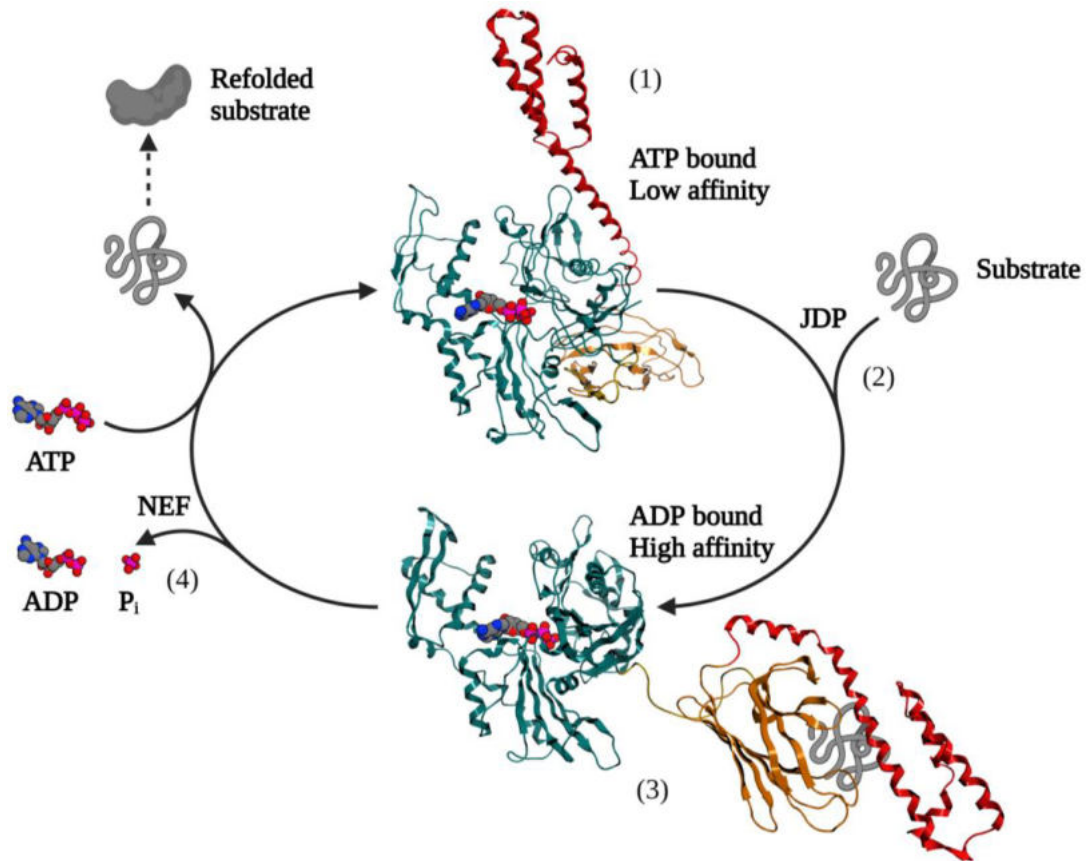


**Figure 1.27** HSP70 catalytic cycle. (1) ATP-bound HSP70 has a low substrate affinity, low ATPase activity. (2) Binding of a co-chaperone, such as a JDP, and a substrate induces dissociation of the NBD (green) and SBD $\beta$  (orange) domains, catalytically activating HSP70 and accelerating the rate of ATP hydrolysis. (3) Hydrolysis of ATP to ADP induces the high affinity conformation of the SBD by allosterically triggering the SBD $\alpha$  lid (red) to dock onto the SBD $\beta$ . (4) Binding of a NEF facilitates ADP dissociation, enabling ATP association, a shift to the low affinity SBD conformation and the release of substrate. Figure adapted from Rosenzweig et al.<sup>110</sup>

ADP/P<sub>i</sub> dissociates slowly from the HSP70-NBD, with a reported off-rate of  $0.05\text{ s}^{-1}$ .<sup>121</sup> Potent product inhibition by ADP/P<sub>i</sub>, in addition to JDP association being required to stimulate catalytic activity, contributes to an extremely slow intrinsic rate of  $\gamma$ -phosphate hydrolysis, approximately 1 ATP molecule every 30 minutes.<sup>111</sup> Interaction of a nucleotide exchange factor (NEF) accelerates the release of ADP and P<sub>i</sub> from the NBD,

which allows for reassociation of an ATP molecule, adoption of the low affinity SBD conformation and consequently release of the substrate.

### 1.3.3 HSP70 and Cancer

Cancer cells are exposed to high levels of stress from maintenance of the oncogenic state, in addition to environmental stresses such as hypoxia, oxidative stress and nutrient deprivation, leading to a dependence on the HSR.<sup>122</sup> Consequently, HSP70 proteins are constitutively overexpressed in a broad range of cancers<sup>123</sup> to counteract the high levels of unfolded proteins and aggregates; this is a form of non-oncogene addiction.<sup>124</sup> Overexpression of the stress-induced HSP72 is associated with increased tumour proliferation and poor prognosis in patients with many cancer types, including breast, colorectal and prostate cancer.<sup>103</sup>

The viability of targeting molecular chaperones for oncology drug discovery has been demonstrated with several HSP90 inhibitors entering the clinic in recent years,<sup>125</sup> culminating in the clinical approval of pimitespib for the treatment of gastrointestinal stromal tumour (GIST).<sup>126</sup> However, modulation of the HSR through inhibition of HSP90 can lead to compensatory upregulation of HSP72, potentially resulting in resistance to HSP90 inhibitor therapy.<sup>127</sup> Consequently, dual targeting of HSP90 and HSP72 may be a viable strategy to reduce cancer cell viability.<sup>128</sup>

Dual siRNA silencing of constitutively-expressed HSC70 and stress-induced HSP72 has been shown to induce tumour-specific apoptosis from degradation of HSP90 client proteins and cell cycle arrest.<sup>129</sup> Intriguingly, the extent of apoptosis from silencing of the two HSP70 isoforms observed was far greater than what was observed for treatment with the HSP90 inhibitor, making HSP70 inhibition an attractive strategy to exploit chaperone dependence in cancer.

### 1.3.4 Targeting HSP70

The addiction of cancer cells to HSP70 proteins has made them a popular drug discovery target.<sup>130</sup> However, despite considerable efforts to develop HSP70-targeting small molecules, very few well-validated inhibitors have been reported.<sup>131</sup> Many reported HSP70 inhibitors either display non-specific interaction with and aggregation of HSP70,<sup>132,133</sup> or were identified from cellular pulldowns and have a poorly-understood



mechanism of action.<sup>104</sup> Only one HSP70-targeting chemotype is well-characterised and has been repeatedly validated by multiple groups, a series of nucleoside-mimetic inhibitors first reported by Massey et al.<sup>134,135</sup>

Discovered through structure-based design, these inhibitors target the ATP binding site within the NBD of HSP72. Beginning from adenosine **35**, the authors substituted a 3,4-dichlorobenzyl moiety at the 8-position of the adenine ring to give **36**, driving a 62-fold boost in potency (Figure 1.28). Introduction of a *p*-cyanobenzyl moiety at the 5'-position of the ribose ring to give VER-155008 **37** further drove improvements in potency, furnishing a  $K_i$  at the limit of detection ( $K_i < 500$  nM) of the biochemical fluorescence polarisation (FP) assay.

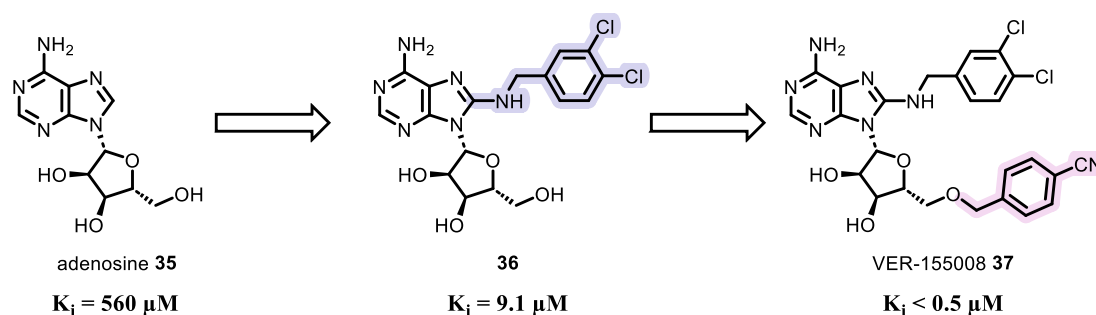


**Figure 1.28** Design of VER-155008 **37** from adenosine **35**, incorporating 8-dichlorobenzyl and 5'-cyanobenzyl moieties for reversible affinity.

VER-155008 **37** was further characterised in HCT116 cells, demonstrating modest downregulation of HSP90 client proteins CRAF and ERBB2 (Figure 1.29).<sup>129</sup> Antiproliferative effects were also observed with a measured  $GI_{50}$  of 5  $\mu\text{M}$  in HCT116 cells; however, in the absence of suitable controls it was unclear whether or not the growth inhibition was *via* an HSP70-dependent mechanism.

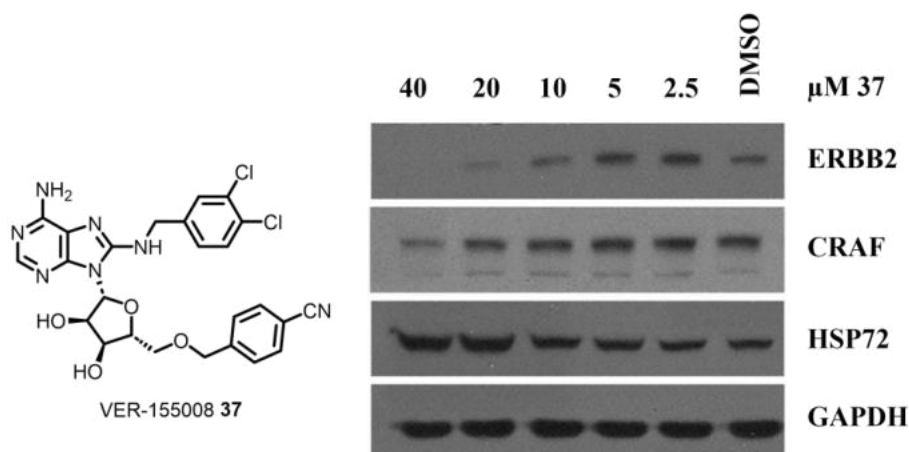


**Figure 1.29** Western blot showing the effect of VER-155008 **37** on levels of ERBB2 and CRAF in HCT116 cells (Massey).

Analysis of the single-crystal x-ray structure of VER-155008 **37** bound to HSP72 showed that in addition to the key 3,4-dichloro and *p*-cyanobenzyl functionalities engaging in  $\pi$ -stacking interactions with Arg-272 and Tyr-15, respectively, the moieties were positioned in a solvent-exposed region of the pocket, desolvating the binding site and stabilising a multitude of hydrogen bonding interactions between the protein and the adenosine core (Figure 1.30).

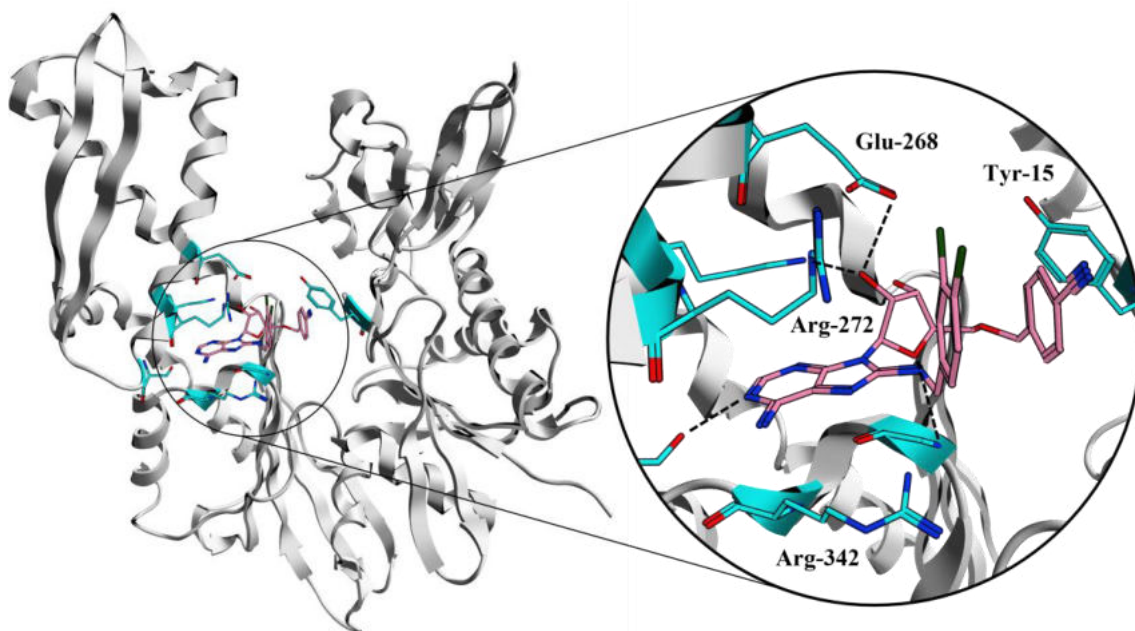


**Figure 1.30** Single crystal x-ray structure of VER-155008 **37** bound to HSP72-NBD (PDB: 4IO8) showing key interactions made within ATP binding pocket.

### 1.3.5 HSP70 is Difficult-To-Drug

Despite demonstrating excellent biochemical potency, VER-155008 **37** showed only modest *in vitro* cell activity.<sup>135</sup> Additionally, to date no ATP-competitive inhibitor of HSP70-NBD has demonstrated *in vivo* activity. The challenges underlying the development of ATP-competitive inhibitors of HSP70 can be summarised through the following main points:

#### 1) High affinity for ATP/ADP

Competition with high affinity, high abundance endogenous substrates can diminish the *in vitro* activity of reversible ligands as the inhibitor is unable to achieve sufficient target occupancy.<sup>13</sup> The HSP70 family is reported to have high affinity for ADP, with  $K_d$  values ranging from 1 – 110 nM depending on the isoform (Table 1.2).

Protein	$K_d$ ( $\mu$ M)
DnaK	0.001 <sup>136</sup>
HSP72	0.082 <sup>115</sup>
HSC70 <sup>a</sup>	0.11 <sup>137</sup>
HSP90	150 <sup>138</sup>

**Table 1.2** Reported  $K_d$  values of ADP for HSP70 isoforms and HSP90. <sup>a</sup> $K_d$  determined for Bovine HSC70.

In contrast, the related ATPase HSP90 is reported to have a ~2300-fold weaker affinity for ADP compared to HSP72.<sup>138</sup> Consequently, the high affinity of ADP for the HSP70 proteins leads to strong product inhibition during the ATPase catalytic cycle, making it challenging to determine reliable values of ATP binding affinity. As the cellular concentrations of ATP are estimated to be 1 – 5 mM,<sup>131</sup> the design of ATP-competitive inhibitors of HSP70 is extremely challenging.

#### 2) Polar binding site

ADP binds to HSP70 with the  $\beta$  and  $\gamma$  phosphate groups buried deeply in a polar pocket (Figure 1.31 A),<sup>116</sup> making a large number of hydrogen binding interactions (Figure 1.26) that are critical to the affinity of the nucleotide.

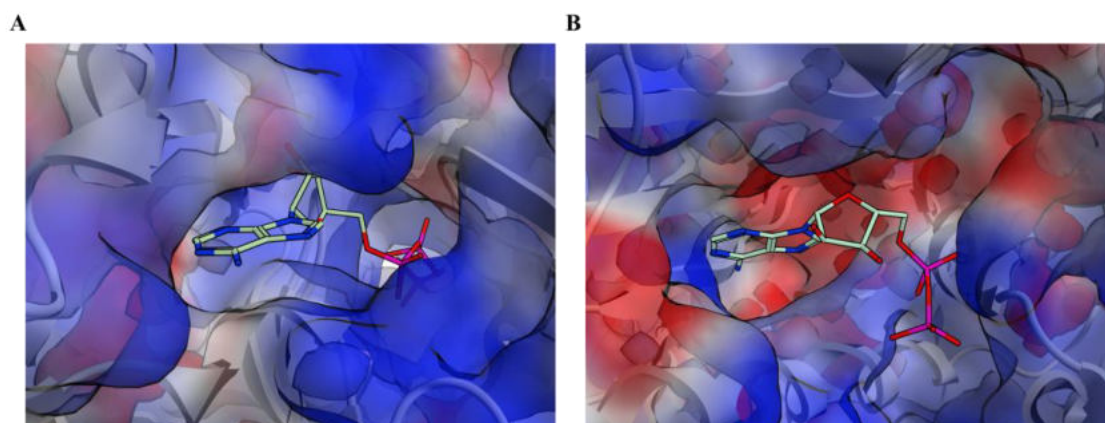


**Figure 1.31** ADP binding modes for **A** HSP72 (PDB: 1S3X) **B** HSP90 (PDB: 1AM1). Red = lipophilic region, blue = hydrophilic region.

Mimicking these interactions with a small molecule inhibitor would require the introduction of highly polar functionalities which would likely compromise the cellular permeability.<sup>139</sup> In contrast, the phosphate groups of HSP90 occupy a solvent exposed region in the ATP binding pocket (Figure 1.31 B).<sup>140</sup>

### 3) Complex conformational dynamics

The NBD of HSP70 is highly flexible and dynamic which can make it challenging to target with structure-based design. When bound to ADP, the NBD adopts a closed conformation in which the two lobes are brought into close proximity. This conformational switch is stabilised through a key salt bridge interaction between Lys-56 and Glu-268 of the IB and IIB subdomains, respectively (Figure 1.32 A).<sup>141</sup> In contrast, when bound to a NEF such as BAG1, this salt bridge is disrupted causing the NBD to adopt an open conformation where the lobes are positioned further apart, causing the ATP binding site to become more solvent exposed and poorly-defined (Figure 1.32 B).

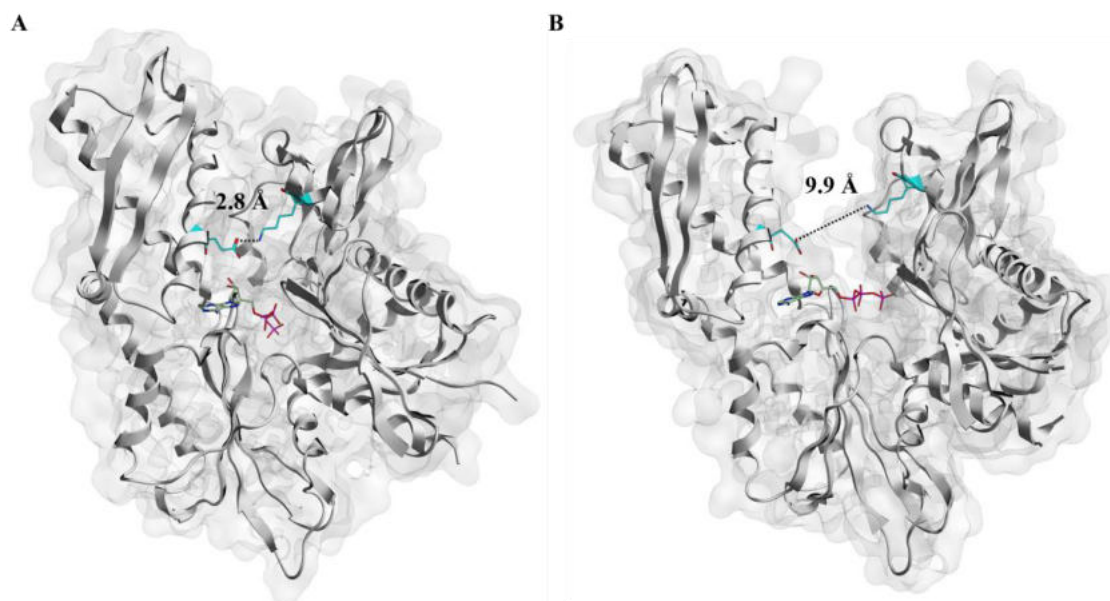


**Figure 1.32** **A** ADP + P<sub>i</sub> bound to closed conformation of HSP72-NBD (PDB: 1S3X), salt bridge between Lys-56 and Glu-268 highlighted. **B** ATP bound to open conformation of HSC70/BAG1 (PDB: 3FZF). BAG1 not shown for clarity.

Our group previously observed a complex structure-activity relationship (SAR) for their class of adenosine-derived inhibitors of HSP70.<sup>142</sup> After extensive efforts to modify the adenine ring of adenosine to generate high affinity ligands, the only scaffold which exhibited submicromolar  $K_d$  values were the 8-*N*-benzyl inhibitors exemplified by compound **38** (Figure 1.33 A). Structural characterisation revealed that the high affinity of the inhibitors was critically dependent on the induction of the closed conformation of the NBD. The 8-*N*-benzyl functionality of **38** was proposed to be desolvating Glu-268 and Lys-56 within the binding pocket, stabilising the key salt bridge and consequently inducing the higher affinity closed conformation (Figure 1.33).

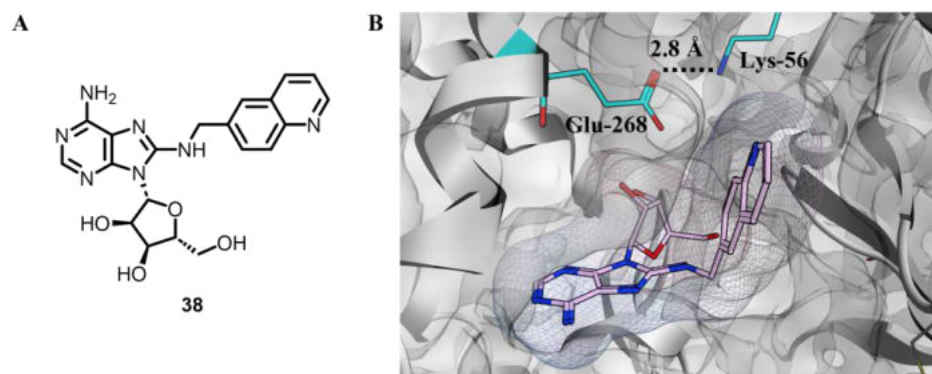


**Figure 1.33** A Structure of **38**. B Single crystal x-ray structure of **38** bound to closed conformation of HSC70-NBD (PDB: 5AR0).

Jones et al. attempted a fragment-based approach to discover a high affinity ligand of the ATP binding pocket, which demonstrated a very low hit rate from the initial fragment screen (<0.1%).<sup>143</sup> Elaboration of a quinazoline hit **39** ( $K_d = 1.4$  mM) resulted in the identification of **40** as the most potent compound in the series ( $K_d = 75$   $\mu$ M), incorporating a ribose-mimetic pentyl group (Figure 1.34 A).

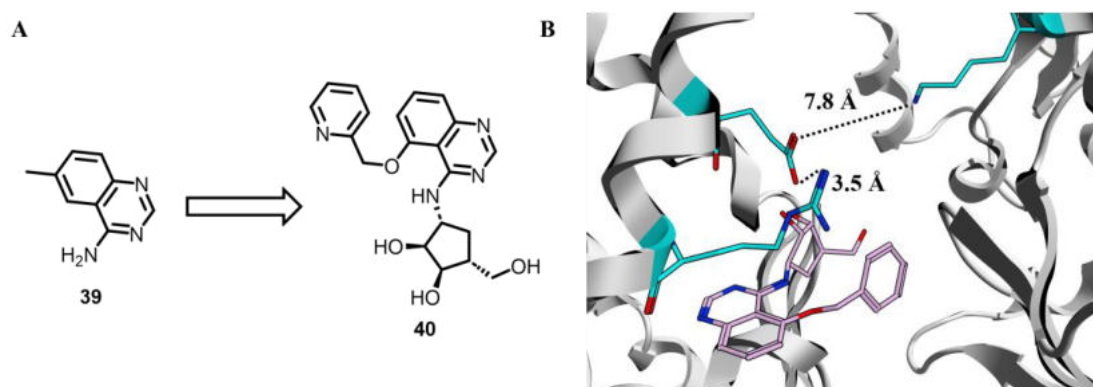


**Figure 1.34** A Design of **40** from initial fragment hit **39**. B Single crystal x-ray structure of analogue of **40** bound to HSP72-NBD (PDB: 5AQX).

Analysis of the binding mode of a close analogue of **40** indicated that an apparent steric clash between the *O*-benzyl group and Arg-272 favours the formation of a salt bridge of the residue with Glu-268, disrupting the Lys-56 – Glu-268 salt bridge and preventing the NBD from adopting the high affinity closed conformation (Figure 1.34 B). The results of this study illustrated the challenge of developing high affinity, non-nucleotide-derived inhibitors of the NBD, owing to the idiosyncratic binding and cooperativity exhibited by adenosine-derivatives that are seemingly required for potency.

### 1.3.6 Lysine-Targeting Covalent Inhibitors of HSP72

We hypothesised that competition with the high affinity, highly abundant substrate of HSP70, ATP, was limiting the cellular activity of the reported nucleoside-derived inhibitors exemplified by VER-155008 **37**. Therefore, within our group, the adenosine-derived TCI **41** was previously designed from reversible ligand **42**, incorporating an acrylate warhead to target the proximal but non-catalytic Cys-17 of HSP72-NBD (Figure 1.35).<sup>144</sup>

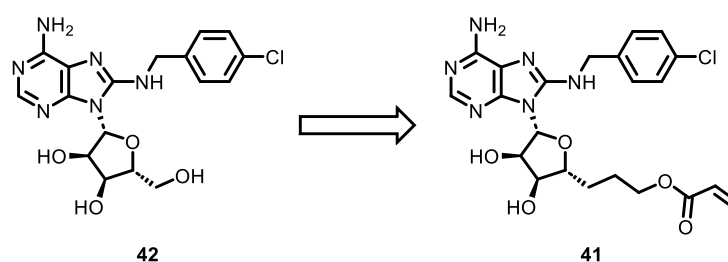


**Figure 1.35** Design of 1<sup>st</sup> generation TCI **41** targeting HSP72-NBD from reversible ligand **42**.

Unexpectedly, extensive characterisation of TCI **41** revealed that no cysteine residue was responsible for adduct formation and the reaction was actually occurring at Lys-56 as the primary pathway. Although no structure of the covalent adduct could be obtained, analysis by x-ray crystallography revealed two distinct binding modes of the reversible complex, which were hypothesised to be crucial for the efficiency of the covalent MoA. In the first binding mode (Figure 1.36 A), denoted as the reversible binding mode, Tyr-15 is in an up-conformation with the acrylate warhead making a  $\pi$ -stacking interaction, blocking the electrophile from reacting with Lys-56. In the second, putative pre-covalent binding mode (Figure 1.36 B), the Tyr-15 flips to a down-conformation enabling the electrophile to be positioned proximally to Lys-56, which would facilitate covalent bond formation. Both binding modes maintain the array of hydrogen bonding and lipophilic interactions with the 8-benzyl adenosine core.

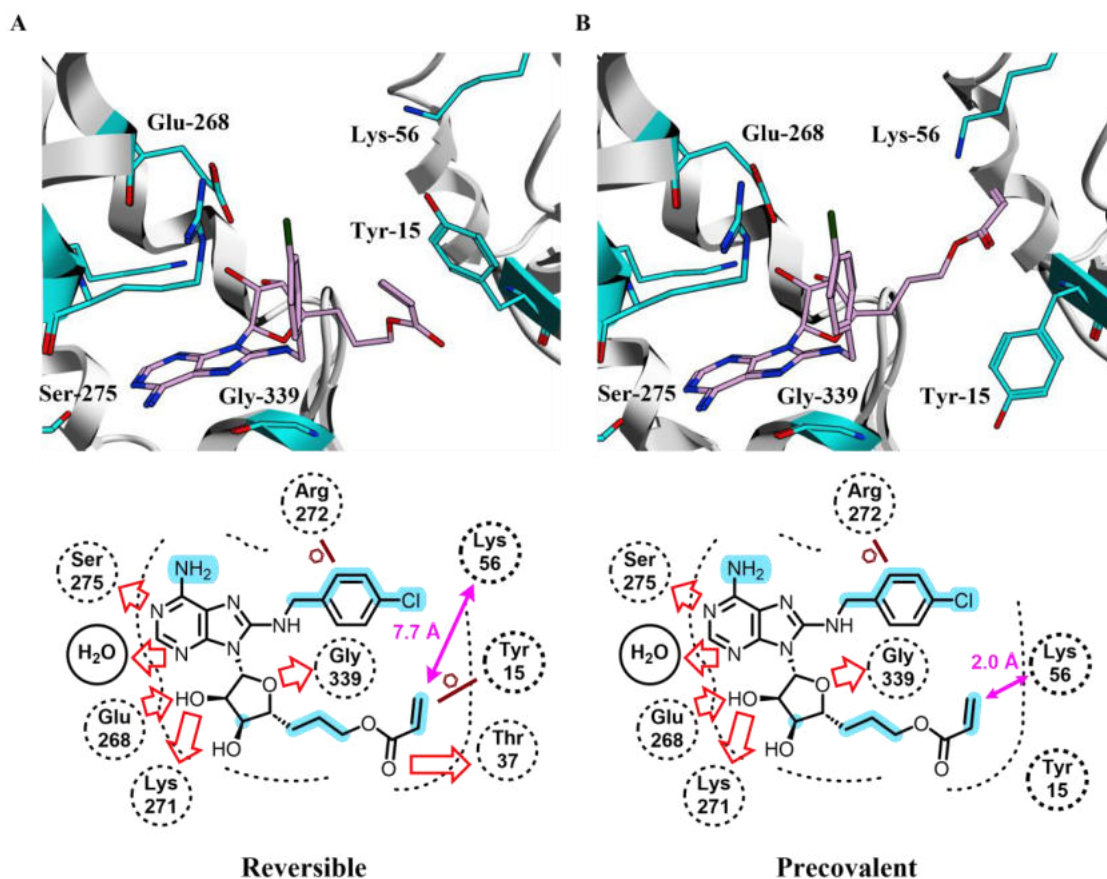


**Figure 1.36** **A** Binding mode of putative reversible complex of TCI **41** with HSP72-NBD (PDB: 5MKR). Tyr-15 sits in an up-conformation, restricting covalent reaction of Lys-56 with the acrylate electrophilic. **B** Binding mode of putative precovalent complex of TCI **41** with HSP72-NBD (PDB: 5MKS). Tyr-15 sits in a down-conformation, with the acrylate warhead positioned in close proximity to Lys-56. Acrylate modelled in to estimate distances as it was not observed due to flexibility. Figures adapted from Pettinger et al.<sup>145</sup>

Kinetic characterisation of the 1<sup>st</sup> generation lysine-TCI **41** revealed that it possessed a modest potency ( $k_{\text{inact}}/K_{\text{I}} = 0.86 \text{ M}^{-1}\text{s}^{-1}$ ), which was driven both by a weak reversible affinity ( $K_{\text{i}} = 18 \text{ }\mu\text{M}$ ) and slow covalent bond formation ( $t_{1/2}^{\infty} = 12 \text{ h}$ ).<sup>145</sup> The design of the 2<sup>nd</sup> generation HSP72 lysine-TCIs aimed to improve the reversible affinity through the incorporation of the 5'-*O*-benzylic ether present in the high affinity reversible inhibitor VER-155008 **37**.<sup>134</sup> To overcome the mismatched reactivity of the hard lysine nucleophile with the soft, cysteine targeting acrylate warhead, a hard sulfonyl fluoride warhead was incorporated into the design of 2<sup>nd</sup> generation TCI **43** (Figure 1.37).



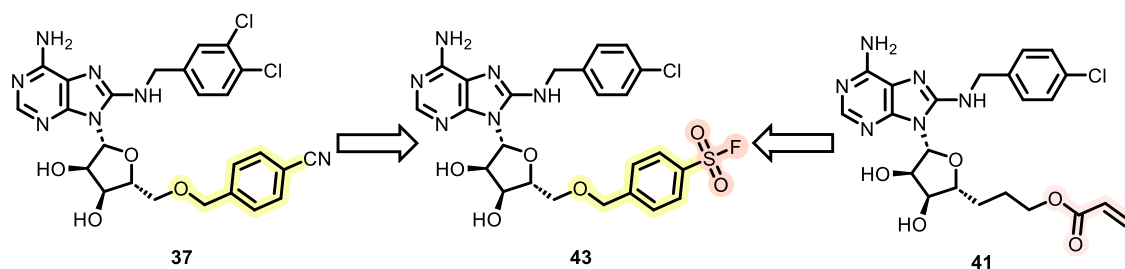
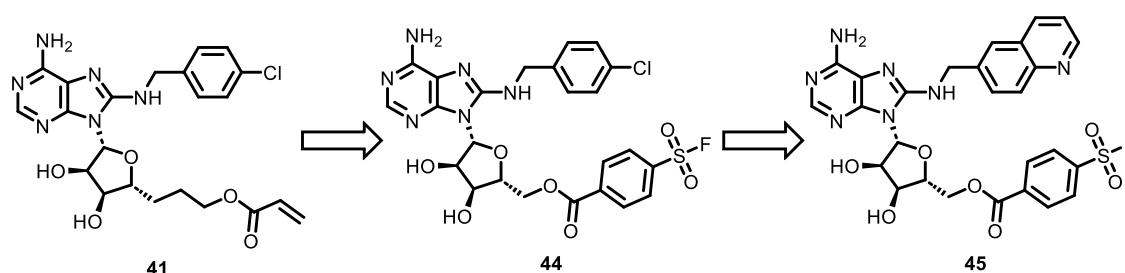


**Figure 1.37** Design of 2<sup>nd</sup> generation HSP72 lysine-TCI **43**, incorporating high reversible affinity scaffold of VER-155008 **37** and optimised hard sulfonyl fluoride warhead to replace acrylate of TCI **41**.

Unfortunately, the existing synthetic methodology for the synthesis of 5'-*O*-benzylic ethers proved to be incompatible with the installation of the sulfonyl fluoride warhead.<sup>145</sup> A more synthetically tractable ester linker was incorporated instead, furnishing 2<sup>nd</sup> generation TCI **44** which exhibited 41-fold improved  $k_{\text{inact}}/K_{\text{I}}$  compared to the first generation TCI **41** (Figure 1.38).



Compound	$k_{\text{inact}}/K_{\text{I}}$ ( $\text{M}^{-1}\text{s}^{-1}$ )	$K_{\text{I}}$ ( $\mu\text{M}$ )	$k_{\text{inact}}$ ( $\text{s}^{-1}$ )	$t_{1/2}^{\infty}$ (min)
acrylate <b>41</b>	$0.86 \pm 0.22$	18	$1.6 \times 10^{-5}$	720
<i>p</i> -SO <sub>2</sub> F <b>44</b>	$35 \pm 1.7$	10	$3.6 \times 10^{-4}$	32
quinoline <b>45</b>	$93 \pm 2.9$	4.7	$4.4 \times 10^{-4}$	26

**Figure 1.38** Design of 2<sup>nd</sup> generation HSP72 lysine-TCIs **44** and **45**, incorporating ester-linked sulfonyl fluoride.

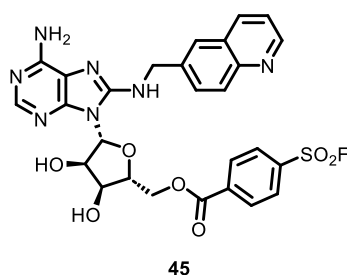
Kinetic analysis of 5'-*O*-ester linked TCI **44** indicated that most of the potency increase was driven by a 23-fold increase in the  $k_{\text{inact}}$ , which validated the switch to the hard sulfonyl fluoride electrophile. However, TCI **44** still only demonstrated modest reversible affinity, with a 1.8-fold improvement in  $K_{\text{I}}$  from the 1<sup>st</sup> generation acrylate **41**. Efforts to improve the potency of this chemotype afforded 8-*N*-quinoline TCI **45**, which exhibited a modest 2.7-fold improved second order rate constant which was driven largely through a 2.1-fold decrease in  $K_{\text{I}}$ .

Reported  $k_{\text{inact}}/K_{\text{I}}$  values for irreversible TCIs typically range from  $10^5 - 10^7 \text{ M}^{-1}\text{s}^{-1}$  for kinase inhibitors,  $10^1 - 10^5 \text{ M}^{-1}\text{s}^{-1}$  for protease inhibitors, and  $10^2 - 10^4 \text{ M}^{-1}\text{s}^{-1}$  for KRAS<sup>G12C</sup> inhibitors.<sup>146</sup> 2<sup>nd</sup> generation HSP72 lysine-TCIs **44** and **45** both exhibit  $k_{\text{inact}}/K_{\text{I}}$  values in the order of  $10^1 \text{ M}^{-1}\text{s}^{-1}$ , which based on the >10,000-fold greater potency of reported ATP-competitive kinase TCIs inhibitors, we concluded was likely insufficient to overcome competition with the high affinity, high abundance substrates ADP and ATP. Consequently, further improvements in the second order rate constant would be required to  $k_{\text{inact}}/K_{\text{I}}$  generate cell active TCIs of HSP72.

## 2 Project Aims

## 2 Project Aims

The overall aim of my project is to validate lysine-targeting covalent inhibition as a strategy to overcome difficult-to-drug targets. Within our group, nucleoside-derived TCIs had been developed targeting Lys-56 of the HSP72-NBD,<sup>145</sup> but we estimated that they displayed  $k_{\text{inact}}/K_{\text{I}}$  values over an order of magnitude too weak to exhibit cellular activity, owing to competition with the high affinity, high abundance natural substrate ATP. Despite displaying rapid covalent bond formation ( $t_{1/2}^{\circ} = 26$  min), *p*-ester-linked sulfonyl fluoride **45** only possessed moderate reversible affinity ( $K_{\text{i}} = 4.7$   $\mu\text{M}$ ) (Figure 2.1).



$k_{\text{inact}}/K_{\text{I}}$ ( $\text{M}^{-1}\text{s}^{-1}$ )	$0.86 \pm 0.22$
$k_{\text{inact}}$ ( $\text{s}^{-1}$ )	$4.4 \times 10^{-4}$
$K_{\text{i}}$ ( $\mu\text{M}$ )	4.7

**Figure 2.1** Structure and kinetic parameters of 2<sup>nd</sup> generation HSP72 lysine-TCI **45**.

These data suggested that the optimal approach to improve the second order rate constant  $k_{\text{inact}}/K_{\text{I}}$  of this chemotype, and consequently obtain cell-active inhibitors, would be through improvements in the reversible affinity of the scaffold. The main project aims were therefore as follows:

- 1) Design and synthesise cell-active irreversible lysine-TCIs of HSP72-NBD, which would primarily involve optimisation of the  $K_{\text{i}}$  from the scaffold of TCI **45**. The high affinity 5'-ether-linked chemotype of reversible inhibitor VER-155008 **37** ( $K_{\text{i}} = 300$  nM)<sup>134</sup> would likely be an appropriate start point (Figure 2.2).

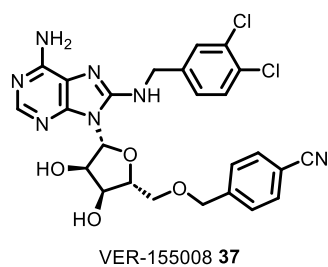


**Figure 2.2** Structure of high reversible affinity HSP72 inhibitor VER-155008 37.

- 2) Investigate the suitability of these cell active inhibitors for probing the phenotype of HSP70 inhibition *in vitro*. Key to this aim will be the design and synthesis of a suitable ABPP probe, which will enable the evaluation of intracellular isoform selectivity for this class of adenosine-derived inhibitors.
- 3) Apply the strategies discovered in the development of HSP72 lysine-TCIs to alternative difficult-to-drug targets.

### 3 Synthesis of HSP72 5'-Ether-Lysine-TCIs

### 3 Synthesis of HSP72 5'-Ether-Lysine-TCIs

#### 3.1 Introduction

##### 3.1.1 Design of 3<sup>rd</sup> Generation HSP72 Lysine-TCIs

2<sup>nd</sup> generation HSP72 lysine-TCI **45** exhibited a 108-fold greater  $k_{\text{inact}}/K_{\text{I}}$  value compared to 1<sup>st</sup> generation HSP72 lysine-TCI **41** (Figure 3.1).<sup>145</sup> However, analysis of the kinetic data indicated that this improvement was largely  $k_{\text{inact}}$ -driven, likely owing to the substitution of the soft acrylate warhead for the hard sulfonyl fluoride warhead, which would react more efficiently with the hard Lys-56 nucleophile.<sup>80</sup>

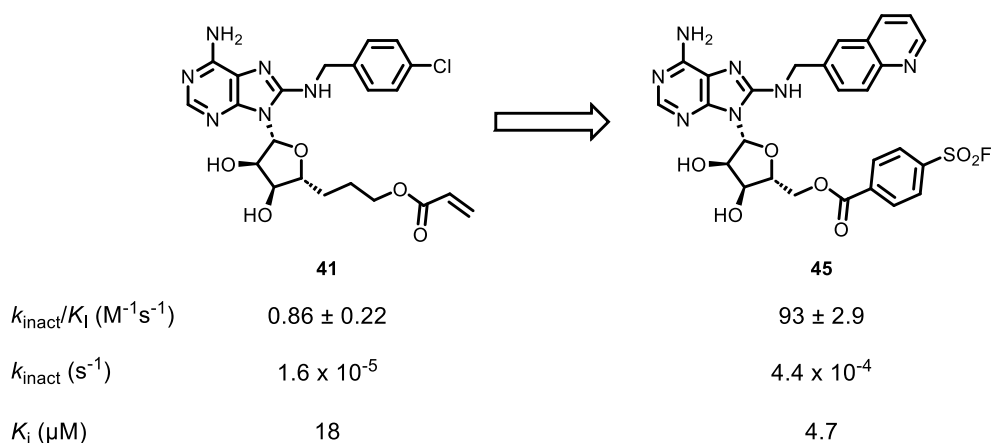


**Figure 3.1** Optimisation of HSP72 lysine-TCIs, from 1<sup>st</sup> generation acrylate **41** to 2<sup>nd</sup> generation sulfonyl fluoride **45**.<sup>145</sup>

To obtain a cell-active HSP72 lysine-TCI, we envisaged that we would require an order of magnitude improvement in  $k_{\text{inact}}/K_{\text{I}}$  to overcome competition with the high affinity, abundance substrate ATP. As TCI **45** displayed a modest  $K_{\text{I}}$  in comparison to its rapid covalent bond formation ( $t_{1/2}^{\text{co}}$  = 26 min), we proposed that improvements in reversible affinity would be the most effective way to drive the necessary improvements in the second order rate constant.

Comparison of the molecular match pairs (MMPs) **46** and **47**, indicates that the switch from a 5'-ester to a 5'-ether resulted in a >18-fold improvement in  $K_{\text{I}}$ , with 5'-ether exhibiting reversible affinity at the resolvable limit of detection for the FP assay (Figure 3.2).<sup>145</sup> The exceptional reversible affinity of **47** was consistent with the SAR reported by Massey et al. for the adenosine-derived 5'-ether chemotype.<sup>134</sup>

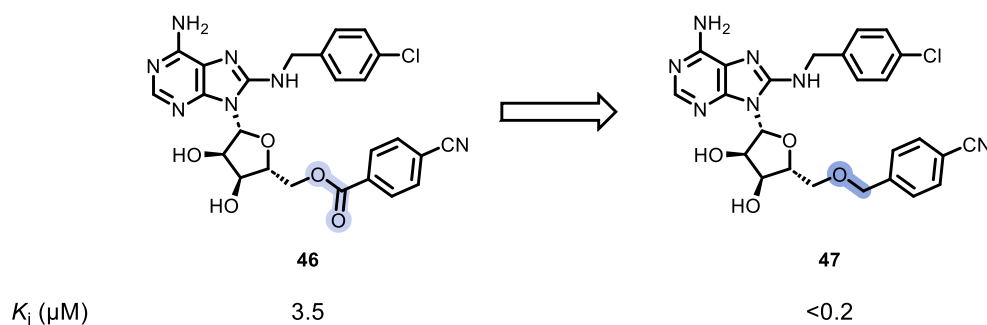


**Figure 3.2** Molecular match-pair analysis of reversible 5'-ester **46** and 5'-ether **47**.

Moreover, a report by Grimster et al. detailed the use of Hammett  $\sigma_m$  and  $\sigma_p$  values to profile the effects of *meta* and *para* substituents on the intrinsic reactivity and hydrolytic stability of aryl sulfonyl fluorides.<sup>147</sup> The authors demonstrated that electron withdrawing groups in the *para* position of aryl sulfonyl fluorides correlate strongly with increased intrinsic reactivity and decreased hydrolytic stability. Decreasing warhead intrinsic reactivity is advantageous, as a high reactivity is associated with idiosyncratic toxicity arising from non-specific labelling of off-target proteins.<sup>72</sup> Replacing the electron-withdrawing ester moiety of TCI **44** for an ether moiety would result in increased electron density at the *para* position of the 5'-benzyl ring, with Hammett  $\sigma_p = 0.45$  for a methyl ester and  $\sigma_p = 0.01$  for a methyl benzylic ether,<sup>148</sup> likely decreasing the intrinsic reactivity and improving the hydrolytic stability of the compound.

Using these data, the design of the 3<sup>rd</sup> generation HSP72 Lysine-TCI **43** involved the incorporation of the high reversible affinity 5'-ether-containing scaffold of **47** in conjunction with the *para*-sulfonyl fluoride of TCI **45** (Figure 3.3). It was hypothesised that this would furnish a TCI with greatly improved  $k_{\text{inact}}/K_I$ , as well as improved stability and decreased intrinsic reactivity, making it a potent and selective cell-active inhibitor of HSP70.



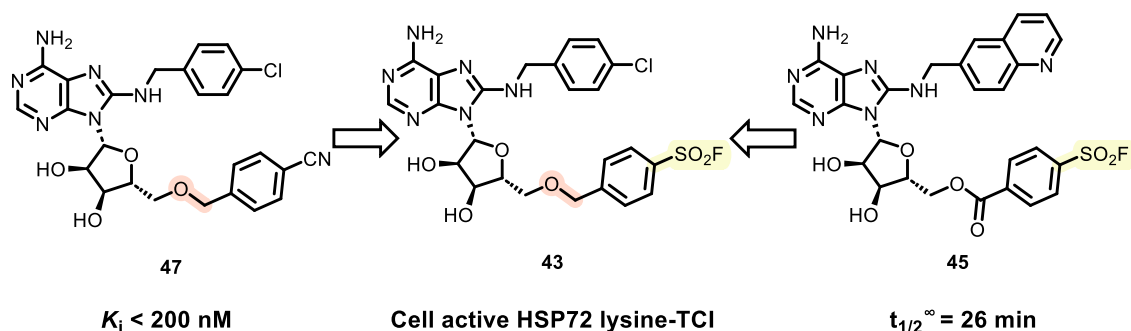
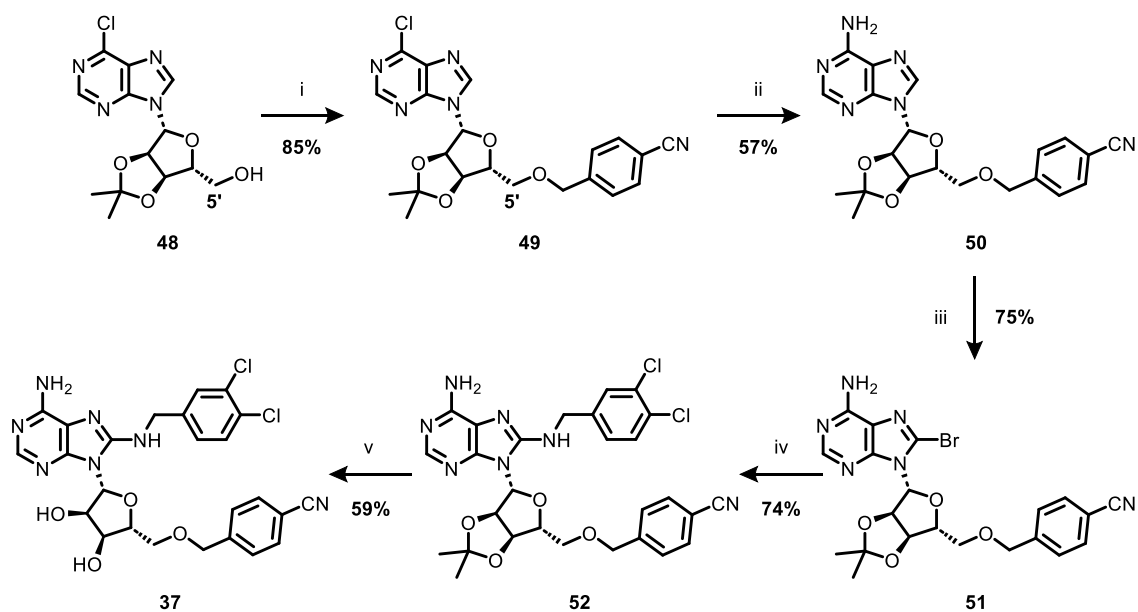


**Figure 3.3** Design strategy for 3<sup>rd</sup> generation HSP72 lysine-TCI **43**.

### 3.1.2 Previous Work Towards the Synthesis of Adenosine-Derived 5'-Ethers

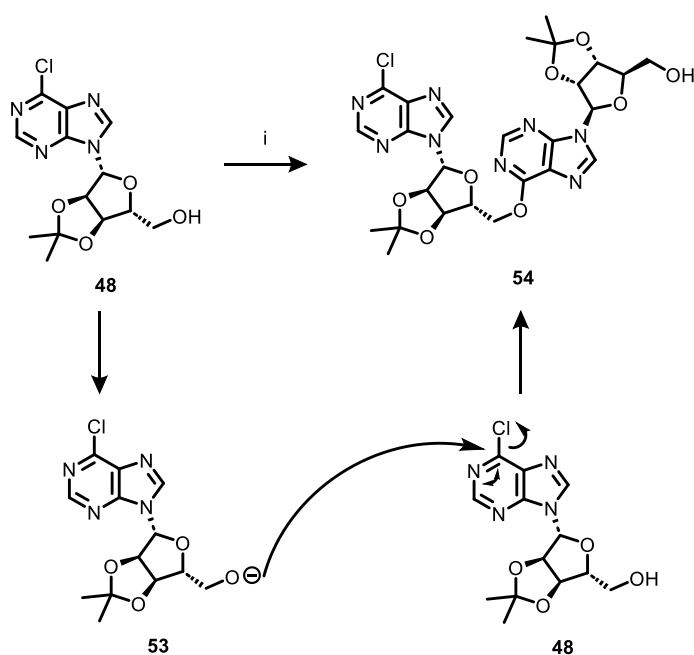
To generate HSP72 TCIs with high reversible affinity, by replacing the 5'-ester linker for a 5'-ether moiety, a protocol to synthesise this key bond would be required. Strategies to synthesise 5'-ethers of adenosine have been explored both in the literature and within our group. The following section is a summary of previous attempts to functionalise the 5'-OH of adenosine with benzylic groups. Massey et al. described the synthesis of a 5'-benzylic ether during their reported synthesis of VER-155008 **37** (Scheme 3.1).<sup>134</sup>



**Scheme 3.1** Synthesis of VER-155008 **37**.<sup>134</sup> Reagents and conditions: i) 4-cyanobenzyl bromide (5 equiv.), NaH (1.1 equiv.), DMF (0.08 M), rt, 30 min; ii) 8N NH<sub>4</sub>OH<sub>(aq)</sub> (62 equiv.), EtOH (0.13 M), 100 °C, 90 mins; iii) Br<sub>2</sub> (2.5 equiv.), 10% Na<sub>2</sub>HPO<sub>4(aq)</sub>:dioxane 1:1 (0.01 M), rt, 1 h; iv) 3,4-dichlorobenzylamine (9.9 equiv.), EtOH (0.13 M), 140 – 150 °C, 2 h; v) TFA:water 1:1 (0.03 M), rt, 3 h (Massey et al.).<sup>134</sup>

Firstly, chloropurine **48** was transformed to 5'-benzylated adenosine **49** and subsequently converted to aniline **50** in moderate yield. This facilitated selective bromination at the 8-position to give **51**, which underwent an  $S_NAr$  reaction with 3,4-dichlorobenzylamine to give **52**. Finally, acidic deprotection of the acetonide gave VER-155008 **37**.

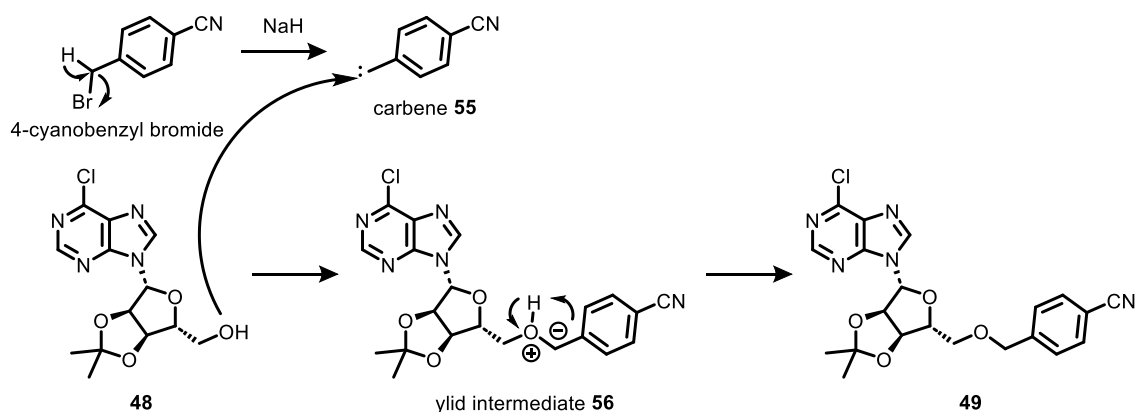
To synthesise the key 5'-benzylic ether, unusually, chloropurine **48** and electrophile 4-cyanobenzyl bromide were combined prior to the addition of sodium hydride. This is in contrast to the conventional Williamson ether synthesis which typically involves the addition of electrophile to a pre-mixed solution of the strong base and alcohol, to form the nucleophilic alkoxide.<sup>149</sup> However, this was not possible in the synthesis of VER-155008 **37**, as previous work within our group showed that pre-treatment of the alcohol with sodium hydride led to the formation of a complex reaction mixture, with full consumption of the starting material. We speculated that following alkoxide formation from deprotonation of **48** with NaH, the intermediate alkoxide **53** underwent facile oligomerisation through attack at the 6-chloropurine moiety to give dimer **54** (Scheme 3.2).



**Scheme 3.2** Proposed mechanism for the degradation of **48** upon pre-stirring with sodium hydride. Reagents and conditions: i) NaH, DMF then 4-(trifluoromethyl)benzyl bromide, rt.

However, Massey et al. did not explain the unorthodox reaction conditions, nor did they provide isolated yields in the synthesis of any analogues other than their lead

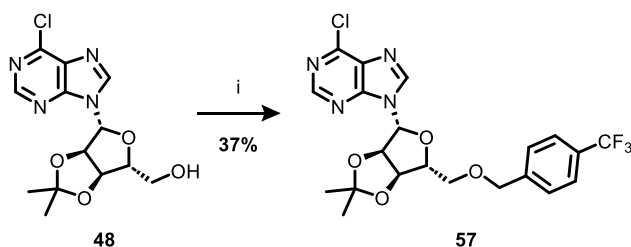
VER-155008 **37**. Analysis of the reported scope<sup>134</sup> of this atypical 5'-benzylation reaction suggested that only electron-deficient benzyl bromides could readily undergo this transformation. Previous attempts within our group to exploit electron rich substituents were also unsuccessful (data not shown). To explain these observations, we propose a plausible alternative mechanistic pathway for the 5'-etherification reaction (Scheme 3.3).



**Scheme 3.3** Plausible mechanism for carbene pathway to form 5'-ether.

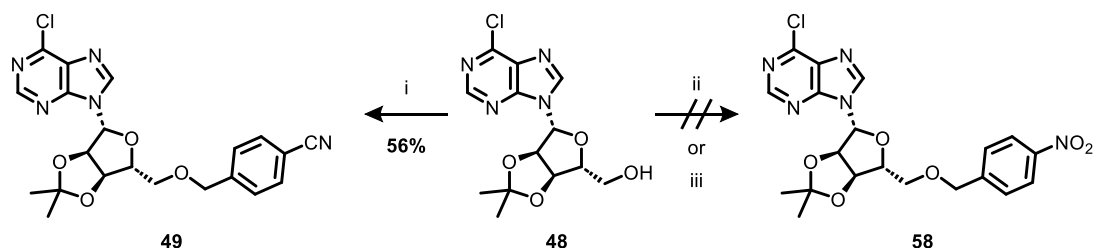
Addition of the strong base sodium hydride to 4-cyanobenzyl bromide initiates the formation of the benzylic carbene **55** through alpha-elimination.<sup>150</sup> The benzylic carbene **55** is stabilised through the electron withdrawing substituents, consistent with the limited scope of this transformation.<sup>151</sup> The carbene **55** then undergoes facile ylid formation to give **56**, followed by proton transfer to give the 5'-ether **49**.<sup>152</sup>

Previously within our team, we attempted to reproduce these conditions for the synthesis of electron-deficient 5'-*O*-benzylated adenosine derivatives. 5'-*para*-CF<sub>3</sub> benzyl ether **57** was isolated in moderate yield following treatment with sodium hydride (Scheme 3.4).<sup>153,154</sup>



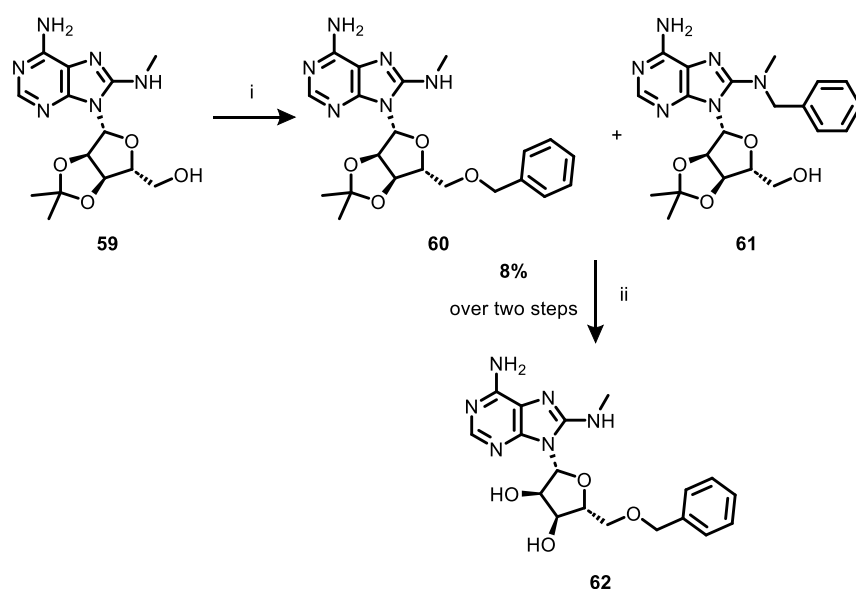
**Scheme 3.4** 5'-etherification to give 5'-*para*-CF<sub>3</sub> benzyl ether **57**.<sup>153</sup> Reagents and conditions: i) 4-(trifluoromethyl)benzyl bromide (1.7 equiv.), NaH (1.1 equiv.), DMF (0.08 M), rt, 4 h.

Within our team we also successfully reproduced the synthesis of *p*-cyanobenzyl intermediate **49** albeit in considerably lower yield than the report in the literature (Scheme 3.5). Unfortunately, we were unable to extend the scope of the reaction to the synthesis of *p*-nitrobenzyl derivative **58**, which could have potentially given access to electron-rich derivatives from reduction of the nitro group (Scheme 3.5).<sup>155</sup>



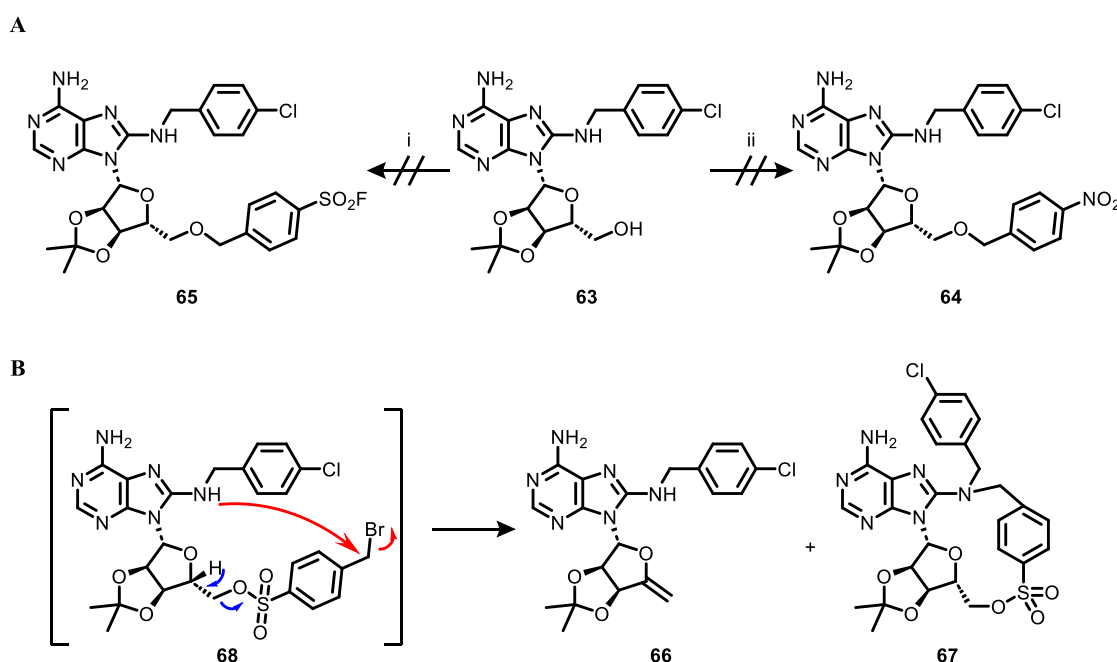
**Scheme 3.5** Attempted 5'-etherifications.<sup>155</sup> Reagents and conditions: i) 4-cyanobenzyl bromide (4 equiv.), NaH (1.1 equiv.), DMF (0.12 M), rt, 45 min; ii) 4-nitrobenzyl bromide, NaH, DMF, rt, 3 h; iii) Ag<sub>2</sub>O, 4-nitrobenzyl bromide, DMF, rt, 5 h.

In a subsequent publication, Massey et al. described a synthetic protocol for late stage functionalisation of 8-*N*-substituted adenosine derivatives, such as 8-*N*-methyl **59**, using Cs<sub>2</sub>CO<sub>3</sub> as a base (Scheme 3.6).<sup>156</sup>



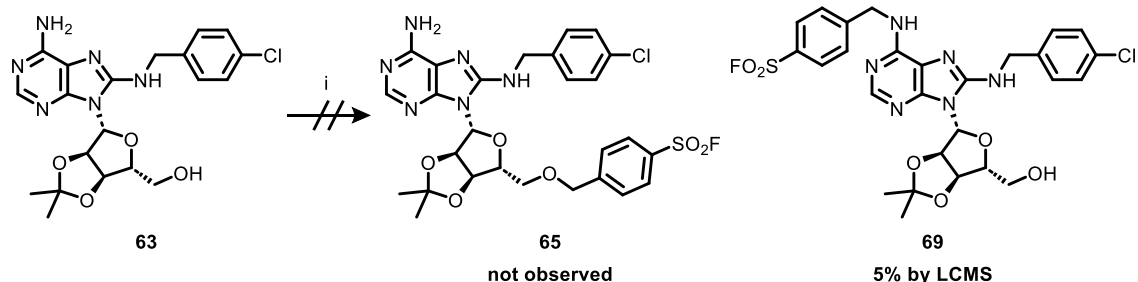
**Scheme 3.6** Synthesis of 5'-*O*-benzylated adenosine derivatives using Cs<sub>2</sub>CO<sub>3</sub> as a base by Massey et al.<sup>156</sup> Reagents and conditions: i) Cs<sub>2</sub>CO<sub>3</sub> (2 equiv.), benzyl chloride (1.15 equiv.), DMF (0.05 M), rt, 72 h; ii) TFA (0.05 M), rt, overnight.

These conditions reportedly led to an inseparable mixture of desired product **60** and undesired 8-*N*-benzylated regioisomer **61**. Whilst they did not state the ratio of the two regioisomers, the undesired regioisomer was reported to decompose in the subsequent acidic deprotection resulting in a poor 8% overall yield of **62** across two steps. Within our team, applying these conditions to 8-*N*-benzyl intermediate **63** in the late-stage introduction of electron-deficient and even electrophile containing benzylic ether substituents, to respectively give *p*-nitro **64** and *p*-SO<sub>2</sub>F **65**, led to a complex reaction mixture apparently resulting from poor chemoselectivity (Scheme 3.7 A).<sup>155</sup> LCMS analysis of the reaction mixture indicated that the major side products had *m/z* values consistent with exocyclic alkene **66** and macrocycle **67**, which were proposed to arise from degradation of transient intermediate **68** (Scheme 3.7 B).



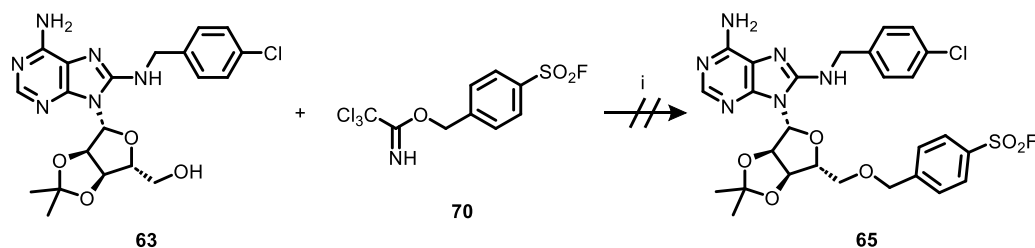
**Scheme 3.7 A** Attempted 5'-etherification with Cs<sub>2</sub>CO<sub>3</sub>.<sup>155</sup> Reagents and conditions: i) C<sub>2</sub>CO<sub>3</sub>, 4-(fluorosulfonyl)benzyl bromide, DMF, rt, 2 h; ii) C<sub>2</sub>CO<sub>3</sub>, 4-nitrobenzyl bromide, DMF, rt, 3 h. **B** Proposed mechanism to side products **66** and **67** from transient intermediate **68** possibly formed from treatment of **63** with Cs<sub>2</sub>CO<sub>3</sub>.

Within our team, 5'-etherification using silver (I) oxide-mediated conditions developed by Hashimoto et al.<sup>157</sup> was then attempted, avoiding the formation of a formal alkoxide that may preferentially react at the sulfonyl fluoride (Scheme 3.8). However, the only recognised product observed from this reaction was 6-*N*-benzylated material **69**.



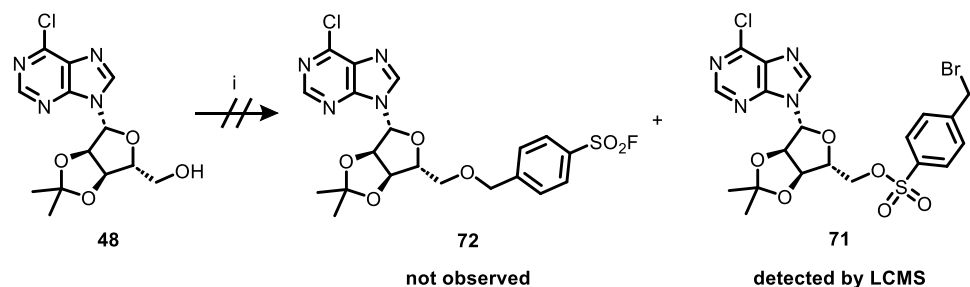
**Scheme 3.8** Silver (I) oxide-mediated conditions for 5'-etherification.<sup>155</sup> Reagents and conditions: *i*) Ag<sub>2</sub>O, 4-(fluorosulfonyl)benzyl bromide, hexane:CH<sub>2</sub>Cl<sub>2</sub> 4:1, 60 °C, 24 h.

Previous efforts within the team also involved attempted etherification under acidic conditions using the corresponding trichloroacetimidate **70** (Scheme 3.9),<sup>158</sup> which led to no reaction occurring and complete re-isolation of starting material.



**Scheme 3.9** Attempted 5'-etherification *via* trichloroacetimidate.<sup>155</sup> Reagents and conditions: *i*) TfOH, CH<sub>2</sub>Cl<sub>2</sub>, 0 °C, 18 h.

Also within the team, basic etherification conditions with sodium hydride first described by Massey et al. were attempted in conjunction with 4-(fluorosulfonyl)benzyl bromide, which led to a complex reaction mixture and a small amount of 5'-sulfonyl ester **71** and none of the desired product **72** being detected in the crude mixture by LCMS (Scheme 3.10).



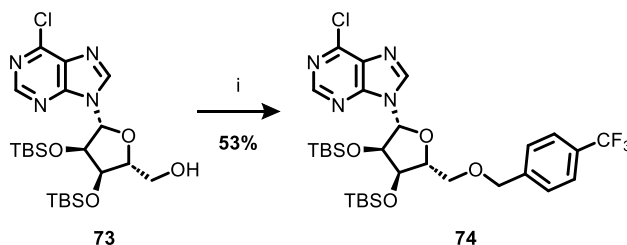
**Scheme 3.10** Attempted 5'-etherification with 4-(fluorosulfonyl)benzyl bromide.<sup>155</sup> Reagents and conditions: *i*) 4-(fluorosulfonyl)benzyl bromide, NaH, DMF, rt, 3 h.

### 3.2 Optimisation of Synthetic Route to Access 5'-Ether

From my analysis of the literature, it was clear that the reported methodologies for the synthesis of 5'-*O*-benzylated adenosine derivatives are not robust, display limited substrate scope and therefore would not be suitable for the synthesis of our proposed class of TCIs. We concluded that our targets would represent a considerable synthetic challenge, in which the inherent reactivity of adenosine must be controlled to enable formation of the desired ether bond, whilst suppressing unwanted oligomerisation and controlling chemoselectivity owing to the multiple nucleophilic sites on the adenosine scaffold.

#### 3.2.1 TBS Protecting Group Strategy

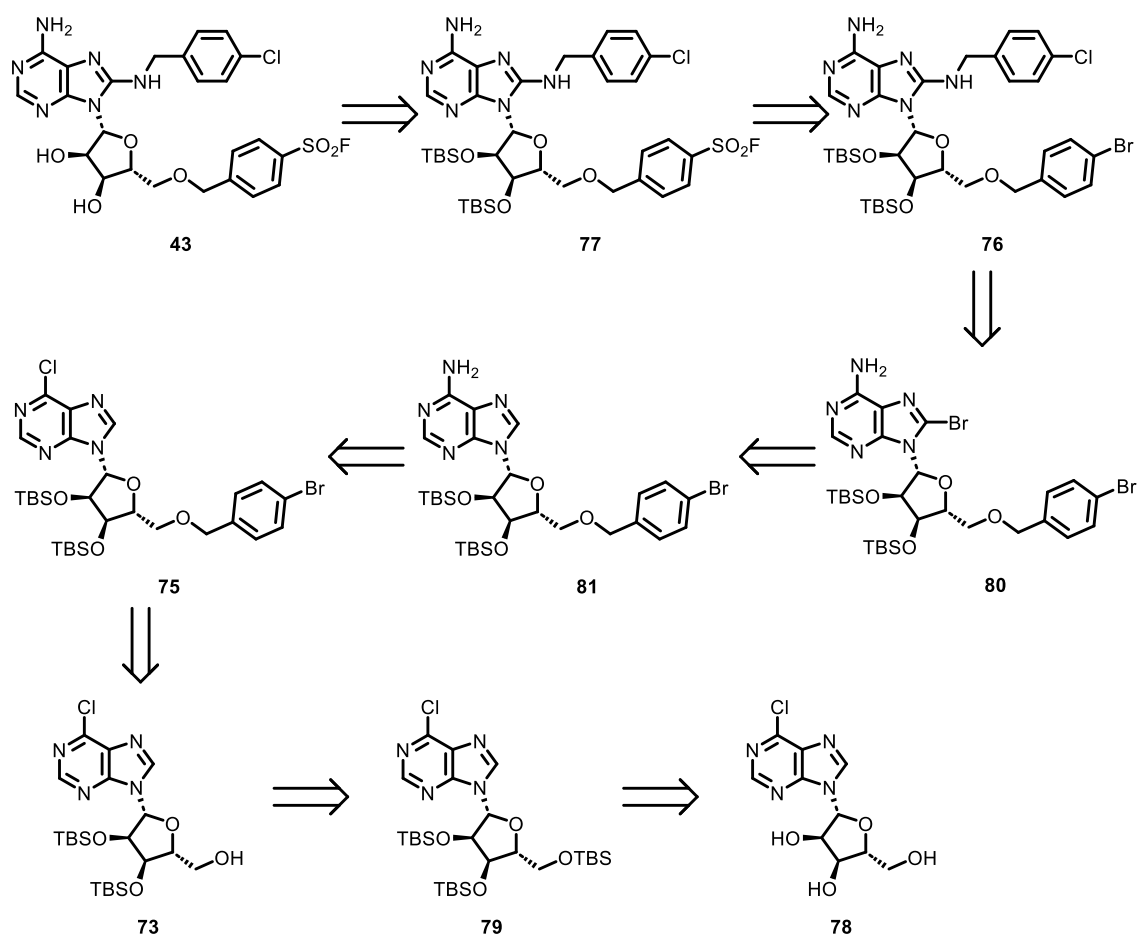
2',3'-Ribose diol protecting groups are important for modulating the reactivity of adenosine derivatives. Work within our group had demonstrated that replacing the commonly used acetonide diol protecting group with two TBS groups to give **73** resulted in a modest improvement in yield from 37% to 53% for the 5'-etherification step with 4-(trifluoromethyl)benzyl bromide giving **74** (Scheme 3.4 and Scheme 3.11).<sup>153</sup>



**Scheme 3.11** 5'-etherification with bis-*O*-TBS protected material.<sup>153</sup> Reagents and conditions: i) NaH (1.3 equiv.), DMF (0.27 M), -78 °C, 15 min *then* 4-(trifluoromethyl)benzyl bromide (2 equiv.), -78 °C to rt, 16 h.

We hypothesised that target TCI **43** could be accessed from 4-bromobenzyl intermediate **75** and that the use of the bis-*O*-TBS protected substrate **73** for the etherification step might allow us to ultimately obtain sufficient isolated 5'-*O*-benzylated material to proceed with this synthetic route. *p*-Bromobenzyl was selected as a functional group for the 5'-etherification owing to its lack of reactive functionalities that could lead to side product formation, as well its possession of a bromine group that could serve as a synthetic handle in late-stage functionalisation and installation of the covalent warhead. We envisaged that late-stage functionalisation would proceed *via* intermediate **76** to give

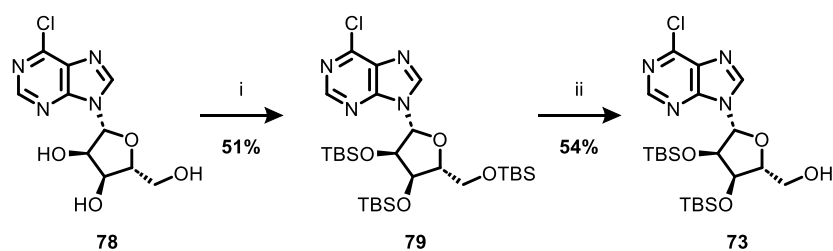
**77** (Scheme 3.12). It was proposed that bis-*O*-TBS protected substrate **73** could be made in two steps from 6-chloropurine riboside **78** via **79** following literature conditions.<sup>153</sup>



**Scheme 3.12** Proposed retrosynthetic route to TCI **43**.

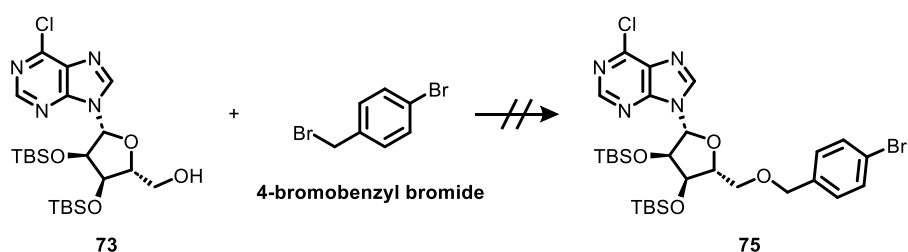
Bis-*O*-TBS protected adenosine **73** was first synthesised in two steps from 6-chloropurine riboside **78** according to the procedure of Evans et al.<sup>153</sup> Riboside **78** was initially tris-*O*-TBS protected with TBSCl to give **79**, before treating with a TFA:H<sub>2</sub>O:THF 1:1:4 mixture to selectively cleave the 5'-*O*-TBS, which gave the desired product **73** in moderate yield (Scheme 3.13).





**Scheme 3.13** Synthesis of bis-*O*-TBS protected riboside **73**. Reagents and conditions: i) TBSCl (6 equiv.), imidazole (7 equiv.), DMF (0.1 M), rt, 20 h; ii) TFA:H<sub>2</sub>O:THF 1:1:4 (0.07 M), 0 °C, 6 h.

The 2',3'-*O*-bis-TBS derivative **73** was then screened for reaction with 4-bromobenzyl bromide to form the 5'-*O*-benzylated target **75** under a range of conditions (Table 3.1).



Entry	Reagents <sup>a</sup>	Temperature	Solvent
1	NaH (1.2 equiv.)	rt	DMF
2	NaH (1.2 equiv.)	-78 °C	DMF:THF 1:1
3	Cs <sub>2</sub> CO <sub>3</sub> (2 equiv.)	rt	DMF
4	Ag <sub>2</sub> O (1.2 equiv.)	rt	DMF
5	TBAB (5 mol%)	rt	toluene: NaOH 2:1 <sup>b</sup>
6	TBAB (5 mol%)	rt	CH <sub>2</sub> Cl <sub>2</sub> :NaOH 2:1 <sup>b</sup>
7	TBAB (5 mol%)	rt	THF:NaOH 2:1 <sup>b</sup>

**Table 3.1** Conditions attempted for etherification reaction. <sup>a</sup>All reactions performed at (0.25 M) with 1 equivalent of 4-bromobenzyl bromide for 18 hours. <sup>b</sup>NaOH 50% (w/w) used, reactions were stirred as heterogeneous mixtures at 1000 rpm.

Treatment with silver (I) oxide resulted in no reaction with only starting material recovered (Table 3.1, Entry 4). In contrast, attempted basic etherification with  $\text{Cs}_2\text{CO}_3$  (Table 3.1, Entry 3), sodium hydride (Table 3.1, Entries 1 and 2) or phase transfer catalysis with tetrabutylammonium bromide (TBAB) and sodium hydroxide<sup>159</sup> (Table 3.1, Entries 5 – 7) all generated a complex and inseparable mixture of products, presumably resulting from oligomerisation of the starting material. The desired product **75** was not observed by LCMS analysis under any of the described reaction conditions.

### 3.2.2 Protecting Group Strategy

From my analysis of previous attempts to synthesise diverse 5'-*O*-benzyl nucleosides and my screening of benzylation conditions following a protecting group swap, it was clear that the formation of the key ether bond would be extremely challenging. The two strategies investigated so far, derivatising the 6-chloropurine without competing oligomerisation and chemoselective 5'-*O*-benzylation that spared the 6-/8-aminoadenine functional groups, had been unsuccessful (Figure 3.4 A). Therefore, we hypothesised that it would be necessary to install multiple protecting groups at the 6- and 8-amino adenine positions in addition to the 2'- and 3'- ribose positions to eliminate the problem of competing nucleophiles (Figure 3.4 B).

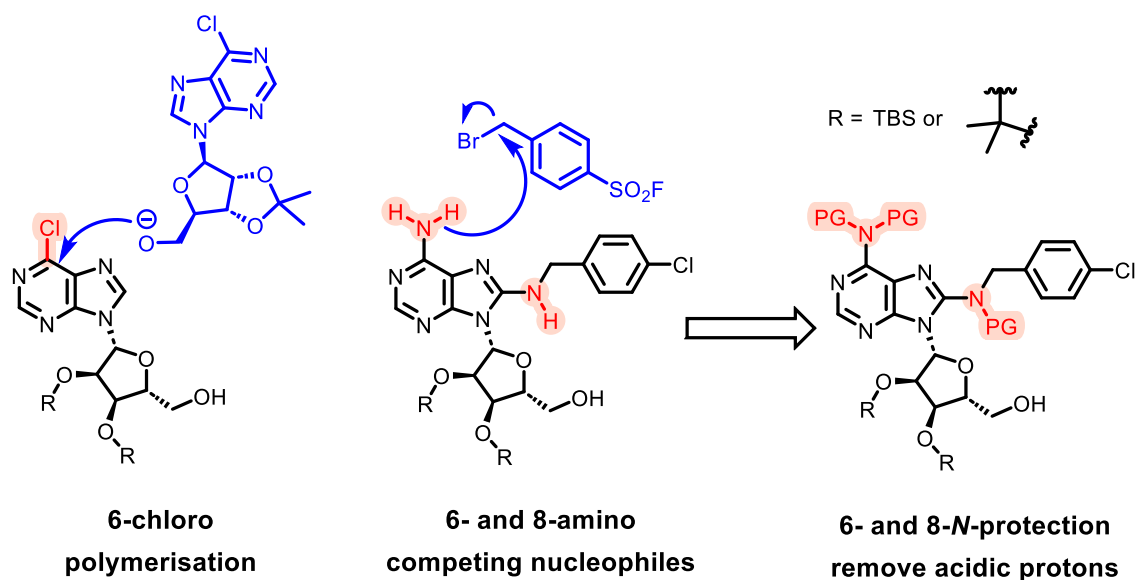
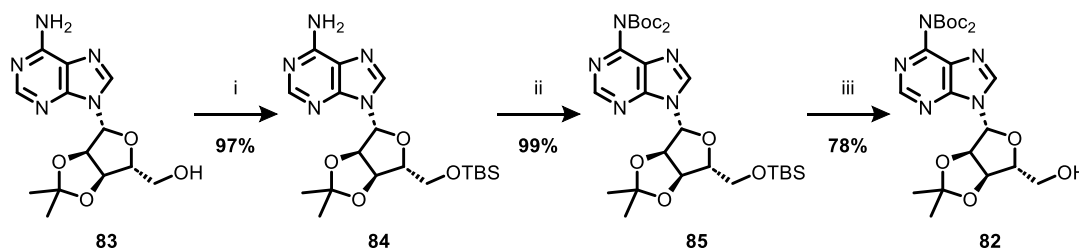


**Figure 3.4** Summary of competing reactive pathways in the attempted synthesis of 5'-*O*-benzylated adenosine derivatives and proposed protecting group strategy to obtain desired reactivity. PG = protecting group.

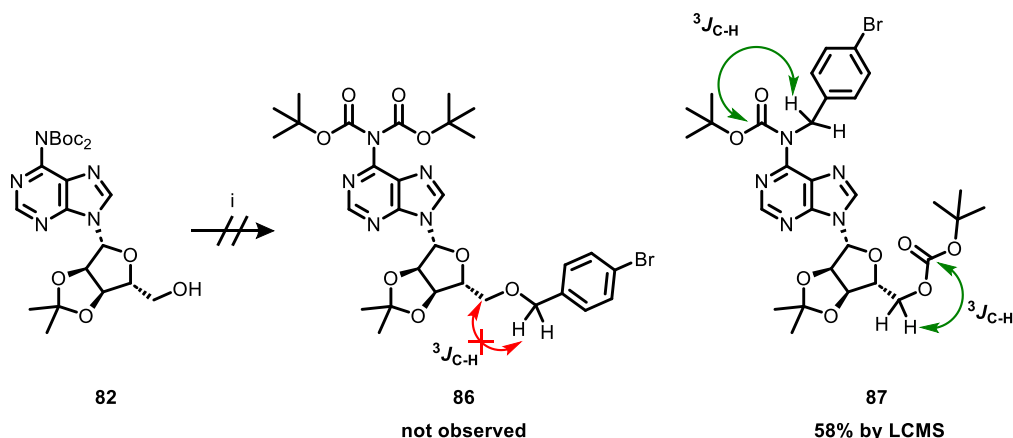
This strategy required protecting groups that would suppress the nucleophilicity of the 6-/8-amino purine to be compatible with the ribose protecting groups and be compatible with late-stage global deprotection in the presence of the base-sensitive sulfonyl fluoride electrophile. We began the study with the *tert*-butyloxycarbonyl (Boc) group, a well-established and robust acid-labile protecting group for anilines.<sup>160</sup> 6-adenine-bis-*N*-Boc derivative **82** was generated in three steps according to literature procedures (Scheme 3.14).<sup>161</sup>



**Scheme 3.14** Synthesis of bis-*N*-Boc intermediate **82**. Reagents and conditions: i) TBSCl (1.2 equiv.), imidazole (2 equiv.), DMF (0.35 M), rt, 20 h; ii) DMAP (0.1 equiv.), Boc<sub>2</sub>O (2.5 equiv.), THF (0.2 M), rt, 3 h; iii) TBAF (1 equiv.), THF (0.12 M), rt, 2 h.

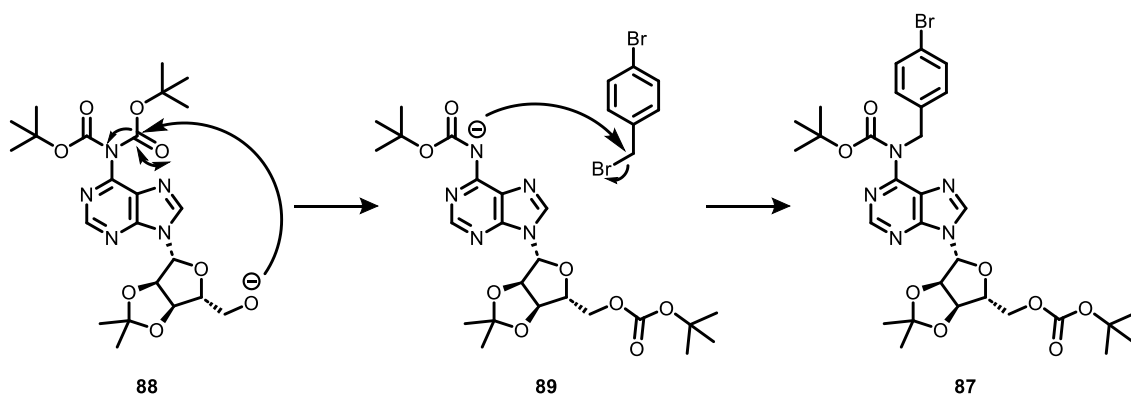
*O*-TBS protection of 2'3'-acetonide adenosine **83** gave the fully ribose-protected adenosine **84** in high yield, which was then subjected to bis-6-*N*-Boc protection using excess Boc-anhydride to give **85** in quantitative yield. Treatment with tetrabutylammonium fluoride (TBAF) resulted in *O*-TBS deprotection to give the key protected precursor **82** in 73% overall yield over three steps.

The bis-6-*N*-Boc protected precursor **82** was then subjected to a reaction with 4-bromobenzyl bromide and sodium hydride under standard Williamson ether synthesis conditions (Scheme 3.15).



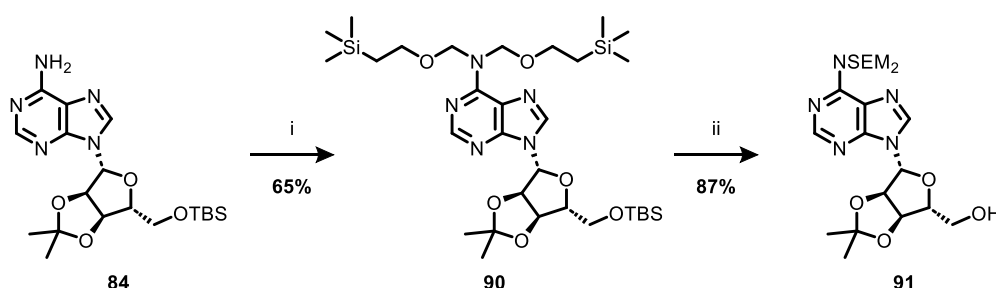
**Scheme 3.15** Attempted synthesis of 5'-*O*-benzylated adenosine **86** led to the formation of 6-*N*-benzylated product **87** which was confirmed through  $^1\text{H}$ - $^{13}\text{C}$  HMBC analysis. Reagents and conditions: i) NaH (1.2 equiv.), THF (0.5 M), 0 °C, 15 min, then 4-bromobenzyl bromide (2 equiv.), 0 °C to rt, 18 h.

Analysis of the crude reaction mixture by LCMS indicated the formation of a product with the correct  $m/z$  for the desired 5'-benzyl-ether **86**. However, analysis of the  $^1\text{H}$  NMR and  $^1\text{H}$ - $^{13}\text{C}$  HMBC spectra showed that this major product was 6-*N*-benzylated adduct **87**. Formation of this undesired product **87** was proposed to occur *via* either intramolecular or intermolecular migration of the *N*-Boc group to the reactive 5'-alkoxide species **88** generated from treatment of **82** with sodium hydride (Scheme 3.16). The resulting anion **89** on the 6-*N* position then reacted with 4-bromobenzyl bromide which was subsequently added into the reaction mixture. We therefore concluded that the bis-*N*-Boc moiety was too labile to function as a suitable protecting group for this reaction.



**Scheme 3.16** Proposed mechanism for the formation of **87**. Alkoxide **88** formed from addition of sodium hydride to **82** initiates Boc transfer, and the resulting anion formed on the 6-*N* position **89** then reacts with 4-bromobenzyl bromide.

To eliminate the risk of migration we required a protecting group that is non-electrophilic. The trimethylsilylethoxymethyl (SEM) group is a silyl protecting group that is non-labile to anionic nucleophiles and has a number of deprotection strategies,<sup>162</sup> making it a potentially viable protecting group for basic etherification protocols. Mono-*O*-TBS protected derivative **84** was reacted with SEMCl under standard conditions, which led to the successful isolation of bis-*N*-SEM product **90** in moderate yield (Scheme 3.17).

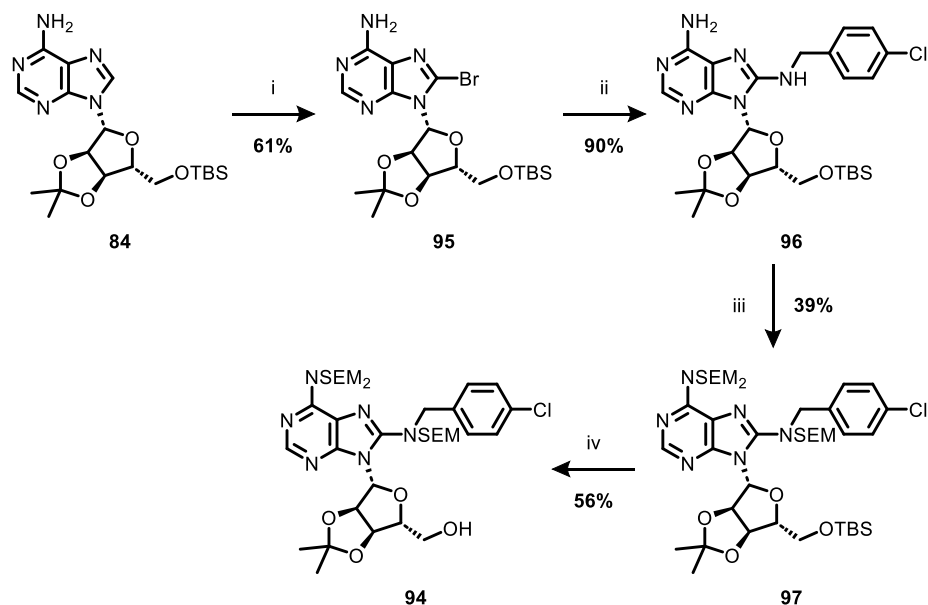


**Scheme 3.17** Synthesis of bis-SEM protected adenosine derivative **91**. Reagents and conditions: i) DIPEA (3 equiv.), SEMCl (3 equiv.), CH<sub>2</sub>Cl<sub>2</sub> (0.3 M), reflux, 3 h; ii) TBAF (1.1 equiv.), THF (0.12 M), 0 °C to rt, 2 h.

Even though *O*-TBS and *N*-SEM are both silyl protecting groups, *O*-TBS can be selectively cleaved using fluoride reagents.<sup>163</sup> 5'-*O*-TBS protected intermediate **90** was treated with TBAF, which selectively gave the free 5'-alcohol **91** in a very high 87% yield. Reaction of this bis-*N*-SEM protected substrate **91** with sodium hydride and 4-bromobenzyl bromide gave the 5'-benzyl ether **92** in an excellent 91% yield, and as

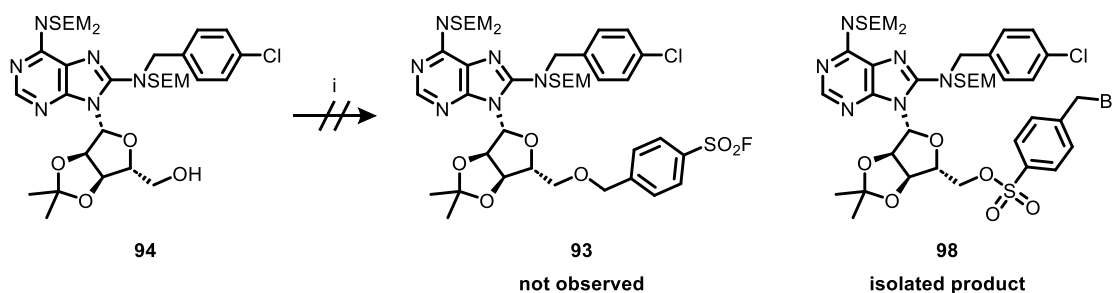


in 61% yield.<sup>145</sup> The  $S_NAr$  reaction of **95** with 4-chlorobenzylamine gave 8-benzyl adenosine **96**. Treatment of **96** with super-stoichiometric amounts of SEMCl resulted in tris-*N*-SEM-protection to give **97**, albeit with longer reaction times than with the corresponding bis-*N*-SEM protection of **84**. Finally, selective *O*-TBS-deprotection afforded intermediate **94** in moderate yield (Scheme 3.20).



**Scheme 3.20** Synthesis of tris-*N*-SEM intermediate **94**. Reagents and conditions: i)  $K_2HPO_4$  (3 equiv.),  $Br_2$  (2.5 equiv.), 1,4-dioxane:H<sub>2</sub>O 1:1 (0.13 M), rt, 24 h; ii) 4-chlorobenzylamine (8 equiv.), EtOH (0.3 M), 160 °C,  $\mu$ wave, 1 h; iii) DIPEA (4.5 equiv.), SEMCl (4.5 equiv.),  $CH_2Cl_2$  (0.3 M), reflux, 30 h; iv) TBAF (1.1 equiv.), THF (0.12 M), 0 °C to rt, 1 h.

Tris-*N*-SEM intermediate **94** was then reacted with sodium hydride and 4-(fluorosulfonyl)benzyl bromide. Unfortunately, purification of the reaction mixture yielded only sulfonyl ester **98**, which was confirmed with HRMS and NMR analysis (Scheme 3.21).



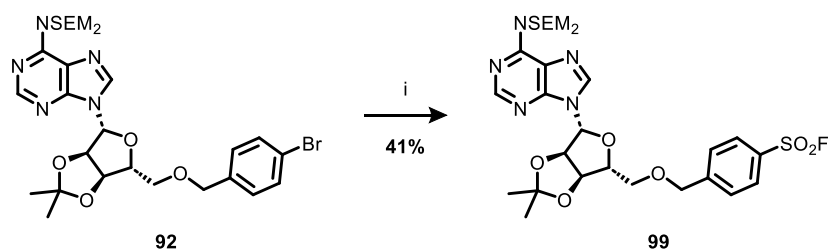
**Scheme 3.21** Attempted synthesis of sulfonyl fluoride **93**. Reagents and conditions: i) NaH (1.2 equiv.), THF (0.5 M), 0 °C, 15 min, *then* 4-(fluorosulfonyl)benzyl bromide (2 equiv.), 0 °C to rt, 18 h.

It was clear that the 5'-alkoxide generated under the reaction conditions preferentially reacts at the sulfonyl fluoride warhead over the desired benzyl bromide; this indicated that the sulfonyl fluoride warhead may have to be introduced after the etherification step to overcome the mismatched reactivity.

### 3.3 Incorporating the Covalent Warhead

#### 3.3.1 Accessing 8-*H* adenosine-derived TCI 101

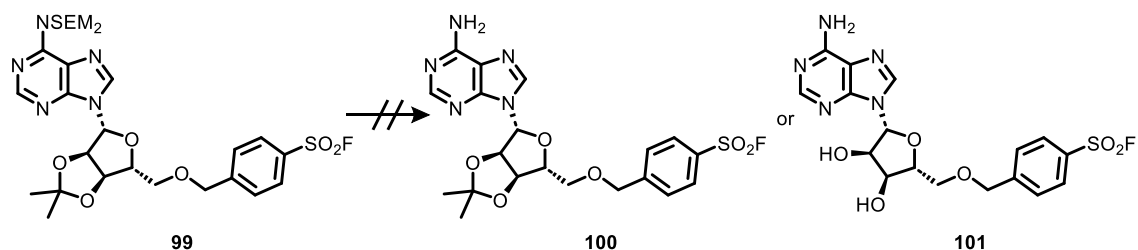
In 2017, Davies et al. described a one-pot palladium-catalysed protocol to access sulfonyl fluorides from the corresponding aryl bromide.<sup>164</sup> The procedure uses 1,4-diazabicyclo[2.2.2]octane bis(sulfur dioxide) adduct (DABSO) as a sulfur dioxide source and *N*-fluorobenzenesulfonimide (NFSI) as an electrophilic fluorination reagent. Application of this protocol to bis-*N*-SEM protected intermediate **92** enabled the isolation of sulfonyl fluoride **99** in moderate yield, despite the multitude of competing functional groups present in the molecule (Scheme 3.22).



**Scheme 3.22** Synthesis of sulfonyl fluoride **99**. Reagents and conditions; i) DABSO (0.6 equiv.), PdCl<sub>2</sub>(AmPhos)<sub>2</sub> (5 mol%), Et<sub>3</sub>N (3 equiv.), isopropanol (0.27 M), 75 °C, 18 h, *then* NFSI (1.5 equiv.), rt, 5 h.



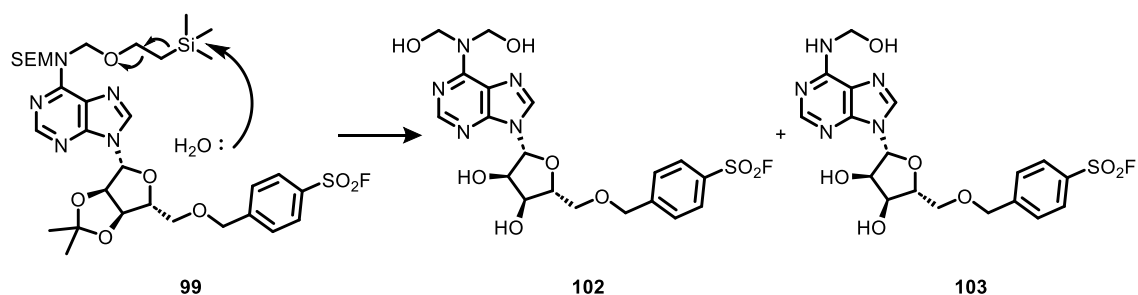
Deprotection of the 6-bis-*N*-SEM group and the ribose acetal, in a manner that would limit hydrolysis of the sulfonyl fluoride electrophile, was now critical to the success of this protecting group strategy. Several conditions were investigated to access **100** or **101** which were all unsuccessful (Table 3.2).



Entry	Reagents <sup>a</sup>	Temperature	Solvent
1	TFA:H <sub>2</sub> O 5:2	rt	-
2	3 M HCl	rt	MeOH
3	3 M HCl	60 °C	MeOH
4	SnCl <sub>4</sub> <sup>a</sup>	rt	CH <sub>2</sub> Cl <sub>2</sub>
5	MeBr <sub>2</sub> , MeNO <sub>2</sub> <sup>c</sup>	rt	Et <sub>2</sub> O
6	TBAF <sup>b</sup>	reflux	THF

**Table 3.2** Conditions attempted for SEM deprotection of **99**. <sup>a</sup>All reactions performed at 0.1 M for 1 h unless otherwise stated. <sup>a2</sup> 2 equivalents used, 72 h reaction time. <sup>b</sup>12 equivalents used. <sup>c</sup>Reaction performed at 0.05 M for 18 h with 15 equivalents of MgBr<sub>2</sub> and 30 equivalents of MeNO<sub>2</sub>.

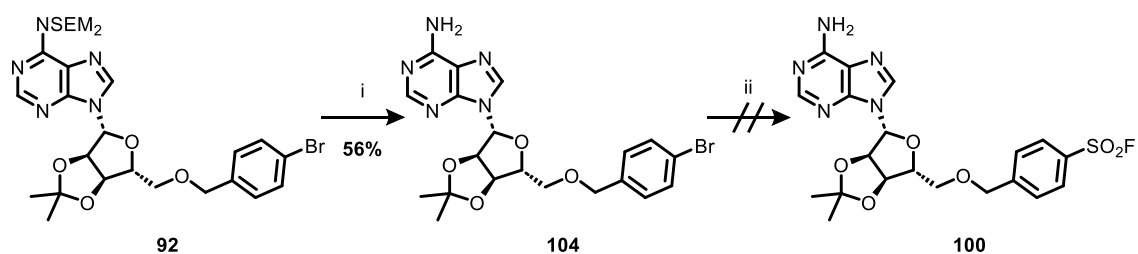
Treatment with Brønsted acids (Table 3.2, Entries 1 – 3) led to partial *N*-SEM cleavage to the corresponding bis- and mono- hemiaminal species **102** and **103** which were detected by LCMS (Scheme 3.23). The use of Lewis acids, including MgBr<sub>2</sub>-mediated conditions detailed by Vakalopoulos and Hoffman<sup>163</sup> (Table 3.2, Entries 4 and 5) generated similar reaction profiles to the Brønsted acid-mediated conditions, with none of the desired product being observed.



**Scheme 3.23** Proposed pathway to hemiaminal intermediates **102** and **103** observed in acidic deprotection of **99**.

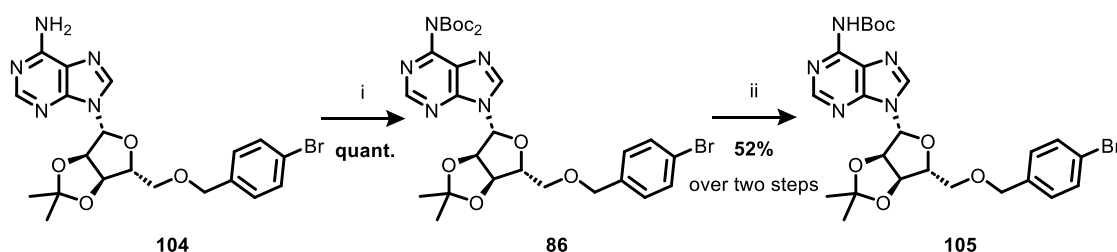
We concluded that forcing reaction conditions would be required to cleave the *N*-SEM group hemiacetal intermediates **102** and **103**.<sup>165,166</sup> Refluxing **99** in THF with TBAF led to a complex reaction mixture with apparent degradation of the starting material (Table 3.2, Entry 6). My screen of deprotection conditions indicated that although loss of the trimethyl silyl group from *N*-SEM was facile, hydrolysis of the bis-hemiaminal **102** and mono-hemiaminal **103** under the reaction conditions was slow.

We speculated that the degradation observed from the attempted SEM-deprotection with TBAF may have arisen from hydrolysis of the sulfonyl fluoride under the reaction conditions (Table 3.2, Entry 6). This suggested that *p*-bromobenzyl intermediate **92** might be deprotected under these conditions as it does not possess the electrophilic sulfonyl fluoride moiety; the SEM-deprotected material **104** could then be converted to a sulfonyl fluoride **100** using the palladium-catalysed conditions.<sup>164</sup> Free aniline **104** was successfully accessed from **92** using an excess of TBAF under refluxing THF in moderate yield. However, attempted palladium-catalysed fluorosulfonation led to no conversion of the starting material (Scheme 3.24).



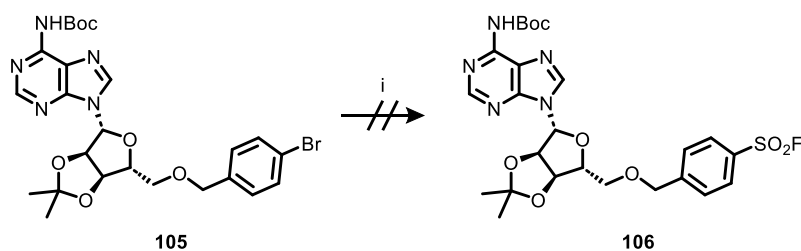
**Scheme 3.24** Attempted synthesis of sulfonyl fluoride **100**. Reagents and conditions: i) TBAF (24 equiv.), THF (0.1 M), reflux, 40 h; ii) DABSO (0.6 equiv.), PdCl<sub>2</sub>(AmPhos)<sub>2</sub> (5 mol%), Et<sub>3</sub>N (3 equiv.), isopropanol (0.27 M), 75 °C, 18 h, then NFSI (1.5 equiv.), rt, 5 h.

Anilines are well-established ligands used in palladium catalysis,<sup>167</sup> so we postulated that free aniline **104** was coordinating to the palladium centre in the reaction mixture preventing turnover of starting material. It was proposed that introduction of an electron withdrawing Boc group on the 6-*N*-position would diminish the capacity of the aniline moiety to act as a ligand and therefore facilitate the desired reaction. *N*-SEM deprotected material **104** was *N*-Boc-protected under standard conditions, which led to a mixture of mono- **105** and bis-*N*-Boc-protected **86** products. Treatment of the crude product with methylamine<sup>168</sup> furnished the desired mono-*N*-Boc intermediate **105** in moderate yield (Scheme 3.25).



**Scheme 3.25** Synthesis of mono-*N*-Boc intermediate **105**. Reagents and conditions: i) DMAP (1.1 equiv.),  $\text{Boc}_2\text{O}$  (5 equiv.), THF (0.2 M), rt, 18 h; ii) methylamine (4 equiv.), methanol (0.1 M), rt, 22 h.

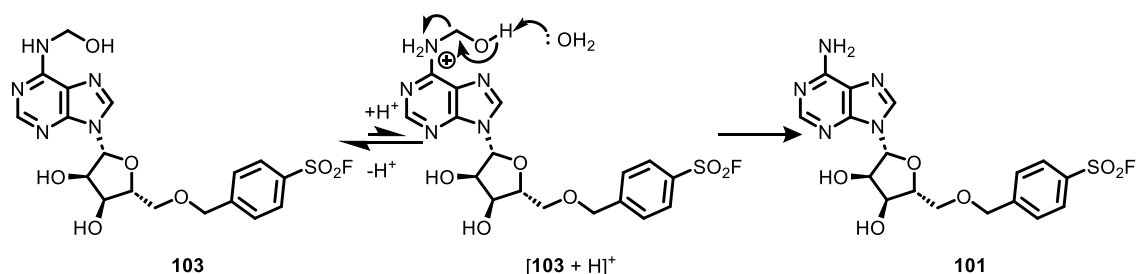
Unfortunately, subjecting **105** to the palladium-catalysed fluorosulfonation conditions resulted in a complex, inseparable mixture (Scheme 3.26).



**Scheme 3.26** Attempted synthesis of sulfonyl fluoride **106**. Reagents and conditions: i) DABSO (0.6 equiv.),  $\text{PdCl}_2(\text{AmPhos})_2$  (5 mol%),  $\text{Et}_3\text{N}$  (3 equiv.), isopropanol (0.27 M), 75 °C, 18 h, then NFSI (1.5 equiv.), rt, 5 h.

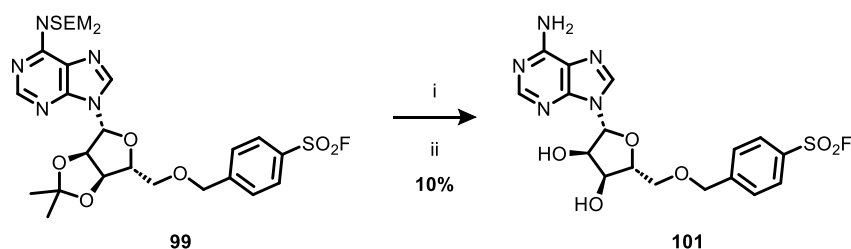
These investigations indicated that a robust, non-labile protecting group such as SEM was also required to enable the conversion of the aryl bromide to a sulfonyl fluoride, as only bis-*N*-SEM sulfonyl fluoride **99** had been successfully isolated. Our efforts therefore turned to enacting the removal of the hemiaminal groups of postulated partially-SEM-

deprotected intermediates **102** and **103**. The apparent stability of these hemiaminal intermediates were hypothesised to be a result of the electron-deficient adenine ring decreasing the  $pK_a$  of the 6-amino group, disfavoured the required protonation step, and consequently the collapse and hydrolysis of the hemiaminal (Scheme 3.27).



**Scheme 3.27** SEM-deprotection of the adenine ring under acidic conditions may require protonation of the 6-amino position, which is possibly disfavoured due to its electron-deficiency.

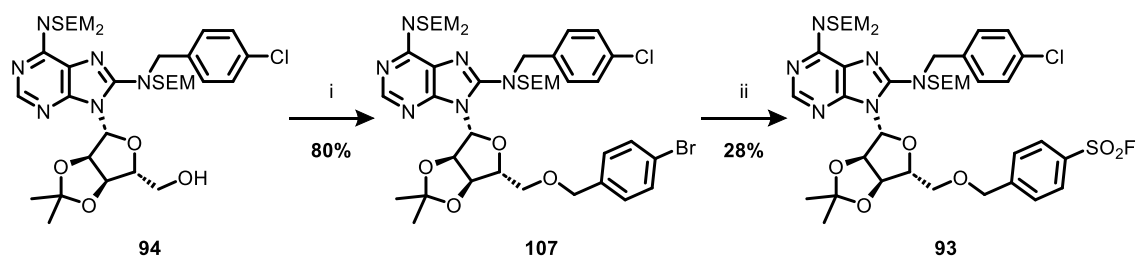
We hypothesised that switching from acidic to basic conditions may be sufficient to cleave the hemiaminal, but mild conditions would be required to circumvent the degradation of the sulfonyl fluoride electrophile. Pleasingly, sequential treatment of bis-*N*-SEM protected sulfonyl fluoride **99** with TFA:water mixture then dilute ammonia furnished the deprotected final product **101**, albeit in a poor yield owing to competing hydrolysis of the sulfonyl fluoride (Scheme 3.28).



**Scheme 3.28** Synthesis of sulfonyl fluoride **101**. Reagents and conditions: i) TFA:H<sub>2</sub>O 5:2 (0.1 M), rt, 1 h; ii) 0.07 N NH<sub>3</sub> in CH<sub>2</sub>Cl<sub>2</sub>:THF 1:1 (0.1 M), rt, 24 h.

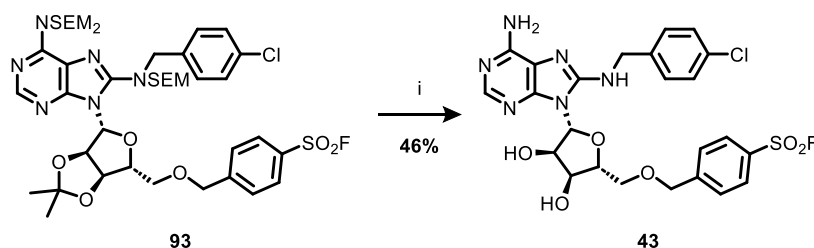
### 3.3.2 Accessing 8-*N*-benzyl adenosine-derived TCI **43**

With ether-linked TCI **101** in hand, my efforts then focussed on the synthesis of TCI **43** with the desired 8-*N*-benzyl functionality. 5'-etherification of *O*-TBS-deprotected derivative **94** with 4-bromobenzyl bromide proceeded cleanly and in high yield. Subsequent conversion of the aryl bromide **107** to a sulfonyl fluoride afforded tris-*N*-SEM intermediate **93** (Scheme 3.29).



**Scheme 3.29** Synthesis of sulfonyl fluoride **93**. Reagents and conditions: i) NaH (1.2 equiv.), THF (0.5 M), 0 °C, 15 min, *then* 4-bromobenzyl bromide (2 equiv.), 0 °C to rt, 18 h; ii) DABSO (0.6 equiv.), PdCl<sub>2</sub>(AmPhos)<sub>2</sub> (5 mol%), Et<sub>3</sub>N (3 equiv.), isopropanol (0.27 M), 75 °C, 18 h, *then* NFSI (1.5 equiv.), rt, 5 h.

It was hypothesised that the 8-*N* functionalisation of tris-*N*-SEM intermediate **93** might enable direct global deprotection of the substrate without additional treatment with mild base, as the additional nitrogen atom at the 8-position increases the electron density of the adenine ring, increasing the basicity of the 6-amino position and thus facilitating full cleavage of the SEM group under acidic conditions. Pleasingly, addition of TFA:water to tris-*N*-SEM sulfonyl fluoride **93** gave the target globally deprotected TCI **43** in moderate yield (Scheme 3.30).



**Scheme 3.30** Synthesis of TCI **43**. Reagents and conditions: i) TFA:H<sub>2</sub>O 5:2 (0.1 M), rt, 1 h.

### 3.4 Conclusions

This chapter has detailed the optimisation towards the synthesis of 5'-ether-linked adenosine derived TCIs, culminating in a new protecting group and sulfonyl fluoride coupling synthetic strategy that furnished 8-*N*-benzyl TCI **43** in 8 steps and 1% overall yield. Whilst extensive efforts to access this chemotype had previously been unsuccessful, incorporation of *N*-SEM protection was sufficiently robust to facilitate ether bond formation. Late-stage conversion of the corresponding aryl bromide to a sulfonyl fluoride was unexpectedly facile; however, the ease of *N*-SEM deprotection proved to be highly dependent on the substitution of the adenine ring.

#### 4 Characterisation of 5'-Ether-Linked HSP72 Lysine-TCIs

## 4 Characterisation of 5'-Ether-Linked HSP72 Lysine-TCIs

### 4.1 Introduction

Following the successful synthesis of the target ether-linked sulfonyl fluoride lysine-TCI **43** (Figure 4.1), the aim was to investigate its binding to HSP72-NBD to validate our design hypothesis. Switching from an ester to an ether linker at the 5'-position should result in high reversible affinity, whilst maintaining efficient covalent bond formation.

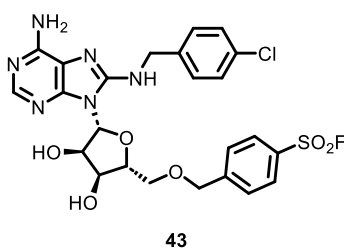


**Figure 4.1** Structure of ether-linked TCI **43**.

Both functional and binding assays can be modified to measure the  $K_I$  and  $k_{inact}$  of a TCI.<sup>146</sup> Binding assays directly measure target-ligand association and dissociation, whereas functional assays quantify binding kinetics *via* a secondary readout of the biological action of the target.<sup>169</sup> Gestwicki et al. described two functional assays for measurement of HSP70 inhibition. A substrate protein refolding assay<sup>170</sup> has been reported utilising the bacterial homologue, DnaK. However, DnaK possesses a catalytic cycle that is tightly regulated by the JDP and NEF co-chaperones, so attempts to measure inhibition using this assay may fail to distinguish between the three components of the trichaperone system, potentially resulting in complex readouts. The ATPase activity assay<sup>171</sup> measures the HSP70-catalysed turnover of ATP to ADP/Pi. Whilst this assay is potentially readily adaptable to estimating the kinetic parameters of covalent bond formation, unfortunately, the very low intrinsic ATPase activity of HSP70, arising from strong product inhibition, makes the estimation of free protein concentration very difficult.<sup>172,173,121</sup> We therefore concluded that neither of these HSP70 assays would be suitable for the characterisation of our lysine-TCIs.

Surface plasmon resonance (SPR) is a biophysical technique that has been used extensively as a binding assay in the characterisation of HSP70 inhibitors.<sup>133,134,142,174</sup> Briefly, HSP70 is immobilised onto a gold layer surface or chip through covalent

attachment utilizing amide bonds with protein surface lysine residues. Small molecules are then passed over the protein-bound surface in running buffer<sup>175</sup> and polarised light is shone on the surface, which produces surface plasmons that convey information about ligand binding to the immobilised protein through the change in mass. The protein-bound surface must be regenerated after each experiment by washing with running buffer to displace bound ligand, which presents a challenge for the characterisation of irreversible TCIs, as a new chip would have to be prepared for each experiment.

Fluorescence Polarisation (FP) has also been frequently applied as a competitive ligand-displacement assay for the characterisation of HSP70 inhibitors.<sup>134,153</sup> Within our group, we previously developed a modification of the standard FP assay, the Time-Dependent Fluorescence Polarisation (TDFP) assay, to assess the binding kinetics of HSP70 inhibitors.<sup>145</sup> As a result of the extensive validation of this assay for characterisation of HSP70 TCIs, it was selected as the primary assay to study 5'-ether sulfonyl fluoride TCI **43**.

## 4.2 Time-Dependent Fluorescent Polarisation Assay

### 4.2.1 Introduction to Fluorescence Polarisation

FP was first applied to screening in 1996, with Jolley detailing the development of an FP assay for the high throughput screening of protease inhibitors.<sup>176</sup> The methodology has since become an increasingly popular tool in small molecule drug discovery, owing to the homogeneous format, low cost, and its ability to examine protein-ligand interactions in solution, without modifications to the protein or the need for enzymatic activity.<sup>177</sup> The principles of FP were first described by Perrin in 1926.<sup>178</sup> Perrin observed that when a fluorescent molecule is excited by plane-polarised light, its emission becomes depolarised from rotational diffusion in solution. The corresponding observed polarisation value ( $P$ ) can be related to the rotational correlation time ( $\theta$ ) and the fluorescence lifetime ( $\tau$ ) (Equation 4.1).

$$\frac{1}{P} - \frac{1}{3} = \left( \frac{1}{P_0} - \frac{1}{3} \right) (1 + \tau/\theta)$$

**Equation 4.1** Equation derived by Perrin relating polarisation ( $P$ ) to polarisation in absence of rotation ( $P_0$ ), the rotational correlation time ( $\theta$ ) and fluorescence lifetime ( $\tau$ ).



Rotational correlation time ( $\theta$ ), which is the time taken for a molecule to rotate one radian,<sup>179</sup> is proportional to the solvent viscosity ( $\eta$ ) and the volume occupied by the fluorescent molecule ( $V$ ) (Equation 4.2).

$$\theta = \frac{\eta V}{RT}$$

**Equation 4.2** Rotational correlation time ( $\theta$ ) is a function of the ideal gas constant ( $R$ ), temperature ( $T$ ), viscosity ( $\eta$ ) and molar volume ( $V$ ).

Consequently, the larger volume a fluorescent molecule occupies, the slower it rotates and thus the light emitted is less depolarised (Equation 4.3).<sup>180</sup>

$$P \propto \theta \propto V$$

**Equation 4.3** Proportionality relationship between polarisation ( $P$ ), rotational correlation time ( $\theta$ ) and molar volume ( $V$ ).

This principle underpins FP when applied to measuring the binding between small molecules and proteins (Figure 4.2).

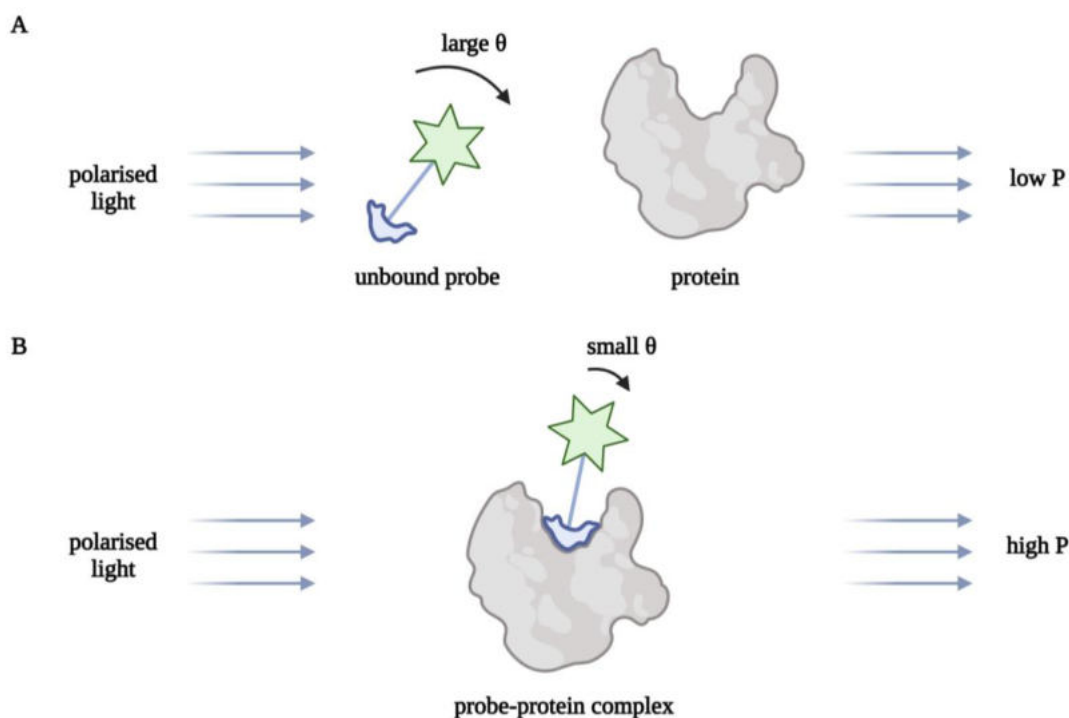


**Figure 4.2** Basic principle of FP. **A** When the fluorescent probe and protein are unbound, the molar volume is smaller and so the probe rotates more quickly, resulting in a greater extent of depolarisation. **B** When the probe and protein are bound, the molar volume is larger and so the probe rotates more slowly, resulting in less depolarisation.

When a small molecule fluorescent probe is unbound in solution, it occupies a small volume, rotates rapidly, leading to a high degree of depolarisation of the emitted light. Conversely, when the probe is bound to the protein in solution, it occupies a larger volume, rotates more slowly, resulting in less depolarisation. Competitive small molecule ligands can displace the FP probe leading to more unbound probe in solution and a correspondingly lower polarisation. For a fixed probe and protein concentration, a competitive inhibitor will displace the FP probe in a concentration-dependent manner. (Figure 4.3).

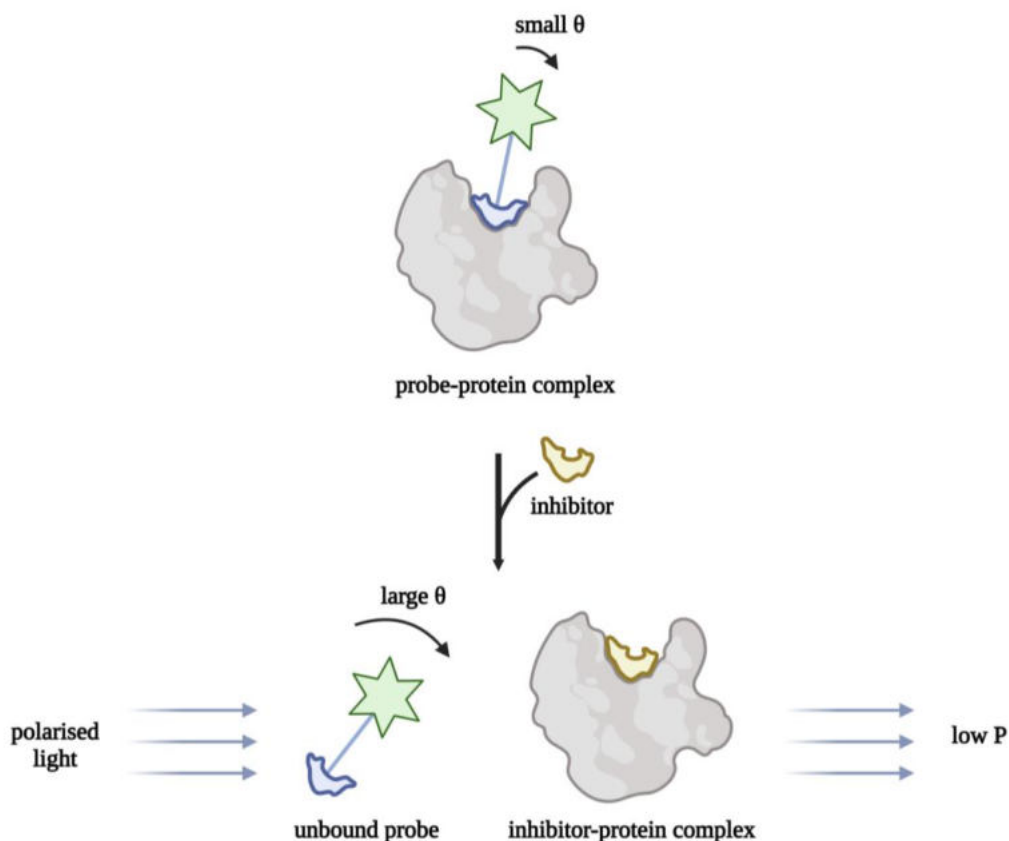


**Figure 4.3** Basic principle of competitive FP experiments. A competitive small molecule ligand displaces the FP-probe, leading to decreased polarisation in the emitted light.

#### 4.2.2 Interpretation of Fluorescence Polarisation Assays

The readout of an FP-assay is quantified in terms of Polarisation (P) or Anisotropy (A), which are normalised intensity measurements.<sup>180</sup> Polarisation and anisotropy contain the same information as they involve identical measurements, but polarisation is typically preferred in drug discovery contexts due to historical convention.<sup>180</sup> Both polarisation and anisotropy are quantified as a dimensionless numbers, but polarisation is typically quoted in units of millipolarisation (mP).<sup>177</sup> Anisotropy can be directly converted to polarisation though Equation 4.4.<sup>181</sup>

$$A = \frac{2P}{3 - P}$$

**Equation 4.4** Relationship between anisotropy (A) and polarisation (P).

Determining an  $IC_{50}$  from an FP experiment involves titration of an inhibitor across a concentration range for a fixed probe and protein concentration and plotting either P or A against [I] (Figure 4.4).

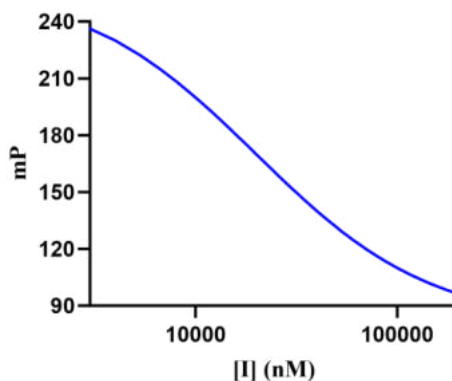


**Figure 4.4** Simulated  $IC_{50}$  data from an FP experiment, plotting raw mP data against inhibitor concentration.

For quantifying the reversible affinity of an inhibitor, the enzyme-inhibitor dissociation constant  $K_i$  is preferred over the  $IC_{50}$ , as unlike the  $K_i$ , the  $IC_{50}$  value is dependent on the probe/substrate concentration and so will vary depending on the chosen assay conditions.<sup>182</sup> The relationship between  $K_i$  and the measured  $IC_{50}$  can be estimated for a typical receptor binding assay, with a purely competitive ligand, using the Cheng-Prusoff equation which corrects for the free probe concentration  $L_f$  and the probe-protein dissociation constant  $K_d$  (Equation 4.5).<sup>183</sup>

$$K_i = \frac{IC_{50}}{1 + \frac{L_f}{K_d}}$$

**Equation 4.5** Cheng-Prusoff equation for the relationship between the  $K_i$  and  $IC_{50}$  of an inhibitor, which is dependent on the free probe concentration ( $L_f$ ) and the probe-protein dissociation constant ( $K_d$ ).

It is appropriate to use the Cheng-Prusoff equation when the following assumptions are satisfied:<sup>169</sup>

- 1) Law of Mass Action applied.
- 2) There is a single class of receptor binding sites.
- 3) There is no depletion of probe.

- 4) The enzyme concentration is  $\ll K_d$  of the probe.
- 5) The assay is at equilibrium or steady state.
- 6) Total and free probe concentrations are equal.

In typical enzyme saturation binding experiments, there is a low proportion of probe bound to protein ( $[\text{probe}] \gg [E]$ ), as the signal is proportional to the product formed rather than the concentration of bound substrate.<sup>169</sup> Consequently the total probe concentration,  $L_0$ , is approximately equal to the free probe concentration,  $L_f$ , as the bound probe concentration  $L_b \ll L_0$ .

However, in an FP assay, the signal is directly proportional to the concentration of bound substrate and therefore the probe bound fraction ( $F_b$ ).  $F_b$  is the proportion of fluorescent probe that is bound to protein and is related to the normalised intensity measurement anisotropy  $A$ , the anisotropy of fully unbound probe  $A_f$ , and the anisotropy of fully bound probe  $A_b$  (Figure 4.5 A).  $F_b$  is related to the functionally equivalent normalised intensity measurement polarisation  $P$  *via* a similar relationship with the polarisation of fully unbound probe  $P_f$  and the polarisation of fully unbound probe  $P_b$  (Figure 4.5 B). Simulating  $F_b$  against  $P$  illustrates how the bound fraction and FP signal are directly proportional to each other (Figure 4.5 C)

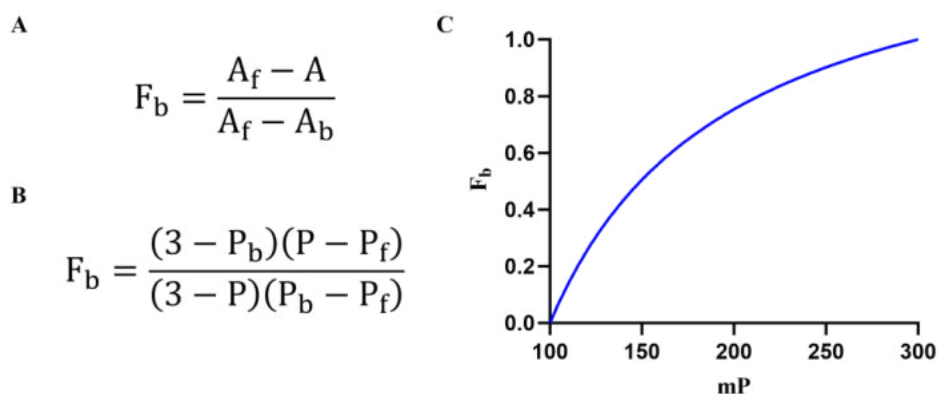


**Figure 4.5** **A** Relationship between  $F_b$  and the measured anisotropy ( $A$ ), the free anisotropy or anisotropy in the absence of protein ( $A_f$ ), and the bound anisotropy or the anisotropy assuming  $F_b = 1$  ( $A_b$ ). **B** Relationship between  $F_b$  and the measured polarisation ( $P$ ), the free polarisation or polarisation in the absence of protein ( $P_f$ ), and the bound polarisation or the polarisation assuming  $F_b = 1$  ( $P_b$ ). **C** Simulated plot of  $F_b$  against  $mP$ , with  $P_f = 0.1$  and  $P_b = 0.3$ .

Consequently, to obtain sufficient signal in an FP assay, a large proportion of the probe must be bound to protein, with assays typically set up with starting  $F_b > 0.8$ .<sup>169</sup> Therefore, the total probe concentration is not equal to the free probe concentration ( $L_0 \neq L_f$ ) due to depletion of probe, and thus the Cheng-Prusoff equation as written correspondingly overestimates values of  $K_i$  from the  $IC_{50}$  for an FP assay.<sup>169</sup> Huang detailed a corrected form of Cheng-Prusoff equation which takes into account the high proportion of probe bound (Equation 4.6).<sup>184</sup> Derived from first principles, this equation describes the relationship between the  $IC_{50}$  and  $K_i$  in terms of the total probe concentration  $L_0$  and the probe  $K_d$ , but also corrects for the probe bound fraction  $F_b$  unlike the Cheng-Prusoff equation.

$$IC_{50} = \left( \frac{F_b K_d}{(1 - F_b)(2 - F_b)} + \frac{F_b L_0}{2} \right) \left( \frac{K_i(2 - F_b)}{K_d F_b} + 1 \right)$$

**Equation 4.6** Huang's corrected relationship between  $K_i$  and  $IC_{50}$ , dependent on probe bound fraction ( $F_b$ ), total probe concentration ( $L_0$ ) and probe-protein dissociation constant ( $K_d$ ).

This equation can be rearranged solving for  $K_i$  (Equation 4.7).

$$K_i = \frac{IC_{50}}{\frac{1}{(1 - F_b)} + \frac{L_0(2 - F_b)}{2K_d}} - K_d \left( \frac{F_b}{2 - F_b} \right)$$

**Equation 4.7** Rearranged form of Equation 4.6, solving for  $K_i$ .

Simulating the Cheng-Prusoff equation (Equation 4.5) and the Huang equation (Equation 4.7) illustrates how the former overestimates the  $K_i$  compared to the latter (Figure 4.6). Thus, for larger  $IC_{50}$  values, the greater the overestimation of the  $K_i$  from the Cheng-Prusoff equation.

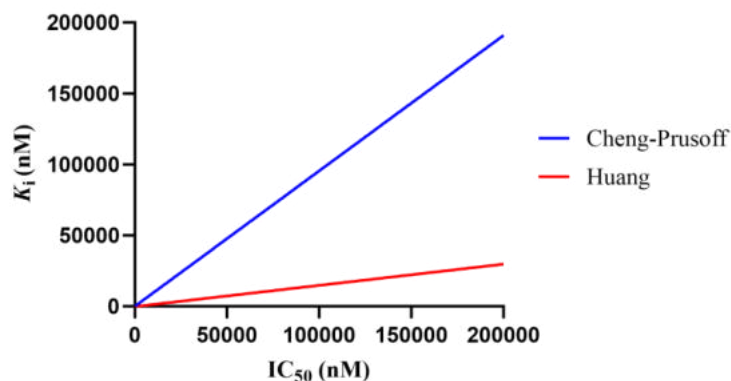


**Figure 4.6** Simulated plots of Cheng-Prusoff (Equation 4.5) and Huang (Equation 4.7) equations,  $K_d = 210$  nM,  $L_0 = 10$  nM,  $F_b = 0.85$ .

Equation 4.7 will be used for the remainder of the thesis for the purpose of converting measured  $IC_{50}$  values to the desired  $K_i$  values and to normalise for changes in bound fraction.

### 4.2.3 Limit of Detection for Fluorescence Polarisation Assays

To carry out an FP assay, a suitable fluorescent probe that can be displaced by the target competitive ligand is required. Fluorescent probes are heterobifunctional molecules containing a protein-of-interest (POI) ligand moiety, a linker that exploits a vector-to-solvent and a fluorophore that is external to the protein and is expected to be independent of binding. The commercially available FP probe ATP-ATTO 488 **108** has been extensively used as a probe for use in HSP70 FP assays (Figure 4.7 A).<sup>153,145</sup> Structurally, ATP-ATTO-488 **108** consists of an ATP unit, which binds to HSP72-NBD, and is attached *via* an alkyl-amide linker to an ATTO 488 fluorophore. Titration of HSP72-NBD using a two-fold dilution series against 10 nM of fluorescent probe **108** and subsequent non-linear regression analysis resulted in a geometric mean probe  $K_d$  of 210 nM ( $pK_d = 6.68 \pm 0.06$ ,  $N = 3$ , mean  $\pm$  SEM) (Figure 4.7 B). The  $K_d$  value determined was consistent with literature reports.<sup>153,144</sup>

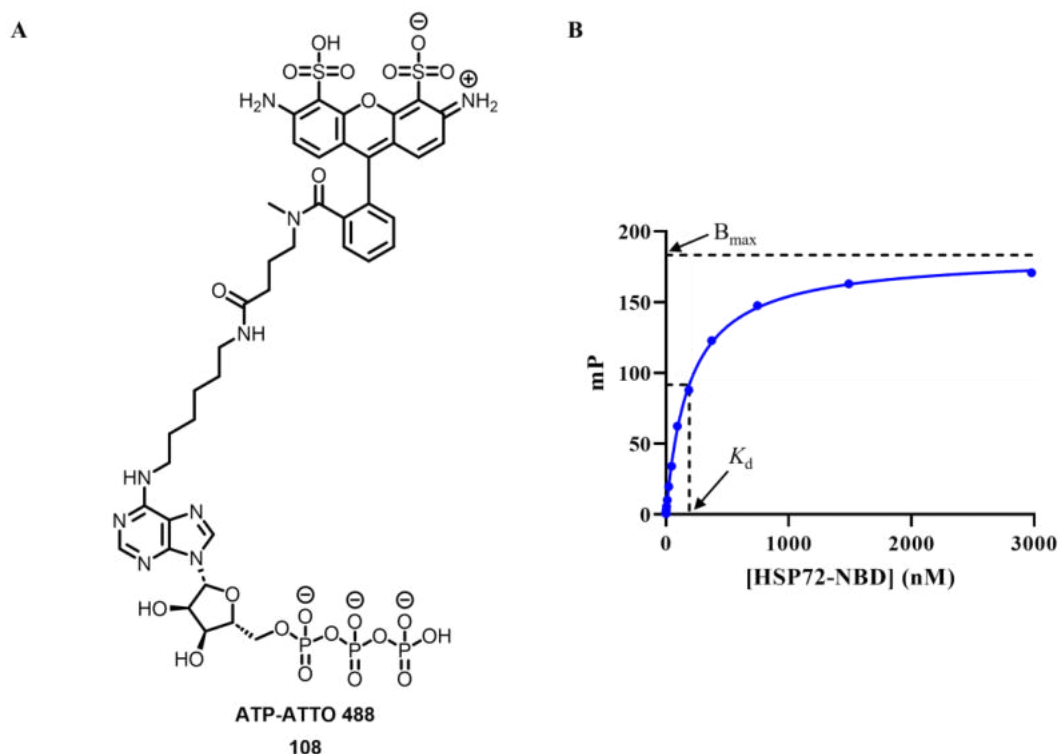


**Figure 4.7**  $K_d$  determination of ATP-ATTO 488 **108** with HSP72-NBD. **A** Structure of **108**. **B** Representative binding isotherm for HSP72-NBD and 10 nM **108**. mP values plotted following subtraction of background polarisation. Assay was performed in triplicate and the mean and standard error plotted using GraphPad Prism 9. The  $K_d$  value was determined as the geometric mean of three independent experiments.

The analysis by Huang outlined that the resolvable limit of an FP assay is determined by the binding affinity of the FP probe.<sup>184</sup> The concentration of protein required in an FP assay is dependent on the probe bound fraction  $F_b$ , the probe  $K_d$ , and total probe concentration  $L_0$  (Equation 4.8).

$$[\text{protein}] = \left( \frac{K_d F_b}{1 - F_b} \right) + F_b L_0$$

**Equation 4.8** Relationship between assay protein concentration, bound fraction ( $F_b$ ), total probe concentration ( $L_0$ ) and probe-protein dissociation constant ( $K_d$ ).

From Equation 4.8, for a fixed total probe concentration ( $L_0$ ) and bound fraction ( $F_b$ ), an increase in probe  $K_d$  will result in an increase in the required total protein concentration. Consequently, weaker affinity probes will require higher total protein concentration in a



FP assay to maintain the same bound fraction ( $F_b$ ). Titration of the inhibitor reduces the free protein concentration and displaces the probe.

Under non-stoichiometric binding conditions,  $IC_{50} \gg [protein]$ , the total concentration of inhibitor and the free concentration of inhibitor are approximately equal, and the enzyme-inhibitor complex concentration is negligible compared to the total inhibitor concentration. However, when the total inhibitor concentration approaches the total protein concentration inhibitor becomes depleted, and these assumptions no longer hold. Therefore,  $IC_{50}$  values below half of the protein concentration as measured by the FP assay cannot be resolved; this is the assay tight-binding limit.<sup>8</sup>

However, simulating the relationship between the calculated  $K_i$  and their respective  $IC_{50}$  values, from a range of probe  $K_d$  values using Equation 4.7 with fixed  $F_b$  and  $L_0$ , also illustrates how the measured  $IC_{50}$  values will increasingly deviate from linearity from their respective  $K_i$  values as they approach the total protein concentration. In this stoichiometric region, small changes in  $IC_{50}$  would result in large changes in ligand  $K_i$  (Figure 4.8).<sup>184</sup>

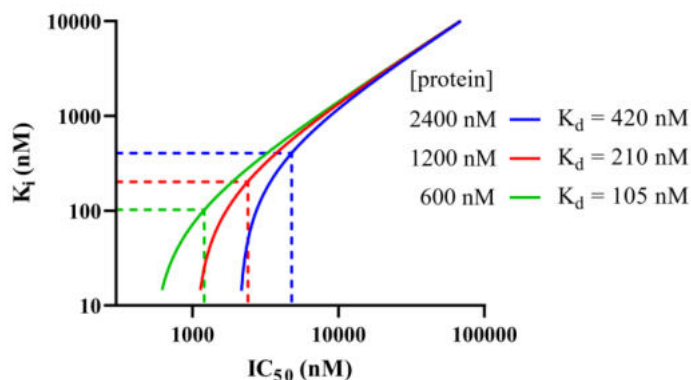


**Figure 4.8** Simulated plot of Equation 4.7, with  $L_0 = 10$  nM,  $F_b = 0.85$ . Dotted lines indicate point of deviation from linearity in stoichiometric region of curve, showing how a lower probe  $K_d$  enables better resolution of lower  $K_i$  values. Data was plotted using GraphPad Prism 9.

To avoid the high noise stoichiometric binding region and improve data interpretation, we selected the resolvable limit of  $IC_{50}$  values to be set at two-fold the total protein concentration. Switching to a higher affinity FP probe will consequently lower the required assay protein concentration for the same bound fraction, and thus lower the resolvable limit of the  $IC_{50}$  and  $K_i$  values. Because of the relationship between total

protein concentration and bound fraction, (Equation 4.8), a lower bound fraction necessitates a lower total protein concentration in the FP assay, which therefore lowers the limit of resolvable  $IC_{50}$  values and the stoichiometric binding region. (Figure 4.9). However, since the signal of an FP assay is directly proportional to the bound fraction, decreasing the  $F_b$  will reduce the signal to noise ratio.<sup>169</sup>

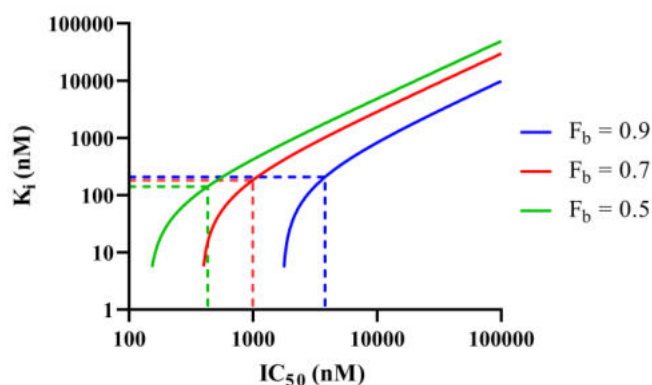


**Figure 4.9** Simulated plot of Equation 4.7, with  $L_0 = 10$  nM,  $K_d = 210$  nM. Dotted lines indicate point of deviation from linearity in stoichiometric region of curve, showing how a lower  $F_b$  enables better resolution of lower  $K_i$  values. Data was plotted using GraphPad Prism 9.

As detailed in the optimisation of the TDFP assay published by our group,<sup>145</sup> the total occupancy of the protein by the inhibitor increases over time when incubated with a TCI, decreasing the free protein concentration that is available to bind the probe. Therefore, protein occupancy by the inhibitor is a combination of reversible occupancy and irreversible covalent occupancy. As the probe bound fraction is related to the total protein concentration, the time-dependent change in  $F_b$  can be used to estimate how the available protein concentration changes over time as the covalent bond forms with the inhibitor ( $k_{obs}$ ), once reversible binding is at equilibrium. Analysis of the relationship between concentration of free protein and binding of the probe ( $F_b$ ) shows at high bound fractions ( $F_b > 0.85$ ), the relationship is non-linear and extremely steep, where small changes in the measured  $F_b$  correspond to large changes in the free protein concentration (Figure 4.10 A). At low bound fraction ( $F_b < 0.4$ ) large changes in  $F_b$  correspond to small changes in the free protein concentration (Figure 4.10 B). For these reasons it would be difficult to use  $F_b$  in these regions to monitor how an irreversible inhibitor changes the free protein concentration over time. At intermediate values of  $F_b$  the relationship is approximately linear (Figure 4.10 C), enabling determination of  $k_{obs}$  values that can be used to derive the

second order rate constant,  $k_{\text{inact}}/K_{\text{I}}$ .  $F_{\text{b}}$  values between 0.7 – 0.85 are selected for the assay conditions to accommodate both reversible displacement of the probe, which rapidly reduces bound fraction, and the time-dependent irreversible covalent bond formation to occur within the pseudo linear portion of the  $F_{\text{b}}$  and free protein concentration relationship.

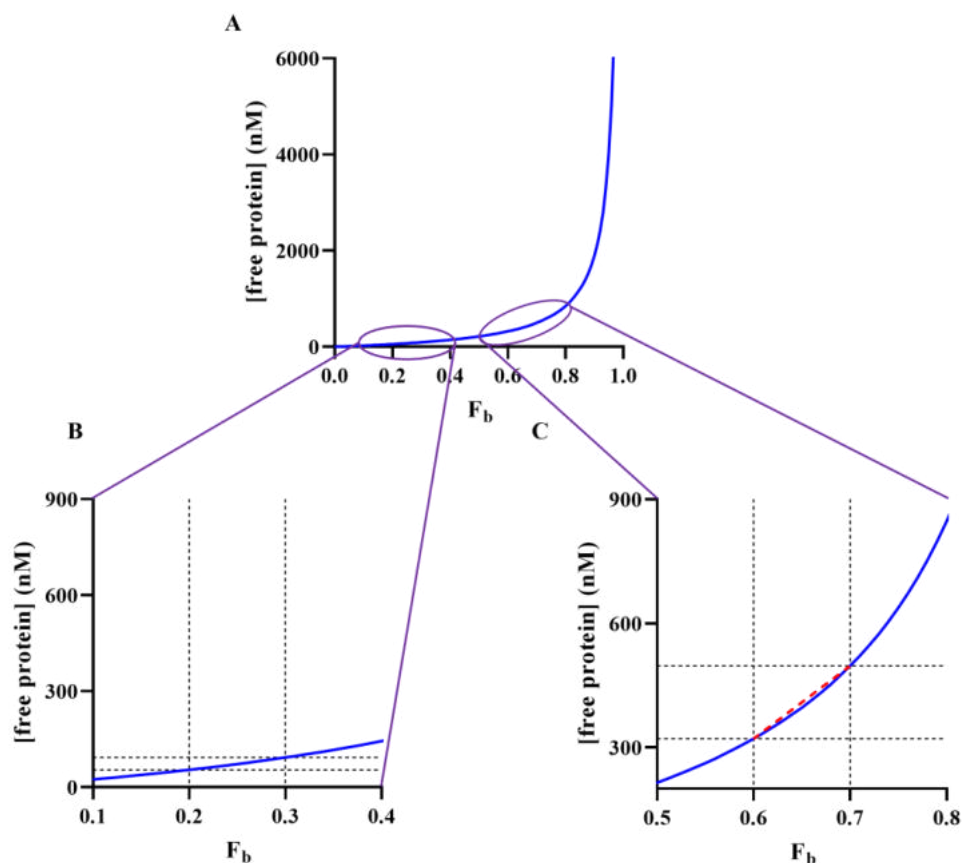
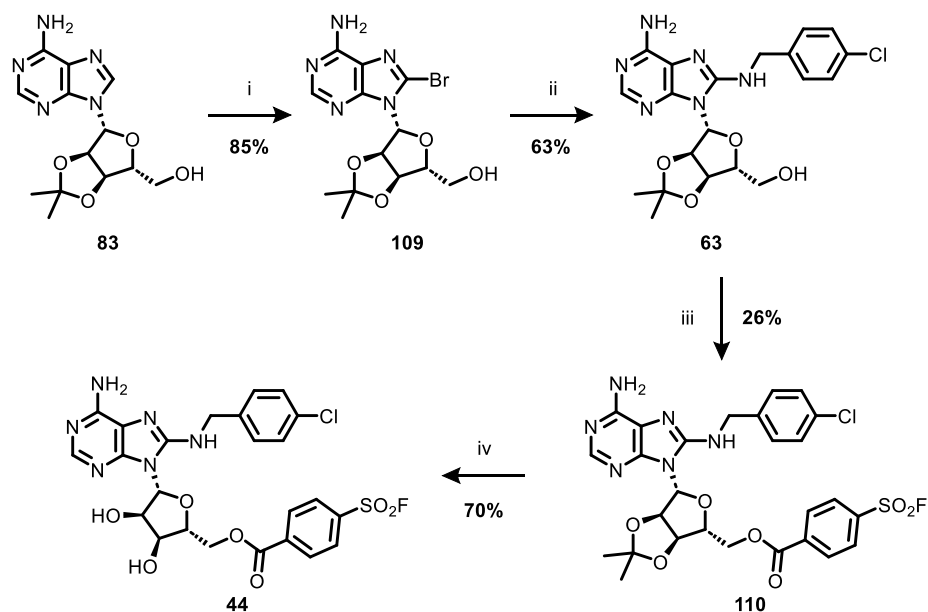


**Figure 4.10** Simulation of Equation 4.8, with  $L_0 = 10$  nM and  $K_d = 210$  nM. **A** Relationship is non-linear at high  $F_{\text{b}}$ , so the assay is highly sensitive to small changes in  $F_{\text{b}}$ . **B** At low  $F_{\text{b}}$ , large changes in  $F_{\text{b}}$  are required for small decreases in free protein concentration. **C** At intermediate  $F_{\text{b}}$ , the relationship between  $F_{\text{b}}$  and [free protein] is approximately linear. Data was plotted using GraphPad Prism 9. Figure adapted from Pettinger et al.<sup>145</sup>

#### 4.2.4 Quantification of Covalent Kinetics

The previously described second generation sulfonyl fluoride lysine-TCI **44** was prepared in 4 steps following the reported procedure (Scheme 4.1).<sup>145</sup> Bromination of 2',3'-*O*-isopropylideneadenosine **83** gave 8-bromo intermediate **109**, which then underwent a nucleophilic aromatic substitution reaction with 4-chlorobenzylamine, to give the 8-*N*-

benzyl intermediate **63**. Esterification with commercially available 4-(fluorosulfonyl)benzoyl chloride gave sulfonyl fluoride **110** in low yield, before acid-mediated deprotection of the 2',3'-acetonide group gave the target TCI **44** in 4 steps and 10% overall yield.



**Scheme 4.1** Synthesis of TCI **44**. Reagents and conditions: i)  $\text{K}_2\text{HPO}_4$  (3 equiv.),  $\text{Br}_2$  (2.5 equiv.), 1,4-dioxane: $\text{H}_2\text{O}$  1:1 (0.13 M), rt, 2 h; ii) 4-chlorobenzylamine (8 equiv.), EtOH (0.3 M), 160 °C,  $\mu$ wave, 1 h; iii) 4-(fluorosulfonyl)benzoyl chloride (1.2 equiv.),  $\text{Et}_3\text{N}$  (1.5 equiv.), DMF (0.1 M), 0 °C, 3 h; iv) TFA: $\text{H}_2\text{O}$  5:2 (0.1 M), rt, 1 h.

The second-generation lysine-TCI **44** was then profiled in the TDFP assay so that its data could be directly compared with the third-generation ether-linked sulfonyl fluoride lysine-TCIs under the same assay conditions and batch of HSP72-NBD protein. Briefly, TCI **44** was incubated with HSP72-NBD and ATP-ATTO 488 probe **108**. Following a 5-minute period to establish reversible equilibrium, a time-dependent increase in the total occupancy of the protein was observed. As the FP probe **108** was displaced over time, there was a time-dependent shift in the measured  $\text{IC}_{50}$  (Figure 4.11 A). The raw mP values were converted to bound fraction, which displayed an apparent linear relationship with respect to incubation time (Figure 4.11 B).<sup>145</sup> Linear regression of this data and extrapolation back to  $t = 0$  provided theoretical estimate of  $F_b$  values in the absence of any covalent labelling, corresponding to the reversible displacement of the probe. These initial  $F_b$  values were plotted against their respective TCI concentrations to obtain an

estimate of the reversible  $IC_{50}$ , which was then converted to the initial  $K_i$  using Equation 4.7 (Figure 4.11 C).

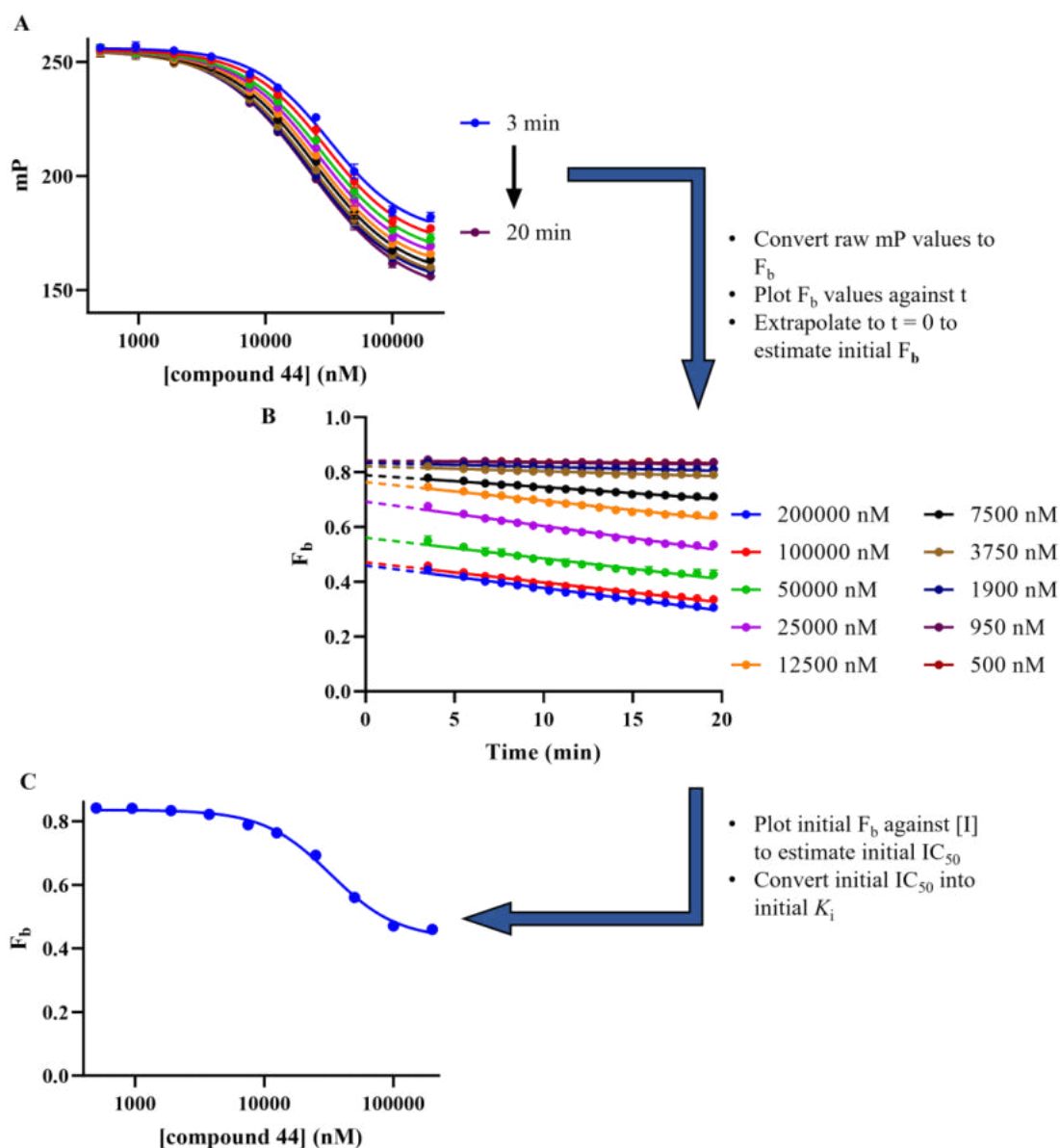
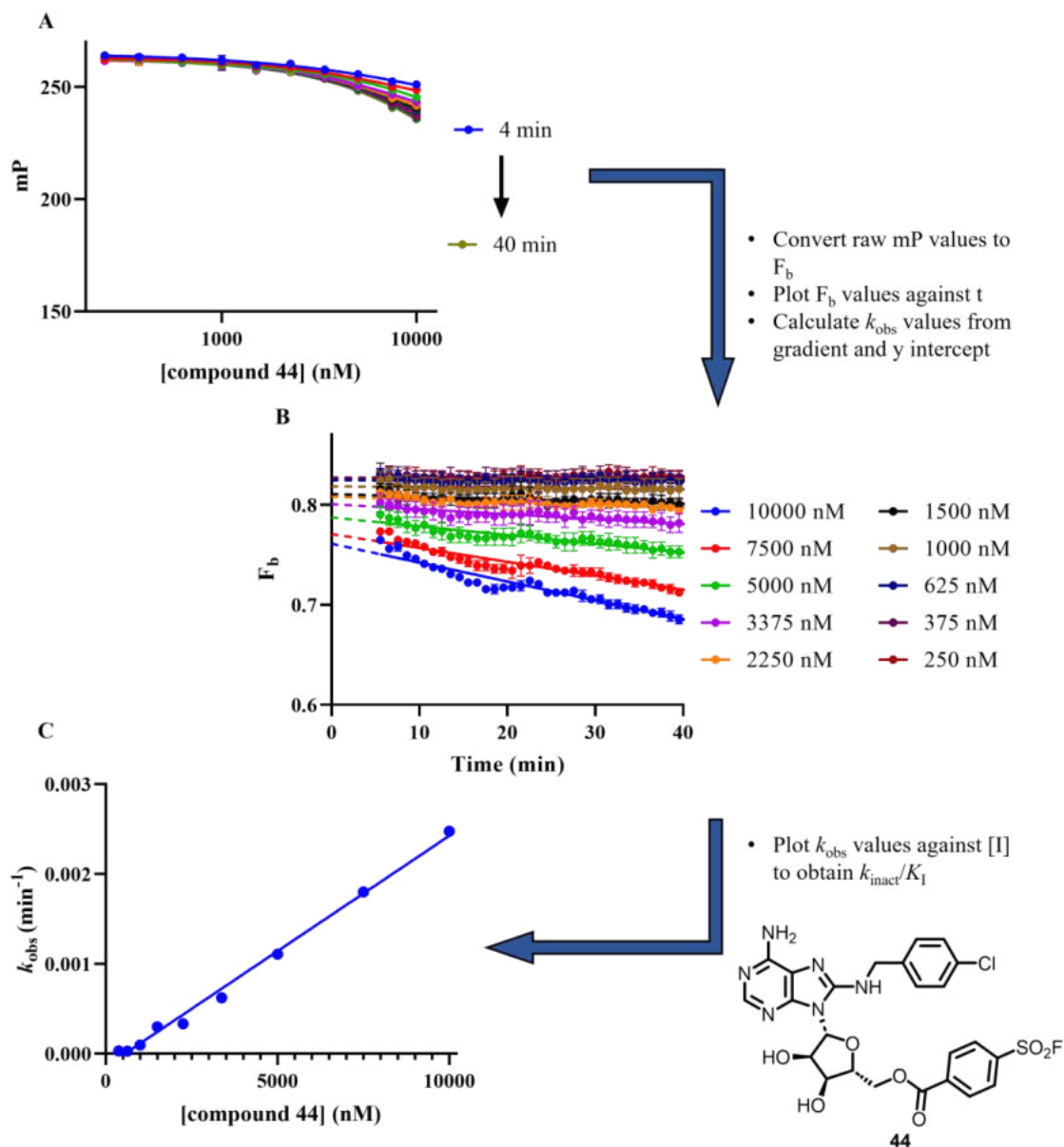


**Figure 4.11** **A** Profiling of TCI **44** in the TDFP assay with HSP72-NBD and ATP-ATTO 488 **108**. [HSP72-NBD] selected so  $F_b = 0.85$ , measurements taken in triplicate every minute for 20 minutes and plotted on same axes. **B** Plotting calculated  $F_b$  values against time enables estimation of initial  $F_b$  through extrapolation to  $t = 0$  (simple linear regression, GraphPad Prism 9). **C** Plot of initial  $F_b$  against  $[I]$  (log(inhibitor) vs. response – variable slope (four parameters), GraphPad Prism 9) allows for estimation of initial  $IC_{50}$ .

Having obtained an estimate of the initial  $IC_{50}$ , a second, focussed titration below these values, to ensure pseudo-first order conditions for the rate of covalent bond formation,

was then performed (Figure 4.12 A).



Compound	Initial $K_i$ ( $\mu\text{M}$ )	$k_{inact}/K_I$ ( $\text{M}^{-1}\text{s}^{-1}$ ) <sup>a</sup>	$k_{inact}$ ( $\text{s}^{-1}$ )	$t_{1/2}^{\infty}$ (h)
5'-ester <b>44</b>	4.7	$5.6 \pm 0.66$	$2.6 \times 10^{-5}$	7.4

**Figure 4.12** A Profiling of TCI **44** in the TDFP assay with HSP72-NBD and ATP-ATTO 488 **108**. [HSP72-NBD] selected so  $F_b = 0.85$ , measurements taken in triplicate every minute for 40 minutes and plotted on same axes, [TCI **44**] < initial  $\text{IC}_{50}$ . **B** Plotting calculated  $F_b$  values against time enables calculation of  $k_{obs}$  (simple linear regression, GraphPad Prism 9). **C** Plot of  $k_{obs}$  against inhibitor concentration (linear regression, GraphPad Prism 9) enables calculation of  $k_{inact}/K_I$ . <sup>a</sup> $k_{inact}/K_I$  values are quoted as mean  $\pm$  SEM of three independent experiments.

Converting the raw mP values to  $F_b$  and then plotting against time enabled the determination of the rate of change of  $F_b$  (Figure 4.12 B). Linear regression gave the gradient in units of  $F_b \cdot \text{min}^{-1}$ ; to determine the  $k_{\text{obs}}$  values in units of  $\text{min}^{-1}$ , the rates of change were subsequently divided by  $F_b$  estimated at  $t = 0$  for each concentration. Finally, a plot of  $k_{\text{obs}}$  against TCI concentration enabled the determination of  $k_{\text{inact}}/K_I$  from linear regression (Figure 4.12 C). The  $k_{\text{inact}}/K_I$  was determined as  $5.6 \pm 0.66$  ( $N = 3$ ). Multiplying by the estimated initial  $K_i$  value with the assumption that  $K_i = K_I$  (Section 1.2.2), allowed for the estimation of  $k_{\text{inact}} = 2.6 \times 10^{-5} \text{ s}^{-1}$  and therefore a half-life at theoretical complete occupancy of  $t_{1/2}^{\infty} = 7.4$  hours. Overall, the  $k_{\text{inact}}/K_I$  values were 5-fold lower than previously observed ( $35 \text{ M}^{-1}\text{s}^{-1}$  vs  $5.6 \text{ M}^{-1}\text{s}^{-1}$ ).<sup>145</sup> The effective protein concentration of each batch of HSP72-NBD can potentially vary depending on the extent of protein misfolding and nucleotide contamination. As the values determined from the TDFP assay, such as the rate of covalent bond formation  $k_{\text{obs}}$ , are dependent on the free protein concentration, it is therefore important to directly compare absolute kinetic parameters only when measured using the same batch of protein.

Profiling 5'-ether-linked third-generation sulfonyl fluoride lysine-TCI **43** in the TDFP assay, the inhibitor displayed a clear time-dependent shift in  $\text{IC}_{50}$  resulting from a rapid displacement of FP probe **108** (Figure 4.13 A), suggesting the inhibitor possessed high reversible affinity. Analysis of the time-dependent change in bound fraction (Figure 4.13 B) illustrated that for high concentrations of the 3<sup>rd</sup> generation TCI **43**, the bound fractions were now approaching zero, which owing to the pseudo-hyperbolic relationship with free concentration (Figure 4.10), suggested only very low free concentrations of protein remained. This was in contrast with 5'-ester-linked TCI **44** (Figure 4.11 B). The rate of change of  $F_b$  was still consistent with rapid covalent bond formation. Therefore, using Equation 4.8, we converted  $F_b$  to the free protein concentration and demonstrated that the 5-ether-linked TCI **43** was exhibiting tight-binding behaviour in the assay (Figure 4.13 C). For the selected  $F_b = 0.85$ , the total protein concentration in the assay is 1200 nM. Therefore for all concentrations of TCI greater than total protein concentration, the extrapolated free protein concentration at  $t = 0$  is below half that of the total protein concentration, which is consistent with a reversible affinity at the assay limit ( $K_i < 200$  nM).<sup>8</sup> Unfortunately, this precluded the determination of the second order rate constant  $k_{\text{inact}}/K_I$ , and therefore the  $k_{\text{inact}}$  value, owing to the stoichiometric binding and ligand depletion.

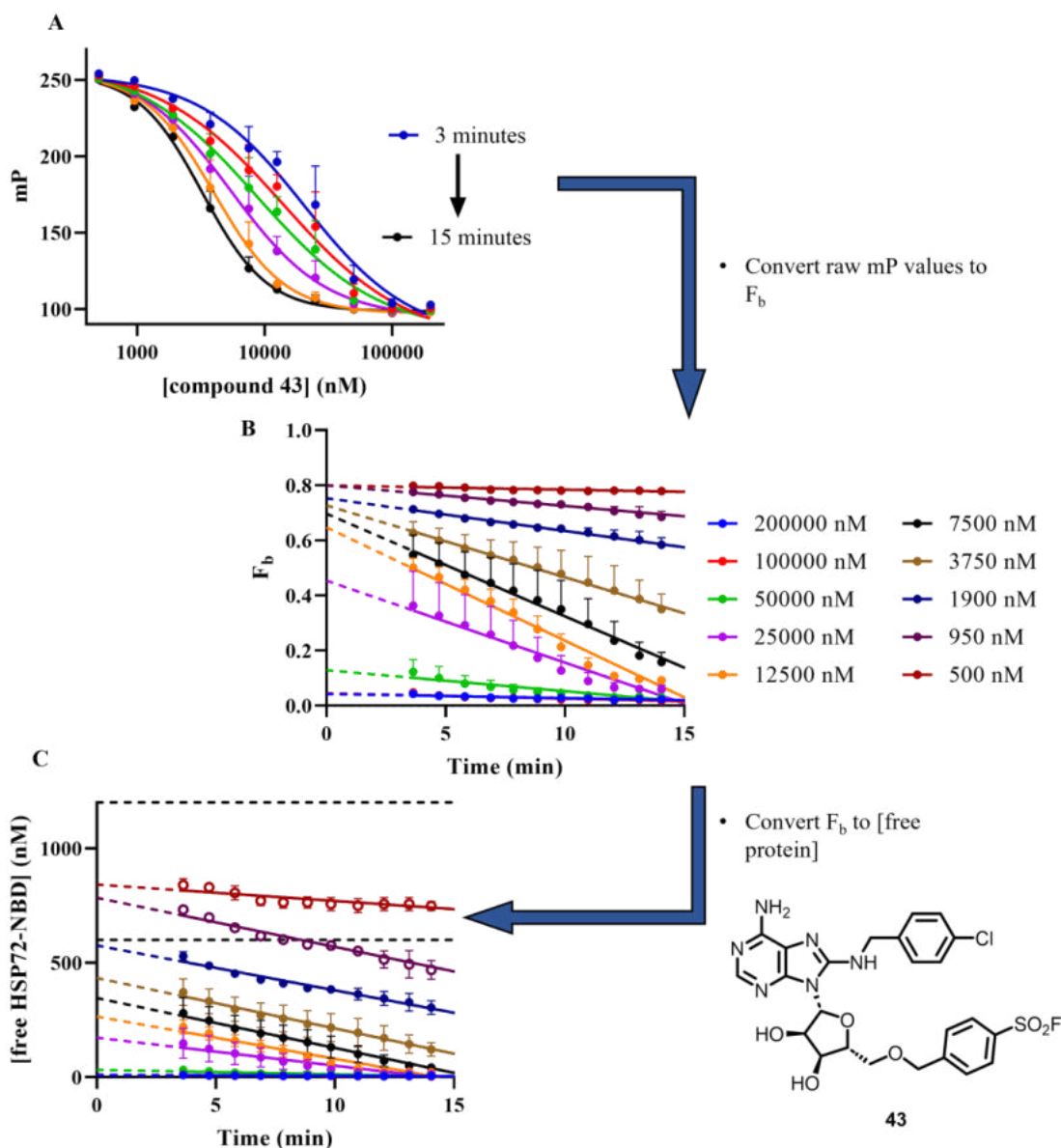


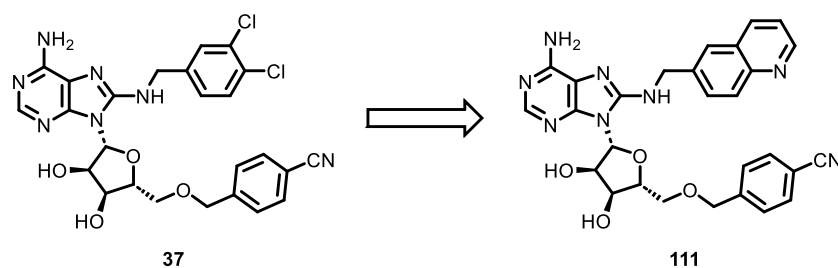
**Figure 4.13** **A** Profiling of TCI **43** in the TDFP assay with HSP72-NBD and ATP-ATTO 488 **108**. [HSP72-NBD] selected so  $F_b = 0.85$ , measurements taken in triplicate every minute for 15 minutes and plotted on same axes. **B** Plot of calculated  $F_b$  values against time. **C**  $F_b$  values converted to [free protein]. Dotted lines indicate [free HSP72-NBD] at 50% and 100% total protein concentration.

#### 4.2.5 Synthesis of 5'-Ether-Linked TCI Analogues

Having demonstrated the potent binding kinetics of TCI **43**, we aimed to generate a library of 5'-ether-linked TCIs to further validate the observed high affinity of this chemotype, and ultimately profile this series in cells. Analysis of the SAR from previously published 8-aminobenzyl group derivatives demonstrated that substitution of dichlorobenzyl



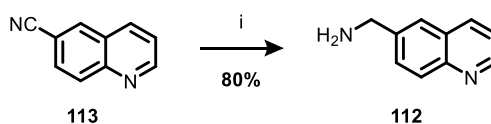
group in **37** for a quinoline moiety in **111** had resulted in an ~6-fold improvement in  $K_d$  when measured by SPR with HSP72 (Table 4.1).<sup>134</sup>



Compound	$K_d$ (nM)
VER-155008 <b>37</b>	300
quinoline <b>111</b>	50

**Table 4.1** Data for reversible analogues **37** and **111** reported by Massey et al.<sup>134</sup> Profiling by SPR indicated that switch from dichlorobenzyl to quinoline moiety at the 8-position drives improvement in  $K_d$ .

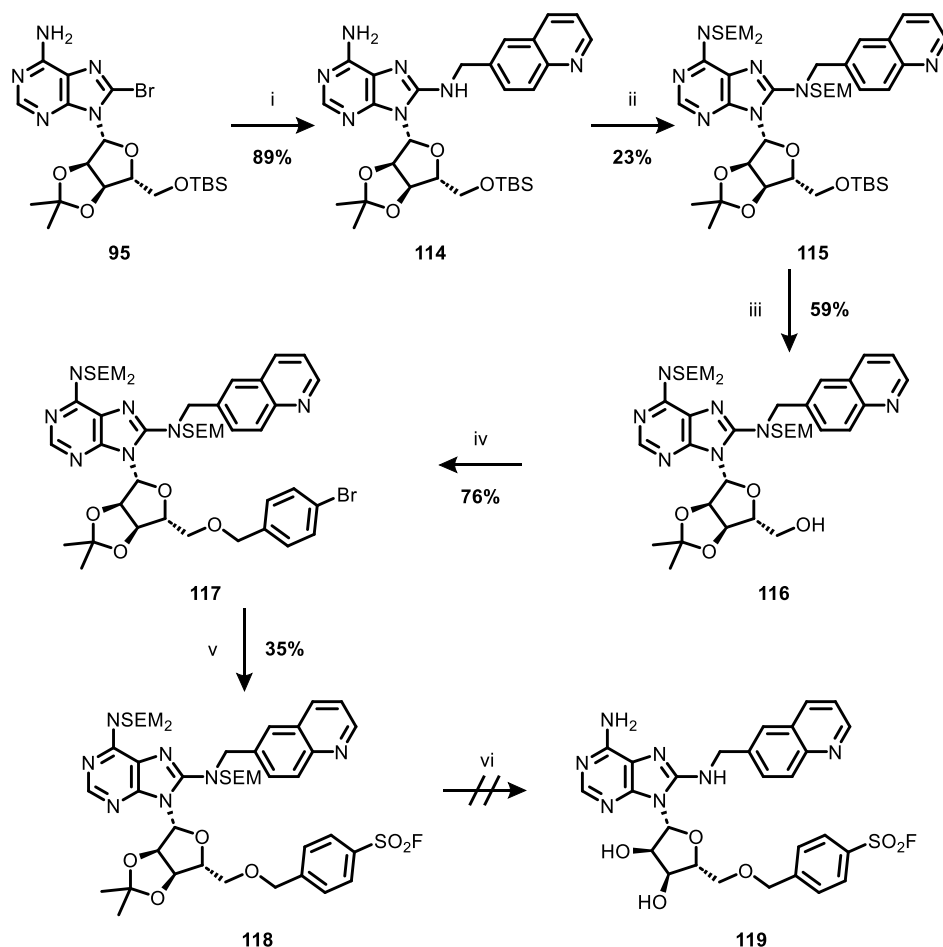
Synthesis of a sulfonyl fluoride MMP to quinoline **111** was commenced; firstly, benzylic amine **112** was prepared from nitrile **113** in high yield *via* hydrogenation with sponge nickel catalyst following a modification of literature conditions (Scheme 4.2).<sup>185</sup>



**Scheme 4.2** Synthesis of benzylic amine **112**. Reagents and conditions: i)  $H_2$  (1 atm), sponge Ni cat, 7 N  $NH_3$  in MeOH (0.6 M), rt, 72 h.

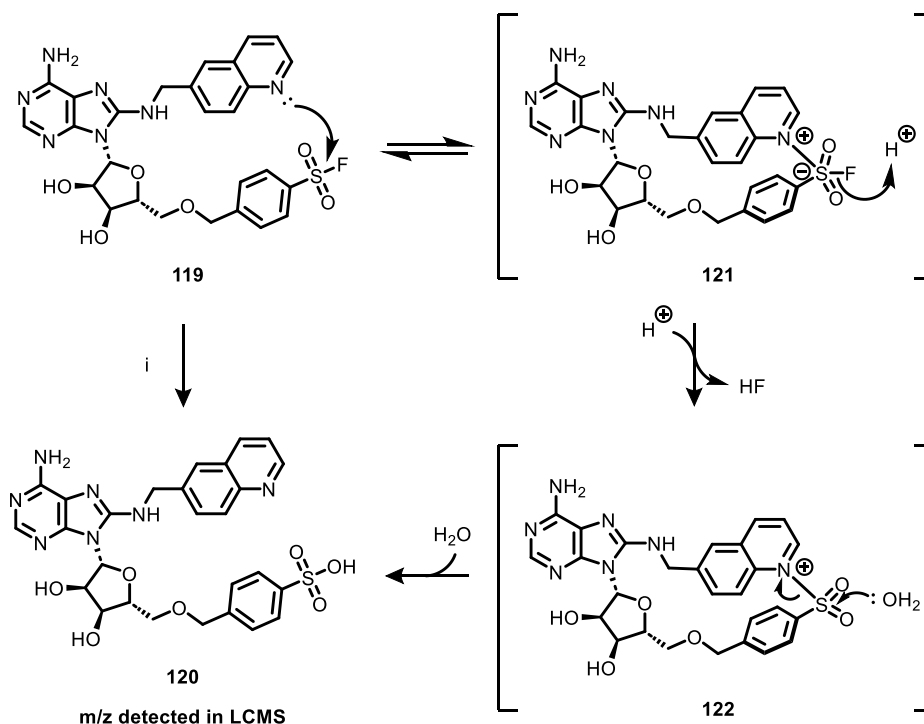
The remaining synthesis proceeded as for chlorobenzyl TCI **43**. Briefly, 8-bromo intermediate **95** underwent an  $S_NAr$  reaction with quinolinic amine **112** to give **114**, which was subsequently tris-*N*-SEM-protected to afford **115**. 5'-*O*-TBS deprotection with TBAF gave **116**, which was followed by sequential etherification with sodium hydride to **117**. Finally, palladium catalysed fluorosulfonation of bromide **117** gave the protected sulfonyl fluoride **118** derivative, in 5 steps and 3% overall yield (Scheme 4.3).

## 4 Characterisation of 5'-Ether-Linked HSP72 Lysine-TCIs



**Scheme 4.3** Attempted synthesis of TCI **119**. Reagents and conditions: i) quinolin-6-ylmethanamine **112** (6.5 equiv.), EtOH (0.3 M), 160 °C,  $\mu$ wave, 1 h; ii) DIPEA (4.5 equiv.), SEMCl (4.5 equiv.), CH<sub>2</sub>Cl<sub>2</sub> (0.3 M), reflux, 18 h; iii) TBAF (1.1 equiv.), THF (0.12 M), 0 °C to rt, 18 h; iv) NaH (1.2 equiv.), THF (0.5 M), 0 °C, 15 min, *then* 4-bromobenzyl bromide (2 equiv.), 0 °C to rt, 18 h; v) DABSO (0.6 equiv.), PdCl<sub>2</sub>(AmPhos)<sub>2</sub> (5 mol%), Et<sub>3</sub>N (3 equiv.), isopropanol (0.27 M), 75 °C, 18 h, *then* NFSI (1.5 equiv.), rt, 5 h; vi) TFA:H<sub>2</sub>O 5:2 (0.1 M), rt, 1 h.

Unfortunately, attempted global deprotection under the acidic hydrolysis conditions, which had been successful in the synthesis of the benzylic sulfonyl fluoride **43**, led to degradation of the starting material, potentially due to hydrolysis of the sulfonyl fluoride electrophile under the reaction conditions. We hypothesised that this degradation was substrate selective; the sulfonyl fluoride group of **119** underwent accelerated hydrolysis to sulfonic acid **120** owing to neighbouring group participation of the proximal quinoline nitrogen under the acidic hydrolysis deprotection reaction conditions (Scheme 4.4).

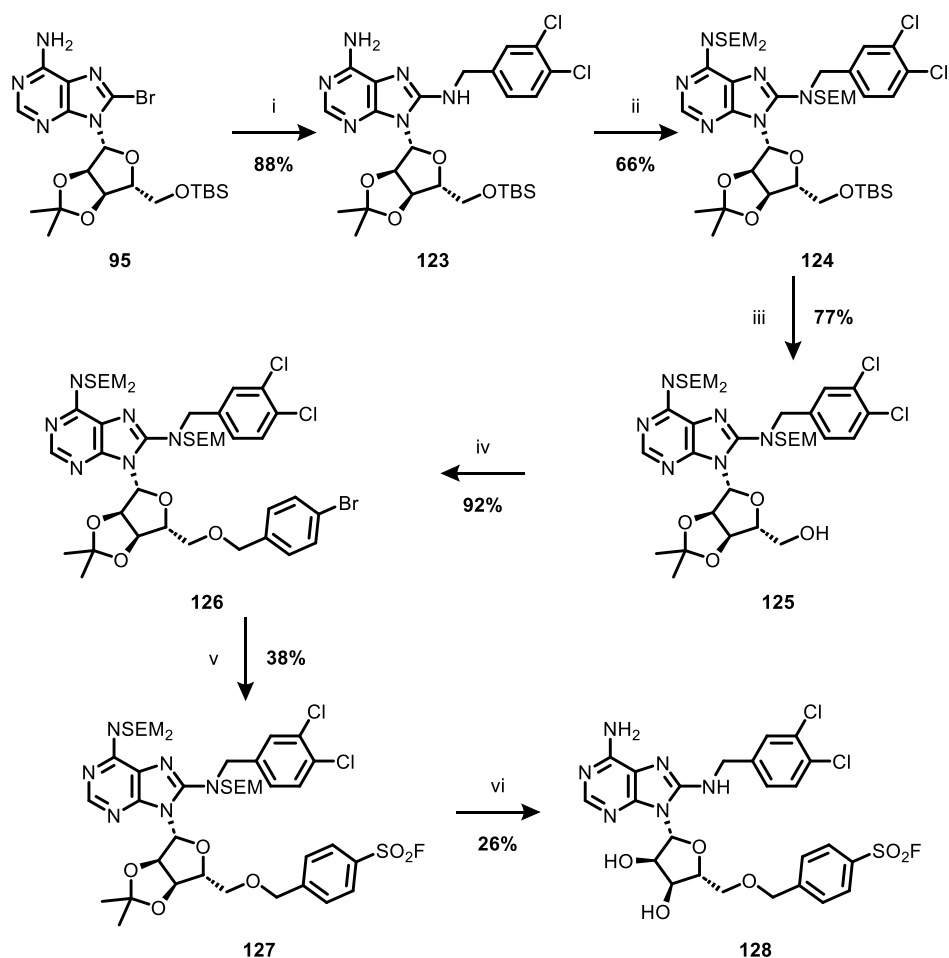


**Scheme 4.4** Plausible mechanism for the degradation of sulfonyl fluoride **119** to sulfonic acid **120**. Quinoline nitrogen attacks intramolecularly into sulfonyl fluoride of **119** leading to the formation of ate-complex **121**, which then decomposes upon treatment of aqueous acid to form sulfone intermediate **122** then sulfonic acid **120**. Reagents and conditions: i) TFA:H<sub>2</sub>O 5:2 (0.1 M), rt, 1 h.

As a plausible mechanism, TCI **119** could undergo intramolecular nucleophilic attack through the quinoline nitrogen into the sulfonyl fluoride functional group, to give the ate-complex **121**. Reaction with acid would then lead to the collapse of the postulated ate-complex **121**, forming HF and a highly reactive sulfone intermediate **122**, which would undergo rapid hydrolysis to give the sulfonic acid by-product **120**. Owing to its apparent acid instability, efforts to synthesise TCI **119** were concluded.

It appeared that neighbouring group participation would be important in the design of potent but stable lysine-targeting covalent inhibitors, as these groups can modulate the intrinsic reactivity of the electrophile. Therefore, we switched the 8-position substituent to the lipophilic 3,4-dichlorobenzyl group, as we hypothesised that removing the nucleophilic quinoline nitrogen would result in a more stable TCI. 8-bromo intermediate **95** was reacted with 3,4-dichlorobenzylamine to form 8-*N*-benzylated intermediate **123** (Scheme 4.5), which then underwent tris-*N*-SEM protection to give protected intermediate **124**. The 5'-*O*-TBS group of **124** was then selectively cleaved to give free

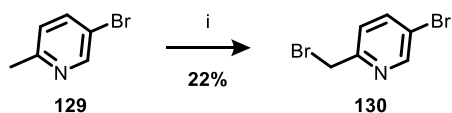
5'-OH **125**. Sequential basic etherification to **126**, then fluorosulfonation to **127**, and finally acidic hydrolysis deprotection gave the desired TCI **128** in acceptable yield, consistent with the role of the 8-position substituent in the intrinsic reactivity of the electrophile.



**Scheme 4.5** Synthesis of TCI **128**. Reagents and conditions: i) 3,4-dichlorobenzylamine (8 equiv.), EtOH (0.3 M), 160 °C,  $\mu$ wave, 1 h; ii) DIPEA (4.5 equiv.), SEMCl (4.5 equiv.), CH<sub>2</sub>Cl<sub>2</sub> (0.3 M), reflux, 22 h; iii) TBAF (1.1 equiv.), THF (0.12 M), 0 °C to rt, 18 h; iv) NaH (1.2 equiv.), THF (0.5 M), 0 °C, 15 min, *then* 4-bromobenzyl bromide (2 equiv.), 0 °C to rt, 18 h; v) DABSO (0.6 equiv.), PdCl<sub>2</sub>(AmPhos)<sub>2</sub> (5 mol%), Et<sub>3</sub>N (3 equiv.), isopropanol (0.27 M), 75 °C, 18 h, *then* NFSI (1.5 equiv.), rt, 5 h; vi) TFA:H<sub>2</sub>O 5:2 (0.1 M), rt, 2 h.

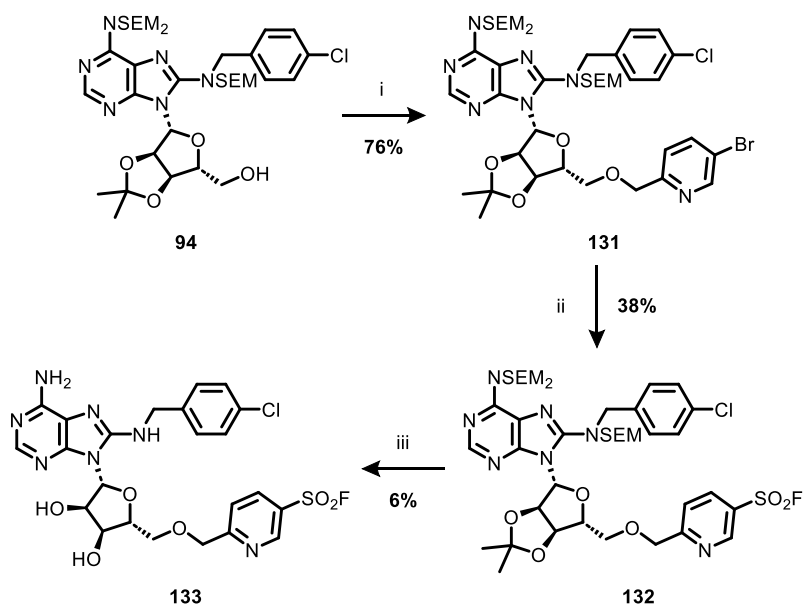
Owing to the limited availability of suitable synthetic methodology prior to our development of the tris-*N*-SEM-8-aminoadenosine strategy to access 5'-*O*-benzylated adenosine-derived HSP70 inhibitors (Section 3.1.2), the SAR of the 5'-*O*-benzyl ring was consequently underexplored. To investigate changes to the 5'-position, we hypothesised that by switching from the benzyl to pyridyl group, we could investigate the SAR of the

ring and probe the effect of a ring heteroatom on the reactivity of the sulfonyl fluoride warhead. The palladium-catalysed cross coupling methodology used to access sulfonyl fluoride TCIs has only previously been described with a limited range of *m*-bromo heteroaryls.<sup>164</sup> Starting from methyl pyridine **129**, pyridyl benzyl bromide **130** was prepared *via* radical bromination with benzoyl peroxide and NBS in low yield (Scheme 4.6).



**Scheme 4.6** Synthesis of 5-bromo-2-(bromomethyl)pyridine **130**. Reagents and conditions: i) benzoyl peroxide (5 mol%), NBS (1.1 equiv.),  $\alpha,\alpha,\alpha$ -trifluorotoluene (0.4 M), 90 °C, 18 h.

Pyridyl bromide **130** was then reacted with tris-*N*-SEM intermediate **94**, to give the 5'-ether substrate **131** in high yield. Substitution of the triethylamine base for *N,N*-dicyclohexylmethylamine and heating to 110 °C in the microwave, a modification of previously described conditions developed for the synthesis of heteroaryl bromides,<sup>164</sup> gave the desired sulfonyl fluoride **132**, albeit as a 3:2 mixture by <sup>1</sup>H NMR with an unidentified impurity. This mixture was carried forward to the acidic hydrolysis deprotection step to give the spectroscopically pure target pyridine TCI **133** following chromatographic purification (Scheme 4.7).



**Scheme 4.7** Synthesis of TCI **133**. Reagents and conditions: i) NaH (1.2 equiv.), THF (0.5 M), 0 °C, 15 min, *then* 5-bromo-2-(bromomethyl)pyridine **130** (2 equiv.), 0 °C to rt, 18 h; ii) DABSO (1 equiv.), PdCl<sub>2</sub>(AmPhos)<sub>2</sub> (5 mol%), *N,N*-dicyclohexylmethylamine (3 equiv.), isopropanol (0.25 M), 110 °C,  $\mu$ wave, 1 h, *then* NFSI (1.5 equiv.), rt, 5 h; iii) TFA:H<sub>2</sub>O 5:2 (0.1 M), rt, 1 h.

#### 4.2.6 Synthesis of 5'-Ether-Linked TCI Controls

The inherent reactivity of covalent inhibitors can lead to non-specific activity.<sup>72</sup> To assess whether this new series of 5'-ether-linked sulfonyl fluoride TCIs were acting in a specific manner, two types of control compounds were required: a reversible control and an irreversible control. The reversible control inhibitor would be required to directly measure the reversible affinity of this class of compounds in the absence of any covalent bond formation. Fluorine is extensively applied as a bioisotere for methyl groups in medicinal chemistry owing to their similar properties;<sup>186</sup> therefore, we hypothesised that a methyl sulfone would be a suitable, non-electrophilic bioisosteric replacement for a sulfonyl fluoride (Figure 4.14).

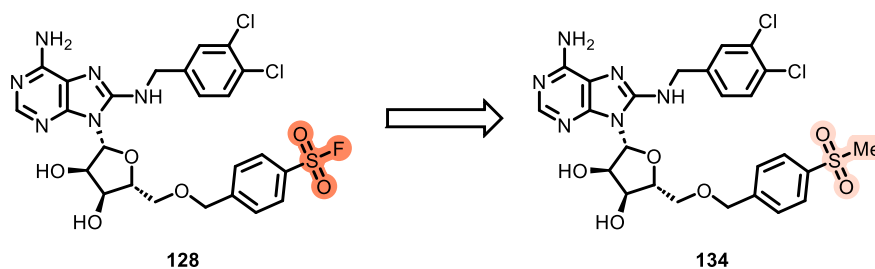
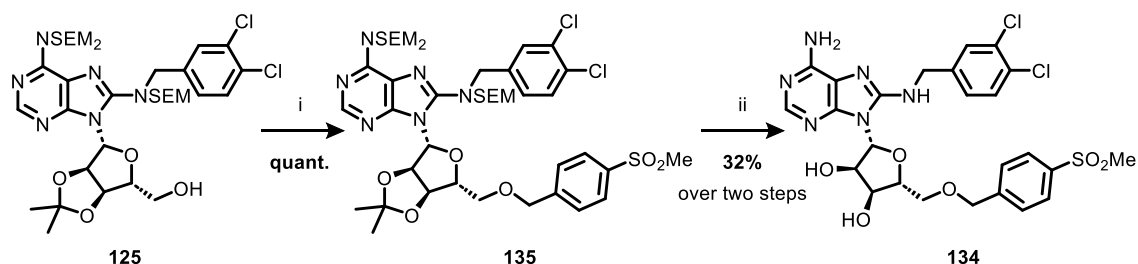


**Figure 4.14** Bioisosteric replacement strategy from TCI **128** to methyl sulfone **134** in the design of a reversible MMP.

The dichlorobenzyl moiety in **134** was included to enable MMP analysis with *p*-cyanobenzyl group in the VER-155008 **37** HSP70 reversible non-covalent inhibitor. Alkylation of tris-*N*-SEM intermediate **125** with 4-(methylsulfonyl)benzyl bromide afforded 5'-*O*-benzylated intermediate **135**; the crude product was then subjected to acidic deprotection with TFA:water to afford the desired reversible control **134** in 32% yield over two steps (Scheme 4.8).



**Scheme 4.8** Synthesis of reversible MMP **134**. Reagents and conditions: i) NaH (1.2 equiv.), THF (0.5 M), 0 °C, 15 min, *then* 4-(methylsulfonyl)benzyl bromide (2 equiv.), 0 °C to rt, 18 h; ii) TFA:H<sub>2</sub>O 5:2 (0.1 M), rt, 1 h.

The irreversible covalent control inhibitor was required to investigate non-specific covalent reactivity of the chemotype. The compound would need to possess the sulfonyl fluoride moiety with similar intrinsic reactivity as the tool TCI **128**, but have very weak reversible affinity for HSP72-NBD. From our analysis of previously described SAR,<sup>142</sup> the bis-8-*N*-alkylation of adenosine-derived HSP70 inhibitor **136** had resulted in a complete loss of measurable reversible affinity with bismethyl **137** (Figure 4.15 A). We therefore hypothesised that a similar modification to our class of lysine-TCIs, to give 8-*N*-methylated compound **138**, would result in a suitable control inhibitor (Figure 4.15 B).

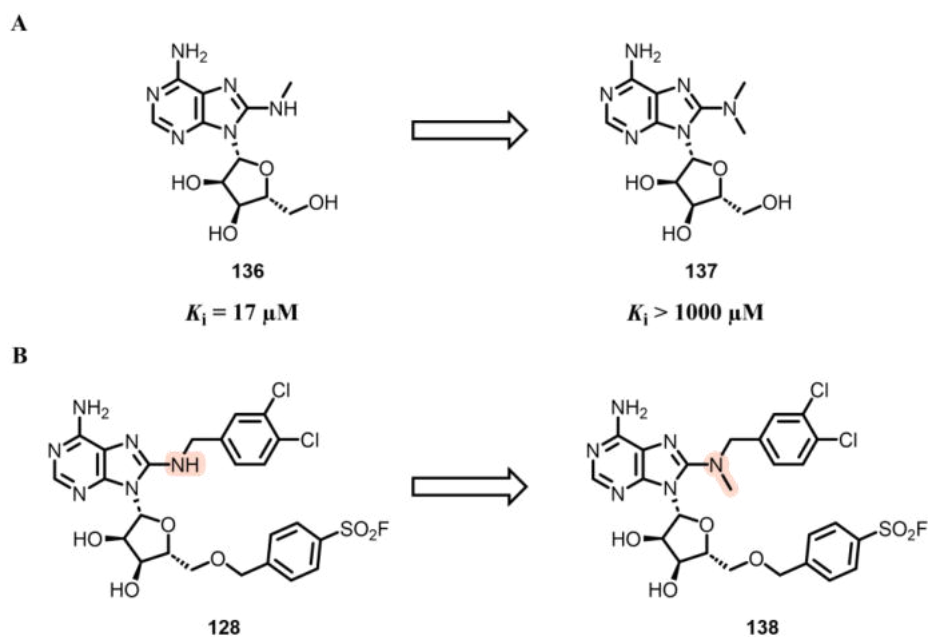
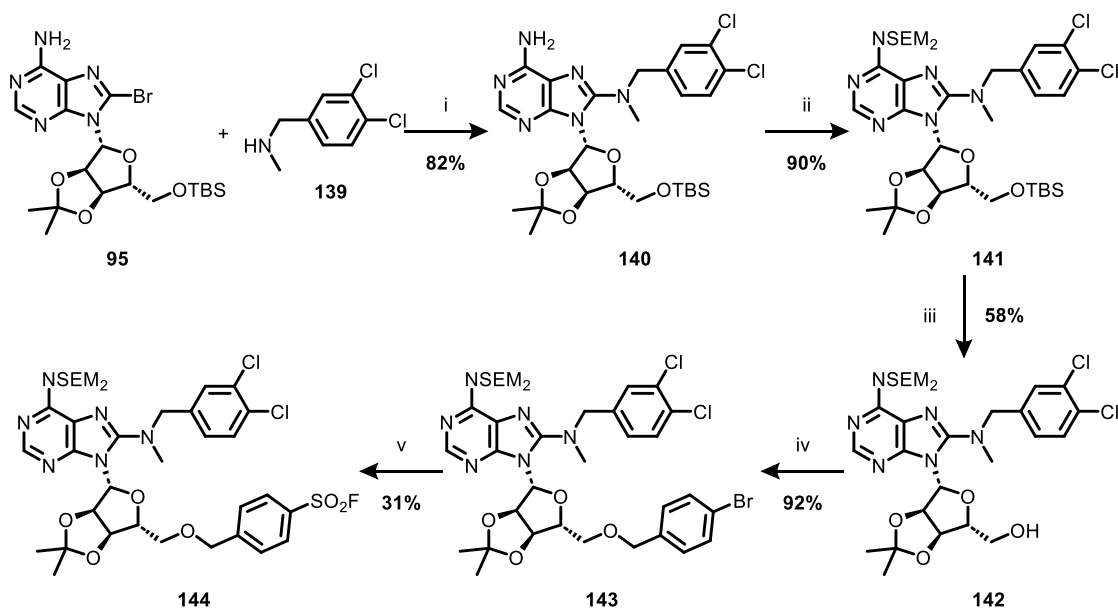


**Figure 4.15 A** MMP analysis showed that switch from mono- to bis-8-*N*-methylation of adenosine-derived HSP70 inhibitors resulted in a loss of all detectable reversible affinity.<sup>142</sup> **B** Design strategy for irreversible control **138**, incorporating *N*-methylation to disrupt reversible binding of the ligand.

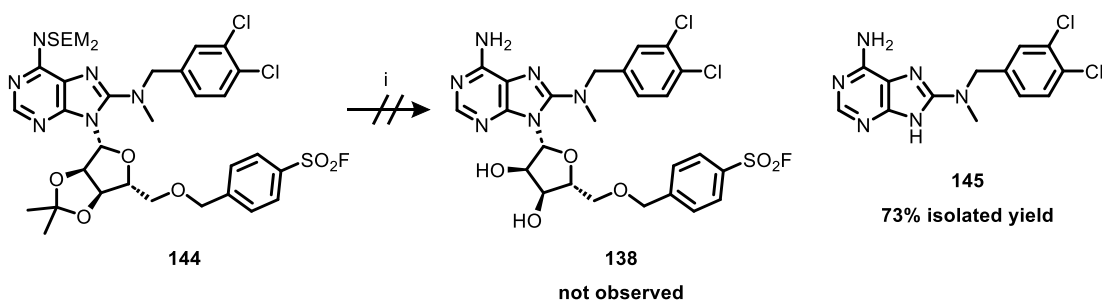
To synthesise the target negative control, *N*-(3,4-dichlorobenzyl)-*N*-methylamine **139** was reacted with 8-bromo intermediate **95** via an  $S_NAr$  reaction to give the 8-*N*-methylated intermediate **140**. Bis 6-*N*-SEM protection gave **141**, which then underwent selective 5'-*O*-TBS deprotection to give **142**. Benzylation under standard conditions gave **143** and was followed by palladium-catalysed fluorosulfonation to give the 6-*N*-protected sulfonyl fluoride **144** (Scheme 4.9).





**Scheme 4.9** Synthesis of sulfonyl fluoride **144**. Reagents and conditions: i) *N*-(3,4-dichlorobenzyl)-*N*-methylamine **139** (8 equiv.), EtOH (0.3 M), 160 °C,  $\mu$ wave, 1 h; ii) DIPEA (4.5 equiv.), SEMCl (4.5 equiv.), CH<sub>2</sub>Cl<sub>2</sub> (0.3 M), reflux, 22 h; iii) TBAF (1.1 equiv.), THF (0.12 M), 0 °C to rt, 4 h; iv) NaH (1.2 equiv.), THF (0.5 M), 0 °C, 15 min, *then* 4-bromobenzyl bromide (2 equiv.), 0 °C to rt, 18 h; v) DABSO (0.6 equiv.), PdCl<sub>2</sub>(AmPhos)<sub>2</sub> (5 mol%), Et<sub>3</sub>N (3 equiv.), isopropanol (0.27 M), 75 °C, 18 h, *then* NFSI (1.5 equiv.), rt, 5 h.

Surprisingly, treatment of **144** under our standard acidic hydrolysis deprotection conditions of TFA:water 5:2, led to complete degradation of the starting material, with the only product isolated from the reaction mixture being the *N*-glycoside-cleaved product **145** (Scheme 4.10).



**Scheme 4.10** Attempted synthesis of irreversible control **138**. Reagents and conditions: i) TFA:H<sub>2</sub>O 5:2 (0.1 M), rt, 1 h.

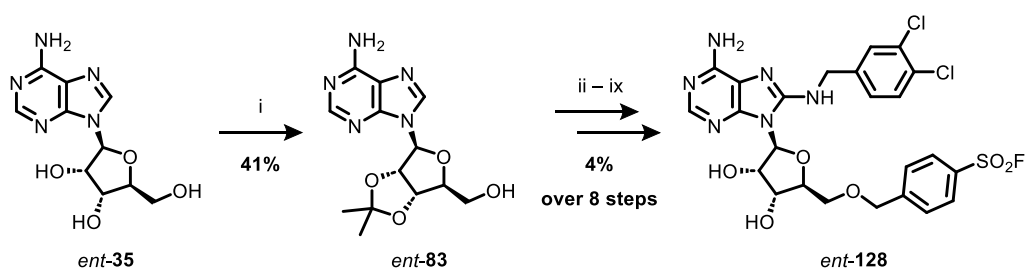
Acid-mediated glycosidic bond cleavage is a well-precedented decomposition pathway for adenosine;<sup>187</sup> however, this side product was not observed in the synthesis of



Unfortunately, all conditions screened led to complete degradation of starting material. Consequently, efforts towards the synthesis of TCI **138** were ceased due to its apparent acid sensitivity.

To design an alternative negative control TCI, we hypothesised that the opposite enantiomer of TCI **128** would possess negligible reversible affinity for HSP72, as inversion of all four stereocentres of the ribose moiety should remove all shape complementarity and disrupt multiple critical hydrogen bonds within the binding site. However, the intrinsic reactivity and stability would be identical to the 5'-ether TCI **128**.

Starting from unnatural L-adenosine *ent*-**35**, acetonide protection of the 2'- and 3'-hydroxyls afforded protected intermediate *ent*-**83**. The remaining eight steps of the synthesis were carried out according to the procedure for TCI **128**, to give the negative control TCI *ent*-**128**.



**Scheme 4.13** Synthesis of irreversible control *ent*-**128**. Reagents and conditions: i) PTSA (10 equiv.), acetone (0.02 M), rt, 18 h; ii) TBSCl (1.2 equiv.), imidazole (2 equiv.), DMF (0.35 M), rt, 16 h; iii)  $K_2HPO_4$  (3 equiv.),  $Br_2$  (2.5 equiv.), 1,4-dioxane:H<sub>2</sub>O 1:1 (0.13 M), rt, 18 h; iv) 3,4-dichlorobenzylamine (8 equiv.), EtOH (0.3 M), 160 °C,  $\mu$ wave, 1 h; v) DIPEA (4.5 equiv.), SEMCl (4.5 equiv.),  $CH_2Cl_2$  (0.3 M), reflux, 18 h; vi) TBAF (1.1 equiv.), THF (0.12 M), 0 °C to rt, 18 h. vii) NaH (1.2 equiv.), THF (0.5 M), 0 °C, 15 min, *then* 4-bromobenzyl bromide (2 equiv.), 0 °C to rt, 18 h; viii) DABSO (0.6 equiv.),  $PdCl_2(AMPHOS)_2$  (5 mol%),  $Et_3N$  (3 equiv.), isopropanol (0.27 M), 75 °C, 18 h, *then* NFSI (1.5 equiv.), rt, 5 h; ix) TFA:H<sub>2</sub>O 5:2 (0.1 M), rt, 2 h.

#### 4.2.7 Characterisation of New Analogues in the TDFP Assay

Following the synthesis of our 5'-ether sulfonyl fluoride library, I began the biochemical assessment of their activity as HSP72-NBD TCIs. Pyridine TCI **133** and dichlorobenzyl TCI **128** were screened in the TDFP assay (Figure 4.16)

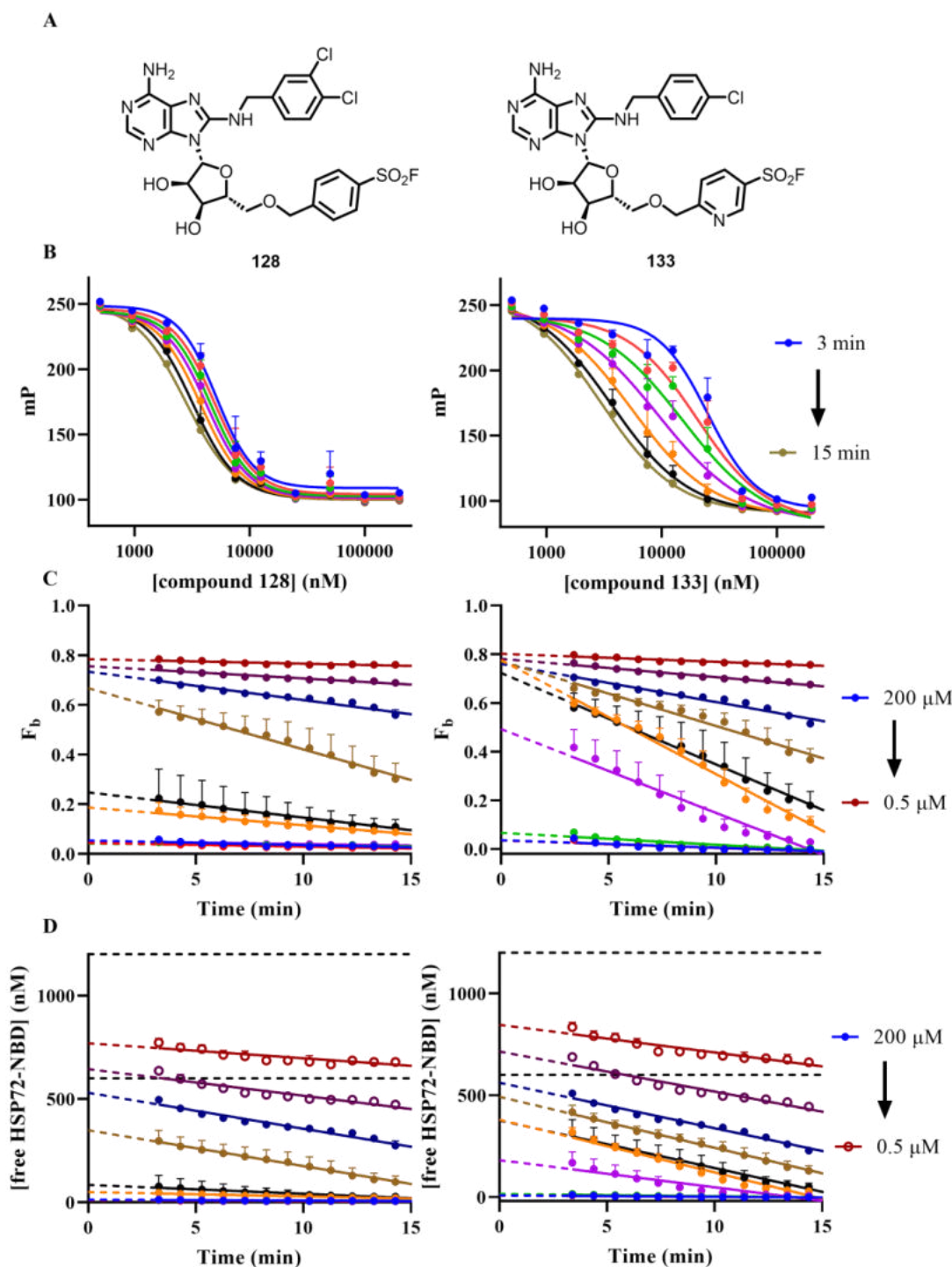


**Figure 4.16** **A** Structures of TCIs **128** and **133**. **B** Profiling of TCIs **128** and **133** in the TDFP assay with HSP72-NBD and ATP-ATTO 488 **108**. [HSP72-NBD] selected so  $F_b = 0.85$ , measurements taken in triplicate every minute for 15 minutes and plotted on same axes. **C** Plot of calculated  $F_b$  values against time, data plotted in GraphPad Prism 9. **D**  $F_b$  values converted to [free protein]. Black dotted lines indicate [free HSP72-NBD] at 50% and 100% total protein concentrations respectively, hollow circles indicate [inhibitor] < [total protein]. Data plotted in GraphPad Prism 9.

Analysis of the bound fraction (Figure 4.16 C) and free protein concentration (Figure 4.16 D) vs time graphs indicated that both compounds displayed affinity consistent with reaching the resolvable limit of the assay ( $K_i < 200$  nM), analogous to the mono-chloro sulfonyl fluoride TCI **43**.

To examine the specificity of this time-dependent binding and formation of the covalent bond, irreversible control *ent-128* was then screened in the TDFP assay (Figure 4.17).

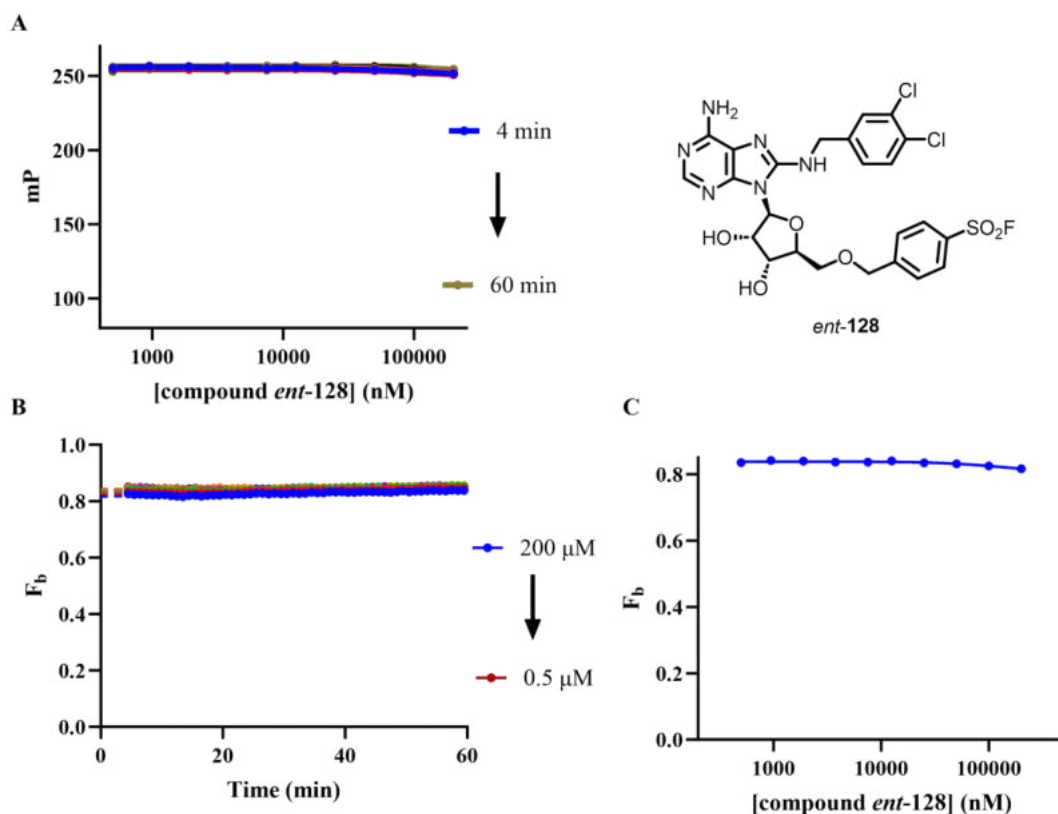
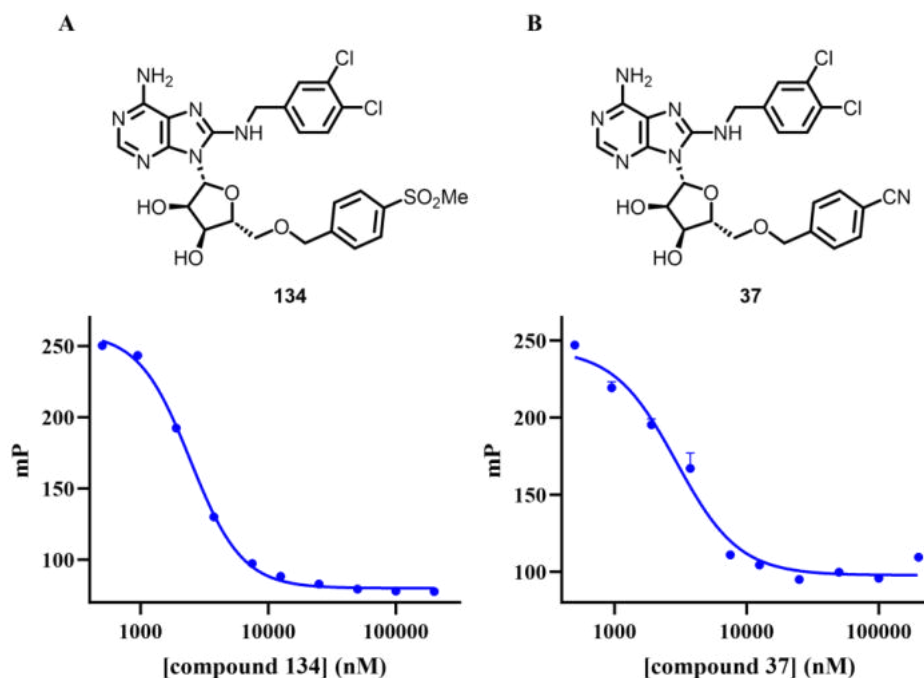


**Figure 4.17** **A** Profiling of irreversible control *ent-128* in the TDFP assay with HSP72-NBD and ATP-ATTO 488 **108**. [HSP72-NBD] selected so  $F_b = 0.85$ , measurements taken in triplicate every minute for 60 minutes and plotted on same axes. **B** Plot of calculated  $F_b$  values against time, y intercepts determined from simple linear regression (GraphPad Prism 9). **C** Plot of initial  $F_b$  against [I] (log(inhibitor) vs. response – variable slope (four parameters), GraphPad Prism 9).

Irreversible control *ent-128* displayed no detectable binding over the time course of the assay, consistent with its predicted negligible reversible affinity (initial  $K_i > 30$   $\mu$ M, Figure 4.17 C) and no time dependent decrease in the bound fraction over 60 minutes was observed (Figure 4.17 B). This result gave us confidence that our high affinity TCIs are

specifically displacing FP probe **108** from the nucleotide binding domain of HSP72 and that reversible occupancy is a requirement for efficient covalent bond formation.

Measurement of the  $K_i$  of reversible control **134** showed a reversible affinity at the resolvable limit of the assay, consistent with our TCIs possessing a high reversible affinity (Figure 4.18 A). VER-155008 **37** also exhibited tight-binding behaviour under the assay conditions (Figure 4.18 B).



Compound	$K_i$ (nM)
methyl sulfone <b>134</b>	<200
VER-155008 <b>37</b>	<200

**Figure 4.18** Measurement of  $K_i$  for reversible analogues with HSP72-NBD and ATP-ATTO 488 **108**. [HSP72-NBD] selected so  $F_b = 0.85$ . Assay was performed in triplicate and the mean and standard error plotted using GraphPad Prism 9. **A** IC<sub>50</sub> curve for methyl sulfone **134**. **B** IC<sub>50</sub> curve for VER-155008 **37**.

#### 4.2.8 Characterisation with Higher Affinity Fluorescent Probe

From the TDFP results, we concluded that the TCIs **43**, **128** and **133** displayed binding activity at the resolvable limit for the assay format, consistent with high reversible affinity. To increase the resolvable range of the TDFP assay, we turned to the HSP72-NBD FP probe **148** derived from 5'-ether-linked reversible inhibitors previously

disclosed by Evans et al. (Figure 4.19 A).<sup>153</sup> The bisaryl FP probe **148** has an ATTO-488 fluorophore in a similar manner to the ATP-derived FP-probe **108** (Figure 4.19 B), but has a reported  $K_d$  that is ~2-fold more potent against HSP72-NBD. We postulated that we would be able to exploit this more potent FP-probe to expand the assay window and obtain initial  $K_i$  for the high reversible affinity HSP70 inhibitors.

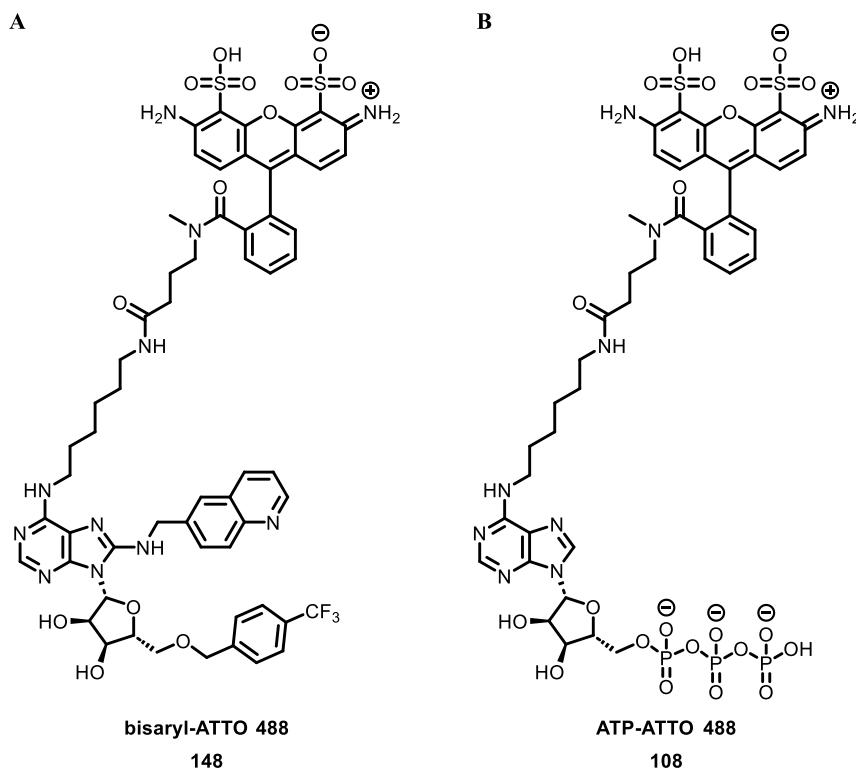
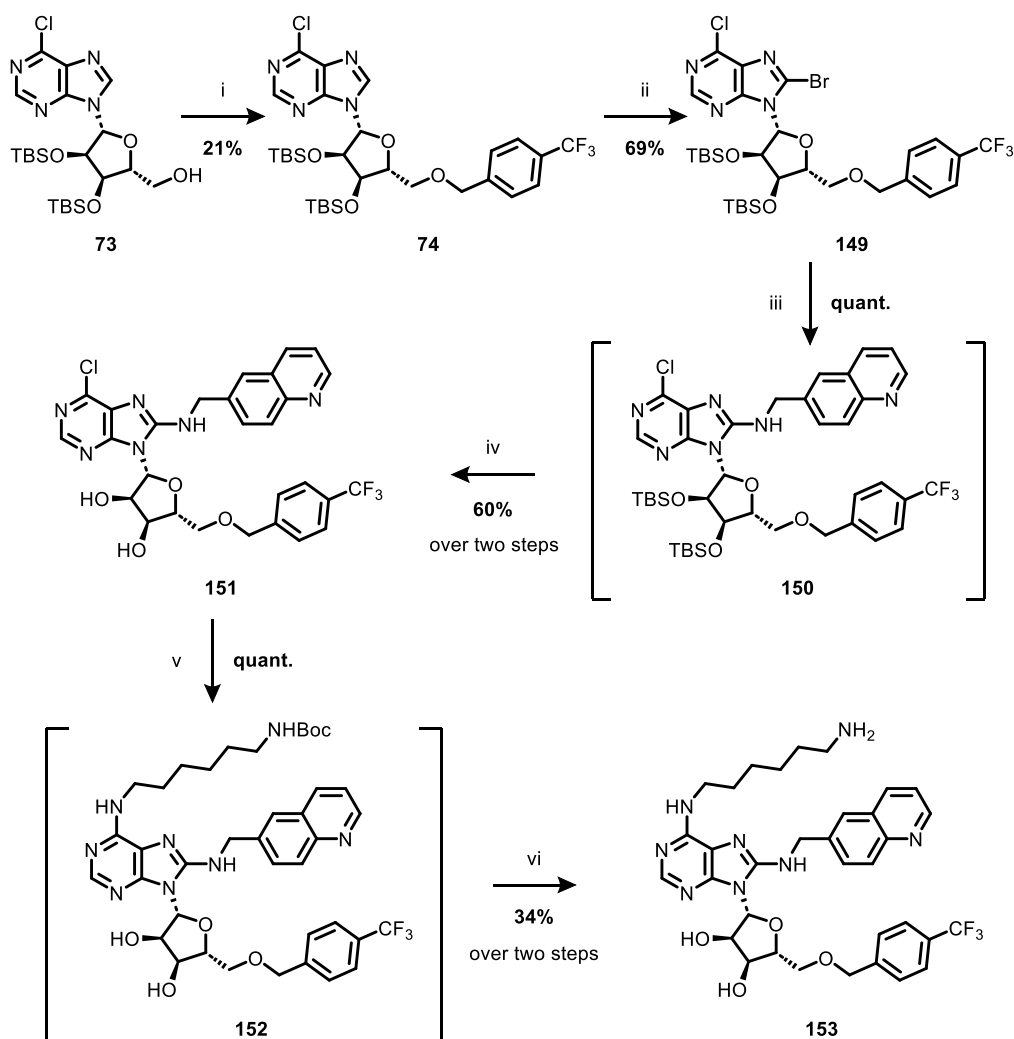


**Figure 4.19** Structure of **A** bisaryl-ATTO 488 **148** **B** ATP-ATTO 488 **108**.

The synthesis of the bisaryl-ATTO 488 FP-probe **148** was carried out *via* an adaptation of the previously described procedure.<sup>153</sup> Briefly, etherification of previously synthesised bis-*O*-TBS intermediate **73** was followed by bromination of the resulting 5'-*O*-ether-linked intermediate **74** to give the 8-bromo intermediate **149**, which was then converted to quinoline **150** *via* S<sub>N</sub>Ar reaction with quinolin-6-ylmethanamine **112**. The crude product was treated with TBAF to yield TBS-deprotected intermediate **151**; an S<sub>N</sub>Ar reaction on this material with *N*-Boc-1,6-hexanediamine gave *N*-Boc protected amine **152**. *N*-Boc-deprotection of the crude product gave free amine **153** in low-moderate yield over two steps (Scheme 4.14).

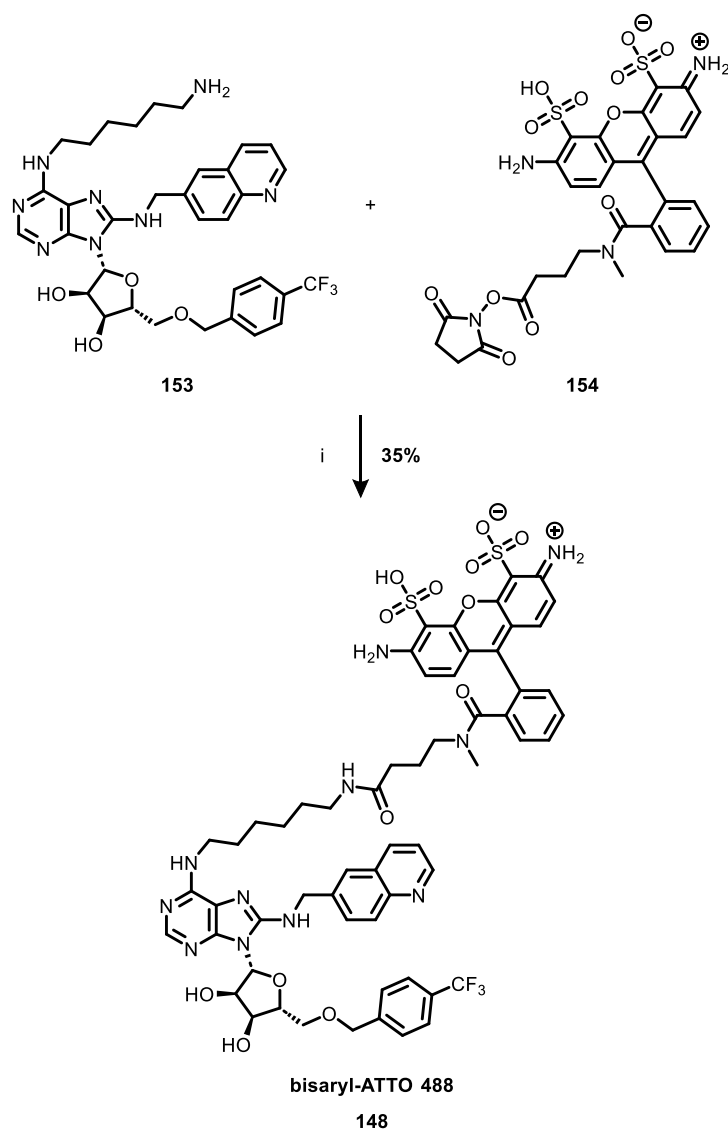
## 4 Characterisation of 5'-Ether-Linked HSP72 Lysine-TCIs



**Scheme 4.14** Synthesis of bisaryl intermediate **153**. Reagents and conditions i) NaH (1.2 equiv.), DMF (0.5 M), -61 °C, 15 min, then 4-(trifluoromethyl)benzyl bromide (2 equiv.), -61 °C to rt, 18 h; ii) LDA (1.4 equiv.), THF (0.14 M), -78 °C, 30 min, then 1,2-dibromotetrachloroethane (2 equiv.), -78 °C, 2 h; iii) quinolin-6-ylmethanamine **112** (1.5 equiv.), Et<sub>3</sub>N (1.5 equiv.), EtOH (0.1 M), 40 °C, 48 h; iv) TBAF (2.2 equiv.), THF (0.1 M), rt, 20 h; v) *N*-Boc-1,6-hexanediamine (5 equiv.), DIPEA (1.2 equiv.), *n*-BuOH (0.5 M), 120 °C,  $\mu$ wave, 2 h; vi) TFA (60 equiv.), CH<sub>2</sub>Cl<sub>2</sub> (0.1 M), rt, 2 h;

Finally, free amine **153** was reacted with ATTO 488 NHS ester **154** and triethylamine to yield bisaryl-ATTO-488 probe **148** in low-moderate yield following purification *via* reverse-phase HPLC (Scheme 4.15).





**Scheme 4.15** Synthesis of bisaryl-ATTO 488 **148**. Reagents and conditions: i) Et<sub>3</sub>N (4 equiv.), DMF (0.025 M), rt, 2 h.

To determine the apparent  $K_d$  of the bisaryl-ATTO 488 FP-probe **148**, 10 nM of **148** underwent titration against HSP72-NBD using a two-fold dilution series, subsequent non-linear regression analysis (Prism 9, one site-specific binding model) revealed a geometric mean probe  $K_d$  of 89 nM ( $pK_d = 7.05 \pm 0.06$ ,  $N = 3$ , mean  $\pm$  SEM) (Figure 4.20 B). The  $K_d$  value determined was consistent with the report by Evans et al.<sup>153</sup>

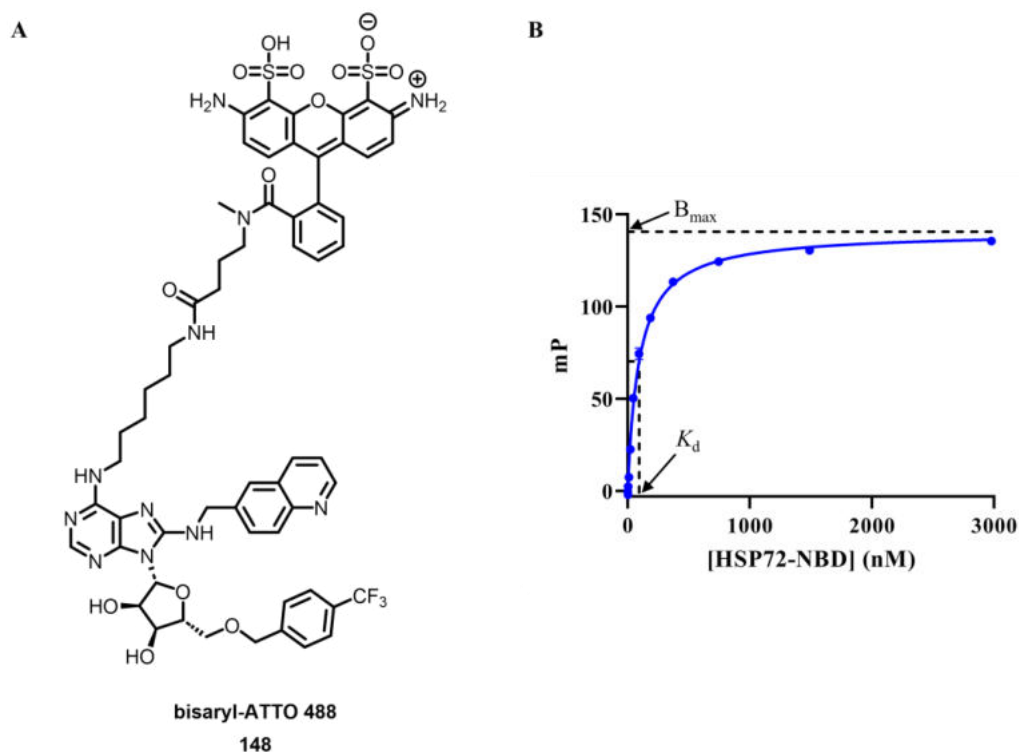
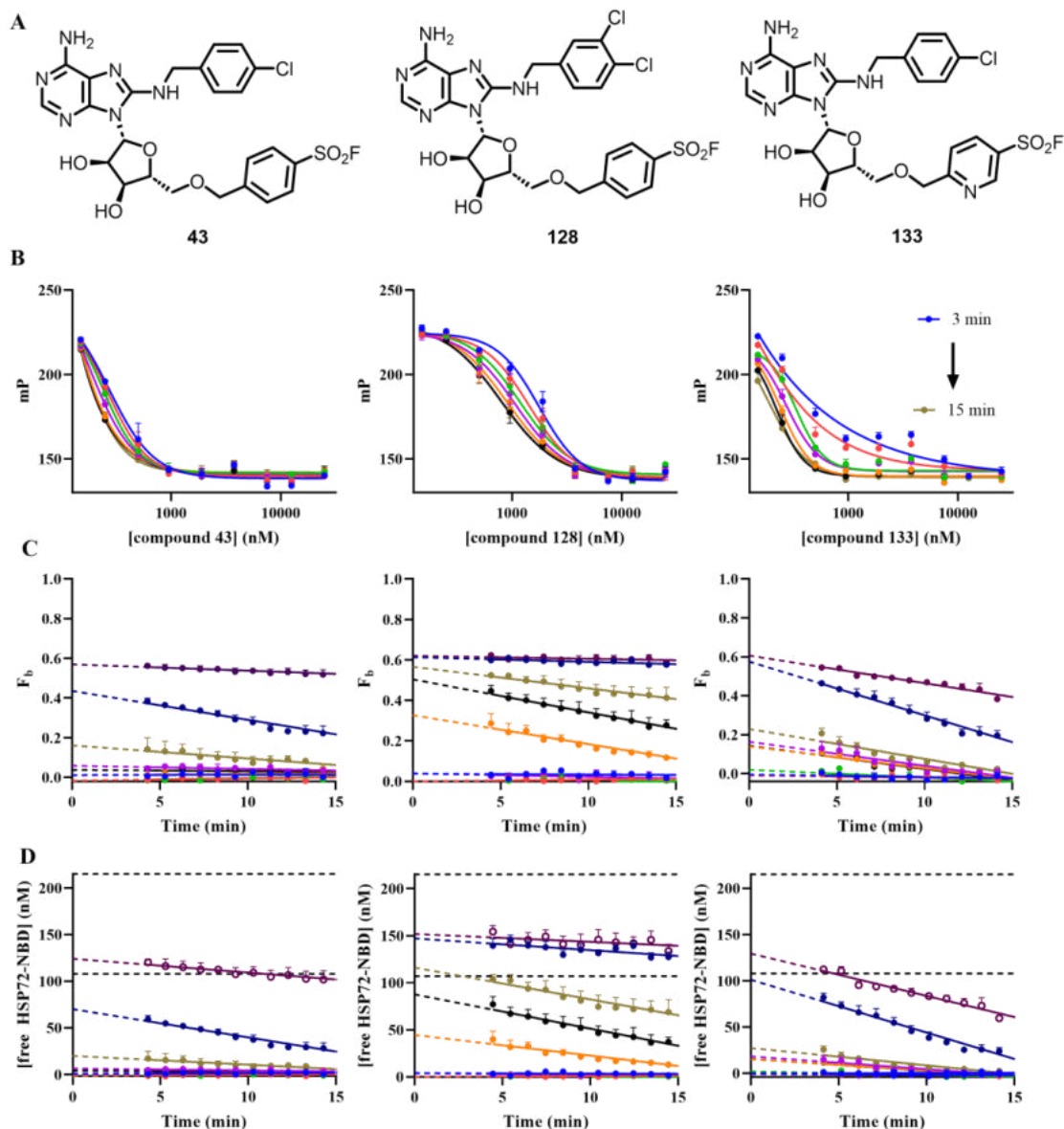


**Figure 4.20**  $K_d$  determination of bisaryl-ATTO 488 **148** with HSP72-NBD. **A** Structure of **148**. **B** Binding isotherm for HSP72-NBD and 10 nM **148**. mP values plotted are after subtraction of background polarisation. Assay was performed in triplicate and the mean and standard error plotted using GraphPad Prism 9.  $K_d$  value was determined as the geometric mean of three independent experiments.

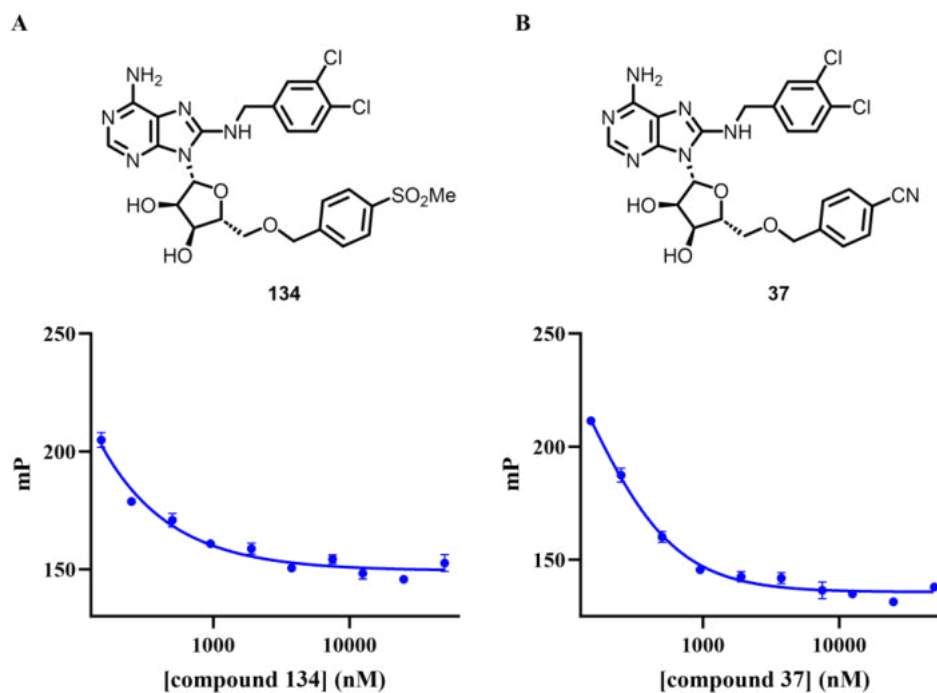
The TDFP assay was then repeated using the bisaryl-ATTO 488 probe **148** to profile the high affinity 5'-ether-linked TCIs **43**, **128** and **133** (Figure 4.21); however, all three TCIs still displayed binding kinetics at the resolvable limit of the assay, revealing stoichiometric binding and ligand depletion (Figure 4.21 C and D). This was consistent with high reversible affinity (initial  $K_i < 80$  nM), and precluded the elucidation of the second order rate constant  $k_{inact}/K_I$ , and therefore the  $k_{inact}$ .



Compound	Initial $K_i$ (nM)
monochloro <b>43</b>	<80
dichloro <b>128</b>	<80
pyridine <b>133</b>	<80

**Figure 4.21** **A** Structures of TCIs **43**, **128** and **133**. **B** Profiling of TCIs **43**, **128** and **133** in the TDFP assay with HSP72-NBD and bisaryl-ATTO 488 **148**. [HSP72-NBD] selected so  $F_b = 0.7$ , measurements taken in triplicate every minute for 15 minutes and plotted on same axes. Different colour lines represent different concentrations of TCIs from 25  $\mu\text{M}$  to 150 nM. **C** Plot of calculated  $F_b$  values against time, data plotted in GraphPad Prism 9. **D**  $F_b$  values converted to [free protein]. Black dotted lines indicate [free HSP72-NBD] at 50% and 100% total protein concentrations respectively, hollow circles indicate [inhibitor] < [total protein]. Data plotted in GraphPad Prism 9.

The reversible analogues methyl sulfone **134** and VER-155008 **37** were also profiled using bisaryl-ATTO 488 **148**, which furnished affinities at the resolvable assay limit ( $K_i < 80$  nM) (Figure 4.22). This corroborated the observed tight-binding behaviour for TCIs **43**, **128** and **133**.



Compound	$K_i$ (nM)
methyl sulfone <b>134</b>	<80
VER-155008 <b>37</b>	<80

**Figure 4.22** Measurement of  $K_i$  for reversible analogues with HSP72-NBD and bisaryl-ATTO 488 **148**. [HSP72-NBD] selected so  $F_b = 0.7$ . Assay was performed in triplicate and the mean and standard error plotted using GraphPad Prism 9. **A** IC<sub>50</sub> curve for methyl sulfone **134**.  $K_i$  value is quoted as the mean of two independent experiments. **B** IC<sub>50</sub> curve for VER-155008 **37**.  $K_i$  value is quoted as the mean of three independent experiments.

Overall, these results were consistent with analogous experiments performed with ATP-ATTO 488 probe **108** (Section 4.2.4 and 4.2.7). Together, they showed that the design strategy of an ester to ether substitution at the 5'-position had successfully furnished high affinity TCIs of HSP72-NBD.

### 4.3 Intact Protein Mass Spectrometry

#### 4.3.1 Introduction to Intact Protein Mass Spectrometry

Intact protein mass spectrometry (IPMS) is a technique that is widely applied in the characterisation of TCIs.<sup>187</sup> In a typical IPMS experiment, recombinant protein is eluted through a liquid chromatography (LC) system and analysed by a mass spectrometry (MS) system with electrospray ionisation (ESI) (Figure 4.23).

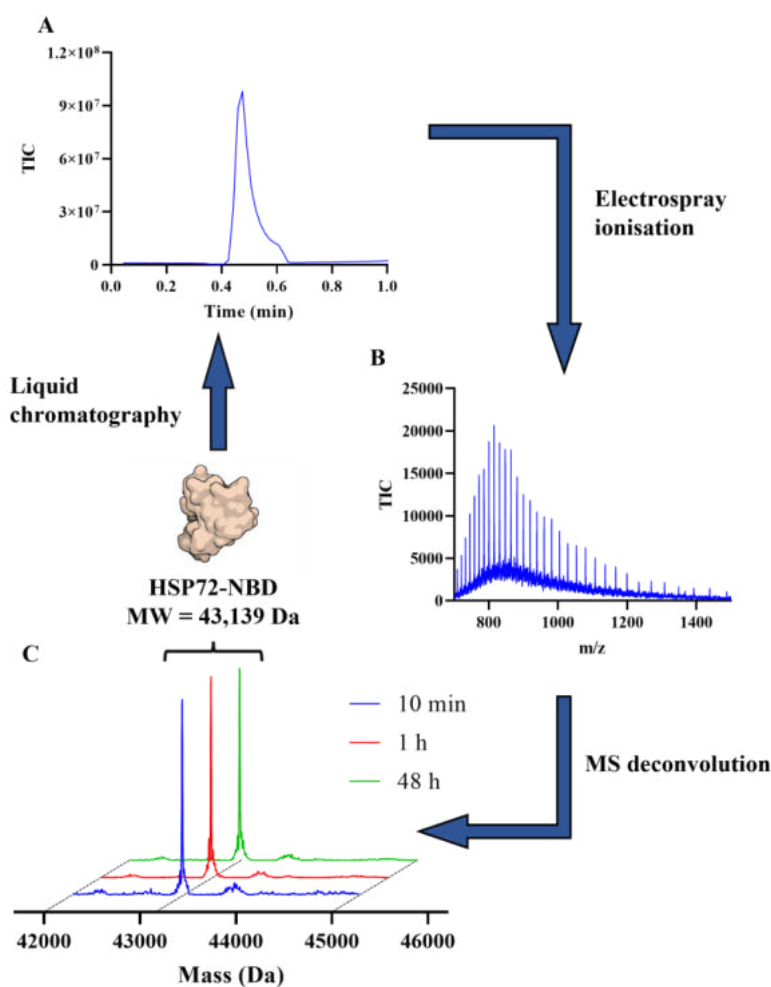


**Figure 4.23** Principle of intact protein mass spectrometry. **A** Recombinant HSP72-NBD is eluted *via* liquid chromatography. **B** The protein is then ionised in a mass spectrometer, resulting in the detection of multiple multiply-charged ions corresponding to  $[M+nH]^{n+}$ . **C**  $m/z$  peaks are computationally deconvoluted to yield a mass. Data plotted in GraphPad Prism 9.

HSP72-NBD was incubated at 0.1 g/mL (2.3  $\mu$ M) in assay buffer at 25 °C and injected into an LCMS system at various time points over a 48 hour period. After the 1 minute LC run (Figure 4.23 A), the protein was ionised into numerous charge states by ESI, which

provided the mass-to-charge ratio ( $m/z$ ) of the multiple ions formed (Figure 4.23 B). The spectrum was deconvoluted algorithmically (Agilent MassHunter Qualitative Analysis) to yield the expected mass of HSP72-NBD (MW = 43,139 Da, Figure 4.23 C). The IPMS clearly showed that the HSP72-NBD construct used was chemically stable over the 48-hour time course of the assay, with no additional peaks being observed. This gave us confidence that the protocol was sufficiently robust to measure covalent adduct formation. However, it was noted that this method provides no information about whether the ternary structure of the protein remained intact across this period, and only indicates whether the primary sequence is modified.

### 4.3.2 Profiling 5'-Ether-Linked TCIs by Intact Protein Mass Spectrometry

To confirm the formation of a covalent bond for the high affinity reversible affinity 5'-ether-linked TCIs, incubation of HSP72-NBD and monochlorobenzyl TCI **43** (2.3  $\mu$ M HSP72-NBD and 20  $\mu$ M TCI **43**) was performed and analysed by IPMS (Figure 4.24).

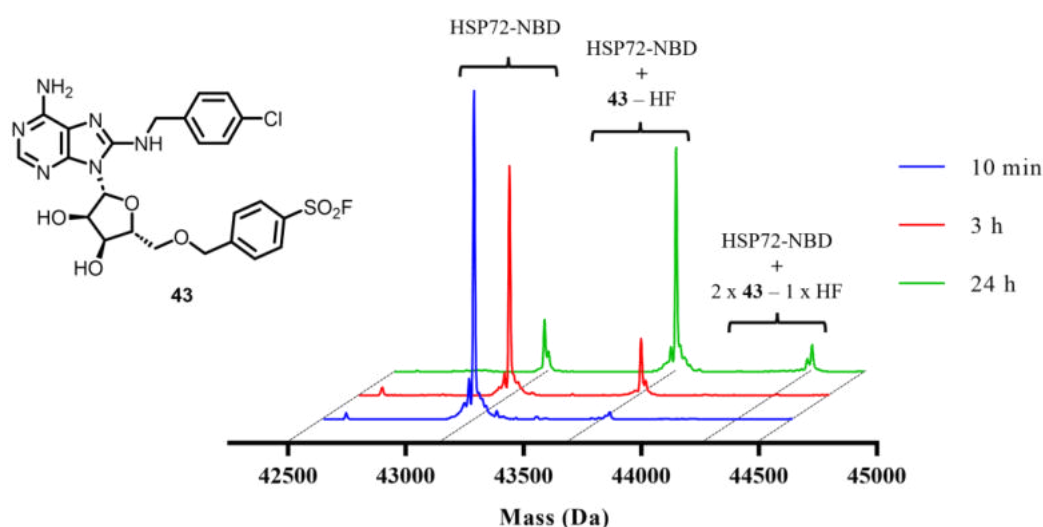


**Figure 4.24** Time-dependent covalent modification of HSP72-NBD with TCI **43** monitored by IPMS. Data plotted in GraphPad Prism 9.

Pleasingly, we observed that over the course of 24 hours the peak of parent HSP72-NBD decreased in intensity. The mass of the major product detected was of HSP72-NBD + TCI **43** – 20 Da, consistent with the expulsion of HF from reaction of the sulfonyl fluoride warhead. It should be noted that the IPMS assay is performed under conditions where the receptor is likely reversibly saturated ( $[I] \gg K_i$ ,  $k_{\text{obs}} = k_{\text{inact}}$ ), therefore the rate of the observed adduct formation was largely dependent on the  $k_{\text{inact}}$ , or the rate of covalent bond

formation within the reversible complex, and not the  $k_{\text{inact}}/K_{\text{I}}$ . A minor peak appeared after 24 hours, with mass consistent with addition of two molecules of TCI **43** but only loss of a single fluorine. It was speculated that this was the result of slow aggregation of labelled HSP72-NBD with the remaining excess TCI **43** in solution. The 8-dichlorobenzyl TCI **128** provided similar results when profiled under these conditions, with the formation of a single covalent adduct being observed (Figure 4.25 A). In contrast, the reversible control **134** demonstrated no covalent adduct over the time course of the experiment as expected (Figure 4.25 B).

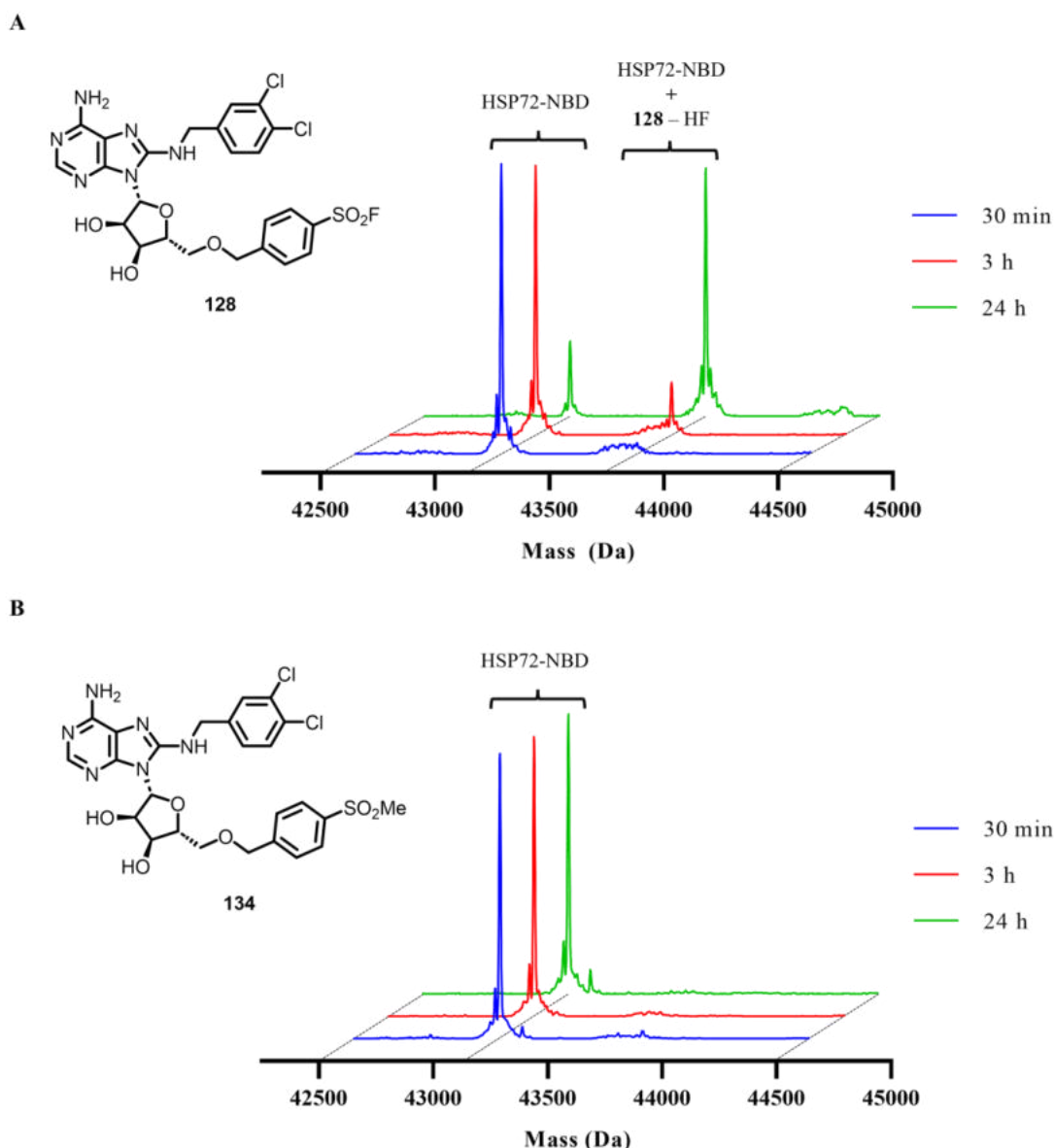


**Figure 4.25** **A** Time-dependent covalent modification of HSP72-NBD (2.3  $\mu$ M) with TCI **128** (20  $\mu$ M) monitored by IPMS. **B** Incubation of HSP72-NBD (2.3  $\mu$ M) with reversible control **134** (20  $\mu$ M) monitored by IPMS. Data plotted in GraphPad Prism 9.

To investigate the specificity of reaction at Lys-56, the sulfonyl fluoride TCI **128** was incubated with K56A HSP72-NBD and although no significant reaction was observed after 3 h, following 24 hour incubation a minor adduct was observed at an apparent slower rate than with WT (wild type) HSP72-NBD (Figure 4.26).



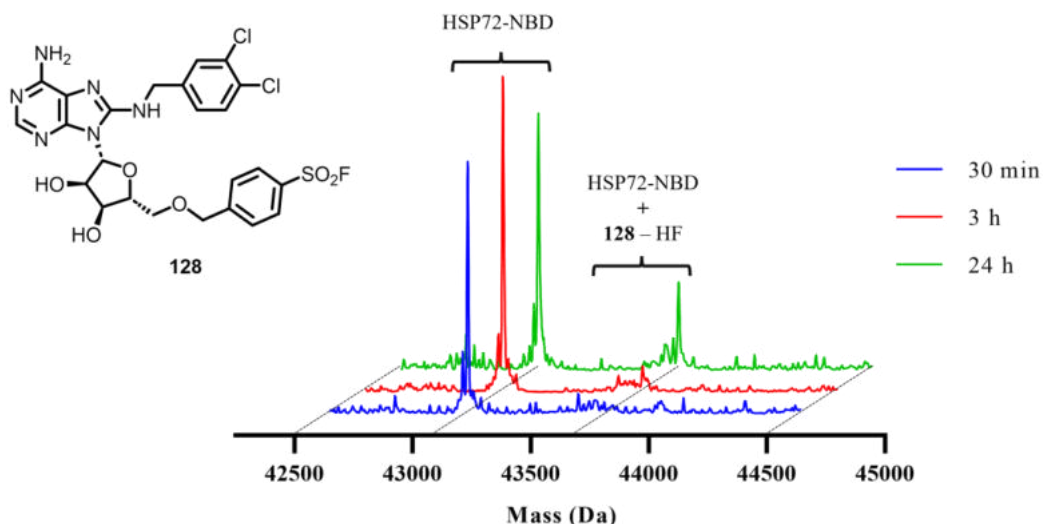


**Figure 4.26** Time-dependent covalent modification of K56A HSP72-NBD (2.3  $\mu$ M) with TCI **128** (20  $\mu$ M) monitored by IPMS. Data plotted in GraphPad Prism 9.

We speculated that a minor reaction pathway that could be resulting from reaction at Tyr-15, which is observed in close proximity to the 5'-*O*-benzyl ring of VER-155008 **37** in the single crystal x-ray structure (PDB: 4IO8) (Figure 4.27).

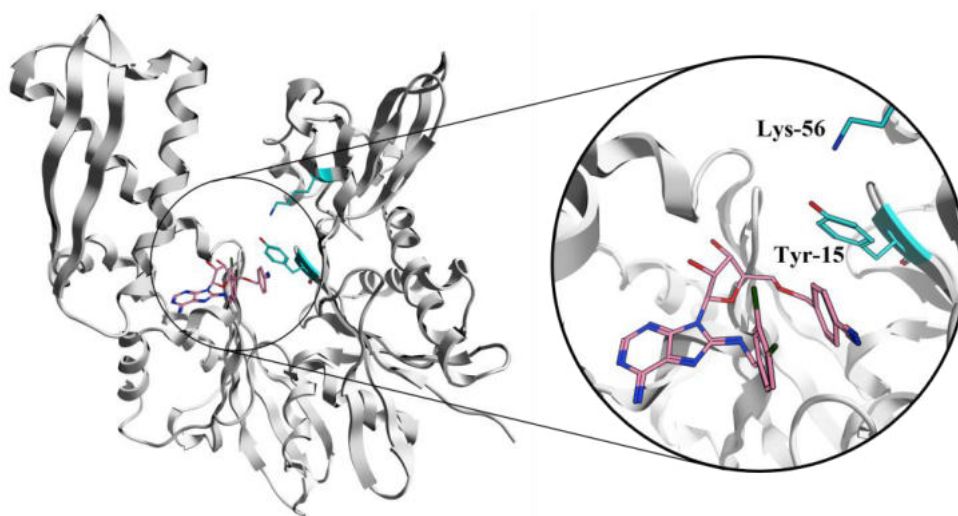


**Figure 4.27** Complex of reversible inhibitor VER-155008 **37** in complex with HSP72-NBD (PDB: 4IO8) illustrates that Tyr-15 exists proximal to 5'-*O*-benzyl ring, making it a potential candidate nucleophile for the minor reaction pathway of TCI **128**.

Sulfonyl fluoride warheads are preceded to react with nucleophilic tyrosine residues<sup>188</sup> in addition to their established lysine reactivity. However, the comparative low

abundance of this adduct, even after 24 hour incubation, suggested that reaction at Lys-56 remained the major pathway.

To confirm that the formation of the minor adduct of **128** with the K56A construct was not as a result of non-specific tagging of the protein, WT-HSP72-NBD was incubated with irreversible negative control *ent-128* (Figure 4.28).

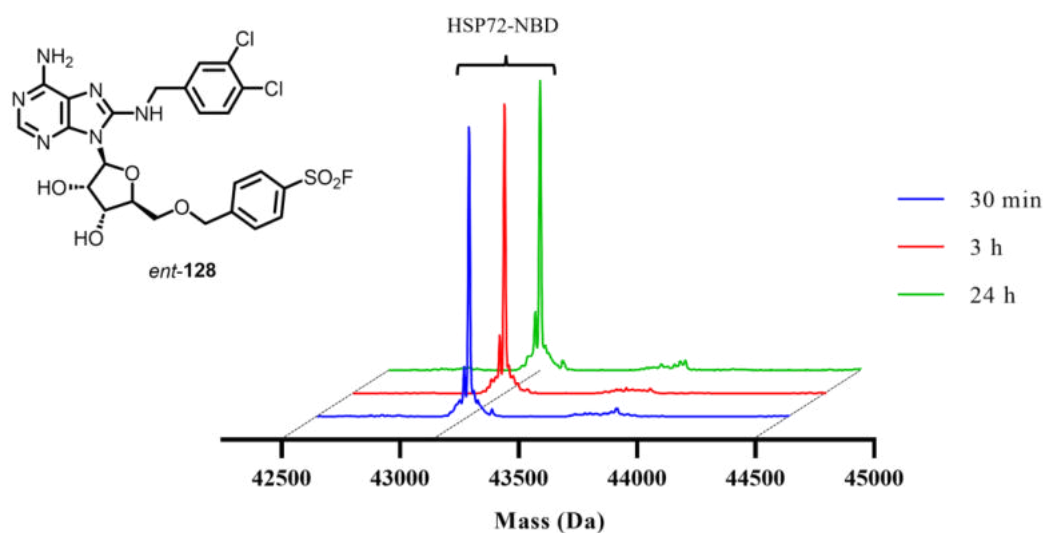


**Figure 4.28** Incubation of WT-HSP72-NBD (2.3  $\mu\text{M}$ ) with irreversible control *ent-128* (20  $\mu\text{M}$ ) monitored by IPMS. Data plotted in GraphPad Prism 9.

No adduct was detected over the time course of the experiment, which indicated that covalent adduct formation in both the wild-type and K56A constructs is specific, consistent with the importance initial reversible binding of the TCI for covalent bond formation.

#### 4.4 Development of Probe for Activity-Based Protein Profiling

##### 4.4.1 Design Hypothesis of Probe for Activity-Based Protein Profiling

Our biochemical FP assay and IPMS data clearly indicated that we had designed and synthesised highly potent HSP72 lysine-TCIs, even though we were unable to quantify the improvement over the second-generation inhibitor, owing to the limits of the resolvable ranges of the assays. A key aim of my project was to develop a probe suitable for use in ABPP from our high affinity chemotype (Section 2) to support the evaluation

of cellular phenotype and HSP70 isoform selectivity. The high activity of the third-generation lysine-TCI **128** was consistent with this aim.

Briefly, the design of an efficient ABPP-probe requires the introduction of a sorting function, such as a clickable terminal alkyne with an appropriate alkyl-linker,<sup>189</sup> to the HSP70 lysine-TCI chemotype, without significantly decreasing potency, to facilitate the enrichment of proteins labelled by the probe in an ABPP experiment.<sup>190</sup> Previously, our group demonstrated that the 6-*N* position of the adenine ring can be successfully modified to access a solvent exposed vector in the development of the FP probe bisaryl-ATTO 488 **148**,<sup>153</sup> which exploits the same solvent-exposed vector as the substrate mimetic ATP-ATTO 488 **108** FP-probe. Analysis of the binding mode of VER-155008 **37** in complex with HSP72-NBD shows that the 6-amino position is positioned near a solvent-exposed cleft at the base of the IIB subdomain (Figure 4.29).

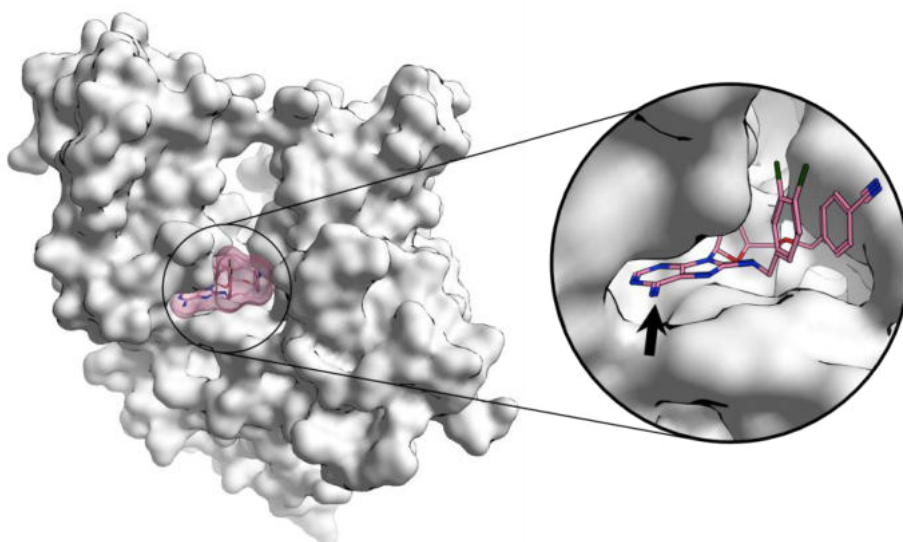


**Figure 4.29** Binding mode of reversible ligand VER-155008 **37** with HSP72-NBD (PDB: 4IO8).<sup>132</sup> Arrow denotes proposed solvent exposed vector from 6-amino position of adenine ring.

By appending the 6-*N*-position of 5'-*O*-linked lysine-TCI **128** with a linker containing a terminal alkyne, we hypothesised that we would obtain a high affinity probe **155** suitable for ABPP experiments in cell lysates and potentially live cancer cells (Figure 4.30).

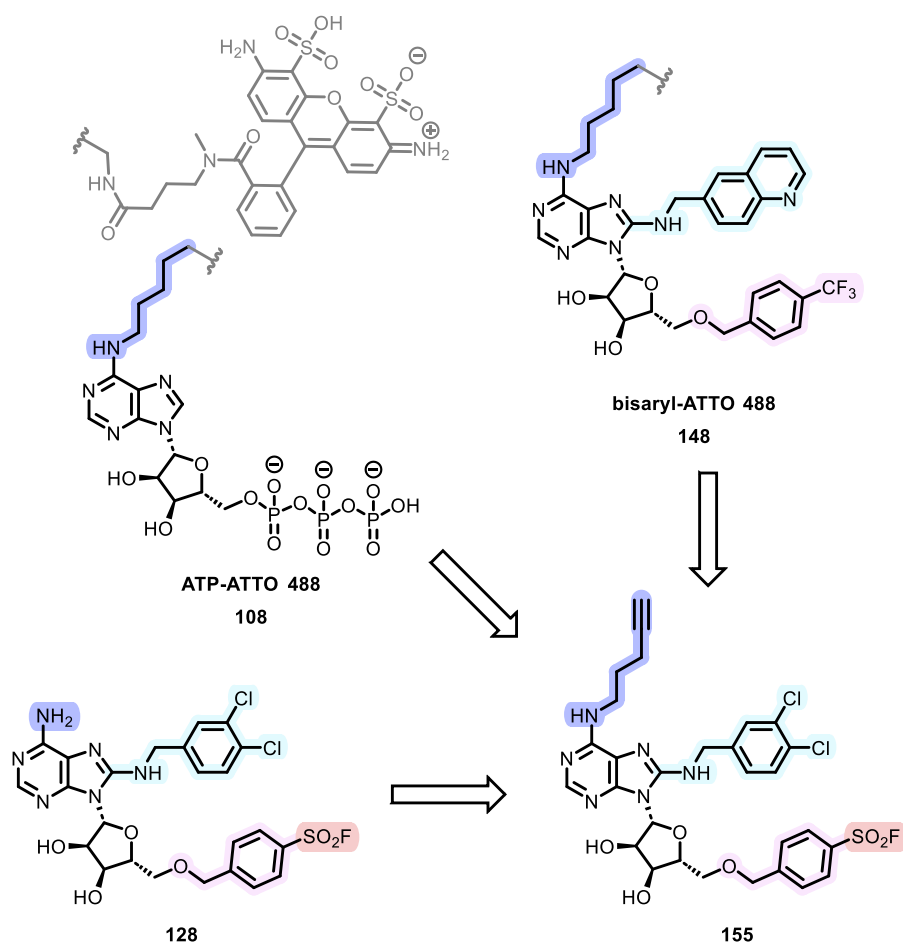
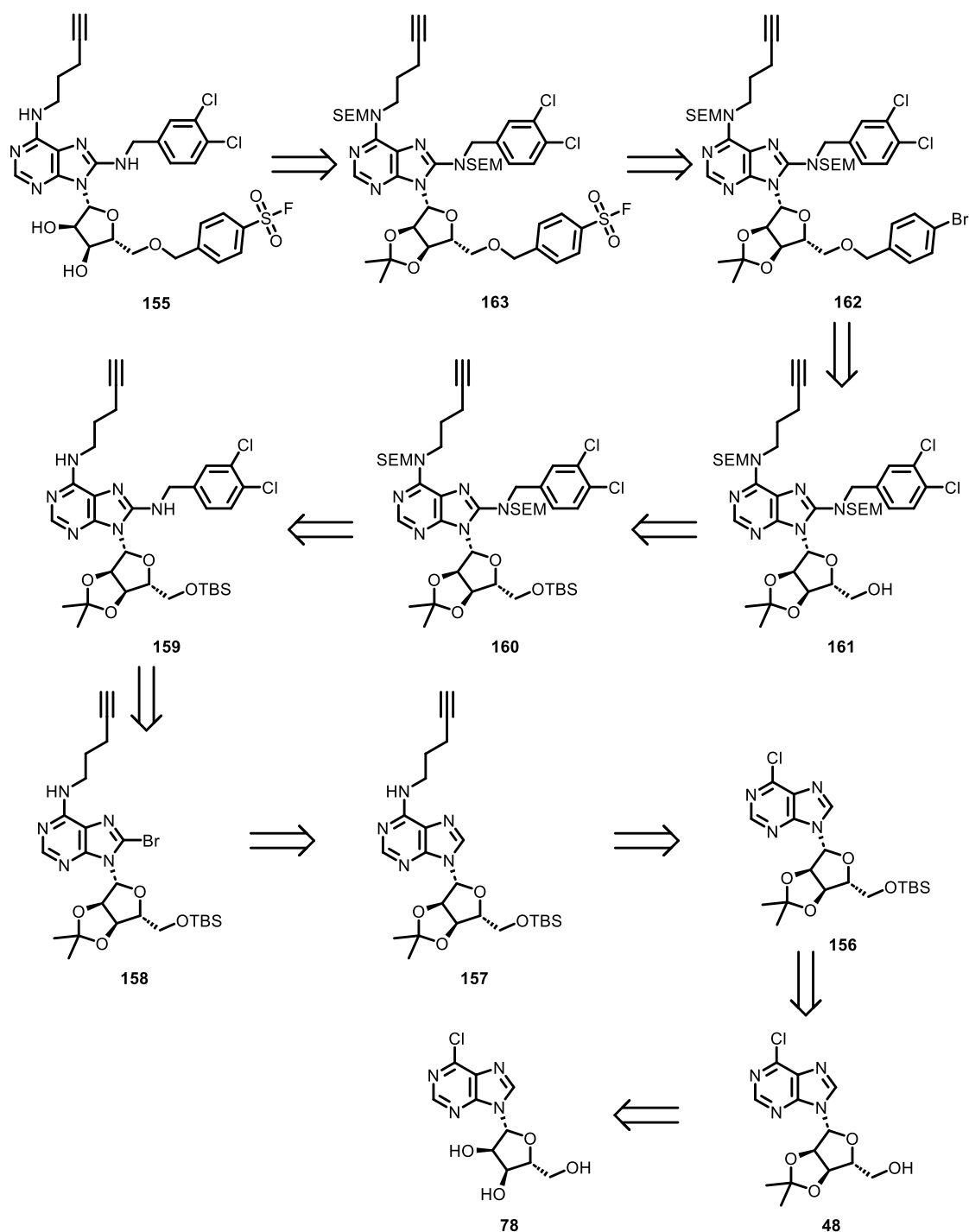


**Figure 4.30** Design strategy for ABPP probe **155**, exploiting solvent exposed vector at the 6-amino position of adenosine, utilised by ATP-ATTO 488 **108** and bisaryl-ATTO 488 **148**, in the modification of high affinity TCI **128**.

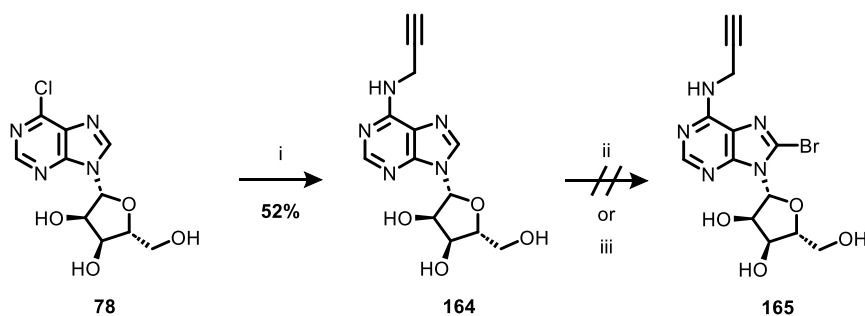
#### 4.4.2 Synthesis of Probe for Activity-Based Protein Profiling

Our aim was to synthesise the ABPP-probe **155** by exploiting an early-stage installation of the alkyne linker *via* an  $S_NAr$  reaction on 6-chloropurine **156**. This would be followed by bromination of the adenine ring of 6-*N*-alkyl **157** to afford **158**. 8-bromo intermediate **158** could then progress through a synthetic route analogous to the synthesis of 8-dichlorobenzyl lysine-TCI **128**, *via*  $S_NAr$  reaction to give **159**, bis-*N*-SEM protection to **160**, *O*-TBS protection to **161**, 5'etherification to **162**, Pd-catalysed fluorosulfonation to **163** and finally a global deprotection to access ABPP probe **155** (Scheme 4.16).



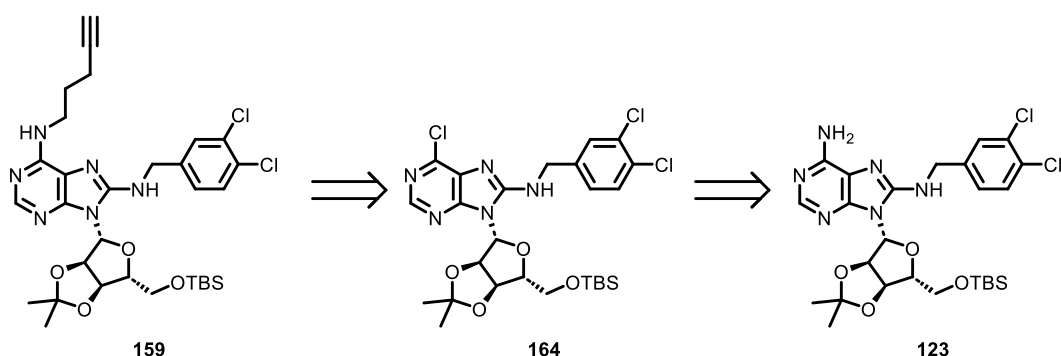
**Scheme 4.16** Proposed retrosynthetic route to ABPP probe **155**.

However, it was uncertain whether the terminal alkyne of 6-*N*-alkylated intermediate **157** could tolerate bromination under the conditions previously required to access 8-bromoadenosine-derived substrates.<sup>145</sup> To investigate the bromination reaction, model substrate **78** was prepared in a single step from 6-chloropurine **164** (Scheme 4.17).



**Scheme 4.17** Synthesis and attempted bromination of model substrate **164**. Reagents and conditions: i) propargyl amine (5 equiv.), EtOH (0.1 M), 60 °C, 18 h; ii) K<sub>2</sub>HPO<sub>4</sub> (3 equiv.), Br<sub>2</sub> (2.5 equiv.), 1,4-dioxane:H<sub>2</sub>O 1:1 (0.13 M), rt, 18 h; iii) NaOAc (5 equiv.), Br<sub>2</sub> (40 equiv.), AcOH (0.25 M), rt, 18 h.

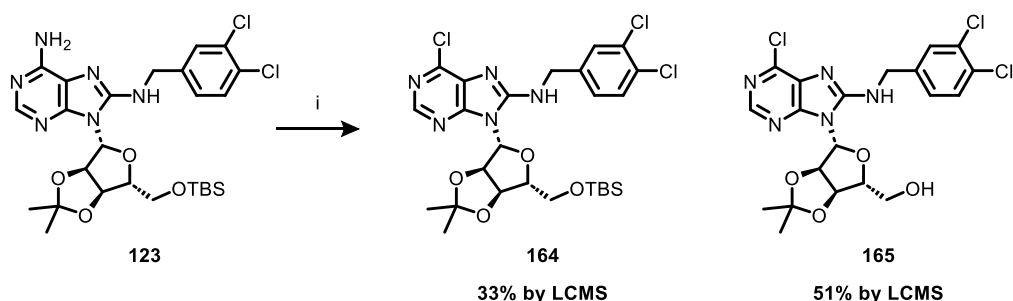
Unfortunately, the attempted bromination of **164**, under both acidic and basic conditions led to the formation of a complex reaction mixture with none of the desired product **165** being observed by LCMS, consistent with polybromination of the starting material **164**. We hypothesised that the terminal alkyne readily underwent bromination under the reaction conditions, owing to its electron rich C-C triple bond. Consequently, the terminal alkyne would have to be installed after the bromination step to circumvent this undesired reactivity. An alternative retrosynthetic strategy was devised to access the key 6-*N*-alkylated intermediate **159**, starting from the previously synthesised intermediate **123**. It was proposed that sequential diazotisation of the 6-amino position of **123** to give 6-chloro **164**, followed by an S<sub>N</sub>Ar reaction with the desired amine would furnish the desired product **159** (Scheme 4.18).



**Scheme 4.18** Alternative retrosynthetic strategy incorporating the late-stage introduction of the alkyne sorting function to access 6-*N*-alkylated intermediate **159**.

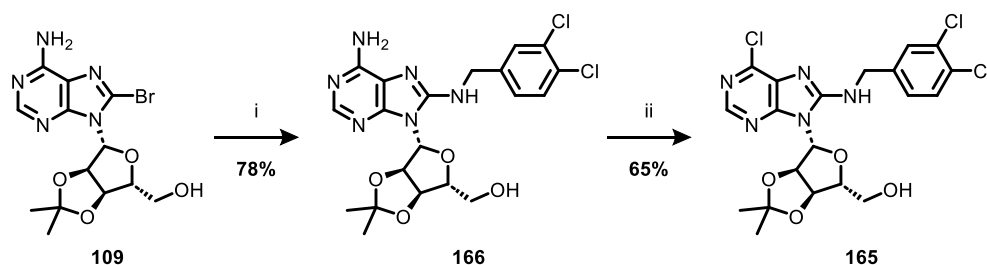
*O*-TBS-protected intermediate **123** was treated with *tert*-butyl nitrite and TMSCl following an adaption of a published procedure.<sup>191</sup> Analysis of the reaction mixture

suggested that the major species observed was the 5'-*O*-TBS-deprotected intermediate **165**, which presumably formed due to the acidity of the reaction mixture. However, both the presence of this side product and a large amount of desired product **164** indicated that the chlorination had been successful (Scheme 4.19).



**Scheme 4.19** Attempted synthesis of intermediate **164**. Reagents and conditions: i) TMSCl (7 equiv.), *t*-BuONO (8 equiv.), CH<sub>2</sub>Cl<sub>2</sub> (0.1 M), rt, 1 h.

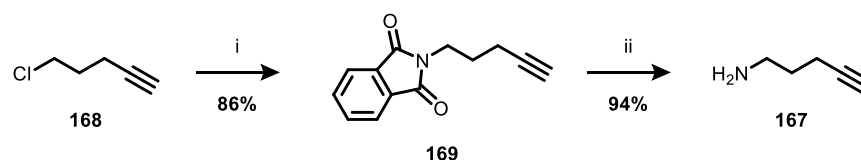
To avoid the formation of the 5'-*O*-TBS-protected and deprotected product mixture, the synthesis was commenced from free 5'-alcohol **109**. The S<sub>N</sub>Ar reaction was carried out at the 8-bromo position of **109** with 3,4-dichlorobenzylamine to afford 8-*N*-benzylated intermediate **166**, which was then successfully transformed into 6-chloro adenosine derivative **165** in moderate yield (Scheme 4.20).



**Scheme 4.20** Synthesis of 6-chloro intermediate **165**. Reagents and conditions: i) 3,4-dichlorobenzylamine (5.1 equiv.), EtOH (0.3 M), 160 °C,  $\mu$ wave, 1 h; ii) TMSCl (7 equiv.), *t*-BuONO (8 equiv.), CH<sub>2</sub>Cl<sub>2</sub> (0.1 M), rt, 3 h.

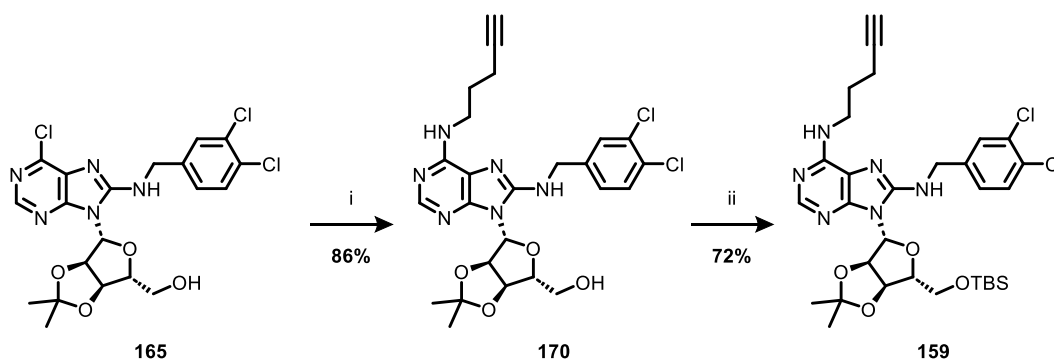
To introduce the alkyne linker group: pent-4-yn-1-amine **167** was accessed in two steps *via* the Gabriel amine synthesis<sup>192</sup> through the reaction of 5-chloro-1-pentyne **168** with phthalimide to give **169**, which then underwent deprotection with hydrazine to afford the desired amine **167** (Scheme 4.21).

#### 4 Characterisation of 5'-Ether-Linked HSP72 Lysine-TCIs



**Scheme 4.21** Gabriel Synthesis of amine **167**. Reagents and conditions: i) phthalimide (1.2 equiv.),  $K_2CO_3$  (1 equiv.), KI (1 mol%), DMF (1 M), 70 °C, 20 h; ii)  $NH_2NH_2 \cdot H_2O$  (13.8 equiv.), EtOH (0.45 M), 70 °C, 2 h.

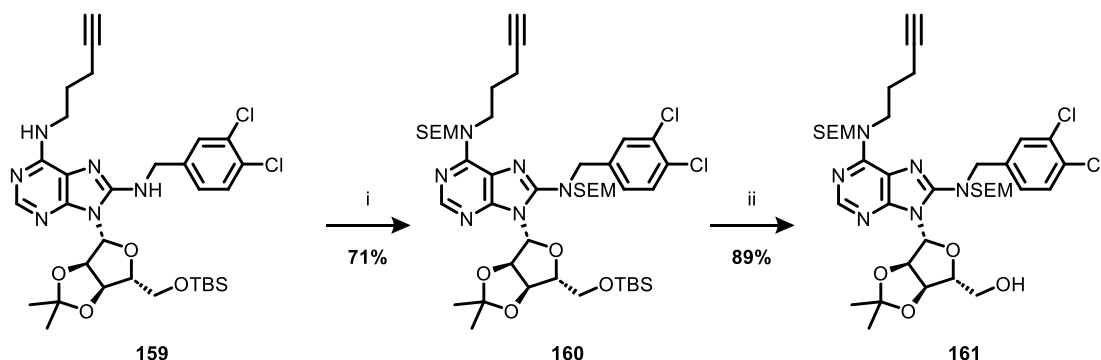
Amine **167** was then reacted with 6-chloro intermediate **165** to yield 6-*N*-alkylated **170**, which was then 5'-*O*-TBS protected to afford key protected intermediate **159** (Scheme 4.22).



**Scheme 4.22** Synthesis of **159**. Reagents and conditions: i) pent-4-yn-1-amine **167** (6 equiv.),  $Et_3N$  (4 equiv.), *n*-BuOH (0.2 M), 100 °C, 20 h; ii) TBSCl (1.2 equiv.), imidazole (2 equiv.), DMF (0.35 M), rt, 20 h.

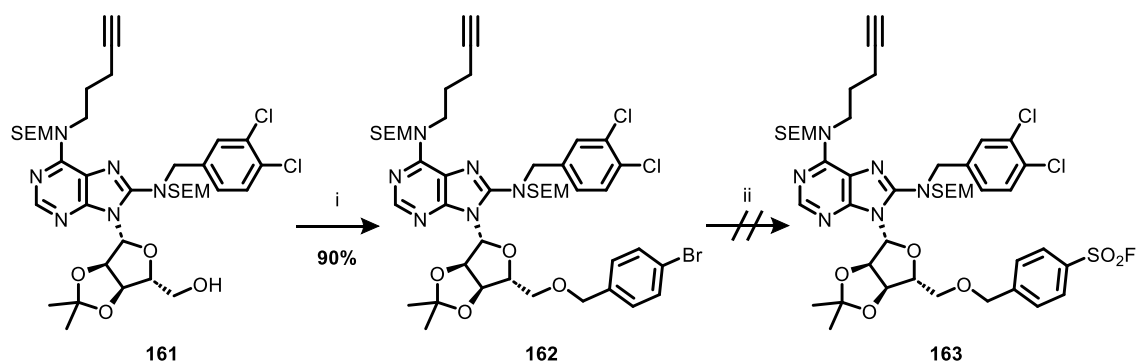
Intermediate **159** was then reacted with SEMCl and DIPEA to afford bis-*N*-SEM protected intermediate **160**, followed by 5'-*O*-TBS-selective deprotection with TBAF to furnish free 5'-alcohol **161** in excellent yield (Scheme 4.23).





**Scheme 4.23** Synthesis of **161**. Reagents and conditions: i) DIPEA (3 equiv.), SEMCl (3 equiv.), CH<sub>2</sub>Cl<sub>2</sub> (0.3 M), reflux, 22 h; ii) TBAF (1.1 equiv.), THF (0.1 M), 0 °C to rt, 24 h.

5'-*O*-benzylation with sodium hydride and 4-bromobenzyl bromide to afford **162** proved highly facile; however, subjecting intermediate **162** to the previously described palladium-catalysed fluorosulfonation conditions<sup>164</sup> resulted in the formation of a complex reaction mixture, with none of the desired product **163** being observed by LCMS or isolated following chromatography (Scheme 4.24).



**Scheme 4.24** Attempted synthesis of **163**. Reagents and conditions: i) NaH (1.2 equiv.), THF (0.5 M), 0 °C, 15 min, then 4-bromobenzyl bromide (2 equiv.), 0 °C to rt, 18 h; ii) DABSO (0.6 equiv.), PdCl<sub>2</sub>(AmPhos)<sub>2</sub> (5 mol%), Et<sub>3</sub>N (3 equiv.), isopropanol (0.27 M), 75 °C, 18 h, then NFSI (1.5 equiv.), rt, 5 h.

We hypothesised that the terminal alkyne of **162** was undergoing side reactions under the palladium-catalysed conditions, potentially *via* oligomerisation through coupling of the aryl bromide and the terminal alkyne.<sup>193</sup> My strategy was therefore to introduce a triisopropylsilyl (TIPS) group as a suitable non-labile, sterically bulky protecting group that would remove the acidic C-H of the terminal alkyne and sterically block palladium-coordination of the C≡C bond (Figure 4.31).

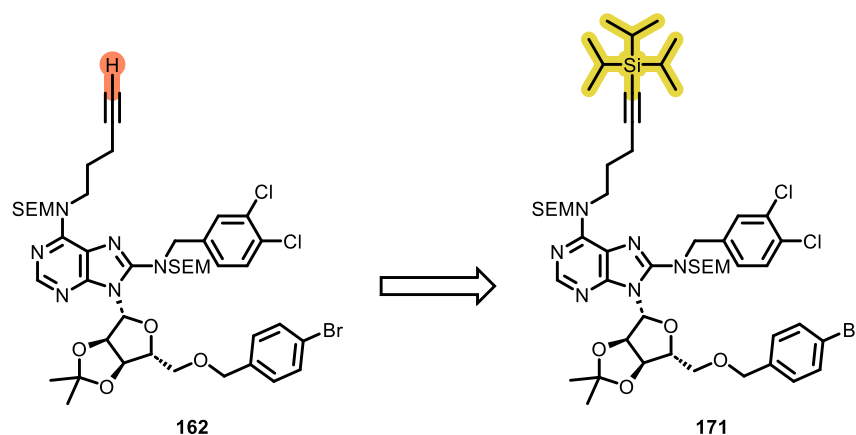
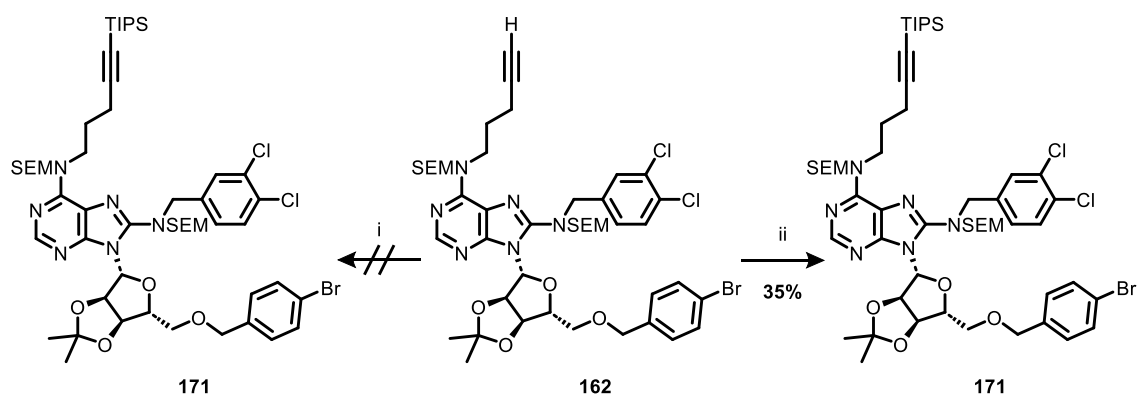


**Figure 4.31** TIPS protection strategy to prevent unwanted reaction of the terminal alkyne under the palladium-catalysed fluorosulfonation conditions.

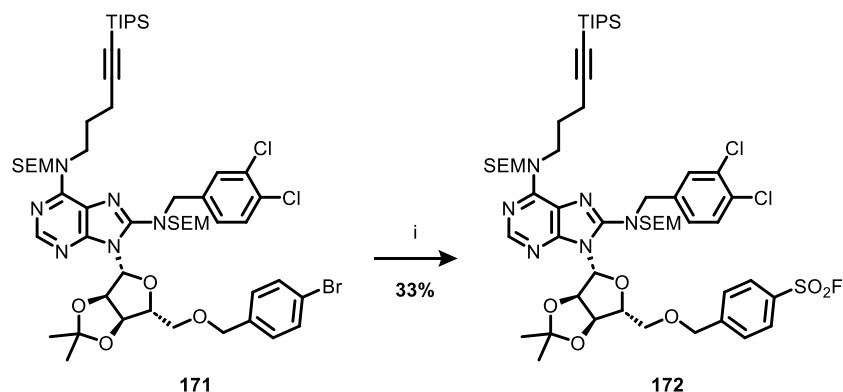
Silyl-protected alkynes are typically accessed through deprotonation of the alkyne C-H with strong base, such as *n*-butyllithium, followed by reaction with the corresponding silyl halide.<sup>160</sup> However, *n*-butyllithium would likely be unsuitable to use with this substrate **162**, owing to competing lithium halogen exchange with the aryl bromide. Lithium hexamethyldisilazane (LiHMDS) is a milder base that has been successfully applied in the TIPS-protection of terminal alkynes.<sup>194,195</sup> However, following treatment of 5'-*O*-benzylated intermediate **162** with LiHMDS and TIPSCl, none of the desired product **171** was observed, with only unreacted starting material being isolated after quenching the reaction mixture (Scheme 4.25).



**Scheme 4.25** Synthesis of TIPS-protected alkyne **171**. Reagents and conditions: i) LiHMDS (1.1 equiv.), THF (0.25 M), -78 °C, 1 h, then TIPSCl (2 equiv.), -78 °C to rt, 18 h; ii) LDA (1.1 equiv.), THF (0.13 M), -78 °C, 1 h, then TIPSOTf (1.2 equiv.), -78 °C, 3 h.

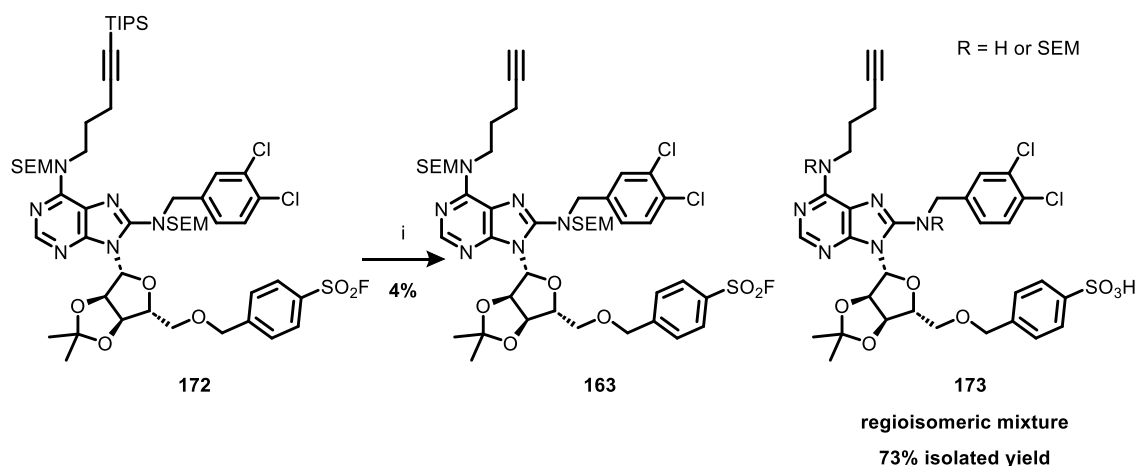
We hypothesised that the LiHMDS was insufficiently basic to deprotonate the substrate **162** (hexamethyldisilazane (HMDS),  $pK_a = 26$  in THF compared to *N,N*-

diisopropylamine,  $pK_a = 36$ ).<sup>196</sup> Switching to the more strongly basic lithium diisopropylamide (LDA) yielded the desired C-TIPS-protected alkyne **171** in low-moderate yield, possibly due to partial SEM cleavage during aqueous workup. Nonetheless, using this procedure sufficient material was accessed to carry forward to the next step. Pleasingly, subjecting C-TIPS-protected substrate **171** to the palladium-catalysed fluorosulfonation conditions yielded the desired sulfonyl fluoride **172** in low-moderate yield (Scheme 4.26).



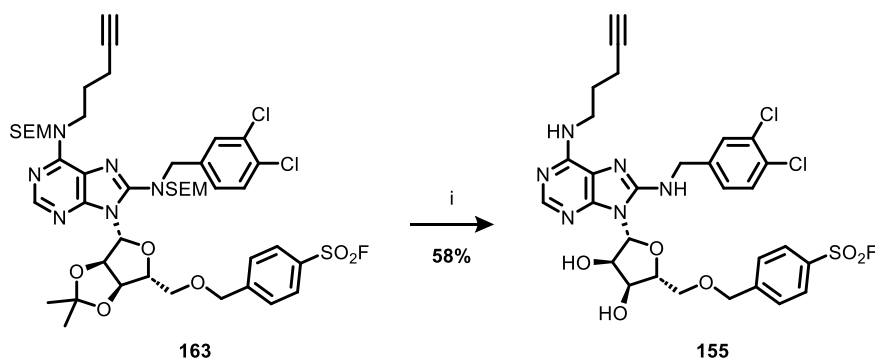
**Scheme 4.26** Synthesis of sulfonyl fluoride **172**. Reagents and conditions: i) DABSO (0.6 equiv.), PdCl<sub>2</sub>(AmPhos)<sub>2</sub> (5 mol%), Et<sub>3</sub>N (3 equiv.), isopropanol (0.27 M), 75 °C, 18 h, then NFSI (1.5 equiv.), rt, 5 h.

It was now critical to remove the C-TIPS-protecting group in a manner that was consistent with base-sensitivity of the sulfonyl-fluoride electrophile. Terminal C-TIPS-alkynes are typically deprotected with basic fluoride sources such as TBAF owing to the acid stability of this group.<sup>160,197</sup> Treatment of sulfonyl fluoride **172** with TBAF led to a poor isolated yield of desired product **163**, with the major side products being an apparent regioisomeric mixture of mono-*N*-SEM deprotected sulfonic acid **173** (Scheme 4.27).



**Scheme 4.27** Synthesis of TIPS-deprotected intermediate **163**. Reagents and conditions: i) TBAF (2 equiv.), THF (0.1 M), 0 °C to rt, 48 h.

Nevertheless, sufficient material could be isolated from this very low yield TBAF-mediated deprotection step such that sulfonyl fluoride **163** could then be deprotected under the previously described mild acidic conditions, to afford the desired ABPP-probe **155** in moderate yield (Scheme 4.28).



**Scheme 4.28** Synthesis of ABPP probe **155**. Reagents and conditions: i) TFA:H<sub>2</sub>O 5:2 (0.1 M), rt, 2 h.

#### 4.4.3 Characterisation of Probe for Activity-Based Protein Profiling

With the desired 6-*N*-alkylated probe **155** in hand, the next task was to characterise it and confirm its biochemical potency prior to its application in proteomics experiments. Profiling **155** via the IPMS assay confirmed the time-dependent formation of a covalent adduct (Figure 4.32).

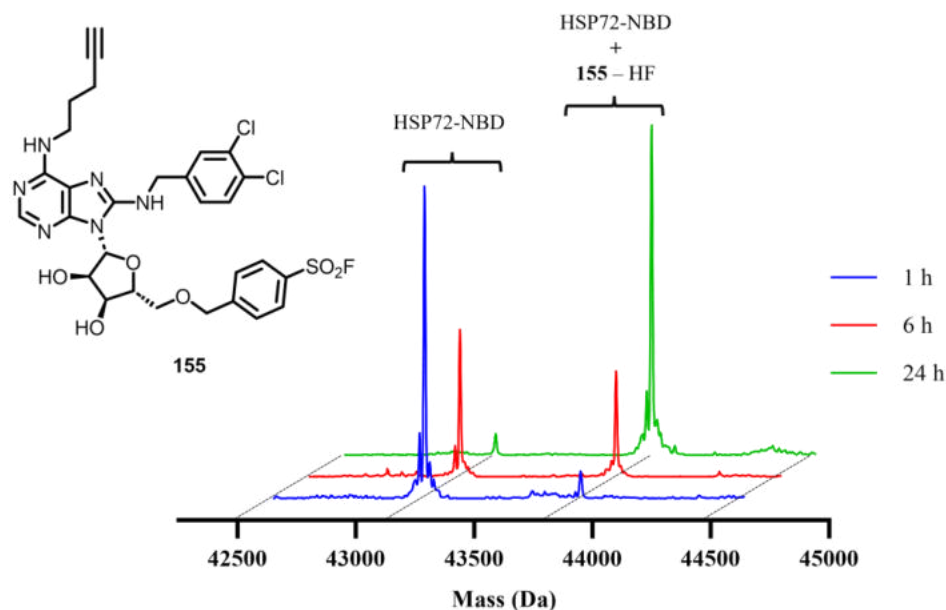
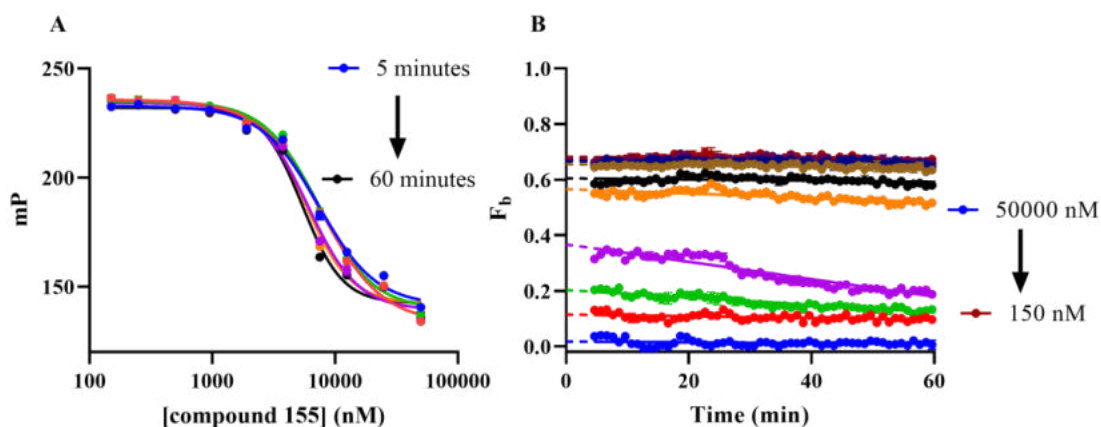


**Figure 4.32** Time-dependent covalent modification of WT HSP72-NBD (2.3  $\mu$ M) with ABPP probe **155** (20  $\mu$ M) monitored by IPMS. Data plotted in GraphPad Prism 9.

However, profiling probe **155** in the TDFP assay unfortunately showed that the compound displayed minimal time-dependence over the assay time course (Figure 4.33).



Compound	$pK_i$	$K_i$ (nM)
6-N-alkyl $SO_2F$ <b>155</b>	$5.9 \pm 0.06$	1300

**Figure 4.33** **A** Profiling of ABPP probe **155** in the TDFP assay with HSP72-NBD and bisaryl-ATTO 488 **148**. [HSP72-NBD] selected so  $F_b = 0.7$ , measurements taken in triplicate every minute for 60 minutes and plotted on same axes. **B** Plot of calculated  $F_b$  values against time, data plotted in GraphPad Prism 9.  $pK_i$  values determined after 60 minutes incubation and are quoted as mean  $\pm$  SEM of three independent experiments.

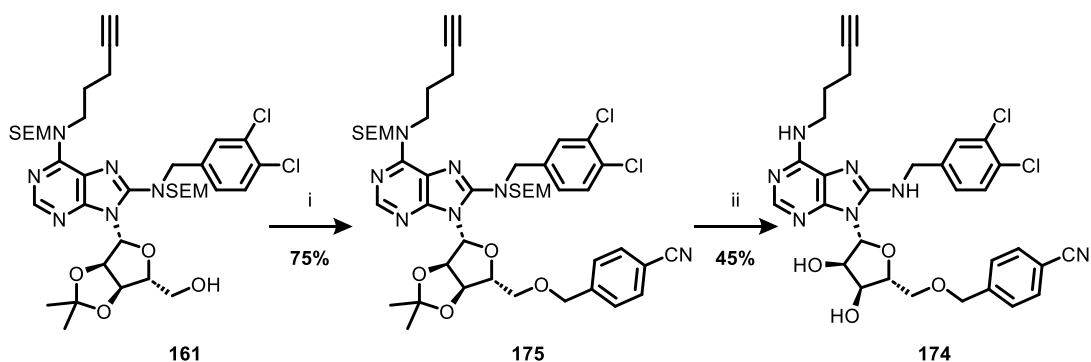
Our analysis of these data suggested that the introduction of the 6-*N*-alkyl group had unexpectedly significantly diminished the reversible affinity of ABPP-probe **155** ( $K_i = 1.3 \mu\text{M}$ ) compared to the corresponding 6- $\text{NH}_2$  MMP **128** (initial  $K_i < 80 \text{ nM}$ ).

The IPMS assay is performed under conditions where the receptor is likely reversibly saturated ( $[I] \gg K_i$ ,  $k_{\text{obs}} = k_{\text{inact}}$ ), thus the IPMS data suggested that the  $k_{\text{inact}}$  of the chemotype had been maintained after introducing the 6-*N*-alkyl group. However, the TDFP assay quantifies rate of change of  $F_b$  under non-saturating conditions, which is dependent on both the  $K_i$  and  $k_{\text{inact}}$  (Equation 4.9).

$$\text{Rate of change of } F_b \propto k_{\text{obs}} = \frac{k_{\text{inact}}[I]}{K_i + [I]}$$

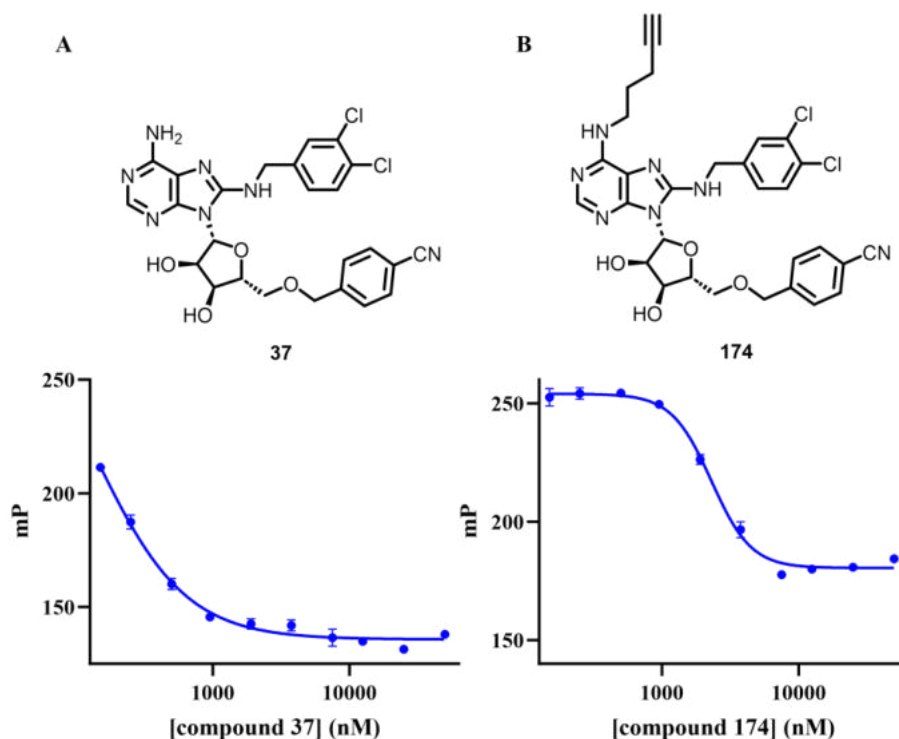
**Equation 4.9** Proportionality relationship between the rate of change of bound fraction and  $k_{\text{obs}}$ .

Therefore, the FP data indicates that the introduction of the 6-*N*-alkyl linker leads to an increase in  $K_i$  and therefore a decrease in  $k_{\text{inact}}/K_i$ , resulting in an effective reversible MoA over the TDFP assay timecourse. To confirm that introduction of the 6-*N*-pentyne results in a loss of reversible affinity for this chemotype, the analogous 6-*N*-alkylated **174**, which is a MMP to VER-155008 **37**, was prepared in two steps from previously synthesised intermediate **161** (Scheme 4.29). First, free alcohol **161** was reacted with 4-cyanobenzyl bromide and sodium hydride to yield 5'-*O*-benzylated intermediate **175**. This intermediate was then deprotected with TFA:water to afford the final compound **174** in moderate yield.



**Scheme 4.29** Synthesis of **174**. Reagents and conditions: i) NaH (1.2 equiv.), THF (0.5 M), 0 °C, 15 min, then 4-cyanobenzyl bromide (2 equiv.), 0 °C to rt, 18 h; ii) TFA:H<sub>2</sub>O 5:2 (0.1 M), rt, 2 h.

Profiling the reversible MMP **174** by fluorescence polarisation indicated that introduction of the alkyne linker resulted in a >8-fold drop off in reversible affinity (Figure 4.34), consistent with the SAR observed for sulfonyl fluorides **128** and **155**.



Compound	p <i>K</i> <sub>i</sub>	<i>K</i> <sub>i</sub> (nM)
6-NH <sub>2</sub> <b>37</b>	>7	<80
6-N-alkyl <b>174</b>	6.2 ± 0.06	630

**Figure 4.34** Measurement of *K*<sub>i</sub> for reversible analogues with HSP72-NBD and bisaryl-ATTO 488 **148**. [HSP72-NBD] selected so *F*<sub>b</sub> = 0.7. Measurements taken in triplicate and the mean and standard error plotted using GraphPad Prism 9. p*K*<sub>i</sub> values are quoted as mean ± SEM of three independent experiments. **A** IC<sub>50</sub> curve for VER-155008 **37**. **B** IC<sub>50</sub> curve for 6-*N*-alkylated reversible MMP **174**.

Together, these data suggested that 6-*N*-alkylation of TCI **128** to give probe **155** resulted in a significant drop off in reversible affinity and therefore the overall potency through the second order rate constant, *k*<sub>inact</sub>/*K*<sub>i</sub>, precluding the use of probe **155** in ABPP experiments. This is contrasted by the high affinity exhibited by the 6-*N*-functionalised FP probes ATP-ATTO 488 **108** and bisaryl-ATTO 488 **148**, which may suggest that the extended linker and fluorophore contribute to their high reversible affinity. Because of the complex SAR and challenging synthesis observed for this chemotype, my efforts to generate a HSP70 ABPP probe were concluded.

## 4.5 Conclusions

This chapter has detailed the biochemical characterisation of 5'-ether-linked lysine-TCIs of HSP72. Profiling of this class of TCIs with two FP probes showed that they exhibit reversible affinities at the resolvable limit for the assay (initial  $K_i < 80$  nM), which was corroborated by corresponding reversible controls. IPMS experiments confirmed the selective formation of a single covalent adduct within the reversible complex, with reaction at Lys-56 as the major pathway.

Finally, with this highly potent class of TCIs in hand, 6-*N*-alkyne-substituted **155** was designed and synthesised for use in ABPP experiments. The synthesis proved non-trivial, owing to side reactions at the terminal alkyne; however, development of a TIPS-protection strategy furnished the desired probe **155** in 12 linear synthetic steps. Unfortunately, biochemical characterisation of this chemotype indicated that inclusion of the alkyne linker results in a significantly diminished reversible affinity such that the probe **155** was not suitable for use in further studies.



## 5 Reactivity-Based Profiling of HSP72 Lysine-TCIs

## 5 Reactivity-Based Profiling of HSP72 Lysine-TCIs

### 5.1 Introduction

The newly synthesised third-generation ether-linked lysine-TCIs had clearly demonstrated considerable improvements in reversible affinity in a manner consistent with the switch from their ester-linked MMPs, progressing us closer to a cell-active HSP70 probe. Even though all covalent biochemical assays have their limitations in characterising inhibition,<sup>146</sup> the TDFP assay had been critical in our development of HSP70 covalent inhibitors from the initial serendipitous discovery, allowing us to determine the kinetic parameters of TCIs that drive occupancy,  $k_{\text{inact}}/K_{\text{I}}$ ,  $K_{\text{I}}$  and  $k_{\text{inact}}$ . Unfortunately, owing to the limited assay window it had been impossible to calculate these parameters for the most potent compounds. Targeting nucleophilic lysine residues and other nucleophilic residues as alternatives to cysteine remains in its infancy.<sup>98</sup> Understanding the impact of electronics and sterics on the electrophile is critical to the optimisation of lysine-TCIs.

As discussed in Section 1.2.2,  $k_{\text{inact}}$  is the pseudo-first order rate constant that describes the irreversible formation of the covalent bond when the binding is saturated, and is modulated by multiple factors, including the warhead intrinsic reactivity.<sup>198</sup> A key aspect of our design strategy towards the third-generation lysine-TCIs had been to reduce intrinsic reactivity of the electrophile, as a higher intrinsic reactivity necessarily leads to increased off-target toxicity arising from non-specific labelling.<sup>72</sup> A report by Grimster et al. detailed the use of Hammett  $\sigma_{\text{m}}$  and  $\sigma_{\text{p}}$  values to investigate the effects of *meta* and *para* substituents on the intrinsic reactivity of aryl sulfonyl fluorides.<sup>147</sup> The authors demonstrated that installing electron withdrawing groups in the *para* position of aryl sulfonyl fluorides correlates strongly with increased warhead intrinsic reactivity. The measured Hammett  $\sigma_{\text{p}}$  values are  $\sigma_{\text{p}} = 0.45$  for a methyl ester and  $\sigma_{\text{p}} = 0.01$  for a methyl benzylic ether,<sup>148</sup> therefore replacing the electron-withdrawing ester moiety of lysine-TCI **44** for an ether moiety should also result in increased electron density at the *para* position of the 5'-benzyl ring, decreasing the intrinsic reactivity of the covalent warhead (Figure 5.1).

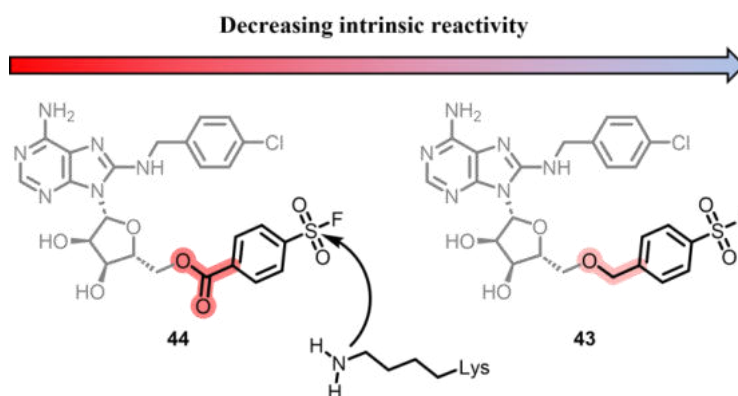


**Figure 5.1** Intrinsic reactivity of sulfonyl fluoride warhead is predicted to decrease with the replacement of *para* electron withdrawing ester for an ether moiety.

However, owing to the high affinity of our compounds, we were unable to assess if this proposed decrease in intrinsic reactivity resulted in a concomitant decrease of the  $k_{\text{inact}}$ . Therefore, our aim was to design a set of moderate reversible affinity HSP70 lysine-TCIs that would be compatible with the available HSP70 assays, allowing us to determine the change in  $k_{\text{inact}}$  following the linker switch from an ester to an ether. We envisaged that substitution of the 8-*N*-benzyl group of **128**, with a group that modulated the reversible affinity of the scaffold, would enable us to resolve the  $k_{\text{inact}}$  whilst retaining the 5'-ether-linked adenosine core that is key for the binding conformation and covalent MoA of this chemotype (Figure 5.2).

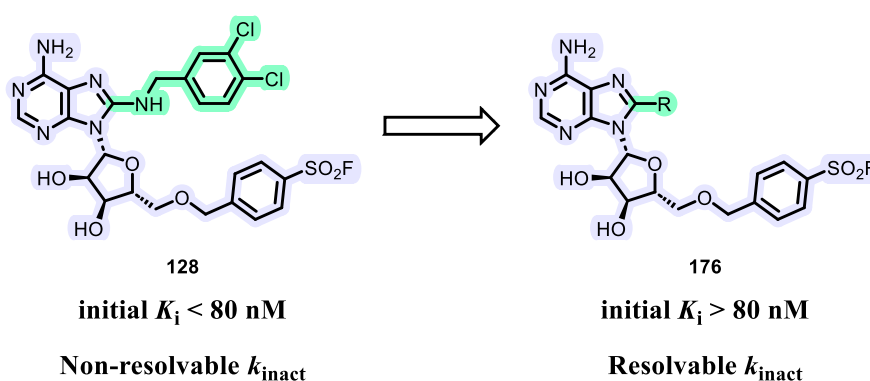


**Figure 5.2** Principle of generating moderate reversible affinity adenosine-derived 5'-ether-linked lysine-TCI **176** from high reversible affinity **128**, R = functional group that confers diminished reversible affinity compared to 8-*N*-benzyl.

## 5.2 Moderate Reversible Affinity 5'-Ether-Linked HSP72 Lysine-TCIs

### 5.2.1 Design of Moderate Reversible Affinity Compounds

The contribution of the 8-*N*-benzyl moiety to the reversible affinity of the chemotype of the adenosine-derived inhibitor **128** is two-fold; firstly, analysis of the binding mode of related high affinity ligand VER-155008 **37** reveals that the lipophilic benzyl group is positioned in a solvent-exposed region of the binding site, desolvating the pocket and facilitating the multitude of hydrogen bonding interactions between the protein and the adenosine core (Figure 5.3). The benzyl group also makes a  $\pi$ -stacking interaction with Arg-272, which contributes to the affinity.<sup>134</sup>

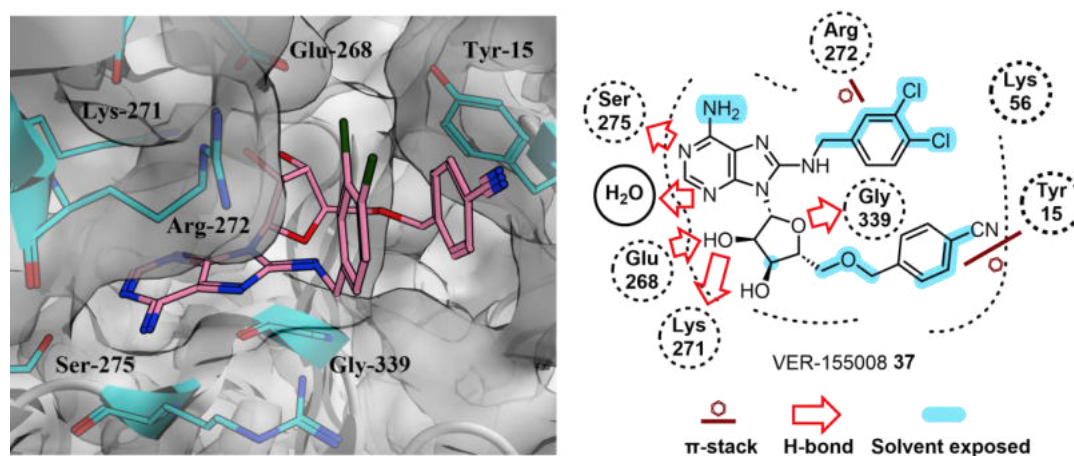


**Figure 5.3** Binding mode of high affinity ligand VER-155008 **37** (PDB: 4IO8) showing hydrogen bonds,  $\pi$ -stacking and solvent-exposed motifs.

Secondly, Cheeseman et al. speculated that the 8-NH group functions as a hydrogen bond donor to the ribose ether oxygen, which stabilises the gauche conformation of adenosine accessed through rotation around the glycosidic N9-C1' bond, and therefore lowers the energy required for the initial binding event.<sup>142</sup> To probe the importance of the 8-*N*-benzyl group to the affinity, the authors analysed adenosine **35** and reversible MMP 8-*N*-benzyl **36** by SPR, demonstrating that this substitution resulted in a 31-fold decrease in reversible affinity (Figure 5.4).<sup>142</sup>

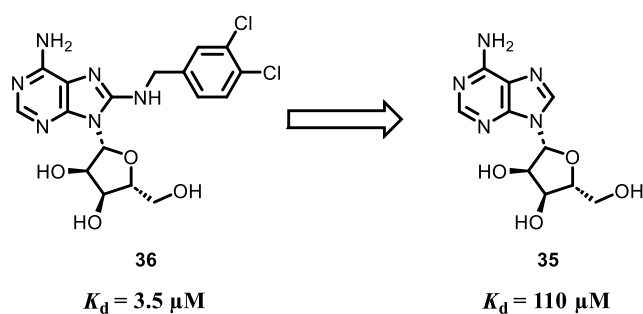


**Figure 5.4** Removal of 8-*N*-benzyl moiety results in large drop off in reversible affinity.<sup>142</sup>  $K_d$  values determined by SPR.<sup>142</sup>

We therefore envisaged that removal of the 8-*N*-benzyl moiety from our high reversible affinity chemotype (initial  $K_i < 80$  nM) would result in a comparable loss of reversible affinity, furnishing TCI **101** with a  $K_i$  within the limit of assay detection (Figure 5.5). 8-*H* TCI **101** had been prepared previously in the development of a synthetic route to access 5'-ether-linked HSP72 lysine-TCIs (Section 3.3.1).

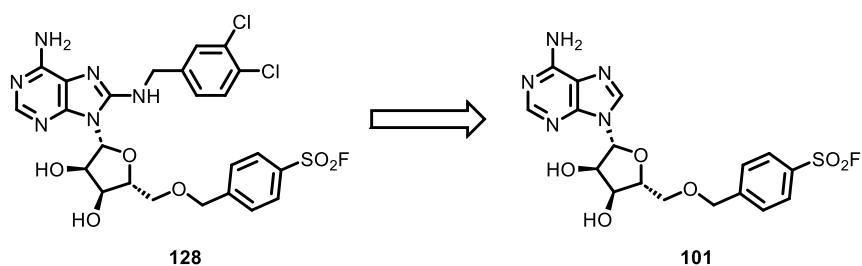


**Figure 5.5** Design of 8-*H* TCI **101** from high affinity TCI **128**.

8-*H* TCI **101** was profiled in the TDFP assay, demonstrating limited dose-dependent displacement of the FP probe (Figure 5.6 A). Analysis of the  $F_b$  against time showed that the probe bound fraction was decreasing in a time-dependent manner consistent with covalent bond formation within the ATP binding site (Figure 5.6 B). However, extrapolation of the bound fraction to  $t = 0$  and plotting these values against inhibitor concentration indicated that TCI **101** was exhibiting poor reversible occupancy under the assay conditions (initial  $IC_{50} > 200 \mu\text{M}$ ) consistent with weak reversible affinity (initial  $K_i > 30 \mu\text{M}$ ) (Figure 5.6 C).

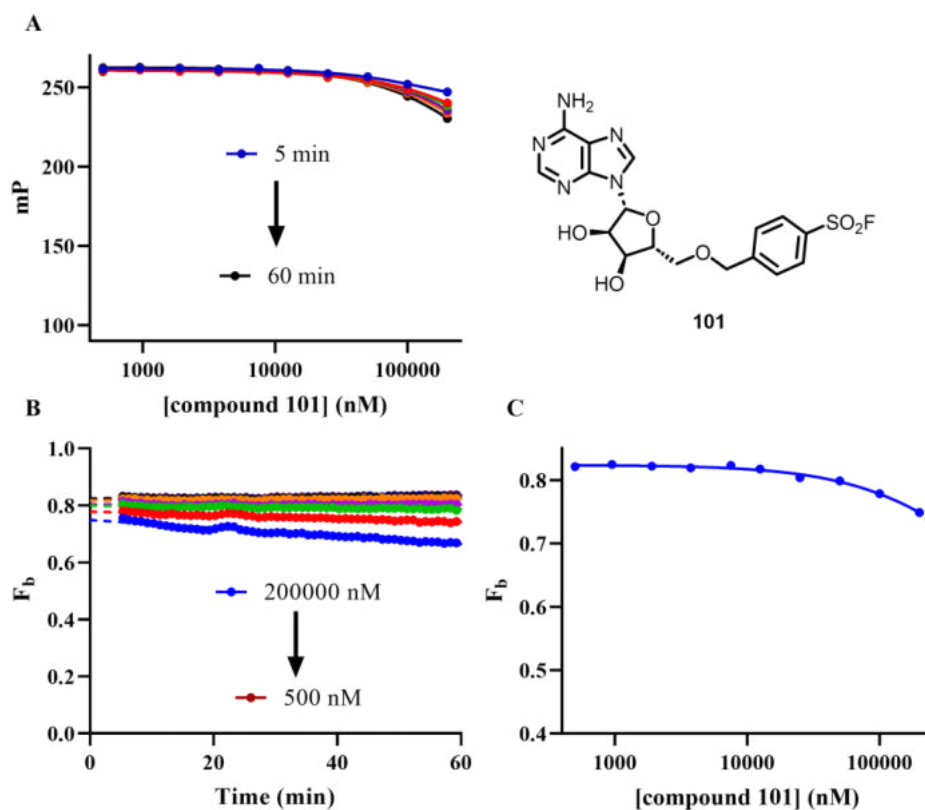
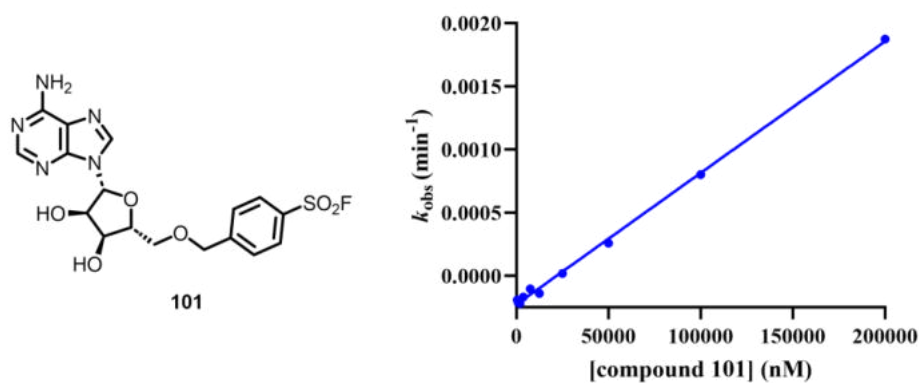


**Figure 5.6** A Profiling of TCI **101** in the TDFP assay with HSP72-NBD and ATP-ATTO 488 **108**. [HSP72-NBD] selected so  $F_b = 0.85$ , measurements taken in triplicate every minute for 60 minutes and plotted on same axes. **B** Plot of calculated  $F_b$  values against time, y-intercepts calculated using simple linear regression (GraphPad Prism 9). **C** Plot of initial  $F_b$  against [I] to determine initial  $IC_{50}$  (log(inhibitor) vs. response – variable slope (four parameters), GraphPad Prism 9).

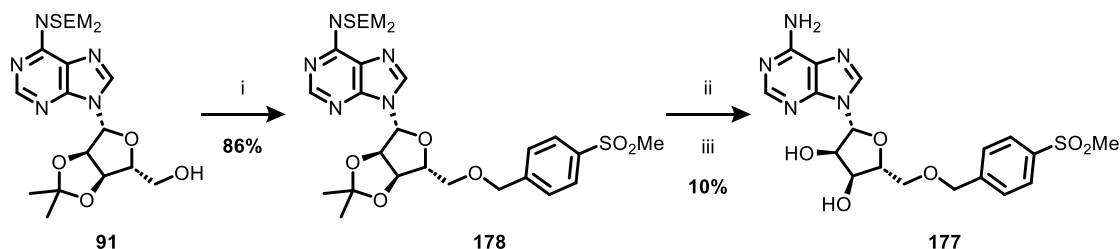
Analysis of the  $F_b$  against time data for 8-*H* TCI **101** enabled the determination of  $k_{inact}/K_I$ ; however, owing to the initial  $IC_{50}$  value exceeding the top concentration of inhibitor tested (200  $\mu$ M), the  $k_{inact}$  could not be precisely calculated (Figure 5.7)



Compound	Initial $K_i$ ( $\mu\text{M}$ )	$k_{\text{inact}}/K_i$ ( $\text{M}^{-1}\text{s}^{-1}$ ) <sup>a</sup>	$k_{\text{inact}}$ ( $\text{s}^{-1}$ )	$t_{1/2}^{\infty}$ (h)
8- <i>H</i> <b>101</b>	>30	$0.17 \pm 0.01$	$> 5.2 \times 10^{-6}$	< 37

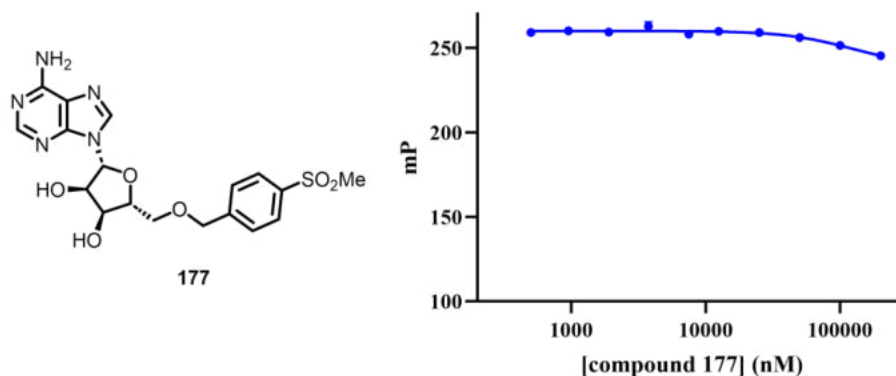
**Figure 5.7** Plot of  $k_{\text{obs}}$  against inhibitor concentration (simple linear regression, GraphPad Prism 9) to determine  $k_{\text{inact}}/K_i$ . <sup>a</sup> $k_{\text{inact}}/K_i$  values are quoted as mean  $\pm$  SEM of three independent experiments.

Unfortunately, these data indicated that substitution of the 8-*N*-benzyl moiety for 8-*H* results in a >375-fold increase in initial  $K_i$ , which would preclude the evaluation of  $k_{\text{inact}}$  for any subsequent 8-*H* analogues. To corroborate the loss of reversible affinity for this chemotype, reversible MMP **177** was prepared from previously synthesised bis-6-*N*-SEM intermediate **91**. Williamson etherification of **91** with 4-(methylsulfonyl)benzyl bromide afforded ether **178**, which was then transformed to the desired deprotected product **177** *via* sequential treatment with TFA:water, followed by dilute aqueous ammonia (Scheme 5.1). The low yield observed in the reaction likely arose from the challenge in fully cleaving the SEM groups owing to the highly electron deficient adenine ring; this was also observed in the synthesis of 8-*H* sulfonyl fluoride **101** (Section 3.3.1).



**Scheme 5.1** Synthesis of 8-*H* reversible MMP **177**. Reagents and conditions: i) NaH (1.2 equiv.), THF (0.5 M), 0 °C, 15 min, then 4-(methylsulfonyl)benzyl bromide (2 equiv.), 0 °C to rt, 18 h. ii) TFA:H<sub>2</sub>O 5:2 (0.1 M), rt, 1 h; iii) 0.07 N NH<sub>3</sub> in CH<sub>2</sub>Cl<sub>2</sub>:THF 1:1 (0.01 M), water, rt, 24 h.

In a similar manner to 8-*H* sulfonyl fluoride **101**, profiling the 8-*H* reversible MMP **177** using the FP-assay showed that this compound also possesses only very weak reversible affinity ( $K_i > 30 \mu\text{M}$ ), with a  $\text{IC}_{50}$  value beyond the top concentration of inhibitor screened ( $\text{IC}_{50} > 200 \mu\text{M}$ ) (Figure 5.8).



Compound	$\text{p}K_i$	$K_i (\mu\text{M})$
8- <i>H</i> $\text{SO}_2\text{Me}$ <b>177</b>	< 4.5	> 30

**Figure 5.8** Measurement of  $K_i$  for reversible MMP **177** with HSP72-NBD and ATP-ATTO 488 **108**. [HSP72-NBD] selected so  $F_b = 0.85$ . Measurements taken in triplicate and the mean and standard error plotted using GraphPad Prism 9.

Together, these data indicated that full removal of the 8-*N*-benzyl moiety of TCI **128** results in an unacceptable decrease in reversible affinity of the scaffold, preventing the evaluation of  $k_{\text{inact}}$ . We hypothesised that substitution of the water-displacing lipophilic benzyl functionality, whilst retaining the key hydrogen bonding 8-NH, would result in a more modest decrease in the reversible affinity furnishing an initial  $K_i$  within the assay window. A re-examination of the SAR for this scaffold indicated that substitution of the 8-*N*-benzyl moiety for an 8-*N*-methyl group in the 5'-OH series resulted in a 5-fold decrease in the reversible affinity when measured using SPR (Figure 5.9).<sup>142</sup>



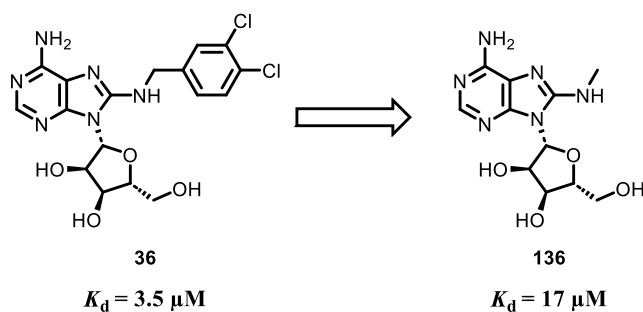


**Figure 5.9** Substitution of the 8-*N*-benzyl moiety for a 8-*N*-methyl group results in a modest decrease in potency.<sup>142</sup>  $K_d$  values determined by SPR.

Our strategy was therefore to synthesise a series of 5'-ether-linked TCIs with 8-*N*-alkyl substituents, with the aim of generating a set of moderate reversible binding compounds to enable the evaluation of  $k_{\text{inact}}$  for the ether-linked sulfonyl fluoride chemotype. Three *N*-alkyl groups were selected to investigate this hypothesis, methyl **179**, ethyl **180** and isopropyl **181** (Figure 5.10).

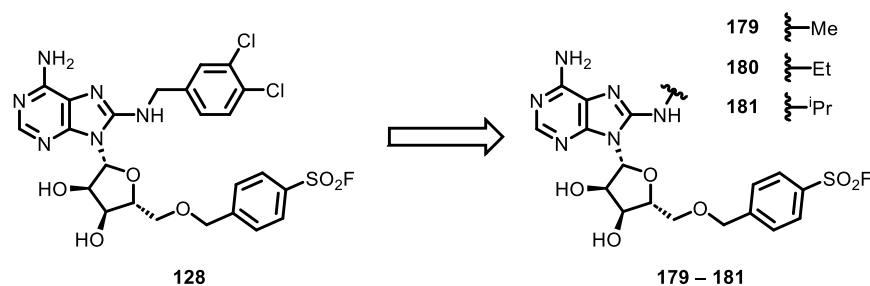
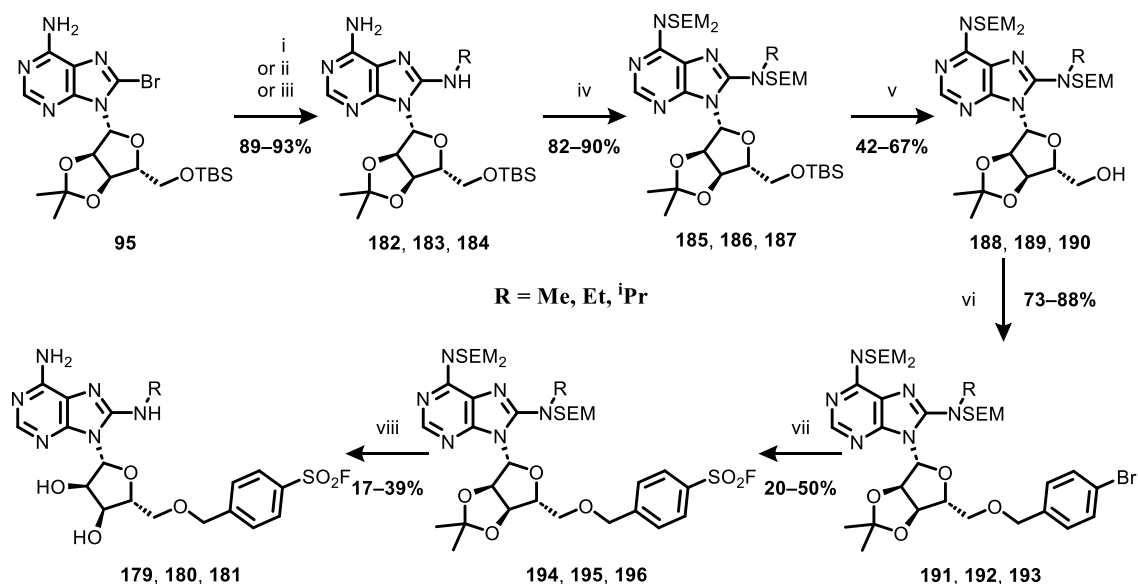


**Figure 5.10** Design strategy for moderate reversible affinity 5'-ether-linked lysine-TCIs, incorporating simple 8-*N*-alkyl groups to attenuate  $K_i$ .

### 5.2.2 Synthesis of Moderate Reversible Affinity Compounds

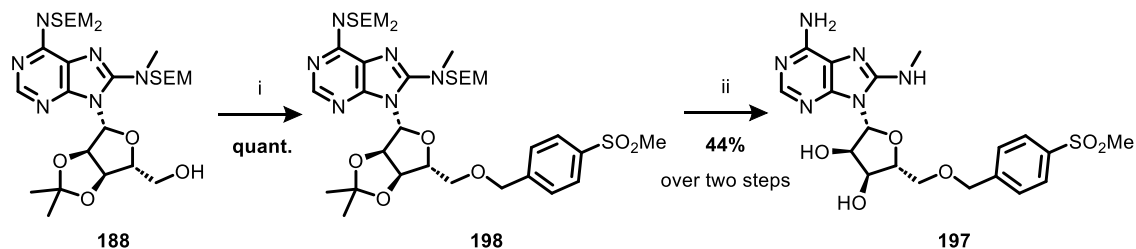
Moderate reversible affinity 5'-ether-linked TCIs were accessed in a similar fashion to the high affinity 8-*N*-benzylated 5'-ether-linked TCIs (Scheme 5.2).



**Scheme 5.2** Synthesis of 8-*N*-alkyl TCIs **179**, **180** and **181**. Reagents and conditions: i) methylamine (26 equiv.) EtOH (0.3 M), 160 °C,  $\mu$ wave, 1 h; ii) ethylamine (10 equiv.), EtOH (0.3 M), 160 °C,  $\mu$ wave, 1 h; iii) isopropylamine (10 equiv.), EtOH (0.3 M), 160 °C,  $\mu$ wave, 1 h; iv) DIPEA (4.5 equiv.), SEMCl (4.5 equiv.), CH<sub>2</sub>Cl<sub>2</sub> (0.3 M), reflux, 18 h; v) TBAF (1.1 equiv.), THF (0.12 M), 0 °C to rt, 2 – 48 h; vi) NaH (1.2 equiv.), THF (0.5 M), 0 °C, 15 min, *then* 4-bromobenzyl bromide (2 equiv.), 0 °C to rt, 18 h; vii) DABSO (0.6 equiv.), PdCl<sub>2</sub>(AmPhos)<sub>2</sub> (5 mol%), Et<sub>3</sub>N (3 equiv.), isopropanol (0.27 M), 75 °C, 18 h, *then* NFSI (1.5 equiv.), rt, 5 h; viii) TFA:H<sub>2</sub>O 5:2 (0.1 M), rt, 1 – 2 h.

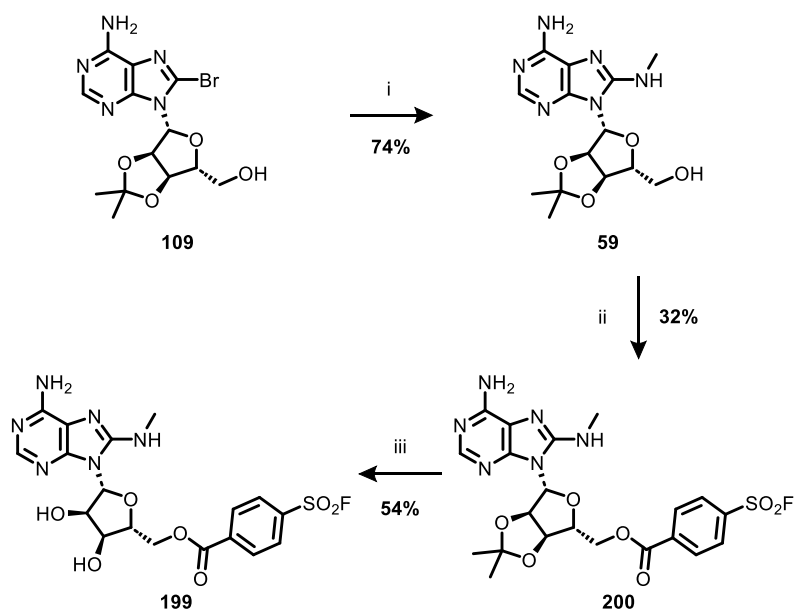
Firstly, the 8-*N*-alkylated intermediates **182**, **183** and **184** were accessed in high yield *via* an S<sub>N</sub>Ar reaction with an excess of the corresponding amine in EtOH. Reaction of these intermediates with SEMCl under standard conditions afforded tris-*N*-SEM protected intermediates **185**, **186** and **187** in excellent yields. Interestingly, these yields were considerably higher than for the corresponding 8-*N*-benzyl series, which we speculated was due to the comparatively decreased steric hindrance on the 8-*N*-position, thus enabling a more facile alkylation with SEMCl. Selective *O*-TBS cleavage with TBAF afforded the corresponding 5'-OH intermediates **188**, **189**, and **190**, which were then reacted with 4-bromobenzyl bromide and sodium hydride to produce 5'-*O*-benzylated intermediates **191**, **192**, and **193**. Finally, sequential fluorosulfonation to give sulfonyl fluorides **194**, **195**, and **196**, was followed by global acidic deprotection to give TCIs **179**, **180**, and **181**. The 8-*N*-methylamine-5'-methyl sulfone reversible control **197** was also prepared in a similar fashion; firstly, the previously synthesised tris-*N*-SEM protected intermediate **188** was reacted with 4-(methylsulfonyl)benzyl bromide under Williamson

etherification conditions to yield 5'-*O*-benzylated intermediate **198**; this intermediate was then subjected to global deprotection with TFA:water to afford reversible MMP **197** (Scheme 5.3).



**Scheme 5.3** Synthesis of reversible control **197**. Reagents and conditions: i) NaH (1.2 equiv.), THF (0.5 M), 0 °C, 15 min, then 4-(methylsulfonyl)benzyl bromide (2 equiv.), 0 °C to rt, 18 h. ii) TFA:H<sub>2</sub>O 5:2 (0.1 M), rt, 1 h.

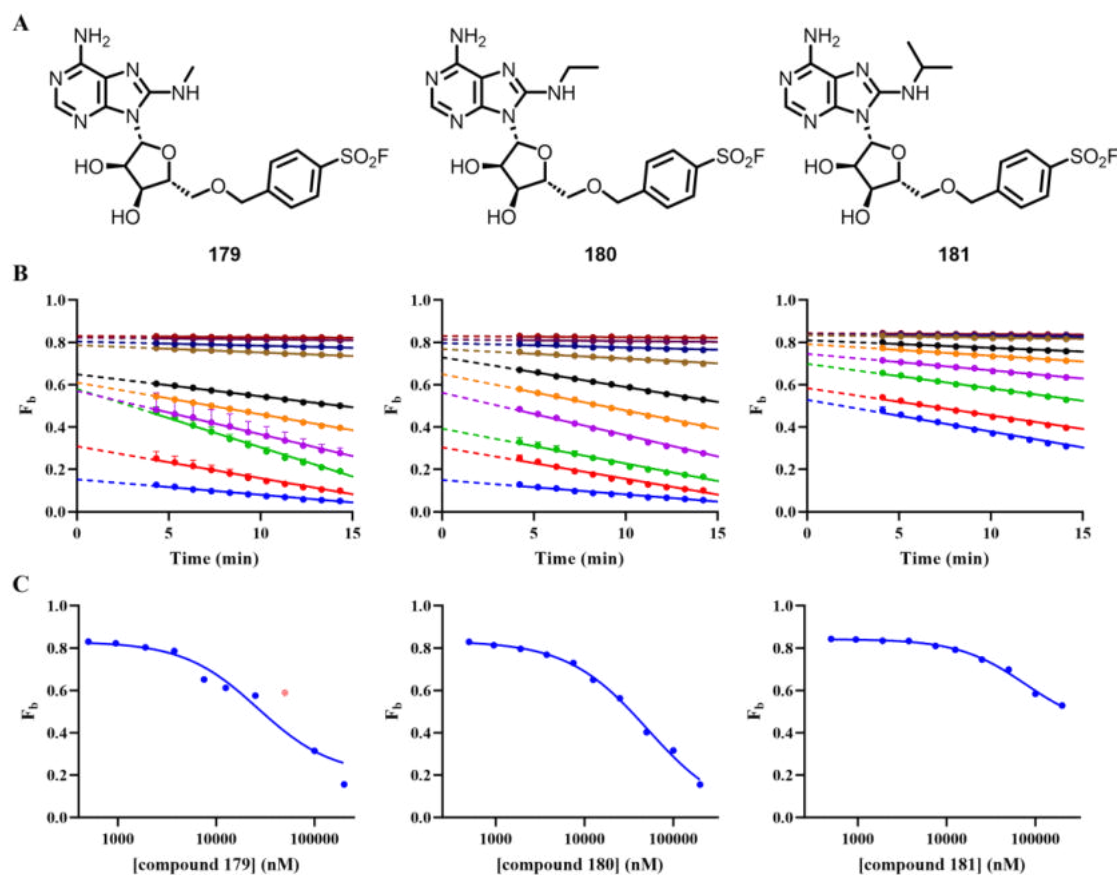
To directly compare the kinetic parameters of 8-*N*-methyl ether-linked TCI **179** with a corresponding ester-linked matched pair, 8-*N*-methyl ester-linked TCI **199** was prepared from previously synthesised 8-bromo intermediate **109**. *N*-methylated intermediate **59** was prepared from **109** via an S<sub>N</sub>Ar reaction with methylamine, which was reacted with 4-(fluorosulfonyl)benzoyl chloride to yield **200**. Acetonide deprotection with TFA:water afforded TCI **199** in three steps and 13% overall yield (Scheme 5.4).



**Scheme 5.4** Synthesis of 8-*N*-methyl ester-linked TCI **199**. Reagents and conditions: i) methylamine (26 equiv.), EtOH (0.3 M), 160 °C,  $\mu$ wave, 1 h; ii) 4-(fluorosulfonyl)benzoyl chloride (1.2 equiv.), Et<sub>3</sub>N (1.5 equiv.), DMF (0.1 M), 0 °C, 3 h; iii) TFA:H<sub>2</sub>O 5:2 (0.1 M), rt, 2 h.

### 5.2.3 Characterisation of Moderate Reversible Affinity Compounds

The next step was to profile TCIs **179**, **180**, and **181** in the TDFP assay to confirm whether our design strategy had furnished 5'-ether-linked HSP72 lysine-TCIs within the desired assay window. (Figure 5.11).



Compound	Initial IC <sub>50</sub> (μM)	Initial K <sub>i</sub> (μM)
<i>N</i> -Me <b>179</b>	35	5.1
<i>N</i> -Et <b>180</b>	51	7.5
<i>N</i> <sup>i</sup> Pr <b>181</b>	150	23

**Figure 5.11** **A** Structures of TCIs **179**, **180** and **181**. **B** Plot of calculated  $F_b$  values against time, y-intercepts calculated using simple linear regression (GraphPad Prism 9). Different colour lines represent different concentrations of TCIs from 200 μM to 500 nM. **C** Plot of initial  $F_b$  against [I] to determine initial IC<sub>50</sub> (log(inhibitor) vs. response – variable slope (four parameters), GraphPad Prism 9). Outlier data point shown in pink.

Pleasingly, these compounds displayed reversible affinities within the limit of assay detection, with initial  $K_i = 5.1$  μM for *N*-methyl TCI **179**, initial  $K_i = 7.5$  μM for *N*-ethyl TCI **180**, and initial  $K_i = 23$  μM for *N*-isopropyl TCI **181**. Following the same process outlined in Section 4.2.4, a second, focussed titration of TCIs **179**, **180**, and **181** at low inhibitor concentrations was then performed (Figure 5.12). Plotting the calculated  $F_b$  values against time enabled the determination of the y-intercept and gradient (Figure 5.12 A). Dividing the gradient by the y-intercept produced values for  $k_{obs}$  in units of min<sup>-1</sup>,

which were replotted against TCI concentration to obtain  $k_{\text{inact}}/K_{\text{I}}$  as the gradient (Figure 5.12 B), which were multiplied by the initial  $K_{\text{I}}$  to estimate values for  $k_{\text{inact}}$ .

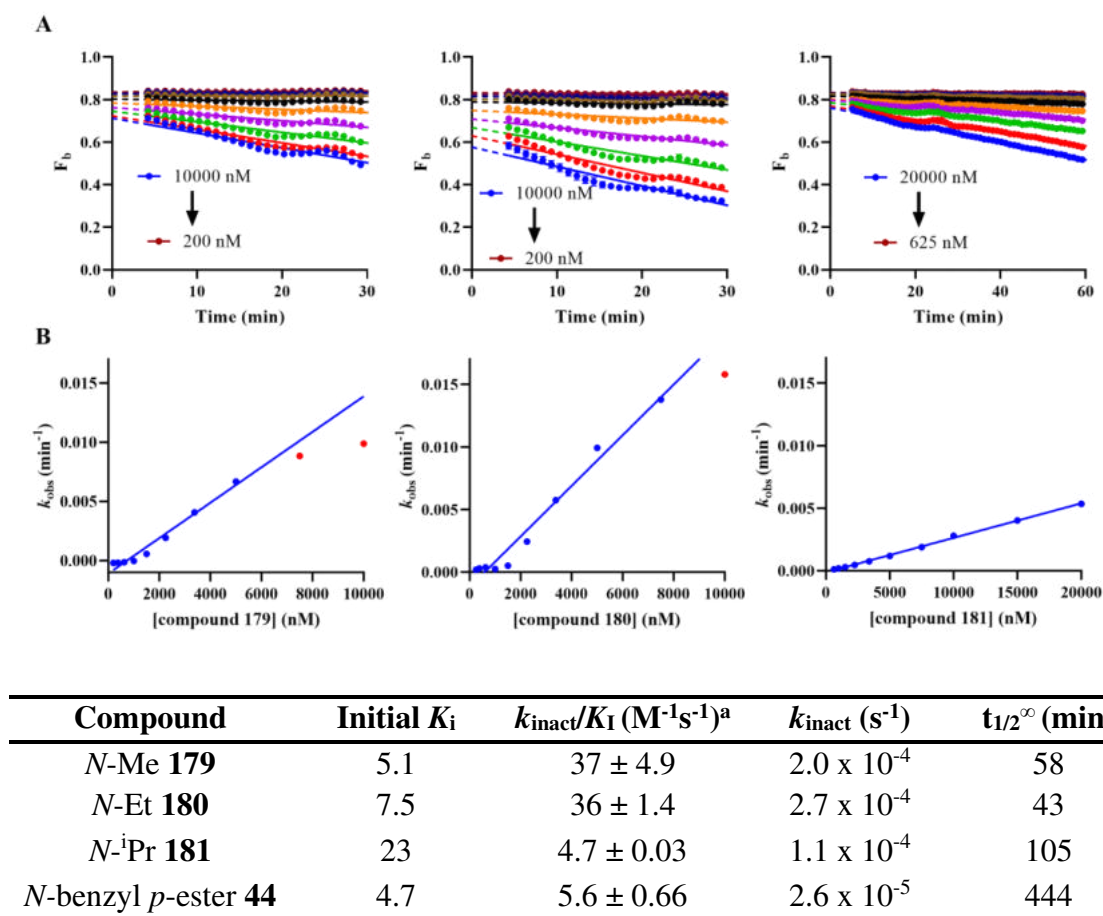
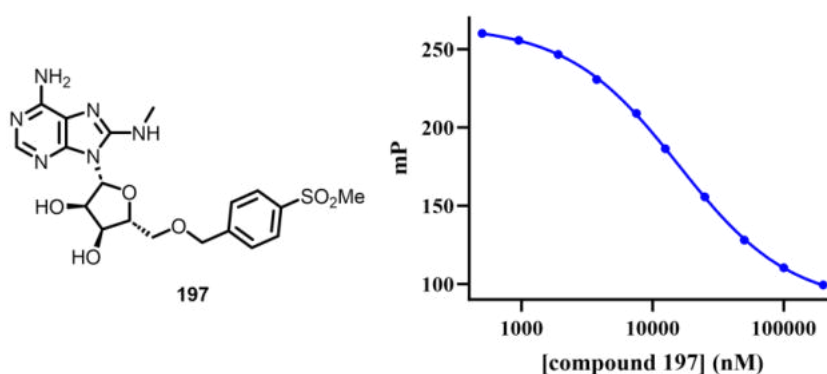


**Figure 5.12** Second, focussed titration of TCIs **179**, **180**, and **181** in the TDFP assay. **A** Plot of calculated  $F_b$  values against time, gradients and y-intercepts calculated using simple linear regression (GraphPad Prism 9). **B** Plot of  $k_{\text{obs}}$  against inhibitor concentration (simple linear regression, GraphPad Prism 9) to determine  $k_{\text{inact}}/K_{\text{I}}$ . Data points that deviate from linearity are red.  $R^2$  values of representative lines are 0.97, 0.97 and 0.998 from left to right. <sup>a</sup> $k_{\text{inact}}/K_{\text{I}}$  values are quoted as mean ± SEM of three independent experiments.

As expected, concentrations screened above the  $K_{\text{I}}$  of their respective inhibitor deviated from linearity and were therefore excluded from the analysis and the remaining points fitted well to a linear model ( $R^2 > 0.97$ ), although at low inhibitor concentrations ( $[I] < 1000$  nM) the measured  $k_{\text{obs}}$  values approached zero likely owing to inhibitor depletion at concentrations at or below  $[\text{protein}]$  (Figure 5.12 C). Interestingly, whilst *N*-methyl TCI **179** and *N*-ethyl TCI **180** appeared equipotent with near-equivalent  $k_{\text{inact}}/K_{\text{I}}$  values, addition of an additional methyl group to give *N*-isopropyl TCI **181** resulted in a ~7.7-fold drop off in  $k_{\text{inact}}/K_{\text{I}}$ . Analysis of the kinetic data implies that this potency decrease is

driven by a 3.1-fold loss of reversible affinity and also a 2.5-fold decrease in  $k_{\text{inact}}$ . However, the most surprising result was obtained when we compared the  $k_{\text{inact}}$  values for TCIs **179**, **180** and **181** to second-generation *N*-monochlorobenzyl *para*-ester TCI **44**, which suggested that the rate of covalent bond formation had been maintained, and possibly even increased by an order of magnitude, despite a predicted decrease in intrinsic reactivity from loss of the ester moiety.

To corroborate the observed initial  $K_i$  values, reversible methyl sulfone-containing MMP **197** was tested in the FP assay, which confirmed that this chemotype exhibits reversible affinity within the window of the assay ( $K_i = 1.6 \mu\text{M}$ , Figure 5.13).



Compound	$pK_i$	$K_i$ ( $\mu\text{M}$ )
<i>N</i> -Me SO <sub>2</sub> Me <b>197</b>	$5.8 \pm 0.07$	1.6

**Figure 5.13** Measurement of  $K_i$  for reversible MMP **197** with HSP72-NBD and ATP-ATTO 488 **108**. [HSP72-NBD] selected so  $F_b = 0.85$ . Measurements taken in triplicate and the mean and standard error plotted using GraphPad Prism 9.  $pK_i$  values are quoted as mean  $\pm$  SEM of three independent experiments.

Analysis of 8-*N*-methyl 5'-ester-linked MMP **199** by the TDFP-assay indicated that despite measurable time dependence consistent with covalent bond formation, it possessed a weak reversible affinity (initial  $K_i > 30 \mu\text{M}$ ) with an initial  $\text{IC}_{50}$  value above the top tested inhibitor concentration (initial  $\text{IC}_{50} > 200 \mu\text{M}$ ) (Figure 5.14).

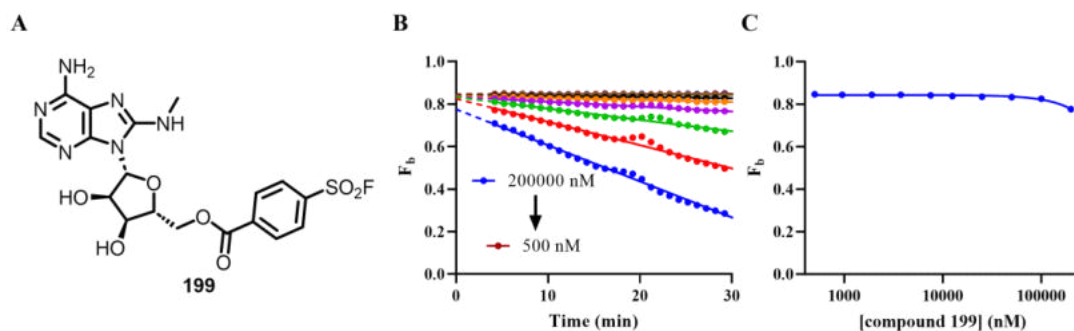
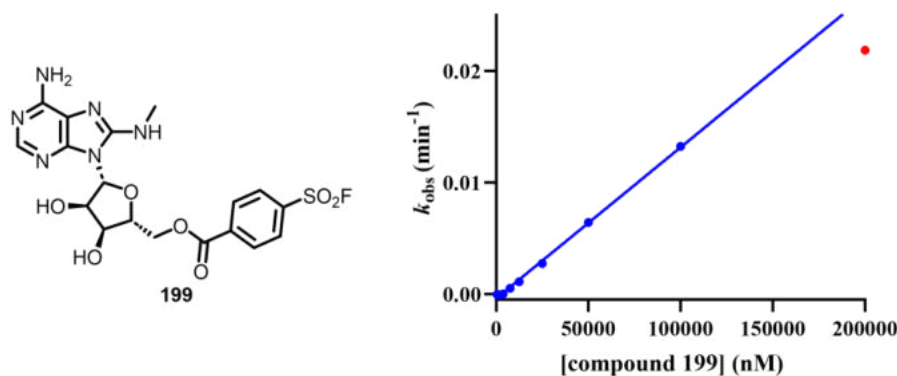


**Figure 5.14** A Structure of TCI **199**. B Plot of calculated  $F_b$  values against time for TCI **199**, y-intercepts calculated using simple linear regression (GraphPad Prism 9). C Plot of initial  $F_b$  against  $[I]$  to determine initial  $IC_{50}$  (log(inhibitor) vs. response – variable slope (four parameters), GraphPad Prism 9).

Calculation of the  $k_{obs}$  values from the gradient and y-intercept of the  $F_b$  vs time plot enabled the determination of  $k_{inact}/K_I$ , but due to the unresolvable reversible affinity,  $k_{inact}$  could not be precisely determined (Figure 5.15).



Compound	Initial $K_i$	$k_{inact}/K_I$ ( $M^{-1}s^{-1}$ ) <sup>a</sup>	$k_{inact}$ ( $s^{-1}$ )	$t_{1/2}^{\infty}$ (h)
<i>N</i> -Me <i>p</i> -ester <b>199</b>	>30	$2.5 \pm 0.1$	$> 7.5 \times 10^{-5}$	< 2.6

**Figure 5.15** Plot of  $k_{obs}$  against inhibitor concentration (simple linear regression, GraphPad Prism 9) to determine  $k_{inact}/K_I$ . Data points that deviate from linearity are red. <sup>a</sup> $k_{inact}/K_I$  values are quoted as mean  $\pm$  SEM of three independent experiments.

Interestingly, the plot of  $k_{obs}$  against TCI **199** concentration appeared to deviate from linearity at the top concentration assayed (200  $\mu$ M), potentially implying the true  $K_i$  value for **199** is between 100 – 200  $\mu$ M.



Together, these data showed that the 5'-ether-linked TCIs possess up to an order of magnitude greater  $k_{\text{inact}}$  values compared to the corresponding 8-*N*-monochlorobenzyl ester-linked TCI **44**, which is unexpected owing to the proposed greater intrinsic reactivity of the sulfonyl fluoride warhead in the presence of the *para*-ester. Increasing  $k_{\text{inact}}$  whilst reducing intrinsic reactivity is highly desirable, as this should result in reduced toxicity from less non-specific labelling of off-targets whilst simultaneously improving the rate of on-target covalent bond formation.

To validate that we had successfully improved  $k_{\text{inact}}$  whilst simultaneously modulating the intrinsic reactivity, we required an assay to quantify and rank the intrinsic reactivity of our TCIs.

### 5.3 Quantification of Intrinsic Reactivity

#### 5.3.1 Introduction

Quantification of the intrinsic reactivity of cysteine-reactive warheads can be achieved through the incubation of the warhead-containing molecule with either *N*-acetyl cysteine or GSH.<sup>199</sup> At physiological pH 7.4, cysteine ( $\text{p}K_{\text{a}} = 8.6$ ) predominately exists (~90%) as the reactive neutral thiol species and the minor hyper reactive anionic thiolate (~10%). In contrast, lysine has a  $\text{p}K_{\text{aH}}$  of 10.4, so predominately exists as the non-reactive cationic ammonium (>99%) species, with a very small (<1%) concentration of the reactive neutral amine species. Whilst the  $\text{p}K_{\text{aH}}$  of lysine residues can be perturbed within the lipophilic environment of protein binding sites, increasing nucleophilic neutral protein concentration, this high basicity represents a significant challenge for the quantification of intrinsic reactivity for lysine-reactive warheads in bulk solvent. The low concentration of neutral lysine under physiological conditions will likely lead to negligible substrate turnover and therefore preclude the evaluation of the half-life and intrinsic reactivity.

Dahal et al. reported that incubation of a variety of warheads, including acrylamides, vinyl sulfones and nitriles, with *N*- $\alpha$ -acetyllysine **201** at pH = 7.4 resulted in no observable reaction between nucleophile and electrophile.<sup>81</sup> Increasing the pH to 10.2, which would correspond to ~50% neutral, nucleophilic lysine in solution, led to significant adduct formation that enabled the quantification of half-life by mass spectrometry (Figure 5.16).

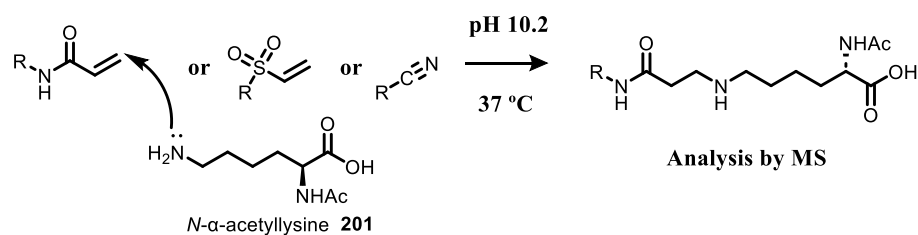
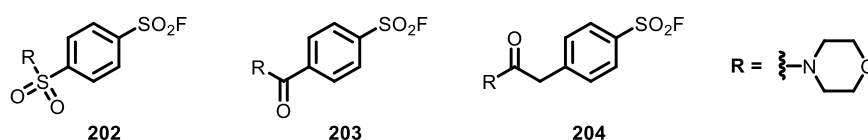


**Figure 5.16** High pH method to quantify intrinsic reactivity of covalent warheads with *N*- $\alpha$ -acetyllysine **201**.<sup>81</sup>

However, increasing the pH by ~3 units compared to physiological conditions, corresponds to a ~1000-fold increase in the concentration of hydroxide ions in solution. A reactivity and stability study of sulfonyl fluorides by Gilbert et al. indicates this moiety is highly sensitive to increases in pH, which would likely make this protocol unsuitable (Table 5.1).<sup>200</sup>



Compound	$t_{1/2}$ (pH 7) (h)	$t_{1/2}$ (pH 8) (h)	$t_{1/2}$ (pH 10) (h)
sulfone <b>202</b>	1.5	0.6	<0.2
phenyl ketone <b>203</b>	7.6	3.1	<0.2
benzyl ketone <b>204</b>	40.5	15.3	<0.2

**Table 5.1** pH dependence of sulfonyl fluoride hydrolytic stability as reported by Gilbert et al.<sup>200</sup> Stability measured at room temperature in PBS buffer (pH = 7 and 8) and bicarbonate buffer (pH = 10).

Gilbert et al. then proceeded to measure the rate of reaction of these electrophiles with monomeric amino acids, *N*- $\alpha$ -acetyllysine, *N*-acetyltyrosine, *N*-acetylhistidine, and *N*-acetylcysteine at pH = 8.0. Under these conditions, they observed significant competing hydrolysis of the sulfonyl fluoride, which complicated their analysis. Grimster et al., in their own investigation of sulfonyl fluoride reactivity with *N*- $\alpha$ -acetyllysine, likewise experienced significant challenges from low reactivity and the competing hydrolysis pathway.<sup>147</sup>

### 5.3.2 Quantifying Hydrolytic Stability by Mass Spectrometry

Because of the challenges in directly measuring the rate of reaction with *N*- $\alpha$ -acetyllysine, our strategy was therefore to measure the hydrolytic stability of the sulfonyl fluoride TCIs and compare the half-lives of substrates possessing either the 5'-ether- and 5'-ester-linker chemotype. The hydrolytic stability of the electrophile in bulk solvent should correlate with the intrinsic reactivity with hard nucleophiles and is an important parameter in successful TCI design.

Incubation of the TCI was performed at pH = 7.4 and 37 °C to mimic physiological conditions and potentially cell-based assays (Figure 5.17 A). Injection into a LC system was performed once an hour across 24 hours, and involved a 10-minute chromatographic separation, with the peaks that eluted between 2 – 5 minutes analysed by MS (Figure 5.17 B). Integration of the mass spectrum across an *m/z* range corresponding to the starting material afforded the Total Ion Count (TIC), which was normalised to the TIC at *t* = 1 hour to give %compound, the relative amount of non-hydrolysed starting material left in solution. %compound decreased in a time-dependent manner over the course of the assay as the sulfonyl fluoride was gradually hydrolysed under the assay conditions (Figure 5.17 C). The rate of hydrolysis can be assumed to follow pseudo first order kinetics ( $d[A]/dt=k[A]$ ), therefore, a plot of the natural logarithm of %compound against time afforded a linear correlation, with the gradient equal to the rate constant of hydrolysis  $k_{\text{hyd}}$  ( $\ln[A]_t=k_{\text{hyd}}t+\ln[A]_0$ ).  $k_{\text{hyd}}$  can also be described as a half-life ( $t_{1/2} = \ln 2/k_{\text{hyd}}$ ) (Figure 5.17 D).

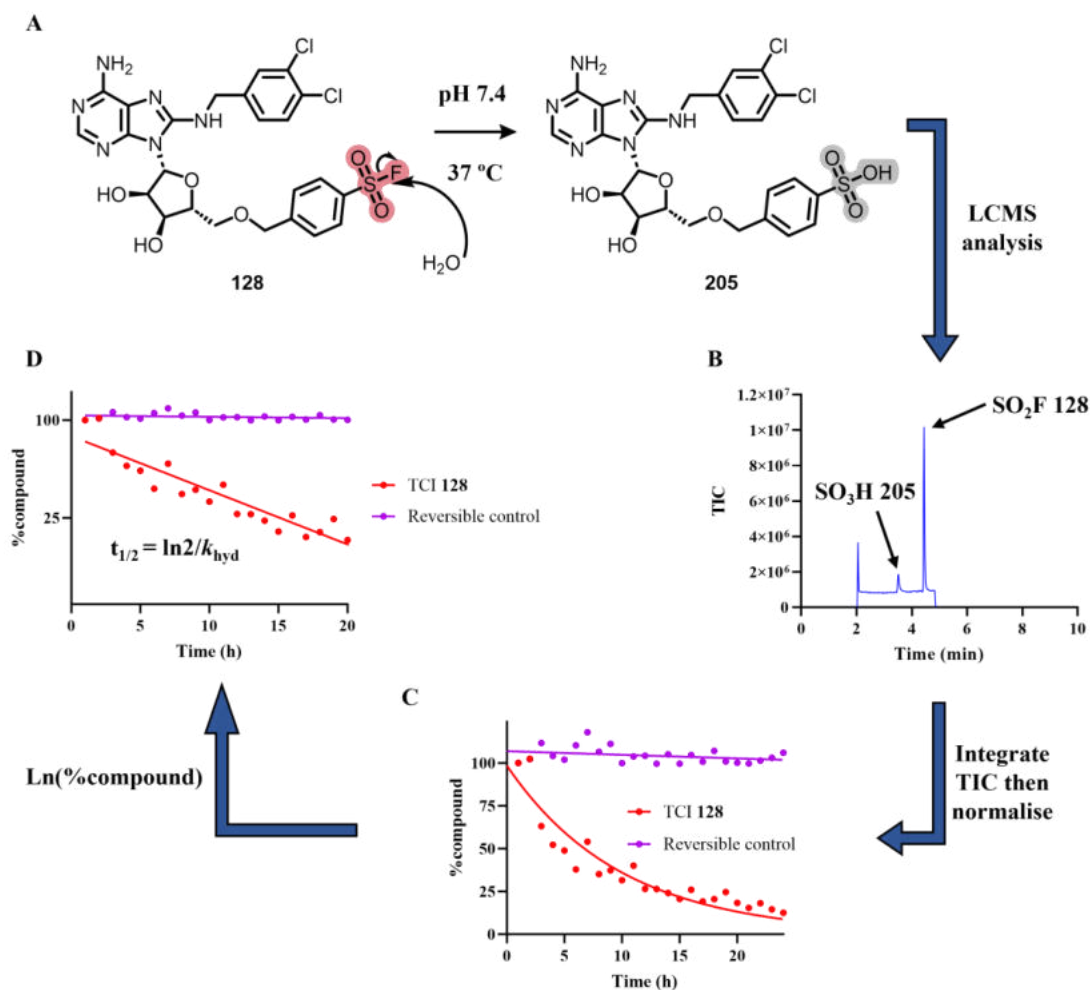
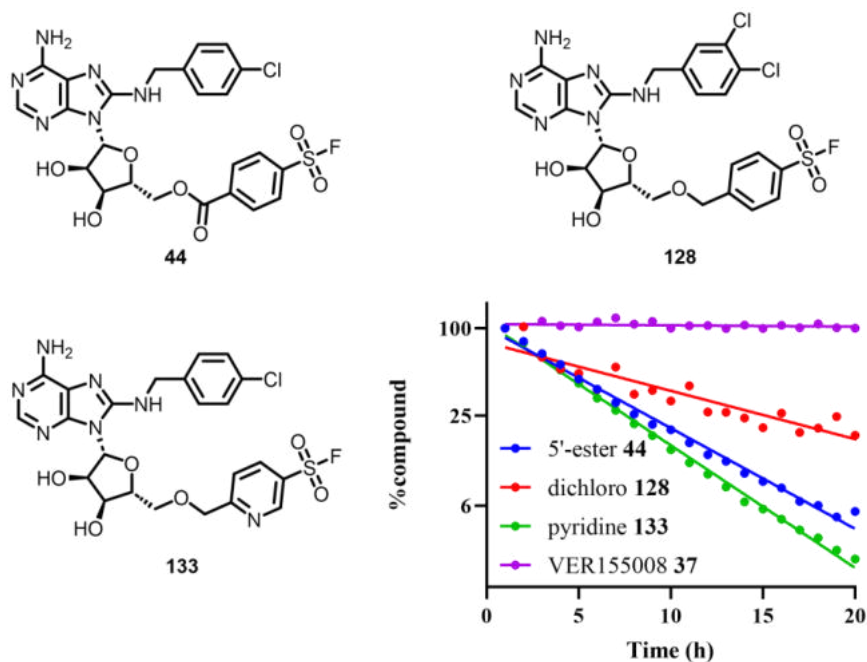


**Figure 5.17** Hydrolytic stability by MS. **A** Compounds are incubated at 50  $\mu$ M in PBS buffer pH 7.4 at 37  $^{\circ}$ C. **B** Injection into LCMS system enables chromatographic separation across a 10 minute gradient, after which eluent is analysed by mass spectrometry. **C** Integration to obtain the TIC, followed by normalisation to %compound gives plot of first order decay. **D**  $\ln(\% \text{compound})$  vs time furnishes linear plot with gradient  $k_{\text{hyd}}$  (simple linear regression, GraphPad Prism 9).

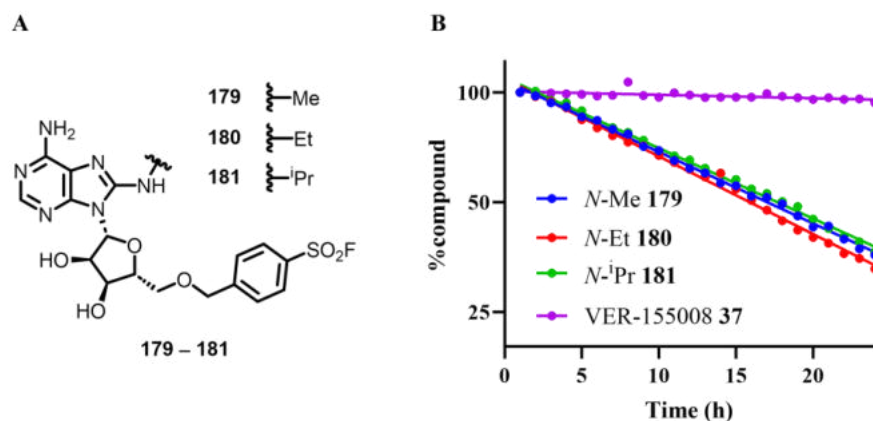
TCIs **44**, **128** and **133** were screened in the hydrolytic stability assay with reversible inhibitor VER-155008 **37** as a control (Figure 5.18). Consistent with the published intrinsic reactivity data, 5'-ester **44** displayed  $\sim$ 2-fold reduced  $t_{1/2}$  compared to 5'-ether **128**. Intriguingly, introduction of a *meta*-nitrogen in pyridine **133** had a similar effect on the rate of hydrolysis as inclusion of the *para*-ester in TCI **44**, which suggests that heteroatoms can effectively act as electron withdrawing groups and increase the intrinsic reactivity of a covalent warhead attached to the same ring system.



Compound	$k_{\text{hyd}} (\text{h}^{-1})$	$t_{1/2} (\text{h})$
5'-ester <b>44</b>	$0.16 \pm 0.007$	$4.4 \pm 0.19$
dichloro <b>128</b>	$0.077 \pm 0.0005$	$9.0 \pm 0.05$
pyridine <b>133</b>	$0.20 \pm 0.002$	$3.5 \pm 0.05$
VER-155008 <b>37</b>	$< 0.02$	$> 24$

**Figure 5.18** Hydrolytic stability of TCIs **44**, **128** and **133** and reversible control VER-155008 **37** at 50  $\mu\text{M}$  in PBS buffer pH 7.4 at 37  $^{\circ}\text{C}$ , with plot of  $\ln(\% \text{compound})$  vs time to determine  $k_{\text{hyd}}$  (simple linear regression, GraphPad Prism 9).  $k_{\text{hyd}}$  and  $t_{1/2}$  values are quoted as mean  $\pm$  SEM of three independent experiments.

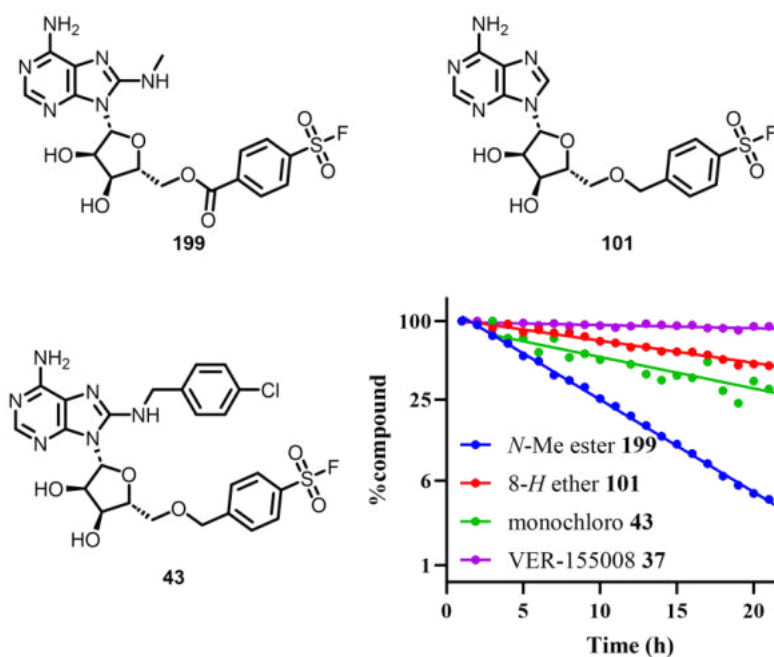
TCIs **179**, **180** and **181** were also profiled in this assay (Figure 5.19).



Compound	$k_{\text{hyd}}$ ( $\text{h}^{-1}$ )	$t_{1/2}$ (h)
<i>N</i> -Me <b>179</b>	$0.044 \pm 0.0007$	$16 \pm 0.27$
<i>N</i> -Et <b>180</b>	$0.047 \pm 0.001$	$15 \pm 0.38$
<i>N</i> - <i>i</i> Pr <b>181</b>	$0.041 \pm 0.002$	$17 \pm 0.63$

**Figure 5.19** A Structures of TCIs **179**, **180**, and **181**. B Hydrolytic stability of TCIs **179**, **180** and **181** at 50 μM in PBS buffer pH 7.4 at 37 °C, with plot of  $\ln(\% \text{compound})$  vs time to determine  $k_{\text{hyd}}$  (simple linear regression, GraphPad Prism 9).  $k_{\text{hyd}}$  and  $t_{1/2}$  values are quoted as mean  $\pm$  SEM of three independent experiments.

TCIs **179**, **180** and **181** exhibited highly congruent hydrolytic stabilities, likely owing to their similar chemical structures. The values of  $t_{1/2}$  observed were ~4-fold higher compared to 5'-ester TCI **44**, which is consistent with the expected decrease in intrinsic reactivity associated with the switch of the *para*-ester-linker for the *para*-benzylic ether-linker. Interestingly, 8-*N*-benzyl MMP **128** displayed ~2-fold reduced  $t_{1/2}$  compared to 8-*N*-methyl TCI **179**, despite possessing the same group on the 5'-benzyl ring. The substituent at the 8-*N* position we had previously shown to have a strong influence on the stability of the covalent warhead in this chemotype, during the attempted synthesis of quinoline TCI **119** (Section 4.2.5), potentially due to increased rate of hydrolysis of the sulfonyl fluoride moiety in the final reaction step, which was expedited by the quinoline group. The 8-*H* TCI **101** and 8-*N*-chlorobenzyl TCI **43** were also profiled in the hydrolytic stability assay to investigate the importance of the 8-position to the hydrolytic stability and compared to the 8-*N*-methylated 5'-ester **199**, to enable direct comparison of its stability with 5'-ether MMP **179** (Figure 5.20).



Compound	$k_{\text{hyd}} \text{ (h}^{-1}\text{)}$	$t_{1/2} \text{ (h)}$
<i>N</i> -Me ester <b>199</b>	$0.17 \pm 0.002$	$4.1 \pm 0.05$
8- <i>H</i> <b>101</b>	$0.040 \pm 0.0003$	$17 \pm 0.14$
monochloro <b>43</b>	$0.061 \pm 0.004$	$11 \pm 0.63$

**Figure 5.20** Hydrolytic stability of TCIs **199**, **101**, and **43** at 50  $\mu\text{M}$  in PBS buffer pH 7.4 at 37  $^{\circ}\text{C}$ , with plot of  $\ln(\% \text{ compound})$  vs time to determine  $k_{\text{hyd}}$  (simple linear regression, GraphPad Prism 9).  $k_{\text{hyd}}$  and  $t_{1/2}$  values are quoted as mean  $\pm$  SEM of three independent experiments.

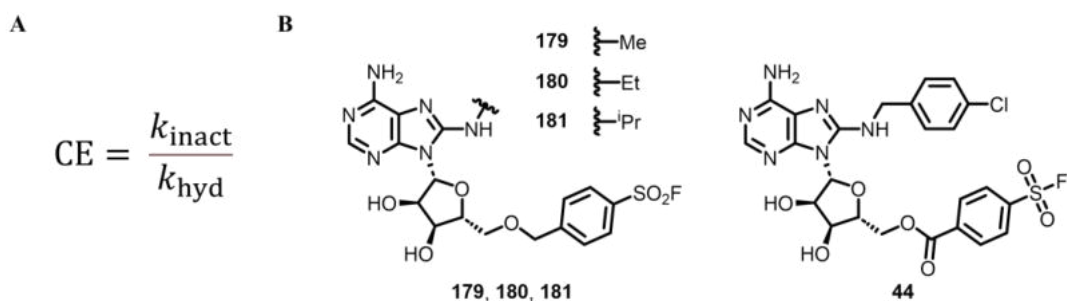
Comparison of 8-*N*-methyl MMPs **179** and **199** shows that 5'-ether **179** has a ~4-fold improved  $t_{1/2}^{\text{int}}$  over 5'-ester **199**, consistent with the anticipated decrease in intrinsic reactivity. Monochlorobenzyl TCI **43** ( $t_{1/2}^{\text{int}} = 11$  h) displays hydrolytic stability congruous with dichlorobenzyl TCI **128** ( $t_{1/2}^{\text{int}} = 9$  h). 8-*H* TCI **101** has hydrolytic stability consistent with 8-*N*-alkyl TCIs **179** – **181**, corroborating the observation that the 8-*N*-benzyl moiety negatively impacts the stability of the 5'-ether TCIs.

### 5.3.3 Covalent Efficiency

The data from the hydrolytic stability assay confirmed that the switch from the 5'-ester- to 5'-ether linker had resulted in a decrease in the intrinsic reactivity of the sulfonyl fluoride warhead. Consequently, the improvements in  $k_{\text{inact}}$  from incorporation of the 5'-ether linker in the HSP72 lysine-TCIs had occurred despite the observed intrinsic reactivity modulation. This corroborates the observation by Gilbert et al., that  $k_{\text{inact}}$  and intrinsic reactivity correlated poorly for their series of  $\text{S}^{\text{IV}}\text{-F}$  electrophiles,<sup>200</sup> and that

other factors, such as the positioning of the warhead within the binding site, can be more important than intrinsic reactivity in determining the magnitude of  $k_{\text{inact}}$ . We speculated that swapping from the 5'-ester to the 5'-ether introduces more conformational flexibility to the 5'-benzyl group, enabling a more favourable alignment between Lys-56 and the covalent warhead, thereby improving the  $k_{\text{inact}}$ .

Modulation of the intrinsic reactivity whilst optimising  $k_{\text{inact}}$  is highly favourable as it involves improving the potency of the TCI whilst decreasing the risk of non-specific covalent labelling of off-target proteins and molecules. However, enhancing the  $k_{\text{inact}}$  alone without a suitable measurement of intrinsic reactivity will fail to capture if an increase in  $k_{\text{inact}}$  is due to optimisation of the on-target binding event or increased electrophilicity of the warhead. To rationalise this improvement in TCI design, we proposed the new metric, Covalent Efficiency (CE), that normalises  $k_{\text{inact}}$  against the intrinsic reactivity, thereby allowing the ranking of compounds within a TCI series. CE can be calculated by taking the ratio of the rate constant for specific covalent bond formation,  $k_{\text{inact}}$ , and a rate constant quantifying intrinsic reactivity, such as  $k_{\text{hyd}}$  (Figure 5.21 A).



Compound	$k_{\text{inact}}$ (s <sup>-1</sup> )	$k_{\text{hyd}}$ (s <sup>-1</sup> )	CE
<i>N</i> -Me <b>179</b>	$2.0 \times 10^{-4}$	$1.2 \times 10^{-5}$	17
<i>N</i> -Et <b>180</b>	$2.7 \times 10^{-4}$	$1.3 \times 10^{-5}$	21
<i>N</i> - <i>i</i> Pr <b>181</b>	$1.1 \times 10^{-4}$	$1.1 \times 10^{-5}$	10
5'-ester <b>44</b>	$2.6 \times 10^{-5}$	$4.4 \times 10^{-5}$	0.59

**Figure 5.21** **A** Equation relating covalent efficiency (CE) to  $k_{\text{inact}}$  and  $k_{\text{hyd}}$ . **B** Structures of TCIs **179**, **180**, **181**, and **44**.

Applying CE to our series of sulfonyl fluoride TCIs (Figure 5.21 B) illustrates how the switch from the 5'-ester to the 5'-ether linker results in a 17 – 36-fold improvement in the covalent efficiency of this series.



## 5.4 Cellular Activity of HSP72 Lysine-Targeting Covalent Inhibitors

### 5.4.1 Stability in Cell Media

Our series of high affinity 5'-ether-linked HSP72 TCIs had been extensively characterised by FP and MS techniques. Notably, we had successfully driven substantial improvements in  $K_i$  through the switch to the 5'-ether chemotype, even though we were unable to quantify the improvement due to the limitations of the assay format. We now hypothesised that the improved efficiency of the third generation TCIs would result in a cell active tool. We selected dichlorobenzyl sulfonyl fluoride TCI **128** as the principal tool compound for *in vitro* profiling, as it was a direct MMP to the reversible inhibitor, VER-155008 **37**.

Sulfonyl fluoride TCI **128** exhibited acceptable hydrolytic stability under the cell assay conditions ( $t_{1/2} = 9.0$  h, pH 7.4, 37 °C), suggesting it would be suitable for a 24-hour incubation (2.7 half-lives) before concentrations of **128** became too low, as the concentration of **128** would be predicted to drop to ~16% across the course of the assay. However, cells are typically grown in media containing various components such as albumin, glucose and amino acids to facilitate cell growth.<sup>201</sup> During cellular respiration, CO<sub>2</sub> is produced as a by-product, which dissolves in the media as carbonic acid. This continuous acidification of the cell culture would be detrimental to cell survival, so the media is buffered with sodium bicarbonate, which neutralises the carbonic acid produced by the cells. Cellular incubation in an atmosphere of 5 – 10% CO<sub>2</sub>, which partially dissolves in the media as carbonic acid, establishes an approximate pH 7.4 buffering system with the sodium bicarbonate, for the maintenance of a stable pH range across the incubation.<sup>202</sup> Within our group, we demonstrated that incubation of standard Dulbecco's Modified Eagle's Medium (DMEM), the cell assay growth media (supplied by Aldrich)<sup>203</sup>, with 10% CO<sub>2</sub> with and without cells leads to a time-dependent decrease in pH, with physiological pH being achieved after 7 days in the presence of cells (Figure 5.22).

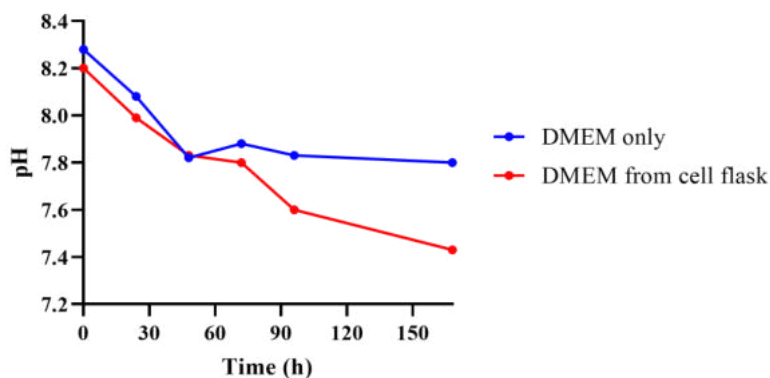
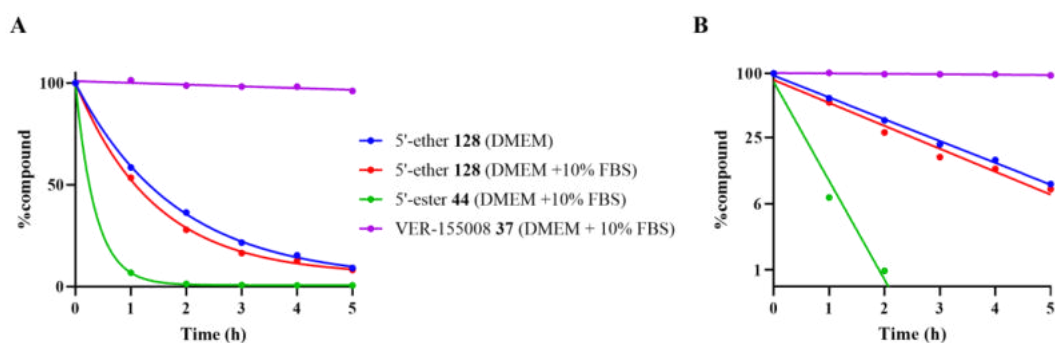


**Figure 5.22** Time-dependent change in pH of DMEM (experiment performed by Marissa Powers).

As demonstrated by Gilbert et al., the aqueous stability of sulfonyl fluoride groups are highly sensitive to increases in pH.<sup>200</sup> The alkalinity of DMEM was measured at pH 8.4, owing to the dissolved bicarbonate. The pH of DMEM would then only be expected to decrease to ~7.4 during the cell assay incubation. To assess how the high pH would affect the stability of our lysine-TCIs, **128** and **44** were assayed for hydrolysis in pH 8.4 DMEM and also compared with 10% foetal bovine serum (FBS) added, a common supplement in animal cell culture media (Figure 5.23).



Compound	$t_{1/2}$ (h)
5'-ether <b>128</b>	1.4 <sup>a</sup>
5'-ether <b>128</b>	1.5
5'-ester <b>44</b>	0.33

**Figure 5.23** **A** Hydrolytic stability of TCIs **128** and **44** at 50  $\mu$ M in DMEM pH 8.4 + 10% FBS at 37  $^{\circ}$ C. **B** Plot of  $\ln(\% \text{compound})$  vs time to determine  $k_{\text{hyd}}$  (simple linear regression, GraphPad Prism 9). <sup>a</sup>Experiment performed in DMEM only.

The 5'-ether-linked sulfonyl fluoride TCI **128** showed significantly reduced stability at pH 8.4 compared to physiological pH 7.4, with a 6.4-fold decrease in  $t_{1/2}$ , which would correspond to <1% remaining after 24 h. Removing the 10% FBS had no significant effect on the observed hydrolytic stability, suggesting that the observed low  $t_{1/2}$  did not arise from degradation due to the serum components. 5'-Ester-linker sulfonyl fluoride TCI **44** displayed negligible hydrolytic stability under these conditions, with a 4.2-fold lower  $t_{1/2}$  compared to 5'-ether TCI **128**, consistent with observed trends in intrinsic reactivity. These data confirmed that use of fresh cell media to probe cellular activity would be unsuitable, as the high pH would lead to rapid degradation of the tool sulfonyl fluoride TCIs. We therefore surmised that the use of media that had been pre-incubated with CO<sub>2</sub> to reach physiological pH would be necessary to circumvent issues with the hydrolytic stability of TCI **128** in cellular assays.

#### 5.4.2 Biomarkers of HSP70 Inhibition

The HSP70 proteins are a family of molecular chaperones which control protein refolding and disaggregation.<sup>103</sup> Inhibition of HSPs, such as HSP70 and HSP90, has previously been shown to result in the destabilisation of client proteins, leading to proteasome-mediated degradation.<sup>128,204</sup> Powers et al. showed that dual knockdown of the HSP70 family members, HSC70 and HSP72, induces degradation of oncogenic HSP90 client proteins CRAF, CDK4 and ERBB2 in the human colon carcinoma cell line, HCT116.<sup>129</sup> Massey et al. had previously incubated the reversible HSP70 inhibitor, VER-155008 **37**, in HCT116 cells for 24 hours, followed by cell lysis and analysis by immunoblotting.<sup>134</sup> VER-155008 **37** exhibited only modest degradation of ERBB2, seemingly requiring total concentrations of **37** >20  $\mu$ M (Figure 5.24). In contrast, analysis of CRAF levels demonstrated that only minimal downregulation was occurring at the top inhibitor concentration tested (40  $\mu$ M), indicating that ERBB2 was a more sensitive biomarker to HSP70 inhibition.

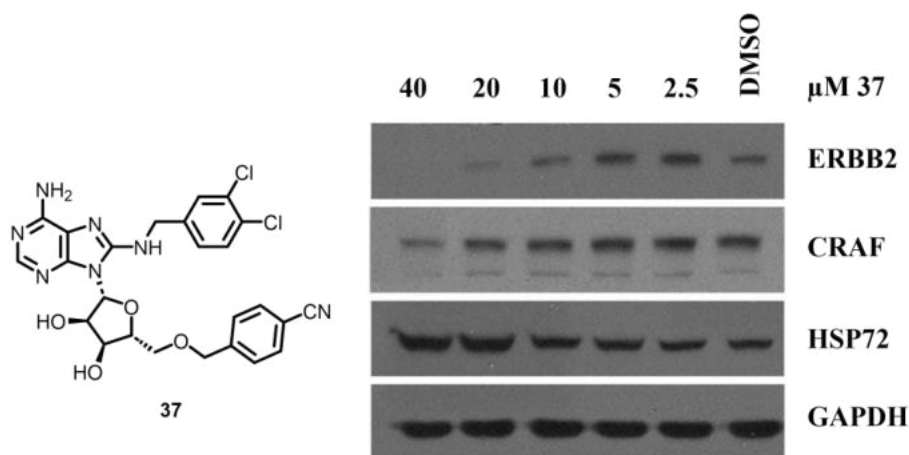


**Figure 5.24** Western blot showing the effect of VER-155008 **37** on levels of ERBB2 and CRAF in HCT116 cells (Massey).<sup>134</sup>

To compare the activity of sulfonyl fluoride TCI **128** versus VER-155008 **37** as intracellular HSP70 inhibitors, we selected ERBB2 as the principal biomarker for investigation, owing to its apparent increased sensitivity compared to CRAF. Using pre-conditioned DMEM growth media at pH 7.4, we then incubated several tool compounds in HCT116 cells for 24 hours, lysed the cells then assessed the protein levels *via* immunoblotting (Figure 5.25).

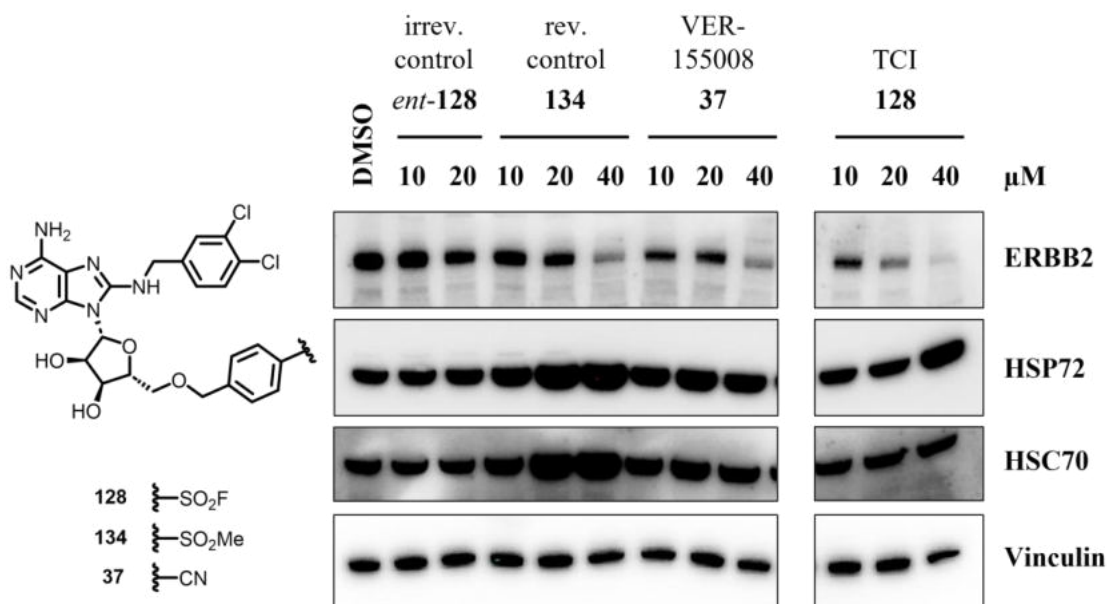


**Figure 5.25** Western blot showing effect of treatment of HCT116 cells with TCI **128** and relevant control compounds (experiment performed by Marissa Powers).

In our hands, VER-155008 **37** displayed degradation of ERBB2 at total concentrations consistent with the report of Massey et al. Pleasingly, TCI **128** exhibited degradation of ERBB2 at similar total concentrations to VER-155008 **37**, demonstrating for the first time that a HSP70 lysine-TCI could act as an inhibitor within cancer cells. Reversible methyl sulfone control **134** also downregulated ERBB2 at similar total concentrations to both TCI **128** and VER-155008 **37**.

Under cell assay conditions, compounds non-specifically bind to serum proteins in the growth media resulting in a smaller fraction of compound being free to cross the cell membrane.<sup>205</sup> The extent of serum protein binding will vary between compounds owing to the binding affinity of each inhibitor for the serum proteins; consequently for a fixed total concentration, the free concentration of inhibitor may vary across a chemical series, confounding analysis when comparing activities using total concentrations. Therefore, it is important to correct total concentrations to free concentrations *via* quantification of the free fraction when comparing the activities of compounds in a cellular assay when serum is present. However, the chemical instability of sulfonyl fluoride-based TCIs precluded the evaluation of the assay free fraction of TCI **128**, so we could not compare with the free concentrations of reversible inhibitors **134** and **37**. Crucially, the opposite enantiomer negative control *ent*-**128** demonstrated no depletion of ERBB2 at all concentrations tested, suggesting that TCI **128** induced degradation of the biomarker in a HSP70-dependent manner.

Although we had demonstrated that a lysine-TCI can function as a cellular inhibitor of HSP70, TCI **128** only degraded ERBB2 at inhibitor total concentrations >10  $\mu\text{M}$  which we concluded was too high to further investigate HSP70 inhibition in a cellular context. Potentially, the hydrolytic instability of the 5'-ether-linked sulfonyl fluoride TCI **128** was still limiting the activity of this compound, even at pH 7.4 in the pre-conditioned media, as hydrolytic decomposition of the inhibitor would limit the intracellular free exposure. Binding of sulfonic acid hydrolysis product **205** to HSP70 could also contribute to the observed degradation of ERBB2 as **128** hydrolyses within the cell under the assay conditions; however, this would be challenging to verify as molecules containing the highly ionisable sulfonic acid group typically exhibit poor cellular permeability,<sup>206</sup> so direct incubation of **205** with HCT116 cells would likely be inconclusive. Additionally, treating the HCT116 cells with 40  $\mu\text{M}$  *ent*-**128** yielded too little protein for analysis owing

to HSP70-independent cytotoxicity. These data suggested that, despite our efforts, the intrinsic reactivity of TCI **128** remained too high for the compound to be progressed as a cellular tool for HSP70 inhibition.

## 5.5 Conclusions

This chapter described our investigation into the reactivity of HSP72 5'-ether-linked sulfonyl fluoride TCIs. The high reversible affinity of this chemotype necessitated the design and synthesis of a series of moderate reversible affinity 8-*N*-alkylated 5'-ether-linked TCIs to enable us to understand the impact of switching to an ether linker on the key kinetic parameters  $k_{\text{inact}}/K_{\text{I}}$  and  $k_{\text{inact}}$ . Surprisingly, these ether-linked TCIs maintained similar  $k_{\text{inact}}$  values to the ester-linked despite an anticipated decrease in intrinsic reactivity. Profiling their hydrolytic stability demonstrated that the improvement in the rate of on-target covalent bond formation occurs despite modulation of intrinsic reactivity. This inspired a new metric, Covalent Efficiency, which normalises the rate of on-target covalent bond formation against the non-specific reactivity of a TCI, to assist future covalent drug discovery projects in triaging hit matter.

We then incubated biochemically potent TCI **128** with HCT116 cells, which demonstrated degradation of HSP70 client protein ERBB2 at similar total concentrations to the reversible HSP70 cellular tool VER-155008 **37**. In contrast, irreversible control *ent*-**128** showed no degradation of ERBB2, indicating that the degradation demonstrated by TCI **128** was occurring in a HSP70-dependent manner. However, the high total concentrations of TCI **128** required to induce ERBB2 degradation, likely owing to hydrolytic instability, in addition to the apparent HSP70-independent cytotoxicity of *ent*-**128**, suggested that sulfonyl fluoride-containing TCIs would be unsuitable to progress as cellular tools.

## 6 Reversible HSP72 Lysine-TCIs

## 6 Reversible HSP72 Lysine-TCIs

### 6.1 Introduction

Extensive characterisation, including profiling in cells, indicated that sulfonyl fluoride-containing TCIs exemplified by TCI **128** were unsuitable to be progressed as cellular probes owing to hydrolytic instability and non-specific cytotoxicity. However, as the 5'-ether scaffold had been demonstrated to possess high reversible affinity ( $K_i < 80$  nM) we proposed that incorporation of an alternative lysine-reactive warhead that would overcome these issues would furnish a suitable cellular tool inhibitor of HSP70.

#### 6.1.1 Alternative Lysine-Reactive Warheads

Alternative warheads that have been successfully applied in the lysine-TCI approach include vinyl sulfones<sup>82</sup> and activated esters (Figure 6.1).<sup>84</sup>

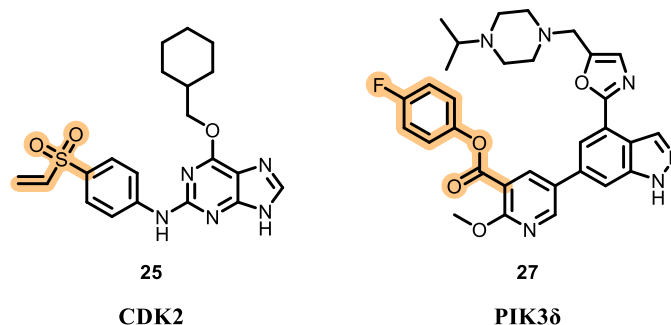


**Figure 6.1** Lysine-TCIs **25** and **27** incorporating a vinyl sulfone warhead, targeting CDK2,<sup>82</sup> and an activated ester warhead, targeting PI3Kδ.<sup>84</sup>

Within our group, activated ester **206** was synthesised for evaluation as a 5'-ether-linked HSP72 lysine-TCI (Figure 6.2 A).<sup>145</sup> Characterisation by FP (Figure 6.2 B) and intact protein mass spectrometry (Figure 6.2 C) respectively demonstrated no time-dependent shift in the  $IC_{50}$  data and no detectable covalent adduct formation, consistent with a non-covalent mechanism of action when binding HSP70.<sup>155</sup>



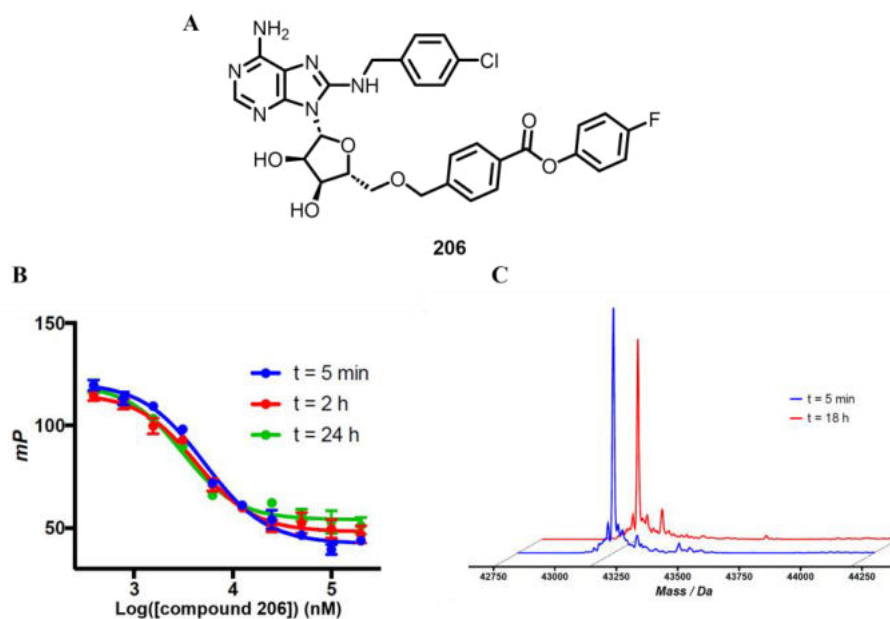


**Figure 6.2** A Structure of activated ester **206**. B Profiling of **206** by FP shows no time dependence consistent with a reversible MoA.<sup>145</sup> C IPMS of **206** incubated with HSP72-NBD shows no detectable covalent adduct formation.<sup>155</sup>

It was proposed that the sterically bulky *p*-fluorophenol leaving group would have to point on a vector-to-solvent to access the pre-covalent binding mode, blocking the nucleophilic attack at the ester carbonyl group by Lys-56, as this reaction must fulfil the requisite Flippin-Lodge (FL) and Bürgi-Dunitz (BD) angles for covalent bond formation (Figure 6.3).<sup>207</sup>

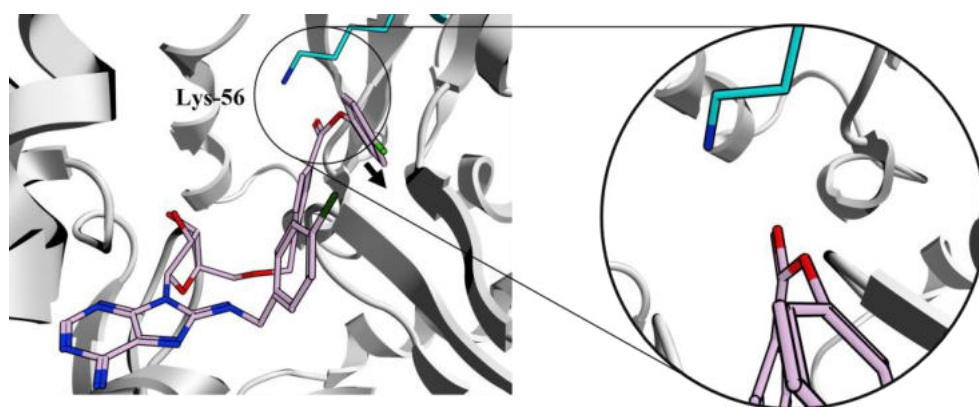


**Figure 6.3** Model of **206** bound to HSP72-NBD, based on single crystal x-ray structure of 1<sup>st</sup> generation acrylate **41** and HSP72-NBD (PDB: 5MKS), showing Lys-56 is incorrectly positioned to attack carbonyl of activated ester. Arrow denotes vector-to-solvent. Model prepared in MOE 2019.

Molecular modelling was performed with a corresponding vinyl sulfone MMP **207**, which suggested that the orientation of inhibitor **207** would likewise be unsuitable to obtain a covalent MoA (Figure 6.4). Analysis of the putative binding mode indicates that the H-bonding interaction of Lys-56 with the sulfone moiety would block access of the nucleophilic residue to the key reacting  $\beta$ -carbon of the vinyl group, preventing covalent bond formation.

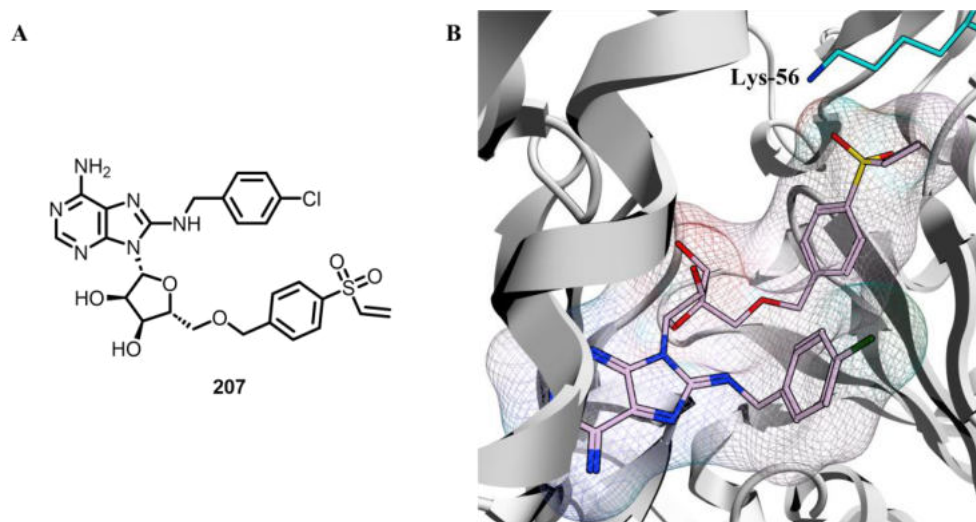


**Figure 6.4** **A** Structure of vinyl sulfone MMP **207**. **B** Model of **207** bound to HSP72-NBD, based on single crystal x-ray structure of 1<sup>st</sup> generation acrylate **41** and HSP72-NBD (PDB: 5MKS), showing how the sulfone group blocks access of Lys-56 to the  $\beta$ -carbon of the vinyl moiety. Model prepared in MOE 2019.

We therefore concluded that the current repertoire of lysine-reactive irreversible covalent warheads were unsuitable to obtain a potent cellular HSP70 tool compound from this chemotype; sulfonyl fluorides owing to their high intrinsic reactivity and chemical instability; and vinyl sulfones and activated esters, owing to their incompatibility with the strict conformational requirements to form a covalent bond with Lys-56. Consequently, an alternative modality would be required to overcome these limitations.

### 6.1.2 Reversible Targeted Covalent Inhibitors

Reversible TCIs represent an alternative paradigm to irreversible TCIs, in which the enzyme-inhibitor covalent complex can dissociate. Reversible TCIs follow a similar two-step mechanism of enzyme inhibition to irreversible TCIs. (Figure 6.5 A).<sup>146</sup> The inhibitor firstly binds reversibly to form the enzyme-inhibitor complex (E·I), which is under

equilibrium and can freely dissociate. The second step is the reaction of the covalent warhead with a nucleophilic amino acid in the binding site to form the inactivated enzyme (E-I), which only occurs at a sufficient rate within the enzyme inhibitor complex.

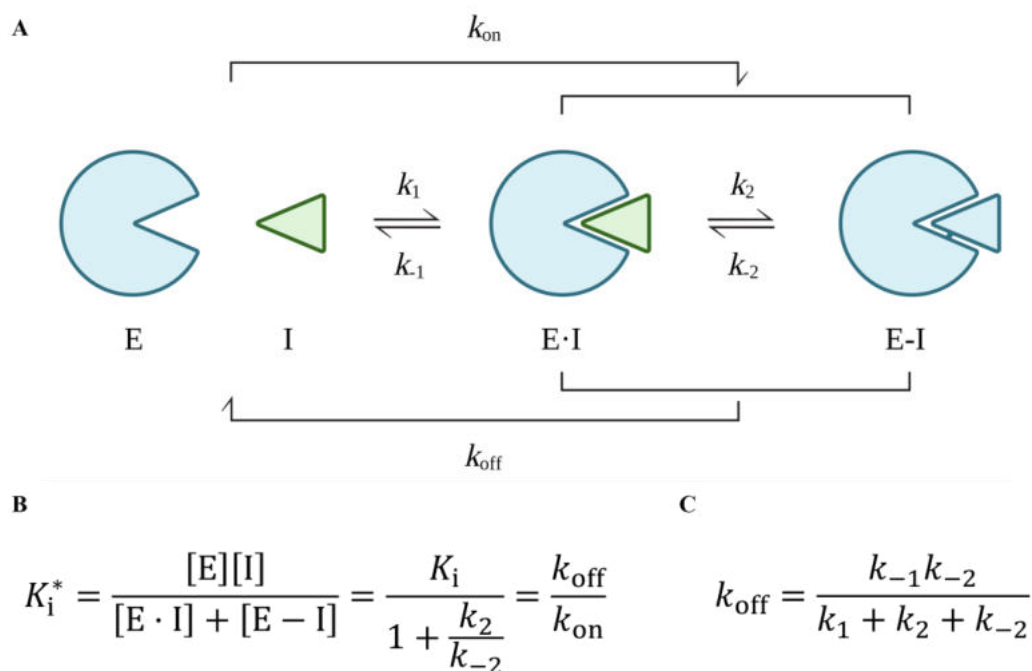


**Figure 6.5 A** Mechanism of reversible TCIs. **B** Definition of the steady state equilibrium constant  $K_i^*$ , the equilibrium constant for the overall reaction  $E + I \rightleftharpoons E \cdot I + E - I$  in terms of the equilibrium constant for the non-covalent reversible complex,  $K_i = k_{-1}/k_1$ , and the microscopic rate constants  $k_2$  and  $k_{-2}$ . **C** Definition of  $k_{\text{off}}$  for reversible TCIs in terms of the microscopic rate constants.

Formation of the non-covalent complex  $E \cdot I$  is governed by the microscopic rate constants  $k_1$  and  $k_{-1}$ , and the inhibition dissociation constant for the non-covalent complex,  $K_i$ , can be expressed in terms of these rate constants ( $K_i = k_{-1}/k_1$ ). Unlike the irreversible case, reaction to form the covalent complex  $E - I$  is reversible, being dependent on covalent association rate constant,  $k_2$ , and the covalent dissociation rate constant,  $k_{-2}$ . The steady state equilibrium constant,  $K_i^*$ , represents the overall reaction  $E + I \rightleftharpoons E \cdot I + E - I$  and thus quantifies the true affinity of a reversible TCI for its target (Figure 6.5 B).  $K_i^*$  can be expressed in terms of  $K_i$  and the microscopic rate constants  $k_2$  and  $k_{-2}$ , and also in terms of the  $k_{\text{off}}$  and  $k_{\text{on}}$ , which are the respective macroscopic rate constants of dissociation ( $E \cdot I + E - I \rightarrow E + I$ ) and association ( $E + I \rightarrow E \cdot I + E - I$ ) for the overall reaction.  $k_{\text{off}}$  can be represented in terms of the microscopic rate constants for the two step reaction (Figure 6.5 C); critically,  $k_{\text{off}}$  is inversely related to the drug-target residence time  $\tau = 1/k_{\text{off}}$ , which is the lifetime of drug-target occupancy.<sup>8</sup> An alternative representation of the drug-target

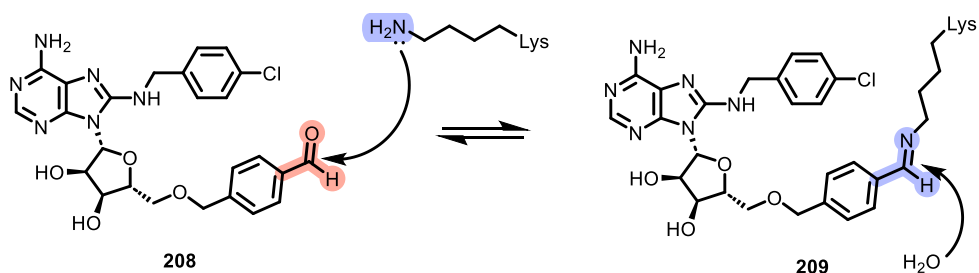
residence time is the dissociative half-life for the receptor–ligand complex  $t_{1/2}^{\text{diss}}$ , which is related to  $k_{\text{off}}$  via the relationship  $t_{1/2}^{\text{diss}} = \ln 2/k_{\text{off}}$ .

Drug-target occupancy drives the pharmacological effect of a small molecule inhibitor,<sup>12</sup> and extended residence times can lead to enhanced pharmacological efficacy.<sup>208</sup> Decreasing the rate of dissociation of the covalent complex ( $k_{-2}$ ), which is typically much slower than  $k_2$ , thus would decrease the overall off-rate of the drug-target complex ( $k_{\text{off}}$ ), leading to an extended residency time. Therefore, improving the potency of a reversible TCI can be achieved by decreasing the off-rate  $k_{\text{off}}$ , accomplished through stabilisation of the covalent complex ( $k_{-2}$ ), as this results in enhanced target occupancy.

Inhibition is considered irreversible when the residency time exceeds the life-time of the enzymatic target.<sup>209</sup> However, irreversible covalent inhibition is associated with idiosyncratic drug toxicity owing to irreversible tagging of off-targets,<sup>210</sup> which may be responsible for the HSP70-independent cytotoxicity observed for our sulfonyl fluoride TCIs. A reversible covalent MoA is therefore potentially advantageous compared to an irreversible covalent MoA, as any off-target adducts that are formed can dissociate ( $k_{\text{off}} > 0$ ), reducing the risk of off-target effects.<sup>211</sup> We envisaged that applying a reversible covalent strategy may increase the target specificity and limit the observed non-specific cytotoxicity of our HSP72 lysine-TCIs.

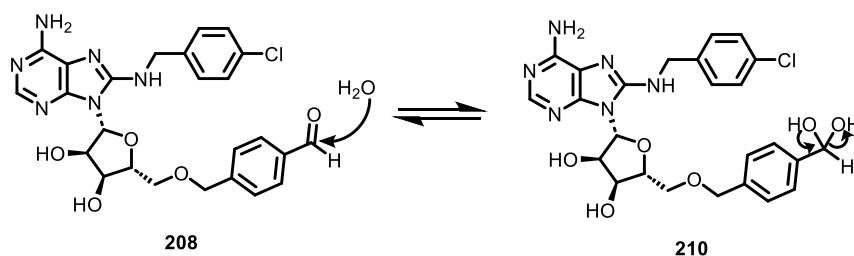
### 6.1.3 Lysine-Targeting Reversible Covalent Inhibition

Aldehydes are reversible covalent warheads which are becoming increasingly popular in covalent drug discovery.<sup>20</sup> Within our group, aldehyde **208** had been previously synthesised as a TCI targeting Lys-56 of HPS72-NBD (Scheme 6.1). Mechanistically, reaction of an aldehyde with lysine is reversible, resulting in the formation of an imine or Schiff base **209**.<sup>212</sup>



**Scheme 6.1** Mechanism of imine formation from reaction of aldehyde **208** with lysine to form lysine adduct **209**.

Aldehydes are potentially attractive covalent warheads owing to their water compatibility; they exist in equilibrium with their hydrate form **210** in aqueous solution (Scheme 6.2).<sup>213</sup>



**Scheme 6.2** aldehyde **208**/hydrate **210** equilibrium in aqueous solution.

Aldehyde **208** was previously profiled *via* FP and IPMS assays, but unfortunately showed no time dependence or evidence of a covalent adduct (Figure 6.6).<sup>155</sup>

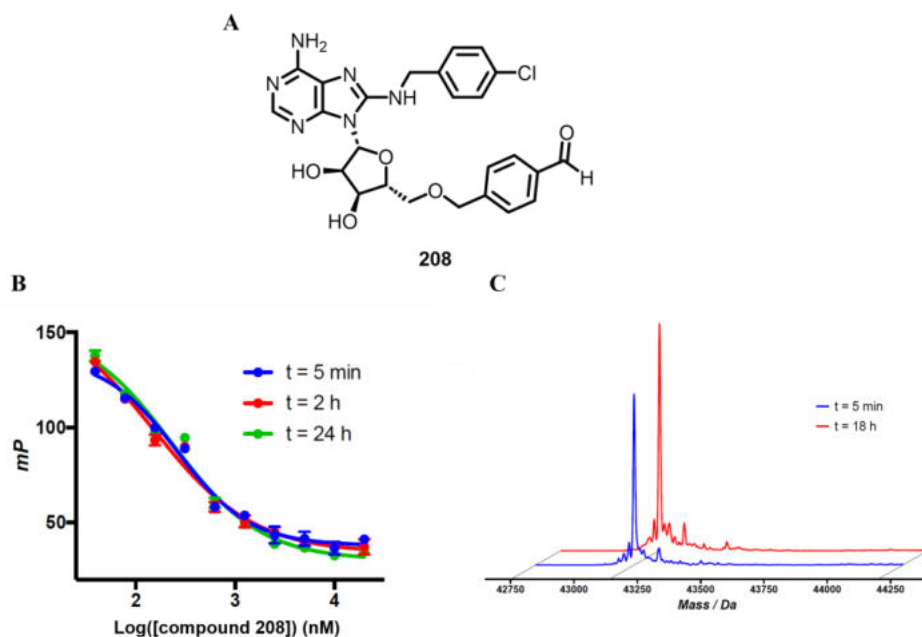


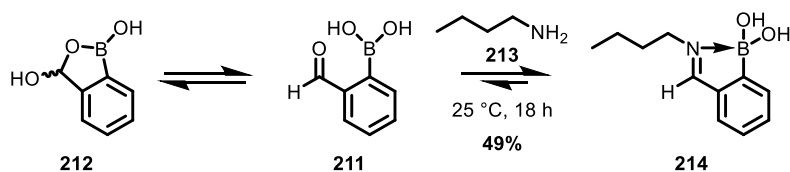
**Figure 6.6** A Structure of aldehyde **208**. B Profiling of **208** by FP shows no time dependence consistent with a reversible MoA.<sup>155</sup> C IPMS of **208** incubated with HSP72-NBD shows no detectable covalent adduct formation.

Applying the reversible covalent model to our lysine-TCI design, whilst aldehyde **208** demonstrated apparent competitive reversible binding in the FP-assay, the lack of observable covalent adduct and time-dependence suggested that the postulated imine adduct was rapidly dissociating in solution, leading to a large  $k_{\text{off}}$  and consequently a minimal enhancement of residency time. Nevertheless, aldehyde **208** appeared to retain the excellent reversible affinity ( $K_i < 200$  nM) of other 5'-ether-linked HSP72 inhibitors even though there appeared to be minimal off-rate suppression associated with the aldehyde warhead. We hypothesised that optimisation of  $k_{\text{off}}$  for aldehyde **208** through stabilisation of the resultant imine adduct may furnish a potent, specific, and hydrolytically stable reversible lysine-TCI of HSP72.

#### 6.1.4 Stabilisation of the Lysine-Aldehyde Adduct

Strategies to stabilise lysine-aldehyde imine adducts involve the incorporation of an Lewis or Brønsted acid functionality *ortho* to the aldehyde moiety, which stabilises the resulting Schiff base through interaction with the imine nitrogen. One well-validated approach is iminoboronate chemistry which employs a boronic acid group<sup>214</sup>. This approach was first detailed in 1968<sup>215</sup> and first applied to modify protein lysine residues

in 2012 by Cal et al.<sup>216</sup> In a model system, they incubated 2-formylboronic acid **211**, which exists in equilibrium with hydrate **212**, with 1-butylamine **213** (Scheme 6.3).



**Scheme 6.3** Model system for imine stabilisation *via ortho*-boronic acid, reacting 1-butylamine **213** with 2-formylboronic acid **211** (Cal et al).<sup>216</sup>

The resulting imine-adduct **214** is thermodynamically stabilised through a robust N-B dative bond.<sup>214,217</sup> The authors then demonstrated *via* MS that 2-formylboronic acid **211** reacts with multiple lysine residues on the surface of proteins such as lysozyme, myoglobin and cytochrome c to form the stabilised Schiff base. This iminoboronate chemistry was successfully applied to develop reversible lysine-TCI **215** targeting a non-catalytic lysine of Mcl-1 forming adduct **216** (Figure 6.7).<sup>218</sup>

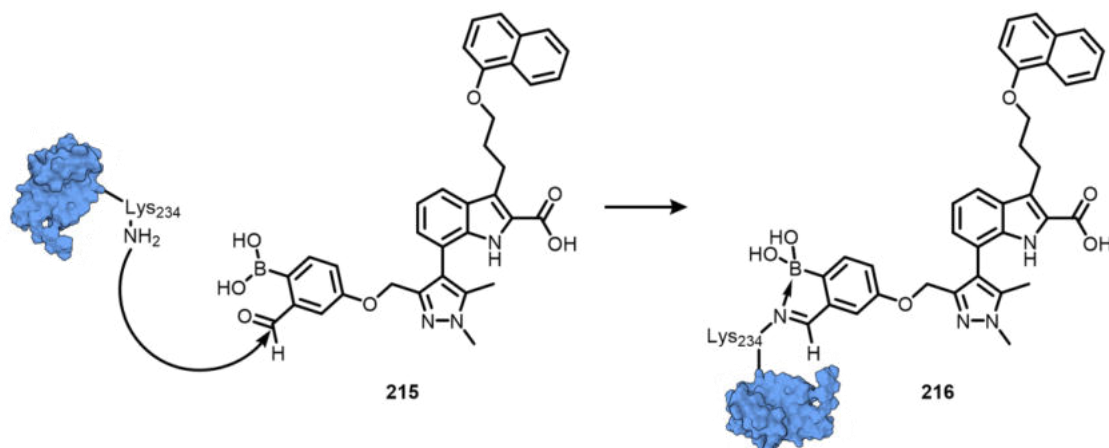


**Figure 6.7** Structure and mechanism of aldehyde boronic acid reversible lysine-TCI **215** targeting Mcl-1.<sup>218</sup>

Reja et al. expanded this concept to design RMR1 **217**, a reversible covalent warhead, which underwent reaction with lysine **218** to form stable diazaborine species **219** with a long residency time, with  $k_{\text{off}} = 2.6 \times 10^{-5} \text{ s}^{-1}$  and therefore  $\tau = 11 \text{ h}$ . (Figure 6.8).<sup>219</sup>

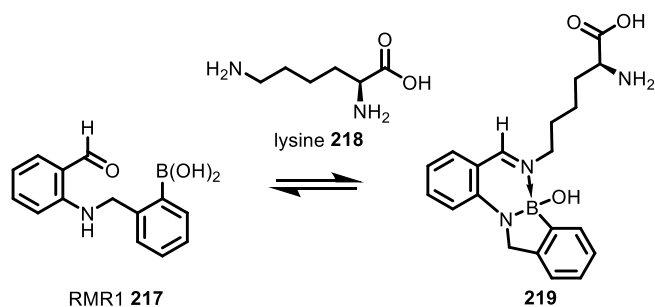


**Figure 6.8** Mechanism for the reaction of RMR1 **217** with lysine.

The authors then appended the RMR1 warhead **217** to a cyclic peptide scaffold to form reversible TCI **220**, targeting SrtA in *Staphylococcus aureus* (Figure 6.9).

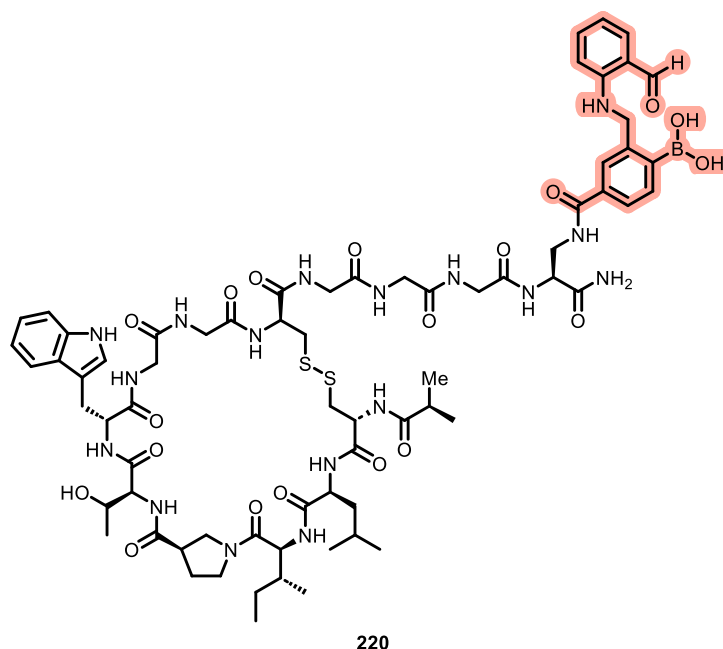


**Figure 6.9** Structure of reversible covalent cyclic peptide **220** targeting SrtA, incorporating RMR1 warhead.

A similar well-precedented strategy to stabilise the Schiff base formed from condensation of an amine with an aldehyde is the incorporation of an *ortho*-phenol moiety, which was first observed in nature in the 1950s in the mechanism of coenzyme pyridoxal 5'-phosphate (PLP) **221**.<sup>220,221</sup> PLP **221** facilitates the transamination reactions of amino acids such as glycine **222**,<sup>222</sup> via the formation of stabilised Schiff base **223** from the salicylaldehyde functionality (Figure 6.10).<sup>223</sup>



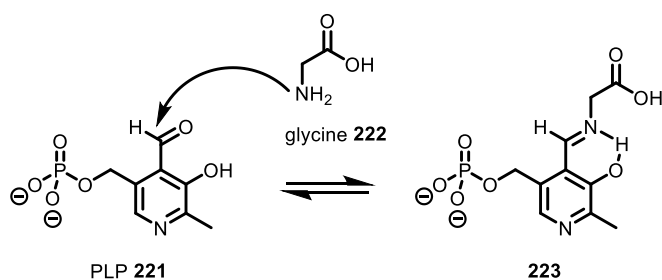


**Figure 6.10** Mechanism of condensation of glycine **222** with PLP **221** to form imine **223** stabilised by intramolecular hydrogen bond.

The resulting imine **223** is stabilised through the formation of a strong intramolecular hydrogen bond from the *ortho*-phenol group.<sup>224</sup> This mechanism was first exploited in drug discovery in 1984 in the development of Velaresol **224**,<sup>225</sup> a salicylaldehyde-derived compound for the treatment of sickle cell disease (Figure 6.11).

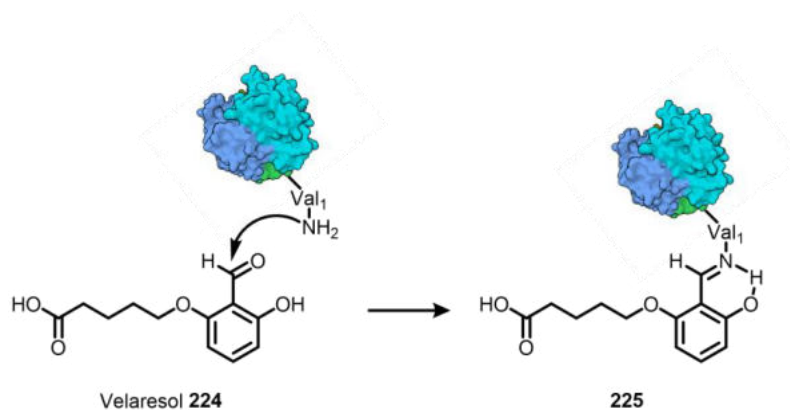


**Figure 6.11** Mechanism of action of Velaresol **224** showing the formation of a stabilised Schiff base **225** from reaction with *N*-terminal valine of HbS.

Mechanistically, the salicylaldehyde warhead of Velaresol **224** forms a stabilised Schiff base **225** with the *N*-terminal valine of sickle haemoglobin (HbS). This chemotype was

adapted in 2016 in the development of Voxelotor **226**, a clinically approved first-in-class oral drug for the treatment of sickle cell anaemia (Figure 6.12).<sup>226,227</sup>

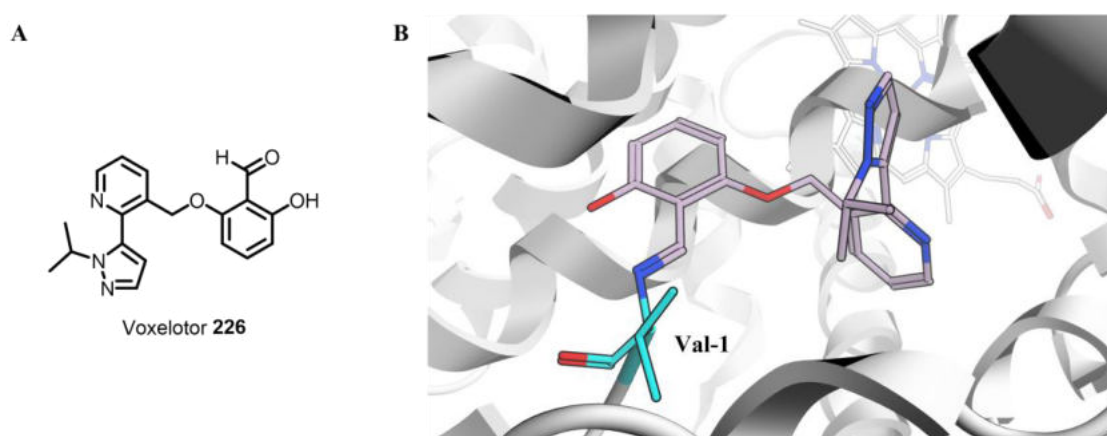


**Figure 6.12** A Structure of Voxelotor **226**. B Single crystal x-ray structure of Voxelotor **226** covalently bound to the *N*-terminal valine of a HbS unit (PDB: 5E83).<sup>228</sup>

The Schiff base formed from condensation of the *N*-terminal valine induces an increase in HbS-O<sub>2</sub> affinity through allosteric modulation.<sup>228</sup> Another application of this MoA was in the development of salicylaldehyde reversible TCI MKC9989 **227** targeting Lys-907 of IRE1 $\alpha$ ,<sup>229</sup> which culminated in the discovery of ORIN1001 **228**<sup>230</sup> which has now entered phase II clinical trials for the treatment of advanced solid tumours (Figure 6.13).<sup>231</sup>

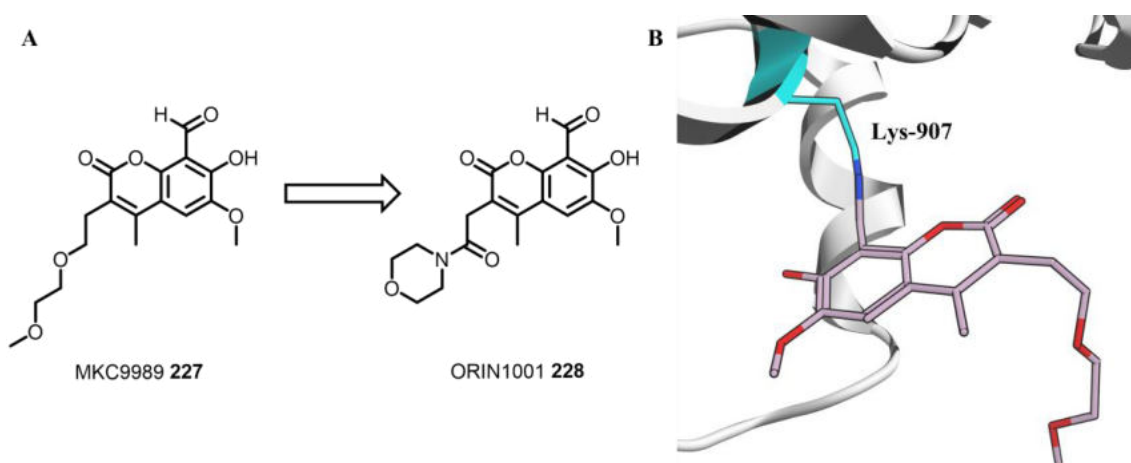


**Figure 6.13** A Optimisation of ORIN1001 **228** from MKC9989 **227**.<sup>230</sup> B Single crystal x-ray structure of MKC9989 **227** covalently bound to Lys-907 of IRE1 $\alpha$  (PDB: 4PL3).<sup>229</sup>

Yao et al. described how an *o*-boronic acid benzaldehyde derivative **229** targeting the catalytic lysine of BCR-ABL, despite showing potent biochemical activity, demonstrated

negligible cellular activity and poor recovery rates, potentially indicating chemical instability of the TCI.<sup>232</sup> However, they noted that by swapping to a *o*-phenol functionality to obtain compound **230**, they observed marked improvements in cellular activity compared to **229** with a measured GI<sub>50</sub> = 56 nM in K562 cells (Figure 6.14).<sup>233</sup> The authors determined that inclusion of the *o*-phenol moiety resulted in an increase in  $t_{1/2}^{\text{diss}}$  from 4 h to 6 h compared to the *des*-phenol MMP.

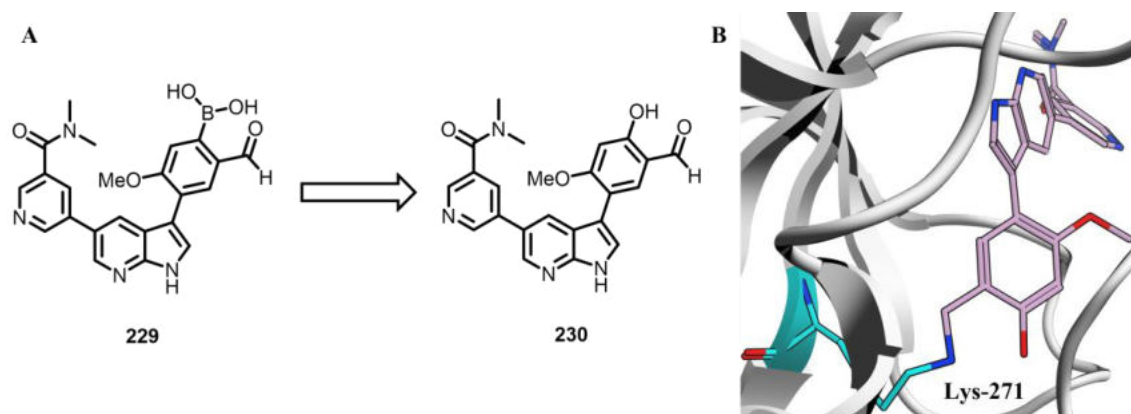


**Figure 6.14** A Design of salicylaldehyde **230** from aldehyde boronic acid **229**. B Single crystal x-ray structure of **230** covalently bound to catalytic lysine of BCR-ABL (PDB: 7W7Y).<sup>233</sup>

Taunton et al. applied chemoproteomic techniques to show that modifying a promiscuous kinase probe with a salicylaldehyde warhead to give YTP-2137 **231** resulted in the engagement of ~100 kinases in cells (Figure 6.15 A).<sup>234</sup>

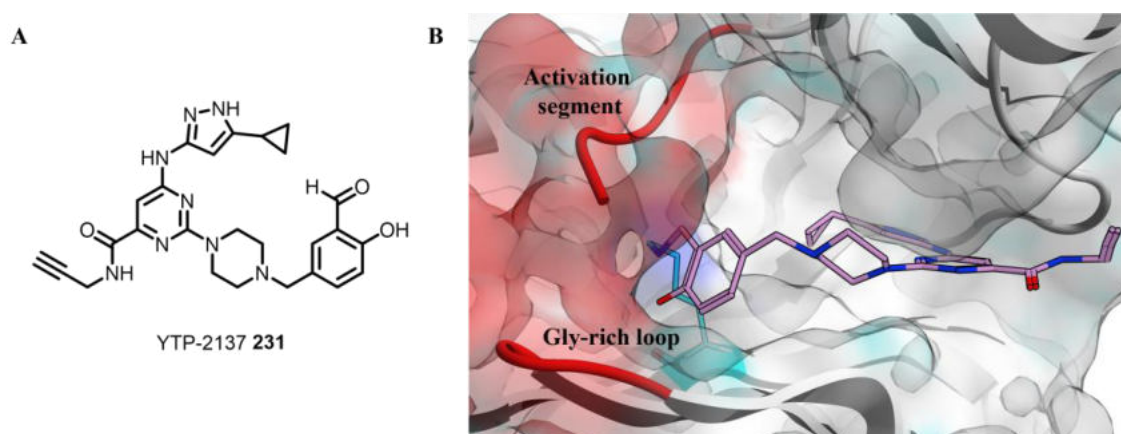


**Figure 6.15** A Structure of YTP-2137 **231**. B Single crystal x-ray structure of YTP-2137 **231** covalently bound to catalytic lysine of AURKA (PDB: 7FIC).<sup>234</sup> Gly-rich loop (bottom left) and activation segment (top left) are shown in red.

Intriguingly however, only six of these kinases exhibited extended residence times, defined by the authors as  $t_{1/2}^{\text{diss}} > 6$  h, when incubated with **231**. Co-crystallisation of **231** with one of these kinases, AURKA, revealed that the Schiff based is shielded from hydrolysis by the glycine-rich loop and the activation segment (Figure 6.15 B).

## 6.2 Design and Synthesis of HSP72 Reversible Lysine-TCI **232**

### 6.2.1 Design of HSP72 Reversible Lysine-TCI **232**

From my analysis of the literature, I concluded that *o*-phenol benzaldehydes are a highly promising functionality for the development of potent and selective lysine-TCIs. Whilst *o*-boronic acid benzaldehydes are also potentially promising in terms of their *in vitro* activity, the oxidative instability of the boronic acid group limits their application in biological systems.<sup>235</sup> Conversely, the clinical approval of Voxelotor **226**,<sup>227</sup> as well as the ongoing phase II study of ORIN1001 **228**,<sup>231</sup> indicate that salicylaldehyde-derived TCIs are suitable for progression to *in vivo* studies and beyond.

Assuming similar reversible and pre-covalent binding modes to sulfonyl fluoride TCI **128**, we hypothesised that the *p*-aldehyde of **208** is suitably positioned to covalently engage with Lys-56 of the HSP72-NBD, and incorporation of an *o*-phenol functionality would furnish reversible TCI **232** with an improved residency time and therefore enhanced potency (Figure 6.16 A). Molecular modelling of salicylaldehyde **232** bound to HSP72-NBD indicated that the aldehyde functionality would be positioned proximal to Lys-56 within the pre-covalent binding mode (Figure 6.16 B)

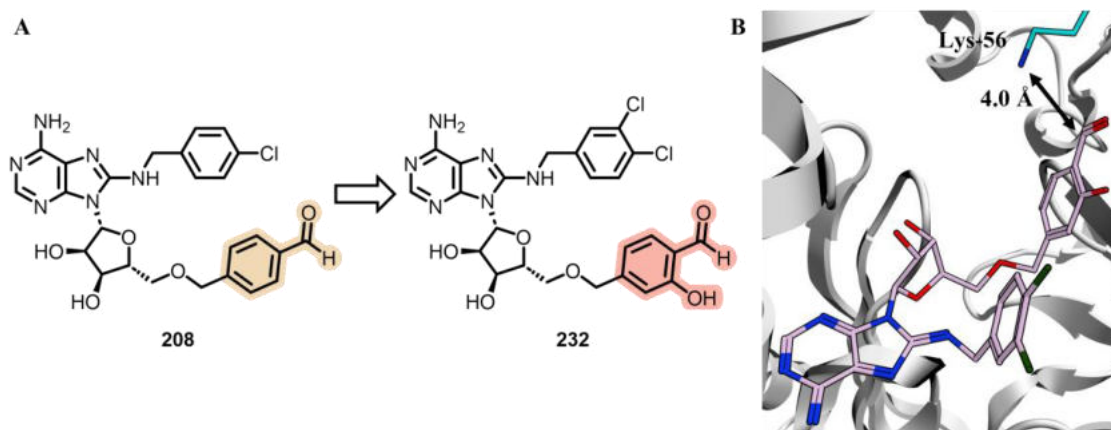
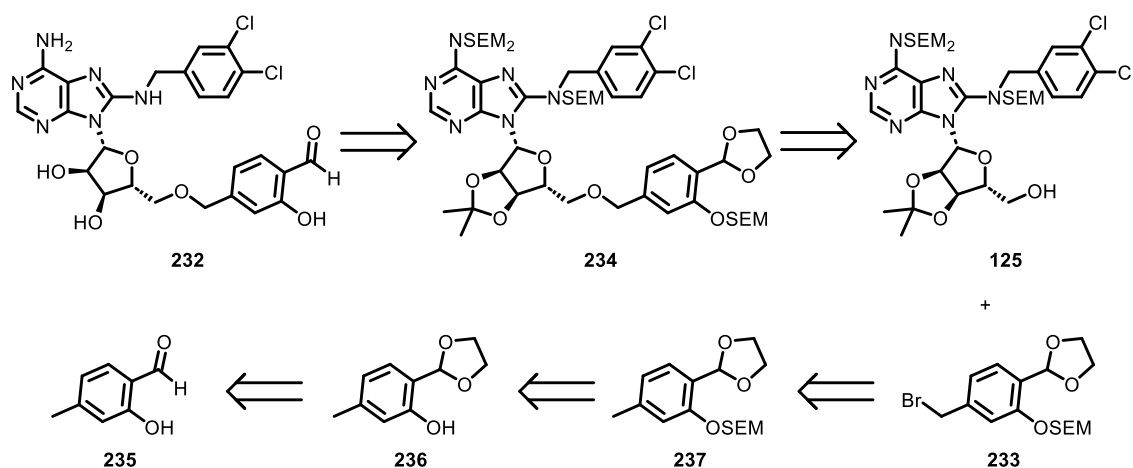


**Figure 6.16** A Design strategy for salicylaldehyde-derived reversible HSP72 lysine-TCI **232**. B Model of **232** bound to HSP72-NBD, based on single crystal x-ray structure of 1<sup>st</sup> generation acrylate **41** and HSP72-NBD (PDB: 5MKS). Model prepared in MOE 2019.

### 6.2.2 Synthesis of HSP72 Reversible Lysine-TCI **232**

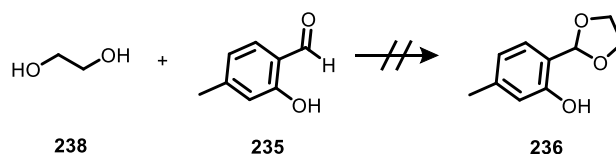
To synthesise the target salicylaldehyde **232**, we envisaged a synthetic strategy incorporating our multi-*N*-SEM-protection approach. This required the synthesis of bespoke benzyl bromide **233**, containing a SEM-protected phenol and acetonide-protected aldehyde that would facilitate direct coupling with previously synthesised intermediate **125** to give 5'-ether **234**. Finally, global deprotection under acidic conditions would yield reversible TCI **232** (Scheme 6.4).



**Scheme 6.4** Retrosynthetic analysis of reversible TCI **232**.

Our synthetic plan was to access benzyl bromide **233** through acetal protection of commercially available aldehyde **235**, SEM protection of the resulting phenol **236** to afford **237**, followed by radical bromination of the tolyl group. Unfortunately, all

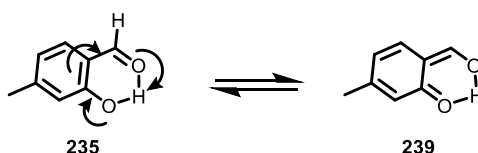
attempted methods for acetal-protection of aldehyde **235** with ethylene glycol **238** were unsuccessful (Table 6.1).



Entry	Conditions	Temperature	Solvent
<b>1</b>	PTSA (2 mol%) <sup>a</sup>	reflux	toluene
<b>2</b>	PTSA (2 mol%) <sup>a,b</sup>	reflux	toluene
<b>3</b>	Bi(OTf) <sub>3</sub> (10 mol%) <sup>c</sup>	80 °C	-

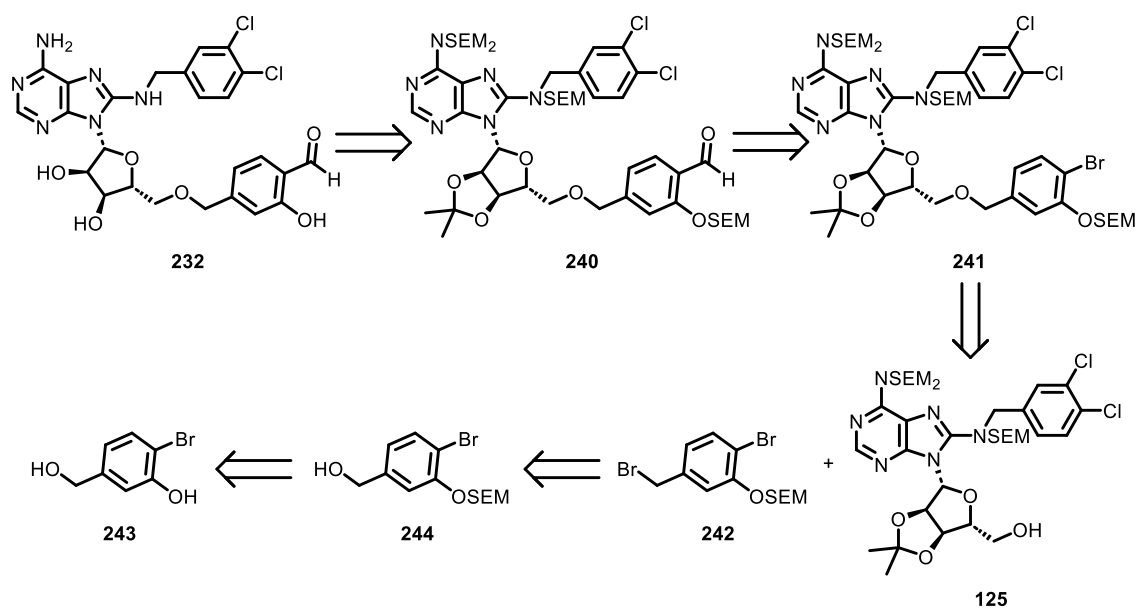
**Table 6.1** Conditions attempted for acetonide protection of **235**. <sup>a</sup>Reactions performed at 0.5 M with 4 equivalents of ethylene glycol **238** and were conducted using a Dean-Stark apparatus. <sup>b</sup>4 Å molecular sieves added to mixture. <sup>c</sup>Reaction performed with 1 equivalent of ethylene glycol **238**.

Application of standard Dean-Stark conditions with and without 4 Å molecular sieves (Table 6.1, Entries 1 and 2), as well as bismuth triflate-mediated conditions<sup>236</sup> (Table 6.1, Entry 3) led to full recovery of starting material. We speculated that the *o*-phenol functionality could be deactivating the aldehyde to nucleophilic attack by ethylene glycol **238**, both through resonance donation to the enol form **239**, and also stabilisation of the aldehyde through intramolecular hydrogen bonding (Scheme 6.5).



**Scheme 6.5** Salicylaldehyde **235** may be deactivated to nucleophilic attack by oxygen nucleophiles owing to keto-enol tautomerism from resonance donation of the phenol into the benzene ring, as well as the formation of an intramolecular hydrogen bond to stabilise the aldehyde.

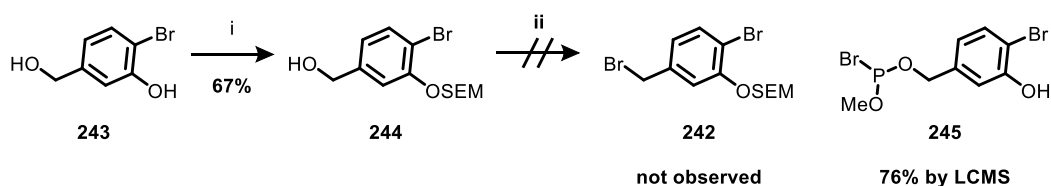
Therefore, an alternative strategy was conceived in which the aldehyde moiety of reversible TCI **232** would be accessed in a late-stage carbonylation approach, *via* tetrakis-SEM protected aldehyde **240** which would be formed from the corresponding bromide **241**, which itself would be accessed from 5'-etherification of free alcohol **125** and benzyl bromide **242** (Scheme 6.6).



**Scheme 6.6** Revised retrosynthetic analysis of reversible TCI **232**.

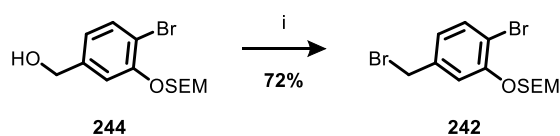
Benzyl bromide **242** would be accessed *via* SEM-protection of the phenol group of commercially available starting material **243** to yield **244**, followed by a bromination to give the key precursor **242**.

By exploiting the  $pK_a$  differential between the phenol and benzylic alcohol, selective *O*-SEM protection was achieved in the presence of sodium hydride and SEMCl to furnish the benzylic alcohol **244** (Scheme 6.7).



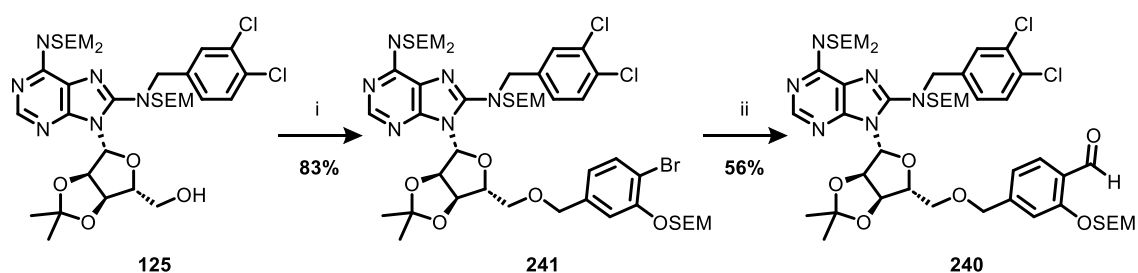
**Scheme 6.7** Attempted synthesis of **242**. Reagents and conditions: i) NaH (1.05 equiv.), THF (0.5 M), 0 °C, 30 min, *then* SEMCl (1.05 equiv.), 0 °C to rt, 22 h; ii) PBr<sub>3</sub> (0.5 equiv.), CH<sub>2</sub>Cl<sub>2</sub> (0.5 M), rt, 2 h.

Unfortunately, treatment of *O*-SEM-protected intermediate **244** with phosphorus tribromide under standard conditions apparently led to majority conversion to phosphonate **245** by LCMS, quenching with methanol, with full cleavage of the *O*-SEM protecting group being observed. Milder Appel conditions were then attempted to preserve the SEM group, which led the isolation of desired benzyl bromide **242** (Scheme 6.8).



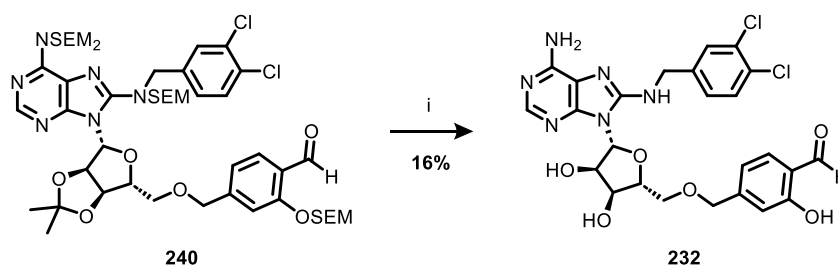
**Scheme 6.8** Synthesis of benzyl bromide **242**. Reagents and conditions: i)  $\text{PPh}_3$  (1.5 equiv.), NBS (1.5 equiv.),  $\text{CH}_2\text{Cl}_2$  (0.25 M),  $0^\circ\text{C}$  to rt, 3 h.

Williamson etherification of tris-*N*-SEM protected intermediate **125** with benzyl bromide **242** afforded the desired tetrakis-SEM protected intermediate **241** in high yield (Scheme 6.9).



**Scheme 6.9** Synthesis of aldehyde **240**. Reagents and conditions: i)  $\text{NaH}$  (1.2 equiv.), THF (0.5 M),  $0^\circ\text{C}$ , 15 min, then (2-((2-bromo-5-(bromomethyl)phenoxy)methoxy)ethyl)trimethylsilane **242** (1.5 equiv.),  $0^\circ\text{C}$  to rt, 18 h; ii)  $n\text{-BuLi}$  (1.2 equiv.), THF (0.5 M),  $-78^\circ\text{C}$ , 10 min, then DMF (2 equiv.),  $-78^\circ\text{C}$ , 3 h.

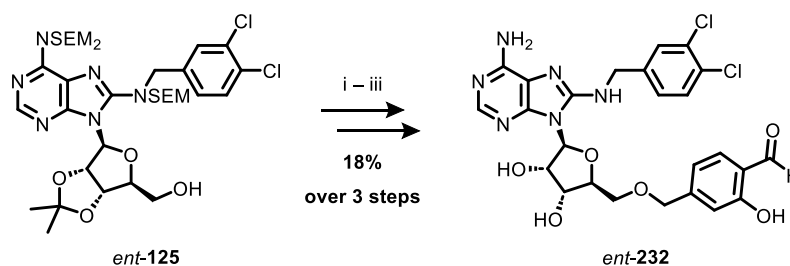
Pleasingly, standard carbonylation conditions, involving lithium-halogen exchange with  $n\text{-BuLi}$  followed by quench with DMF, afforded the desired aldehyde intermediate **240** in moderate yield despite the dense functionalisation of starting material **241**. Finally, global acid deprotection furnished reversible salicylaldehyde derived TCI **232** (Scheme 6.10).



**Scheme 6.10** Synthesis of reversible TCI **232**. Reagents and conditions: i) TFA: $\text{H}_2\text{O}$  5:2 (0.1 M), rt, 1 h.



Irreversible negative control, *ent*-**232**, was accessed in the same fashion as active TCI **232** beginning from previously synthesised intermediate *ent*-**125** (Scheme 6.11).



**Scheme 6.11** Synthesis of *ent*-**232**. Reagents and conditions: i) NaH (1.2 equiv.), THF (0.5 M), 0 °C, 15 min, *then* (2-((2-bromo-5-(bromomethyl)phenoxy)methoxy)ethyl)trimethylsilane **242** (1.5 equiv.), 0 °C to rt, 18 h; ii) *n*-BuLi (1.2 equiv.), THF (0.5 M), -78 °C, 10 min, *then* DMF (2 equiv.), -78 °C, 2 h; iii) TFA:H<sub>2</sub>O 5:2 (0.1 M), rt, 3 h.

### 6.3 Characterisation of Reversible Lysine-TCI **232**

#### 6.3.1 Characterising Reversible Lysine-TCI **232** in the TDFP Assay

With salicylaldehyde-derived TCI **232** in hand, we aimed to profile it in the TDFP assay to investigate if time-dependence would be observed. To our delight, profiling **232** with ATP-ATTO 488 **108** as the FP-probe and HSP72-NBD, demonstrated a time-dependent shift in the bound fraction/effective free protein concentration consistent with stable covalent bond formation (Figure 6.17).

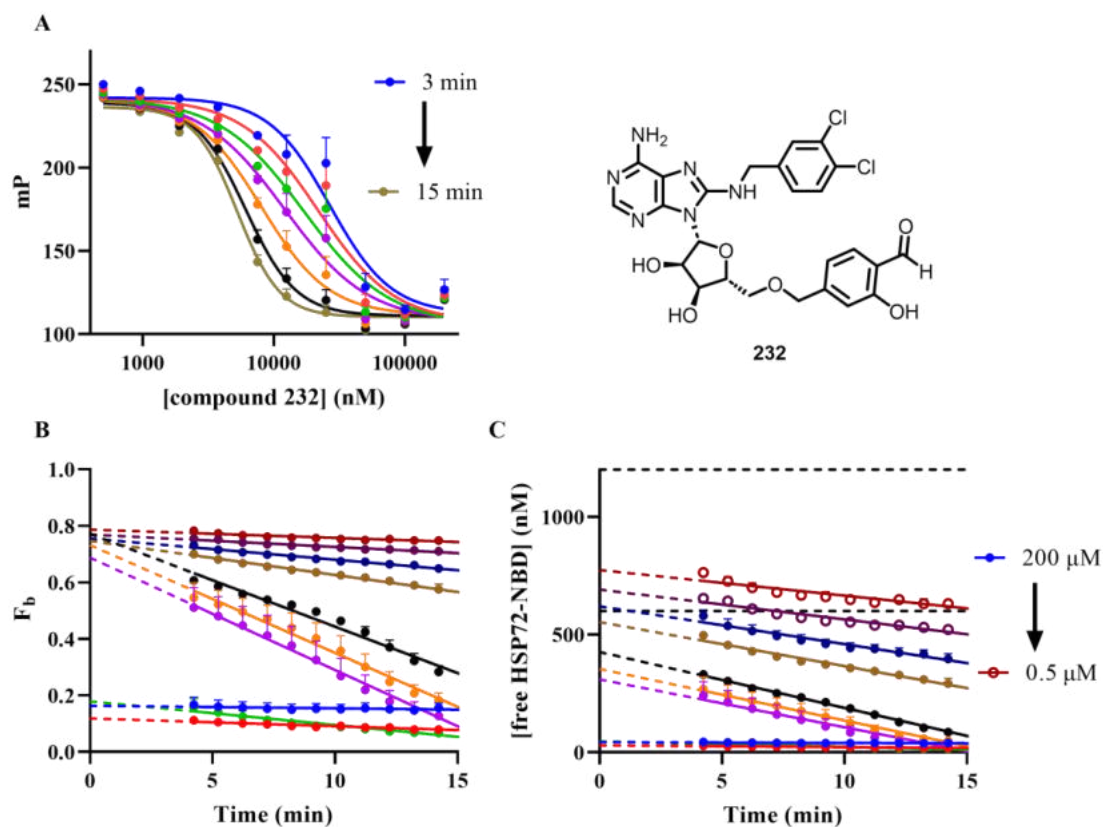


**Figure 6.17** A Profiling of reversible TCI **232** in the TDFP assay with HSP72-NBD and ATP-ATTO 488 **108**. [HSP72-NBD] selected so  $F_b = 0.85$ , measurements taken in triplicate every minute for 15 minutes and plotted on same axes. **B** Plot of calculated  $F_b$  values against time, data plotted in GraphPad Prism 9. Different colour lines represent different concentrations of TCIs from 200  $\mu\text{M}$  to 500 nM. **C**  $F_b$  values converted to [free protein]. Black dotted lines indicate [free HSP72-NBD] at 50% and 100% total protein concentration, hollow circles indicate [inhibitor] < [total protein]. Data plotted in GraphPad Prism 9.

In addition to the observed time dependence, reversible TCI **232** expectedly exhibited binding kinetics at the limit of the detection of the assay which precluded evaluation of any individual kinetic parameters. Reversible TCI **232** was also examined in the TDFP-assay in conjunction with the more potent bisaryl-ATTO 488 **148** FP-probe, in which time-dependent displacement of the FP probe was also observed (Figure 6.18).

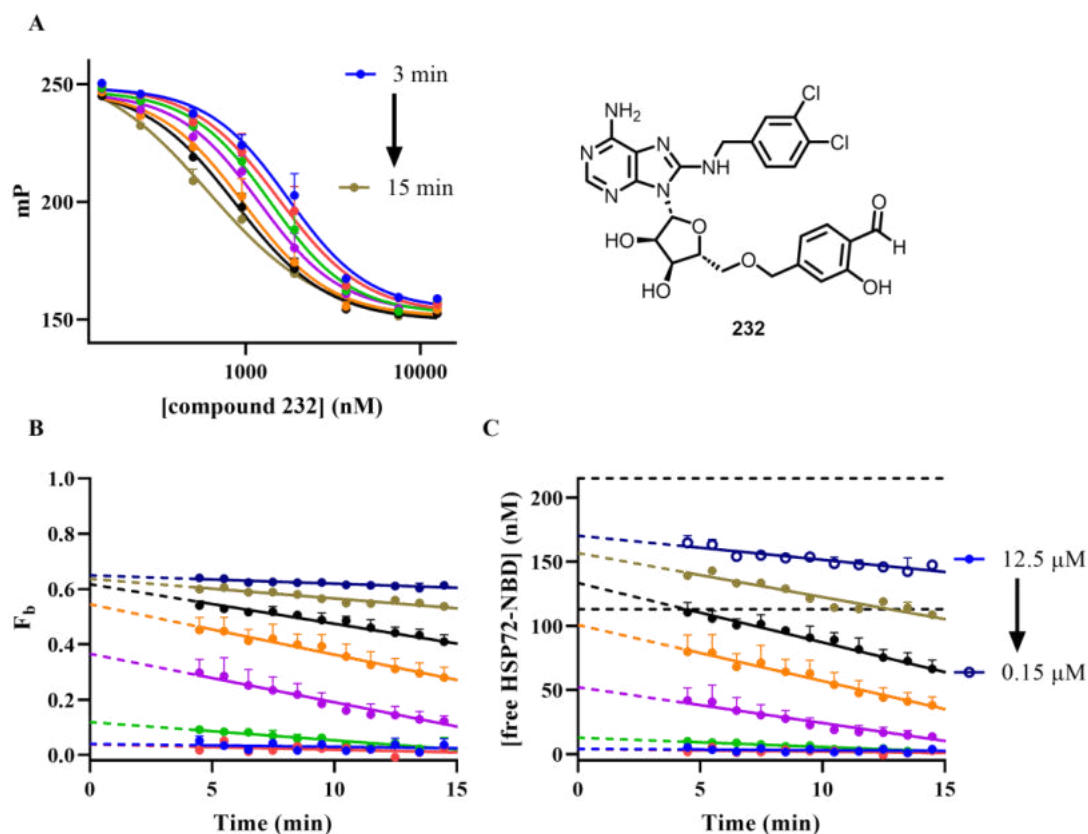


**Figure 6.18** **A** Profiling of reversible TCI **232** in the TDFP assay with HSP72-NBD and bisaryl-ATTO 488 **148**. [HSP72-NBD] selected so  $F_b = 0.7$ , measurements taken in triplicate every minute for 15 minutes and plotted on same axes. **C** Plot of calculated  $F_b$  values against time, data plotted in GraphPad Prism 9. Different colour lines represent different concentrations of TCIs from 12.5  $\mu\text{M}$  to 150 nM. **D**  $F_b$  values converted to [free protein]. Black dotted lines indicate [free HSP72-NBD] at 50% and 100% total protein concentration, hollow circles indicate [inhibitor] < [total protein]. Data plotted in GraphPad Prism 9.

Under these conditions, reversible lysine-TCI **232** exhibited kinetics at the resolvable limit of the assay format, consistent with the high reversible affinity ( $K_i < 80$  nM) observed for this chemotype. As expected, irreversible control *ent*-**232** displayed no displacement of the FP probe over the assay timecourse, consistent with negligible reversible affinity (Figure 6.19).

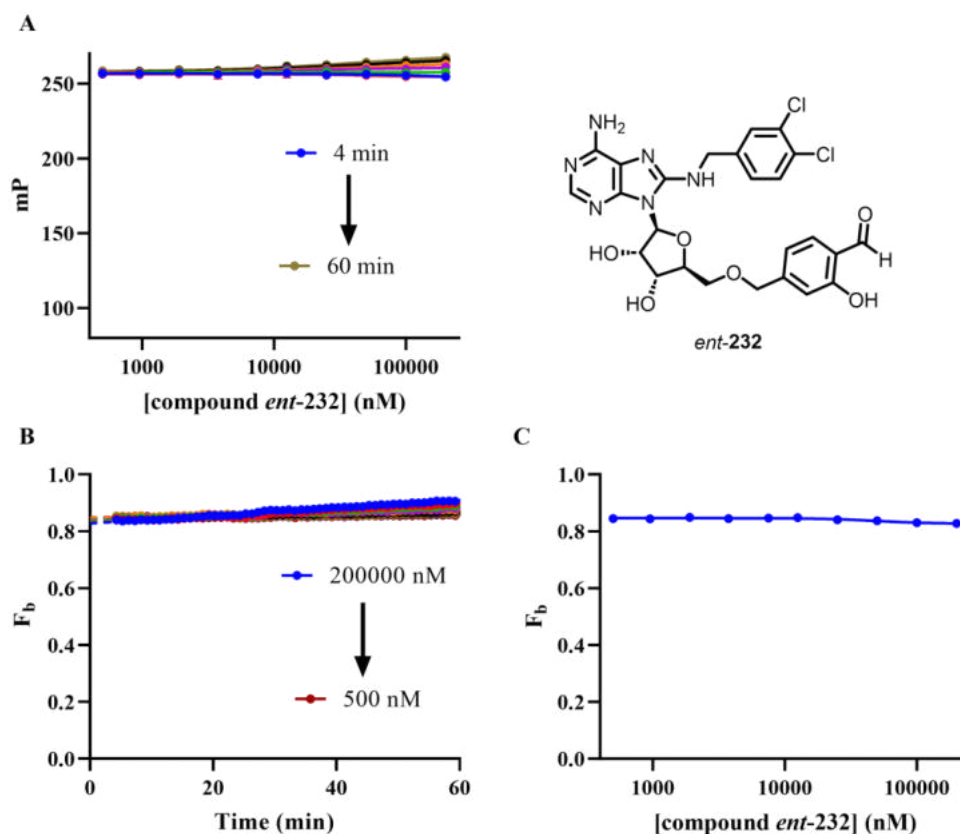
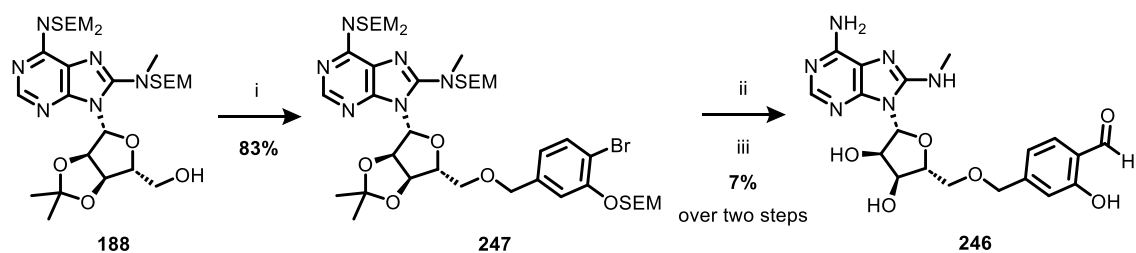


**Figure 6.19** **A** Profiling of irreversible control *ent-232* in the TDFP assay with HSP72-NBD and ATP-ATTO 488 **108**. [HSP72-NBD] selected so  $F_b = 0.85$ , measurements taken in triplicate every minute for 60 minutes and plotted on same axes. **B** Plot of calculated  $F_b$  values against time, y intercepts determined from simple linear regression (GraphPad Prism 9). **C** Plot of initial  $F_b$  against [I] (log(inhibitor) vs. response – variable slope (four parameters), GraphPad Prism 9).

The FP assay can in principle be applied to evaluate the individual kinetic parameters  $k_{on}$  and  $k_{off}$  for reversible covalent inhibitors;<sup>237</sup> however, as salicylaldehyde **232** exhibited binding kinetics at the limit of assay detection, we were unable to quantify how the inclusion of the salicylaldehyde warhead improved the potency of *o*-phenol TCI **232** relative to *des*-phenol aldehyde **208**. We therefore aimed to generate a moderate affinity reversible TCI by applying the 8-*N*-benzyl swap to 8-*N*-methyl strategy from Section 5.2.1, which would furnish a reversible covalent inhibitor with affinity within the assay window to facilitate an analysis of the binding kinetics of this chemotype.

TCI **246** was accessed in three steps from previously synthesised tris-*N*-SEM intermediate **188**, via 5-*O*'-benzylation to give **247**, carbonylation with *n*-BuLi and DMF and finally a global deprotection to afford the desired final product **246** (Scheme 6.12).



**Scheme 6.12** Synthesis of **246**. Reagents and conditions: i) NaH (1.2 equiv.), THF (0.5 M), 0 °C, 15 min, *then* 2-((2-bromo-5-(bromomethyl)phenoxy)methoxy)ethyl)trimethylsilane **242** (1.5 equiv.), 0 °C to rt, 18 h; ii) n-BuLi (1.2 equiv.), THF (0.5 M), -78 °C, 10 min, *then* DMF (2 equiv.), -78 °C, 3 h; iii) TFA:H<sub>2</sub>O 5:2 (0.1 M), rt, 1 h.

Unexpectedly, 8-*N*-methyl reversible TCI **246** also exhibited affinity at the resolvable limit of the assay window, prohibiting further kinetic analysis. However, comparison with the methyl sulfone reversible control **197** indicated that inclusion of the salicylaldehyde warhead had enhanced affinity at least >8.0-fold (Figure 6.20).

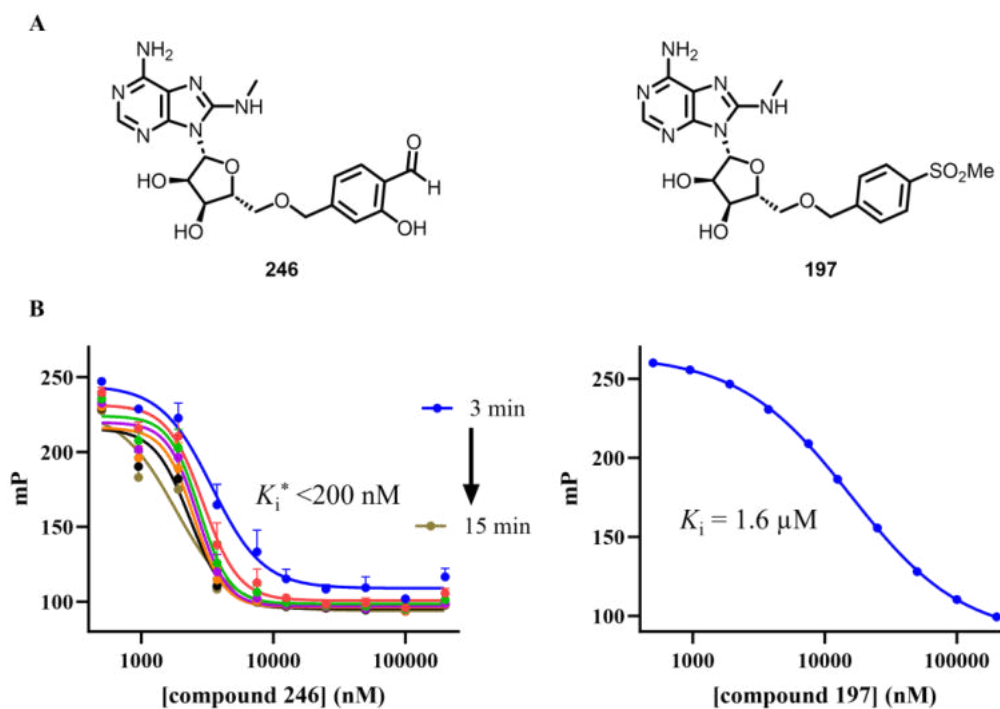


**Figure 6.20** A Structures of reversible TCI **246** and reversible methyl sulfone **197**. B Profiling of **246** and **197** in the TDFP assay with HSP72-NBD and ATP-ATTO 488 **108**.

### 6.3.2 Characterising Reversible Lysine-TCI **232** by Intact Protein-MS

With high biochemical potency and time-dependence demonstrated in the TDFP-assay, our next aim was to profile salicylaldehyde **232** by IPMS to ascertain whether the postulated Schiff base covalent adduct could be detected. Pleasingly, we observed time-dependent formation of a single adduct corresponding to addition of TCI **232** with loss of 18 Da, consistent with the formation of the critical imine and subsequent expulsion of a water molecule (Figure 6.21).

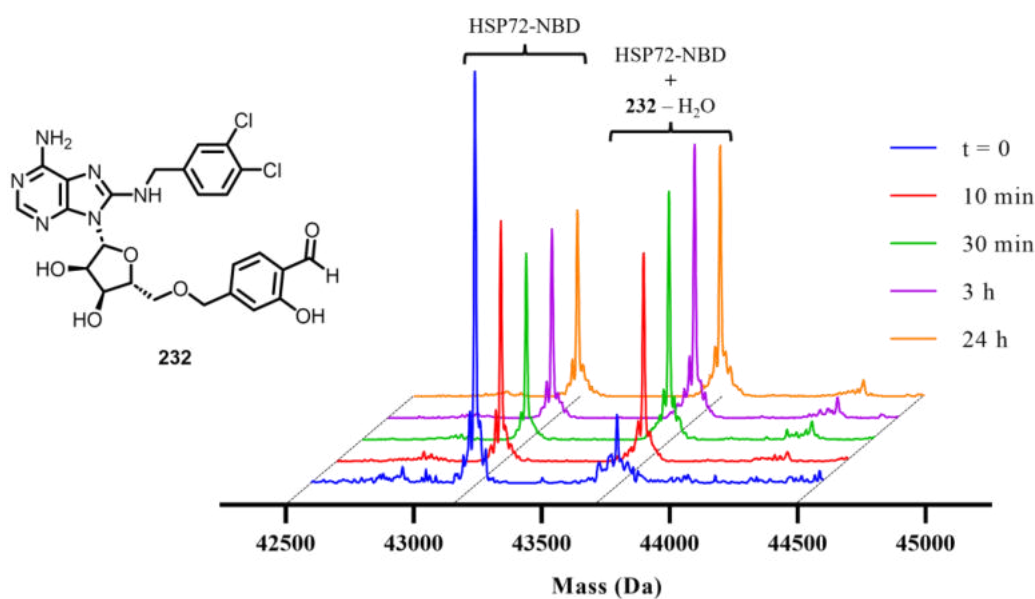


**Figure 6.21** Time-dependent covalent modification of WT HSP72-NBD (2.3  $\mu$ M) with reversible TCI **232** (20  $\mu$ M) monitored by IPMS. Data plotted in GraphPad Prism 9.

Adduct formation occurred rapidly, with significant protein labelling observed after 10 minutes of incubation. The ratio of labelled to unlabelled protein AUC appeared to remain constant at approximately 3:2 after 30 minutes, consistent with the system reaching equilibrium after this time. This is consistent with a reversible covalent MoA, as an irreversible TCI would display a continuous time-dependent increase in the adduct peak as observed for sulfonyl fluoride MMP **128**.

To probe the reversibility of the adduct, a solution of HSP72-NBD and reversible TCI **232** was prepared and incubated for 24 hours, after which irreversible TCI **128** was dosed in and the resultant mixture was monitored by IPMS in a 48 hour timecourse (Figure 6.22).

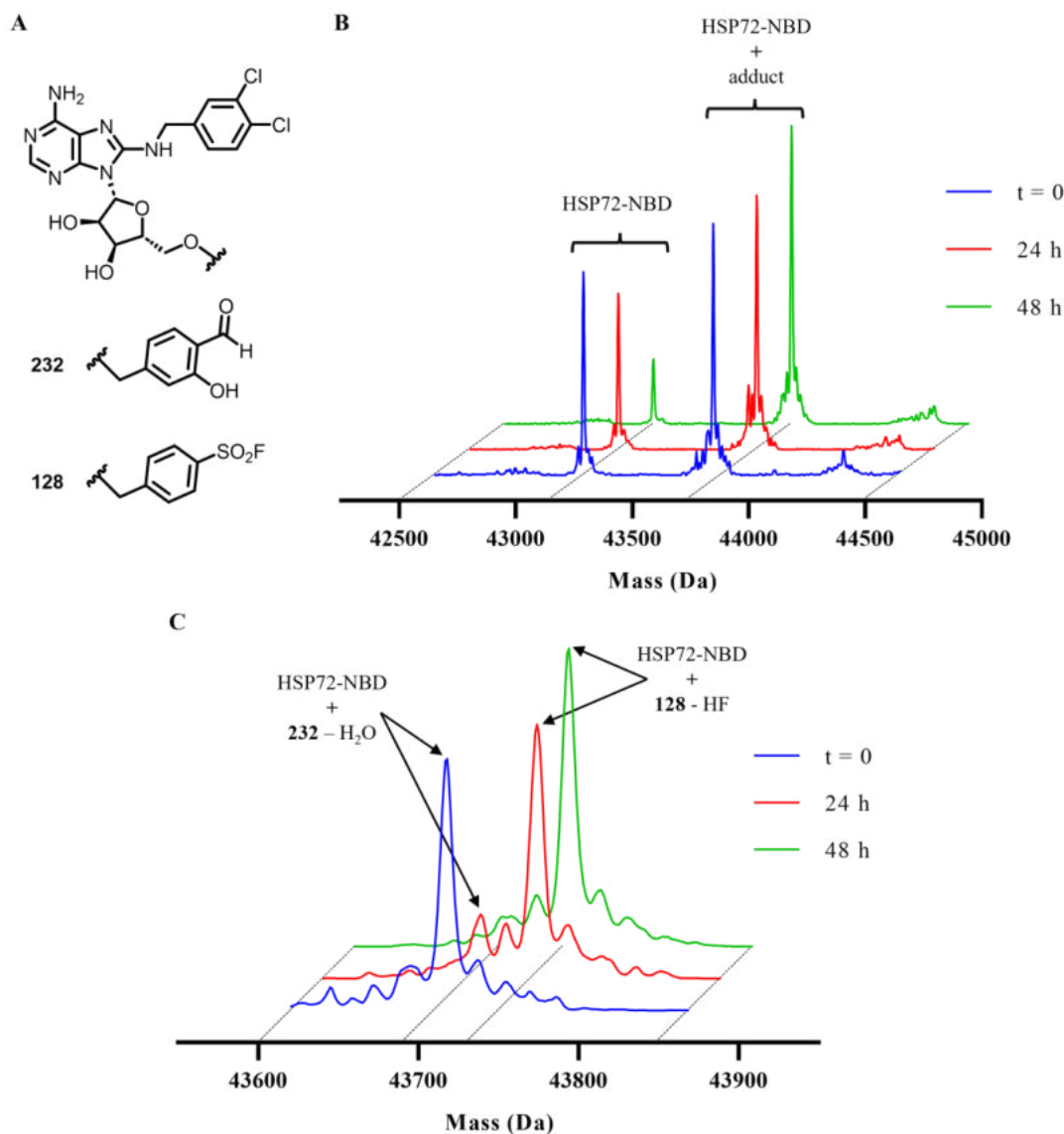


**Figure 6.22** A Structures of reversible TCI **232** and irreversible TCI **128**. B Time-dependent covalent modification of WT HSP72-NBD (2.3  $\mu$ M) pre-incubated with reversible TCI **232** (20  $\mu$ M) for 24 hours, after which irreversible TCI **128** (20  $\mu$ M) was added and monitored by IPMS across a 48 hour timecourse. C Zoom of IPMS trace. Data plotted in GraphPad Prism 9.

The peak corresponding to the Schiff base adduct of TCI **232** decreased in magnitude over time, whilst a new peak corresponding to the irreversible adduct of sulfonyl fluoride **128** simultaneously increased over the assay timecourse. This demonstrated that the adduct of salicylaldehyde **232** and HSP72-NBD is reversible, as the decrease in effective protein concentration arising from the formation of the irreversible adduct of TCI **128** appeared to lead to its gradual dissociation from the protein.

To probe whether covalent reaction was selectively occurring at Lys-56, reversible TCI **232** was incubated with the K56A construct of HSP72-NBD (Figure 6.23).

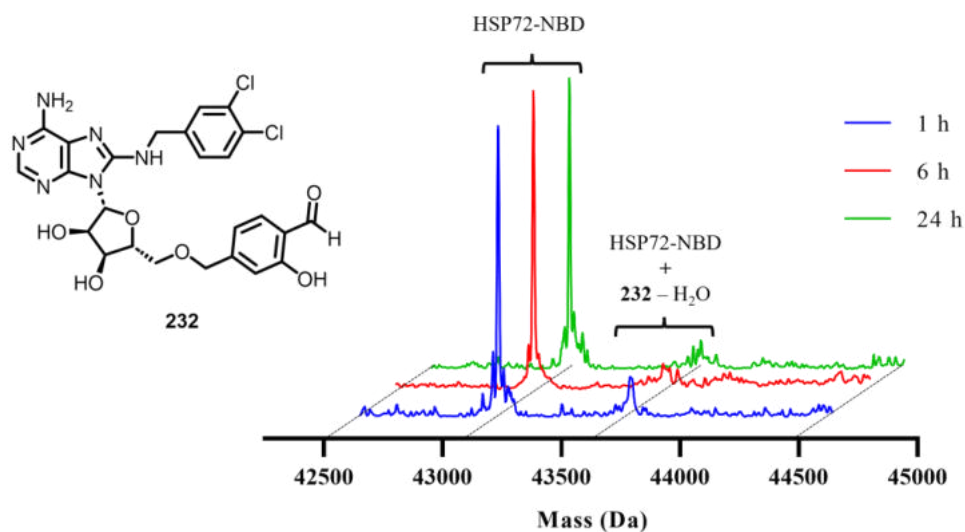


**Figure 6.23** Incubation of K56A HSP72-NBD (2.3  $\mu\text{M}$ ) with reversible TCI **232** (20  $\mu\text{M}$ ) monitored by IPMS. Data plotted in GraphPad Prism 9.

As expected, the point mutation of Lys-56 to an alanine residue resulted in a near-complete loss of adduct formation, with only a minor adduct being detected in the IPMS.

Importantly, incubation of irreversible control *ent*-**232** with wild-type HSP72-NBD furnished a similar profile in the IPMS assay, demonstrating that reversible binding of TCI **232** is critical to the covalent reaction (Figure 6.24).



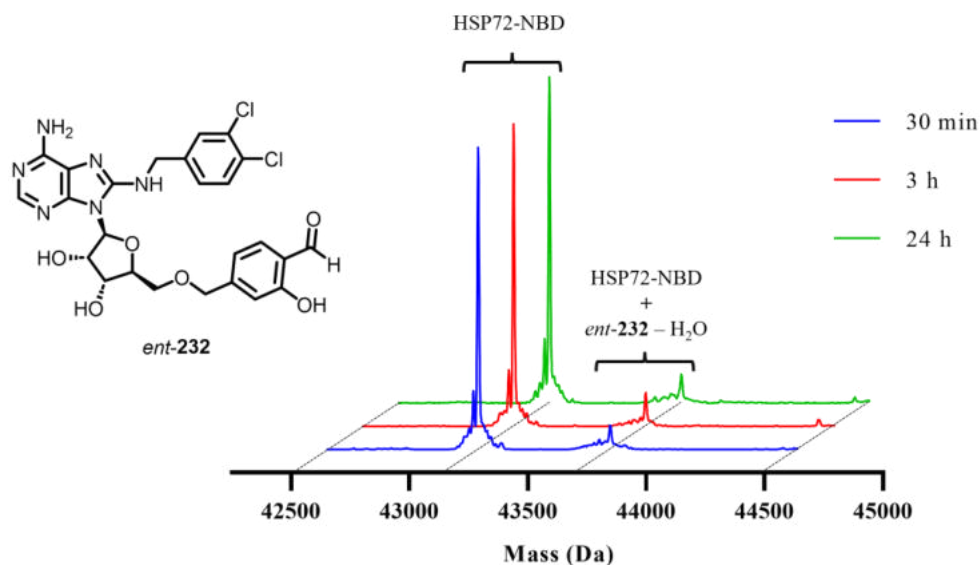


**Figure 6.24** Incubation of WT HSP72-NBD (2.3  $\mu$ M) with irreversible control *ent-232* (20  $\mu$ M) monitored by IPMS. Data plotted in GraphPad Prism 9.

#### 6.4 Biological Profiling of Reversible TCI 232

Our analysis indicated that reversible TCI **232**, incorporating a hydrolytically stable salicylaldehyde warhead, had potentially improved residency times compared to aldehyde **208** in the IPMS assay, and displayed clear time-dependence in the TDFP assay. The fourth generation reversible TCI **232** was therefore progressed for assessment as a HSP70 inhibitor in the in HCT116 cell line. Following a 24-hour incubation in pre-conditioned pH 7.4 media with VER-155008 **37**, irreversible TCI **128** and reversible TCI **232**, the cells were lysed and protein levels were assessed by immunoblotting (Figure 6.25).

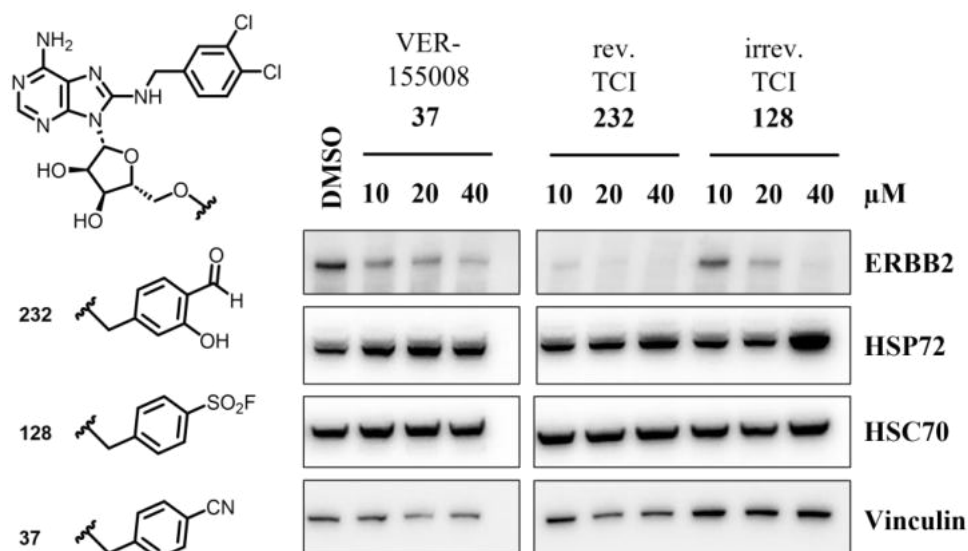


**Figure 6.25** Western blot showing biomarker response of HCT116 cells with reversible TCI **232**, irreversible TCI **128** and VER-155008 **37** (experiment performed by Marissa Powers).

To our delight, reversible TCI **232** demonstrated apparent complete degradation of ERBB2 down to 10  $\mu\text{M}$  total concentration, which represented a substantial improvement over both the previous cellular probe VER-155008 **37** as well as the third generation irreversible TCI **128**, when comparing total concentrations.

As discussed in Chapter 5, when comparing activities in cellular assays it is important to correct for the free fraction, as the free concentration of inhibitor may vary according to the different binding affinities of each compound for serum proteins contained in the cell media. Phenolic and aldehyde-containing compounds, such as reversible TCI **232**, often display significant binding to serum proteins such as albumin,<sup>238,239</sup> which consequently decreases their free concentration at equilibrium.<sup>240</sup> To assess the extent of serum protein binding and therefore correct for the free concentration of inhibitor in subsequent cell experiments, VER-155008 **37** and reversible TCI **232** were submitted to Pharmidex for profiling *via* rapid equilibrium dialysis in the cell assay conditions (Table 6.2). In brief, two compartments separated by a dialysis membrane were charged with compound, DMEM and FBS in the first compartment and only DMEM in the second compartment. After a four hour incubation, the two compartments were analysed by MS for quantitative detection of the parent compound.

Compound	%free <sup>a</sup>
VER-155008 <b>37</b>	29 (23 – 36)
Reversible TCI <b>232</b>	2.2 (1.9 – 2.6)

**Table 6.2** %free determined for VER-155008 **37** and reversible TCI **232** under cell assay conditions (experiment performed by Pharmidex). <sup>a</sup>%free values quoted as geometric mean (90% confidence intervals) of three independent experiments.

As expected, reversible TCI **232** displayed a greater extent of serum protein binding compared to VER-155008 **37**. We then performed a dose-down of VER-155008 **37** and the reversible TCI **232** with HCT116 cells to probe the extent of ERBB2 degradation at lower concentrations (Figure 6.26).

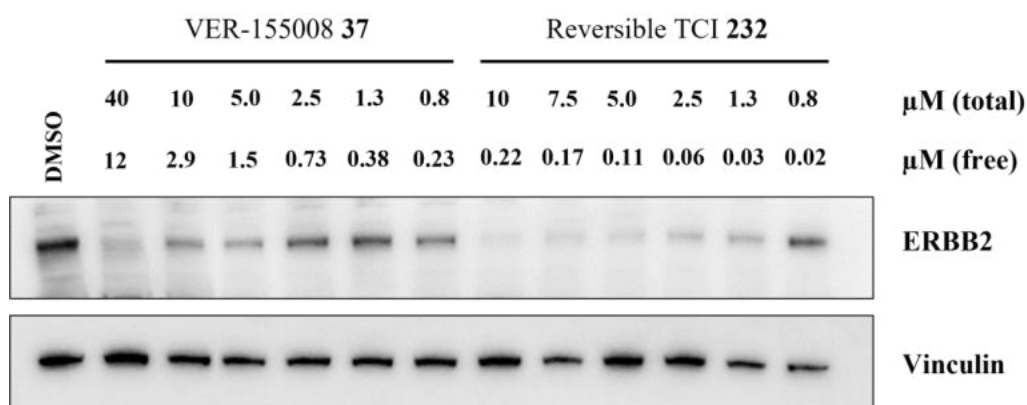


**Figure 6.26** Western blot showing effect of reversible TCI **232** and VER-155008 **37** on ERBB2 levels (experiment performed by Marissa Powers). Total concentrations have been converted to free concentrations through correction with %free = 2.2 for **232** and 29 for **37**.

Pleasingly, we observed significant ERBB2 degradation down to 30 nM free concentration for reversible TCI **232**, in contrast to 12 μM for VER-155008 **37**. This corresponds to a ~400-fold increase in cellular potency from incorporation of the salicylaldehyde warhead into the high reversible affinity 5'-ether scaffold.

## 6.5 Conclusions and Future Work

This chapter has detailed the design, synthesis, and characterisation of reversible HSP72 lysine-TCIs, which has culminated in the discovery of salicylaldehyde-derived reversible TCI **232**. Synthetic optimisation towards the salicylaldehyde chemotype involved the synthesis of a bespoke benzyl bromide intermediate **232**, which, after sodium hydride-

mediated coupling to the corresponding alcohol, was transformed to the desired aldehyde through a late-stage carbonylation approach.

Characterisation of salicylaldehyde reversible-TCI **232** demonstrated exceptional biochemical potency as well as high selectivity for the key reacting residue Lys-56 of the HSP72-NBD. Notably, unlike with the corresponding aldehyde **208**, time-dependent formation of the Schiff base adduct was directly observed *via* mass spectrometry, consistent with an improvement in residency time owing to the inclusion of the *o*-phenol moiety. Crucially, this potency increase was exploited to obtain a clear improvement in activity for the degradation of the key HSP70 client protein ERBB2, compared to previous state-of-the-art compound VER-155008 **37**.

We therefore propose that the salicylaldehyde TCI, designated CCT400591 **232**, has the potential to be an important small molecule tool for investigating the effects of HSP70 inhibition *in vitro*. Future efforts will involve determining the selectivity of **232** across the 13 family members of HSP70,<sup>103</sup> and quantitative proteomic profiling to understand its degradation profile.<sup>241</sup>

CCT400591 **232** and the reversible lysine-targeting strategy could function as a suitable start-point for a drug discovery campaign towards a clinically approved HSP70 inhibitor. Whilst the clinical approval of Voxelotor **226**<sup>227</sup> indicates that salicylaldehyde-derived drugs can be progressed onto the market, we anticipate that modifications to improve the properties of CCT400591 **232** would be necessary to obtain a suitable drug candidate. Possible modifications include a reduction in hydrogen bond donor (HBD) count,<sup>242</sup> such as substitution of the non-critical HBD at the 6-NH<sub>2</sub>, substitution of the glycosidic bond that is susceptible to both enzymatic and spontaneous cleavage,<sup>243</sup> and further optimisation of both the scaffold and reversible covalent warhead, although this approach would also require the development of new biochemical assays to quantify the kinetic and thermodynamics of binding (Figure 6.27).

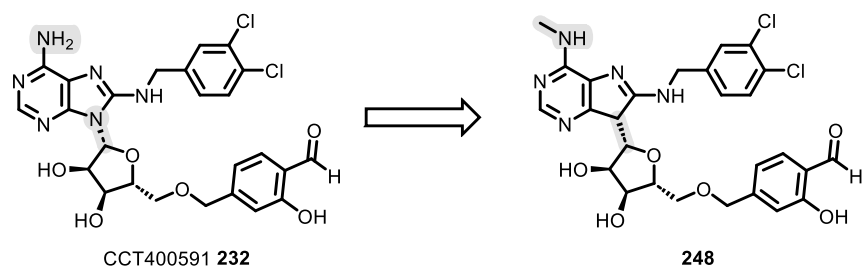


**Figure 6.27** Possible optimisation of lead compound CCT400591 **232** towards drug candidate molecule **248**.

## 7 Lysine-Targeting Covalent Inhibitors of EGFR

## 7 Lysine-Targeting Covalent Inhibitors of EGFR

### 7.1 Introduction

A principal aim of my project had been to expand the scope of the lysine-targeting covalent inhibitor approach to other difficult-to-drug targets beyond HSP70. A key challenge in the development of small molecule targeted therapies is the appearance of secondary resistance mutations, which render the therapies ineffectual.<sup>244</sup> TCIs have been successfully applied to overcome resistance mutations for targets in oncology,<sup>15</sup> one of the most successful approaches being for the epidermal growth factor receptor.<sup>20</sup>

#### 7.1.1 Epidermal Growth Factor Receptor

EGFR is a receptor tyrosine kinase (RTK)<sup>245</sup> which has a critical role in regulating the proliferation and survival of epithelial cells.<sup>246</sup> Structurally, RTKs such as EGFR are membrane-bound and consist of an extracellular ligand-binding region, which in EGFR consists of domains I – IV, a transmembrane domain and an intracellular region comprising an ATP-binding tyrosine kinase domain (TKD) and a C-terminal tail (Figure 7.1 A).<sup>247</sup>

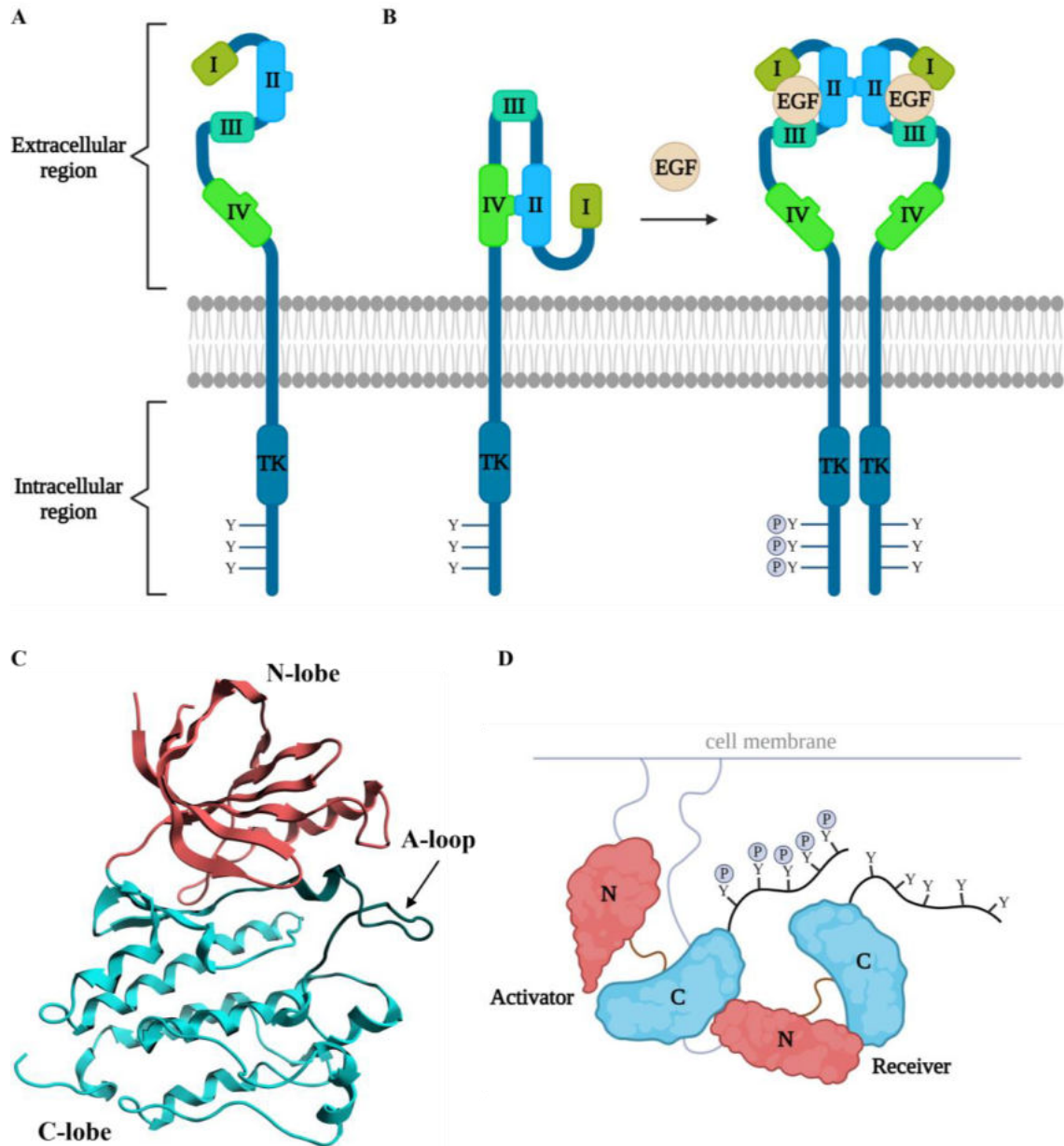


**Figure 7.1** **A** Cartoon representation of the structure of the Epidermal Growth Factor Receptor, consisting of an extracellular region (Domains I – IV), transmembrane domain and the intracellular region containing the tyrosine kinase domain and C-terminal chain. **B** Mechanism of EGFR activation. Binding of ligands such as EGF to Domain I and III triggers dimerisation of EGFR monomers through disruption of the II and IV tethering, which brings TKDs in close proximity enabling autophosphorylation. **C** Single crystal x-ray structure of EGFR TKD in an inactive conformation (PDB: 4HJO) showing N-lobe (scarlet), C-lobe (turquoise) and activation loop. **D** Activation of the TKD occurs through formation of asymmetric dimer, in which activator TKD induces allosteric activation of receiver TKD, triggering trans-autophosphorylation of activator C-terminal tail.



Mechanistically, the EGFR monomer exists in an auto-inhibited form in which domains II and IV are tethered together *via* intramolecular interactions. Binding of a ligand, such as the Epidermal Growth Factor (EGF), to Domains I and III induces a conformational change, which disrupts the tethering of II and IV, leading to the exposure of a dimerization arm of II.<sup>248</sup> This enables the dimerization of the two EGFR monomers through interaction of the Domain II of each unit, bringing the TKDs of the intracellular region into close proximity (Figure 7.1 B).

The TKD of EGFR consists of two lobes, the N-lobe and the C-lobe (Figure 7.1 C). Unlike many other RTKs, activation of the TKD of EGFR does not require phosphorylation of its activation loop (A-loop);<sup>249</sup> instead, interaction of the close proximity TKDs within the dimer allows one TKD, the activator, to induce an allosteric activation in the second domain, the receiver.<sup>250</sup> The receiver TKD then *trans*-phosphorylates the tyrosine residues present in the C-terminal tail of the activator, which act as sites to recruit and activate downstream signalling proteins (Figure 7.1 D).<sup>247</sup>

Primary mutations in the EGFR TKD are heavily implicated as oncogenic drivers in non-small cell lung cancer (NSCLC), with reported incidence rates of ~25%.<sup>251</sup> Of these, 51% were accounted for by the L858R mutation,<sup>252</sup> which results in constitutive activation of the TKD. Substitution of Leu858 for an arginine residue destabilises an autoinhibitory interaction between the  $\alpha$ -helix of the A-loop and the  $\alpha$ C helix of the N-lobe. This results in a shift to the conformation present in the active TKD and consequently activation of signalling independent of ligand-binding to the extracellular region (Figure 7.2).<sup>250</sup>

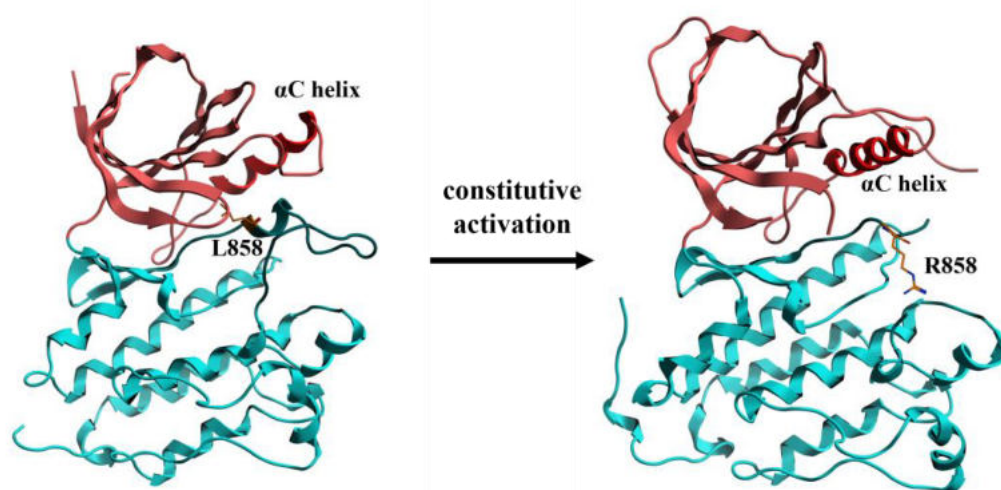


**Figure 7.2** L858R mutation results in constitutive activation of the EGFR TKD through loss of an autoinhibitory interaction between the  $\alpha$ -helix of the A-loop (teal) and the  $\alpha$ C helix of the N-lobe (red) (PDB: 4HJO and 2EB3).

### 7.1.2 Small Molecule Inhibitors of the EGFR Tyrosine Kinase Domain

Gefitinib **249**<sup>253</sup> and erlotinib **250**<sup>254</sup> are ATP-competitive reversible tyrosine kinase inhibitors (TKIs) targeting L858R EGFR (Figure 7.3).

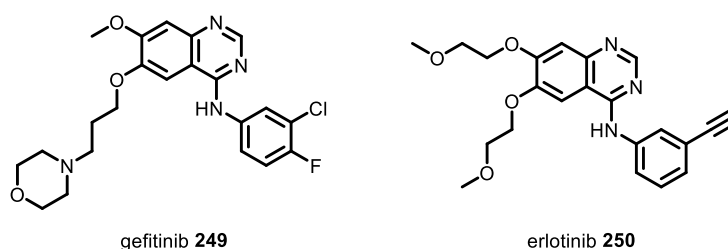


**Figure 7.3** Structures of gefitinib **249** and erlotinib **250**, 1<sup>st</sup> generation TKIs of L858R EGFR.

Despite impressive initial efficacy in patients with NSCLC harbouring L858R EGFR driver mutation, inevitably, resistance to these therapies develops, often through the acquisition of the T790M or “gatekeeper” mutation.<sup>255</sup> This threonine 790 to methionine residue substitution results in a ~10-fold increase of the ATP affinity of the TKD, resulting in a loss of efficacy from competition with this high affinity endogenous substrate.<sup>256</sup> Additionally, the T790M mutation results in a 1500 – 1700-fold loss of reversible affinity of **249** and **250** for T790M/L858R EGFR compared to L858R EGFR, and crucially a 120 – 150-fold reduced affinity compared to WT EGFR, resulting in a loss of therapeutic index.<sup>257</sup> To overcome the increased substrate competition and loss of

reversible affinity, the 2<sup>nd</sup> generation TKI afatinib **251** was designed incorporating an acrylamide warhead targeting the non-catalytic Cys-797 in the active site of EGFR (Figure 7.4).<sup>258</sup>

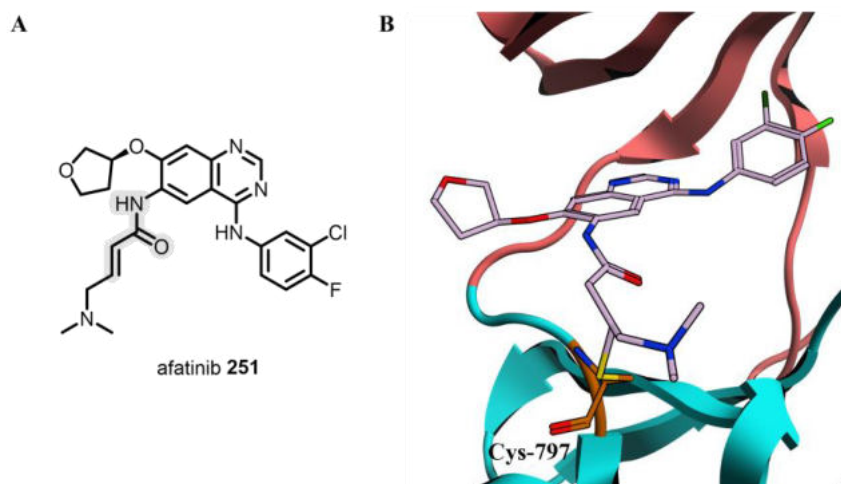


**Figure 7.4** A Structure of afatinib **251**. B Single crystal x-ray structure of afatinib **251** covalently bound to Cys-797 of the TKD of WT EGFR (PDB: 4G5J).

Following clinical approval of afatinib in 2013,<sup>259</sup> several EGFR TKIs incorporating this scaffold and acrylamide warhead have been developed, including dacomitinib **252** and neratinib **253** (Figure 7.5).<sup>260</sup>

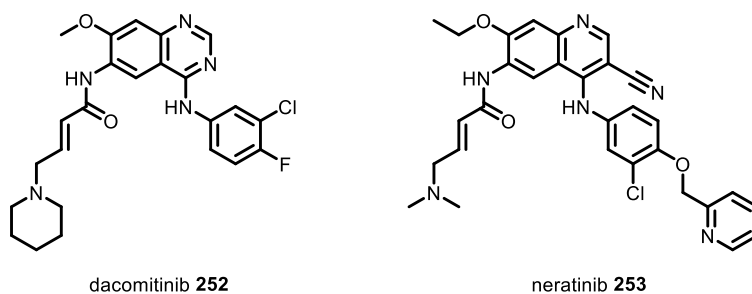


**Figure 7.5** Structures of dacomitinib **252** and neratinib **253**, 2<sup>nd</sup> generation TKIs of L858R/T790M EGFR.

However, treatment of patients with these 2<sup>nd</sup> generation EGFR TKIs is associated with severe dose-limiting toxicities which limits their application.<sup>261,262</sup> Analysis of the kinetic data demonstrated that afatinib **251** and dacomitinib **252** display ~10-fold and ~60-fold greater  $k_{\text{inact}}/K_{\text{I}}$  for WT EGFR over L858R/T790M EGFR,<sup>257</sup> respectively, suggesting that the observed toxicities are as a result of this therapeutic index.<sup>263</sup>

In an effort to develop a WT-sparing EGFR TKI, Finlay et al. disclosed the discovery of osimertinib **12** in 2014 (Figure 7.6 A),<sup>264</sup> which was ultimately approved as a first-line treatment for metastatic NSCLC.<sup>265</sup>

Biochemically, osimertinib **12** displays a 45-fold greater  $k_{\text{inact}}/K_i$  for L858R/T790M EGFR over WT, which is largely driven by a difference in  $K_i$  (17-fold).<sup>257</sup> Comparatively, afatinib **251** and dacomitinib **252** exhibit a respective 14-fold and 53-fold decrease in reversible affinity for L858R/T790M EGFR compared to WT. This may be rationalised through an examination of their binding modes, as the more extended binding mode of the aminoquinazoline chemotype of afatinib **251** may result in a steric clash when Thr-790 is substituted to methionine; conversely, the indole ring of osimertinib **12** points away from Thr-790 to make VdW interactions with residues in the phosphate-binding loop (P-loop), preventing a possible steric clash. (Figure 7.6 B).

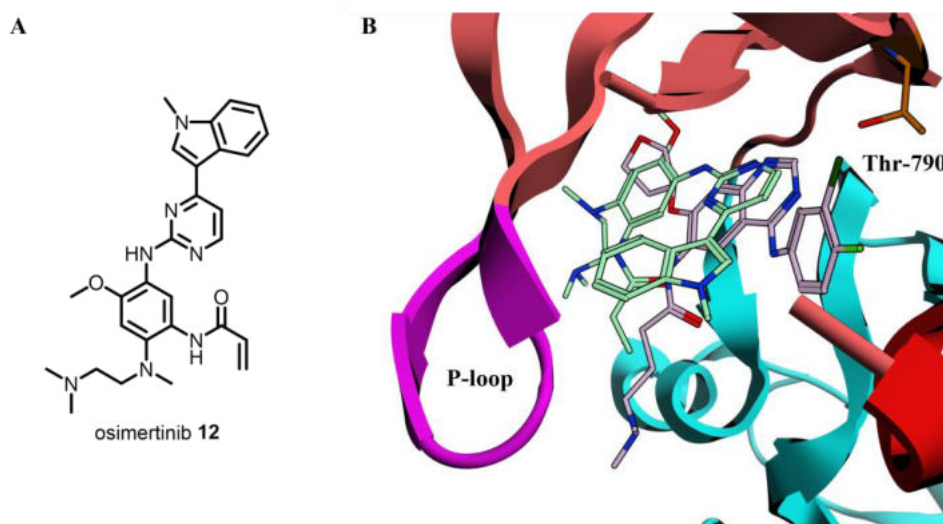


**Figure 7.6** A Structure of osimertinib **12**. B Overlay of single crystal x-ray structures of afatinib **251** (PDB: 4G5J) and osimertinib **12** (PDB: 4ZAU) bound to WT EGFR TKD. *N*-benzyl moiety of afatinib **251** is orientated towards Thr-790 which could introduce a steric clash in T790M EGFR, whilst the corresponding indole moiety of osimertinib **12** is positioned away from Thr-790 towards the hydrophobic P-loop (magenta).

The improved WT selectivity of osimertinib **12** enables a higher recommended dose compared to 2<sup>nd</sup> generation EGFR TKIs.<sup>266</sup> However, despite demonstrated efficacy in NSCLC with an EGFR L858R/T790M oncogene addiction and improvements in safety profile, acquired resistance to osimertinib **12** inevitably develops.<sup>267</sup> 14 – 40% of the observed resistance is from the mutation of the critical Cys-797 to a serine residue,<sup>268,269</sup>

which results in a loss of the covalent MoA as the serine residue is insufficiently nucleophilic towards the acrylamide warhead.

Despite considerable efforts being dedicated to the development of 4<sup>th</sup> generation reversible TKIs,<sup>270</sup> discovery of a targeted therapy for NSCLC with L858R/T790M/C797S or “triple mutant” (TM) EGFR oncogene addiction remains an unmet clinical need. We proposed that applying the lysine-targeting covalent inhibitor strategy in the development of a TKI targeting TM EGFR will re-acquire a covalent MoA for this chemotype and therefore overcome the C797S resistance mutation.

### 7.1.3 Targeting the Catalytic Lysine of EGFR

The catalytic lysine residue is critical to the key enzymatic process of protein kinases, the transfer of the  $\gamma$ -phosphate of ATP to the substrate protein.<sup>271</sup> For this reason, the catalytic lysine is conserved across the protein kinome,<sup>85</sup> and it is correspondingly not susceptible to secondary mutation as a resistance mechanism. Development of lysine-TCIs targeting the catalytic lysine of kinases is now a validated approach, with reversible lysine-TCIs of BCR-ABL being reported<sup>233</sup> in addition to a probe based on a promiscuous kinase scaffold (Section 6.1.4).<sup>234</sup> Irreversible lysine-TCIs of **27**<sup>272</sup> and **254**<sup>84</sup> targeting the catalytic Lys-779 of phosphoinositide 3-kinase  $\delta$  (PI3K $\delta$ ) have also been reported, incorporating an activated ester and acetyl ester warhead, respectively (Figure 7.7).

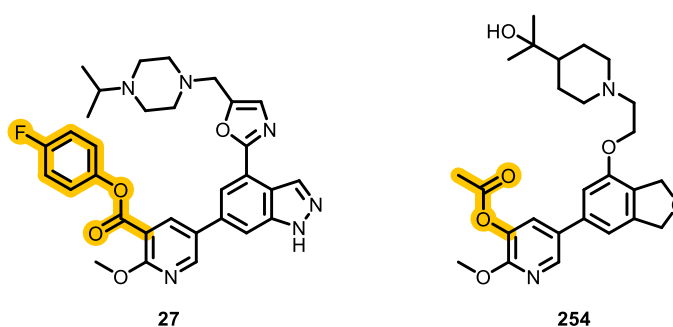


**Figure 7.7** Structures of TCIs **27** and **254** targeting the catalytic lysine of PI3K $\delta$ .

Shen et al. applied a novel prediction tool to calculate the  $pK_a$  of 18 kinase catalytic lysine residues, determining only 50% of the lysine residues to be reactive (>10% neutral lysine residue at physiological pH).<sup>273</sup> Intriguingly, the catalytic lysine of EGFR, Lys-745, was determined to be hyper-reactive, owing to its calculated  $pK_a$  of 7.3, corresponding to

~50% neutral lysine at pH 7.4. We hypothesised that Lys-745 would therefore be a highly suitable residue to target with the lysine-TCI approach.

Taunton et al. demonstrated with their broad spectrum kinase probe XO44 **255**, that Lys-745 can irreversibly covalently engage with a sulfonyl fluoride warhead (Figure 7.8).<sup>274</sup>

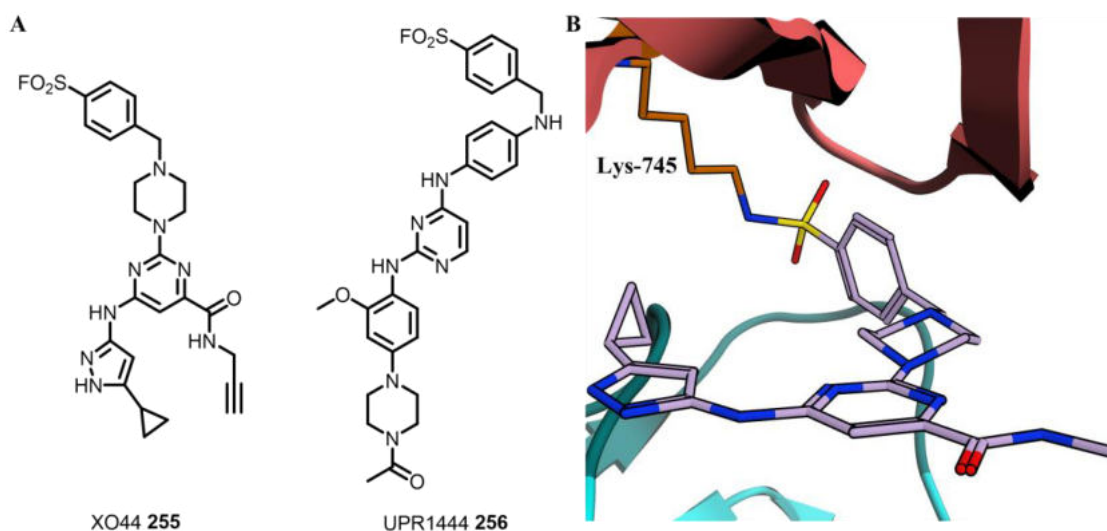


**Figure 7.8** A Structures of lysine-reactive probes XO44 **255** and UPR1444 **256**. B Single crystal x-ray structure of XO44 **255** covalently bound to catalytic lysine of EGFR (PDB: 5U8L).<sup>274</sup>

The authors showed that XO44 **255** covalently engages 133 kinases in live cells owing to the non-selective reversible scaffold. In an effort to develop a selective lysine-TCI of TM EGFR, Ferlenghi et al. designed sulfonyl fluoride-derived probe UPR1444 **256** (Figure 7.8 A), which showed time-dependent inhibition of TM EGFR as well as evidence of covalent labelling by trypsin digest-MS.<sup>275</sup> However, in addition to not displaying persistent target engagement in cells, consistent with a non-covalent MoA, UPR1444 **256** only possessed a modest selectivity improvement over promiscuous probe XO44 **255** when screened in a small sixteen member kinase panel.

## 7.2 Design and Synthesis of 1<sup>st</sup> Generation Lysine-TCIs of EGFR

### 7.2.1 Design of 1<sup>st</sup> Generation EGFR Lysine-TCIs

My analysis of the literature indicated that the catalytic lysine of EGFR, Lys-745, could potentially be covalently engaged by a S(VI)-F electrophile. However, existing chemical entities XO44 **255** and UPR1444 **256** displayed poor selectivity for EGFR over other members of the kinome. In contrast, 3<sup>rd</sup> generation TCI osimertinib **12** displays excellent

off-target kinase selectivity,<sup>264</sup> indicating that its indole-aminopyrimidine core would be a suitable start point for the development of an EGFR lysine-TCI. We therefore proposed that modification of the osimertinib **12** scaffold with a S(VI)-F warhead positioned to engage with Lys-745 would furnish a potent and selective lysine-TCI of TM EGFR.

We hypothesised that appending a phenyl vector and a fluorosulfonate warhead to the 1-*N*-position of the indole would result in the optimal reversible binding geometry to facilitate covalent engagement (Figure 7.9 A); this was supported by molecular modelling that positioned Lys-745 in close proximity to the warhead within the reversible binding mode (Figure 7.9 B).

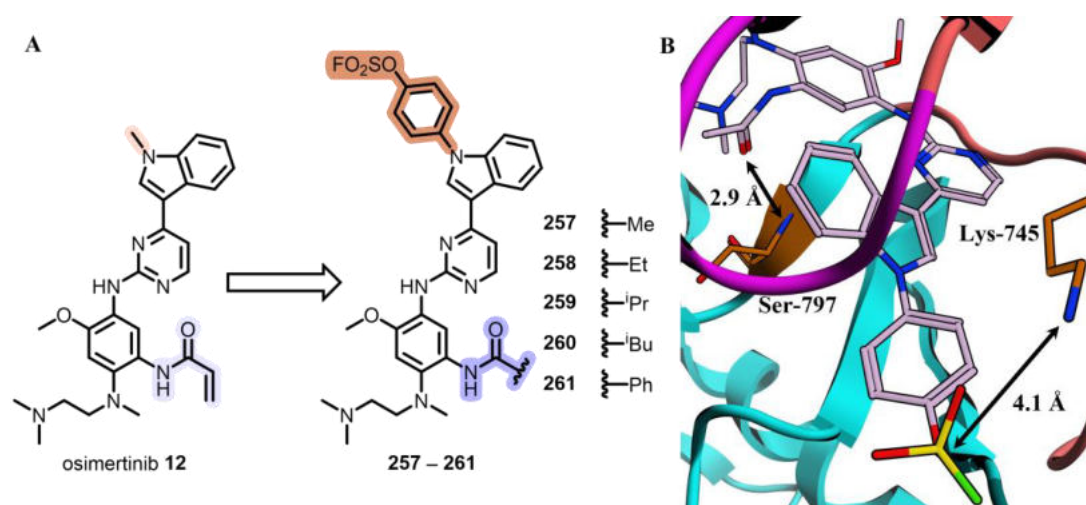
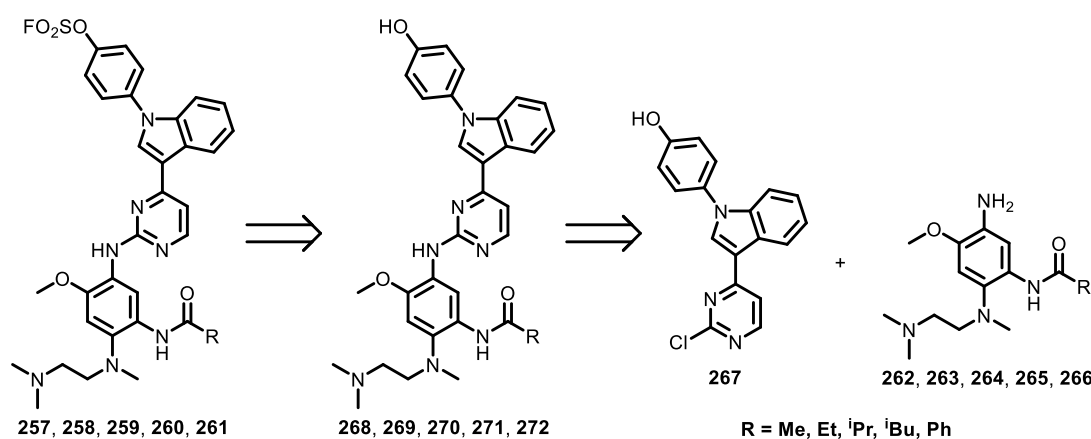


**Figure 7.9** **A** Design strategy for EGFR lysine-TCIs, incorporating phenyl fluorosulfonate warhead. Various alkyl groups were selected to probe effect of increasing lipophilicity and steric bulk in polar serine pocket. **B** Model of **257** bound to TM EGFR, based on single crystal x-ray structure of osimertinib **12** and WT EGFR (PDB: 4ZAU), showing orientation of fluorosulfonate warhead towards key catalytic lysine. Carbonyl of acetyl amide makes hydrogen bonding interaction with the backbone N-H of Ser-797. Model prepared in MOE 2019.

Additionally, we hypothesised that retention of a polar amide functionality may yield additional selectivity for TM over WT EGFR, as the polar Ser-797 residue would likely form more favourable interactions compared to the lipophilic Cys-797. This was supported by our model, which indicated that the acetyl amide of **257** was predicted to make a H-bonding interaction with the amide backbone of Ser-797 (Figure 7.9 B). To investigate this, we designed a series of phenyl fluorosulfonate TCIs **257**, **258**, **259**, **260**, and **261**, incorporating a variety of alkyl functionalities to probe the effect of steric bulk and lipophilicity in this part of the binding pocket.

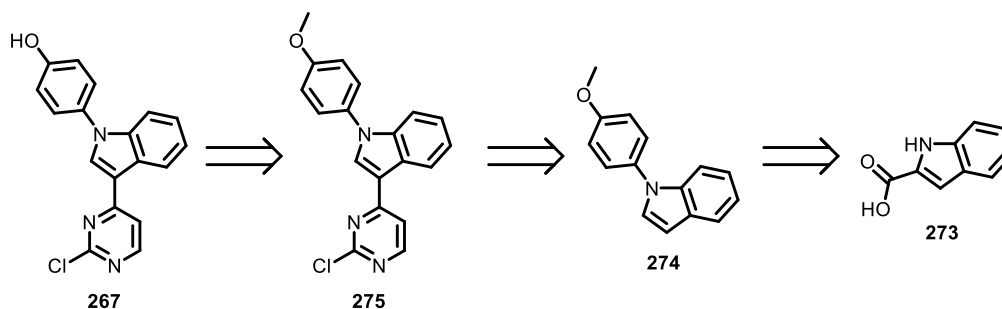
### 7.2.2 Synthesis of 1<sup>st</sup> Generation EGFR Lysine-TCIs

To expedite the synthesis of the 1<sup>st</sup> generation EGFR lysine-TCI library, we proposed that a modular approach would enable variation of the lower portion of the TCI containing the amide-functionality, through an  $S_NAr$  reaction of the tetrasubstituted anilines **262**, **263**, **264**, **265**, and **266**, via common intermediate **267**, to yield intermediates **268**, **269**, **270**, **271**, and **272**. Finally, a late-stage conversion of the phenol intermediates would give fluorosulfonates **257**, **258**, **259**, **260**, and **261** (Scheme 7.1).



**Scheme 7.1** Retrosynthetic analysis of TCIs **257** – **261**, involving a late-stage  $S_NAr$  then fluorosulfonation approach.

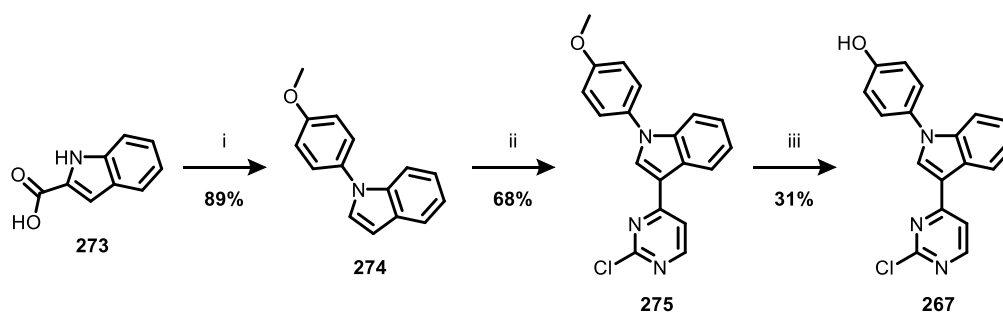
Phenolic intermediate **267** was proposed to be accessible from commercial indole **273**, involving an *N*-arylation to previously reported compound **274**,<sup>276</sup> followed by a sequential  $S_NAr$  reaction to **275** then an *O*-demethylation protocol (Scheme 7.2).



**Scheme 7.2** Retrosynthetic analysis of common phenolic intermediate **267**.

1-(4-methoxyphenyl)-1*H*-indole **274** was first synthesised from 2-indolecarboxylic acid **273** via a copper catalysed decarboxylative *N*-arylation according to a literature procedure,<sup>276</sup> and was obtained in excellent yield (Scheme 7.3).

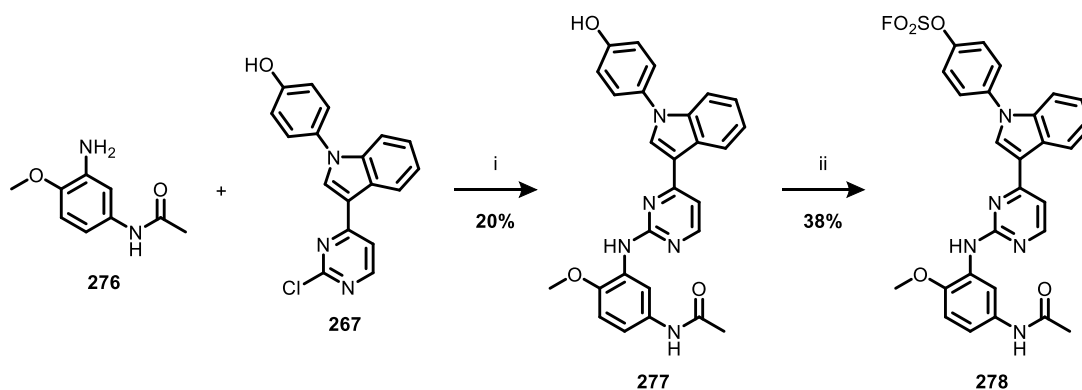




**Scheme 7.3** Synthesis of common phenolic intermediate **267**. Reagents and conditions: i) 4-iodoanisole (1 equiv.),  $K_3PO_4$  (2 equiv.),  $Cu_2O$  (10 mol%), NMP (0.2 M), 160 °C, 6 days; ii) 2,4-dichloropyrimidine (1 equiv.),  $FeCl_3$  (1 equiv.), DME (0.5 M), 60 °C, 20 h; iii)  $BBr_3$  (2.2 equiv.),  $CH_2Cl_2$  (0.2 M), -78 °C to rt, 18 h.

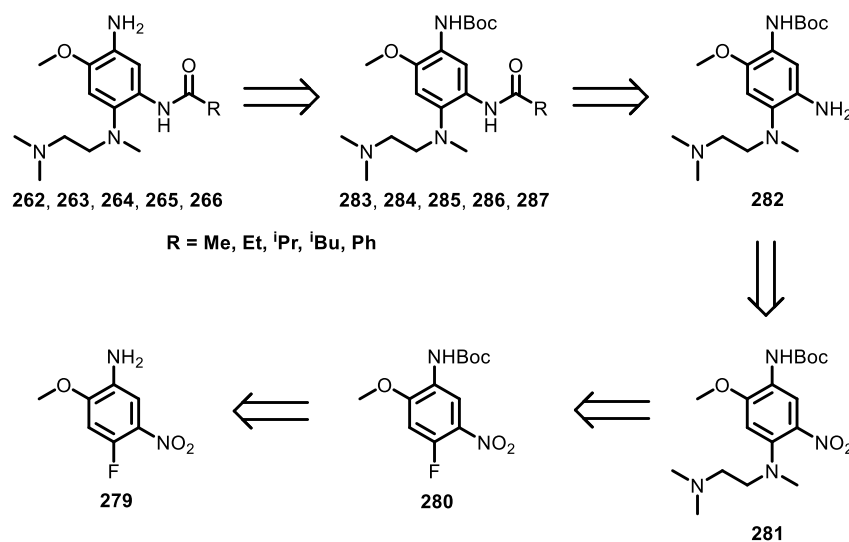
Subsequent regioselective  $S_NAr$  reaction with 2,4-dichloropyrimidine<sup>277</sup> exploiting stoichiometric iron (III) chloride, based on a procedure by Butterworth et al.,<sup>278</sup> furnished the chloro-pyrimidine **275** in moderate yield. Demethylation of **275** with  $BBr_3$  under standard conditions generated material that was challenging to purify due to its poor solubility, but ultimately afforded phenol **267** in low yield.

With key intermediate **267** in hand, I next aimed to perform the critical  $S_NAr$  reaction to assemble the fully elaborated scaffold prior to installation of the warhead. Commercially available aniline **276** was selected as a model substrate for this reaction, owing to its structural similarity to anilines **262**, **263**, **264**, **265**, and **266**, but the absence of an amine functionality, which would also enable investigation of the importance of this group to the overall SAR.  $S_NAr$  reaction was carried out following a modification of a literature protocol,<sup>279</sup> enabling the isolation of intermediate **277** in low yield, owing to incomplete substrate turnover and apparent degradation of the starting material, as observed by LCMS (Scheme 7.4).



**Scheme 7.4** Synthesis of TCI **278**. Reagents and conditions: i) Aniline **276** (1 equiv.), PTSA (1 equiv.), isobutanol (0.1 M), 60 °C, 6 days; ii) AISF (1.2 equiv.), DBU (2.2 equiv.), THF:DMSO 5:1 (0.1 M), rt, 1 h.

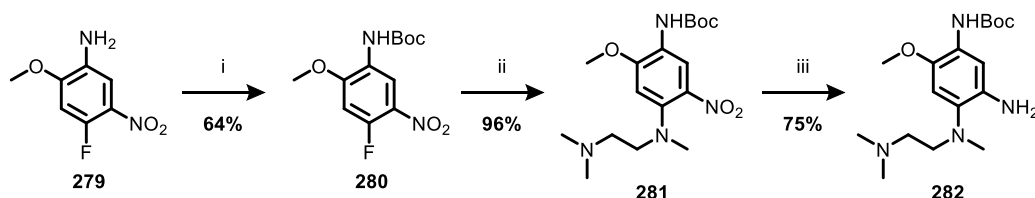
Finally, reaction of phenol **277** with [4-(acetylamino)phenyl]imidodisulfonyl difluoride (AISF)<sup>280</sup> in the presence of DBU afforded fluorosulfonate **278**, the first target molecule for testing as an EGFR lysine-TCI. We next aimed to enact the synthesis of the library of anilines containing the diverse set of amide functionalities, which were proposed to be prepared *via* a 5-step sequence beginning from commercially available aniline **279** (Scheme 7.5).



**Scheme 7.5** Retrosynthetic analysis of aniline library **262**, **263**, **264**, **265**, and **266**.

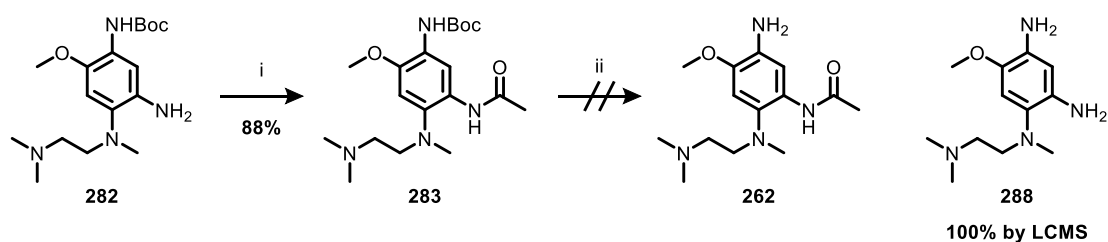
Sequential *N*-Boc protection to **280**, S<sub>N</sub>Ar reaction to give **281**, then nitro reduction in accordance with literature protocols,<sup>281</sup> would afford intermediate **282**. Diversification through amide coupling to intermediates **283**, **284**, **285**, **286**, and **287** followed by *N*-Boc deprotection would yield the fully functionalised anilines **262**, **263**, **264**, **265**, and **266**.

Common intermediate **282** was accessed *via* a sequence of trivial transformations (Scheme 7.6). *N*-Boc protection of aniline **279** gave **280** in good yield, which was followed by S<sub>N</sub>Ar reaction with *N,N,N'*-trimethylethylenediamine to yield **281** in excellent yield. Finally, mild hydrogenation of this substrate with Pd/C under 1 atm of H<sub>2</sub> gave aniline **282** in high yield.



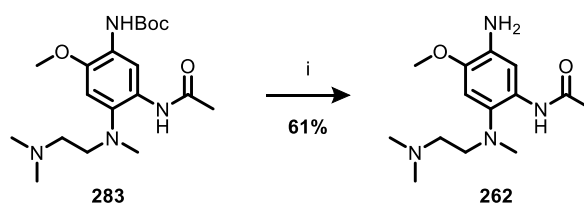
**Scheme 7.6** Synthesis of common aniline intermediate **282**. Reagents and conditions: i) DMAP (10 mol%), Boc<sub>2</sub>O (1.2 equiv.), CH<sub>2</sub>Cl<sub>2</sub> (0.43 M), 0 °C to rt, 18 h; ii) DIPEA (1 equiv.), *N,N,N'*-trimethylethylenediamine (1.15 equiv.), DMA (0.3 M), 60 °C, 2 h; iii) Pd/C, H<sub>2</sub> (1 atm), rt, 4 h.

Exploration of the synthetic route to acetyl amide **262** began with reaction of aniline **282** with acetyl chloride under standard conditions to give intermediate **283**; however, attempted *N*-Boc deprotection with HCl in methanol led to degradation of the starting material with full conversion to bis-aniline **288**, which was confirmed through LCMS and NMR analysis (Scheme 7.7).



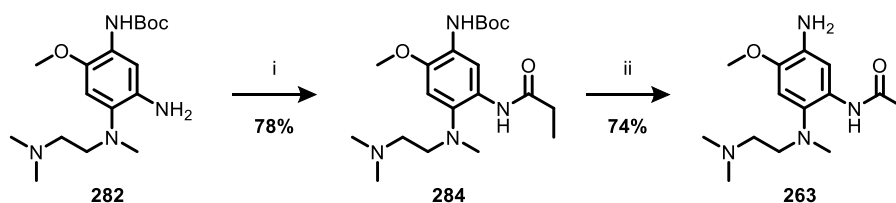
**Scheme 7.7** Attempted synthesis of aniline **262**. Reagents and conditions: i) acetyl chloride (1 equiv.), Et<sub>3</sub>N (1.1 equiv.), CH<sub>2</sub>Cl<sub>2</sub> (0.5 M), 0 °C to rt, 18 h; ii) 3M HCl in MeOH (0.3 M), rt, 20 h.

To circumvent unwanted hydrolysis of the amide, milder conditions were attempted using iodotrimethylsilane (TMSI), a mild dealkylating reagent for carbamates.<sup>282</sup> Pleasingly, treatment of *N*-Boc intermediate **283** with TMSI afforded the desired *N*-Boc-deprotected intermediate **262** in high yield (Scheme 7.8).



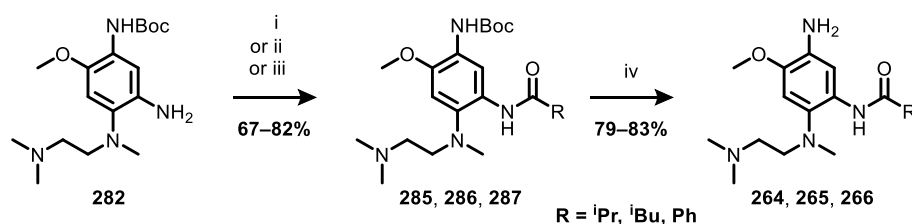
**Scheme 7.8** Synthesis of **262**. Reagents and conditions: i) TMSI (7 equiv.), CH<sub>2</sub>Cl<sub>2</sub> (0.3 M), reflux, 7 days.

Propanyl intermediate **263** was accessed in a similar fashion, *via* reaction of **282** with propanoyl chloride to give **284**, followed by treatment with TMSI to form *N*-Boc deprotected product **263** (Scheme 7.9).



**Scheme 7.9** Synthesis of **263**. Reagents and conditions: i) propanoyl chloride (1 equiv.), Et<sub>3</sub>N (1.1 equiv.), CH<sub>2</sub>Cl<sub>2</sub> (0.5 M), 0 °C to rt, 70 h; ii) TMSI (2.4 equiv.), CH<sub>2</sub>Cl<sub>2</sub> (0.3 M), reflux, 2 h.

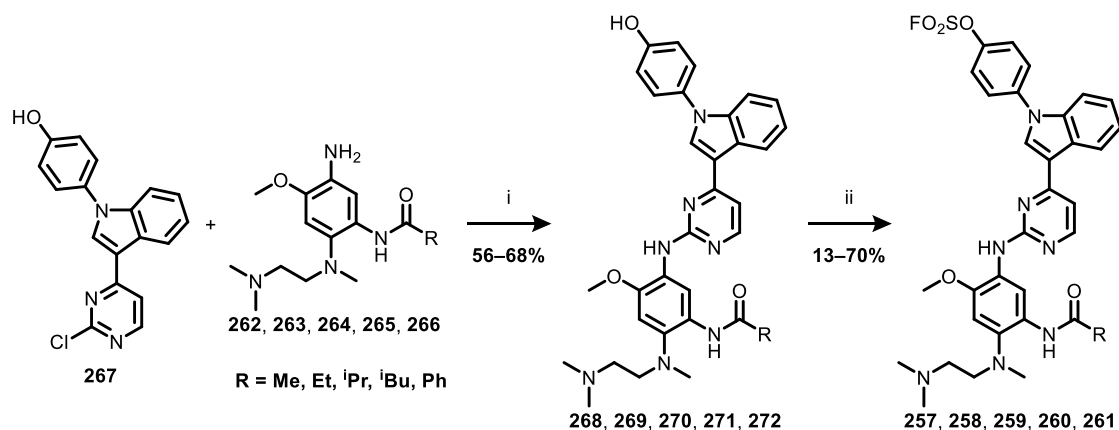
The remaining anilines **264**, **265** and **266** were accessed following reaction with the corresponding acyl chloride to give **285**, **286** and **287**, followed by *in situ* formation of TMSI with TMSCl and lithium iodide (Scheme 7.10).



**Scheme 7.10** Synthesis of **264**, **265** and **266**. Reagents and conditions: i) isobutyryl chloride (1 equiv.), Et<sub>3</sub>N (1 equiv.), CH<sub>2</sub>Cl<sub>2</sub> (0.5 M), 0 °C to rt, 3 h ii) isovaleryl chloride (1 equiv.), Et<sub>3</sub>N (1.1 equiv.), CH<sub>2</sub>Cl<sub>2</sub> (0.5 M), 0 °C to rt, 24 h iii) benzoyl chloride (1.1 equiv.), Et<sub>3</sub>N (1.1 equiv.), CH<sub>2</sub>Cl<sub>2</sub> (0.5 M), 0 °C to rt, 3 h; ii) TMSCl (2.4 equiv.), LiI (2.4 equiv.), CH<sub>2</sub>Cl<sub>2</sub> (0.3 M), reflux, 3 h.

S<sub>N</sub>Ar reaction of chloropyrimidine **267** with the corresponding anilines **262** – **266** was carried out in *tert*-butanol instead of isobutanol to minimise nucleophilic degradation of starting material. Pleasingly, precursors **268**, **269**, **270**, **271**, and **272** were acquired in

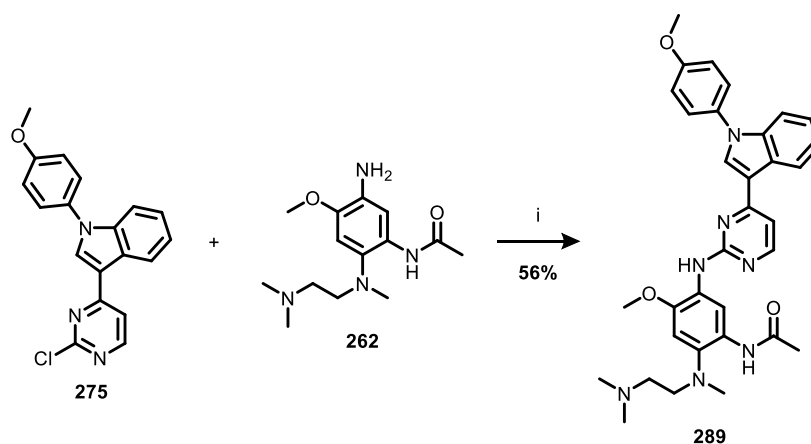
considerably improved yields compared to the low yielding  $S_NAr$  reaction to give **277** (Scheme 7.11). Finally, fluorosulfonation with AISF afforded the desired final compounds **257**, **258**, **259**, **260**, and **261** in low to high yields.



**Scheme 7.11** Synthesis of TCIs **257** – **261**. Reagents and conditions: i) anilines **262** – **266** (1 equiv.), PTSA (1 equiv.), *tert*-butanol (0.1 M), 100 °C, 36 – 72 h; ii) AISF (1.2 equiv.), DBU (2.2 equiv.), THF:DMSO 5:1 (0.1 M), rt, 1 – 24 h.

### 7.2.3 Synthesis of 1<sup>st</sup> Generation EGFR Lysine-TCI Controls

With fluorosulfonates **257**, **258**, **259**, **260**, and **261** in hand, the next aim was to access suitable reversible and irreversible controls to examine the specificity of this series of postulated TCIs. Reversible control **289**, containing the anisole linker with no covalent warhead, was synthesised in one step from previously-obtained intermediates **262** and **275** in moderate yield (Scheme 7.12).



**Scheme 7.12** Synthesis of reversible control **289**. Reagents and conditions: i) Aniline **262** (1 equiv.), PTSA (1 equiv.), *tert*-butanol (0.1 M), 100 °C, 48 h.

The hinge-binding motif of small molecule kinase inhibitors are generally required for potent inhibition of the enzymatic target.<sup>283</sup> For osimertinib **12**, this motif comprises the aminopyrimidine core, which makes interactions with the amide backbone of Met-793,<sup>284</sup> therefore, *N*-alkylation of the aniline functionality would likely impede the reversible binding of fluorosulfonate **257** (Figure 7.10).

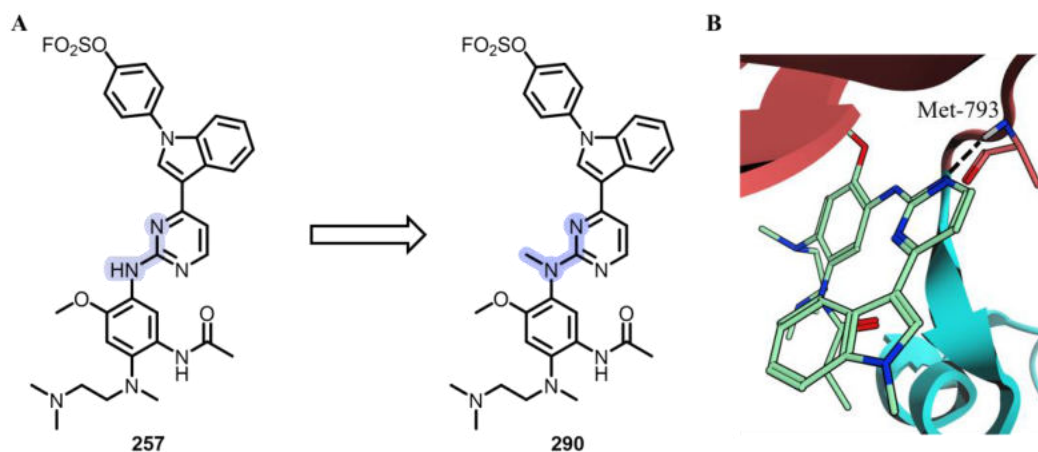
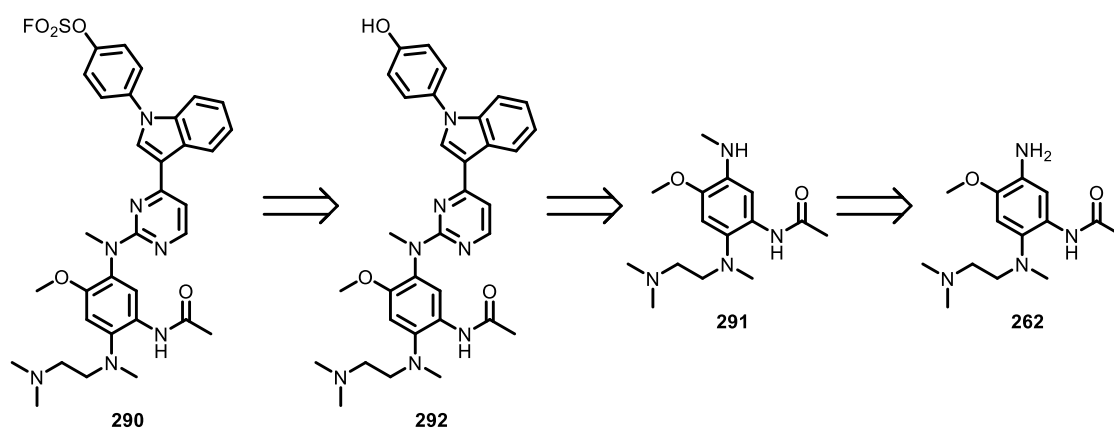


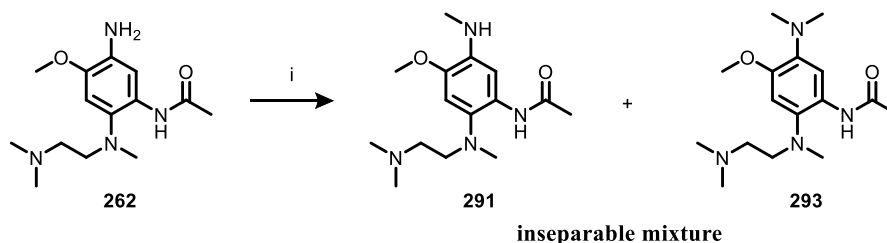
**Figure 7.10** A Design of irreversible control **290**, incorporating *N*-methylation of aminopyrimidine hinge binder to obstruct reversible binding of scaffold. B Single crystal x-ray structure of osimertinib **12** bound to WT-EGFR, showing hinge-binding interaction of the Met-793 backbone with the pyrimidine ring of **12** (PDB: 4ZAU).

We hypothesised that irreversible control **290** would be accessible from late-stage aniline **262**, which could be selectively mono-alkylated to *N*-methyl aniline **291** and then subjected to S<sub>N</sub>Ar reaction with chloropyrimidine **267** to yield key penultimate step intermediate **292** (Scheme 7.13).



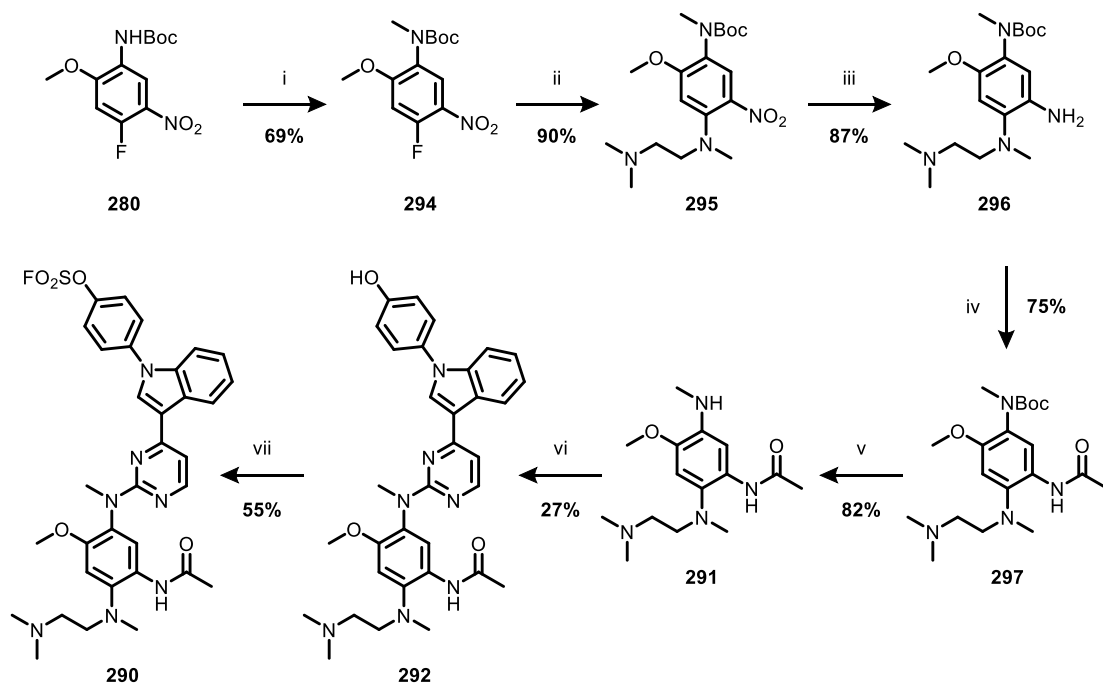
**Scheme 7.13** Retrosynthetic analysis of irreversible control **290**.

Unfortunately, attempted reductive amination of aniline **262** lead to the formation of an inseparable mixture of desired mono-*N*-methylated product **291**, bis-*N*-methylated product **293** and starting material **262** (Scheme 7.15).



**Scheme 7.14** Attempted synthesis of **291**. Reagents and conditions: i) formaldehyde (2.3 equiv.), NaBH<sub>3</sub>CN (2 equiv.), MeOH (0.05 M), rt, 20 h.

Selective mono-*N*-methylation was ultimately accomplished through reaction of previously synthesised *N*-Boc intermediate **280** with sodium hydride and methyl iodide (Scheme 7.15). The remainder of the synthesis was accomplished in an analogous fashion to other analogues of these series. Firstly, S<sub>N</sub>Ar reaction of **294** with *N,N,N'*-trimethylethylenediamine gave amine **295**, which was hydrogenated to aniline **296** and then coupled with acetyl chloride to give amide **297**. *N*-Boc-deprotection of **297** furnished free aniline **291**, which was reacted with chloropyrimidine **267** via S<sub>N</sub>Ar reaction to give intermediate **292** in low yield. The lower yield for the synthesis of **292** compared to that of **268**, **269**, **270**, **271**, and **272** was a result of incomplete substrate turnover, likely owing to the steric-hindrance associated with nucleophilic attack by the secondary aniline decelerating the reaction. Finally, fluorosulfonation of **292** with AISF afforded the desired irreversible control **290** in moderate yield.



**Scheme 7.15** Synthesis of irreversible control **290**. Reagents and conditions: i) NaH (1.2 equiv.), THF (0.5 M), 0 °C, 1 h, *then* MeI (1.5 equiv.), 0 °C to rt, 18 h; ii) DIPEA (1 equiv.), *N,N,N'*-trimethylethylenediamine (1.15 equiv.), DMA (0.3 M), 60 °C, 2 h; iii) Pd/C, H<sub>2</sub> (1 atm), rt, 2 h; iv) acetyl chloride (1 equiv.), Et<sub>3</sub>N (1.1 equiv.), CH<sub>2</sub>Cl<sub>2</sub> (0.5 M), 0 °C to rt, 18 h; v) TMSCl (2.4 equiv.), LiI (2.4 equiv.), CH<sub>2</sub>Cl<sub>2</sub> (0.3 M), reflux, 3 h; vi) chloropyrimidine **267** (1 equiv.), PTSA (1 equiv.), *tert*-butanol (0.1 M), 100 °C, 48 h; vii) AISF (1.2 equiv.), DBU (2.2 equiv.), THF:DMSO 5:1 (0.1 M), rt, 3 h.

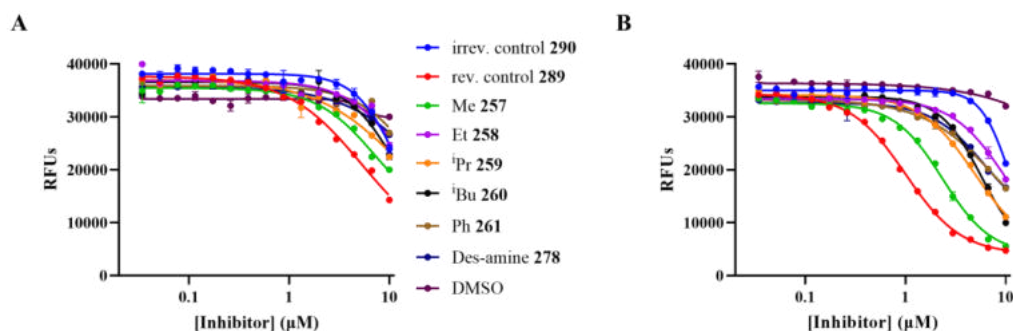
#### 7.2.4 Characterisation of 1<sup>st</sup> Generation EGFR Lysine-TCIs

With a complete set of targets and controls in hand, the next aim was to demonstrate a covalent mechanism of action. We incubated fluorosulfonates **257**, **258**, **259**, **260**, and **261** and irreversible control **290** with recombinant EGFR TKD, then subsequently analysed the samples by IPMS. Unfortunately, no adduct formation was observed for any of the compounds tested (data not shown) suggesting that TCIs **257**, **258**, **259**, **260**, and **261** were not binding covalently to the enzyme.

To investigate whether the compounds were still binding reversibly to EGFR, we screened TCIs **257**, **258**, **259**, **260**, **261** and **278**, as well as reversible control **289** and irreversible control **290** in the AssayQuant<sup>®</sup> Omnia assay.<sup>285</sup> Briefly, this assay measures EGFR activity through the binding and phosphorylation of a peptide containing a sulfonamido-oxine (sox) fluorophore. Phosphorylation of the sox peptide initiates an



increase in fluorescence intensity, measured in relative fluorescence units (RFUs). Consequently, inhibition of EGFR results in less phosphorylation of the sox peptide, corresponding to a lower fluorescence signal. TCIs **257** – **261** displayed dose-dependent reduction in EGFR activity, consistent with reversible binding to the protein (Scheme 7.15).



Compound	WT IC <sub>50</sub> (μM)	TM IC <sub>50</sub> (μM)
irrev. control <b>290</b>	>10	>10
rev. control <b>289</b>	5.3	1.0
Me <b>257</b>	7.1	2.3
Et <b>258</b>	>10	9.8
<sup>i</sup> Pr <b>259</b>	>10	5.0
<sup>i</sup> Bu <b>260</b>	>10	5.6
Ph <b>261</b>	>10	7.9
des-amine <b>278</b>	>10	6.1

**Figure 7.11** Inhibitory activities of fluorosulfonates **257**, **258**, **259**, **260**, **261** and **278**, irreversible control **290** and reversible control **289**, determined from plot of RFUs against [I] (log(inhibitor) vs. response – variable slope (four parameters, GraphPad Prism 9). Measurements taken in duplicate and the mean and standard error plotted using GraphPad Prism 9. Data reported is of N = 1 biological replicates. Experiments performed by Omar Alkhatib. **A** Inhibition against WT EGFR. **B** Inhibition against TM EGFR.

Pleasingly, the majority of compounds tested exhibited concentration-dependent inhibition of EGFR function, suggesting that the phenyl fluorosulfonate vector does not abrogate binding, although quantitative comparison of the data would require a greater number of biological replicates.

For an activity assay performed with an irreversible covalent inhibitor, the reaction progress curve will eventually reach a plateau as the concentration of free protein approaches zero over time, leading to no substrate turnover. (Figure 7.12).<sup>8</sup>

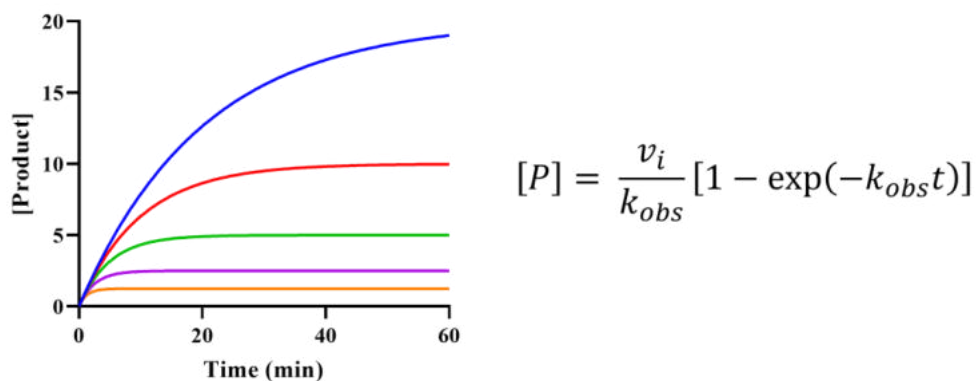


**Figure 7.12** Simulated enzyme reaction progress curve in the presence of an irreversible TCI, with  $v_i = 1 \text{ min}^{-1}$  and a range of  $k_{obs}$  values from  $0.05 - 0.8 \text{ min}^{-1}$ . Equation obtained from Copeland (2013).<sup>8</sup>

Unfortunately, fluorosulfonate **257** exhibited pseudolinear reaction progress consistent with a reversible mechanism of action (Figure 7.13 A). Some curvature was observed at the later time points tested; however, reversible control **289** possessed a similar profile indicating that this apparent deviation from linearity was not because of covalent binding (Figure 7.13 B). We speculated that this curvature arose from the recombinant EGFR TKD protein gradually decomposing under the assay conditions.

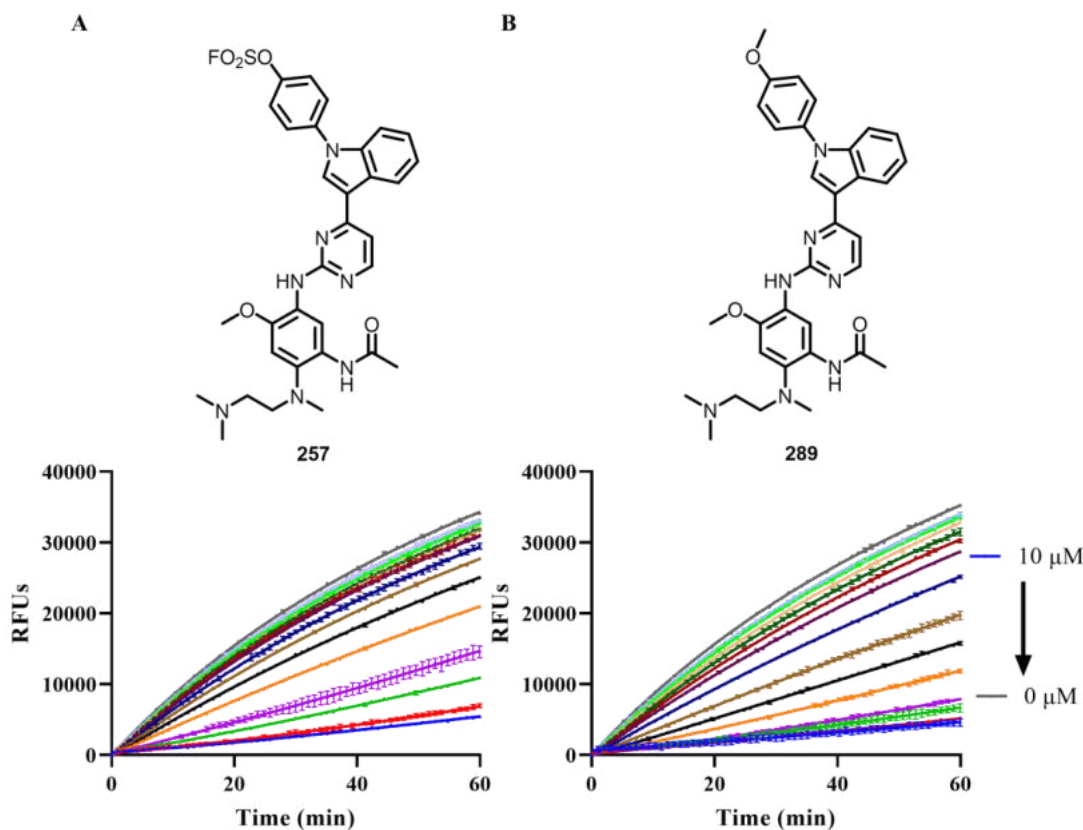


**Figure 7.13** Progress curve analysis of **257** and **289** incubated with TM EGFR, measurements taken in duplicate every minute for 60 minutes and plotted on same axes. Data plotted in GraphPad Prism 9. Experiments performed by Omar Alkhatib. **A** Progress curve of fluorosulfonate **257**. **B** Progress curve of reversible control **289**.

Together, our data suggested that whilst reversible binding to the protein was maintained for this chemotype, fluorosulfonates **257**, **258**, **259**, **260**, and **261** were behaving as reversible inhibitors of EGFR, with no evidence of a covalent MoA.

### 7.3 Design and Synthesis of 2<sup>nd</sup> Generation EGFR Lysine-TCIs

#### 7.3.1 Design of 2<sup>nd</sup> Generation EGFR Lysine-TCIs

Two hypotheses were suggested to explain the lack of a covalent MoA for the 1<sup>st</sup> generation EGFR lysine-TCIs. Firstly, aryl fluorosulfonates are reported as possessing reduced intrinsic reactivity compared to the corresponding sulfonyl fluoride,<sup>286</sup> so we hypothesised that the warhead of these inhibitors may be insufficiently reactive to form a covalent bond with Lys-745 of EGFR. Secondly, it was noted that the rigidity of *N*-phenyl

linker of inhibitors **257**, **258**, **259**, **260**, and **261** would reduce conformational flexibility to the warhead, potentially impeding the optimal positioning to the reacting residue.

We therefore designed a second generation of osimertinib **12**-derived inhibitors **298**, **299**, **300**, and **301** targeting Lys-745 incorporating the more intrinsically reactive sulfonyl fluoride warhead, in conjunction with a variety of linker lengths to probe the effect of increasing conformational flexibility on the feasibility of covalent bond formation (Figure 7.14). By employing our optimised TM-selective acetyl amide group, we aimed to retain the reversible affinity and WT selectivity of our scaffold. Finally, we aimed to probe the importance of the indole group to the biochemical potency and improve the synthetic tractability of this series through an indole to pyrazole scaffold hop.

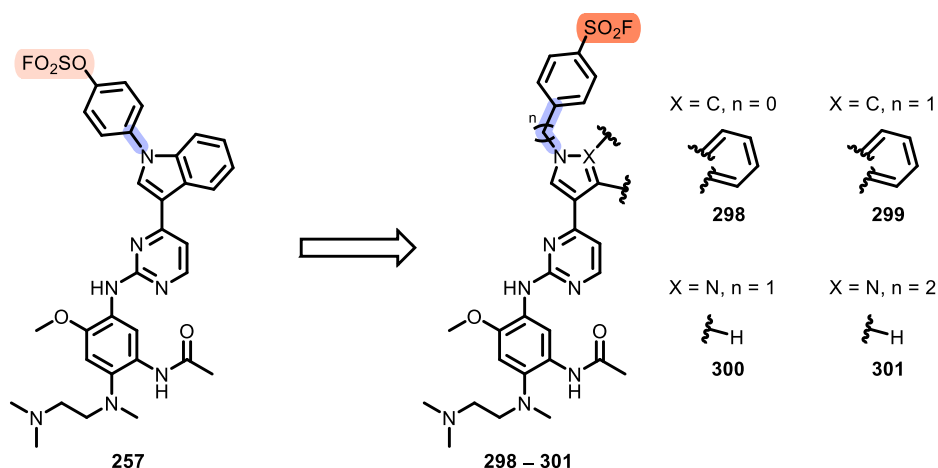
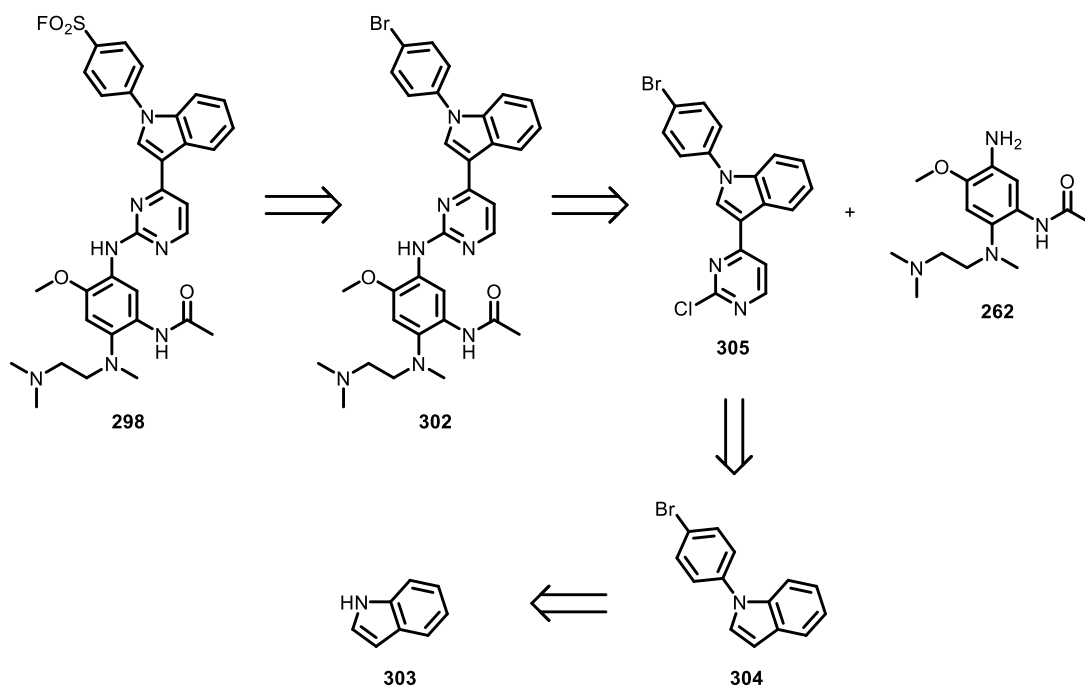


**Figure 7.14** Design strategy of 2<sup>nd</sup> generation EGFR lysine-TCIs incorporating a sulfonyl fluoride warhead, a variety of linker lengths as well as an indole to pyrazole scaffold hop.

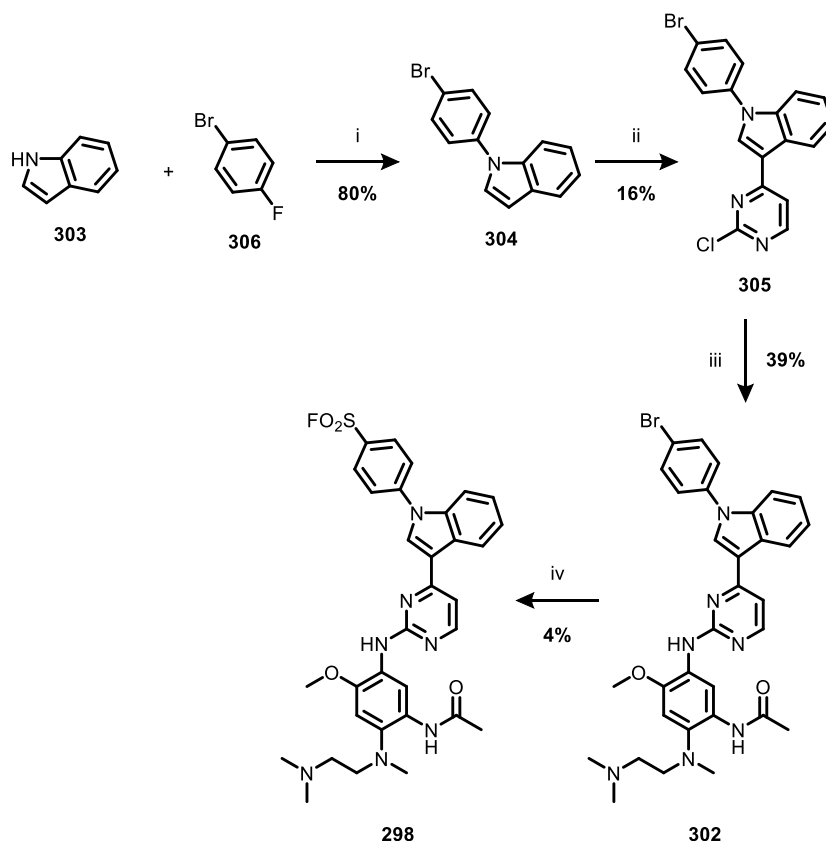
### 7.3.2 Synthesis of 2<sup>nd</sup> Generation EGFR Lysine-TCIs

Indole-derived TCI **298** was proposed to be accessible from a late-stage fluorosulfonation approach from aryl bromide **302**, which would be accessed from *N*-arylation of indole **303** to give **304**, followed by subsequent S<sub>N</sub>Ar reaction to give chloropyrimidine **305**, and then reaction with aniline **262** (Scheme 7.16).



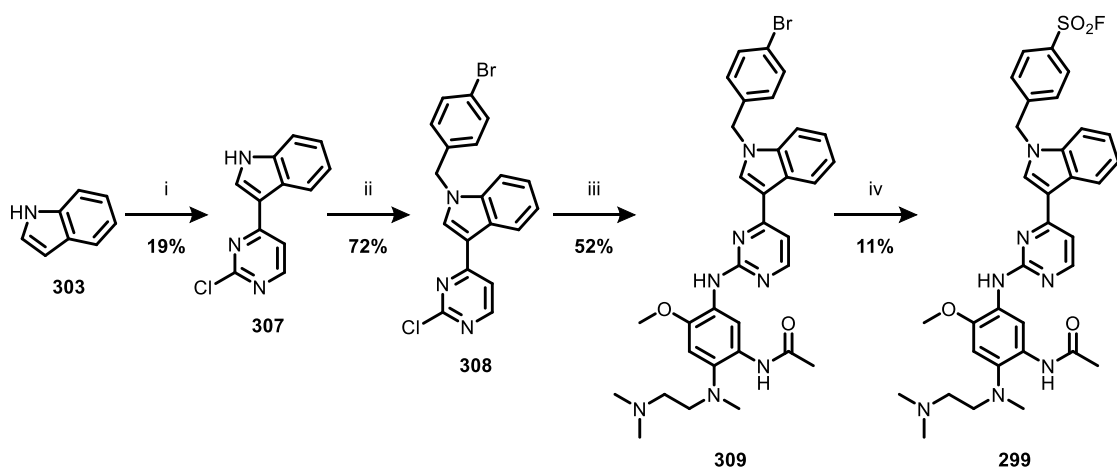
**Scheme 7.16** Retrosynthetic analysis of TCI **298**.

*N*-arylated indole **304** was first accessed from an S<sub>N</sub>Ar reaction of unactivated fluorobenzene **306** with indole **303** via a procedure first detailed by Diness and Fairlie (Scheme 7.17).<sup>287</sup> Indole **304** was then reacted with 2,4-chloropyrimidine in the presence of iron (III) chloride to give 2-chloropyrimidine **305** in low yield, which was challenging to purify owing to the poor solubility of the substrate. An S<sub>N</sub>Ar reaction of **305** with acetyl aniline **262** yielded aminopyrimidine **302**. To access the final sulfonyl fluoride **298**, I employed a modification of the previously reported palladium-catalysed fluorosulfonation conditions.<sup>164</sup> To overcome the poor solubility of **302** in organic solvents, the reaction was performed at 110 °C under microwave irradiation instead of a thermal reaction at 75 °C, which furnished TCI **298** albeit in poor yield.



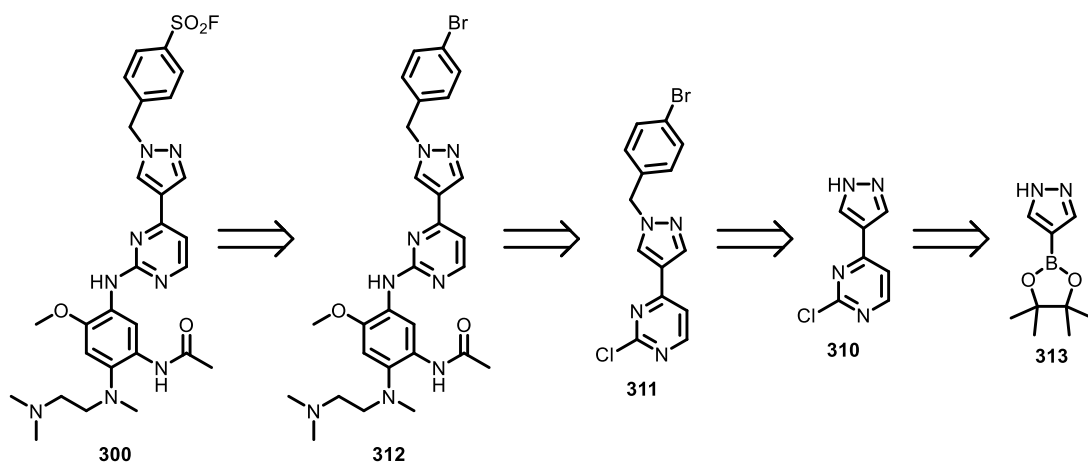
**Scheme 7.17** Synthesis of TCI **298**. Reagents and conditions: i) 1-bromo-4-fluorobenzene (2 equiv.), K<sub>3</sub>PO<sub>4</sub> (5 equiv.), DMF (0.1 M), reflux, 18 h; ii) 2,4-dichloropyrimidine (1 equiv.), FeCl<sub>3</sub> (1 equiv.), DME (0.5 M), 80 °C, 72 h; iii) aniline **262** (1 equiv.), PTSA (1 equiv.), *tert*-butanol (0.1 M), 100 °C, 36 h; iv) DABSO (0.6 equiv.), PdCl<sub>2</sub>(AmPhos)<sub>2</sub> (5 mol%), Et<sub>3</sub>N (3 equiv.), isopropanol (0.27 M), 110 °C,  $\mu$ wave, 18 h, *then* NFSI (1.5 equiv.), rt, 5 h.

*N*-benzylated indole **299** was accessed following a similar synthetic route. Firstly, 3-(2-chloropyrimidin-4-yl)-1*H*-indole **307** was synthesised in low yield according to literature conditions, through deprotonation of indole **303** with methyl magnesium bromide, followed by addition of 2,4-dichloropyrimidine (Scheme 7.18).<sup>264</sup> *N*-benzylation of the indole 1-*N*-position of **307** was accomplished through sodium hydride-mediated conditions to give *N*-benzyl intermediate **308** in high yield, which was combined with previously synthesised aniline **262** in an S<sub>N</sub>Ar reaction to give aminopyrimidine **309**. Finally, application of the modified palladium-catalysed fluorosulfonation conditions furnished sulfonyl fluoride **299** in low yield.



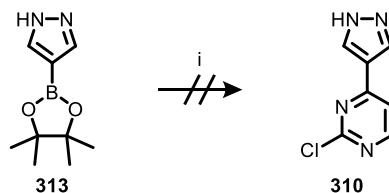
**Scheme 7.18** Synthesis of TCI **299**. Reagents and conditions: i) MeMgBr (1.1 equiv.), DCE (0.25 M), 0 °C, 15 min, *then* 2,4-dichloropyrimidine (2 equiv.), 0 °C to rt, 18 h; ii) NaH (2.25 equiv.), DMF (0.5 M), 0 °C, 15 min, *then* 4-bromobenzyl bromide (2 equiv.), 0 °C to rt, 18 h; iii) aniline **262** (1 equiv.), PTSA (1 equiv.), *tert*-butanol (0.1 M), 100 °C, 18 h; iv) DABSO (0.6 equiv.), PdCl<sub>2</sub>(AmPhos)<sub>2</sub> (5 mol%), Et<sub>3</sub>N (3 equiv.), isopropanol (0.27 M), 110 °C,  $\mu$ wave, 18 h, *then* NFSI (1.5 equiv.), rt, 5 h.

We similarly proposed that pyrazole-derived TCI **300** could be prepared from an analogous *N*-alkylation of pyrazole **310**, followed by S<sub>N</sub>Ar reaction of the resulting intermediate **311** to aminopyrimidine **312**, followed by late-stage fluorosulfonation of the aryl bromide (Scheme 7.19). Pyrazole **310** would be accessed from commercially available boronic ester **313**.



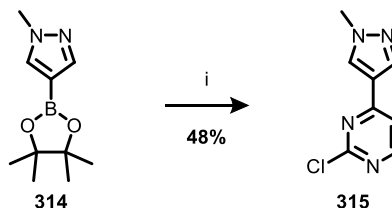
**Scheme 7.19** Retrosynthetic analysis of TCI **300**.

Unfortunately, attempted Suzuki coupling of boronic ester **313** with 2,4-dichloropyrimidine generated a complex reaction mixture with none of the desired product detected by LCMS (Scheme 7.20).



**Scheme 7.20** Attempted synthesis of **310**. Reagents and conditions: i) 2,4-dichloropyrimidine (1 equiv.),  $K_2CO_3$  (2 equiv.),  $PdCl_2(dtbpf)$  (5 mol%), MeCN:water 1:1 (0.2 M), 80 °C, 18 h.

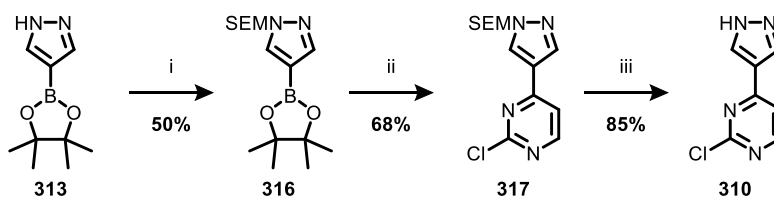
We hypothesised that the complex reaction mixture formed because of competing reactivity of the 1-*N* position of the pyrazole. Therefore, we proposed that protection of the 1-*N* position would facilitate successful Suzuki coupling, which was supported by the successful reaction of 1-*N*-methyl pyrazole boronic ester **314** with 2,4-dichloropyrimidine to give **315** (Scheme 7.21).



**Scheme 7.21** Synthesis of **315**. Reagents and conditions: i) 2,4-dichloropyrimidine (1 equiv.),  $K_2CO_3$  (2 equiv.),  $PdCl_2(dtbpf)$  (5 mol%), MeCN:water 1:1 (0.2 M), 80 °C, 18 h.

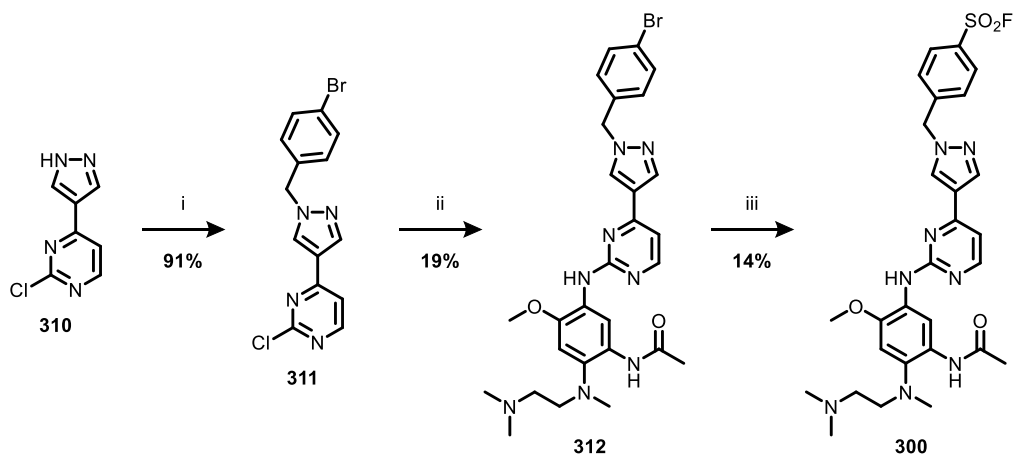
Encouraged by this result, we employed a *N*-SEM protection strategy to access key pyrazole intermediate **310**. Reaction of boronic ester **313** with SEMCl and potassium carbonate following a modification of literature conditions<sup>288</sup> afforded *N*-SEM protected pyrazole **316** (Scheme 7.22). Pleasingly, *N*-SEM protected pyrazole **316** underwent successful Suzuki coupling with 2,4-dichloropyrimidine, giving 4-arylated pyrazole **317** in high yield. Finally, acidic deprotection with HCl in 1,4-dioxane afforded key intermediate **310** in high yield.





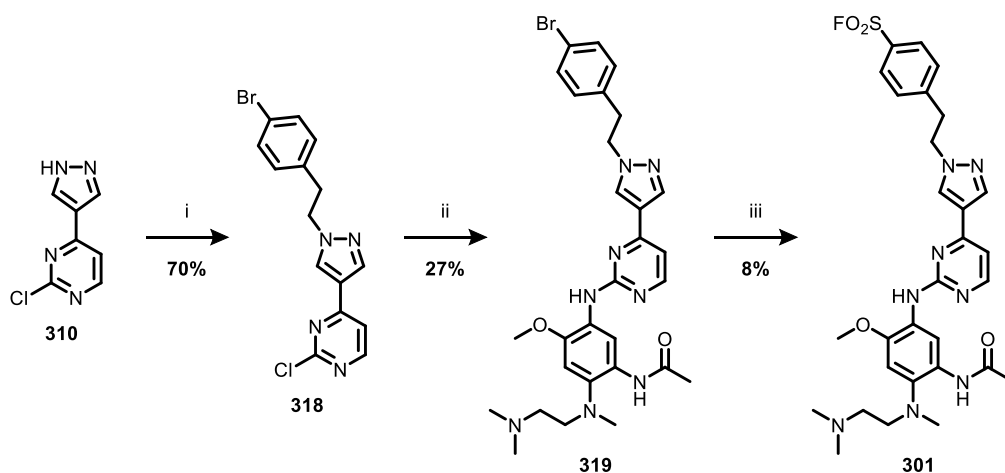
**Scheme 7.22** Synthesis of **310**. Reagents and conditions: i)  $K_2CO_3$  (2 equiv.), SEMCl (1.1 equiv.), NMP (0.6 M), rt, 20 h; ii) 2,4-dichloropyrimidine (1 equiv.),  $K_2CO_3$  (2 equiv.),  $PdCl_2(dtbpf)$  (5 mol%), MeCN:water 1:1 (0.2 M), 80 °C, 18 h; iii) 1.6 M HCl in 1,4-dioxane (0.15 M), rt, 18h.

4-arylated pyrazole **310** was then alkylated with 4-bromobenzyl bromide to give aryl bromide **311** in excellent yield, which underwent an  $S_NAr$  reaction with aniline **262** to give aminopyrimidine **312**. This was finally converted to sulfonyl fluoride **300** in low yield under palladium-catalysed conditions (Scheme 7.23).



**Scheme 7.23** Synthesis of TCI **300**. Reagents and conditions: i)  $K_2CO_3$  (2 equiv.), DMF (0.5 M), rt, 30 min, then 4-bromobenzyl bromide (2 equiv.), 0 °C to rt, 18 h; ii) aniline **262** (1 equiv.), PTSA (1 equiv.), *tert*-butanol (0.1 M), 100 °C, 48 h; iii) DABSO (0.6 equiv.),  $PdCl_2(AmPhos)_2$  (5 mol%),  $Et_3N$  (3 equiv.), isopropanol (0.25 M), 110 °C,  $\mu$ wave, 18 h, then NFSI (1.5 equiv.), rt, 5 h.

Phenethyl-linked TCI **301** was accessed in a similar fashion, *via* alkylation of 4-arylated pyrazole **310** with 4-bromophenethyl bromide to give **318**, then an  $S_NAr$  reaction with aniline **262** to give aminopyrimidine **319**, and finally palladium-catalysed fluorosulfonation to give **301** in 3 steps and 2% overall yield (Scheme 7.24).



**Scheme 7.24** Synthesis of TCI **301**. Reagents and conditions: i) K<sub>2</sub>CO<sub>3</sub> (2 equiv.), DMF (0.5 M), rt, 30 min, *then* 4-bromophenethyl bromide (2 equiv.), 0 °C to rt, 18 h; ii) aniline **262** (1 equiv.), PTSA (1 equiv.), *tert*-butanol (0.1 M), 100 °C, 18 h; iii) DABSO (0.6 equiv.), PdCl<sub>2</sub>(AmPhos)<sub>2</sub> (5 mol%), Et<sub>3</sub>N (3 equiv.), isopropanol (0.27 M), 110 °C,  $\mu$ wave, 18 h, *then* NFSI (1.5 equiv.), rt, 5 h.

### 7.3.3 Characterisation of 2<sup>nd</sup> Generation EGFR Lysine-TCIs

With the second generation sulfonyl fluorides in hand, we next aimed to investigate if our design strategy had successfully furnished compounds with a covalent MoA. We proceeded to investigate the compounds through incubation with recombinant WT EGFR TKD followed by IPMS analysis of the samples. Pleasingly, incubation of sulfonyl fluoride **298** showed some time-dependent covalent modification of the TKD consistent with addition of compound with loss of HF, consistent with reaction of the enzyme with the covalent warhead (Figure 7.15), in contrast to the corresponding fluorosulfonate MMP **257** for which no adduct was observed. This supported our hypothesis that a more intrinsically reactive electrophile would enable a covalent MoA. Only a single adduct was detected, which was in accordance with selective reaction at Lys-745 within the reversible complex.

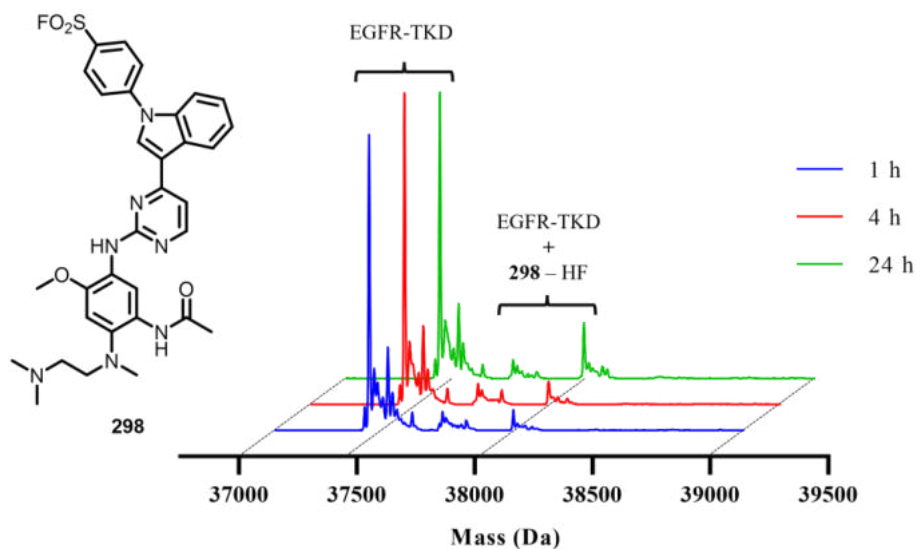


**Figure 7.15** Time-dependent covalent modification of WT EGFR TKD (500 nM) with TCI **298** (10  $\mu$ M) monitored by IPMS. Experiment performed by Marcus Ladds. Data plotted in GraphPad Prism 9.

Intriguingly, addition of an additional carbon atom in the linker to give *N*-benzyl TCI **299** resulted in an apparently enhanced rate of adduct formation (Figure 7.16).

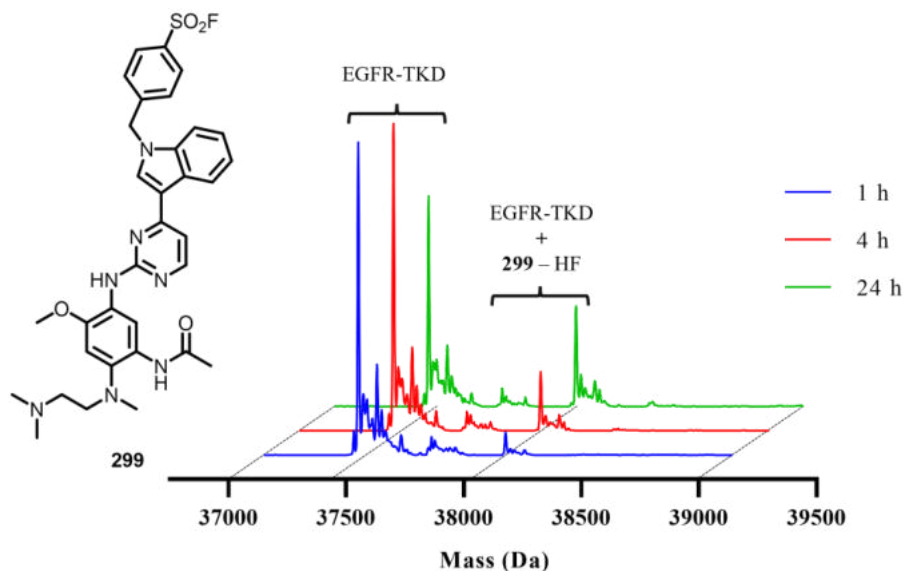


**Figure 7.16** Time-dependent covalent modification of WT EGFR TKD (500 nM) with TCI **299** (10  $\mu$ M) monitored by IPMS. Experiment performed by Marcus Ladds. Data plotted in GraphPad Prism 9.

This confirmed the rationale for our design strategy, as it indicated that introduction of flexibility to the phenyl linker enabled more favourable orientation of the covalent warhead towards Lys-745, thus increasing  $k_{\text{inact}}$ .

*N*-benzyl pyrazole **300** also displayed some covalent adduct formation with EGFR TKD, but demonstrated limited time-dependent increase after 30 minutes (Figure 7.17).

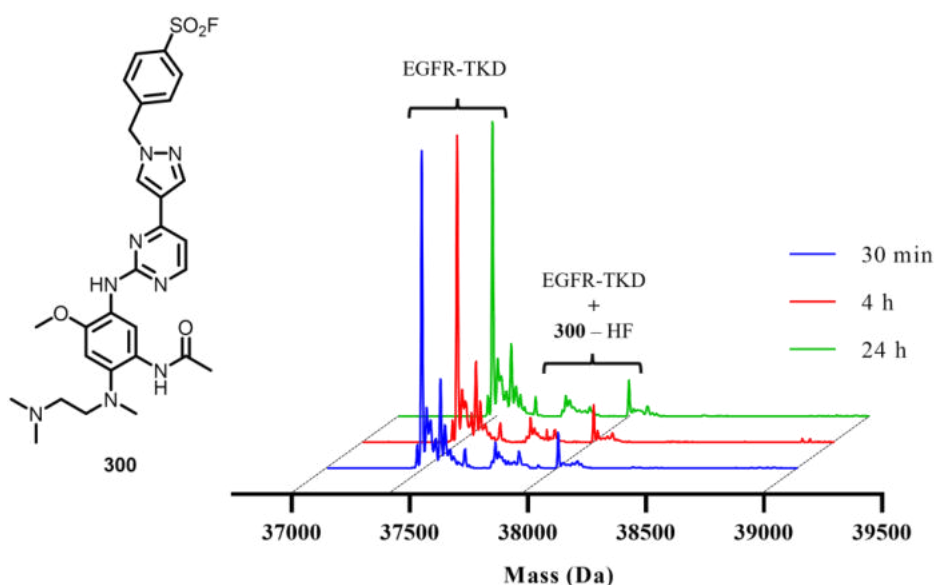


**Figure 7.17** Time-dependent covalent modification of WT EGFR TKD (500 nM) with TCI **300** (10  $\mu\text{M}$ ) monitored by IPMS. Experiment performed by Marcus Ladds. Data plotted in GraphPad Prism 9.

In contrast, phenethyl-linked sulfonyl fluoride **301** displayed the greatest extent of adduct formation of all the TCIs tested (Figure 7.18). This was consistent with the observation that an increased linker length led to an apparent improvement in the  $k_{\text{inact}}$  of the TCIs, likely owing to the longer linker facilitating a more optimal orientation of the covalent warhead. However, further biochemical characterisation would be required to evaluate the precise  $K_i$  and  $k_{\text{inact}}$  values of the second generation library of EGFR lysine-TCIs. Pleasingly, mono-labelled adduct formation was also observed for TCI **301**, suggesting that this adduct was forming selectively and not as a result of non-specific labelling of EGFR TKD.

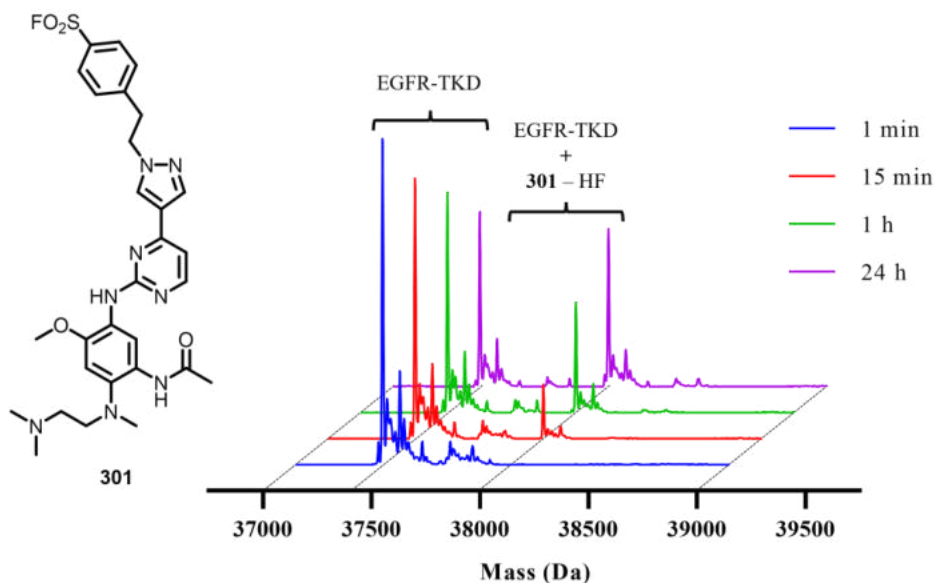


**Figure 7.18** Time-dependent covalent modification of WT EGFR TKD (500 nM) with TCI **301** (10  $\mu$ M) monitored by IPMS. Experiment performed by Marcus Ladds. Data plotted in GraphPad Prism 9.

#### 7.4 Conclusions and Future Work

This chapter has detailed the design and synthesis of osimertinib **12**-derived irreversible TCIs targeting the catalytic Lys-745 of the EGFR TKD. The syntheses of fluorosulfonate-derived inhibitors **257**, **258**, **259**, **260**, and **261** were achieved in 7 linear steps by applying a convergent synthetic strategy. However, biochemical profiling indicated that whilst inhibitors **257**, **258**, **259**, **260**, and **261** maintained selective reversible inhibition of TM EGFR over WT EGFR, no evidence of covalent adduct formation was observed, despite the inclusion of a lysine-reactive warhead.

We adopted a two-fold strategy to obtain a covalent MoA, which culminated in the design of a second generation TCI library, incorporating a more reactive sulfonyl fluoride warhead and a variety of linker lengths in an effort to improve  $k_{\text{inact}}$ . Incubation with EGFR TKD pleasingly demonstrated selective single adduct formation for all compounds tested, with the most rapid labelling observed for highly flexible phenethyl-linked TCI **301**.

Future work will involve extensive kinetic characterisation of the 2<sup>nd</sup> generation EGFR lysine-TCI library through progress curve analysis, as well as further characterisation to

confirm Lys-745 as the reacting residue which will include the production of a K745A construct of EGFR TKD.

## 8 Experimental

## 8 Experimental

### 8.1 Chemical Synthesis

#### 8.1.1 General Information

Unless otherwise stated, all reagents were purchased from commercial suppliers (Sigma-Aldrich, Alfa Aesar, Fluorochem, Apollo Scientific, Strem Chemicals, ATTO-TEC, Tokyo Chemical Industry, Carbosynth and Combi-Blocks) and used without further purification. Unless otherwise stated, solvents were used without prior drying/degassing. Reactions requiring anhydrous conditions are clearly stated and were conducted after heat-drying of the appropriate reaction vessel (round bottom two-neck flasks) and under an inert atmosphere of nitrogen or argon. Microwave reactions were performed using a Biotage Initiator Microwave Synthesizer. Thin-layer chromatography (TLC) was performed on pre-coated aluminium sheets of silica (60 F254 nm, Merck) and visualised using short-wave UV light and/or permanganate stain and/or vanillin stain and/or 2,4-dinitrophenylhydrazine stain. Column chromatography was performed on a Biotage Isolera purification system using Biotage Sfär Silica D Duo and Biotage® Sfär KP-Amino D cartridges and for normal phase and Biotage Sfär C18 D Duo cartridges for reverse-phase chromatography. Infrared spectra were recorded on a Bruker Alpha-p FT-IR spectrometer. Absorption maxima ( $V_{\max}$ ) are quoted in wavenumbers ( $\text{cm}^{-1}$ ). Optical rotations were recorded on a Bellingham & Stanley Ltd. ADP440 Polarimeter with a path length of 0.1 dm, using a light emitting diode with interference filter (298 nm). Concentrations ( $c$ ) are quoted in g/100 mL.

$^1\text{H}$  NMR spectra were recorded on a Bruker AMX500 (500 MHz) or Bruker AMX600 (600 MHz) spectrometers using an internal deuterium lock. Chemical shifts are quoted in parts per million (ppm) using the following internal references:  $\text{CDCl}_3$  ( $\delta\text{H}$  7.26),  $\text{CD}_2\text{Cl}_2$  ( $\delta\text{H}$  5.32),  $\text{DMSO-d}_6$  ( $\delta\text{H}$  2.50), acetone- $\text{d}_6$  ( $\delta\text{H}$  2.05) and  $\text{CD}_3\text{CN}$  ( $\delta\text{H}$  1.94). Signal multiplicities are recorded as singlet (s), doublet (d), triplet (t), quartet (q), quintet (quint), septet (sept), multiplet (m), doublet of doublets (dd), triplet of doublets (td), doublet of triplets (dt), apparent (app.), or broad (br.). Coupling constants,  $J$ , are measured to the nearest 0.1 Hz.  $^{13}\text{C}$  NMR spectra were recorded on Bruker AMX500 (126 MHz) or Bruker AMX600 (151 MHz) spectrometers using an internal deuterium lock. Chemical shifts are quoted to 0.01 ppm, using the following internal references:  $\text{CD}_3\text{CN}$



( $\delta$ C 118.26), CDCl<sub>3</sub> ( $\delta$ C 77.16), CD<sub>2</sub>Cl<sub>2</sub> ( $\delta$ C 53.84), acetone-d<sub>6</sub> ( $\delta$ C 29.84) and DMSO-d<sub>6</sub> ( $\delta$ C 39.52).

LCMS and HRMS analyses were recorded on an Agilent 1200 series HPLC and diode array detector coupled to a 6210 time-of-flight mass spectrometer with dual multimode APCI/ESI source. For LCMS extended mass (100 – 1000 amu), analytical separation was carried out at 30 °C on a Merck Chromolith Flash column (RP-18e, 25 x 2 mm) using a flow rate of 0.75 mL/min in a 4-minute gradient elution with detection at 254 nm. The mobile phase was a mixture of methanol (solvent A) and water (solvent B), both containing formic acid at 0.1%. Gradient elution was as follows: 5:95 (A/B) to 100:0 (A/B) over 2.5 min, 100:0 (A/B) for 1 min, and then reversion back to 5:95 (A/B) over 0.1 min, finally 5:95 (A/B) for 0.4 min. HRMS references: caffeine [M+H]<sup>+</sup> 195.087652; hexakis(2,2-difluoroethoxy)phosphazene [M+H]<sup>+</sup> 622.02896; and hexakis(1*H*,1*H*,3*H*-tetrafluoropentoxy)phosphazene [M+H]<sup>+</sup> 922.009798. For standard LCMS, analytical separation was carried out at 40 °C on a Merck Chromolith Flash column (RP-18e, 25 x 2 mm) using a flow rate of 1.5 mL/min in a 2-minute gradient elution with detection at 254 nm. The mobile phase was a mixture of methanol (solvent A) and water (solvent B), both containing formic acid at 0.1%. Gradient elution was as follows: 5:95 (A/B) to 100:0 (A/B) over 1.25 min, 100:0 (A/B) for 0.5 min, and then reversion back to 5:95 (A/B) over 0.05 min, finally 5:95 (A/B) for 0.2 min.

### 8.1.2 Chemistry Experimental Procedures

#### Chapters 3 – 6

The standard adenosine numbering has been used throughout this thesis and experimental section for analogues of adenosine (Figure 8.1). Additional groups extending from the adenine ring are numbered without a superscript, and groups extending from the ribose ring are numbered with a ‘ superscript.

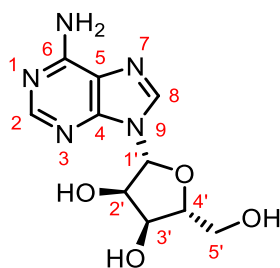


**Figure 8.1** Standard numbering of adenosine.

### General procedure A — nucleophilic aromatic substitution of 8-bromoadenosine

A glass microwave vial equipped with magnetic stirrer was charged with either 8-bromo-9-((3*aR*,4*R*,6*R*,6*aR*)-6-(((*tert*-butyldimethylsilyl)oxy)methyl)-2,2-dimethyltetrahydrofuro[3,4-*d*][1,3]dioxol-4-yl)-9*H*-purin-6-amine **95** (1 equiv.) or ((3*aR*,4*R*,6*R*,6*aR*)-6-(6-amino-8-bromo-9*H*-purin-9-yl)-2,2-dimethyltetrahydrofuro[3,4-*d*][1,3]dioxol-4-yl)methanol **109** (1 equiv.), amine (5.1 – 26 equiv.) and ethanol (0.3 M). The mixture was heated to 160 °C under microwave irradiation for 1 hour, after which the solvent was removed under reduced pressure. The crude mixture was redissolved in EtOAc and 1% AcOH (v/v) solution and the phases were separated. The organic phase was washed with 1% AcOH (v/v) solution (×3), sat. NaHCO<sub>3</sub> solution (×3), dried over MgSO<sub>4</sub>, filtered and concentrated under reduced pressure. The crude product was purified by flash column chromatography to yield the desired products.

### General procedure B — *N*-SEM protection of 8-*N* substituted adenosine derivatives

A two-neck round bottom flask equipped with magnetic stirrer and reflux condenser was charged with the corresponding 8-*N* substituted adenosine derivative (1 equiv.), CH<sub>2</sub>Cl<sub>2</sub> (0.3 M), and *N,N*-diisopropylethylamine (3 – 4.5 equiv.) under flow of nitrogen. 2-(trimethylsilyl)ethoxymethylchloride (3 – 4.5 equiv.) was then added dropwise and the mixture was heated to reflux. After stirring at reflux for 3 – 30 hours, the solvent was removed under reduced pressure and the crude mixture was purified by flash column chromatography to yield the desired products.

**General procedure C — *O*-TBS deprotection of *N*-SEM protected adenosine derivatives**

A two-neck round bottom flask equipped with magnetic stirrer was charged with the corresponding *N*-SEM protected adenosine derivative (1 equiv.) and THF (0.1 – 0.12 M) under flow of nitrogen. The mixture was cooled to 0 °C and TBAF (1 M in THF, 1.1 equiv.) was added dropwise, after which the mixture was allowed to warm up to room temperature. After stirring at room temperature for 1 - 48 hours the solvent was removed under reduced pressure, the crude mixture was redissolved in EtOAc and water and the phases were separated. The organic phase was washed with water (×3), dried over MgSO<sub>4</sub>, filtered, and concentrated under reduced pressure. The crude product was purified by flash column chromatography to yield the desired products.

**General procedure D — 5'-*O* etherification of *N*-SEM protected adenosine derivatives**

A two-neck round bottom flask heat-dried under vacuum and equipped with magnetic stirrer was charged with the corresponding *O*-TBS-deprotected *N*-SEM protected adenosine derivatives (1 equiv.) and THF (0.5 M) under flow of nitrogen. The mixture was cooled to 0 °C and sodium hydride (60% in mineral oil, 1.2 equiv.) was added and stirred for 15 minutes. The corresponding benzyl bromide (2 equiv.) was then added, after which the mixture was allowed to warm up to room temperature. After stirring at room temperature for 18 hours, the reaction mixture was quenched with methanol and the solvent was removed under reduced pressure. The crude mixture was purified by flash column chromatography to yield the desired products.

**General procedure E — palladium catalysed synthesis of sulfonyl fluorides from aryl bromides**

Adapted from a procedure developed by Willis and coworkers.<sup>164</sup>

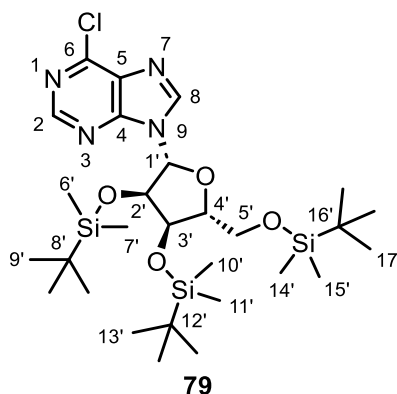
A glass microwave vial equipped with magnetic stirrer was charged with the corresponding aryl bromide (1 equiv.), DABSO (0.6 equiv.), PdCl<sub>2</sub>(AmPhos)<sub>2</sub> (5 mol%), and degassed and backfilled with argon four times. Isopropanol (0.27 M) was added to the mixture, which was then degassed and backfilled with argon four times, after which triethylamine (3 equiv.) was added and the mixture was heated to 75 °C. After stirring at

75 °C for 18 hours, the reaction mixture was cooled to room temperature and NFSI (1.5 equiv.) was added and the reaction mixture was stirred for a further 5 hours. The solvent was removed under reduced pressure, and the crude residue was redissolved in EtOAc and filtered through celite. The filtrate was washed with sat. Na<sub>2</sub>S<sub>2</sub>O<sub>3</sub> solution (×1), brine (×1), dried over MgSO<sub>4</sub>, filtered, and concentrated under reduced pressure. The crude product was purified by flash column chromatography to yield the desired products.

### General procedure F — global deprotection of adenosine derivatives

A glass vial equipped with magnetic stirrer was charged with the corresponding adenosine derivative (1 equiv.) and TFA:water 5:2 (v/v) mixture (0.1 M). After stirring at room temperature for 30 minutes – 3 hours, the reaction mixture was diluted with toluene and concentrated under reduced pressure. The crude mixture was purified by flash column chromatography to yield the desired products.

### 9-((2*R*,3*R*,4*R*,5*R*)-3,4-bis((*tert*-butyldimethylsilyl)oxy)-5-(((*tert*-butyldimethylsilyl)oxy)methyl)tetrahydrofuran-2-yl)-6-chloro-9*H*-purine (**79**)

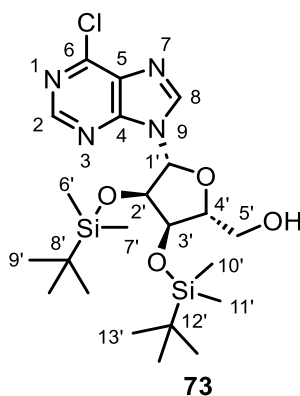


A two-neck round bottom flask equipped with magnetic stirrer was charged with (2*R*,3*R*,4*S*,5*R*)-2-(6-chloropurin-9-yl)-5-(hydroxymethyl)tetrahydrofuran-3,4-diol **78** (1.0 g, 3.49 mmol, 1 equiv.), DMF (35 mL, 0.1 M), *tert*-butyldimethylsilyl chloride (3.2 g, 20.9 mmol, 6 equiv.), and imidazole (0.24 g, 3.49 mmol, 1 equiv.) under flow of nitrogen. After stirring at room temperature for 20 hours, the reaction mixture was precipitated with water (50 mL), and the resultant solid was recrystallised from boiling methanol to yield **79** (1.1 g, 51%) as a white crystalline solid. <sup>1</sup>H NMR (500 MHz, CDCl<sub>3</sub>) δ = 8.74 (s, 1H, H<sub>2</sub>), 8.55 (s, 1H, H<sub>8</sub>), 6.13 (d, *J* = 4.9 Hz, 1H, H<sub>1'</sub>), 4.59 (app. t, *J* = 4.6 Hz, 1H, H<sub>2'</sub>), 4.31 (app. t, *J* = 4.0 Hz, 1H, H<sub>3'</sub>), 4.17 – 4.14 (m, 1H, H<sub>4'</sub>), 4.02

(dd,  $J = 11.5, 3.5$  Hz, 1H, H5'a), 3.81 (dd,  $J = 11.5, 2.5$  Hz, 1H, H5'b), 0.96 (s, 9H, SiC(CH<sub>3</sub>)<sub>3</sub>), 0.94 (s, 9H, SiC(CH<sub>3</sub>)<sub>3</sub>), 0.79 (s, 9H, SiC(CH<sub>3</sub>)<sub>3</sub>), 0.16 (s, 3H, SiCH<sub>3</sub>), 0.15 (s, 3H, SiCH<sub>3</sub>), 0.11 (s, 3H, SiCH<sub>3</sub>), 0.10 (s, 3H, SiCH<sub>3</sub>), -0.03 (s, 3H, SiCH<sub>3</sub>) -0.24 (s, 3H, SiCH<sub>3</sub>); <sup>13</sup>C NMR (126 MHz, CDCl<sub>3</sub>)  $\delta = 152.10$  (C2), 151.67 (C4), 151.17 (C6), 144.23 (C8), 132.25 (C5), 88.74 (C1'), 85.89 (C4'), 76.55 (C2'), 71.98 (C3'), 62.55 (C5'), 26.27 (3C, SiC(CH<sub>3</sub>)<sub>3</sub>), 25.97 (3C, SiC(CH<sub>3</sub>)<sub>3</sub>), 25.77 (3C, SiC(CH<sub>3</sub>)<sub>3</sub>), 18.72 (SiCH<sub>3</sub>), 18.23 (SiCH<sub>3</sub>), 17.98 (SiCH<sub>3</sub>), -4.24 (SiCH<sub>3</sub>), -4.50 (SiCH<sub>3</sub>), -4.56 (SiCH<sub>3</sub>), -4.90 (SiCH<sub>3</sub>), -5.17 (SiCH<sub>3</sub>), -5.21 (SiCH<sub>3</sub>); HRMS (ESI+)  $m/z$  calculated for C<sub>28</sub>H<sub>54</sub><sup>35</sup>ClN<sub>4</sub>O<sub>4</sub>Si<sub>3</sub> (M+H)<sup>+</sup> 629.3136, found 629.3161.

The spectroscopic and analytical data were in agreement with literature values.<sup>153</sup>

**((2*R*,3*R*,4*R*,5*R*)-3,4-bis(*tert*-butyldimethylsilyloxy)-5-(6-chloro-9*H*-purin-9-yl)tetrahydrofuran-2-yl)methanol (73)**

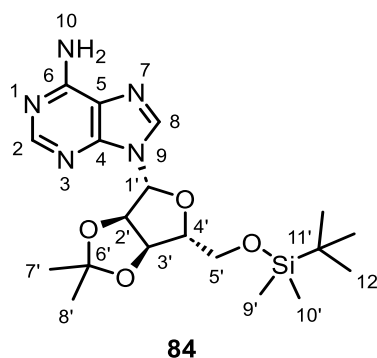


A two-neck round bottom flask equipped with magnetic stirrer was charged with 9-(((2*R*,3*R*,4*R*,5*R*)-3,4-bis(*tert*-butyldimethylsilyloxy)-5-(((*tert*-butyldimethylsilyloxy)methyl)tetrahydrofuran-2-yl)-6-chloro-9*H*-purine **79** (990 mg, 1.57 mmol, 1 equiv.) and THF (16.8 mL, 0.09 M) under flow of nitrogen. The mixture was cooled to 0 °C and TFA:water 1:1 mixture (8.4 mL) was added. After stirring at 0 °C for 6 hours, the reaction mixture was quenched with sat. NaHCO<sub>3</sub> solution (50 mL), diluted with EtOAc (75 mL) and the phases were separated. The aqueous phase was extracted with EtOAc (3 × 75 mL) and the resultant combined organic layers were washed with brine (3 × 100 mL), dried over MgSO<sub>4</sub>, filtered, and concentrated under reduced pressure. The crude product was purified by normal phase column chromatography on silica (100% cyclohexane to EtOAc:cyclohexane 10:90 gradient) to yield **73** (440 mg, 54%) as a white solid. <sup>1</sup>H NMR (600 MHz, CDCl<sub>3</sub>)  $\delta = 8.77$  (s, 1H, H2), 8.20 (s, 1H, H8), 5.88 (d,  $J = 7.8$  Hz, 1H, H1'),

4.98 (dd,  $J = 7.8, 4.5$  Hz, 1H, H2'), 4.34 (app. d,  $J = 4.5$  Hz, 1H, H3'), 4.20 – 4.18 (m, 1H, H4'), 3.95 (dd,  $J = 13.1, 1.8$  Hz, 1H, H5'a), 3.73 (dd,  $J = 13.1, 1.6$  Hz, 1H, H5'b), 0.95 (s, 9H, SiC(CH<sub>3</sub>)<sub>3</sub>), 0.74 (s, 9H, SiC(CH<sub>3</sub>)<sub>3</sub>), 0.13 (s, 3H, SiCH<sub>3</sub>), 0.12 (s, 3H, SiCH<sub>3</sub>), -0.13 (s, 3H, SiCH<sub>3</sub>), -0.65 (s, 3H, SiCH<sub>3</sub>); <sup>13</sup>C NMR (151 MHz, CDCl<sub>3</sub>)  $\delta = 152.68$  (C4), 151.55 (C2), 150.67 (C6), 145.79 (C8), 133.74 (C5), 91.45 (C1'), 89.65 (C4'), 74.26 (C2'), 73.85 (C3'), 63.00 (C5'), 25.94 (3C, SiC(CH<sub>3</sub>)<sub>3</sub>), 25.75 (3C, SiC(CH<sub>3</sub>)<sub>3</sub>), 18.21 (SiC(CH<sub>3</sub>)<sub>3</sub>), 17.91 (SiC(CH<sub>3</sub>)<sub>3</sub>), -4.41 (SiCH<sub>3</sub>), -4.43 (SiCH<sub>3</sub>), -4.46 (SiCH<sub>3</sub>), -5.73 (SiCH<sub>3</sub>); HRMS (ESI+)  $m/z$  calculated for C<sub>22</sub>H<sub>40</sub><sup>35</sup>ClN<sub>4</sub>O<sub>4</sub>Si<sub>2</sub> (M+H)<sup>+</sup> 515.2277, found 515.2271.

The spectroscopic and analytical data were in agreement with literature values.<sup>153</sup>

**9-((3*aR*,4*R*,6*R*,6*aR*)-6-(((*tert*-butyldimethylsilyl)oxy)methyl)-2,2-dimethyltetrahydrofuro[3,4-*d*][1,3]dioxol-4-yl)-9*H*-purin-6-amine (**84**)**

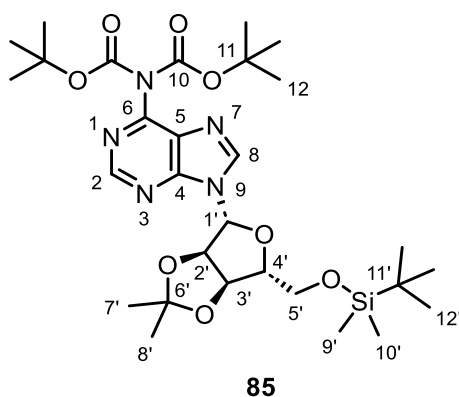


A two-neck round bottom flask equipped with magnetic stirrer was charged with 2',3'-*O*-isopropylideneadenosine **83** (30.0 g, 97.6 mmol, 1 equiv.), DMF (279 mL, 0.35 M), *tert*-butyldimethylsilyl chloride (17.7 g, 117 mmol, 1.2 equiv.), and imidazole (13.3 g, 195 mmol, 2 equiv.) under flow of nitrogen. After stirring for at room temperature for 20 hours, the reaction mixture was precipitated with water (600 mL), and the resultant solid was filtered and washed with water (10 x 200 mL) to yield **84** (40.0 g, 97%) as a white solid. <sup>1</sup>H NMR (600 MHz, CDCl<sub>3</sub>)  $\delta = 8.38$  (s, 1H, H2), 8.06 (s, 1H, H8), 6.17 (d,  $J = 2.5$  Hz, 1H, H1'), 5.80 (s, 2H, H10), 5.27 (dd,  $J = 6.2, 2.5$  Hz, 1H, H2'), 4.95 (dd,  $J = 6.2, 2.5$  Hz, 1H, H3'), 4.44 – 4.41 (m, 1H, H4'), 3.88 (dd,  $J = 11.2, 3.9$  Hz, 1H, H5'a), 3.76 (dd,  $J = 11.2, 4.2$  Hz, 1H, H5'b), 1.63 (s, 3H, H7'), 1.40 (s, 3H, H8'), 0.84 (s, 9H, H12'), 0.02 (s, 3H, H9'), 0.01 (s, 3H, H10'); <sup>13</sup>C NMR (151 MHz, CDCl<sub>3</sub>)  $\delta = 155.31$  (C6), 152.91 (C2), 149.58 (C4), 139.58 (C8), 120.24 (C5), 114.24 (C6'), 91.73 (C1'), 87.54

(C4'), 85.16 (C2'), 81.64 (C3'), 63.70 (C5'), 27.38 (C7'), 25.99 (3C, C12'), 25.54 (C8'), 18.47 (C11'), -5.31 (C9'), -5.39 (C10'); **HRMS** (ESI+)  $m/z$  calculated for  $C_{19}H_{32}N_5O_4Si$  (M+H)<sup>+</sup> 422.2218, found 422.2235.

The spectroscopic and analytical data were in agreement with literature values.<sup>289</sup>

**tert-butyl** (*tert*-butoxycarbonyl)(9-((3*aR*,4*R*,6*R*,6*aR*)-6-(((*tert*-butyldimethylsilyl)oxy)methyl)-2,2-dimethyltetrahydrofuro[3,4-*d*][1,3]dioxol-4-yl)-9*H*-purin-6-yl)carbamate (**85**)

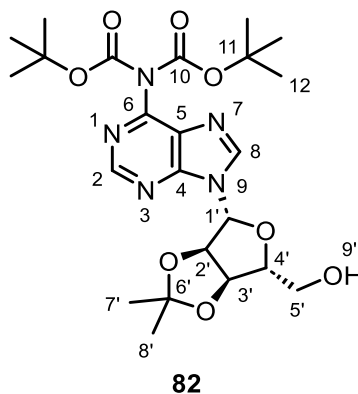


A two-neck round bottom flask equipped with magnetic stirrer was charged with 9-((3*aR*,4*R*,6*R*,6*aR*)-6-(((*tert*-butyldimethylsilyl)oxy)methyl)-2,2-dimethyltetrahydrofuro[3,4-*d*][1,3]dioxol-4-yl)-9*H*-purin-6-amine **84** (1.2 g, 2.85, 1 equiv.), THF (14.2 mL, 0.2 M), and 4-dimethylaminopyridine (35.0 mg, 0.28 mmol, 0.1 equiv.) under flow of nitrogen. Di-*tert*-butyl dicarbonate (1.69 mL, 7.11 mmol, 2.5 equiv.) was added dropwise, and the mixture was stirred at room temperature. After stirring at room temperature at 3 hours, the solvent was removed under reduced pressure and the crude mixture was purified by normal phase column chromatography on silica (100%  $CH_2Cl_2$  to methanol: $CH_2Cl_2$  5:95 gradient) to yield **85** (1.76 g, 99%) as a yellow oil. **<sup>1</sup>H NMR** (500 MHz,  $CDCl_3$ )  $\delta$  = 8.88 (s, 1H, H2), 8.35 (s, 1H, H8), 6.25 (d,  $J$  = 2.6 Hz, 1H, H1'), 5.22 (dd,  $J$  = 6.1, 2.6 Hz, 1H, H2'), 4.96 (dd,  $J$  = 6.1, 2.5 Hz, 1H, H3'), 4.47 – 4.43 (m, 1H, H4'), 3.90 (dd,  $J$  = 11.2, 3.6 Hz, 1H, H5'a), 3.79 (dd,  $J$  = 11.3, 4.0 Hz, 1H, H5'b), 1.65 (s, 3H, H7'), 1.43 (s, 18H, H12), 1.41 (s, 3H, H8'), 0.86 (s, 9H, H12'), 0.03 (s, 3H, H9'), 0.02 (s, 3H, H10'); **<sup>13</sup>C NMR** (126 MHz,  $CDCl_3$ )  $\delta$  = 152.75 (C6), 152.38 (C2), 150.54 (2C, C10), 150.52 (C4), 143.46 (C8), 129.57 (C5), 114.45 (C6'), 91.80 (C1'), 87.46 (C4'), 85.25 (C2'), 83.89 (2C, C11), 81.53 (C3'), 63.67 (C5'), 27.94 (6C, C12), 27.40 (C7'), 26.04 (3C, C12'), 25.52 (C8'), 18.51 (C11'), -5.27 (C9'), -5.35

(C10'); **HRMS** (ESI+)  $m/z$  calculated for  $C_{29}H_{48}N_5O_8Si$  ( $M+Na$ )<sup>+</sup> 644.3092, found 644.3083.

The spectroscopic and analytical data were in agreement with literature values.<sup>290</sup>

**tert-butyl** (tert-butoxycarbonyl)(9-((3*aR*,4*R*,6*R*,6*aR*)-6-(hydroxymethyl)-2,2-dimethyltetrahydrofuro[3,4-*d*][1,3]dioxol-4-yl)-9*H*-purin-6-yl)carbamate (**82**)



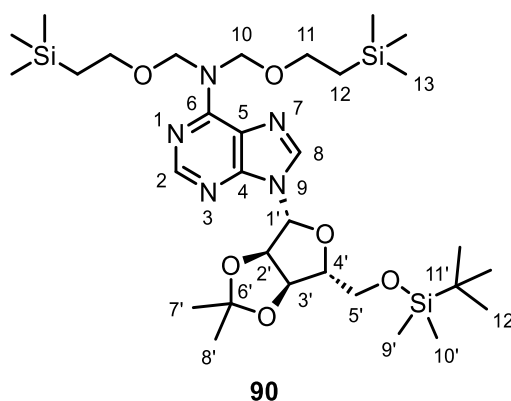
A two-neck round bottom flask equipped with magnetic stirrer was charged with *tert*-butyl (tert-butoxycarbonyl)(9-((3*aR*,4*R*,6*R*,6*aR*)-6-(((*tert*-butyldimethylsilyl)oxy)methyl)-2,2-dimethyltetrahydrofuro[3,4-*d*][1,3]dioxol-4-yl)-9*H*-purin-6-yl)carbamate **85** (1.76 g, 2.83 mmol, 1 equiv.) and THF (23.6 mL, 0.12 M) under flow of nitrogen. TBAF (2.83 mL, 1 M in THF, 2.83 mmol, 1 equiv.) was added slowly to the mixture, which was then stirred at room temperature. After stirring at room temperature for 2 hours, then solvent was removed under reduced pressure and the crude mixture was redissolved in EtOAc (100 mL) and water (100 mL) and the phases were separated. The organic phase was washed with water (3 × 100 mL), dried over  $MgSO_4$ , filtered, and concentrated under reduced pressure. The crude product was purified by normal phase column chromatography on silica (EtOAc:cyclohexane 5:95 to 20:80 gradient) to yield **82** (1.1 g, 78%) as a white foam. **<sup>1</sup>H NMR** (500 MHz,  $CDCl_3$ )  $\delta$  = 8.84 (s, 1H, H2), 8.13 (s, 1H, H8), 5.94 (d,  $J$  = 4.9 Hz, 1H, H1'), 5.38 (app. d,  $J$  = 10.9 Hz, 1H, H9'), 5.23 – 5.20 (m, 1H, H2'), 5.12 (dd,  $J$  = 6.0, 1.5 Hz, 1H, H3'), 4.56 – 4.54 (m, 1H, H4'), 4.01 – 3.96 (m, 1H, H5'a), 3.85 – 3.78 (m, 1H, H5'b), 1.65 (s, 3H, H7'), 1.47 (s, 18H, H12), 1.39 (s, 3H, H8'); **<sup>13</sup>C NMR** (126 MHz,  $CDCl_3$ )  $\delta$  = 151.97 (C6), 151.83 (C2), 151.49 (C4), 150.47 (2C, C10), 144.38 (C8), 130.52 (C5), 114.47 (C6'), 94.31 (C1'), 86.28 (C4'), 84.26 (2C, C11), 83.16 (C2'), 81.69 (C3'), 63.46 (C5'), 27.95 (6C,



C12), 27.75 (C7'), 25.37 (C8'); **HRMS** (ESI+)  $m/z$  calculated for  $C_{23}H_{34}N_5O_8$  (M+H)<sup>+</sup> 508.2402, found 508.2420;

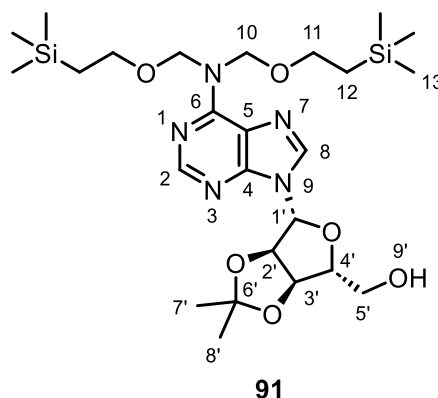
The spectroscopic and analytical data were in agreement with literature values.<sup>290</sup>

**9-((3*aR*,4*R*,6*R*,6*aR*)-6-(((*tert*-butyldimethylsilyl)oxy)methyl)-2,2-dimethyltetrahydrofuro[3,4-*d*][1,3]dioxol-4-yl)-*N*-((3,3-dimethylbutoxy)methyl)-*N*-((2-(trimethylsilyl)ethoxy)methyl)-9*H*-purin-6-amine (90)**



**90** was prepared following general procedure B, with 9-((3*aR*,4*R*,6*R*,6*aR*)-6-(((*tert*-butyldimethylsilyl)oxy)methyl)-2,2-dimethyltetrahydrofuro[3,4-*d*][1,3]dioxol-4-yl)-9*H*-purin-6-amine **84** (5.00 g, 11.9 mmol, 1 equiv.),  $CH_2Cl_2$  (39.5 mL, 0.3 M), 2-(trimethylsilyl)ethoxymethylchloride (6.30 mL, 35.6 mmol, 3 equiv.) and *N,N*-diisopropylethylamine (6.20 mL, 35.6 mmol, 3 equiv.) for 3 hours. Purification by normal phase column chromatography on silica (EtOAc:cyclohexane 5:95 to 15:85 gradient) yielded **90** (5.29 g, 65%) as a colourless oil. **<sup>1</sup>H NMR** (500 MHz,  $CDCl_3$ )  $\delta$  = 8.44 (s, 1H, H2), 8.01 (s, 1H, H8), 6.13 (d,  $J$  = 2.4 Hz, 1H, H1'), 5.54 (s br, 4H, H10), 5.25 (dd,  $J$  = 6.3, 2.4 Hz, 1H, H2'), 4.95 (dd,  $J$  = 6.3, 2.6 Hz, 1H, H3'), 4.41 – 4.38 (m, 1H, H4'), 3.86 (dd,  $J$  = 11.1, 4.1 Hz, 1H, H5'a), 3.75 (dd,  $J$  = 11.1, 4.4 Hz, 1H, H5'b), 3.65 – 3.59 (m, 4H, H11), 1.61 (s, 3H, H7'), 1.38 (s, 3H, H8') 0.99 – 0.89 (m, 4H, H12), 0.83 (s, 9H, H12'), 0.00 (s, 3H, H9'), -0.01(s, 3H, H10') -0.05 (s, 18H, H13); **<sup>13</sup>C NMR** (126 MHz,  $CDCl_3$ )  $\delta$  = 154.68 (C6), 152.40 (C2), 151.00 (C4), 138.43 (C8), 120.72 (C5), 114.15 (C6'), 91.52 (C1'), 87.48 (C4'), 85.05 (C2'), 81.61 (C3'), 76.34 (2C, C10), 65.42 (2C, C11), 63.61 (C5'), 27.35 (C7'), 25.99 (3C, C12'), 25.54 (C8'), 18.44 (C11'), 18.27 (2C, C12), -1.27 (6C, C13), -5.31 (C9'), -5.40 (C10'); **HRMS** (ESI+)  $m/z$  calculated for  $C_{32}H_{60}N_5O_6Si_2$  (M+H)<sup>+</sup> 682.3846, found 682.3823.

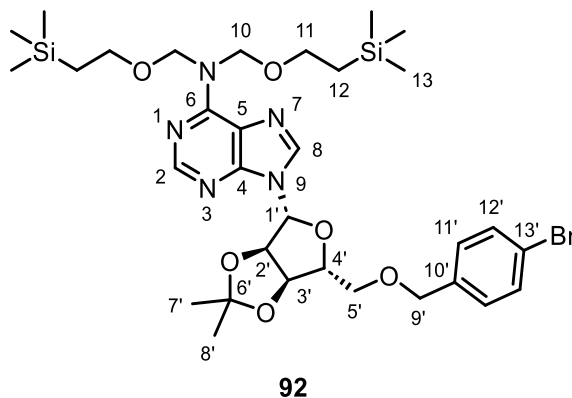
**((3*aR*,4*R*,6*R*,6*aR*)-6-(6-(bis((2-(trimethylsilyl)ethoxy)methyl)amino)-9*H*-purin-9-yl)-2,2-dimethyltetrahydrofuro[3,4-*d*][1,3]dioxol-4-yl)methanol (91)**



**91** was prepared following general procedure C, with 9-((3*aR*,4*R*,6*R*,6*aR*)-6-(((*tert*-butyldimethylsilyl)oxy)methyl)-2,2-dimethyltetrahydrofuro[3,4-*d*][1,3]dioxol-4-yl)-*N*-((3,3-dimethylbutoxy)methyl)-*N*-((2-(trimethylsilyl)ethoxy)methyl)-9*H*-purin-6-amine **90** (5.25 g, 7.69 mmol, 1 equiv.), THF (64.1 mL, 0.12 M) and TBAF (8.46 mL, 1 M in THF, 8.46 mmol, 1.1 equiv.) for 1 hour. Purification by normal phase column chromatography on silica (EtOAc:cyclohexane 5:95 to 50:50 gradient) yielded **91** (3.79 g, 87%) as a colourless oil. <sup>1</sup>H NMR (600 MHz, CDCl<sub>3</sub>) δ = 8.38 (s, 1H, H<sub>2</sub>), 7.83 (s, 1H, H<sub>8</sub>), 6.54 (app. d, *J* = 11.9 Hz, 1H, H<sub>9'</sub>), 5.84 (d, *J* = 5.0 Hz, 1H, H<sub>1'</sub>), 5.54 (s br, 4H, H<sub>10</sub>), 5.22 (app. t, *J* = 5.4 Hz, 1H, H<sub>2'</sub>), 5.13 – 5.10 (m, 1H, H<sub>3'</sub>), 4.55 – 4.52 (m, 1H, H<sub>4'</sub>), 3.99 – 3.94 (m, 1H, H<sub>5'a</sub>), 3.82 – 3.75 (m, 1H, H<sub>5'b</sub>), 3.67 – 3.61 (m, 4H, H<sub>11</sub>), 1.65 (s, 3H, H<sub>7'</sub>), 1.38 (s, 3H, H<sub>8'</sub>), 0.97 – 0.93 (m, 4H, H<sub>12</sub>), -0.03 (s, 18H, H<sub>13</sub>); <sup>13</sup>C NMR (151 MHz, CDCl<sub>3</sub>) δ = 155.30 (C<sub>6</sub>), 151.79 (C<sub>2</sub>), 150.00 (C<sub>4</sub>), 139.60 (C<sub>8</sub>), 121.85 (C<sub>5</sub>), 114.13 (C<sub>6'</sub>), 94.53 (C<sub>1'</sub>), 86.14 (C<sub>4'</sub>), 82.84 (C<sub>2'</sub>), 81.84 (C<sub>3'</sub>), 65.69 (2C, C<sub>11</sub>), 63.66 (C<sub>5'</sub>), 27.84 (C<sub>7'</sub>), 25.40 (C<sub>8'</sub>), 18.33 (2C, C<sub>12</sub>), -1.24 (6C, C<sub>13</sub>);\* HRMS (ESI+) *m/z* calculated for C<sub>25</sub>H<sub>46</sub>N<sub>5</sub>O<sub>6</sub>Si<sub>2</sub> (M+H)<sup>+</sup> 568.2981, found 568.2967.

\*C<sub>10</sub> not observed in spectrum.

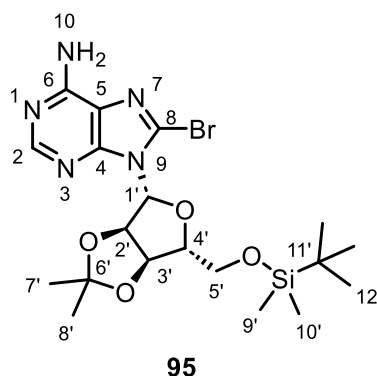
**9-((3*aR*,4*R*,6*R*,6*aR*)-6-(((4-bromobenzyl)oxy)methyl)-2,2-dimethyltetrahydrofuro[3,4-*d*][1,3]dioxol-4-yl)-*N,N*-bis((2-(trimethylsilyl)ethoxy)methyl)-9*H*-purin-6-amine (92)**



**92** was prepared following general procedure D, with ((3*aR*,4*R*,6*R*,6*aR*)-6-(6-(bis((2-(trimethylsilyl)ethoxy)methyl)amino)-9*H*-purin-9-yl)-2,2-dimethyltetrahydrofuro[3,4-*d*][1,3]dioxol-4-yl)methanol **91** (3.75 g, 6.60 mmol, 1 equiv.), THF (13.2 mL, 0.5 M), sodium hydride (317 mg, 60% in mineral oil, 7.92 mmol, 1.2 equiv.) and 4-bromobenzyl bromide (3.30 g, 13.20 mmol, 2 equiv.). Purification by normal phase column chromatography on silica (EtOAc:cyclohexane 5:95 to 25:75 gradient) yielded **92** (4.42 g, 91%) as a colourless oil. <sup>1</sup>H NMR (600 MHz, CDCl<sub>3</sub>) δ = 8.41 (s, 1H, H2), 7.97 (s, 1H, H8), 7.44 – 7.39 (m, 2H, H12'), 7.12 – 7.07 (m, 2H, H11'), 6.17 (d, *J* = 2.3 Hz, 1H, H1'), 5.55 (s br, 4H, H10), 5.32 (dd, *J* = 6.3, 2.3 Hz, 1H, H2'), 4.99 (dd, *J* = 6.3, 2.9 Hz, 1H, H3'), 4.49 – 4.46 (m, 1H, H4'), 4.46 – 4.39 (m, 2H, H9') 3.71 – 3.59 (m, 6H, H5', H11), 1.62 (s, 3H, H7'), 1.39 (s, 3H, H8'), 1.00 – 0.93 (m, 4H, H12), -0.03 (s, 18H, H13); <sup>13</sup>C NMR (151 MHz, CDCl<sub>3</sub>) δ = 154.72 (C6), 152.44 (C2), 151.06 (C4), 138.64 (C8), 136.53 (C10'), 131.71 (2C, C12'), 129.52 (2C, C11'), 121.93 (C13'), 120.76 (C5), 114.41 (C6'), 91.35 (C1'), 86.11 (C4'), 84.84 (C2'), 81.96 (C3'), 72.92 (C9'), 70.48 (C5'), 65.58 (2C, C12), 27.37 (C7'), 25.59 (C8'), 18.33 (2C, C11), -1.23 (6C, C13);\* HRMS (ESI+) *m/z* calculated for C<sub>32</sub>H<sub>51</sub><sup>79</sup>BrN<sub>5</sub>O<sub>6</sub>Si<sub>2</sub> (M+H)<sup>+</sup> 736.2556, found 736.2633.

\*C10 not observed in spectrum.

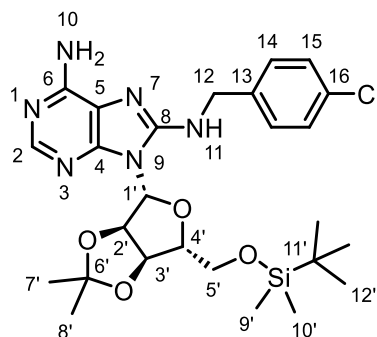
**8-bromo-9-((3*aR*,4*R*,6*R*,6*aR*)-6-(((*tert*-butyldimethylsilyl)oxy)methyl)-2,2-dimethyltetrahydrofuro[3,4-*d*][1,3]dioxol-4-yl)-9*H*-purin-6-amine (95)**



A two-neck round bottom flask equipped with magnetic stirrer was charged with 9-((3*aR*,4*R*,6*R*,6*aR*)-6-(((*tert*-butyldimethylsilyl)oxy)methyl)-2,2-dimethyltetrahydrofuro[3,4-*d*][1,3]dioxol-4-yl)-9*H*-purin-6-amine **84** (9.77 g, 23.2 mmol, 1 equiv.) and 1,4-dioxane (77.3 mL, 0.25 M) under flow of nitrogen. A separate flask equipped with magnetic stirrer was charged with K<sub>2</sub>HPO<sub>4</sub> (12.1 g, 69.5 mmol, 3 equiv.), water (77.3 mL), and bromine (2.97 mL, 57.9 mmol, 2.5 equiv.), and the resultant solution was slowly transferred *via* syringe into the first mixture. After stirring at room temperature for 24 hours, the reaction mixture was quenched with sat. Na<sub>2</sub>S<sub>2</sub>O<sub>3</sub> solution (200 mL), diluted with EtOAc (100 mL) and the phases were separated. The aqueous phase was extracted with EtOAc (3 × 250 mL) and the resultant combined organic layers were washed with brine (2 × 250 mL), dried over MgSO<sub>4</sub>, filtered, and concentrated under reduced pressure. The crude product was purified by normal phase column chromatography on silica (EtOAc:cyclohexane 10:90 to 40:60 gradient) to yield **95** (7.02 g, 61%) as an off-white solid. <sup>1</sup>H NMR (600 MHz, CDCl<sub>3</sub>) δ = 8.28 (s, 1H, H2), 6.18 (d, *J* = 1.9 Hz, 1H, H1'), 5.79 (dd, *J* = 6.3, 1.9 Hz, 1H, H2'), 5.51 (s br, 2H, H10), 5.15 (dd, *J* = 6.3, 3.2 Hz, 1H, H3'), 4.29 (app. td, *J* = 6.5, 3.2 Hz, 1H, H4'), 3.74 (dd, *J* = 10.6, 6.7 Hz, 1H, H5'a), 3.64 (dd, *J* = 10.6, 6.4 Hz, 1H, H5'a), 1.61 (s, 3H, H7'), 1.41 (s, 3H, H8'), 0.83 (s, 9H, H12'), -0.05 (s, 3H, H8'), -0.06 (s, 3H, H9'); <sup>13</sup>C NMR (151 MHz, CDCl<sub>3</sub>) δ = 154.24 (C6), 153.09 (C2), 150.70 (C4), 128.22 (C8), 120.38 (C5), 114.16 (C6'), 91.76 (C1'), 88.39 (C4'), 83.04 (C2'), 82.32 (C3'), 63.29 (C5'), 27.35 (C7'), 26.01 (3C, C12'), 25.63 (C8'), 18.51 (C9'), -5.23 (C10'), -5.29 (C11'); HRMS (ESI+) *m/z* calculated for C<sub>19</sub>H<sub>31</sub><sup>79</sup>BrN<sub>5</sub>O<sub>4</sub>Si (M+H)<sup>+</sup> 500.1323, found 500.1333.

The spectroscopic and analytical data were in agreement with literature values.<sup>291</sup>

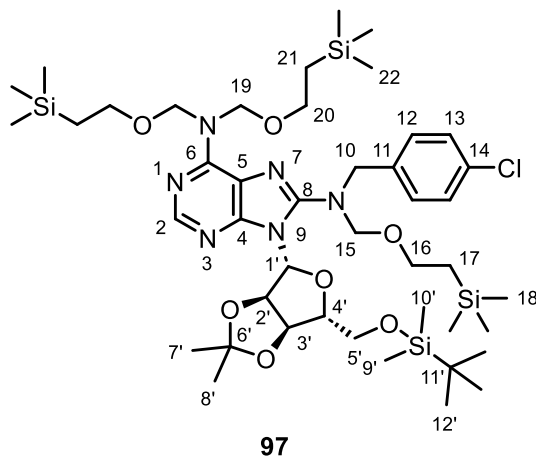
**9-((3*aR*,4*R*,6*R*,6*aR*)-6-(((*tert*-butyldimethylsilyl)oxy)methyl)-2,2-dimethyltetrahydrofuro[3,4-*d*][1,3]dioxol-4-yl)-*N*8-(4-chlorobenzyl)-9*H*-purine-6,8-diamine (**96**)**



**96**

**96** was prepared following general procedure A, with 8-bromo-9-((3*aR*,4*R*,6*R*,6*aR*)-6-(((*tert*-butyldimethylsilyl)oxy)methyl)-2,2-dimethyltetrahydrofuro[3,4-*d*][1,3]dioxol-4-yl)-9*H*-purin-6-amine **95** (4.00 g, 7.99 mmol, 1 equiv.), ethanol (26.6 mL, 0.3 M) and 4-chlorobenzylamine (7.78 mL, 63.9 mmol, 8 equiv.). Purification by normal phase column chromatography on silica (100% CH<sub>2</sub>Cl<sub>2</sub> to methanol: CH<sub>2</sub>Cl<sub>2</sub> 10:90 gradient) then reverse phase column chromatography on C18 (methanol:water +0.1% formic acid 40:60 to 100% methanol gradient) yielded **96** (4.03 g, 90%) as a pink solid. <sup>1</sup>H NMR (600 MHz, CDCl<sub>3</sub>) δ = 8.17 (s, 1H, H2), 7.34 – 7.26 (m, 4H, H14, H15), 6.07 (d, *J* = 3.1 Hz, 1H, H1'), 5.61 (app. t, *J* = 5.95 Hz, 1H, H11), 5.57 (dd, *J* = 6.6 Hz, 3.1 Hz, 1H, H2'), 5.15 (s br, 2H, H10), 4.93 (dd, *J* = 6.6, 3.3 Hz, 1H, H3'), 4.68 (dd, *J* = 15.3, 7.0 Hz, 1H, H12a), 4.61 (dd, *J* = 15.3, 4.9 Hz, 1H, H12b), 4.24 – 4.20 (m, 1H, H4'), 3.77 (dd, *J* = 11.3, 4.2 Hz, 1H, H5'a), 3.68 (dd, *J* = 11.3, 4.0 Hz, 1H, H5'b), 1.61 (s, 3H, H7'), 1.39 (s, 3H, H8'), 0.82 (s, 9H, H12'), -0.04 (s, 6H, H9', H10'); <sup>13</sup>C NMR (151 MHz, CDCl<sub>3</sub>) δ = 152.17 (C6), 151.94 (C8), 150.26 (C4), 150.14 (C2), 137.35 (C13), 133.28 (C16), 128.90 (2C, C15), 128.72 (2C, C14), 117.74 (C5), 114.77 (C6'), 89.16 (C1'), 85.96 (C4'), 82.37 (C2'), 80.43 (C3'), 62.84 (C5'), 46.12 (C12), 27.34 (C7'), 26.05 (3C, C12'), 25.55 (C8'), 18.70 (C11'), -5.21 (C9'), -5.35 (C10'); HRMS (ESI+) *m/z* calculated for C<sub>26</sub>H<sub>38</sub><sup>35</sup>ClN<sub>6</sub>O<sub>4</sub>Si (M+H)<sup>+</sup> 561.2407, found 561.2407.

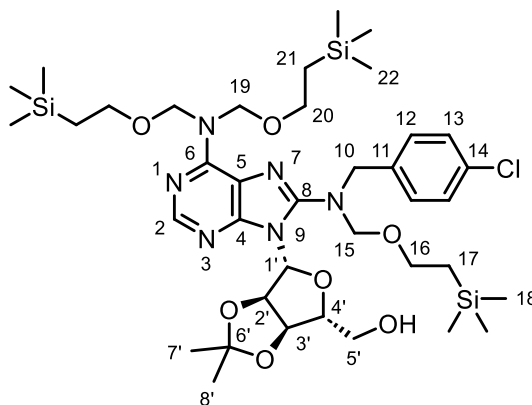
**9-((3*aR*,4*R*,6*R*,6*aR*)-6-(((*tert*-butyldimethylsilyl)oxy)methyl)-2,2-dimethyltetrahydrofuro[3,4-*d*][1,3]dioxol-4-yl)-*N*8-(4-chlorobenzyl)-*N*6,*N*8-tris((2-(trimethylsilyl)ethoxy)methyl)-9*H*-purine-6,8-diamine (**97**)**



**97** was prepared following general procedure B, with 9-((3*aR*,4*R*,6*R*,6*aR*)-6-(((*tert*-butyldimethylsilyl)oxy)methyl)-2,2-dimethyltetrahydrofuro[3,4-*d*][1,3]dioxol-4-yl)-*N*8-(4-chlorobenzyl)-9*H*-purine-6,8-diamine **96** (3.81 g, 6.78 mmol, 1 equiv.), CH<sub>2</sub>Cl<sub>2</sub> (22.5 mL, 0.3 M), 2-(trimethylsilyl)ethoxymethylchloride (5.40 mL, 30.5 mmol, 4.5 equiv.) and *N,N*-diisopropylethylamine (5.32 mL, 30.5 mmol, 4.5 equiv.) for 30 hours. Purification by normal phase column chromatography on silica (EtOAc:cyclohexane 1:99 to 10:90 gradient) yielded **97** (2.54 g, 39%) as a yellow oil. <sup>1</sup>H NMR (600 MHz, CDCl<sub>3</sub>) δ = 8.30 (s, 1H, H<sub>2</sub>), 7.36 – 7.26 (m, 4H, H<sub>12</sub>, H<sub>13</sub>), 6.07 (d, *J* = 1.9 Hz, 1H, H<sub>1'</sub>), 5.64 (dd, *J* = 6.2, 1.9 Hz, 1H, H<sub>2'</sub>), 5.60 – 5.50 (m, 2H, H<sub>19a</sub>), 5.47 – 5.33 (m, 2H, H<sub>19b</sub>), 5.19 (dd, *J* = 6.2, 2.9 Hz, 1H, H<sub>3'</sub>), 4.77 – 4.59 (m, 4H, H<sub>10</sub>, H<sub>15</sub>), 4.28 (app. td, *J* = 7.0, 2.9 Hz, 1H, H<sub>4'</sub>), 3.95 – 3.91 (m, 1H, H<sub>5'a</sub>), 3.73 – 3.69 (m, 1H, H<sub>5'b</sub>), 3.65 – 3.60 (m, 4H, H<sub>20</sub>), 3.55 – 3.49 (m, 2H, H<sub>16</sub>), 1.60 (s, 3H, H<sub>7'</sub>) 1.40 (s, 3H, H<sub>8'</sub>), 0.99 – 0.93 (m, 4H, H<sub>21</sub>), 0.93 – 0.89 (m, 2H, H<sub>17</sub>), 0.88 (s, 9H, H<sub>12'</sub>), 0.01 (s, 3H, H<sub>9'</sub>), 0.00 (s, 3H, H<sub>10'</sub>), -0.01 (s, 27H, H<sub>18</sub>, H<sub>22</sub>); <sup>13</sup>C NMR (151 MHz, CDCl<sub>3</sub>) δ = 152.71 (C<sub>6</sub>), 152.63 (C<sub>8</sub>), 151.40 (C<sub>4</sub>), 150.37 (C<sub>2</sub>), 136.00 (C<sub>11</sub>), 133.35 (C<sub>14</sub>), 130.21 (2C, C<sub>13</sub>), 128.74 (2C, C<sub>12</sub>), 117.98 (C<sub>5</sub>), 113.54 (C<sub>6'</sub>), 90.24 (C<sub>1'</sub>), 88.26 (C<sub>4'</sub>), 83.05 (C<sub>2'</sub>), 82.90 (C<sub>3'</sub>), 81.53 (C<sub>15</sub>), 66.00 (C<sub>16</sub>), 65.21 (2C, C<sub>20</sub>), 63.45 (C<sub>5'</sub>), 52.78 (C<sub>10</sub>), 27.30 (C<sub>7'</sub>), 26.04 (C<sub>12'</sub>), 25.59 (C<sub>8'</sub>), 18.49 (C<sub>11'</sub>), 18.33 (2C, C<sub>21</sub>), 18.15 (C<sub>17</sub>), -1.22 (6C, C<sub>22</sub>), -1.26 (3C, C<sub>18</sub>), -5.10 (C<sub>9'</sub>), -5.19 (C<sub>10'</sub>);\* HRMS (ESI+) *m/z* calculated for C<sub>44</sub>H<sub>80</sub><sup>35</sup>ClN<sub>6</sub>O<sub>7</sub>Si<sub>4</sub> (M+H)<sup>+</sup> 951.4849, found 951.4863.

\*C19 not observed in spectrum.

**((3*aR*,4*R*,6*R*,6*aR*)-6-(6-(bis((2-(trimethylsilyl)ethoxy)methyl)amino)-8-(4-chlorobenzyl)((2-(trimethylsilyl)ethoxy)methyl)amino)-9*H*-purin-9-yl)-2,2-dimethyltetrahydrofuro[3,4-*d*][1,3]dioxol-4-yl)methanol (94)**

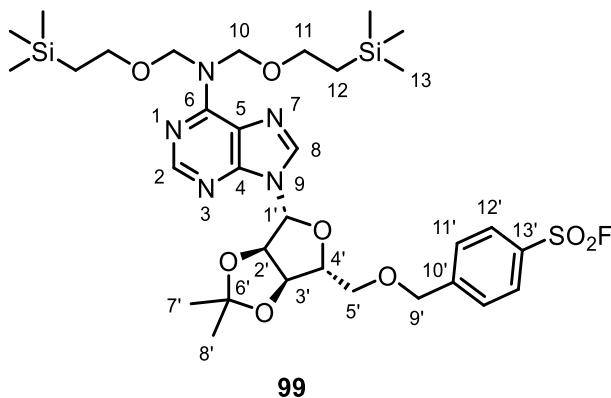


**94**

**94** was prepared following general procedure C, with 9-((3*aR*,4*R*,6*R*,6*aR*)-6-(((*tert*-butyldimethylsilyl)oxy)methyl)-2,2-dimethyltetrahydrofuro[3,4-*d*][1,3]dioxol-4-yl)-*N*8-(4-chlorobenzyl)-*N*6,*N*6,*N*8-tris((2-(trimethylsilyl)ethoxy)methyl)-9*H*-purine-6,8-diamine **97** (2.51 g, 2.64 mmol, 1 equiv.) and THF (22.0 mL, 0.12 M), TBAF (2.91 mL, 1 M in THF, 2.91 mmol, 1.1 equiv.) for 1 hour. Purification by normal phase column chromatography on silica (EtOAc:cyclohexane 5:95 to 30:70 gradient) yielded **94** (1.23 g, 56%) as a colourless oil. <sup>1</sup>H NMR (600 MHz, acetone-*d*<sub>6</sub>) δ = 8.21 (s, 1H, H2), 7.50 – 7.43 (m, 2H, H12), 7.36 – 7.25 (m, 2H, H13), 6.11 (d, *J* = 4.6 Hz, 1H, H1'), 5.59 – 5.40 (m, 6H, H2', H9', H19), 5.11 (dd, *J* = 5.9, 1.8 Hz, 1H, H3'), 4.88 – 4.79 (m, 2H, H15), 4.79 – 4.72 (m, 2H, H10), 4.40 – 4.37 (m, 1H, H4'), 3.80 (app. dt, *J* = 12.2, 3.0 Hz, 1H, H5'a), 3.72 – 3.66 (m, 1H, H5'b), 3.64 – 3.60 (m, 4H, H20), 3.59 – 3.55 (m, 2H, H16) 1.61 (s, 3H, H7'), 1.39 (s, 3H, H8'), 0.93 – 0.87 (m, 6H, H17, H21), -0.03 (s, 18H, H22), -0.04 (s, 9H, H18); <sup>13</sup>C NMR (151 MHz, acetone-*d*<sub>6</sub>) δ = 154.05 (C6), 153.25 (C8), 151.99 (C4), 150.74 (C2), 137.89 (C11), 133.53 (C14), 131.19 (2C, C12), 129.36 (2C, C13), 119.11 (C5), 114.54 (C6'), 92.39 (C1'), 87.15 (C4'), 83.77 (C15), 83.03 (C2'), 83.00 (C3'), 66.80 (C16), 65.65 (2C, C20), 63.84 (C5'), 53.65 (C10), 28.00 (C7'), 25.71 (C8'), 18.77 (2C, C21), 18.61 (C17), -1.03 (6C, C22), -1.13 (3C, C18);\* HRMS (ESI+) *m/z* calculated for C<sub>38</sub>H<sub>66</sub><sup>35</sup>ClN<sub>6</sub>O<sub>7</sub>Si<sub>3</sub> (M+H)<sup>+</sup> 837.3984, found 837.3907.

\*C19 not observed in spectrum.

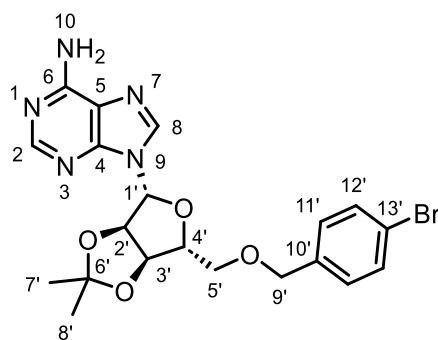
**4-(((3*aR*,4*R*,6*R*,6*aR*)-6-(6-(bis((2-(trimethylsilyl)ethoxy)methyl)amino)-9*H*-purin-9-yl)-2,2-dimethyltetrahydrofuro[3,4-*d*][1,3]dioxol-4-yl)methoxy)methyl)benzenesulfonyl fluoride (**99**)**



**99** was prepared following general procedure E, with 9-((3*aR*,4*R*,6*R*,6*aR*)-6-(((4-bromobenzyl)oxy)methyl)-2,2-dimethyltetrahydrofuro[3,4-*d*][1,3]dioxol-4-yl)-*N,N*-bis((2-(trimethylsilyl)ethoxy)methyl)-9*H*-purin-6-amine **92** (1.02 g, 1.38 mmol, 1 equiv.), isopropanol (5.10 mL, 0.27 M), DABSO (199 mg, 0.83 mmol, 0.6 equiv.), PdCl<sub>2</sub>(AmPhos)<sub>2</sub> (48.9 mg, 0.07 mmol, 5 mol%), triethylamine (0.58 mL, 4.14 mmol, 3 equiv.) and NFSI (653 mg, 2.07 mmol, 1.5 equiv.). Purification by normal phase column chromatography on silica (EtOAc:cyclohexane 5:95 to 40:60 gradient) yielded **99** (423 mg, 41%) as a pale yellow oil. <sup>1</sup>H NMR (600 MHz, acetone-*d*<sub>6</sub>) δ = 8.32 (s, 1H, H2), 8.30 (s, 1H, H8), 8.03 – 8.00 (m, 2H, H12'), 7.68 – 7.65 (m, 2H, H11'), 6.28 (d, *J* = 2.3 Hz, 1H, H1'), 5.71 – 5.41 (m, 5H, H2', H10), 5.17 (dd, *J* = 6.1, 2.9 Hz, 1H, H3'), 4.72 (s, 2H, H9'), 4.49 (app. td, *J* = 4.8, 2.9 Hz, 1H, H4'), 3.85 (dd, *J* = 10.6, 4.4 Hz, 1H, H5'a), 3.78 (dd, *J* = 10.6, 5.1 Hz, 1H, H5'b), 3.68 – 3.63 (m, 4H, H11), 1.58 (s, 3H, H7'), 1.37 (s, 3H, H8'), 0.94 – 0.89 (m, 4H, H12), -0.04 (s, 18H, H13); <sup>13</sup>C NMR (151 MHz, acetone-*d*<sub>6</sub>) δ = 155.53 (C4), 152.64 (C2), 151.90 (C6), 148.65 (C10'), 140.34 (C8), 132.22 (d, *J*<sub>C-F</sub> = 24.2 Hz, C13'), 129.30 (2C, C12'), 129.29 (2C, C11'), 121.14 (C5), 114.46 (C6'), 91.54 (C1'), 86.79 (C4'), 85.16 (C2'), 82.83 (C3'), 76.60 (2C, C10), 72.49 (C9'), 71.76 (C5'), 65.56 (2C, C11), 27.51 (C7'), 25.57 (C8'), 18.60 (2C, C12), -1.21 (6C, C13); <sup>19</sup>F NMR (471 MHz, acetone-*d*<sub>6</sub>) δ = 65.11; HRMS (ESI+) *m/z* calculated for C<sub>32</sub>H<sub>50</sub>FN<sub>5</sub>NaO<sub>8</sub>SSi<sub>2</sub> (M+Na)<sup>+</sup> 762.2795, found 762.2731.



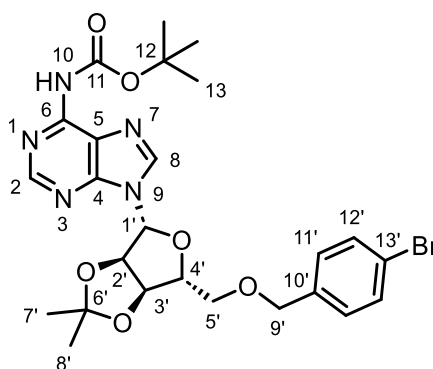
**9-((3*aR*,4*R*,6*R*,6*aR*)-6-(((4-bromobenzyl)oxy)methyl)-2,2-dimethyltetrahydrofuro[3,4-*d*][1,3]dioxol-4-yl)-9*H*-purin-6-amine (104)**



**104**

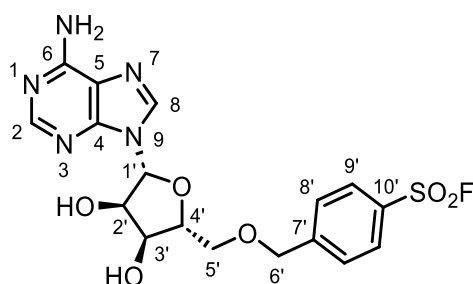
A two-neck round bottom flask equipped with magnetic stirrer and reflux condenser was charged with 9-((3*aR*,4*R*,6*R*,6*aR*)-6-(((4-bromobenzyl)oxy)methyl)-2,2-dimethyltetrahydrofuro[3,4-*d*][1,3]dioxol-4-yl)-*N,N*-bis((2-(trimethylsilyl)ethoxy)methyl)-9*H*-purin-6-amine **92** (1.00 g, 1.36 mmol, 1 equiv.), THF (13.6 mL, 0.1 M) and TBAF (32.6 mL, 1 M in THF, 32.6 mmol, 24 equiv.) under flow of nitrogen. The mixture was heated to reflux for 40 hours, after which the solvent was removed under reduced pressure. The crude mixture was redissolved in EtOAc (100 mL) and water (100 mL) and the phases were separated. The organic phase was washed with water (3 × 100 mL), dried over MgSO<sub>4</sub>, filtered, and concentrated under reduced pressure. The crude product was purified by normal phase column chromatography on silica (100% CH<sub>2</sub>Cl<sub>2</sub> to methanol:CH<sub>2</sub>Cl<sub>2</sub> 10:90 gradient) to yield **104** (361 mg, 56%) as a colourless gel. **<sup>1</sup>H NMR** (600 MHz, acetone-*d*<sub>6</sub>) δ = 8.17 (s, 2H, H2, H8), 7.48 – 7.45 (m, 2H, H12'), 7.25 – 7.22 (m, 2H, H11'), 6.65 (s br, 2H, H10), 6.21 (d, *J* = 2.4 Hz, 1H, H1'), 5.49 (dd, *J* = 6.1, 2.4 Hz, 1H, H2'), 5.11 (dd, *J* = 6.1, 2.8 Hz, 1H, H3'), 4.49 (s, 2H, H9'), 4.43 (app. td, *J* = 4.9, 2.8 Hz, 1H, H4'), 3.73 (dd, *J* = 10.5, 4.7 Hz, 1H, H5'a), 3.65 (dd, *J* = 10.5, 5.1 Hz, 1H, H5'b), 1.57 (s, 3H, H7'), 1.36 (s, 3H, H8'); **<sup>13</sup>C NMR** (151 MHz, acetone-*d*<sub>6</sub>) δ = 157.20 (C6), 153.72 (C2), 150.33 (C4), 140.58 (C8), 138.62 (C10'), 132.12 (2C, C12'), 130.40 (2C, C11'), 121.71 (C13'), 120.69 (C5), 114.32 (C6'), 91.37 (C1'), 86.69 (C4'), 85.14 (C2'), 82.96 (C3'), 72.88 (C9'), 71.24 (C5'), 27.50 (C7'), 25.55 (C8'); **HRMS** (ESI+) *m/z* calculated for C<sub>20</sub>H<sub>23</sub><sup>79</sup>BrN<sub>5</sub>O<sub>4</sub> (M+H)<sup>+</sup> 476.0928, found 476.0907.

*tert*-butyl (9-((3*aR*,4*R*,6*R*,6*aR*)-6-(((4-bromobenzyl)oxy)methyl)-2,2-dimethyltetrahydrofuro[3,4-*d*][1,3]dioxol-4-yl)-9*H*-purin-6-yl)carbamate (**105**)

**105**

A two-neck round bottom flask was charged with 9-((3*aR*,4*R*,6*R*,6*aR*)-6-(((4-bromobenzyl)oxy)methyl)-2,2-dimethyltetrahydrofuro[3,4-*d*][1,3]dioxol-4-yl)-9*H*-purin-6-amine **104** (100 mg, 0.21 mmol, 1 equiv.), THF (1.05 mL, 0.2 M), and 4-dimethylaminopyridine (28.2 mg, 0.23 mmol, 1.1 equiv.) under flow of nitrogen. Di-*tert*-butyl dicarbonate (0.25 mL, 1.05 mmol, 5 equiv.) was added dropwise, and the mixture was stirred at room temperature. After stirring at room temperature at 18 hours, the solvent was removed under reduced pressure and the crude mixture was eluted through a silica plug (methanol:CH<sub>2</sub>Cl<sub>2</sub> 5:95), concentrated under reduced pressure and the crude residue was redissolved in methanol (2.10 mL, 0.1 M) and methylamine (0.42 mL, 2 M in THF, 0.84 mmol, 4 equiv.). After stirring at room temperature for 22 hours, the solvent was removed under reduced pressure and the crude mixture was purified by normal phase column chromatography on silica (100% CH<sub>2</sub>Cl<sub>2</sub> to methanol:CH<sub>2</sub>Cl<sub>2</sub> 10:90 gradient) to yield **105** (63 mg, 52%) as a white foam. <sup>1</sup>H NMR (500 MHz, acetone-*d*<sub>6</sub>) δ = 8.80 (s br, 1H, H10), 8.53 (s, 1H, H2), 8.39 (s, 1H, H8), 7.47 – 7.44 (m, 2H, H12'), 7.22 – 7.19 (m, 2H, H11'), 6.29 (d, *J* = 2.3 Hz, 1H, H1'), 5.51 (dd, *J* = 6.1, 2.3 Hz, 1H, H2'), 5.12 (dd, *J* = 6.1, 2.6 Hz, 1H, H3'), 4.50 – 4.47 (m, 3H, H4', H9'), 3.75 (dd, *J* = 10.7, 4.3 Hz, 1H, H5'a), 3.67 (dd, *J* = 10.7, 4.9 Hz, 1H, H5'b), 1.57 (s, 3H, H7'), 1.54 (s, 9H, H13), 1.37 (s, 3H, H8'); <sup>13</sup>C NMR (126 MHz, acetone-*d*<sub>6</sub>) δ = 152.81 (C2), 152.02 (C6), 151.06 (C11), 151.00 (C4), 142.93 (C8), 138.47 (C10'), 132.14 (2C, C12'), 130.45 (2C, C11'), 124.07 (C5), 121.78 (C13'), 114.36 (C6'), 91.82 (C1'), 87.01 (C4'), 85.32 (C2'), 82.95 (C3'), 81.37 (C12), 72.92 (C9'), 71.25 (C5'), 28.32 (3C, C13), 27.48 (C7'), 25.53 (C8'); HRMS (ESI+) *m/z* calculated for C<sub>25</sub>H<sub>31</sub><sup>79</sup>BrN<sub>5</sub>O<sub>6</sub> (M+H)<sup>+</sup> 576.1452, found 576.1453.

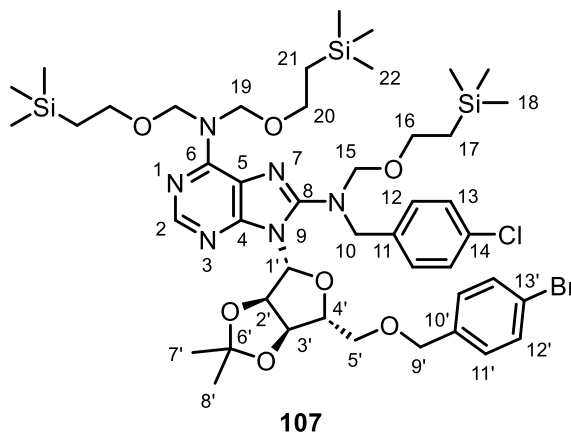
**4-(((2*R*,3*S*,4*R*,5*R*)-5-(6-amino-9*H*-purin-9-yl)-3,4-dihydroxytetrahydrofuran-2-yl)methoxy)methyl)benzenesulfonyl fluoride (101)**



**101**

A glass vial equipped with magnetic stirrer was charged with 4-(((3*aR*,4*R*,6*R*,6*aR*)-6-(6-(bis((2-(trimethylsilyl)ethoxy)methyl)amino)-9*H*-purin-9-yl)-2,2-dimethyltetrahydrofuro[3,4-*d*][1,3]dioxol-4-yl)methoxy)methyl)benzenesulfonyl fluoride **99** (80 mg, 0.11 mmol, 1 equiv.) and TFA:water 5:2 (v/v) mixture (1.10 mL, 0.1 M). After stirring at room temperature for 1 hour, the reaction mixture was diluted with water (10 mL) and the aqueous phase was extracted with EtOAc (3 × 10 mL). The resultant combined organic layers were washed with brine (1 × 15 mL), dried over MgSO<sub>4</sub>, filtered and concentrated under reduced pressure. The crude residue was redissolved in CH<sub>2</sub>Cl<sub>2</sub>:THF 1:1 mixture (1 mL) and 7 N ammonia in methanol solution (10 μL) was added. After stirring at room temperature for 24 hours, the solvent was removed under reduced pressure and the crude product was purified by normal phase column chromatography on silica (100% CH<sub>2</sub>Cl<sub>2</sub> to 15:85 methanol:CH<sub>2</sub>Cl<sub>2</sub> gradient) then reverse phase column chromatography on C18 (methanol:water +0.1% formic acid 40:60 to 80:20 gradient) to yield **101** (5.0 mg, 11%) as a white solid. <sup>1</sup>H NMR (500 MHz, CD<sub>2</sub>Cl<sub>2</sub>) δ = 8.27 (s, 1H, H2), 8.23 (s, 1H, H8), 7.98 (app. d, *J* = 8.2 Hz, 2H, H9'), 7.58 (app. d, *J* = 8.2 Hz, 2H, H8'), 6.03 (d, *J* = 3.5 Hz, 1H, H1'), 4.77 – 4.69 (m, 2H, H6'), 4.47 (app. t, *J* = 3.9 Hz, 1H, H2'), 4.42 (app. t, *J* = 5.2 Hz, 1H, H3'), 4.32 – 4.28 (m, 1H, H4'), 3.93 (dd, *J* = 10.9, 2.7 Hz, 1H, H5'a), 3.80 (dd, *J* = 10.9, 3.3 Hz, 1H, H5'b); <sup>13</sup>C NMR (126 MHz, CD<sub>2</sub>Cl<sub>2</sub>) δ = 154.53 (C6), 150.05 (C2), 148.98 (C4), 147.15 (C7'), 140.15 (C8), 132.30 (d, *J*<sub>C-F</sub> = 24.7 Hz, C10'), 129.04 (2C, C9'), 128.53 (2C, C8'), 119.83 (C5), 90.37 (C1'), 84.46 (C4'), 75.68 (C2'), 72.67 (C6'), 70.70 (C3'), 70.44 (C5'); <sup>19</sup>F NMR (471 MHz, CD<sub>2</sub>Cl<sub>2</sub>) δ = 65.41 **HRMS** (ESI+) *m/z* calculated for C<sub>17</sub>H<sub>19</sub>FN<sub>5</sub>O<sub>6</sub>S (M+H)<sup>+</sup> 440.1035, found 440.1037.

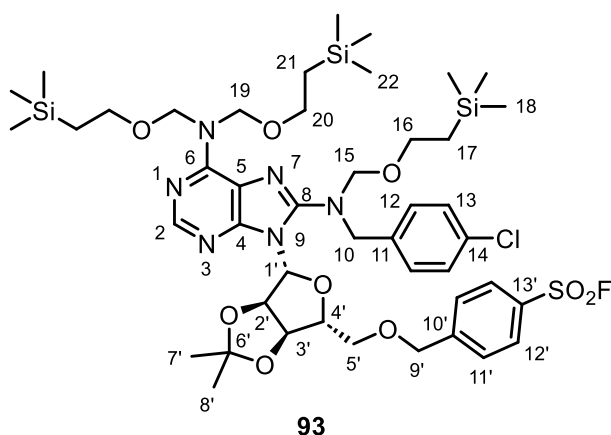
**9-((3*aR*,4*R*,6*R*,6*aR*)-6-(((4-bromobenzyl)oxy)methyl)-2,2-dimethyltetrahydrofuro[3,4-*d*][1,3]dioxol-4-yl)-*N*8-(4-chlorobenzyl)-*N*6,*N*6,*N*8-tris((2-(trimethylsilyl)ethoxy)methyl)-9*H*-purine-6,8-diamine (**107**)**



**107** was prepared following general procedure D, with ((3*aR*,4*R*,6*R*,6*aR*)-6-(6-(bis((2-(trimethylsilyl)ethoxy)methyl)amino)-8-((4-chlorobenzyl)((2-(trimethylsilyl)ethoxy)methyl)amino)-9*H*-purin-9-yl)-2,2-dimethyltetrahydrofuro[3,4-*d*][1,3]dioxol-4-yl)methanol **94** (500 mg, 0.60 mmol, 1 equiv.), THF (1.20 mL 0.5 M), sodium hydride (28.7 mg, 60% in mineral oil, 0.72 mmol, 1.2 equiv.) and 4-bromobenzyl bromide (298 mg, 1.19 mmol, 2 equiv.). Purification by normal phase column chromatography on silica (EtOAc:cyclohexane 1:99 to 20:80 gradient) yielded **107** (481 mg, 80%) as a colourless oil. <sup>1</sup>H NMR (500 MHz, acetone-*d*<sub>6</sub>) δ = 8.17 (s, 1H, H2), 7.48 – 7.42 (m, 4H, H12', H13), 7.34 – 7.31 (m, 2H, H12), 7.22 – 7.19 (m, 2H, H11'), 6.18 (d, *J* = 2.0 Hz, 1H, H1'), 5.65 (dd, *J* = 6.3, 2.0 Hz, 1H, H2'), 5.59 – 5.40 (m, 4H, H19), 5.20 (dd, *J* = 6.3, 3.2 Hz, 1H, H3'), 4.90 (d, *J* = 10.2 Hz, 1H, H15a), 4.85 (d, *J* = 14.6 Hz, 1H, H10a), 4.80 (d, *J* = 10.2 Hz, 1H, H15b), 4.68 (d, *J* = 14.6 Hz, 1H, H10b), 4.51 – 4.44 (m, 2H, H9'), 4.38 (app. td, *J* = 6.4, 3.2 Hz, 1H, H4'), 3.79 (dd, *J* = 10.2, 6.0 Hz, 1H, H5'a), 3.69 – 3.60 (m, 5H, H5'b, H20), 3.59 – 3.54 (m, 2H, H16), 1.56 (s, 3H, H7'), 1.34 (s, 3H, H8'), 0.93 – 0.88 (m, 6H, H17, H21), -0.04 (s, 18H, H22), -0.05 (s, 9H, H18); <sup>13</sup>C NMR (126 MHz, acetone-*d*<sub>6</sub>) δ = 153.59 (C6), 153.27 (C8), 152.16 (C4), 150.83 (C2), 138.94 (C10'), 137.79 (C11), 133.44 (C14), 132.06 (2C, C12'), 131.21 (2C, C13), 130.24 (2C, C11'), 129.24 (2C, C12), 121.58 (C13'), 118.61 (C5), 114.29 (C6'), 90.74 (C1'), 87.32 (C4'), 83.70 (C2'), 83.55 (C3'), 83.10 (C15), 76.70 (2C, C19), 72.75 (C9'), 71.08 (C5'), 66.45 (C16), 65.47 (2C, C20), 53.66 (C10), 27.55 (C7'), 25.58 (C8'), 18.67 (2C, C21),

18.56 (C17), -1.14 (6C, C22), -1.20 (3C, C18); **HRMS** (ESI+)  $m/z$  calculated for  $C_{45}H_{71}^{79}Br^{35}ClN_6O_7Si_3$  (M+H)<sup>+</sup> 1005.3558, found 1005.3553.

**4-(((3a*R*,4*R*,6*R*,6a*R*)-6-(6-(bis((2-(trimethylsilyl)ethoxy)methyl)amino)-8-((4-chlorobenzyl)((2-(trimethylsilyl)ethoxy)methyl)amino)-9*H*-purin-9-yl)-2,2-dimethyltetrahydrofuro[3,4-*d*][1,3]dioxol-4-yl)methoxy)methyl)benzenesulfonyl fluoride (93)**

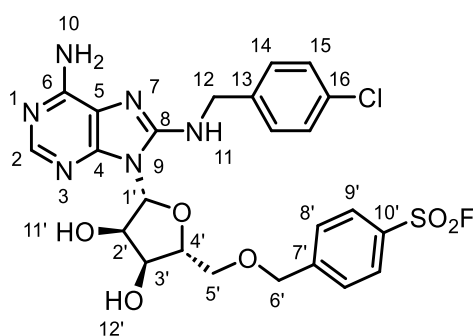


**93** was prepared following general procedure E, with 9-((3a*R*,4*R*,6*R*,6a*R*)-6-(((4-bromobenzyl)oxy)methyl)-2,2-dimethyltetrahydrofuro[3,4-*d*][1,3]dioxol-4-yl)-*N*8-(4-chlorobenzyl)-*N*6,*N*6,*N*8-tris((2-(trimethylsilyl)ethoxy)methyl)-9*H*-purine-6,8-diamine **107** (470 mg, 0.47 mmol, 1 equiv.), isopropanol (1.73 mL, 0.27 M), DABSO (67.3 mg, 0.28 mmol, 0.6 equiv.), PdCl<sub>2</sub>(AmPhos)<sub>2</sub> (16.5 mg, 0.02 mmol, 5 mol%), triethylamine (0.20 mL, 1.40 mmol, 3 equiv.) and NFSI (221 mg, 0.70 mmol, 1.5 equiv.). Purification by normal phase column chromatography on silica (EtOAc:cyclohexane 5:95 to 40:60 gradient) yielded **93** (130 mg, 28%) as a pale yellow oil. **<sup>1</sup>H NMR** (500 MHz, acetone-*d*<sub>6</sub>)  $\delta$  = 8.19 (s, 1H, H2), 8.05 – 8.01 (m, 2H, H12'), 7.71 – 7.67 (m, 2H, H11'), 7.50 – 7.47 (m, 2H, H13), 7.36 – 7.33 (m, 2H, H12), 6.22 (d,  $J$  = 2.1 Hz, 1H, H1'), 5.69 (dd,  $J$  = 6.3, 2.1 Hz, 1H, H2'), 5.60 – 5.40 (m, 4H, H19), 5.27 (dd,  $J$  = 6.3, 3.3 Hz, 1H, H3'), 4.94 (d,  $J$  = 10.2 Hz, 1H, H15a), 4.87 (d,  $J$  = 14.6 Hz, 1H, H10a), 4.82 (d,  $J$  = 10.2 Hz, 1H, H15b), 4.77 – 4.67 (m, 3H, H9', H10b), 4.45 (app. td,  $J$  = 6.3, 3.3 Hz, 1H, H4'), 3.91 (dd,  $J$  = 10.4, 5.7 Hz, 1H, H5'a), 3.80 (dd,  $J$  = 10.4, 6.7 Hz, 1H, H5'b), 3.66 – 3.62 (m, 4H, H20), 3.62 – 3.57 (m, 2H, H16), 1.58 (s, 3H, H7'), 1.37 (s, 3H, H8'), 0.95 – 0.89 (m, 6H, H17, H21), -0.02 (s, 18H, H22), -0.04 (s, 9H, H18); **<sup>13</sup>C NMR** (126 MHz, acetone-*d*<sub>6</sub>)  $\delta$  = 153.60 (C6), 153.27 (C8), 152.17 (C4), 150.85 (C2), 149.11 (C10'), 137.79 (C11), 133.44 (C14), 131.20 (2C, C13), 129.28 (2C, C12), 129.24 (2C, C12'), 129.09 (2C,

C11'), 118.63 (C5), 114.40 (C6'), 90.74 (C1'), 87.21 (C4'), 83.72 (C2'), 83.39 (C3'), 83.16 (C15), 76.70 (C19), 72.37 (C9'), 71.64 (C5'), 66.47 (C16), 65.46 (2C, C20), 53.69 (C10), 27.57 (C7'), 25.58 (C8'), 18.65 (2C, C21), 18.55 (C17), -1.16 (6C, C22), -1.23 (3C, C18);\*  $^{19}\text{F}$  NMR (471 MHz, acetone- $d_6$ )  $\delta$  = 65.14; HRMS (ESI+)  $m/z$  calculated for  $\text{C}_{45}\text{H}_{71}^{35}\text{ClF}_6\text{O}_9\text{SSi}_3$  (M+H) $^+$  1009.3978, found 1009.4010.

\*C13' not observed in spectrum.

**4-((((2*R*,3*S*,4*R*,5*R*)-5-(6-amino-8-((4-chlorobenzyl)amino)-9*H*-purin-9-yl)-3,4-dihydroxytetrahydrofuran-2-yl)methoxy)methyl)benzenesulfonyl fluoride (43)**

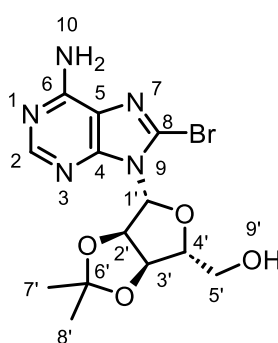


**43**

**43** was prepared following a modification of general procedure F, with 4-((((3*aR*,4*R*,6*R*,6*aR*)-6-(6-(bis((2-(trimethylsilyl)ethoxy)methyl)amino)-8-((4-chlorobenzyl)((2-(trimethylsilyl)ethoxy)methyl)amino)-9*H*-purin-9-yl)-2,2-dimethyltetrahydrofuro[3,4-*d*][1,3]dioxol-4-yl)methoxy)methyl)benzenesulfonyl fluoride **93** (125 mg, 0.12 mmol, 1 equiv.), and TFA:water 5:2 (v/v) mixture (1.24 mL, 0.1 M). After stirring at room temperature for 1 hour, the reaction mixture was diluted with water (10 mL) and the aqueous phase was extracted with EtOAc (3 × 10 mL). The resultant combined organic layers were washed with brine (1 × 15 mL), dried over  $\text{MgSO}_4$ , filtered and concentrated under reduced pressure. Purification by normal phase column chromatography on silica (100%  $\text{CH}_2\text{Cl}_2$  to 15:85 methanol: $\text{CH}_2\text{Cl}_2$  gradient) then reverse phase column chromatography on C18 (methanol:water +0.1% formic acid 20:80 to 80:20 gradient) yielded **43** (33 mg, 46%) as a white solid.  $^1\text{H}$  NMR (500 MHz, DMSO- $d_6$ )  $\delta$  = 8.04 – 8.00 (m, 2H, H9'), 7.99 (s, 1H, H2), 7.61 – 7.56 (m, 2H, H8'), 7.33 – 7.29 (m, 5H, H11, H14, H15), 7.00 (s br, 2H, H10), 5.88 (d,  $J$  = 5.5 Hz, 1H, H1'), 5.43 (s br, 1H, H11'), 5.26 (s br, 1H, H12'), 4.93 (app. t,  $J$  = 5.5 Hz, 1H, H2'), 4.62 (s, 2H, H6'), 4.50 (d,  $J$  = 6.0 Hz, 2H, H12), 4.34 (app. t,  $J$  = 4.9 Hz, 1H, H3'), 4.08 – 4.04 (m,

1H, H4'), 3.80 (dd,  $J = 10.9, 3.1$  Hz, 1H, H5'a), 3.69 (dd,  $J = 10.9, 4.7$  Hz, 1H, H5'b);  $^{13}\text{C}$  NMR (126 MHz, DMSO- $d_6$ )  $\delta = 151.85$  (C4), 150.82 (C6), 149.56 (C8), 147.65 (C7'), 146.99 (C2), 138.48 (C13), 131.34 (C16), 130.21 (d,  $J_{\text{C-F}} = 23.1$  Hz, C10'), 128.88 (2C, C14), 128.38 (2C, C9'), 128.28 (2C, C8'), 128.12 (2C, C15), 116.94 (C5), 87.17 (C1'), 82.89 (C4'), 71.12 (C6'), 70.61 (C2'), 70.54 (C5'), 70.19 (C3'), 44.68 (C12);  $^{19}\text{F}$  NMR (471 MHz, DMSO- $d_6$ )  $\delta = 66.66$ ; HRMS (ESI+)  $m/z$  calculated for  $\text{C}_{24}\text{H}_{25}^{35}\text{ClFN}_6\text{O}_6\text{S}$  (M+H) $^+$  579.1223, found 579.1222.

**((3a*R*,4*R*,6*R*,6a*R*)-6-(6-amino-8-bromo-9*H*-purin-9-yl)-2,2-dimethyltetrahydrofuro[3,4-*d*][1,3]dioxol-4-yl)methanol (109)**



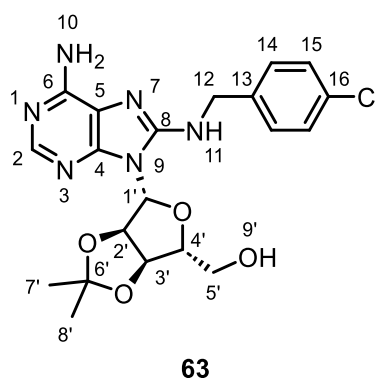
**109**

A two-neck round bottom flask equipped with magnetic stirrer was charged with 2',3'-*O*-isopropylideneadenosine **83** (4.00 g, 13.0 mmol, 1 equiv.) and 1,4-dioxane (52.1 mL, 0.25 M) under flow of nitrogen. A separate flask equipped with magnetic stirrer was charged with  $\text{K}_2\text{HPO}_4$  (6.80 g, 39.0 mmol, 3 equiv.), water (52.1 mL), and bromine (1.67 mL, 32.5 mmol, 2.5 equiv.), and the resultant solution was slowly transferred *via* syringe into the first mixture. After stirring at room temperature for 2 hours, the reaction mixture was quenched with sat.  $\text{Na}_2\text{S}_2\text{O}_3$  solution (50 mL), diluted with EtOAc (100 mL) and the phases were separated. The aqueous phase was extracted with EtOAc (2  $\times$  100 mL) and the resultant combined organic layers were washed with brine (1  $\times$  100 mL), dried over  $\text{MgSO}_4$ , filtered, and concentrated under reduced pressure. The crude product was purified by normal phase column chromatography on silica (100%  $\text{CH}_2\text{Cl}_2$  to methanol: $\text{CH}_2\text{Cl}_2$  10:90 gradient) to yield **109** (4.27 g, 85%) as a light brown solid.  $^1\text{H}$  NMR (600 MHz, DMSO- $d_6$ )  $\delta = 8.15$  (s, 1H, H2), 7.55 (s br, 2H, H10), 6.02 (d,  $J = 2.6$  Hz, 1H, H1'), 5.66 (dd,  $J = 6.3, 2.6$  Hz, 1H, H2'), 5.12 (app. t,  $J = 6.0$  Hz, 1H, H9'), 5.03 (dd,  $J = 6.3, 3.0$  Hz, 1H, H3'), 4.16 (app. td,  $J = 5.9, 3.0$  Hz, 1H, H4'), 3.54 – 3.49 (m, 1H, H5'a), 3.46 – 3.40 (m, 1H, H5'b), 1.55 (s, 3H, H7'), 1.33 (s, 3H, H8');  $^{13}\text{C}$  NMR

(151 MHz, DMSO- $d_6$ )  $\delta$  = 155.05 (C6), 152.82 (C2), 149.75 (C4), 126.39 (C8), 119.29 (C5), 113.22 (C6'), 90.98 (C1'), 87.16 (C4'), 81.92 (C2'), 81.61 (C3'), 61.47 (C5'), 27.13 (C7'), 25.24 (C8'); **HRMS** (ESI+)  $m/z$  calculated for  $C_{13}H_{17}^{79}BrN_5O_4$  (M+H) $^+$  386.0458, found 386.0473.

The spectroscopic and analytical data were in agreement with literature values.<sup>145</sup>

**((3a*R*,4*R*,6*R*,6a*R*)-6-(6-amino-8-((4-chlorobenzyl)amino)-9*H*-purin-9-yl)-2,2-dimethyltetrahydrofuro[3,4-*d*][1,3]dioxol-4-yl)methanol (63)**

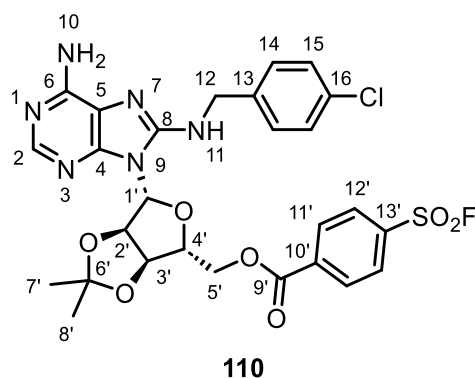


**63** was prepared following general procedure A, with ((3a*R*,4*R*,6*R*,6a*R*)-6-(6-amino-8-bromo-9*H*-purin-9-yl)-2,2-dimethyltetrahydrofuro[3,4-*d*][1,3]dioxol-4-yl)methanol **109** (2.00 g, 5.18 mmol, 1 equiv.), ethanol (17.2 mL, 0.3 M) and 4-chlorobenzylamine (4.90 mL, 40.3 mmol, 7.8 equiv.). Purification by normal phase column chromatography on silica (100%  $CH_2Cl_2$  to methanol:  $CH_2Cl_2$  10:90 gradient) then reverse phase column chromatography on C18 (methanol:water +0.1% formic acid 40:60 to 100% methanol gradient) yielded **63** (1.46 g, 63%) as an orange solid.  **$^1H$  NMR** (600 MHz, DMSO- $d_6$ )  $\delta$  = 7.93 (s, 1H, H2), 7.61 (t,  $J$  = 5.9 Hz, 1H, H11), 7.42 – 7.35 (m, 4H, H14, H15), 6.56 (s br, 2H, H10), 6.08 (d,  $J$  = 3.5 Hz, 1H, H1'), 5.47 (dd,  $J$  = 6.3, 3.5 Hz, 1H, H2'), 5.43 (s br, 1H, H9'), 4.98 (dd,  $J$  = 6.3, 2.8 Hz, 1H, H3'), 4.58 (dd,  $J$  = 15.5, 5.9 Hz, 1H, H12a), 4.53 (dd,  $J$  = 15.5, 5.9 Hz, 1H, H12b), 4.19 – 4.15 (m, 1H, H4'), 3.57 (dd,  $J$  = 11.8, 4.6 Hz, 1H, H5'a), 3.52 (dd,  $J$  = 11.8, 3.6 Hz, 1H, H5'b), 1.55 (s, 3H, H7'), 1.32 (s, 3H, H8');  **$^{13}C$  NMR** (151 MHz, DMSO- $d_6$ )  $\delta$  = 152.59 (C6), 150.99 (C8), 149.25 (C4), 148.94 (C2), 138.77 (C13), 131.30 (C16), 129.18 (2C, C14), 128.16 (2C, C15), 117.00 (C5), 113.18 (C6'), 87.92 (C1'), 85.40 (C4'), 81.40 (C2'), 81.16 (C3'), 61.36 (C5'), 44.75 (C12), 27.15 (C7'), 25.27 (C8'); **HRMS** (ESI+)  $m/z$  calculated for  $C_{20}H_{24}^{35}ClN_6O_4$  (M+H) $^+$  447.1542, found 447.1557.



The spectroscopic and analytical data were in agreement with literature values.<sup>145</sup>

**((3*aR*,4*R*,6*R*,6*aR*)-6-(6-amino-8-((4-chlorobenzyl)amino)-9*H*-purin-9-yl)-2,2-dimethyltetrahydrofuro[3,4-*d*][1,3]dioxol-4-yl)methyl 4-(fluorosulfonyl)benzoate (110)**

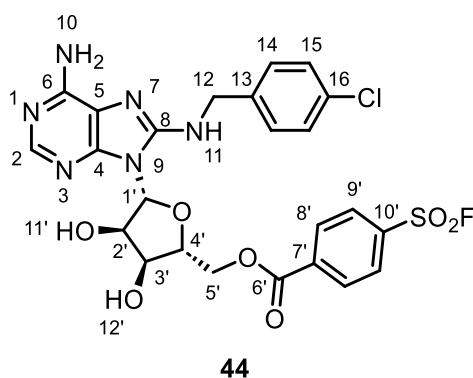


A two-neck round bottom flask equipped with magnetic stirrer was charged with ((3*aR*,4*R*,6*R*,6*aR*)-6-(6-amino-8-((4-chlorobenzyl)amino)-9*H*-purin-9-yl)-2,2-dimethyltetrahydrofuro[3,4-*d*][1,3]dioxol-4-yl)methanol **63** (500 mg, 1.12 mmol, 1 equiv.) and DMF (11.2 mL, 0.1 M) under flow of nitrogen. The mixture was cooled to 0 °C, and 4-(fluorosulfonyl)benzoyl chloride (299 mg, 1.34 mmol, 1.2 equiv.) and triethylamine (0.23 mL, 1.68 mmol, 1.5 equiv.) were added in sequence. After stirring at 0 °C for 3 hours, the reaction mixture was quenched with water (30 mL), diluted with EtOAc (20 mL) and the phases were separated. The aqueous phase was extracted with EtOAc (2 × 20 mL) and the resultant combined organic layers were washed with 10% LiCl (w/v) solution (3 × 30 mL), dried over MgSO<sub>4</sub>, filtered, and concentrated under reduced pressure. The crude product was purified by normal phase column chromatography on silica (100% CH<sub>2</sub>Cl<sub>2</sub> to methanol:CH<sub>2</sub>Cl<sub>2</sub> 10:90 gradient) then reverse phase column chromatography on C18 (acetonitrile:water +0.1% formic acid 20:80 to 80:20 gradient) to yield **110** (187 mg, 26%) as a white solid. <sup>1</sup>H NMR (600 MHz, CDCl<sub>3</sub>) δ = 8.11 (s, 1H, H2), 8.07 – 8.03 (m, 2H, H11'), 8.01 – 7.97 (m, 2H, H12'), 7.31 – 7.28 (m, 4H, H14, H15), 6.11 (dd, *J* = 6.1, 1.2 Hz, 1H, H2'), 5.90 (d, *J* = 1.2 Hz, 1H, H1'), 5.22 (s br, 2H, H10), 5.17 (dd, *J* = 6.1, 3.2 Hz, 1H, H3'), 5.02 (t, *J* = 5.6 Hz, 1H, H11), 4.63 (dd, *J* = 14.5, 6.1 Hz, 1H, H12a), 4.57 – 4.48 (m, 3H, H4', H5'a, H12b), 4.39 (dd, *J* = 11.9, 5.9 Hz, 1H, H5'b), 1.60 (s, 3H, H7'), 1.44 (s, 3H, H8'); <sup>13</sup>C NMR (151 MHz, CDCl<sub>3</sub>) δ = 164.03 (C9'), 152.23 (C6), 151.84 (C8), 149.86 (C2), 149.81 (C4), 137.05 (d, *J*<sub>C-F</sub> = 25.5 Hz, C13'), 136.68 (C13), 135.61 (C10'), 133.76 (C16), 130.71 (2C,

C11'), 129.25 (2C, C14), 129.06 (2C, C15), 128.55 (2C, C12'), 117.87 (C5), 114.48 (C6'), 89.62 (C1'), 85.41 (C4'), 82.51 (C2'), 81.69 (C3'), 64.86 (C5'), 46.60 (C12), 27.24 (C7'), 25.55 (C8');  $^{19}\text{F}$  NMR (471 MHz,  $\text{CDCl}_3$ )  $\delta = 65.64$ ; HRMS (ESI+)  $m/z$  calculated for  $\text{C}_{27}\text{H}_{27}^{35}\text{ClFN}_6\text{O}_7\text{S}$  ( $\text{M}+\text{H}$ ) $^+$  633.1329, found 633.1343.

The spectroscopic and analytical data were in agreement with literature values.<sup>145</sup>

**((2*R*,3*S*,4*R*,5*R*)-5-(6-amino-8-((4-chlorobenzyl)amino)-9*H*-purin-9-yl)-3,4-dihydroxytetrahydrofuran-2-yl)methyl 4-(fluorosulfonyl)benzoate (**44**)**

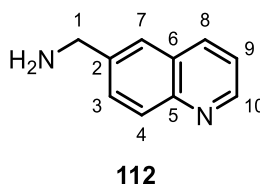


**44** was prepared following general procedure F, with ((3*aR*,4*R*,6*R*,6*aR*)-6-(6-amino-8-((4-chlorobenzyl)amino)-9*H*-purin-9-yl)-2,2-dimethyltetrahydrofuro[3,4-*d*][1,3]dioxol-4-yl)methyl 4-(fluorosulfonyl)benzoate **110** (150 mg, 0.24 mmol, 1 equiv.), and TFA:water 5:2 (v/v) mixture (2.37 mL, 0.1 M) for 30 minutes. Purification by normal phase column chromatography on silica (100%  $\text{CH}_2\text{Cl}_2$  to 10:90 methanol: $\text{CH}_2\text{Cl}_2$  gradient) yielded **44** (98 mg, 70%) as a white solid.  $^1\text{H}$  NMR (600 MHz,  $\text{DMSO-d}_6$ )  $\delta = 8.24 - 8.21$  (m, 2H, H9'), 8.16 - 8.13 (m, 2H, H8'), 8.00 (s, 1H, H2), 7.85 (s br, 1H, H11), 7.49 (s br, 2H, H10), 7.40 - 7.33 (m, 4H, H14, H15), 5.85 (d,  $J = 4.2$  Hz, 1H, H1'), 5.53 (s br, 1H, H11'), 5.40 (s br, 1H, H12'), 5.11 (app. t,  $J = 4.8$  Hz, 1H, H2'), 4.69 (dd,  $J = 12.0, 3.2$  Hz, 1H, H5'a), 4.62 - 4.52 (m, 3H, H3', H12), 4.47 (dd,  $J = 12.0, 5.2$  Hz, 1H, H5'b), 4.19 (app. td,  $J = 5.6, 3.3$  Hz, 1H, H4');  $^{13}\text{C}$  NMR (151 MHz,  $\text{DMSO-d}_6$ )  $\delta = 163.82$  (C6'), 152.64 (C8), 148.92 (C2), 138.36 (C13), 136.12 (C7'), 135.28 (d,  $J_{\text{C-F}} = 23.6$  Hz, C10'), 131.42 (C16), 130.75 (2C, C8'), 129.20 (2C, C14), 128.84 (2C, C15), 128.13 (C9'), 87.84 (C1'), 80.90 (C4'), 70.96 (C2'), 69.65 (C3'), 64.76 (C5'), 44.78 (C12)\*;  $^{19}\text{F}$  NMR (471 MHz,  $\text{DMSO-d}_6$ )  $\delta = 66.05$  HRMS (ESI+)  $m/z$  calculated for  $\text{C}_{24}\text{H}_{23}^{35}\text{ClFN}_6\text{O}_7\text{S}$  ( $\text{M}+\text{H}$ ) $^+$  593.1016, found 593.1036.

\*C4, C5 and C6 not observed in spectrum.

The spectroscopic and analytical data were in agreement with literature values.<sup>145</sup>

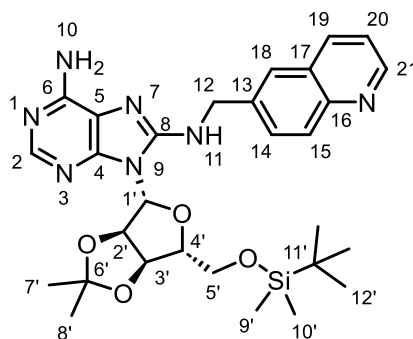
### quinolin-6-ylmethanamine (**112**)



A two-neck round bottom flask equipped with magnetic stirrer was charged with quinoline-6-carbonitrile **113** (5 g, 32.4 mmol, 1 equiv.), 7 N ammonia in methanol (54.0 mL, 0.6 M) and sponge nickel catalyst (1 g, 50% aqueous slurry) under flow of nitrogen. The flask was degassed and backfilled with hydrogen three times, and then stirred at room temperature. After stirring at room temperature for 72 hours, the flask was degassed and backfilled with nitrogen, the reaction mixture was then filtered through celite and concentrated under reduced pressure. The crude residue was purified by normal phase column chromatography on silica (methanol:CH<sub>2</sub>Cl<sub>2</sub> + 0.07 N ammonia in methanol 1:99 to 15:95 gradient) to yield **112** (4.11 g, 80%) as a brown oil. **<sup>1</sup>H NMR** (600 MHz, DMSO-d<sub>6</sub>) δ = 8.83 (dd, *J* = 4.2, 1.5 Hz, 1H, H10), 8.30 (app. d, *J* = 7.9 Hz, 1H, H8), 7.95 (d, *J* = 8.6 Hz, 1H, H4), 7.87 (app. s, 1H, H7), 7.75 (dd, *J* = 8.6, 1.6 Hz, 1H, H3), 7.49 (dd, *J* = 7.9, 4.2 Hz, 1H, H9), 3.91 (s, 2H, H1); **<sup>13</sup>C NMR** (151 MHz, DMSO-d<sub>6</sub>) δ = 149.72 (C10), 146.94 (C5), 142.62 (C2), 135.62 (C8), 129.69 (C3), 128.56 (C4), 127.76 (C6), 124.67 (C7), 121.38 (C9), 45.49 (C1); **HRMS** (ESI+) *m/z* calculated for C<sub>10</sub>H<sub>11</sub>N<sub>2</sub> (M+H)<sup>+</sup> 159.0917, found 159.0927.

The spectroscopic and analytical data were in agreement with literature values.<sup>185</sup>

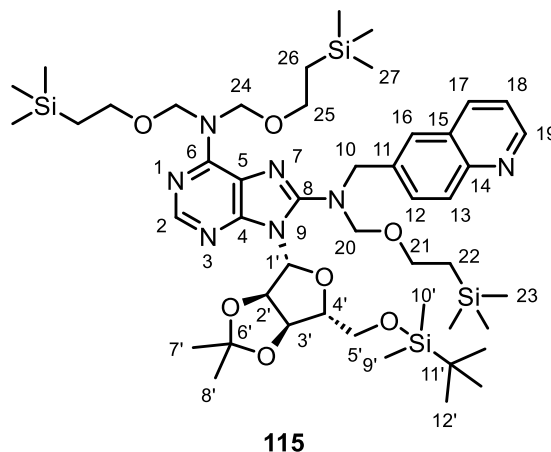
**9-((3*aR*,4*R*,6*R*,6*aR*)-6-(((*tert*-butyldimethylsilyl)oxy)methyl)-2,2-dimethyltetrahydrofuro[3,4-*d*][1,3]dioxol-4-yl)-*N*8-(quinolin-6-ylmethyl)-9*H*-purine-6,8-diamine (**114**)**



**114**

**114** was prepared following general procedure A, with 8-bromo-9-((3*aR*,4*R*,6*R*,6*aR*)-6-(((*tert*-butyldimethylsilyl)oxy)methyl)-2,2-dimethyltetrahydrofuro[3,4-*d*][1,3]dioxol-4-yl)-9*H*-purin-6-amine **95** (2.00 g, 4.00 mmol, 1 equiv.), ethanol (13.3 mL, 0.3 M) and quinolin-6-ylmethanamine **112** (4.10 g, 25.9 mmol, 6.5 equiv.). Purification by normal phase column chromatography on silica (100% CH<sub>2</sub>Cl<sub>2</sub> to methanol: CH<sub>2</sub>Cl<sub>2</sub> 10:90 gradient) yielded **114** (2.06 g, 89%) as a pink foam. <sup>1</sup>H NMR (600 MHz, acetone-*d*<sub>6</sub>) δ = 8.85 (dd, *J* = 4.2, 1.7 Hz, 1H, H21), 8.25 (d, *J* = 8.2 Hz, 1H, H19), 8.01 – 7.99 (m, 2H, H2, H15), 7.98 (app. s, 1H, H18), 7.86 (dd, *J* = 8.7, 1.9 Hz, 1H, H14), 7.45 (dd, *J* = 8.2, 4.2 Hz, 1H, H20), 6.78 (t, *J* = 5.8 Hz, 1H, H11), 6.07 (d, *J* = 2.0 Hz, 1H, H1'), 5.98 (s br, 2H, H10), 5.89 (dd, *J* = 6.2, 2.0 Hz, 1H, H2'), 5.10 (dd, *J* = 6.2, 2.8 Hz, 1H, H3'), 4.96 – 4.88 (m, 2H, H12), 4.18 (app. td, *J* = 6.1, 2.8 Hz, 1H, H4'), 3.73 (dd, *J* = 10.5, 6.4 Hz, 1H, H5'a), 3.64 (dd, *J* = 10.5, 5.7 Hz, 1H, H5'b), 1.52 (s, 3H, H7'), 1.36 (s, 3H, H8'), 0.81 (s, 9H, H12'), -0.06 (s, 3H, H9'), -0.07 (s, 3H, H10'); <sup>13</sup>C NMR (151 MHz, acetone-*d*<sub>6</sub>) δ = 153.84 (C6), 152.73 (C8), 151.00 (C21), 150.70 (C4), 150.15 (C2), 148.81 (C16), 138.99 (C13), 136.40 (C19), 130.33 (C14), 130.32 (C15), 129.04 (C17), 126.80 (C18), 122.25 (C20), 118.72 (C5), 114.09 (C6'), 89.69 (C1'), 88.30 (C4'), 83.43 (C2'), 82.91 (C3'), 64.08 (C5'), 46.92 (C12), 27.41 (C7'), 26.24 (3C, C12'), 25.59 (C8'), 18.90 (C11'), -5.16 (C9'), -5.33 (C10'); HRMS (ESI+) *m/z* calculated for C<sub>29</sub>H<sub>40</sub>N<sub>7</sub>O<sub>4</sub>Si (M+H)<sup>+</sup> 578.2906, found 578.2905.

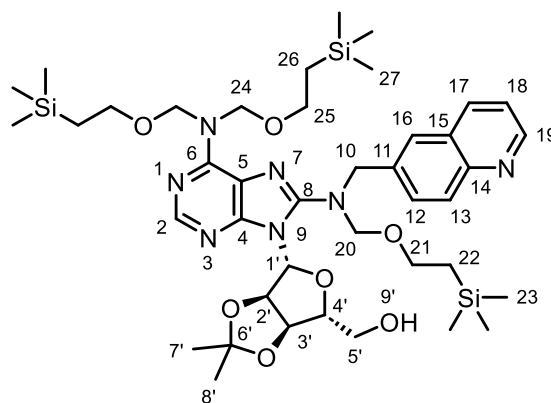
**9-((3*aR*,4*R*,6*R*,6*aR*)-6-(((*tert*-butyldimethylsilyl)oxy)methyl)-2,2-dimethyltetrahydrofuro[3,4-*d*][1,3]dioxol-4-yl)-*N*8-(quinolin-6-ylmethyl)-*N*6,*N*6,*N*8-tris((2-(trimethylsilyl)ethoxy)methyl)-9*H*-purine-6,8-diamine (**115**)**



**115** was prepared following general procedure B, with 9-((3*aR*,4*R*,6*R*,6*aR*)-6-(((*tert*-butyldimethylsilyl)oxy)methyl)-2,2-dimethyltetrahydrofuro[3,4-*d*][1,3]dioxol-4-yl)-*N*8-(quinolin-6-ylmethyl)-9*H*-purine-6,8-diamine **114** (2.00 g, 3.46 mmol, 1 equiv.), CH<sub>2</sub>Cl<sub>2</sub> (11.5 mL, 0.3 M), 2-(trimethylsilyl)ethoxymethylchloride (2.76 mL, 15.6 mmol, 4.5 equiv.) and *N,N*-diisopropylethylamine (2.71 mL, 15.6 mmol, 4.5 equiv.) for 18 hours. Purification by normal phase column chromatography on silica (100% CH<sub>2</sub>Cl<sub>2</sub> to methanol:CH<sub>2</sub>Cl<sub>2</sub> 10:90 gradient) yielded **115** (764 mg, 23%) as a red gel. <sup>1</sup>H NMR (600 MHz, acetone-*d*<sub>6</sub>) δ = 8.86 (dd, *J* = 4.1, 1.8 Hz, 1H, H19), 8.26 – 8.22 (m, 2H, H2, H17), 8.00 (d, *J* = 8.8 Hz, 1H, H13), 7.96 (app. s, 1H, H16), 7.84 (dd, *J* = 8.8, 1.9 Hz, 1H, H12), 6.84 (dd, *J* = 8.3, 4.1 Hz, 1H, H18), 6.26 (d, *J* = 2.0 Hz, 1H, H1'), 5.69 (dd, *J* = 6.3, 2.0 Hz, 1H, H2'), 5.63 – 5.34 (m, 4H, H24), 5.20 (dd, *J* = 6.3, 2.9 Hz, 1H, H3'), 5.07 (d, *J* = 14.6 Hz, 1H, H10a), 4.96 (d, *J* = 10.2 Hz, 1H, H20a), 4.92 – 4.86 (m, 2H, H10b, H20b), 4.26 (app. td, *J* = 6.9, 2.9 Hz, 1H, H4'), 3.96 (dd, *J* = 10.4, 7.2 Hz, 1H, H5'a), 3.78 (dd, *J* = 10.4, 6.4 Hz, 1H, H5'b), 3.68 – 3.57 (m, 6H, H21, H25), 1.56 (s, 3H, H7'), 1.35 (s, 3H, H8'), 1.05 – 0.83 (m, 15H, H12', H22, H26), 0.01 – -0.08 (m, 33H, H9', H10', H23, H27); <sup>13</sup>C NMR (151 MHz, acetone-*d*<sub>6</sub>) δ = 153.64 (C6), 153.47 (C8), 152.15 (C4), 151.18 (C19), 150.82 (C2), 148.90 (C14), 137.19 (C11), 136.45 (C17), 130.80 (C12), 130.45 (C13), 129.00 (C15), 128.03 (C16), 122.33 (C18), 118.65 (C5), 114.11 (C6'), 91.05 (C1'), 89.03 (C4'), 83.74 (C2'), 83.53 (C3'), 83.12 (C20), 76.41 (C24), 66.45 (C21), 65.42 (2C, C25), 64.25 (C5'), 54.18 (C10), 27.55 (C7'), 26.26 (3C, C12'), 25.59 (C8'), 18.88 (C11'), 18.61 (2C, C26), 18.58 (C22), -1.17 (6C, C27), -1.19 (3C, C23), -

5.04 (C9'), -5.14 (C10'); **HRMS** (ESI+)  $m/z$  calculated for  $C_{47}H_{82}N_7O_7Si_4$  (M+H)<sup>+</sup> 968.5347, found 968.5348.

**((3aR,4R,6R,6aR)-6-(6-(bis((2-(trimethylsilyl)ethoxy)methyl)amino)-8-((quinolin-6-ylmethyl)((2-(trimethylsilyl)ethoxy)methyl)amino)-9H-purin-9-yl)-2,2-dimethyltetrahydrofuro[3,4-d][1,3]dioxol-4-yl)methanol (116)**

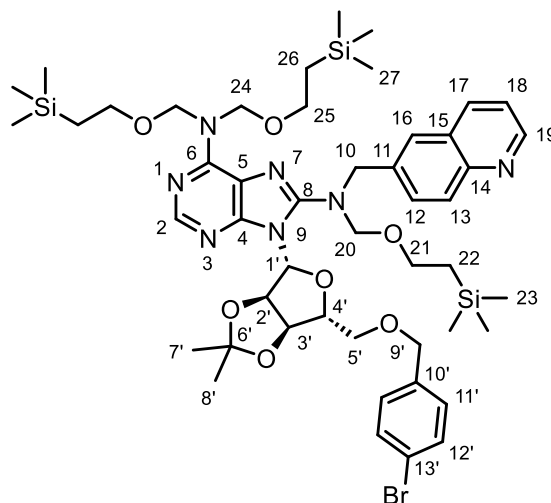


**116**

**116** was prepared following general procedure C, with 9-((3aR,4R,6R,6aR)-6-(((tert-butyl)dimethylsilyl)oxy)methyl)-2,2-dimethyltetrahydrofuro[3,4-d][1,3]dioxol-4-yl)-N8-(quinolin-6-ylmethyl)-N6,N6,N8-tris((2-(trimethylsilyl)ethoxy)methyl)-9H-purine-6,8-diamine **115** (750 mg, 0.77 mmol, 1 equiv.), THF (6.45 mL, 0.12 M) and TBAF (0.85 mL, 1 M in THF, 0.85 mmol, 1.1 equiv.) for 18 hours. Purification by normal phase column chromatography on silica (100%  $CH_2Cl_2$  to methanol: $CH_2Cl_2$  10:90 gradient) yielded **116** (387 mg, 59%) as an orange oil. **<sup>1</sup>H NMR** (600 MHz, acetone- $d_6$ )  $\delta$  = 8.85 (dd,  $J$  = 4.2, 1.7 Hz, 1H, H19), 8.24 (app. d,  $J$  = 8.3 Hz, 1H, H17), 8.21 (s, 1H, H2), 7.99 (d,  $J$  = 8.8 Hz, 1H, H13), 7.96 (app. s, 1H, H16), 7.83 (dd,  $J$  = 8.8, 1.9 Hz, H12), 7.46 (dd,  $J$  = 8.3, 4.2 Hz, 1H, H18), 6.21 (d,  $J$  = 4.4 Hz, 1H, H1'), 5.58 – 5.38 (m, 6H, H2', H9', H24), 5.12 (dd,  $J$  = 5.9, 1.7 Hz, 1H, H3'), 5.02 (d,  $J$  = 14.6 Hz, 1H, H10a), 4.97 – 4.91 (m, 2H, H10b, H20a), 4.87 (d,  $J$  = 10.5 Hz, 1H, H20b), 4.42 – 4.39 (m, 1H, H4'), 3.83 – 3.78 (m, 1H, H5'a), 3.73 – 3.56 (m, 7H, H5'b, H21, H25), 1.62 (s, 3H, H7'), 1.39 (s, 3H, H8'), 0.97 – 0.80 (m, 6H, H22, H26), -0.04 (s, 9H, H23), -0.06 (s, 18H, H27); **<sup>13</sup>C NMR** (151 MHz, acetone- $d_6$ )  $\delta$  = 153.93 (C6), 153.24 (C8), 151.88 (C4), 151.17 (C2), 150.61 (C19), 148.91 (C14), 137.14 (C11), 136.43 (C17), 130.71 (C12), 130.45 (C13), 129.03 (C15), 127.81 (C16), 122.34 (C18), 119.02 (C5), 114.44 (C6'), 92.36 (C1'), 87.02 (C4'), 83.75 (C20), 82.90 (C2'), 82.88 (C3'), 76.55 (2C, C24), 66.71 (C21), 65.51 (2C,

C25), 63.74 (C5'), 54.09 (C10), 27.94 (C7'), 25.63 (C8'), 18.59 (2C, C26), 18.50 (C22), -1.17 (6C, C27), -1.25 (3C, C23); **HRMS** (ESI+) *m/z* calculated for C<sub>41</sub>H<sub>68</sub>N<sub>7</sub>O<sub>7</sub>Si<sub>3</sub> (M+H)<sup>+</sup> 854.4483, found 854.4462.

**9-((3*aR*,4*R*,6*R*,6*aR*)-6-(((4-bromobenzyl)oxy)methyl)-2,2-dimethyltetrahydrofuro[3,4-*d*][1,3]dioxol-4-yl)-*N*8-(quinolin-6-ylmethyl)-*N*6,*N*6,*N*8-tris((2-(trimethylsilyl)ethoxy)methyl)-9*H*-purine-6,8-diamine (**117**)**

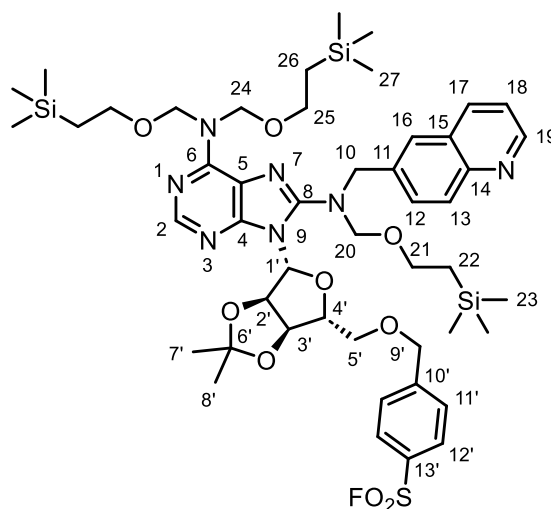


**117**

**117** was prepared following general procedure D, with ((3*aR*,4*R*,6*R*,6*aR*)-6-(6-(bis((2-(trimethylsilyl)ethoxy)methyl)amino)-8-((quinolin-6-ylmethyl)((2-(trimethylsilyl)ethoxy)methyl)amino)-9*H*-purin-9-yl)-2,2-dimethyltetrahydrofuro[3,4-*d*][1,3]dioxol-4-yl)methanol **116** (380 mg, 0.44 mmol, 1 equiv.), THF (0.89 mL, 0.5 M), sodium hydride (21.3 mg, 60% in mineral oil, 0.53 mmol, 1.2 equiv.) and 4-bromobenzyl bromide (222 mg, 0.89 mmol, 2 equiv.). Purification by normal phase column chromatography on silica (100% CH<sub>2</sub>Cl<sub>2</sub> to methanol:CH<sub>2</sub>Cl<sub>2</sub> 5:95 gradient) yielded **117** (345 mg, 76%) as an orange oil. **<sup>1</sup>H NMR** (600 MHz, acetone-*d*<sub>6</sub>) δ = 8.85 (dd, *J* = 4.2, 1.6 Hz, 1H, H19), 8.23 (app. d, *J* = 8.3 Hz, 1H, H17), 8.16 (s, 1H, H2), 7.99 (d, *J* = 8.8 Hz, 1H, H13), 7.96 (app. s, 1H, H16), 7.84 (dd, *J* = 8.8, 1.8 Hz, 1H, H12), 7.46 – 7.41 (m, 3H, H12', H18), 7.22 – 7.18 (m, 2H, H11'), 6.27 (d, *J* = 1.9 Hz, 1H, H1'), 5.68 (dd, *J* = 6.4, 1.9 Hz, 1H, H2'), 5.59 – 5.37 (m, 4H, H24), 5.20 (dd, *J* = 6.4, 3.1 Hz, 1H, H3'), 5.07 (d, *J* = 14.7 Hz, 1H, H10a), 4.97 (d, *J* = 10.3 Hz, 1H, H20a), 4.91 (d, *J* = 14.7 Hz, 1H, H10b), 4.87 (d, *J* = 10.3 Hz, 1H, H20b), 4.51 – 4.45 (m, 2H, H9'), 4.40 (app. td, *J* = 6.4, 3.3 Hz, 1H, H4'), 3.80 (dd, *J* = 10.4, 5.9 Hz, 1H, H5'a), 3.68 (dd, *J* = 10.4, 6.8 Hz,

1H, H5'b), 3.63 – 3.58 (m, 6H, H21, H25), 1.56 (s, 3H, H7'), 1.35 (s, 3H, H8'), 0.94 – 0.83 (m, 6H, H22, H26), -0.04 (s, 9H, H23), -0.06 (s, 18H, H27);  $^{13}\text{C}$  NMR (151 MHz, acetone- $d_6$ )  $\delta$  = 153.60 (C6), 153.39 (C8), 152.19 (C4), 151.18 (C2), 150.84 (C19), 148.91 (C14), 138.93 (C10'), 137.17 (C11), 136.45 (C17), 132.05 (2C, C12), 130.81 (C12), 130.46 (C13), 130.24 (2C, C11), 129.01 (C15), 128.03 (C16), 122.33 (C18), 121.57 (C13'), 118.65 (C5), 114.35 (C6'), 90.82 (C1'), 87.25 (C4'), 83.69 (C2'), 83.51 (C3'), 83.23 (C20), 76.58 (2C, C24), 72.74 (C9'), 71.08 (C5'), 66.49 (C21), 65.44 (2C, C25), 54.22 (C10), 27.57 (C7'), 25.59 (C8'), 18.61 (2C, C26), 18.57 (C22), -1.16 (3C, C23), -1.20 (6C, C27); HRMS (ESI+)  $m/z$  calculated for  $\text{C}_{48}\text{H}_{73}^{79}\text{BrN}_7\text{O}_7\text{Si}_3$  (M+H) $^+$  1022.4057, found 1022.4034.

**4-(((3a*R*,4*R*,6*R*,6a*R*)-6-(6-(bis((2-(trimethylsilyl)ethoxy)methyl)amino)-8-((quinolin-6-ylmethyl)((2-(trimethylsilyl)ethoxy)methyl)amino)-9*H*-purin-9-yl)-2,2-dimethyltetrahydrofuro[3,4-*d*][1,3]dioxol-4-yl)methoxy)methyl)benzenesulfonyl fluoride (118)**



**118**

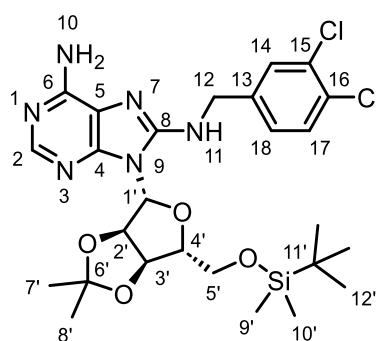
**118** was prepared following general procedure E, with 9-((3a*R*,4*R*,6*R*,6a*R*)-6-(((4-bromobenzyl)oxy)methyl)-2,2-dimethyltetrahydrofuro[3,4-*d*][1,3]dioxol-4-yl)-*N*8-(quinolin-6-ylmethyl)-*N*6,*N*6,*N*8-tris((2-(trimethylsilyl)ethoxy)methyl)-9*H*-purine-6,8-diamine **117** (340 mg, 0.33 mmol, 1 equiv.), isopropanol (1.23 mL, 0.27 M), DABSO (47.9 mg, 0.20 mmol, 0.6 equiv.), PdCl<sub>2</sub>(AmPhos)<sub>2</sub> (11.8 mg, 0.02 mmol, 5 mol%), triethylamine (0.14 mL, 1.00 mmol, 3 equiv.) and NFSI (157 mg, 0.50 mmol, 1.5 equiv.). Purification by normal phase column chromatography on silica (EtOAc:cyclohexane 5:95



to 40:60 gradient) yielded **118** (119 mg, 35%) as a yellow oil.  $^1\text{H NMR}$  (600 MHz, acetone- $d_6$ )  $\delta$  = 8.85 (d,  $J$  = 4.2, 1.7 Hz, 1H, H19), 8.23 (app. d,  $J$  = 8.3 Hz, 1H, H17), 8.16 (s, 1H, H2), 8.02 – 7.95 (m, 4H, H12', H13, H16), 7.85 (dd,  $J$  = 8.6, 1.9 Hz, 1H, H12), 7.68 – 7.65 (m, 2H, H11'), 7.45 (dd,  $J$  = 8.3, 4.1 Hz, 1H, H18), 6.30 (d,  $J$  = 2.10 Hz, 1H, H1'), 5.69 (dd,  $J$  = 6.3, 2.1 Hz, 1H, H2'), 5.59 – 5.39 (m, 4H, H24), 5.24 (dd,  $J$  = 6.3, 3.2 Hz, 1H, H3'), 5.08 (d,  $J$  = 14.6 Hz, 1H, H10a), 4.98 (d,  $J$  = 10.3 Hz, 1H, H20a), 4.92 (d,  $J$  = 14.6 Hz, 1H, H10b), 4.87 (d,  $J$  = 10.3 Hz, 1H, H20b), 4.75 – 4.67 (m, 2H, H9'), 4.45 (app. td,  $J$  = 6.4, 3.3 Hz, 1H, H4'), 3.91 (dd,  $J$  = 10.6, 5.6 Hz, 1H, H5'a), 3.80 (dd,  $J$  = 10.6, 6.8 Hz, 1H, H5'b), 3.63 – 3.58 (m, 6H, H21, H25), 1.58 (s, 3H, H7'), 1.36 (s, 3H, H8'), 0.93 – 0.84 (m, 6H, H22, H26), -0.05 (s, 9H, H23), -0.07 (s, 18H, H27);  $^{13}\text{C NMR}$  (151 MHz, acetone- $d_6$ )  $\delta$  = 153.61 (C6), 153.38 (C8), 152.20 (C4), 151.19 (C19), 150.85 (C2), 149.11 (C10), 148.90 (C14), 137.17 (C11), 136.44 (C17), 132.04 (C13')\*, 130.80 (C12), 130.46 (C13), 129.27 (2C, C12'), 129.08 (2C, C11'), 129.00 (C15), 128.03 (C16), 122.33 (C18), 118.68 (C5), 114.45 (C6'), 90.82 (C1'), 87.15 (C4'), 83.71 (C2'), 83.35 (C3'), 83.30 (C20), 76.68 (2C, C24), 72.37 (C9'), 71.64 (C5'), 66.51 (C21), 65.44 (2C, C25), 54.26 (C10), 27.60 (C7'), 25.60 (C8'), 18.60 (2C, C26), 18.56 (C22), -1.17 (6C, C27), -1.22 (3C, C23);  $^{19}\text{F NMR}$  (471 MHz, acetone- $d_6$ )  $\delta$  = 65.11; **HRMS** (ESI+)  $m/z$  calculated for  $\text{C}_{48}\text{H}_{72}\text{FN}_7\text{NaO}_9\text{SSi}_3$  ( $\text{M}+\text{Na}$ ) $^+$  1048.4296, found 1048.4315.

\*C13' observed as broad singlet/weak doublet and so it is reported as a singlet due to non-resolvable  $J_{\text{C-F}}$ -coupling.

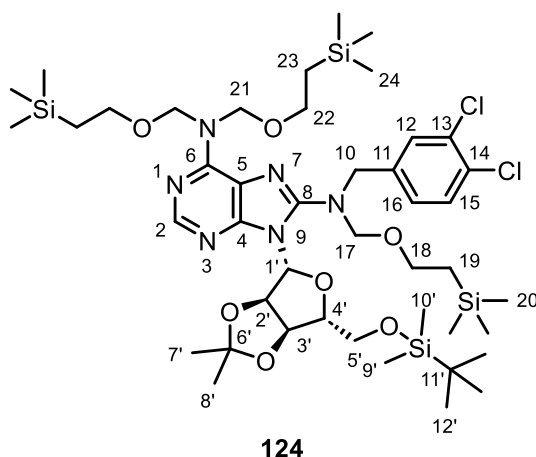
**9-((3a*R*,4*R*,6*R*,6a*R*)-6-(((*tert*-butyldimethylsilyl)oxy)methyl)-2,2-dimethyltetrahydrofuro[3,4-*d*][1,3]dioxol-4-yl)-*N*8-(3,4-dichlorobenzyl)-9*H*-purine-6,8-diamine (**123**)**



**123**

**123** was prepared following general procedure A, with 8-bromo-9-((3*aR*,4*R*,6*R*,6*aR*)-6-(((*tert*-butyldimethylsilyl)oxy)methyl)-2,2-dimethyltetrahydrofuro[3,4-*d*][1,3]dioxol-4-yl)-9*H*-purin-6-amine **95** (2.6 g, 5.20 mmol, 1 equiv.), ethanol (17.3 mL, 0.3 M) and 3,4-dichlorobenzylamine (5.54 mL, 41.6 mmol, 8 equiv.). Purification by normal phase column chromatography on silica (100% CH<sub>2</sub>Cl<sub>2</sub> to methanol:CH<sub>2</sub>Cl<sub>2</sub> 15:85 gradient) yielded **123** (2.73 g, 88%) as an orange foam. <sup>1</sup>H NMR (600 MHz, CDCl<sub>3</sub>) δ = 8.12 (s, 1H, H2), 7.39 (d, *J* = 1.7 Hz, 1H, H14), 7.34 (d, *J* = 8.3 Hz, 1H, H17), 7.14 (dd, *J* = 8.3, 1.7 Hz, 1H, H18), 6.11 (d, *J* = 3.2 Hz, 1H, H1'), 5.90 (app. t, *J* = 5.8 Hz, 1H, H11), 5.67 (s br, 2H, H10), 5.51 (dd, *J* = 6.6, 3.2 Hz, 1H, H2'), 4.93 (dd, *J* = 6.6, 3.4 Hz, 1H, H3'), 4.63 (dd, *J* = 15.9, 6.9 Hz, 1H, H12a), 4.55 (dd, *J* = 15.9, 4.8 Hz, 1H, H12b), 4.23 – 4.20 (m, 1H, H4'), 3.81 (dd, *J* = 11.3, 3.8 Hz, 1H, H5'a), 3.71 (dd, *J* = 11.3, 3.8 Hz, 1H, H5'b), 1.59 (s, 3H, H7'), 1.38 (s, 3H, H8'), 0.81 (s, 9H, H12'), -0.04 (s, 6H, H9', H10'); <sup>13</sup>C NMR (151 MHz, CDCl<sub>3</sub>) δ = 152.23 (C6), 151.67 (C8), 150.02 (C4), 149.66 (C2), 139.18 (C13), 132.69 (C16), 131.31 (C15), 130.58 (C17), 129.13 (C14), 126.54 (C18), 117.48 (C5), 114.84 (C6'), 89.01 (C1'), 85.80 (C4'), 82.41 (C2'), 80.25 (C3'), 62.80 (C5'), 45.56 (C12), 27.29 (C7'), 26.00 (3C, C12'), 25.50 (C8'), 18.67 (C11'), -5.20 (C9'), -5.37 (C10'); HRMS (ESI+) *m/z* calculated for C<sub>26</sub>H<sub>37</sub><sup>35</sup>Cl<sub>2</sub>N<sub>6</sub>O<sub>4</sub>Si (M+H)<sup>+</sup> 595.2017, found 595.2028; [α]<sub>D</sub><sup>25</sup> = -14 ° (c = 0.5, CHCl<sub>3</sub>)

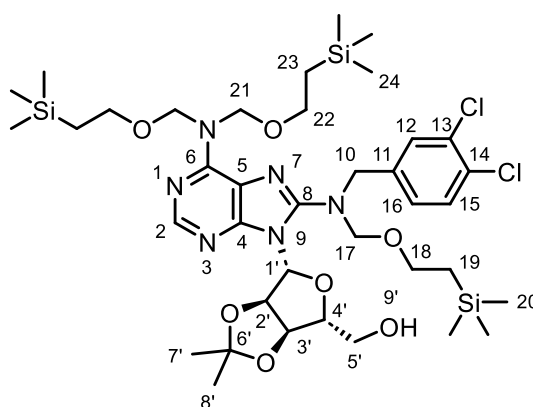
**9-((3*aR*,4*R*,6*R*,6*aR*)-6-(((*tert*-butyldimethylsilyl)oxy)methyl)-2,2-dimethyltetrahydrofuro[3,4-*d*][1,3]dioxol-4-yl)-*N*8-(3,4-dichlorobenzyl)-*N*6,*N*6,*N*8-tris((2-(trimethylsilyl)ethoxy)methyl)-9*H*-purine-6,8-diamine (**124**)**



**124** was prepared following general procedure B, with 9-((3*aR*,4*R*,6*R*,6*aR*)-6-(((*tert*-butyldimethylsilyl)oxy)methyl)-2,2-dimethyltetrahydrofuro[3,4-*d*][1,3]dioxol-4-yl)-*N*8-

(3,4-dichlorobenzyl)-9*H*-purine-6,8-diamine **123** (2.00 g, 3.36 mmol, 1 equiv.), CH<sub>2</sub>Cl<sub>2</sub> (11.2 mL, 0.3 M), 2-(trimethylsilyl)ethoxymethylchloride (2.67 mL, 15.1 mmol, 4.5 equiv.) and *N,N*-diisopropylethylamine (2.63 mL, 15.1 mmol, 4.5 equiv.) for 22 hours. Purification by normal phase column chromatography on silica (EtOAc:cyclohexane 1:99 to 15:85 gradient) yielded **124** (2.20 g, 66%) as a colourless oil. <sup>1</sup>H NMR (600 MHz, acetone-d<sub>6</sub>) δ = 8.26 (s, 1H, H2), 7.67 (d, *J* = 1.9 Hz, 1H, H12), 7.50 (d, *J* = 8.2 Hz, 1H, H15), 7.43 (dd, *J* = 8.2, 1.9 Hz, 1H, H16), 6.19 (d, *J* = 1.9 Hz, 1H, H1'), 5.67 (dd, *J* = 6.3, 1.9 Hz, 1H, H2'), 5.61 – 5.36 (m, 4H, H21), 5.20 (dd, *J* = 6.3, 2.8 Hz, 1H, H3'), 4.94 – 4.83 (m, 3H, H10a, H17), 4.71 – 4.67 (m, 1H, H10b), 4.25 (app. td, *J* = 6.8, 2.8 Hz, 1H, H4'), 3.93 (dd, *J* = 10.7, 7.0 Hz, 1H, H5'a), 3.76 (dd, *J* = 10.5, 6.4 Hz, 1H, H5'b), 3.64 – 3.57 (m, 6H, H18, H22), 1.56 (s, 3H, H7'), 1.35 (s, 3H, H8'), 0.95 – 0.88 (m, 6H, H19, H23), 0.86 (s, 9H, H12'), -0.02 – -0.03 (m, 15H, H9', H10', H20), -0.04 (s, 18H, H24); <sup>13</sup>C NMR (151 MHz, acetone-d<sub>6</sub>) δ = 153.64 (C6), 153.13 (C8), 152.17 (C4), 150.86 (C2), 140.17 (C11), 132.60 (C14), 131.53 (C13), 131.43 (C12), 131.28 (C15), 129.46 (C16), 118.57 (C5), 114.08 (C6'), 90.96 (C1'), 89.04 (C4'), 83.68 (C2'), 83.52 (C3'), 83.39 (C17), 76.52 (2C, C21), 66.43 (C18), 65.46 (2C, C22), 64.21 (C5'), 53.37 (C10), 27.55 (C7'), 26.25 (C12'), 25.58 (C8'), 18.88 (C11'), 18.64 (2C, C23), 18.57 (C19), -1.15 (6C, C24), -1.21 (3C, C20), -5.06 (C9'), -5.15 (C10'); HRMS (ESI+) *m/z* calculated for C<sub>44</sub>H<sub>79</sub><sup>35</sup>Cl<sub>2</sub>N<sub>6</sub>O<sub>7</sub>Si<sub>4</sub> (M+H)<sup>+</sup> 985.4459, found 985.4472.

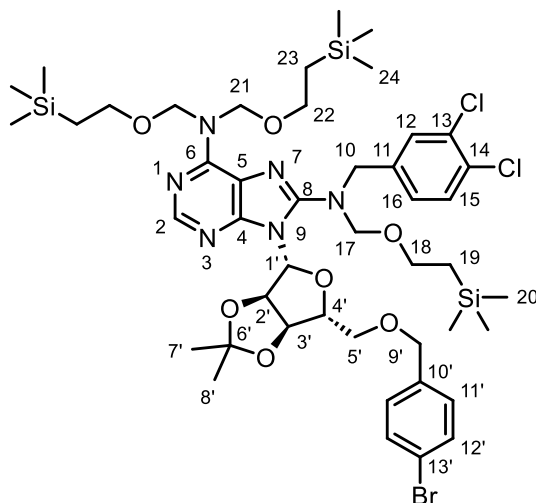
**((3*aR*,4*R*,6*R*,6*aR*)-6-(6-(bis((2-(trimethylsilyl)ethoxy)methyl)amino)-8-((3,4-dichlorobenzyl)((2-(trimethylsilyl)ethoxy)methyl)amino)-9*H*-purin-9-yl)-2,2-dimethyltetrahydrofuro[3,4-*d*][1,3]dioxol-4-yl)methanol (125)**



125

**125** was prepared following general procedure C, with 9-((3*aR*,4*R*,6*R*,6*aR*)-6-(((*tert*-butyldimethylsilyl)oxy)methyl)-2,2-dimethyltetrahydrofuro[3,4-*d*][1,3]dioxol-4-yl)-*N*8-(3,4-dichlorobenzyl)-*N*6,*N*6,*N*8-tris((2-(trimethylsilyl)ethoxy)methyl)-9*H*-purine-6,8-diamine **124** (2.18 g, 2.21 mmol, 1 equiv.), THF (22.1 mL, 0.1 M) and TBAF (2.43 mL, 1 M in THF, 2.43 mmol, 1.1 equiv.) for 18 hours. Purification by normal phase column chromatography on silica (EtOAc:cyclohexane 5:95 to 50:50 gradient) yielded **125** (1.48 g, 77%) as a colourless oil. **<sup>1</sup>H NMR** (600 MHz, CD<sub>3</sub>CN)  $\delta$  = 8.19 (s, 1H, H2), 7.57 (d,  $J$  = 1.8 Hz, 1H, H12), 7.43 (d,  $J$  = 8.3 Hz, 1H, H15), 7.32 (dd,  $J$  = 8.3, 1.8 Hz, 1H, H16), 6.03 (d,  $J$  = 4.8 Hz, 1H, H1'), 5.47 (dd,  $J$  = 10.7, 2.3 Hz, 1H, H9'), 5.40 (app. s, 4H, H21), 5.35 (app. t,  $J$  = 5.2 Hz, 1H, H2'), 5.07 (dd,  $J$  = 5.9, 1.3 Hz, 1H, H3'), 4.80 (d,  $J$  = 10.5 Hz, 1H, H17a), 4.71 (d,  $J$  = 10.5 Hz, 1H, H17b), 4.68 (d,  $J$  = 14.9 Hz, 1H, H10a), 4.64 (d, 14.9 Hz, 1H, H10b), 4.39 – 4.36 (m, 1H, H4'), 3.77 (app. dt,  $J$  = 12.5, 2.4 Hz, 1H, H5'a), 3.71 – 3.65 (m, 1H, H5'b), 3.57 – 3.53 (m, 4H, H22), 3.52 – 3.48 (m, 2H, H18), 1.61 (s, 3H, H7'), 1.35 (s, 3H, H8'), 0.88 – 0.83 (m, 6H, H19, H23), -0.07 (s, 18H, H24), -0.08 (s, 9H, H20); **<sup>13</sup>C NMR** (151 MHz, CD<sub>3</sub>CN)  $\delta$  = 153.88 (C6), 152.84 (C8), 151.84 (C4), 150.69 (C2), 140.11 (C11), 132.64 (C14), 131.43 (C13), 131.27 (C15), 131.21 (C12), 129.29 (C16), 119.12 (C5), 114.64 (C6'), 92.48 (C1'), 86.68 (C4'), 84.26 (C17), 82.81 (C2'), 82.75 (C3'), 77.14 (2C, C21), 66.88 (C18), 65.68 (2C, C22), 63.76 (C5'), 53.27 (C10), 27.84 (C7'), 25.60 (C8'), 18.60 (2C, C23), 18.41 (C19), -1.35 (6C, C24), -1.42 (3C, C20); **HRMS** (ESI+)  $m/z$  calculated for C<sub>38</sub>H<sub>65</sub><sup>35</sup>Cl<sub>2</sub>N<sub>6</sub>O<sub>7</sub>Si<sub>3</sub> (M+H)<sup>+</sup> 871.3594, found 871.3581;  $[\alpha]_D^{25} = -9^\circ$  (c = 0.5, CHCl<sub>3</sub>).

**9-((3*aR*,4*R*,6*R*,6*aR*)-6-(((4-bromobenzyl)oxy)methyl)-2,2-dimethyltetrahydrofuro[3,4-*d*][1,3]dioxol-4-yl)-*N*8-(3,4-dichlorobenzyl)-*N*6,*N*6,*N*8-tris((2-(trimethylsilyl)ethoxy)methyl)-9*H*-purine-6,8-diamine (**126**)**

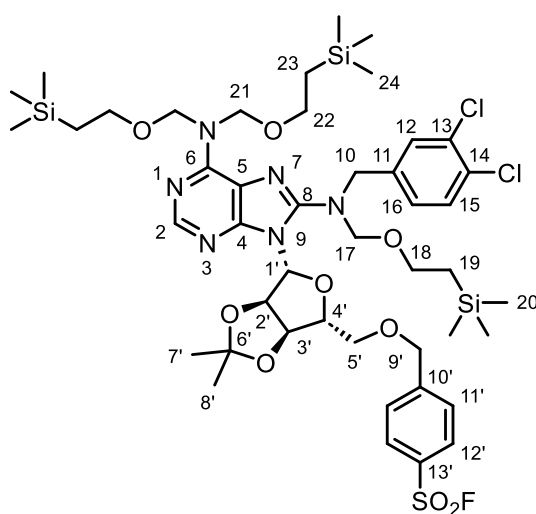


**126**

**126** was prepared following general procedure D, with ((3*aR*,4*R*,6*R*,6*aR*)-6-(6-(bis((2-(trimethylsilyl)ethoxy)methyl)amino)-8-((3,4-dichlorobenzyl)((2-(trimethylsilyl)ethoxy)methyl)amino)-9*H*-purin-9-yl)-2,2-dimethyltetrahydrofuro[3,4-*d*][1,3]dioxol-4-yl)methanol **125** (500 mg, 0.57 mmol, 1 equiv.), THF (1.15 mL, 0.5 M), sodium hydride (27.5 mg, 60% in mineral oil, 0.69 mmol, 1.2 equiv.) and 4-bromobenzyl bromide (287 mg, 1.15 mmol, 2 equiv.). Purification by normal phase column chromatography on silica (EtOAc:cyclohexane 5:95 to 20:70 gradient) yielded **126** (549 mg, 92%) as a colourless oil. <sup>1</sup>H NMR (600 MHz, CD<sub>3</sub>CN) δ = 8.11 (s, 1H, H2), 7.57 (d, *J* = 2.0 Hz, 1H, H12), 7.43 (d, *J* = 8.3 Hz, 1H, H15), 7.41 – 7.38 (m, 2H, H12'), 7.31 (dd, *J* = 8.3, 2.0 Hz, 1H, H16), 7.13 – 7.10 (m, 2H, H11'), 6.09 (d, *J* = 2.0 Hz, 1H, H1'), 5.58 (dd, *J* = 6.3, 2.0 Hz, 1H, H2'), 5.51 – 5.30 (m, 4H, H21), 5.12 (dd, *J* = 6.3, 3.2 Hz, 1H, H3'), 4.81 (d, *J* = 10.4 Hz, 1H, H17a), 4.75 (d, *J* = 14.9 Hz, 1H, H10a), 4.72 (d, *J* = 10.4 Hz, 1H, H17b), 4.58 (d, *J* = 14.9 Hz, 1H, H10b), 4.44 – 4.38 (m, 2H, H9'), 4.34 – 4.31 (m, 1H, H4'), 3.69 (dd, *J* = 10.1, 5.8 Hz, 1H, H5'a), 3.61 (dd, *J* = 10.1, 7.0 Hz, 1H, H5'b), 3.58 – 3.54 (m, 4H, H22), 3.51 – 3.47 (m, 2H, H18), 1.54 (s, 3H, H7'), 1.32 (s, 3H, H8'), 0.88 – 0.82 (m, 6H, H19, H23), -0.08 (s, 18H, C24), -0.09 (s, 9H, C20); <sup>13</sup>C NMR (151 MHz, CD<sub>3</sub>CN) δ = 153.45 (C6), 153.15 (C8), 152.24 (C4), 150.85 (C2), 140.13 (C11), 138.80 (C10'), 132.62 (C14), 132.13 (2C, C12'), 131.45 (C13), 131.39 (C12), 131.29 (C15), 130.34 (2C, C11'), 129.41 (C16), 121.67 (C13'), 118.66 (C5), 114.50 (C6'), 90.69

(C1'), 87.29 (C4'), 83.73 (C2'), 83.56 (C17), 83.41 (C3'), 77.30 (2C, C21), 72.76 (C9'), 70.93 (C5'), 66.59 (C18), 65.61 (2C, C22), 53.46 (C10), 27.46 (C7'), 25.57 (C8'), 18.62 (2C, C23), 18.49 (C19), -1.33 (6C, C24), -1.36 (3C, C20); **HRMS** (ESI+)  $m/z$  calculated for  $C_{45}H_{70}^{79}Br^{35}Cl_2N_6O_7Si_3$  (M+H)<sup>+</sup> 1039.3169, found 1039.3166;  $[\alpha]_D^{25} = -26^\circ$  ( $c = 0.5$ ,  $CHCl_3$ ).

**4-(((3*aR*,4*R*,6*R*,6*aR*)-6-(6-(bis((2-(trimethylsilyl)ethoxy)methyl)amino)-8-((3,4-dichlorobenzyl)((2-(trimethylsilyl)ethoxy)methyl)amino)-9*H*-purin-9-yl)-2,2-dimethyltetrahydrofuro[3,4-*d*][1,3]dioxol-4-yl)methoxy)methyl)benzenesulfonyl fluoride (127)**

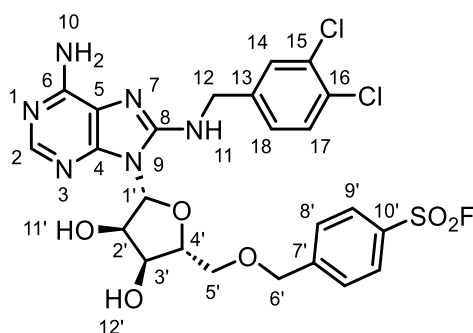


127

**127** was prepared following general procedure E, with 9-((3*aR*,4*R*,6*R*,6*aR*)-6-(((4-bromobenzyl)oxy)methyl)-2,2-dimethyltetrahydrofuro[3,4-*d*][1,3]dioxol-4-yl)-*N*8-(3,4-dichlorobenzyl)-*N*6,*N*6,*N*8-tris((2-(trimethylsilyl)ethoxy)methyl)-9*H*-purine-6,8-diamine **126** (549 mg, 0.53 mmol, 1 equiv.), isopropanol (1.95 mL, 0.27 M), DABSO (76.0 mg, 0.32 mmol, 0.6 equiv.), PdCl<sub>2</sub>(AmPhos)<sub>2</sub> (18.7 mg, 0.03 mmol, 5 mol%), triethylamine (0.22 mL, 1.58 mmol, 3 equiv.) and NFSI (249 mg, 0.79 mmol, 1.5 equiv.). Purification by normal phase column chromatography on silica (EtOAc:cyclohexane 1:99 to 25:75 gradient) yielded **127** (209 mg, 38%) as a pale yellow oil. <sup>1</sup>H NMR (600 MHz, CD<sub>3</sub>CN)  $\delta$  = 8.11 (s, 1H, H2), 7.94 – 7.91 (m, 2H, H12'), 7.57 (d,  $J = 1.9$  Hz, 1H, H12), 7.55 – 7.52 (m, 2H, H11'), 7.43 (d,  $J = 8.3$  Hz, 1H, H15), 7.31 (dd,  $J = 8.3, 1.9$  Hz, 1H, H16), 6.11 (d,  $J = 2.1$  Hz, 1H, H1'), 5.61 (dd,  $J = 6.3, 2.1$  Hz, 1H, H2'), 5.49 – 5.29 (m, 4H, H21), 5.17 (dd,  $J = 6.3, 3.3$  Hz, 1H, H3'), 4.83 (d,  $J = 10.4$  Hz, 1H, H17a), 4.76 (d,  $J$

= 14.8 Hz, 1H, H10a), 4.73 (d,  $J = 10.3$  Hz, 1H, H17b), 4.64 – 4.56 (m, 3H, H9', H10b), 4.40 – 4.35 (m, 1H, H4'), 3.78 (dd,  $J = 10.2, 5.5$  Hz, 1H, H5'a), 3.70 (dd,  $J = 10.2, 7.0$  Hz, 1H, H5'b), 3.57 – 3.53 (m, 4H, H22), 3.51 – 3.47 (m, 2H, H18), 1.56 (s, 3H, H7'), 1.34 (s, 3H, H8'), 0.87 – 0.82 (m, 6H, H19, H23), -0.08 (s, 18H, H24), -0.09 (s, 9H, H20);  $^{13}\text{C}$  NMR (151 MHz,  $\text{CD}_3\text{CN}$ )  $\delta = 153.46$  (C6), 153.14 (C8), 152.26 (C4), 150.88 (C2), 148.99 (C10'), 140.12 (C11), 132.62 (C14), 131.91 (d,  $J_{\text{C-F}} = 23.9$  Hz, C13'), 131.45 (C13), 131.37 (C12), 131.28 (C15), 129.40 (C16), 129.33 (2C, C12'), 129.08 (2C, C11'), 118.68 (C5), 114.59 (C6'), 90.70 (C1'), 87.14 (C4'), 83.71 (C17), 83.63 (C2'), 83.25 (C3'), 77.36 (2C, C21), 72.38 (C9'), 71.51 (C5), 66.61 (C18), 65.60 (2C, C22), 53.48 (C10), 27.47 (C7'), 25.57 (C8'), 18.59 (2C, C23), 18.47 (2C, C19), -1.36 (6C, C24), -1.40 (3C, C20);  $^{19}\text{F}$  NMR (471 MHz,  $\text{CD}_3\text{CN}$ )  $\delta = 65.01$ ; HRMS (ESI+)  $m/z$  calculated for  $\text{C}_{45}\text{H}_{70}^{35}\text{Cl}_2\text{FN}_6\text{O}_9\text{SSi}_3$  (M+H) $^+$  1043.3588, found 1043.3574.

**4-(((2*R*,3*S*,4*R*,5*R*)-5-(6-amino-8-((3,4-dichlorobenzyl)amino)-9*H*-purin-9-yl)-3,4-dihydroxytetrahydrofuran-2-yl)methoxy)methyl)benzenesulfonyl fluoride (128)**

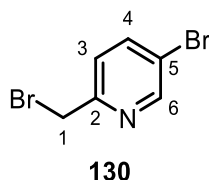


**128**

**128** was prepared following general procedure F, with 4-(((3*aR*,4*R*,6*R*,6*aR*)-6-(6-(bis((2-(trimethylsilyl)ethoxy)methyl)amino)-8-((3,4-dichlorobenzyl)((2-(trimethylsilyl)ethoxy)methyl)amino)-9*H*-purin-9-yl)-2,2-dimethyltetrahydrofuro[3,4-*d*][1,3]dioxol-4-yl)methoxy)methyl)benzenesulfonyl fluoride **127** (200 mg, 0.19 mmol, 1 equiv.), and TFA:water 5:2 (v/v) mixture (1.69 mL, 0.1 M) for 2 hours. Purification by normal phase column chromatography on silica (100%  $\text{CH}_2\text{Cl}_2$  to 15:85 methanol: $\text{CH}_2\text{Cl}_2$  gradient) then reverse phase column chromatography on C18 (acetonitrile:water +0.1% formic acid 10:90 to 50:50 gradient) yielded **128** (31 mg, 26%) as a white solid.  $^1\text{H}$  NMR (600 MHz,  $\text{DMSO-d}_6$ )  $\delta = 8.03 - 7.99$  (m, 2H, H9'), 7.92 (s, 1H, H18), 7.60 – 7.56 (m, 2H, H8'), 7.53 – 7.50 (m, 2H, H14, H17), 7.31 – 7.26 (m, 2H, H11, H18), 6.66 (s br, 2H, H10), 5.86 (d,  $J = 5.4$  Hz, 1H, H1'), 5.32 (d,  $J = 5.0$  Hz, 1H, H11'), 5.24 (d,  $J = 3.8$  Hz,

1H, H12'), 4.98 (app. q,  $J = 4.9$  Hz, 1H, H2'), 4.64 (s, 2H, H6'), 4.50 (d,  $J = 5.9$  Hz, 2H, H12), 4.38 – 3.34 (m, 1H, H3'), 4.07 – 4.04 (m, 1H, H4'), 3.81 (dd,  $J = 10.9, 3.2$  Hz, 1H, H5'a), 3.70 (dd,  $J = 10.9, 4.8$  Hz, 1H, H5'b);  $^{13}\text{C}$  NMR (151 MHz, DMSO- $d_6$ )  $\delta = 152.01$  (C6), 151.40 (C8), 149.75 (C4), 148.35 (C2), 147.71 (C7'), 140.97 (C13), 130.80 (C16), 130.35 (C17), 130.16 (d,  $J_{\text{C-F}} = 23.2$  Hz, C10'), 129.25 (C15), 128.96 (C14), 128.36 (2C, C9'), 128.22 (2C, C8'), 127.42 (C18), 116.94 (C5), 87.17 (C1'), 82.78 (C4'), 71.12 (C6'), 70.59 (C5'), 70.55 (C2'), 70.20 (C3'), 44.32 (C12);  $^{19}\text{F}$  NMR (471 MHz, DMSO- $d_6$ )  $\delta = 66.69$ ; HRMS (ESI+)  $m/z$  calculated for  $\text{C}_{24}\text{H}_{24}^{35}\text{Cl}_2\text{FN}_6\text{O}_6\text{S}$  (M+H) $^+$  613.0834, found 613.0845.

### 5-bromo-2-(bromomethyl)pyridine (**130**)

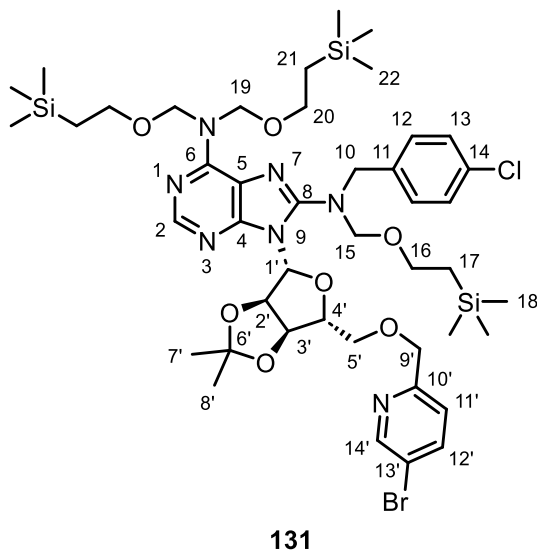


A two-neck round bottom flask equipped with magnetic stirrer and reflux condenser was charged with 5-bromo-2-methylpyridine **129** (500 mg, 2.91 mmol, 1 equiv.),  $\alpha,\alpha,\alpha$ -trifluorotoluene (7.27 mL, 0.4 M), NBS (569 mg, 3.20 mmol, 1.1 equiv.) and benzoyl peroxide (46.9 mg, 75 wt% in water, 0.14 mmol, 5 mol%) under flow of nitrogen. The mixture was heated to 90 °C for 18 hours, after which the mixture was cooled to room temperature, filtered, and the filtrate concentrated under reduced pressure. The crude residue was purified by normal phase column chromatography on silica (EtOAc:cyclohexane 1:99 to 20:80 gradient) to yield **130** (162 mg, 22%) as a brown paste.  $^1\text{H}$  NMR (600 MHz,  $\text{CDCl}_3$ )  $\delta = 8.63$  (d,  $J = 2.2$  Hz, 1H, H6), 7.82 (dd,  $J = 8.3, 2.2$  Hz, 1H, H4), 7.35 (d,  $J = 8.3$  Hz, 1H, H3), 4.50 (s, 2H, H1);  $^{13}\text{C}$  NMR (151 MHz,  $\text{CDCl}_3$ )  $\delta = 155.53$  (C2), 150.89 (C6), 139.84 (C4), 124.88 (C3), 120.25 (C5), 32.89 (C1); HRMS (ESI+)  $m/z$  calculated for  $\text{C}_6\text{H}_6^{79}\text{Br}_2\text{N}$  (M+H) $^+$  249.8862, found 249.8866.

The spectroscopic and analytical data were in agreement with literature values.<sup>292</sup>



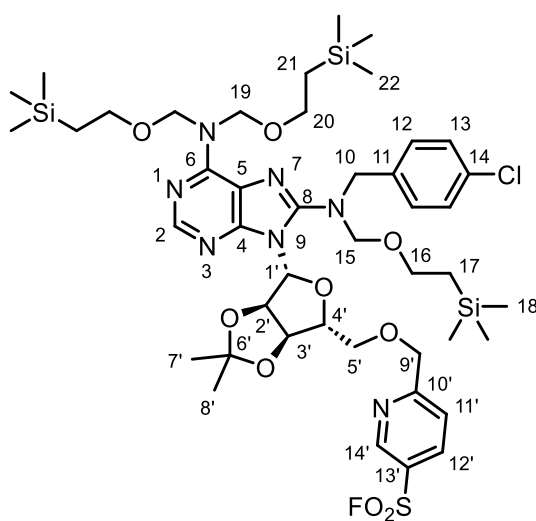
**9-((3a*R*,4*R*,6*R*,6a*R*)-6-(((5-bromopyridin-2-yl)methoxy)methyl)-2,2-dimethyltetrahydrofuro[3,4-*d*][1,3]dioxol-4-yl)-*N*8-(4-chlorobenzyl)-*N*6,*N*6,*N*8-tris((2-(trimethylsilyl)ethoxy)methyl)-9*H*-purine-6,8-diamine (**131**)**



**131** was prepared following general procedure D, with ((3a*R*,4*R*,6*R*,6a*R*)-6-(6-(bis((2-(trimethylsilyl)ethoxy)methyl)amino)-8-((4-chlorobenzyl)((2-(trimethylsilyl)ethoxy)methyl)amino)-9*H*-purin-9-yl)-2,2-dimethyltetrahydrofuro[3,4-*d*][1,3]dioxol-4-yl)methanol **94** (650 mg, 0.78 mmol, 1 equiv.), THF (1.55 mL, 0.5 M), sodium hydride (37.2 mg, 60% in mineral oil, 0.93 mmol, 1.2 equiv.) and 5-bromo-2-(bromomethyl)pyridine **130** (389 mg, 1.55 mmol, 2 equiv.). Purification by normal phase column chromatography on silica (EtOAc:cyclohexane 1:99 to 20:80 gradient) yielded **131** (592 mg, 76%) as a yellow oil. <sup>1</sup>H NMR (600 MHz, acetone-*d*<sub>6</sub>) δ = 8.53 – 8.50 (m, 1H, H14'), 8.17 (s, 1H, H2), 7.86 – 7.81 (m, 1H, H12'), 7.49 – 7.44 (m, 2H, H13), 7.35 – 7.31 (m, 3H, H11', H12), 6.21 – 6.18 (m, 1H, H1'), 5.69 – 5.65 (m, 1H, H2'), 5.62 – 5.37 (m, 4H, H19), 5.25 – 5.21 (m, 1H, H3'), 4.92 (d, *J* = 10.3 Hz, 1H, H15a), 4.86 (d, *J* = 14.7 Hz, 1H, H10a), 4.80 (d, *J* = 10.3 Hz, 1H, H15b), 4.68 (d, *J* = 14.7 Hz, 1H, H10b), 4.59 – 4.49 (m, 2H, H9'), 4.45 – 4.40 (m, 1H, H4'), 3.89 – 3.85 (m, 1H, H5'a), 3.79 – 3.74 (m, 1H, H5'b), 3.66 – 3.60 (m, 4H, H20), 3.60 – 3.55 (m, 2H, H16), 1.57 (s, 3H, H7'), 1.35 (s, 3H, H8'), 0.93 – 0.87 (m, 6H, H17, H21), -0.02 – -0.06 (s, 29H, H18, H22) <sup>13</sup>C NMR (151 MHz, acetone-*d*<sub>6</sub>) δ = 158.52 (C10'), 153.57 (C6), 153.27 (C8), 152.13 (C4), 150.82 (C2), 150.50 (C14'), 139.83 (C12'), 137.78 (C11), 133.43 (C14), 131.20 (2C, C12), 129.24 (2C, C13), 123.51 (C11'), 119.52 (C13'), 118.58 (C5), 114.30 (C6'), 90.74 (C1'), 87.31 (C4'), 83.73 (C2'), 83.44 (C3'), 83.10 (C15), 76.59 (2C, C19), 73.98

(C9'), 71.67 (C5'), 66.44 (C16), 65.45 (2C, C20), 53.65 (C10), 27.54 (C7'), 25.57 (C8'), 18.65 (2C, C21), 18.55 (C17), -1.14 (6C, C22), -1.22 (3C, C18); **HRMS** (ESI+) *m/z* calculated for C<sub>44</sub>H<sub>70</sub><sup>79</sup>Br<sup>35</sup>ClN<sub>7</sub>O<sub>7</sub>Si<sub>3</sub> (M+H)<sup>+</sup> 1006.3511, found 1006.3550.

**6-(((3*aR*,4*R*,6*R*,6*aR*)-6-(6-(bis((2-(trimethylsilyl)ethoxy)methyl)amino)-8-((4-chlorobenzyl)((2-(trimethylsilyl)ethoxy)methyl)amino)-9*H*-purin-9-yl)-2,2-dimethyltetrahydrofuro[3,4-*d*][1,3]dioxol-4-yl)methoxy)methyl)pyridine-3-sulfonyl fluoride (132)**



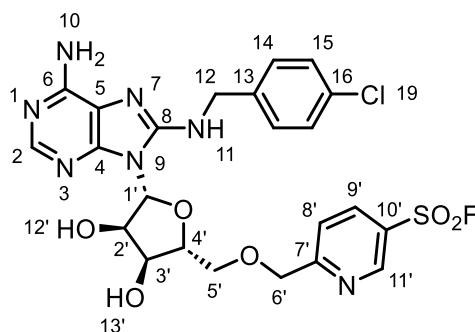
**132**

A glass microwave vial equipped with magnetic stirrer was charged with 9-(((3*aR*,4*R*,6*R*,6*aR*)-6-(((5-bromopyridin-2-yl)methoxy)methyl)-2,2-dimethyltetrahydrofuro[3,4-*d*][1,3]dioxol-4-yl)-*N*8-(4-chlorobenzyl)-*N*6,*N*6,*N*8-tris((2-(trimethylsilyl)ethoxy)methyl)-9*H*-purine-6,8-diamine **131** (576 mg, 0.57 mmol, 1 equiv.), DABSO (137 mg, 0.57 mmol, 1 equiv.), PdCl<sub>2</sub>(AmPhos)<sub>2</sub> (20.2 mg, 0.03 mmol, 5 mol%), and degassed and backfilled with argon four times. Isopropanol (2.29 mL, 0.25 M) was added to the mixture, which was then degassed and backfilled with argon four times, after which *N,N*-dicyclohexylmethylamine (0.38 mL, 1.71 mmol, 3 equiv.) was added and the mixture was heated to 110 °C under microwave irradiation. After stirring at 110 °C for 1 hour, the reaction mixture was cooled to room temperature and NFSI (270 mg, 0.86 mmol, 1.5 equiv.) was added and the reaction mixture was stirred for a further 5 hours. The reaction mixture was diluted with water (30 mL) and EtOAc (30 mL) and the phases were separated. The aqueous phase was extracted with EtOAc (2 × 30 mL) and the resultant combined organic layers were dried over MgSO<sub>4</sub>, filtered, and

concentrated under reduced pressure. The crude product was purified by normal phase column chromatography on silica (EtOAc:cyclohexane 10:90 to 30:70 gradient) to yield **132** (222 mg, 38%) as a pale yellow oil. Product is 2:3 mixture of impurity:desired product by LCMS, carried forward onto next step without further purification. **<sup>1</sup>H NMR** (600 MHz, acetone-*d*<sub>6</sub>)  $\delta$  = 9.09 (app. s, 1H, H14'), 8.39 (dd, *J* = 8.4, 2.4 Hz, 1H, H12'), 8.18 (s, 1H, H2), 7.82 (d, *J* = 8.4 Hz, 1H, H11'), 7.49 – 7.45 (m, 2H, H13), 7.34 – 7.31 (m, 2H, H12), 6.23 – 6.21 (m, 1H, H1'), 5.70 – 5.67 (m, 1H, H2'), 5.62 – 5.38 (m, 4H, H19), 5.28 (dd, *J* = 6.3, 3.3 Hz, 1H, H3'), 4.92 (d, *J* = 10.3 Hz, 1H, H15a), 4.89 – 4.72 (m, 4H, H9', H10a, H15b), 4.62 (d, *J* = 14.6 Hz, 1H, H10b), 4.49 – 4.45 (m, 1H, H4'), 4.01 – 3.97 (m, 1H, H5'a), 3.91 – 3.86 (m, 1H, H5'b), 3.64 – 3.56 (m, 6H, H16, H20), 1.58 (s, 3H, H7'), 1.36 (s, 3H, H8'), 0.92 – 0.88 (m, 6H, H17, H21), -0.04 (s, 18H, H22), -0.05 (s, 9H, H18); **<sup>13</sup>C NMR** (151 MHz, acetone-*d*<sub>6</sub>)  $\delta$  = 168.25 (C10'), 153.58 (C6), 153.25 (C8), 152.17 (C4), 150.87 (C2), 148.98 (C14'), 137.82 (2C, C11, C12'), 133.42 (C14), 131.18(2C, C12), 129.24 (2C, C13), 122.26 (C11'), 118.46 (C5), 114.43 (C6'), 90.73 (C1'), 87.15 (C4'), 83.71 (C2'), 83.26 (C3'), 83.17 (C15), 76.68 (2C, C19), 74.01 (C9'), 72.05 (C5'), 66.48 (C16), 65.45 (2C, C20), 53.68 (C10), 27.58 (C7'), 25.59 (C8'), 18.63 (2C, C21), 18.54 (C17), -1.16 (6C, C22), -1.24 (3C, C18);\* **<sup>19</sup>F NMR** (471 MHz, acetone-*d*<sub>6</sub>)  $\delta$  = 66.84; **HRMS** (ESI+) *m/z* calculated for C<sub>44</sub>H<sub>70</sub><sup>35</sup>ClFN<sub>7</sub>O<sub>9</sub>SSi<sub>3</sub> (M+H)<sup>+</sup> 1010.3931, found 1010.3934.

\*C13' not observed in spectrum.

**6-((((2*R*,3*S*,4*R*,5*R*)-5-(6-amino-8-((4-chlorobenzyl)amino)-9*H*-purin-9-yl)-3,4-dihydroxytetrahydrofuran-2-yl)methoxy)methyl)pyridine-3-sulfonyl fluoride (133)**

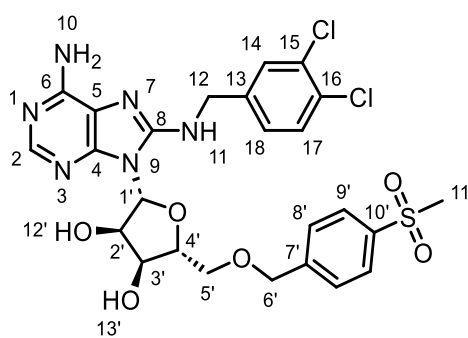


**133**

**133** was prepared following general procedure F, with 6-((((3*aR*,4*R*,6*R*,6*aR*)-6-(6-(bis((2-(trimethylsilyl)ethoxy)methyl)amino)-8-((4-chlorobenzyl)((2-

(trimethylsilyl)ethoxy)methyl)amino)-9*H*-purin-9-yl)-2,2-dimethyltetrahydrofuro[3,4-*d*][1,3]dioxol-4-yl)methoxy)methyl)pyridine-3-sulfonyl fluoride **132** (222 mg, 0.22 mmol, 1 equiv.), and TFA:water 5:2 (v/v) mixture (1.24 mL, 0.1 M) for 1 hour. Purification by normal phase column chromatography on silica (100% CH<sub>2</sub>Cl<sub>2</sub> to 15:85 methanol:CH<sub>2</sub>Cl<sub>2</sub> gradient) then reverse phase column chromatography on C18 (methanol:water +0.1% formic acid 30:70 to 70:30 gradient) yielded **133** (8 mg, 6%) as a white solid. **<sup>1</sup>H NMR** (600 MHz, DMSO-*d*<sub>6</sub>) δ = 9.14 (d, *J* = 2.2 Hz, 1H, H11'), 8.43 (dd, *J* = 8.4, 2.2 Hz, 1H, H9'), 7.88 (s, 1H, H2), 7.62 (d, *J* = 8.4 Hz, 1H, H8'), 7.34 – 7.28 (m, 4H, H14, H15), 7.19 (t, *J* = 6.0 Hz, 1H, H11), 6.49 (s br, 2H, H10), 5.87 (d, *J* = 5.5 Hz, 1H, H1'), 5.39 (d, *J* = 5.8 Hz, 1H, H12'), 5.23 (d, *J* = 5.3 Hz, 1H, H13'), 4.98 (app. q, *J* = 5.6 Hz, 1H, H2'), 4.69 (s, 2H, H6'), 4.57 – 4.49 (m, 2H, H12), 4.38 (app. q, *J* = 5.1 Hz, 1H, H3'), 4.08 – 4.05 (m, 1H, H4'), 3.87 (dd, *J* = 10.9, 3.0 Hz, 1H, H5'a), 3.77 (dd, *J* = 10.9, 4.8 Hz, 1H, H5'b); **<sup>13</sup>C NMR** (151 MHz, DMSO-*d*<sub>6</sub>) δ = 166.49 (C7'), 152.45 (C6), 151.45 (C8), 149.85 (C4), 148.85 (C2), 148.08 (C11'), 138.76 (C13), 137.24 (C9'), 131.26 (C16), 128.94 (2C, C14), 128.09 (2C, C15), 127.28 (d, *J*<sub>C-F</sub> = 23.9 Hz, C10'), 121.46 (C8'), 117.00 (C5), 87.11 (C1'), 82.73 (C4'), 72.66 (C6'), 70.89 (C5'), 70.54 (C2'), 70.17 (C3'), 44.74 (C12); **<sup>19</sup>F NMR** (471 MHz, DMSO-*d*<sub>6</sub>) δ = 68.32; **HRMS** (ESI+) *m/z* calculated for C<sub>23</sub>H<sub>24</sub><sup>35</sup>ClF<sub>7</sub>O<sub>6</sub>S (M+H)<sup>+</sup> 580.1176, found 580.1177.

**(2*R*,3*R*,4*S*,5*R*)-2-(6-amino-8-((3,4-dichlorobenzyl)amino)-9*H*-purin-9-yl)-5-(((4-(methylsulfonyl)benzyl)oxy)methyl)tetrahydrofuran-3,4-diol (134)**

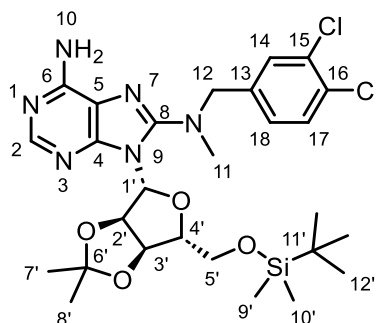


**134**

A two-neck round bottom flask heat-dried under vacuum and equipped with magnetic stirrer was charged with ((3*aR*,4*R*,6*R*,6*aR*)-6-(6-(bis((2-(trimethylsilyl)ethoxy)methyl)amino)-8-((3,4-dichlorobenzyl)((2-(trimethylsilyl)ethoxy)methyl)amino)-9*H*-purin-9-yl)-2,2-dimethyltetrahydrofuro[3,4-*d*][1,3]dioxol-4-yl)methanol **125** (208 mg, 0.24 mmol, 1 equiv.) and THF (0.48 mL, 0.5

M) under flow of nitrogen. The mixture was cooled to 0 °C and sodium hydride (11.4 mg, 60% in mineral oil, 0.29 mmol, 1.2 equiv.) was added and stirred for 15 minutes. 1-(bromomethyl)-4-methanesulfonylbenzene (119 mg, 0.48 mmol, 2 equiv.) was then added, after which the mixture was allowed to warm up to room temperature. After stirring at room temperature for 18 hours, the reaction mixture was quenched with methanol and the solvent was removed under reduced pressure. The crude mixture was eluted through a silica plug (EtOAc:cyclohexane 20:80), concentrated under reduced pressure and the crude residue was redissolved in TFA:water 5:2 (v/v) mixture (2.4 mL). After stirring at room temperature for 1 hour, the mixture was diluted with toluene (20 mL) and concentrated under reduced pressure. The crude product was purified by reverse phase column chromatography on C18 (methanol:water +0.1% formic acid 20:80 to 100% methanol gradient) then normal phase column chromatography on silica (100% CH<sub>2</sub>Cl<sub>2</sub> to methanol:CH<sub>2</sub>Cl<sub>2</sub> 15:85 gradient) to yield **134** (45 mg, 31%) as a white solid. **<sup>1</sup>H NMR** (600 MHz, DMSO-d<sub>6</sub>) δ = 7.90 (s, 1H, H2), 7.85 – 7.82 (m, 2H, H9'), 7.56 – 7.54 (m, 2H, H14, H17), 7.48 – 7.44 (m, 2H, H8'), 7.31 (dd, *J* = 8.3, 1.9 Hz, 1H, H18), 7.24 (t, *J* = 5.9 Hz, 1H, H11), 6.50 (s br, 2H, H10), 5.84 (d, *J* = 5.4 Hz, 1H, H1'), 5.39 (d, *J* = 5.8 Hz, 1H, H12'), 5.21 (d, *J* = 5.3 Hz, 1H, H13'), 4.99 (app. q, *J* = 5.5 Hz, 1H, H2'), 4.59 – 4.51 (m, 3H, H6', H12a), 4.45 (dd, *J* = 15.9, 5.7 Hz, 1H, H12b), 4.33 (app. q, *J* = 5.0 Hz, 1H, H3'), 4.06 – 4.02 (m, 1H, H4'), 3.77 (dd, *J* = 10.7, 3.2 Hz, 1H, H5'a), 3.65 (dd, *J* = 10.7, 4.9 Hz, 1H, H5'b), 3.19 (s, 3H, H11'); **<sup>13</sup>C NMR** (151 MHz, DMSO-d<sub>6</sub>) δ = 152.57 (C6), 151.23 (C8), 149.86 (C4), 149.01 (C2), 144.10 (C7'), 141.13 (C13), 139.80 (C10'), 130.81 (C16), 130.40 (C14), 129.24 (C15), 129.04 (C17), 127.68 (2C, C8'), 127.51 (C18), 126.93 (2C, C9'), 116.94 (C5), 87.10 (C1'), 82.77 (C4'), 71.43 (C6'), 70.47 (C2'), 70.42 (C5'), 70.28 (C3'), 44.30 (C12), 43.56 (C11'); **HRMS** (ESI+) *m/z* calculated for C<sub>25</sub>H<sub>27</sub><sup>35</sup>Cl<sub>2</sub>N<sub>6</sub>O<sub>6</sub>S (M+H)<sup>+</sup> 609.1084, found 609.1100.

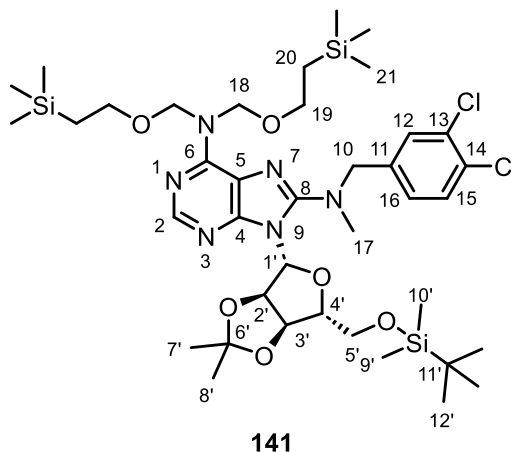
**9-((3*aR*,4*R*,6*R*,6*aR*)-6-(((*tert*-butyldimethylsilyl)oxy)methyl)-2,2-dimethyltetrahydrofuro[3,4-*d*][1,3]dioxol-4-yl)-*N*8-(3,4-dichlorobenzyl)-*N*8-methyl-9*H*-purine-6,8-diamine (**140**)**



**140**

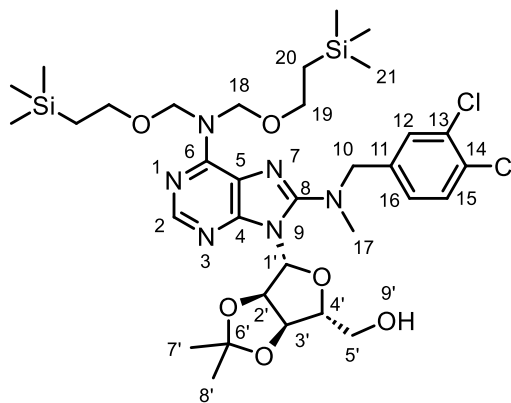
**140** was prepared following general procedure A, with 8-bromo-9-((3*aR*,4*R*,6*R*,6*aR*)-6-(((*tert*-butyldimethylsilyl)oxy)methyl)-2,2-dimethyltetrahydrofuro[3,4-*d*][1,3]dioxol-4-yl)-9*H*-purin-6-amine **95** (1.90 g, 3.80 mmol, 1 equiv.), ethanol (12.7 mL, 0.3 M) and *N*-(3,4-dichlorobenzyl)-*N*-methylamine **139** (5.77 g, 30.4 mmol, 8 equiv.). Purification by normal phase column chromatography on silica (100% CH<sub>2</sub>Cl<sub>2</sub> to methanol:CH<sub>2</sub>Cl<sub>2</sub> 10:90 gradient) then reverse phase column chromatography on C18 (acetonitrile:water +0.1% formic acid 40:60 to 100% acetonitrile gradient) yielded **140** (1.90 g, 82%) as a white solid. <sup>1</sup>H NMR (600 MHz, DMSO-*d*<sub>6</sub>) δ = 8.05 (s, 1H, H2), 7.62 (d, *J* = 8.2 Hz, 1H, H17), 7.61 (d, *J* = 1.8 Hz, 1H, H14), 7.33 (dd, *J* = 8.2, 1.8 Hz, 1H, H18), 6.99 (s, 2H, H10), 5.92 (d, *J* = 2.0 Hz, 1H, H1'), 5.63 (dd, *J* = 6.3, 2.0 Hz, 1H, H2'), 5.04 (dd, *J* = 6.3, 2.8 Hz, 1H, H3'), 4.45 (d, *J* = 15.0 Hz, 1H, H12a), 4.41 (d, *J* = 15.0 Hz, 1H, H12b), 4.13 (app. td, *J* = 6.7, 2.8 Hz, 1H, H4'), 3.82 (dd, *J* = 10.5, 6.4 Hz, 1H, H5'a), 3.69 (dd, *J* = 10.5, 7.0 Hz, 1H, H5'b), 2.84 (s, 3H, H11), 1.46 (s, 3H, H7'), 1.30 (s, 3H, H8'), 0.77 (s, 9H, H12'), -0.11 (s, 3H, H9'), -0.12 (s, 3H, H10'); <sup>13</sup>C NMR (151 MHz, DMSO-*d*<sub>6</sub>) δ = 154.33 (C6), 154.26 (C8), 150.94 (C2), 149.00 (C4), 138.32 (C13), 131.11 (C16), 130.64 (C17), 130.11 (C14), 130.03 (C15), 128.52 (C18), 116.36 (C5), 112.92 (C6'), 89.36 (C1'), 87.19 (C4'), 81.95 (C2'), 81.77 (C3'), 62.95 (C5'), 56.60 (C12), 39.93 (C11'), 26.89 (C7'), 25.68 (3C, C12'), 25.25 (C8'), 17.94 (C11'), -5.45 (C9'), -5.52 (C10'); HRMS (ESI+) *m/z* calculated for C<sub>27</sub>H<sub>39</sub><sup>35</sup>Cl<sub>2</sub>N<sub>6</sub>O<sub>4</sub>Si (M+H)<sup>+</sup> 609.2174, found 609.2170;

**9-((3*aR*,4*R*,6*R*,6*aR*)-6-(((*tert*-butyldimethylsilyl)oxy)methyl)-2,2-dimethyltetrahydrofuro[3,4-*d*][1,3]dioxol-4-yl)-*N*8-(3,4-dichlorobenzyl)-*N*8-methyl-*N*6,*N*6-bis((2-(trimethylsilyl)ethoxy)methyl)-9*H*-purine-6,8-diamine (**141**)**



**141** was prepared following general procedure B, with 9-((3*aR*,4*R*,6*R*,6*aR*)-6-(((*tert*-butyldimethylsilyl)oxy)methyl)-2,2-dimethyltetrahydrofuro[3,4-*d*][1,3]dioxol-4-yl)-*N*8-(3,4-dichlorobenzyl)-*N*8-methyl-9*H*-purine-6,8-diamine **140** (1.80 g, 2.95 mmol, 1 equiv.), CH<sub>2</sub>Cl<sub>2</sub> (9.84 mL, 0.3 M), 2-(trimethylsilyl)ethoxymethylchloride (1.57 mL, 8.89 mmol, 3 equiv.) and *N,N*-diisopropylethylamine (1.54 mL, 8.89 mmol, 3 equiv.) for 22 hours. Purification by normal phase column chromatography on silica (EtOAc:cyclohexane 1:99 to 15:85 gradient) yielded **141** (2.30 g, 90%) as a colourless oil. <sup>1</sup>H NMR (600 MHz, CD<sub>3</sub>CN) δ = 8.21 (s, 1H, H2), 7.56 (d, *J* = 2.0 Hz, 1H, H12), 7.49 (d, *J* = 8.3 Hz, 1H, H15), 7.29 (dd, *J* = 8.3, 2.0 Hz, 1H, H16), 5.99 (d, *J* = 1.9 Hz, 1H, H1'), 5.64 (dd, *J* = 6.3, 1.9 Hz, 1H, H2'), 5.42 (s br, 4H, H18), 5.11 (dd, *J* = 6.3, 2.9 Hz, 1H, H3'), 4.50 (d, *J* = 15.1 Hz, 1H, H10a), 4.44 (d, *J* = 15.1 Hz, 1H, H10b), 4.18 (app. td, *J* = 6.8, 2.9 Hz, 1H, H4'), 3.85 (dd, *J* = 10.8, 6.4 Hz, 1H, H5'a), 3.73 (dd, *J* = 10.8, 6.9 Hz, 1H, H5'b), 3.60 – 3.55 (m, 4H, H19), 2.94 (s, 3H, H17), 1.49 (s, 3H, H7'), 1.33 (s, 3H, H8'), 0.89 – 0.85 (m, 4H, H20), 0.81 (s, 9H, H12'), -0.07 (s, 18H, H21), -0.08 (s, 3H, H9'), -0.09 (s, 3H, H10'); <sup>13</sup>C NMR (151 MHz, CD<sub>3</sub>CN) δ = 155.61 (C8), 153.32 (C6), 152.42 (C4), 150.73 (C2), 139.52 (C11), 132.78 (C14), 131.61 (C13), 131.45 (C15), 131.16 (C12), 129.19 (C16), 118.70 (C5), 114.20 (C6'), 90.98 (C1'), 89.18 (C4'), 83.77 (C2'), 83.37 (C3'), 77.27 (2C, C18), 65.50 (2C, C19), 64.28 (C5'), 57.71 (C10), 40.95 (C17), 27.31 (C7'), 26.16 (3C, C12'), 25.60 (C8'), 18.90 (C11'), 18.60 (2C, C20), -1.33 (6C, C21), -5.18 (C9'), -5.22 (C10'); HRMS (ESI+) *m/z* calculated for C<sub>39</sub>H<sub>67</sub><sup>35</sup>Cl<sub>2</sub>N<sub>6</sub>O<sub>6</sub>Si<sub>3</sub> (M+H)<sup>+</sup> 869.3801, found 869.3807.

**((3*aR*,4*R*,6*R*,6*aR*)-6-(6-(bis((2-(trimethylsilyl)ethoxy)methyl)amino)-8-((3,4-dichlorobenzyl)(methyl)amino)-9*H*-purin-9-yl)-2,2-dimethyltetrahydrofuro[3,4-*d*][1,3]dioxol-4-yl)methanol (142)**

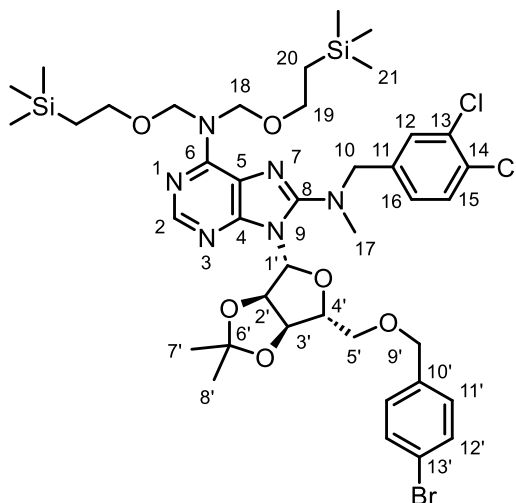


142

**142** was prepared following general procedure C, with 9-((3*aR*,4*R*,6*R*,6*aR*)-6-(((*tert*-butyldimethylsilyl)oxy)methyl)-2,2-dimethyltetrahydrofuro[3,4-*d*][1,3]dioxol-4-yl)-*N*8-(3,4-dichlorobenzyl)-*N*8-methyl-*N*6,*N*6-bis((2-(trimethylsilyl)ethoxy)methyl)-9*H*-purine-6,8-diamine **141** (2.30 g, 2.64 mmol, 1 equiv.), THF (26.4 mL, 0.1 M) and TBAF (2.91 mL, 1 M in THF, 2.91 mmol, 1.1 equiv.) for 4 hours. Purification by normal phase column chromatography on silica (EtOAc:cyclohexane 5:95 to 40:60 gradient) yielded **142** (1.15 g, 58%) as a colourless oil. <sup>1</sup>H NMR (600 MHz, CD<sub>3</sub>CN) δ = 8.19 (s, 1H, H2), 7.57 (d, *J* = 1.9 Hz, 1H, H12), 7.48 (d, *J* = 8.2 Hz, 1H, H15), 7.31 (dd, *J* = 8.2, 1.9 Hz, 1H, H16), 5.97 (d, *J* = 4.9 Hz, 1H, H1'), 5.61 (dd, *J* = 10.6, 2.2 Hz, 1H, H9'), 5.48 – 5.34 (m, 5H, H2', H18), 5.07 (dd, *J* = 6.0, 1.5 Hz, 1H, H3'), 4.47 – 4.40 (m, 2H, H10), 4.36 (app. q, *J* = 1.7 Hz, 1H, H4'), 3.77 (app. dt, *J* = 12.5, 2.3 Hz, 1H, H5'a), 3.70 – 3.65 (m, 1H, H5'b), 3.60 – 3.55 (m, 4H, H19), 2.92 (s, 3H, H17), 1.49 (s, 3H, H7'), 1.33 (s, 3H, H8'), 0.89 – 0.86 (m, 4H, H20), -0.07 (s, 18H, H21); <sup>13</sup>C NMR (151 MHz, CD<sub>3</sub>CN) δ = 155.31 (C8), 153.69 (C6), 152.05 (C4), 150.47 (C2), 139.48 (C11), 132.80 (C14), 131.58 (C13), 131.44 (C15), 131.07 (C12), 129.13 (C16), 119.16 (C5), 114.58 (C6'), 92.55 (C1'), 86.70 (C4'), 82.99 (C2'), 82.73 (C3'), 77.24 (2C, C18), 65.60 (2C, C19), 63.76 (C5'), 57.88 (C10), 41.64 (C17), 27.65 (C7'), 25.53 (C8'), 18.58 (2C, C20), -1.37 (6C, C21); HRMS (ESI+) *m/z* calculated for C<sub>33</sub>H<sub>53</sub><sup>35</sup>Cl<sub>2</sub>N<sub>6</sub>O<sub>6</sub>Si<sub>2</sub> (M+H)<sup>+</sup> 755.2937, found 755.2940.



**9-((3*aR*,4*R*,6*R*,6*aR*)-6-(((4-bromobenzyl)oxy)methyl)-2,2-dimethyltetrahydrofuro[3,4-*d*][1,3]dioxol-4-yl)-*N*8-(3,4-dichlorobenzyl)-*N*8-methyl-*N*6,*N*6-bis((2-(trimethylsilyl)ethoxy)methyl)-9*H*-purine-6,8-diamine (**143**)**

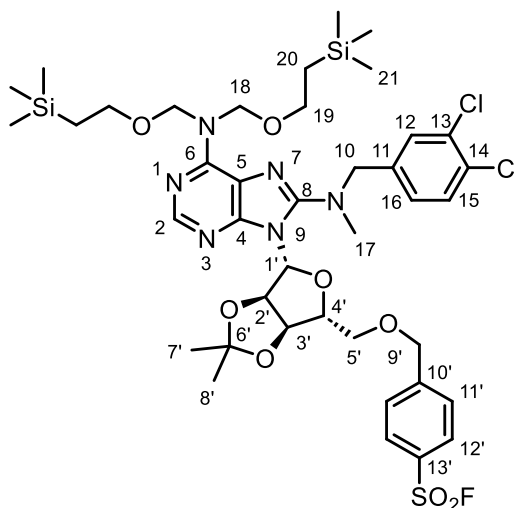


**143**

**143** was prepared following general procedure D, with ((3*aR*,4*R*,6*R*,6*aR*)-6-(6-(bis((2-(trimethylsilyl)ethoxy)methyl)amino)-8-((3,4-dichlorobenzyl)(methyl)amino)-9*H*-purin-9-yl)-2,2-dimethyltetrahydrofuro[3,4-*d*][1,3]dioxol-4-yl)methanol **142** (1.10 g, 1.46 mmol, 1 equiv.), THF (2.91 mL, 0.5 M), sodium hydride (70.0 mg, 60% in mineral oil, 1.75 mmol, 1.2 equiv.) and 4-bromobenzyl bromide (727 mg, 2.91 mmol, 2 equiv.). Purification by normal phase column chromatography on silica (EtOAc:cyclohexane 1:99 to 25:75 gradient) yielded **143** (1.24 g, 92%) as a colourless oil. <sup>1</sup>H NMR (600 MHz, CD<sub>3</sub>CN) δ = 8.11 (s, 1H, H2), 7.55 (d, *J* = 1.9 Hz, 1H, H12), 7.46 (d, *J* = 8.3, 1H, H15), 7.39 – 7.36 (m, 1H, H12'), 7.28 (dd, *J* = 8.3, 1.9 Hz, 1H, H16), 7.12 – 7.09 (m, 2H, H11'), 5.98 (d, *J* = 2.0 Hz, 1H, H1'), 5.60 (dd, *J* = 6.3, 2.0 Hz, 1H, H2'), 5.48 – 5.35 (s br, 4H, H18), 5.10 (dd, *J* = 6.3, 3.1 Hz, 1H, H3'), 5.40 (d, *J* = 15.1 Hz, 1H, H10a), 4.45 – 4.40 (m, 2H, H9'a, H10b), 4.37 (d, *J* = 12.5 Hz, 1H, H9'b), 4.33 – 4.29 (m, 1H, H4'), 3.70 (dd, *J* = 10.4, 5.6 Hz, 1H, H5'a), 3.63 (dd, *J* = 10.4, 7.3 Hz, 1H, H5'b), 3.60 – 3.56 (m, 4H, H19), 2.93 (s, 3H, H17), 1.49 (s, 3H, H7'), 1.32 (s, 3H, H8'), 0.89 – 0.85 (m, 4H, H20), -0.07 (s, 18H, H21); <sup>13</sup>C NMR (151 MHz, CD<sub>3</sub>CN) δ = 155.49 (C8), 153.26 (C6), 152.41 (C4), 150.67 (C2), 139.44 (C11), 138.78 (C10'), 132.77 (C14), 132.09 (2C, C12'), 131.62 (C13), 131.44 (C15), 131.18 (C12), 130.36 (2C, C11'), 129.22 (C16), 121.68 (C13'), 118.7 (C5), 114.45 (C6'), 90.83 (C1'), 87.27 (C4'), 83.68 (C2'), 83.39 (C3'), 77.38 (2C, C18), 72.74 (C9'), 70.92 (C5'), 65.52 (2C, C19), 57.68 (C10), 40.94 (C17), 27.30 (C7'),

25.56 (C8'), 18.59 (2C, C20), -1.36 (6C, C21); **HRMS** (ESI+)  $m/z$  calculated for  $C_{40}H_{58}^{79}Br^{35}Cl_2N_6O_6Si_2$  (M+H)<sup>+</sup> 923.2511, found 923.2521;  $[\alpha]_D^{25} = -9^\circ$  (c = 0.5, CHCl<sub>3</sub>).

**4-(((3a*R*,4*R*,6*R*,6a*R*)-6-(6-(bis((2-(trimethylsilyl)ethoxy)methyl)amino)-8-((3,4-dichlorobenzyl)(methyl)amino)-9*H*-purin-9-yl)-2,2-dimethyltetrahydrofuro[3,4-*d*][1,3]dioxol-4-yl)methoxy)methyl)benzenesulfonyl fluoride (144)**

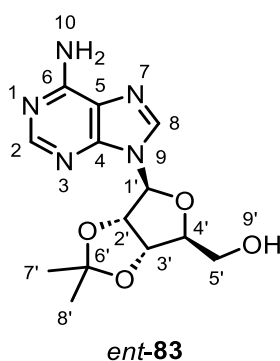


**144**

**144** was prepared following general procedure E, with 9-((3a*R*,4*R*,6*R*,6a*R*)-6-(((4-bromobenzyl)oxy)methyl)-2,2-dimethyltetrahydrofuro[3,4-*d*][1,3]dioxol-4-yl)-*N*8-(3,4-dichlorobenzyl)-*N*8-methyl-*N*6,*N*6-bis((2-(trimethylsilyl)ethoxy)methyl)-9*H*-purine-6,8-diamine **143** (800 mg, 0.87 mmol, 1 equiv.), isopropanol (3.20 mL, 0.27 M), DABSO (125 mg, 0.52 mmol, 0.6 equiv.), PdCl<sub>2</sub>(AmPhos)<sub>2</sub> (30.6 mg, 0.04 mmol, 5 mol%), triethylamine (0.36 mL, 2.59 mmol, 3 equiv.) and NFSI (409 mg, 1.30 mmol, 1.5 equiv.). Purification by normal phase column chromatography on silica (EtOAc:cyclohexane 1:99 to 30:70 gradient) yielded **144** (252 mg, 31%) as a pale yellow oil. **<sup>1</sup>H NMR** (600 MHz, CD<sub>3</sub>CN)  $\delta$  = 8.12 (s, 1H, H2), 7.93 – 7.90 (m, 2H, H12'), 7.55 – 7.51 (m, 3H, H11', H12), 7.45 (d,  $J$  = 8.2 Hz, 1H, H15), 7.28 (dd,  $J$  = 8.2, 2.0 Hz, 1H, H16), 6.00 (d,  $J$  = 2.0 Hz, 1H, H1'), 5.62 (dd,  $J$  = 6.3, 2.0 Hz, 1H, H2'), 5.40 (s br, 4H, H18), 5.15 (dd,  $J$  = 6.3, 3.1 Hz, 1H, H3'), 4.62 (d,  $J$  = 13.8 Hz, 1H, H9'a), 4.57 (d,  $J$  = 13.8 Hz, 1H, H9'b), 4.52 (d,  $J$  = 15.2 Hz, 1H, H10a), 4.43 (d,  $J$  = 15.2 Hz, 1H, H10b), 4.38 – 4.34 (m, 1H, H4'), 3.80 (dd,  $J$  = 10.4, 5.4 Hz, 1H, H5'a), 3.73 (dd,  $J$  = 10.4, 7.2 Hz, 1H, H5'b), 3.59 – 3.55 (m, 4H, H19), 2.93 (s, 3H, H17), 1.51 (s, 3H, H7'), 1.33 (s, 3H, H8'), 0.88 – 0.84 (m, 4H,

H<sub>2</sub>O), -0.08 (s, 18H, H<sub>2</sub>1); <sup>13</sup>C NMR (151 MHz, CD<sub>3</sub>CN) δ = 155.48 (C<sub>8</sub>), 153.27 (C<sub>6</sub>), 152.45 (C<sub>4</sub>), 150.71 (C<sub>2</sub>), 148.97 (C<sub>10'</sub>), 139.40 (C<sub>11</sub>), 132.77 (C<sub>14</sub>), 131.90 (d, *J*<sub>C-F</sub> = 24.2 Hz, C<sub>13'</sub>), 131.62 (C<sub>13</sub>), 131.44 (C<sub>15</sub>), 131.16 (C<sub>12</sub>), 129.29 (2C, C<sub>12'</sub>), 129.21 (C<sub>16</sub>), 129.10 (2C, C<sub>11'</sub>), 118.72 (C<sub>5</sub>), 114.55 (C<sub>6'</sub>), 90.84 (C<sub>1'</sub>), 87.12 (C<sub>4'</sub>), 83.65 (C<sub>2'</sub>), 83.24 (C<sub>3'</sub>), 77.40 (2C, C<sub>18</sub>), 72.38 (C<sub>9'</sub>), 71.52 (C<sub>5'</sub>), 65.50 (2C, C<sub>19</sub>), 57.67 (C<sub>10</sub>), 40.96 (C<sub>17</sub>), 27.32 (C<sub>7'</sub>), 25.57 (C<sub>8'</sub>), 18.57 (2C, C<sub>20</sub>), -1.38 (6C, C<sub>21</sub>); <sup>19</sup>F NMR (471 MHz, CD<sub>3</sub>CN) δ = 65.03; HRMS (ESI+) *m/z* calculated for C<sub>40</sub>H<sub>58</sub><sup>35</sup>Cl<sub>2</sub>FN<sub>6</sub>O<sub>8</sub>SSi<sub>2</sub> (M+H)<sup>+</sup> 927.2931, found 927.2939; [α]<sub>D</sub><sup>25</sup> = -30 ° (c = 0.5, CHCl<sub>3</sub>).

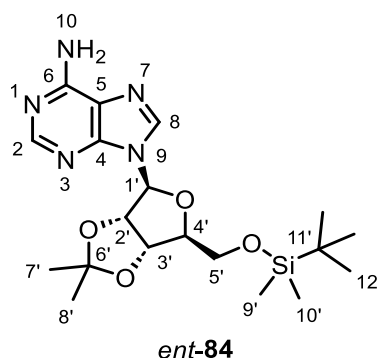
**((3a*S*,4*S*,6*S*,6a*S*)-6-(6-amino-9*H*-purin-9-yl)-2,2-dimethyltetrahydrofuro[3,4-*d*][1,3]dioxol-4-yl)methanol (*ent*-83)**



A two-neck round bottom flask equipped with magnetic stirrer was charged with L-adenosine *ent*-35 (2.24 g, 8.37 mmol, 1 equiv.), acetone (419 mL, 0.02 M), *p*-toluenesulfonic acid monohydrate (15.9 g, 83.7 mmol, 10 equiv.) under flow of nitrogen. After stirring at room temperature for 18 hours, the reaction mixture was neutralised with sat. NaHCO<sub>3</sub> solution (250 mL) and the acetone was removed under reduced pressure. The aqueous phase was extracted with EtOAc (3 × 100 mL) and the resultant combined organic layers were washed with water (100 mL), brine (100 mL), dried over MgSO<sub>4</sub>, filtered, and concentrated under reduced pressure. The crude product was purified by normal phase column chromatography on silica (100% CH<sub>2</sub>Cl<sub>2</sub> to methanol:CH<sub>2</sub>Cl<sub>2</sub> 15:85 gradient) to yield *ent*-83 (1.05 g, 41%) as a white solid. <sup>1</sup>H NMR (600 MHz, DMSO-*d*<sub>6</sub>) δ = 8.34 (s, 1H, H<sub>8</sub>), 8.15 (s, 1H, H<sub>2</sub>), 7.34 (s, 2H, H<sub>10</sub>), 6.12 (d, *J* = 3.1 Hz, 1H, H<sub>1'</sub>), 5.34 (dd, *J* = 6.2, 3.1 Hz, 1H, H<sub>2'</sub>), 5.23 (app. t, *J* = 5.3 Hz, 1H, H<sub>9'</sub>), 4.96 (dd, *J* = 6.2, 2.5 Hz, 1H, H<sub>3'</sub>), 4.23 – 4.19 (app. td, *J* = 4.9, 2.5 Hz, 1H, H<sub>4'</sub>), 3.59 – 3.49 (m, 2H, H<sub>5'</sub>), 1.54 (s, 3H, H<sub>7'</sub>), 1.32 (s, 3H, H<sub>8'</sub>); <sup>13</sup>C NMR (151 MHz, DMSO-*d*<sub>6</sub>) δ = 156.15 (C<sub>6</sub>), 152.64 (C<sub>2</sub>), 148.82 (C<sub>4</sub>), 139.69 (C<sub>8</sub>), 119.10 (C<sub>5</sub>), 113.05 (C<sub>6'</sub>), 89.61 (C<sub>1'</sub>),

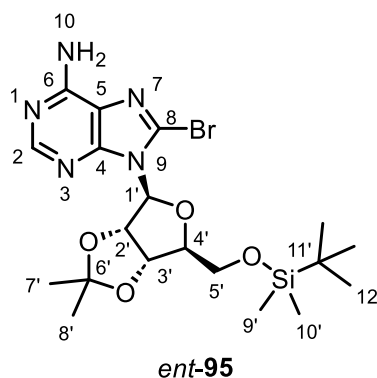
86.35 (C4'), 83.22 (C2'), 81.36 (C3'), 61.58 (C5'), 27.09 (C7'), 25.20 (C8'); **HRMS** (ESI+)  $m/z$  calculated for  $C_{13}H_{18}N_5O_4$  (M+H)<sup>+</sup> 308.1353, found 308.1358.

**9-((3a*S*,4*S*,6*S*,6a*S*)-6-(((*tert*-butyldimethylsilyl)oxy)methyl)-2,2-dimethyltetrahydrofuro[3,4-*d*][1,3]dioxol-4-yl)-9*H*-purin-6-amine (*ent*-**84**)**



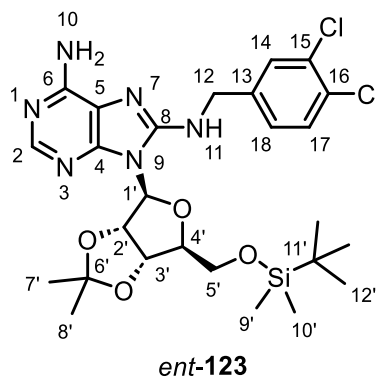
A two-neck round bottom flask equipped with magnetic stirrer was charged with ((3a*S*,4*S*,6*S*,6a*S*)-6-(6-amino-9*H*-purin-9-yl)-2,2-dimethyltetrahydrofuro[3,4-*d*][1,3]dioxol-4-yl)methanol *ent*-**83** (1.04 g, 3.38 mmol, 1 equiv.), DMF (9.67 mL, 0.35 M), *tert*-butyldimethylsilyl chloride (612 mg, 4.06 mmol, 1.2 equiv.), and imidazole (461 mg, 6.77 mmol, 2 equiv.) under flow of nitrogen. After stirring for at room temperature for 16 hours, the reaction mixture was diluted with water (60 mL) and EtOAc (60 mL) and the phases were separated. The aqueous phase was extracted with EtOAc (2 × 60 mL) and the resultant combined organic layers were washed with LiCl 10% (w/v) solution (3 × 100 mL), dried over MgSO<sub>4</sub>, filtered, and concentrated under reduced pressure. The crude product was purified by normal phase column chromatography on silica (100% CH<sub>2</sub>Cl<sub>2</sub> to methanol:CH<sub>2</sub>Cl<sub>2</sub> 10:90 gradient) to yield *ent*-**84** (1.27 g, 89%) as a white solid. **<sup>1</sup>H NMR** (600 MHz, CDCl<sub>3</sub>) δ = 8.37 (s, 1H, H8), 8.11 (s, 1H, H2), 6.31 (s br, 2H, H10), 6.17 (d, *J* = 2.5 Hz, 1H, H1'), 5.23 (dd, *J* = 6.2, 2.5 Hz, 1H, H2'), 4.93 (dd, *J* = 6.2, 2.3 Hz, 1H, H3'), 4.47 – 4.44 (m, 1H, H4'), 3.89 (dd, *J* = 11.3, 3.7 Hz, 1H, H5'a), 3.77 (dd, *J* = 11.3, 3.9 Hz, 1H, H5'b), 1.63 (s, 3H, H7'), 1.40 (s, 3H, H8'), 0.83 (s, 9H, H12'), 0.02 – 0.00 (m, 6H, H9', H10'); **<sup>13</sup>C NMR** (151 MHz, CDCl<sub>3</sub>) δ = 154.59 (C6), 151.23 (C2), 149.33 (C4), 140.00 (C8), 120.05 (C5), 114.29 (C6'), 92.00 (C1'), 87.64 (C4'), 85.31 (C2'), 81.64 (C3'), 63.74 (C5'), 27.36 (C7'), 25.97 (3C, C12'), 25.50 (C8'), 18.45 (C11'), -5.33 (C9'), -5.41 (C10'); **HRMS** (ESI+)  $m/z$  calculated for  $C_{19}H_{32}N_5O_4Si$  (M+H)<sup>+</sup> 422.2218, found 422.2214.

**8-bromo-9-((3*aS*,4*S*,6*S*,6*aS*)-6-(((*tert*-butyldimethylsilyl)oxy)methyl)-2,2-dimethyltetrahydrofuro[3,4-*d*][1,3]dioxol-4-yl)-9*H*-purin-6-amine (*ent*-95)**



A two-neck round bottom flask equipped with magnetic stirrer was charged with 9-((3*aS*,4*S*,6*S*,6*aS*)-6-(((*tert*-butyldimethylsilyl)oxy)methyl)-2,2-dimethyltetrahydrofuro[3,4-*d*][1,3]dioxol-4-yl)-9*H*-purin-6-amine *ent*-84 (1.22 g, 2.89 mmol, 1 equiv.) and 1,4-dioxane (11.6 mL, 0.25 M) under flow of nitrogen. A separate flask equipped with magnetic stirrer was charged with K<sub>2</sub>HPO<sub>4</sub> (1.51 g, 8.68 mmol, 3 equiv.), water (11.6 mL), and bromine (0.37 mL, 7.23 mmol, 2.5 equiv.), and the resultant solution was slowly transferred *via* syringe into the first mixture. After stirring at room temperature for 18 hours, the reaction mixture was quenched with sat. Na<sub>2</sub>S<sub>2</sub>O<sub>3</sub> solution (20 mL), diluted with EtOAc (50 mL) and the phases were separated. The aqueous phase was extracted with EtOAc (2 × 50 mL) and the resultant combined organic layers were washed with brine (50 mL), dried over MgSO<sub>4</sub>, filtered, and concentrated under reduced pressure. The crude product was purified by normal phase column chromatography on silica 100% CH<sub>2</sub>Cl<sub>2</sub> to methanol:CH<sub>2</sub>Cl<sub>2</sub> 10:90 gradient) to yield *ent*-95 (1.17 g, 81%) as a brown foam. <sup>1</sup>H NMR (600 MHz, CDCl<sub>3</sub>) δ = 8.29 (s, 1H, H2), 6.60 (s br, 2H, H10), 6.18 (d, *J* = 2.2 Hz, 1H, H1'), 5.71 (dd, *J* = 6.3, 2.2 Hz, 1H, H2'), 5.11 (d, *J* = 6.3, 3.5 Hz, 1H, H3'), 4.28 (app. td, *J* = 6.2, 3.5 Hz, 1H, H4'), 3.75 (dd, *J* = 10.8 Hz, 6.4 Hz, 1H, H5'a), 3.66 (dd, *J* = 10.8, 6.2 Hz, 1H, H5'b), 1.62 (s, 3H, H7'), 1.40 (s, 3H, H8'), 0.84 (s, 9H, H12'), -0.03 (s, 3H, H9'), -0.04 (s, 3H, H10'); <sup>13</sup>C NMR (151 MHz, CDCl<sub>3</sub>) δ = 152.16 (C6), 150.15 (C4), 148.12 (C2), 129.76 (C8), 120.08 (C5), 114.68 (C6'), 91.85 (C1'), 88.04 (C4'), 82.89 (C1'), 81.76 (C2'), 63.09 (C5'), 27.38 (C7'), 25.98 (3C, C12'), 25.61 (C8'), 18.51 (C11'), -5.23 (C10'), -5.25 (C11'); HRMS (ESI+) *m/z* calculated for C<sub>19</sub>H<sub>31</sub><sup>79</sup>BrN<sub>5</sub>O<sub>4</sub>Si (M+H)<sup>+</sup> 500.1323, found 500.1335.

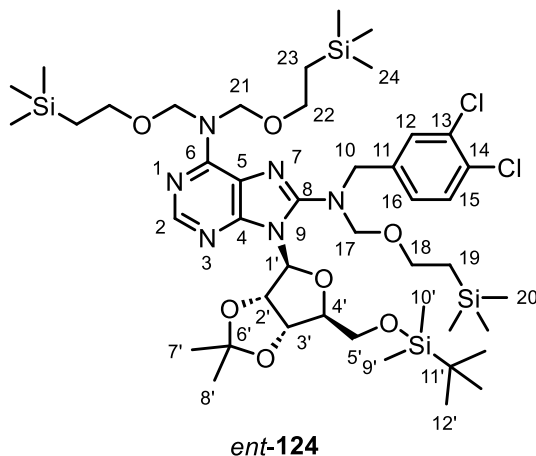
**9-((3a*S*,4*S*,6*S*,6a*S*)-6-(((*tert*-butyldimethylsilyl)oxy)methyl)-2,2-dimethyltetrahydrofuro[3,4-*d*][1,3]dioxol-4-yl)-*N*8-(3,4-dichlorobenzyl)-9*H*-purine-6,8-diamine (*ent*-123)**



*ent*-123 was prepared following general procedure A, with 8-bromo-9-((3a*S*,4*S*,6*S*,6a*S*)-6-(((*tert*-butyldimethylsilyl)oxy)methyl)-2,2-dimethyltetrahydrofuro[3,4-*d*][1,3]dioxol-4-yl)-9*H*-purin-6-amine *ent*-95 (1.15 g, 2.30 mmol, 1 equiv.), ethanol (7.66 mL, 0.3 M) and 3,4-dichlorobenzylamine (2.45 mL, 18.4 mmol, 8 equiv.). Purification by normal phase column chromatography on silica (100% CH<sub>2</sub>Cl<sub>2</sub> to methanol:CH<sub>2</sub>Cl<sub>2</sub> 15:85 gradient) yielded *ent*-123 (1.26 g, 92%) as an orange foam. <sup>1</sup>H NMR (600 MHz, CDCl<sub>3</sub>) δ = 8.15 (s, 1H, H2), 7.42 – 7.38 (m, 2H, H14, H17), 7.18 (app. d, *J* = 8.3 Hz, 1H, H18), 6.72 (s br, 2H, H10), 6.40 (s br, 1H, H11), 6.15 (d, *J* = 4.0 Hz, 1H, H1'), 5.32 (dd, *J* = 6.4, 4.0 Hz, 1H, H2'), 4.89 (d, *J* = 6.4, 3.1 Hz, 1H, H3'), 4.73 (dd, *J* = 16.0, 7.2 Hz, 1H, H12a), 4.59 (dd, *J* = 16.0, 4.6 Hz, 1H, H12b), 4.34 – 4.31 (m 1H, H4'), 3.91 (dd, *J* = 11.6, 2.8 Hz, 1H, H5'a), 3.82 (dd, *J* = 11.6, 2.9 Hz, 1H, H5'b), 1.64 (s, 3H, H7'), 1.40 (s, 3H, H8'), 0.83 (s, 9H, H12'), 0.01 – 0.00 (m, 6H, H9', H10'); <sup>13</sup>C NMR (151 MHz, CDCl<sub>3</sub>) δ = 152.48 (C8), 149.29 (C4), 148.93 (C2), 138.37 (C13), 132.98 (C16), 131.76 (C15), 130.84 (C17), 128.99 (C14), 126.48 (C18), 115.36 (C6'), 89.70 (C1'), 85.56 (C4'), 82.44 (C2'), 80.01 (C3'), 63.06 (C5'), 45.66 (C12), 27.43 (C7'), 26.05 (3C, C12'), 25.54 (C8'), 18.80 (C11'), -5.04 (C9'), -5.30 (C10');\* HRMS (ESI+) *m/z* calculated for C<sub>26</sub>H<sub>37</sub><sup>35</sup>Cl<sub>2</sub>N<sub>6</sub>O<sub>4</sub>Si (M+H)<sup>+</sup> 595.2017, found 595.2029.

\*C5 and C6 not observed in spectrum.

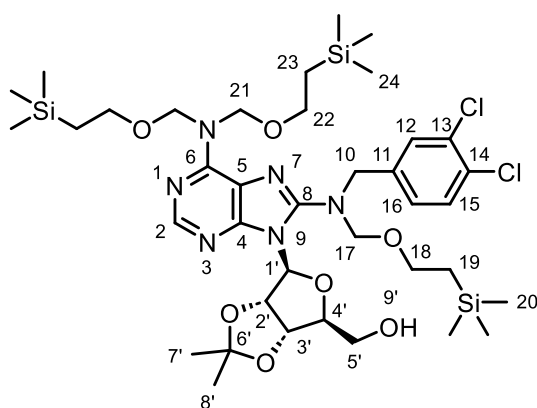
**9-((3a*S*,4*S*,6*S*,6a*S*)-6-(((*tert*-butyldimethylsilyl)oxy)methyl)-2,2-dimethyltetrahydrofuro[3,4-*d*][1,3]dioxol-4-yl)-*N*8-(3,4-dichlorobenzyl)-*N*6,*N*6,*N*8-tris((2-(trimethylsilyl)ethoxy)methyl)-9*H*-purine-6,8-diamine (*ent*-124)**



*ent*-124 was prepared following general procedure B, with 9-((3a*S*,4*S*,6*S*,6a*S*)-6-(((*tert*-butyldimethylsilyl)oxy)methyl)-2,2-dimethyltetrahydrofuro[3,4-*d*][1,3]dioxol-4-yl)-*N*8-(3,4-dichlorobenzyl)-9*H*-purine-6,8-diamine *ent*-123 (1.26 g, 2.12 mmol, 1 equiv.), CH<sub>2</sub>Cl<sub>2</sub> (7.05 mL, 0.3 M), 2-(trimethylsilyl)ethoxymethylchloride (1.68 mL, 9.52 mmol, 4.5 equiv.) and *N,N*-Diisopropylethylamine (1.66 mL, 9.52 mmol, 4.5 equiv.) for 18 hours. Purification by normal phase column chromatography on silica (EtOAc:cyclohexane 1:99 to 10:90 gradient) yielded *ent*-124 (1.33 g, 64%) as a yellow oil. <sup>1</sup>H NMR (600 MHz, CD<sub>3</sub>CN) δ = 8.21 (s, 1H, H2), 7.57 (d, *J* = 2.0 Hz, 1H, H12), 7.43 (d, *J* = 8.2 Hz, 1H, H15), 7.31 (dd, *J* = 8.2, 2.0 Hz, 1H, H16), 6.09 (d, *J* = 1.8 Hz, 1H, H1'), 5.62 (dd, *J* = 6.3, 1.8 Hz, 1H, H2'), 5.54 – 5.27 (m, 4H, H21), 5.13 (dd, *J* = 6.3, 3.0 Hz, 1H, H3'), 4.81 (d, *J* = 10.4 Hz, 1H, H17a), 4.77 – 4.72 (m, 2H, H10a, H17b), 4.58 (d, *J* = 14.9 Hz, 1H, H10b), 4.19 (app. td, *J* = 6.8, 3.0 Hz, 1H, H4'), 3.85 (dd, *J* = 10.7, 7.0 Hz, 1H, H5'a), 3.71 (dd, *J* = 10.7, 6.5 Hz, 1H, H5'b), 3.57 – 3.53 (m, 4H, H22), 3.52 – 3.48 (m, 2H, H18), 1.54 (s, 3H, H7'), 1.33 (s, 3H, H8'), 0.88 – 0.84 (m, 6H, H19, H23), 0.83 (s, 9H, H12'), -0.05 – -0.09 (m, 33H, H9', H10', H20, H24); <sup>13</sup>C NMR (151 MHz, CD<sub>3</sub>CN) δ = 153.48 (C6), 153.25 (C8), 152.24 (C4), 150.88 (C2), 140.14 (C11), 132.60 (C14), 131.43 (C13), 131.39 (C12), 131.27 (C15), 129.40 (C16), 118.65 (C5), 114.24 (C6'), 90.86 (C1'), 89.08 (C4'), 83.80 (C2'), 83.45 (C17), 83.39 (C3'), 77.14 (2C, C21), 66.55 (C18), 65.58 (2C, C22), 64.25 (C5'), 53.41 (C10), 27.45 (C7'), 26.19 (3C, C12'), 25.58 (C8'), 18.91 (C11'), 18.61 (2C, C23), 18.58 (C19), -1.33 (6C, C24), -1.36 (3C,

C20), -5.10 (C9'), -5.19 (C10'); **HRMS** (ESI+)  $m/z$  calculated for  $C_{44}H_{79}^{35}Cl_2N_6O_7Si_4$  (M+H)<sup>+</sup> 985.4459, found 985.4464.

**((3a*S*,4*S*,6*S*,6a*S*)-6-(6-(bis((2-(trimethylsilyl)ethoxy)methyl)amino)-8-((3,4-dichlorobenzyl)((2-(trimethylsilyl)ethoxy)methyl)amino)-9*H*-purin-9-yl)-2,2-dimethyltetrahydrofuro[3,4-*d*][1,3]dioxol-4-yl)methanol (*ent*-125)**



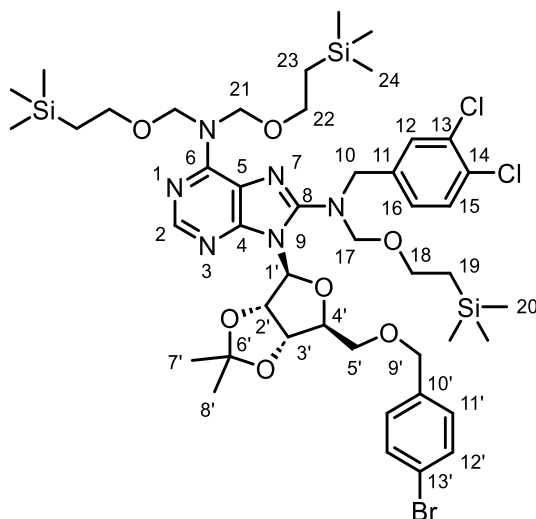
*ent*-125

*ent*-125 was prepared following general procedure C, with 9-((3a*S*,4*S*,6*S*,6a*S*)-6-(((*tert*-butyldimethylsilyl)oxy)methyl)-2,2-dimethyltetrahydrofuro[3,4-*d*][1,3]dioxol-4-yl)-*N*8-(3,4-dichlorobenzyl)-*N*6,*N*6,*N*8-tris((2-(trimethylsilyl)ethoxy)methyl)-9*H*-purine-6,8-diamine *ent*-124 (1.33 g, 1.35 mmol, 1 equiv.), THF (13.5 mL, 0.1 M) and TBAF (1.48 mL, 1 M in THF, 1.48 mmol, 1.1 equiv.) for 18 hours. Purification by normal phase column chromatography on silica (EtOAc:cyclohexane 5:95 to 30:70 gradient) yielded *ent*-125 (743 mg, 63%) as a yellow oil. **<sup>1</sup>H NMR** (600 MHz, CD<sub>3</sub>CN)  $\delta$  = 8.19 (s, 1H, H2), 7.57 (d,  $J$  = 1.9 Hz, 1H, H12), 7.43 (d,  $J$  = 8.3 Hz, 1H, H15), 7.32 (dd,  $J$  = 8.3, 1.9 Hz, 1H, H16), 6.04 (d,  $J$  = 4.9 Hz, 1H, H1'), 5.47 (dd,  $J$  = 10.7, 2.2 Hz, 1H, H9'), 5.40 (s br, 4H, H21), 5.35 (app. t,  $J$  = 5.3 Hz, 1H, H2'), 5.07 (dd,  $J$  = 6.0, 1.5 Hz, 1H, H3'), 4.80 (d,  $J$  = 10.6 Hz, 1H, H17a), 4.71 (d,  $J$  = 10.6 Hz, 1H, H17b), 4.68 (d,  $J$  = 14.9 Hz, 1H, H10a), 4.63 (d,  $J$  = 14.9 Hz, 1H, H10b), 4.39 – 4.36 (m, 1H, H4'), 3.77 (app. dt,  $J$  = 12.4, 2.5 Hz, 1H, H5'a), 3.71 – 3.65 (m, 1H, H5'b), 3.57 – 3.53 (m, 4H, H22), 3.52 – 3.47 (m, 2H, H18), 1.61 (s, 3H, H7'), 1.35 (s, 3H, H8'), 0.88 – 0.83 (m, 6H, H19, H23), -0.07 (s, 18H, H24), -0.08 (s, 9H, H20); **<sup>13</sup>C NMR** (151 MHz, CD<sub>3</sub>CN)  $\delta$  = 153.89 (C6), 152.85 (C8), 151.85 (C4), 150.70 (C2), 140.11 (C11), 132.65 (C14), 131.45 (C13), 131.28 (C15), 131.22 (C12), 129.30 (C16), 119.13 (C5), 114.65 (C6'), 92.49 (C1'), 86.70 (C4'), 84.26 (C17), 82.83 (C2'), 82.76 (C3'), 77.11 (2C, C21), 66.89 (C18), 65.69 (2C, C22), 63.78



(C5'), 53.29 (C10), 27.86 (C7'), 25.62 (C8'), 18.62 (2C, C23), 18.43 (C19), -1.33 (6C, C24), -1.40 (3C, C20); **HRMS** (ESI+)  $m/z$  calculated for  $C_{38}H_{65}^{35}Cl_2N_6O_7Si_3$  (M+H)<sup>+</sup> 871.3594, found 871.3596;  $[\alpha]_D^{25} = +12^\circ$  ( $c = 0.5$ ,  $CHCl_3$ ).

**9-((3a*S*,4*S*,6*S*,6a*S*)-6-(((4-bromobenzyl)oxy)methyl)-2,2-dimethyltetrahydrofuro[3,4-*d*][1,3]dioxol-4-yl)-*N*8-(3,4-dichlorobenzyl)-*N*6,*N*6,*N*8-tris((2-(trimethylsilyl)ethoxy)methyl)-9*H*-purine-6,8-diamine (*ent*-126)**

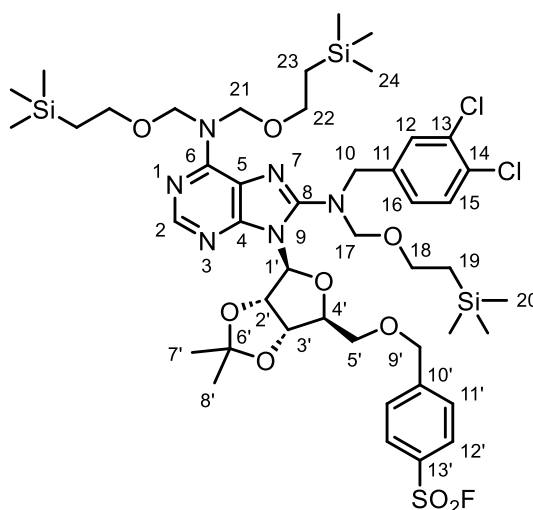


*ent*-126

*ent*-126 was prepared following general procedure D, with ((3a*S*,4*S*,6*S*,6a*S*)-6-(6-(bis((2-(trimethylsilyl)ethoxy)methyl)amino)-8-((3,4-dichlorobenzyl)((2-(trimethylsilyl)ethoxy)methyl)amino)-9*H*-purin-9-yl)-2,2-dimethyltetrahydrofuro[3,4-*d*][1,3]dioxol-4-yl)methanol *ent*-125 (660 mg, 0.76 mmol, 1 equiv.), THF (1.51 mL, 0.5 M), sodium hydride (36.3 mg, 60% in mineral oil, 0.91 mmol, 1.2 equiv.) and 4-bromobenzyl bromide (378 mg, 1.51 mmol, 2 equiv.). Purification by normal phase column chromatography on silica (EtOAc:cyclohexane 5:95 to 20:80 gradient) yielded *ent*-126 (780 mg, 99%) as a pale yellow oil. **<sup>1</sup>H NMR** (600 MHz,  $CD_3CN$ )  $\delta = 8.11$  (s, 1H, H2), 7.57 (d,  $J = 1.7$  Hz, 1H, H12), 7.43 (d,  $J = 8.3$  Hz, 1H, H15), 7.41 – 7.37 (m, 2H, H12'), 7.31 (dd,  $J = 8.3, 1.7$  Hz, 1H, H16), 7.13 – 7.10 (m, 2H, H11'), 6.09 (d,  $J = 1.8$  Hz, 1H, H1'), 5.58 (dd,  $J = 6.4, 1.8$  Hz, 1H, H2'), 5.54 – 5.27 (m, 4H, H21), 5.12 (dd,  $J = 6.4, 3.3$  Hz, 1H, H3'), 4.81 (d,  $J = 10.4$  Hz, 1H, 17a), 4.75 (d,  $J = 14.8$  Hz, 1H, H10a), 4.72 (d,  $J = 10.4$  Hz, 1H, H17b), 4.58 (d,  $J = 14.8$  Hz, 1H, H10b), 4.44 – 4.37 (m, 2H, H9'), 4.33 (app. td,  $J = 6.4, 3.3$  Hz, 1H, H4'), 3.69 (dd,  $J = 10.2, 5.8$  Hz, 1H, H5'a), 3.61 (dd,  $J = 10.2, 7.0$  Hz, 1H, H5'b), 3.58 – 3.54 (m, 4H, H22), 3.51 – 3.47 (m, 2H, H18),

1.54 (s, 3H, H7'), 1.32 (s, 3H, H8'), 0.89 – 0.82 (m, 6H, H19, H23), -0.08 (s, 18H, H24), -0.09 (s, 9H, H20); <sup>13</sup>C NMR (151 MHz, CD<sub>3</sub>CN) δ = 153.44 (C6), 153.14(C8), 152.23 (C4), 150.84 (C2), 140.12 (C11), 138.79 (C10'), 132.61 (C14), 132.12 (2C, C12'), 131.44 (C13), 131.38 (C12), 131.28 (C15), 130.33 (2C, C11'), 129.40 (C16), 121.66 (C13'), 118.65 (C5), 114.49 (C6'), 90.68 (C1'), 87.28 (C4'), 83.72 (C2'), 83.55 (C17), 83.40 (C3'), 77.30 (2C, C21), 72.75 (C9'), 70.92 (C5'), 66.58 (C18), 65.60 (2C, C22), 53.45 (C10), 27.44 (C7'), 25.55 (C8'), 18.61 (2C, C23), 18.48 (C19), -1.34 (6C, C24), -1.38 (3C, C20); HRMS (ESI+) m/z calculated for C<sub>45</sub>H<sub>70</sub><sup>79</sup>Br<sup>35</sup>Cl<sub>2</sub>N<sub>6</sub>O<sub>7</sub>Si<sub>3</sub> (M+H)<sup>+</sup> 1039.3169, found 1039.3187. [α]<sub>D</sub><sup>25</sup> = +26 ° (c = 0.5, CHCl<sub>3</sub>).

**4-(((3a*S*,4*S*,6*S*,6a*S*)-6-(6-(bis((2-(trimethylsilyl)ethoxy)methyl)amino)-8-((3,4-dichlorobenzyl)((2-(trimethylsilyl)ethoxy)methyl)amino)-9*H*-purin-9-yl)-2,2-dimethyltetrahydrofuro[3,4-*d*][1,3]dioxol-4-yl)methoxy)methyl)benzenesulfonyl fluoride (*ent*-127)**

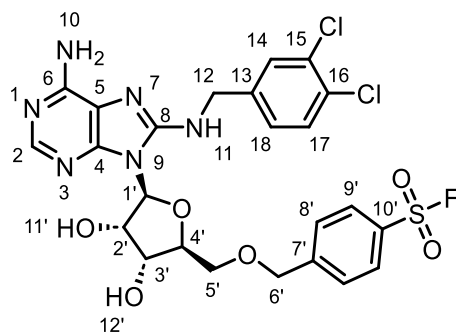


*ent*-127

*ent*-127 was prepared following general procedure E, with 9-(((3a*S*,4*S*,6*S*,6a*S*)-6-(((4-bromobenzyl)oxy)methyl)-2,2-dimethyltetrahydrofuro[3,4-*d*][1,3]dioxol-4-yl)-*N*8-(3,4-dichlorobenzyl)-*N*6,*N*6,*N*8-tris((2-(trimethylsilyl)ethoxy)methyl)-9*H*-purine-6,8-diamine *ent*-126 (770 mg, 0.74 mmol, 1 equiv.), isopropanol (2.74 mL, 0.27 M), DABSO (107 mg, 0.44 mmol, 0.6 equiv.), PdCl<sub>2</sub>(AmPhos)<sub>2</sub> (26.2 mg, 0.04 mmol, 5 mol%), triethylamine (0.31 mL, 2.22 mmol, 3 equiv.) and NFSI (350 mg, 1.11 mmol, 1.5 equiv.). Purification by normal phase column chromatography on silica (EtOAc:cyclohexane 1:99 to 20:80 gradient) yielded *ent*-127 (274 mg, 35%) as a yellow oil. <sup>1</sup>H NMR (600 MHz,

CD<sub>3</sub>CN)  $\delta$  = 8.11 (s, 1H, H2), 7.94 – 7.90 (m, 2H, H12'), 7.57 (d,  $J$  = 1.8 Hz, 1H, H12), 7.55 – 7.52 (m, 2H, H11'), 7.42 (d,  $J$  = 8.3 Hz, 1H, H15), 7.31 (dd,  $J$  = 8.3, 1.8 Hz, 1H, H16), 6.11 (d,  $J$  = 1.9 Hz, 1H, H1'), 5.61 (dd,  $J$  = 6.3, 1.9 Hz, H2'), 5.52 – 5.28 (m, 4H, H21), 5.17 (dd,  $J$  = 6.3, 3.3 Hz, 1H, H3'), 4.83 (d,  $J$  = 10.4 Hz, 1H, H17a), 4.76 (d,  $J$  = 14.9 Hz, 1H, H10a), 4.73 (d,  $J$  = 10.4 Hz, 1H, H17b), 4.64 – 4.55 (m, 3H, H9', H10b), 4.39 – 4.35 (m, 1H, H4'), 3.78 (dd,  $J$  = 10.5, 5.6 Hz, 1H, H5'a), 3.70 (dd,  $J$  = 10.5, 7.0 Hz, 1H, H5'b), 3.57 – 3.53 (m, 4H, H22), 3.51 – 3.47 (m, 2H, H18), 1.56 (s, 3H, H7'), 1.33 (s, 3H, H8'), 0.88 – 0.81 (m, 6H, H19, H23), -0.08 (s, 18H, H24), -0.10 (s, 9H, H20); <sup>13</sup>C NMR (151 MHz, CD<sub>3</sub>CN)  $\delta$  = 153.45 (C6), 153.14 (C8), 152.25 (C4), 150.87 (C2), 148.98 (C10'), 140.11 (C11), 132.61 (C14), 131.90 (d,  $J_{C-F}$  = 24.2 Hz, C13'), 131.44 (C13), 131.36 (C12), 131.27 (C15), 129.39 (C16), 129.32 (C12'), 129.07 (2C, C11'), 118.67 (2C, C5), 114.58 (C6'), 90.69 (C1'), 87.13 (C4'), 83.70 (C2'), 83.61 (C17), 83.23 (C3'), 77.24 (2C, C21), 72.37 (C9'), 71.50 (C5'), 66.59 (C18), 65.58 (2C, C22), 53.47 (C10), 27.46 (C7'), 25.56 (C8'), 18.58 (2C, C23), 18.46 (C19), -1.36 (6C, C24), -1.41 (C20); <sup>19</sup>F NMR (471 MHz, CD<sub>3</sub>CN)  $\delta$  = 65.02; HRMS (ESI+)  $m/z$  calculated for C<sub>45</sub>H<sub>70</sub><sup>35</sup>Cl<sub>2</sub>FN<sub>6</sub>O<sub>9</sub>SSi<sub>3</sub> (M+H)<sup>+</sup> 1043.3588, found 1043.3588.

**4-(((2*S*,3*R*,4*S*,5*S*)-5-(6-amino-8-((3,4-dichlorobenzyl)amino)-9*H*-purin-9-yl)-3,4-dihydroxytetrahydrofuran-2-yl)methoxy)methyl)benzenesulfonyl fluoride (*ent*-128)**

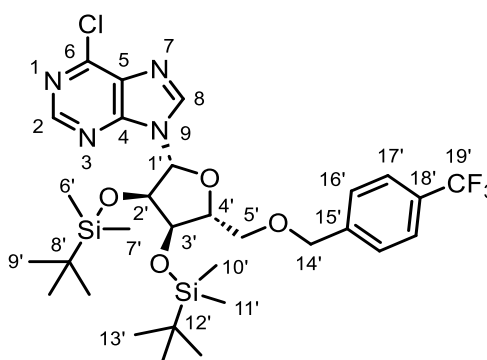


*ent*-128

*ent*-128 was prepared following general procedure F, with 4-(((3*aS*,4*S*,6*S*,6*aS*)-6-(6-bis((2-(trimethylsilyl)ethoxy)methyl)amino)-8-((3,4-dichlorobenzyl)((2-(trimethylsilyl)ethoxy)methyl)amino)-9*H*-purin-9-yl)-2,2-dimethyltetrahydrofuro[3,4-*d*][1,3]dioxol-4-yl)methoxy)methyl)benzenesulfonyl fluoride *ent*-127 (270 mg, 0.26 mmol, 1 equiv.), and TFA:water 5:2 (v/v) mixture (2.59 mL, 0.1 M) for 2 hours. Purification by normal phase column chromatography on silica (100% CH<sub>2</sub>Cl<sub>2</sub> to 15:85 methanol:CH<sub>2</sub>Cl<sub>2</sub> gradient) then reverse phase column chromatography on C18

(acetonitrile:water +0.1% formic acid 5:95 to 50:50 gradient) yielded *ent*-**128** (68 mg, 43%) as a white solid.  $^1\text{H NMR}$  (600 MHz, DMSO- $d_6$ )  $\delta$  = 8.02 – 7.99 (m, 2H, H9'), 7.93 (s, 1H, H2), 7.60 – 7.56 (m, 2H, H8'), 7.53 – 7.50 (m, 2H, H14, H17), 7.31 – 7.26 (m, 2H, H11, H18), 6.67 (s, 2H, H10), 5.86 (d,  $J$  = 5.4 Hz, 1H, H1'), 5.42 (d,  $J$  = 5.0 Hz, 1H, H11'), 5.24 (app. s, 1H, H12'), 4.98 (app. q,  $J$  = 4.8 Hz, 1H, H2'), 4.64 (s, 2H, H6'), 4.50 (d,  $J$  = 6.0 Hz, 1H, H12), 4.38 – 4.34 (m, 1H, H3'), 4.08 – 4.04 (m, 1H, H4'), 3.81 (dd,  $J$  = 10.8, 3.0 Hz, 1H, H5'a), 3.70 (dd,  $J$  = 10.8, 4.7 Hz, 1H, H5'b);  $^{13}\text{C NMR}$  (151 MHz, DMSO- $d_6$ )  $\delta$  = 151.97 (C6), 151.41 (C8), 149.75 (C4), 148.30 (C2), 147.70 (C7'), 140.96 (C13), 130.80 (C16), 130.35 (C17), 130.17 (d,  $J_{\text{C-F}}$  = 23.4 Hz, C10'), 129.26 (C15), 128.96 (C14), 128.36 (2C, C9'), 128.22 (2C, C8'), 127.42 (C18), 116.93 (C5), 87.17 (C1'), 82.79 (C4'), 71.13 (C6'), 70.59 (C5'), 70.55 (C2'), 70.20 (C3'), 44.32 (C12);  $^{19}\text{F NMR}$  (471 MHz, DMSO- $d_6$ )  $\delta$  = 66.69; **HRMS** (ESI+)  $m/z$  calculated for  $\text{C}_{24}\text{H}_{24}^{35}\text{Cl}_2\text{FN}_6\text{O}_6\text{S}$  (M+H) $^+$  613.0834, found 613.0848.

**9-((2*R*,3*R*,4*R*,5*R*)-3,4-bis((*tert*-butyldimethylsilyl)oxy)-5-(((4-(trifluoromethyl)benzyl)oxy)methyl)tetrahydrofuran-2-yl)-6-chloro-9*H*-purine (74)**



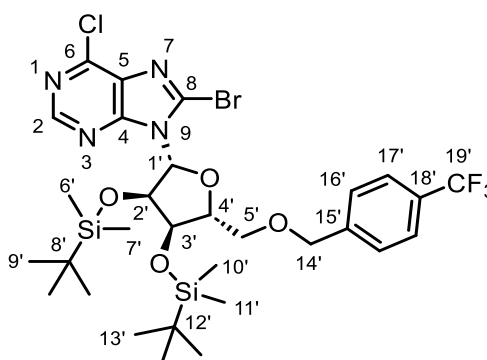
**74**

A two-neck round bottom flask heat-dried under vacuum and equipped with magnetic stirrer was charged with ((2*R*,3*R*,4*R*,5*R*)-3,4-bis((*tert*-butyldimethylsilyl)oxy)-5-(6-chloro-9*H*-purin-9-yl)tetrahydrofuran-2-yl)methanol (2.00 g, 3.88 mmol, 1 equiv.) **73** and DMF (7.76 mL, 0.5 M) under flow of nitrogen. The mixture was cooled to -61 °C and sodium hydride (186 mg, 60% in mineral oil, 4.66 mmol, 1.2 equiv.) was added and stirred for 15 minutes. 1-(bromomethyl)-4-(trifluoromethyl)benzene (1.86 g, 7.76 mmol, 2 equiv.) was then added, after which the mixture was allowed to warm up to room temperature. After stirring at room temperature for 18 hours, the reaction mixture was quenched with methanol and the solvent was removed under reduced pressure. The crude

product was purified by normal phase column chromatography on silica (EtOAc:cyclohexane 1:99 to 30:70 gradient) to yield **74** (543 mg, 21%) as a white foam.  $^1\text{H NMR}$  (600 MHz,  $\text{CDCl}_3$ )  $\delta$  = 8.73 (s, 1H, H2), 8.57 (s, 1H, H8), 7.64 (app. d,  $J$  = 8.1 Hz, 2H, H17'), 7.46 (d,  $J$  = 8.1 Hz, 2H, H16'), 6.08 (d,  $J$  = 3.7 Hz, 1H, H1'), 4.68 (s, 2H, H14'), 4.58 (app. t,  $J$  = 3.9 Hz, 1H, H2'), 4.36 (app. t,  $J$  = 4.6 Hz, 1H, H3'), 4.28 – 4.25 (m, 1H, H4'), 3.92 (dd,  $J$  = 10.7, 3.0 Hz, 1H, H5'a), 3.70 (dd,  $J$  = 10.7, 2.7 Hz, 1H, H5'b), 0.90 (s, 9H,  $\text{SiC}(\text{CH}_3)_3$ ), 0.83 (s, 9H,  $\text{SiC}(\text{CH}_3)_3$ ), 0.06 (s, 3H,  $\text{SiCH}_3$ ), 0.05 (s, 3H,  $\text{SiCH}_3$ ), 0.00 (s, 3H,  $\text{SiCH}_3$ ), -0.10 (s, 3H,  $\text{SiCH}_3$ );  $^{13}\text{C NMR}$  (151 MHz,  $\text{CDCl}_3$ )  $\delta$  = 152.08 (C2), 151.39 (C6), 151.22 (C4), 144.22 (C8), 141.39 (C15'), 132.33 (C5), 130.48 (q,  $J_{\text{C-F}}$  = 32.5 Hz, C18'), 127.96 (2C, C16'), 125.79 (q,  $J_{\text{C-F}}$  = 3.8 Hz, 2C, C17'), 124.17 (q,  $J_{\text{C-F}}$  = 272.0 Hz, C19'), 89.44 (C1'), 83.59 (C4'), 76.18 (C2'), 73.11 (C14'), 71.58 (C3'), 69.07 (C5'), 25.92 (3C,  $\text{SiC}(\text{CH}_3)_3$ ), 25.80 (3C,  $\text{SiC}(\text{CH}_3)_3$ ), 18.19 ( $\text{SiC}(\text{CH}_3)_3$ ), 18.04 ( $\text{SiC}(\text{CH}_3)_3$ ), -4.22 ( $\text{SiCH}_3$ ), -4.59 ( $\text{SiCH}_3$ ), -4.69 ( $\text{SiCH}_3$ ), -4.79 ( $\text{SiCH}_3$ ); **HRMS** (ESI+)  $m/z$  calculated for  $\text{C}_{30}\text{H}_{45}^{35}\text{ClF}_3\text{N}_4\text{O}_4\text{Si}_2$  (M+H) $^+$  673.2614, found 673.2624.

The spectroscopic and analytical data were in agreement with literature values.<sup>153</sup>

**9-((2*R*,3*R*,4*R*,5*R*)-3,4-bis((*tert*-butyldimethylsilyl)oxy)-5-(((4-(trifluoromethyl)benzyl)oxy)methyl)tetrahydrofuran-2-yl)-8-bromo-6-chloro-9*H*-purine (149)**



**149**

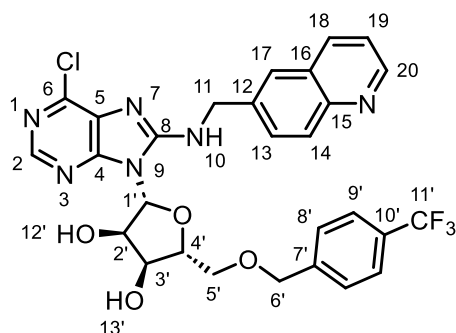
A glass microwave vial heat-dried under vacuum and equipped with magnetic stirrer was charged with 9-((2*R*,3*R*,4*R*,5*R*)-3,4-bis((*tert*-butyldimethylsilyl)oxy)-5-(((4-(trifluoromethyl)benzyl)oxy)methyl)tetrahydrofuran-2-yl)-6-chloro-9*H*-purine **74** (530 mg, 0.79 mmol, 1 equiv.) and THF (5.61 mL, 0.14 M) under flow of nitrogen. The mixture was cooled to -78 °C and LDA (551  $\mu\text{L}$ , 2 M in THF, 1.10 mmol, 1.4 equiv.) was added and stirred for 30 minutes. 1,2-dibromotetrachloroethane (513 mg, 1.57 mmol, 2

equiv.) was then added as a solution in THF (2.27 mL), after which the mixture was stirred for a further 2 hours at -78 °C. The reaction mixture was quenched with sat. NH<sub>4</sub>Cl solution (40 mL), diluted with EtOAc (50 mL) and the phases were separated. The aqueous phase was extracted with EtOAc (2 × 50 mL) and the resultant combined organic layers were dried over MgSO<sub>4</sub>, filtered, and concentrated under reduced pressure. The crude product was purified by normal phase column chromatography on silica (EtOAc:cyclohexane 1:99 to 20:80 gradient) to yield **149** (407 mg, 69%) as a yellow oil. **<sup>1</sup>H NMR** (600 MHz, CDCl<sub>3</sub>) δ = 8.60 (s, 1H, H2), 7.56 (app. d, *J* = 8.1 Hz, 2H, H17'), 7.35 (app. d, *J* = 8.1 Hz, 2H, H16'), 6.05 (d, *J* = 5.2 Hz, 1H, H1'), 5.30 (app. t, *J* = 4.8 Hz, 1H, H2'), 4.63 – 4.59 (m, 2H, H3', H14'a), 4.54 (d, *J* = 12.6 Hz, 1H, H14'b), 4.28 – 4.24 (m, 1H, H4'), 3.83 (dd, *J* = 10.6, 5.2 Hz, 1H, H5'a), 3.72 (dd, *J* = 10.6, 5.7 Hz, 1H, H5'b), 0.95 (s, 9H, SiC(CH<sub>3</sub>)<sub>3</sub>), 0.80 (s, 9H, SiC(CH<sub>3</sub>)<sub>3</sub>), 0.15 (s, 3H, SiCH<sub>3</sub>), 0.14 (s, 3H, SiCH<sub>3</sub>), -0.05 (s, 3H, SiCH<sub>3</sub>), -0.35 (s, 3H, SiCH<sub>3</sub>); **<sup>13</sup>C NMR** (151 MHz, CDCl<sub>3</sub>) δ = 152.24 (C4), 151.57 (C2), 150.21 (C6), 142.12 (C15'), 135.62 (C8), 132.62 (C5), 127.43 (2C, C16'), 125.43 (q, *J*<sub>C-F</sub> = 3.6 Hz, 2C, C17'), 91.43 (C1'), 84.40 (C4'), 72.79 (C14'), 72.72 (C2'), 72.56 (C3'), 70.04 (C5'), 25.98 (3C, SiC(CH<sub>3</sub>)<sub>3</sub>), 25.77 (3C, SiC(CH<sub>3</sub>)<sub>3</sub>), 18.23 (SiC(CH<sub>3</sub>)<sub>3</sub>), 17.97 (SiC(CH<sub>3</sub>)<sub>3</sub>), -4.23 (SiCH<sub>3</sub>), -4.38 (SiCH<sub>3</sub>), -4.50 (SiCH<sub>3</sub>), -4.91 (SiCH<sub>3</sub>);\* **HRMS** (ESI+) *m/z* calculated for C<sub>30</sub>H<sub>44</sub><sup>79</sup>Br<sup>35</sup>ClF<sub>3</sub>N<sub>4</sub>O<sub>4</sub>Si<sub>2</sub> (M+H)<sup>+</sup> 751.1720, found 751.1741.

\*C18' and C19' not observed in spectrum.

The spectroscopic and analytical data were in agreement with literature values.<sup>153</sup>

**(2*R*,3*R*,4*S*,5*R*)-2-(6-chloro-8-((quinolin-6-ylmethyl)amino)-9*H*-purin-9-yl)-5-(((4-(trifluoromethyl)benzyl)oxy)methyl)tetrahydrofuran-3,4-diol (151)**

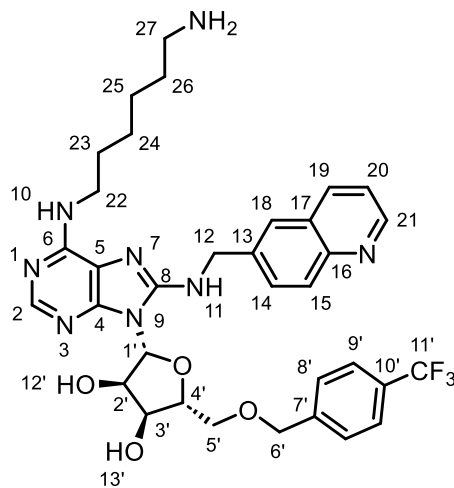


**151**

A two-neck round bottom flask equipped with magnetic stirrer and reflux condenser was charged with 9-((2*R*,3*R*,4*R*,5*R*)-3,4-bis((*tert*-butyldimethylsilyl)oxy)-5-(((4-(trifluoromethyl)benzyl)oxy)methyl)tetrahydrofuran-2-yl)-8-bromo-6-chloro-9*H*-purine **149** (400 mg, 0.53 mmol, 1 equiv.), ethanol (5.32 mL, 0.1 M), quinoline-6-ylmethanamine **112** (0.11 mL, 0.80 mmol, 1.5 equiv.) and triethylamine (0.11 mL, 0.80 mmol, 1.5 equiv.) under flow of nitrogen. The mixture was heated to 40 °C for 48 hours, after which the solvent was removed under reduced pressure and the crude mixture was eluted through a silica plug (EtOAc:cyclohexane 30:70), concentrated under reduced pressure and the crude residue (335 mg, 0.40 mmol) was redissolved in THF (4.04 mL, 0.1 M) and TBAF (0.89 mL, 1 M in THF, 0.89 mmol, 2.2 equiv.). After stirring at room temperature for 20 hours, the reaction mixture was quenched with methanol, concentrated under reduced pressure and purified by normal phase column chromatography on silica (100% CH<sub>2</sub>Cl<sub>2</sub> to 10:90 methanol:CH<sub>2</sub>Cl<sub>2</sub> gradient) to yield **151** (194 mg, 60%) as an off-white solid. **<sup>1</sup>H NMR** (600 MHz, DMSO-*d*<sub>6</sub>) δ = 8.85 (dd, *J* = 4.2, 1.7 Hz, 1H, H20), 8.34 (s, 1H, H2), 8.27 (app. d, *J* = 8.4 Hz, 1H, H18), 8.15 (t, *J* = 5.9 Hz, 1H, H10), 7.98 (d, *J* = 8.7 Hz, 1H, H14), 7.83 (app. s, 1H, H17), 7.73 (dd, *J* = 8.7, 2.0 Hz, 1H, H13), 7.56 – 7.53 (m, 2H, H9'), 7.49 (dd, *J* = 8.4, 4.2 Hz, 1H, H19), 7.36 – 7.32 (m, 2H, H8'), 6.01 (d, *J* = 5.5 Hz, 1H, H1'), 5.54 (d, *J* = 5.5 Hz, 1H, H12'), 5.32 (d, *J* = 5.2 Hz, 1H, H13'), 5.02 (app. q, *J* = 5.5 Hz, 1H, H2'), 4.82 (dd, *J* = 15.8, 6.0 Hz, 1H, H11a), 4.77 (dd, *J* = 15.8, 5.7 Hz, 1H, H11b), 4.54 – 4.48 (m, 2H, H6'), 4.38 – 4.34 (m, 1H, H3'), 4.12 – 4.09 (m, 1H, H4'), 3.78 (dd, *J* = 10.8, 3.1 Hz, 1H, H5'a), 3.66 (dd, *J* = 10.8, 4.5 Hz, 1H, H5'b); **<sup>13</sup>C NMR** (151 MHz, DMSO-*d*<sub>6</sub>) δ = 155.37 (C8), 153.20 (C4), 150.25 (C20), 147.54 (C2), 147.09 (C15), 142.71 (C7'), 141.03 (C6), 137.08 (C12), 135.72 (C18), 131.41 (C5), 129.08 (C14), 129.07 (C13), 127.94 (q, *J*<sub>C-F</sub> = 31.7 Hz, C10'), 127.61 (C16), 127.53 (2C, C8'), 125.40 (C17), 124.98 (q, *J*<sub>C-F</sub> = 3.9 Hz, 2C, C9'), 124.15 (q, *J*<sub>C-F</sub> = 271.9 Hz, C11'), 121.60 (C19), 87.50 (C1'), 83.31 (C4'), 71.45 (C6'), 70.61 (C2'), 70.32 (C3'), 70.14 (C5'), 45.34 (C11); **HRMS** (ESI+) *m/z* calculated for C<sub>28</sub>H<sub>25</sub><sup>35</sup>ClF<sub>3</sub>N<sub>6</sub>O<sub>4</sub> (M+H)<sup>+</sup> 601.1572, found 601.1591;

The spectroscopic and analytical data were in agreement with literature values.<sup>153</sup>

**(2*R*,3*R*,4*S*,5*R*)-2-(6-((6-aminohexyl)amino)-8-((quinolin-6-ylmethyl)amino)-9*H*-purin-9-yl)-5-(((4-(trifluoromethyl)benzyl)oxy)methyl)tetrahydrofuran-3,4-diol (153)**



**153**

A glass microwave vial equipped with magnetic stirrer was charged with (2*R*,3*R*,4*S*,5*R*)-2-(6-chloro-8-((quinolin-6-ylmethyl)amino)-9*H*-purin-9-yl)-5-(((4-(trifluoromethyl)benzyl)oxy)methyl)tetrahydrofuran-3,4-diol **151** (400 mg, 0.53 mmol, 1 equiv.), n-butanol (0.62 mL, 0.5 M), *N*-Boc-1,6-hexanediamine (0.35 mL, 1.54 mmol, 5 equiv.) and *N,N*-diisopropylethylamine (64  $\mu$ L, 0.37 mmol, 1.2 equiv.) under flow of nitrogen. The mixture was heated to 120  $^{\circ}$ C under microwave irradiation for 2 hours, after which the solvent was removed under reduced pressure and the crude mixture was eluted through a silica plug (methanol:CH<sub>2</sub>Cl<sub>2</sub> 10:90), concentrated under reduced pressure and the crude residue (170 mg, 0.22 mmol) was redissolved in CH<sub>2</sub>Cl<sub>2</sub> (2.18 mL, 0.1 M) and TFA (1 mL, 13.1 mmol, 60 equiv.). After stirring for 2 hours at room temperature, the solvent was removed under reduced pressure and the crude product was purified by reverse phase column chromatography on C18 (acetonitrile:water +0.1% formic acid 5:95 to 40:60 gradient) to yield **153** (125 mg, 34%) as an off-white solid. <sup>1</sup>H NMR (600 MHz, DMSO-d<sub>6</sub>)  $\delta$  = 8.84 (dd,  $J$  = 4.2, 1.7 Hz, 1H, H21), 8.24 (app. d,  $J$  = 8.4 Hz, 1H, H19), 7.97 – 7.93 (m, 2H, H2, H15), 7.80 (app s, 1H, H18), 7.69 (dd,  $J$  = 8.7, 1.7 Hz, 1H, H14), 7.56 – 7.52 (m, 2H, H9'), 7.47 (dd,  $J$  = 8.4, 4.2 Hz, 1H, H20), 7.38 – 7.34 (m, 2H, H8'), 7.24 (t,  $J$  = 5.7 Hz, 1H, H11), 6.86 (t,  $J$  = 6.1 Hz, 1H, H10), 5.93 (d,  $J$  = 5.7 Hz, 1H, H1'), 5.54 (s br, 1H, H12'), 5.28 (s br, 1H, H13'), 4.96 (t,  $J$  = 5.6 Hz, 1H, H2'), 4.74 – 4.63 (m, 2H, H12), 4.54 – 4.48 (m, 2H, H6'), 4.36 – 4.32 (m, 1H, H3'), 4.08 – 4.04 (m, 1H, H4'),

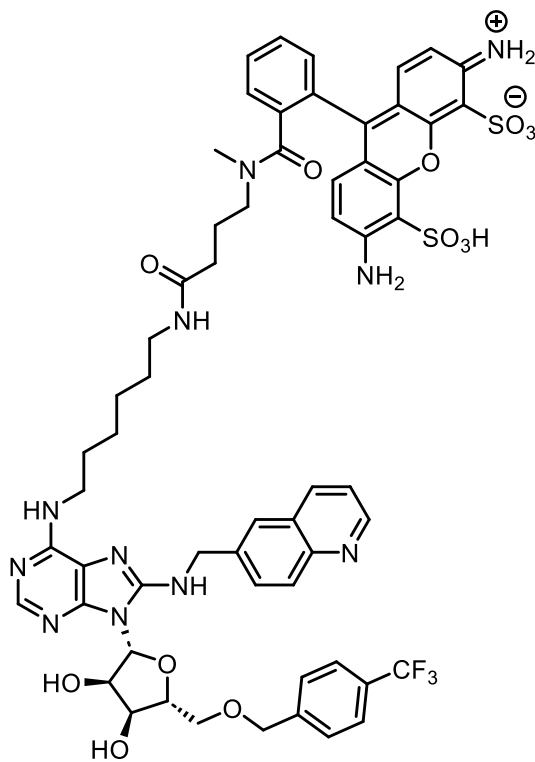


3.77 (dd,  $J = 10.9, 2.9$  Hz, 1H, H5'a), 3.65 (dd,  $J = 10.9, 4.4$  Hz, 1H, H5'b), 3.52 (s br, 2H, H22), 2.71 (app. t,  $J = 7.5$  Hz, 2H, H27), 1.57 – 1.41 (m, 4H, H23, H26), 1.31 – 1.19 (m, 4H, H24, H25);  $^{13}\text{C}$  NMR (151 MHz, DMSO- $d_6$ )  $\delta = 151.60$  (C6), 151.23 (C8), 150.08 (C21), 149.22 (C4), 148.98 (C2), 147.03 (C16), 142.77 (C7'), 138.10 (C13), 135.64 (C19), 129.14 (C14), 128.87 (C15), 127.92 (q,  $J_{\text{C-F}} = 31.8$  Hz, C10'), 127.60 (3C, C8', C17), 125.12 (C18), 124.99 (q,  $J_{\text{C-F}} = 3.8$  Hz, 2C, C9'), 124.17 (q,  $J_{\text{C-F}} = 271.7$  Hz, C11'), 121.52 (C20), 116.99 (C5), 86.99 (C1'), 82.84 (C4'), 71.47 (C6'), 70.59 (C2'), 70.33 (2C, C3', C5'), 45.28 (C12), 39.82 (C22)\*, 38.89 (C27), 29.41 (C23), 27.38 (C26), 25.96 (C24), 25.64 (C25); HRMS (ESI+)  $m/z$  calculated for  $\text{C}_{34}\text{H}_{40}\text{F}_3\text{N}_8\text{O}_4$  (M+H) $^+$  681.3119, found 681.3132.

\*Signal present in  $^1\text{H}$ - $^{13}\text{C}$  HMBC but is under solvent signal in 1D  $^{13}\text{C}$  spectrum.

The spectroscopic and analytical data were in agreement with literature values.<sup>153</sup>

**6-amino-9-(2-((4-((6-((9-((2*R*,3*R*,4*S*,5*R*)-3,4-dihydroxy-5-(((4-(trifluoromethyl)benzyl)oxy)methyl)tetrahydrofuran-2-yl)-8-((quinolin-6-ylmethyl)amino)-9*H*-purin-6-yl)amino)hexyl)amino)-4-oxobutyl)(methyl)carbamoyl)phenyl)-3-iminio-5-sulfo-8*a*,10*a*-dihydro-3*H*-xanthene-4-sulfonate (**148**)**

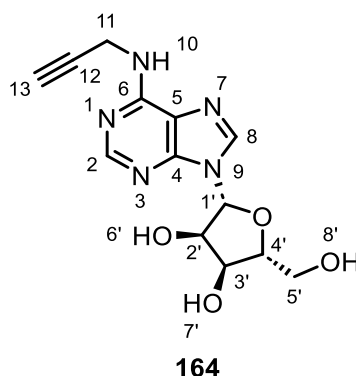


**148**

A glass microwave vial equipped with magnetic stirrer was charged with (2*R*,3*R*,4*S*,5*R*)-2-(6-((6-aminohexyl)amino)-8-((quinolin-6-ylmethyl)amino)-9*H*-purin-9-yl)-5-(((4-(trifluoromethyl)benzyl)oxy)methyl)tetrahydrofuran-3,4-diol **153** (4.9 mg, 7.3  $\mu$ mol, 1 equiv.), DMF (0.29 mL, 0.025 M) and triethylamine (4  $\mu$ L, 2.9  $\mu$ mol, 4 equiv.), ATTO 488 NHS ester **154** (5.0 mg, 7.3  $\mu$ mol, 1 equiv.) was then added as a solution in DMF (0.19 mL), after which the mixture was stirred for 2 hours at room temperature protected from light. The reaction mixture was directly purified by reverse phase column chromatography on C18 (acetonitrile:water +0.1% formic acid 10:90 to 50:50 gradient) to yield **148** (3.2 mg, 35%) as a red solid. **HRMS** (ESI+) *m/z* calculated for C<sub>59</sub>H<sub>62</sub>F<sub>3</sub>N<sub>11</sub>O<sub>13</sub>S<sub>2</sub> (M+2H)<sup>+</sup> 626.6956, found 626.6953.

The spectroscopic and analytical data were in agreement with literature values.<sup>153</sup>

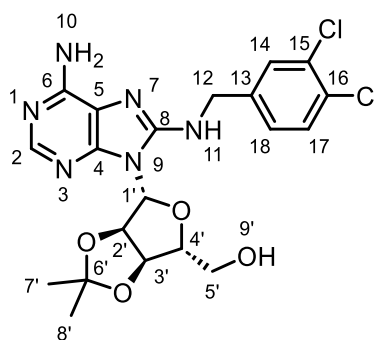
**(2*R*,3*S*,4*R*,5*R*)-2-(hydroxymethyl)-5-(6-(prop-2-yn-1-ylamino)-9*H*-purin-9-yl)tetrahydrofuran-3,4-diol (164)**



A two-neck round bottom flask equipped with magnetic stirrer was charged with (2*R*,3*R*,4*S*,5*R*)-2-(6-chloropurin-9-yl)-5-(hydroxymethyl)tetrahydrofuran-3,4-diol **78** (2.00 g, 6.98 mmol, 1 equiv.), ethanol (70.0 mL, 0.1 M) and propargyl amine (2.23 mL, 34.9 mmol, 5 equiv.) under flow of nitrogen. The mixture was heated to 60 °C for 18 hours, after which the reaction mixture was cooled to room temperature and the resultant precipitate was filtered and washed with ethanol (3 × 20 mL) to yield **164** (1.10 g, 52%) as a white solid. **<sup>1</sup>H NMR** (600 MHz, DMSO-*d*<sub>6</sub>) δ = 8.40 (s, 1H, H8), 8.28 (s br, 1H, H2), 8.25 (s br, 1H, H10), 5.90 (d, *J* = 6.1 Hz, 1H, H1'), 5.44 (d, *J* = 6.2 Hz, 1H, H6'), 3.55 – 3.51 (m, 1H, H8'), 5.18 (d, *J* = 4.7 Hz, 1H, H7'), 4.63 – 4.59 (m, 1H, H2'), 4.25 (s br, 2H, H11), 4.17 – 4.13 (m, 1H, H3'), 3.98 – 3.94 (m, 1H, H4'), 3.67 (app. dt, *J* = 12.1, 4.2 Hz, 1H, H5'a), 3.58 – 3.53 (m, 1H, H5'b), 3.03 (app. s, 1H, H13); **<sup>13</sup>C NMR** (151 MHz, DMSO-*d*<sub>6</sub>) δ = 153.92 (C6), 152.23 (C2), 148.81 (C4), 140.19 (C8), 119.95 (C5), 87.87 (C1'), 85.84 (C4'), 81.83 (C12), 73.53 (C2'), 72.35 (C13), 70.58 (C3'), 61.60 (C5'), 29.10 (C11); **HRMS** (ESI+) *m/z* calculated for C<sub>13</sub>H<sub>16</sub>N<sub>5</sub>O<sub>4</sub> (M+H)<sup>+</sup> 306.1197, found 306.1203.

The spectroscopic and analytical data were in agreement with literature values.<sup>293</sup>

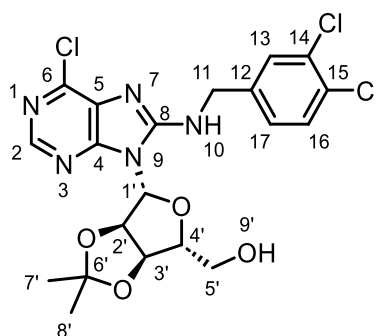
**((3*aR*,4*R*,6*R*,6*aR*)-6-(6-amino-8-((3,4-dichlorobenzyl)amino)-9*H*-purin-9-yl)-2,2-dimethyltetrahydrofuro[3,4-*d*][1,3]dioxol-4-yl)methanol (166)**



**166**

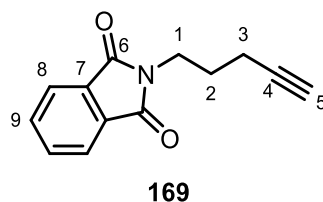
**166** was prepared following general procedure A, with ((3*aR*,4*R*,6*R*,6*aR*)-6-(6-amino-8-bromo-9*H*-purin-9-yl)-2,2-dimethyltetrahydrofuro[3,4-*d*][1,3]dioxol-4-yl)methanol **109** (9.50 g, 24.6 mmol, 1 equiv.), ethanol (82.0 mL, 0.3 M) and 3,4-dichlorobenzylamine (19.0 mL, 126 mmol, 5.1 equiv.). Purification by normal phase column chromatography on silica (100% CH<sub>2</sub>Cl<sub>2</sub> to methanol:CH<sub>2</sub>Cl<sub>2</sub> 10:90 gradient) then reverse phase column chromatography on C18 (methanol:water +0.1% formic acid 40:60 to 100% methanol gradient) yielded **166** (9.23 g, 78%) as an off-white foam. <sup>1</sup>H NMR (600 MHz, DMSO-*d*<sub>6</sub>) δ = 7.94 (s, 1H, H2), 7.64 (t, *J* = 6.0 Hz, 1H, H11), 7.62 (d, *J* = 2.0 Hz, 1H, H14), 7.58 (d, *J* = 8.3 Hz, 1H, H17), 7.38 (dd, *J* = 8.3, 2.0 Hz, 1H, H18), 6.59 (s, 2H, H10), 6.08 (d, *J* = 3.4 Hz, 1H, H1'), 5.49 (dd, *J* = 6.3, 3.4 Hz, 1H, H2'), 5.42 (s br, 1H, H9'), 4.98 (dd, *J* = 6.3, 2.7 Hz, 1H, H3'), 4.60 – 4.52 (m, 2H, H12), 4.19 – 4.16 (m, 1H, H4'), 3.57 – 3.50 (m, 2H, H5'), 1.55 (s, 3H, H7'), 1.32 (s, 3H, H8'); <sup>13</sup>C NMR (151 MHz, DMSO-*d*<sub>6</sub>) δ = 152.66 (C6), 150.84 (C8), 149.25 (C4), 149.05 (C2), 141.06 (C13), 130.81 (C16), 130.44 (C17), 129.29 (C15), 129.24 (C14), 127.71 (C18), 116.93 (C5), 113.17 (C6'), 87.97 (C1'), 85.49 (C4'), 81.44 (C2'), 81.19 (C3'), 61.35 (C5'), 44.38 (C12), 27.14 (C7'), 25.25 (C8'); HRMS (ESI+) *m/z* calculated for C<sub>20</sub>H<sub>23</sub><sup>35</sup>Cl<sub>2</sub>N<sub>6</sub>O<sub>4</sub> (M+H)<sup>+</sup> 481.1152, found 481.1162.

**((3a*R*,4*R*,6*R*,6a*R*)-6-(6-chloro-8-((3,4-dichlorobenzyl)amino)-9*H*-purin-9-yl)-2,2-dimethyltetrahydrofuro[3,4-*d*][1,3]dioxol-4-yl)methanol (165)**



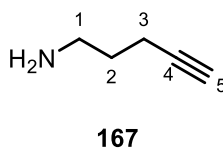
**165**

A two-neck round bottom flask equipped with magnetic stirrer was charged with ((3a*R*,4*R*,6*R*,6a*R*)-6-(6-amino-8-((3,4-dichlorobenzyl)amino)-9*H*-purin-9-yl)-2,2-dimethyltetrahydrofuro[3,4-*d*][1,3]dioxol-4-yl)methanol **166** (9.20 g, 19.1 mmol, 1 equiv.) and CH<sub>2</sub>Cl<sub>2</sub> (191 mL, 0.1 M) under flow of nitrogen. To the resulting suspension was slowly added chlorotrimethylsilane (17.0 mL, 134 mmol, 7 equiv.) followed by *tert*-butyl nitrite (18.2 mL, 153 mmol, 8 equiv.). After stirring at room temperature for 3 hours, the reaction mixture was quenched with sat. NaHCO<sub>3</sub> solution (200 mL) and the phases were separated. The aqueous phase was extracted with CH<sub>2</sub>Cl<sub>2</sub> (200 mL) and the resultant combined organic layers were dried over MgSO<sub>4</sub>, filtered, and concentrated under reduced pressure. The crude product was purified by normal phase column chromatography on silica (100% CH<sub>2</sub>Cl<sub>2</sub> to methanol:CH<sub>2</sub>Cl<sub>2</sub> 10:90 gradient) then reverse phase column chromatography on C18 (methanol:water +0.1% formic acid 40:60 to 100% methanol gradient) to yield **165** (6.23 g, 65%) as an orange foam. <sup>1</sup>H NMR (600 MHz, DMSO-*d*<sub>6</sub>) δ = 8.49 (t, *J* = 5.9 Hz, 1H, H10), 8.40 (s, 1H, H2), 7.65 (d, *J* = 1.9 Hz, 1H, H13), 7.61 (d, *J* = 8.3 Hz, 1H, H16), 7.38 (dd, *J* = 8.3, 1.9 Hz, 1H, H17), 6.20 (d, *J* = 3.0 Hz, 1H, H1'), 5.58 (dd, *J* = 6.3, 3.0 Hz, 1H, H2'), 5.32 (s br, 1H, H9'), 5.01 (dd, *J* = 6.3, 3.0 Hz, 1H, H3'), 4.64 (d, *J* = 5.9 Hz, 2H, H11), 4.22 – 4.19 (m, 1H, H4'), 3.51 (app. d, *J* = 4.8 Hz, 2H, H5'), 1.55 (s, 3H, H7'), 1.33 (s, 3H, H8'); <sup>13</sup>C NMR (151 MHz, DMSO-*d*<sub>6</sub>) δ = 154.81 (C8), 152.74 (C4), 147.65 (C2), 141.12 (C6), 140.07 (C12), 131.35 (C5), 130.91 (C15), 130.57 (C16), 129.59 (C14), 129.40 (C13), 127.72 (C17), 113.23 (C6'), 88.22 (C1'), 86.32 (C4'), 81.62 (C2'), 81.12 (C3'), 61.15 (C5'), 44.43 (C11), 27.08 (C7'), 25.22 (C8'); HRMS (ESI+) *m/z* calculated for C<sub>20</sub>H<sub>21</sub><sup>35</sup>Cl<sub>3</sub>N<sub>5</sub>O<sub>4</sub> (M+H)<sup>+</sup> 500.0654, found 500.0669. [α]<sub>D</sub><sup>25</sup> = -6 ° (c = 0.5, CHCl<sub>3</sub>).

**2-(pent-4-yn-1-yl)isoindoline-1,3-dione (169)**

A two-neck round bottom flask equipped with magnetic stirrer was charged with 5-chloro-1-pentyne **168** (5.17 mL, 48.8 mmol, 1 equiv.), DMF (48.8 mL, 1 M), phthalimide (8.61 g, 58.5 mmol, 1.2 equiv.),  $K_2CO_3$  (6.73 g, 48.8 mmol, 1 equiv.) and KI (80.9 mg, 0.49 mmol, 1 mol%) under flow of nitrogen. The mixture was heated to 70 °C for 20 hours, after which the reaction mixture was diluted with water (300 mL) and EtOAc (100 mL) and the phases were separated. The aqueous phase was extracted with EtOAc (2 × 100 mL) and the resultant combined organic layers were washed with LiCl 10% (w/v) solution (3 × 100 mL), dried over  $MgSO_4$ , filtered, and concentrated under reduced pressure. The crude product was purified by normal phase column chromatography on silica (100%  $CH_2Cl_2$  isocratic) to yield **169** (8.90 g, 86%) as a white solid.  $^1H$  NMR (600 MHz,  $CDCl_3$ )  $\delta$  = 7.85 – 7.82 (m, 2H, H8), 7.72 – 7.69 (m, 2H, H9), 3.79 (t,  $J$  = 7.2 Hz, 2H, H1), 2.26 (td,  $J$  = 7.1, 2.7 Hz, 2H, H3), 1.95 – 1.88 (m, 3H, H2, H5);  $^{13}C$  NMR (151 MHz,  $CDCl_3$ )  $\delta$  = 168.48 (2C, C6), 134.06 (2C, C9), 132.23 (2C, C7), 123.36 (2C, C8), 83.10 (C4), 69.13 (C5), 37.27 (C1), 27.40 (C2), 16.40 (C3); HRMS (ESI+)  $m/z$  calculated for  $C_{13}H_{12}NO_2$  (M+H)<sup>+</sup> 214.0863, found 214.0874.

The spectroscopic and analytical data were in agreement with literature values.<sup>294</sup>

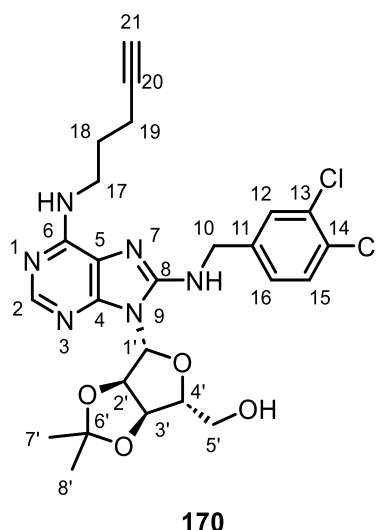
**pent-4-yn-1-amine (167)**

A two-neck round bottom flask equipped with magnetic stirrer was charged with 2-(pent-4-yn-1-yl)isoindoline-1,3-dione **169** (7.68 g, 36.0 mmol, 1 equiv.), ethanol (80.0 mL, 0.45 M) and hydrazine monohydrate (37.2 mL, 499 mmol, 13.8 equiv.) under flow of nitrogen. The mixture was heated to 70 °C for 2 hours, after which the reaction mixture was diluted with water (100 mL) and acidified to pH = 2 with 2M HCl solution. The resultant white

precipitate was filtered off and the filtrate was concentrated under reduced pressure. The crude residue was redissolved in 10 M NaOH, the aqueous phase was extracted with CH<sub>2</sub>Cl<sub>2</sub> (2 × 200 mL) and the resultant combined organic layers were dried over MgSO<sub>4</sub>, filtered, and concentrated under reduced pressure to yield **167** (2.82 g, 94%) as a pale yellow liquid. <sup>1</sup>H NMR (600 MHz, CDCl<sub>3</sub>) δ = 2.81 (t, *J* = 6.9 Hz, 2H, H1), 2.26 (td, *J* = 7.0, 2.7 Hz, 2H, H3), 1.95 (t, *J* = 2.7 Hz, 1H, H5), (app. quint, *J* = 7.0 Hz, 2H, H2); <sup>13</sup>C NMR (151 MHz, CDCl<sub>3</sub>) δ = 84.07 (C4), 68.71 (C5), 41.15 (C1), 32.11 (C2), 15.99 (C3); HRMS *m/z* not observed due to low molecular weight. IR (thin layer film) ν/cm<sup>-1</sup> = 3301 (H-C≡C), 2116 (C≡C).

The spectroscopic and analytical data were in agreement with literature values.<sup>295</sup>

**((3*aR*,4*R*,6*R*,6*aR*)-6-(8-((3,4-dichlorobenzyl)amino)-6-(pent-4-yn-1-ylamino)-9*H*-purin-9-yl)-2,2-dimethyltetrahydrofuro[3,4-*d*][1,3]dioxol-4-yl)methanol (170)**

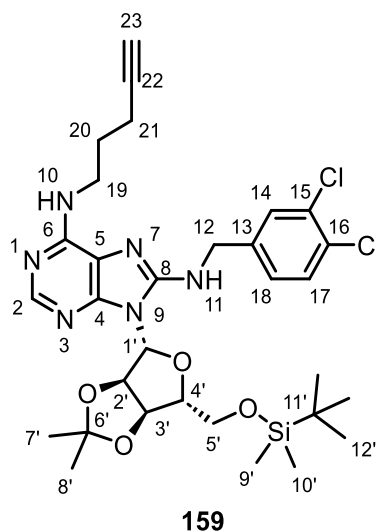


A two-neck round bottom flask equipped with magnetic stirrer and reflux condenser was charged with ((3*aR*,4*R*,6*R*,6*aR*)-6-(6-chloro-8-((3,4-dichlorobenzyl)amino)-9*H*-purin-9-yl)-2,2-dimethyltetrahydrofuro[3,4-*d*][1,3]dioxol-4-yl)methanol **165** (5.00 g, 9.98 mmol, 1 equiv.), n-butanol (49.9 mL, 0.2 M), pent-4-yn-1-amine **167** (4.98 g, 59.9 mmol, 6 equiv.) and triethylamine (5.57 mL, 39.9 mmol, 4 equiv.) under flow of nitrogen. The mixture was heated to 100 °C for 20 hours, after which the solvent was removed under reduced pressure and the crude mixture was purified by normal phase column chromatography on silica (100% CH<sub>2</sub>Cl<sub>2</sub> to methanol:CH<sub>2</sub>Cl<sub>2</sub> 10:90 gradient) to yield **170** (4.73 g, 86%) as an orange foam. <sup>1</sup>H NMR (600 MHz, CDCl<sub>3</sub>) δ = 8.15 (s br, 1H, H2),

7.49 – 7.47 (m, 1H, H12), 7.39 (d,  $J = 8.2$  Hz, 1H, H15), 7.22 (app. d,  $J = 8.2$  Hz, 1H, H16), 6.00 – 5.94 (m, 1H, H1'), 5.11 (app. t,  $J = 5.0$  Hz, 1H, H2'), 5.03 (dd,  $J = 6.2, 2.0$  Hz, 1H, H3'), 4.62 (dd,  $J = 15.1, 5.5$  Hz, 1H, H10a), 4.56 (dd,  $J = 15.1, 5.5$  Hz, 1H, H10b), 4.41 – 4.39 (m, 1H, H4'), 3.99 (app. d,  $J = 12.0$  Hz, 1H, H5'a), 3.83 (app. d,  $J = 12.0$  Hz, 1H, H5'b), 3.75 (app. s br, 2H, H17), 2.31 (td,  $J = 7.0, 2.6$  Hz, 2H, H19), 1.97 (t,  $J = 2.6$  Hz, 1H, H20), 1.90 (app. quint,  $J = 6.9$  Hz, 2H, H18), 1.62 (s, 3H, H7'), 1.36 (s, 3H, H8');  $^{13}\text{C}$  NMR (151 MHz  $\text{CDCl}_3$ )  $\delta = 148.82$  (C8), 138.66 (C11), 132.82 (C14), 131.78 (C13), 130.75 (C15), 129.73 (C12), 127.16 (C16), 114.77 (C6'), 90.59 (C1'), 85.27 (C4'), 83.60 (C20), 82.85 (C2'), 81.03 (C3'), 69.27 (C21), 62.61 (C5'), 46.12 (C10), 40.33 (C17), 28.70 (C18), 27.66 (C7'), 25.39 (C8'), 16.15 (C19);\* **HRMS** (ESI+)  $m/z$  calculated for  $\text{C}_{25}\text{H}_{29}^{35}\text{Cl}_2\text{N}_6\text{O}_4$  (M+H) $^+$  547.1622, found 547.1634; **IR** (thin layer film)  $\nu/\text{cm}^{-1} = 3276$  (H-C $\equiv$ C).

\*C2, C4, C5, and C6 not observed in spectrum.

**9-((3a*R*,4*R*,6*R*,6a*R*)-6-(((*tert*-butyldimethylsilyl)oxy)methyl)-2,2-dimethyltetrahydrofuro[3,4-*d*][1,3]dioxol-4-yl)-*N*8-(3,4-dichlorobenzyl)-*N*6-(pent-4-yn-1-yl)-9*H*-purine-6,8-diamine (159)**



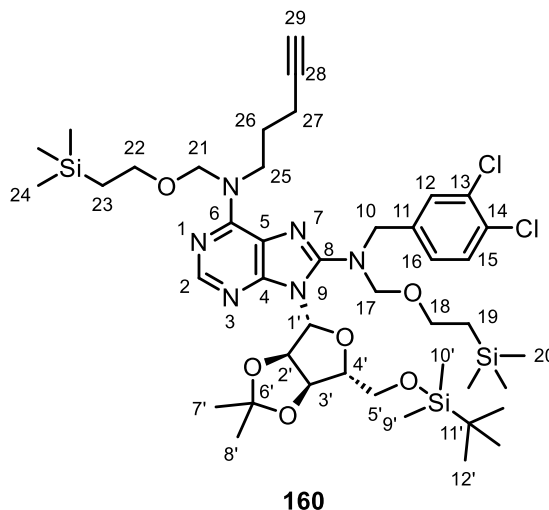
A two-neck round bottom flask equipped with magnetic stirrer was charged with ((3a*R*,4*R*,6*R*,6a*R*)-6-(8-((3,4-dichlorobenzyl)amino)-6-(pent-4-yn-1-ylamino)-9*H*-purin-9-yl)-2,2-dimethyltetrahydrofuro[3,4-*d*][1,3]dioxol-4-yl)methanol **170** (4.72 g, 8.62 mmol, 1 equiv.), DMF (24.6 mL, 0.35 M), *tert*-butyldimethylsilyl chloride (1.56 g, 10.3 mmol, 1.2 equiv.), and imidazole (1.17 g, 17.2 mmol, 2 equiv.) under flow of nitrogen.



After stirring for at room temperature for 20 hours, the reaction mixture was diluted with water (200 mL) and EtOAc (100 mL) and the phases were separated. The aqueous phase was extracted with EtOAc (100 mL) and the resultant combined organic layers were washed with LiCl 10% (w/v) solution ( $3 \times 100$  mL), dried over  $\text{MgSO}_4$ , filtered, and concentrated under reduced pressure. The crude product was purified by normal phase column chromatography on silica (EtOAc:cyclohexane 5:95 to 50:50 gradient) to yield **159** (4.10 g, 72%) as a yellow solid.  **$^1\text{H NMR}$**  (600 MHz,  $\text{CD}_3\text{CN}$ )  $\delta$  = 8.02 (s, 1H, H2), 7.58 (app. s, 1H, H14), 7.46 (d,  $J$  = 8.3 Hz, 1H, H17), 7.34 (app. d,  $J$  = 8.2 Hz, 1H, H18), 6.05 (t,  $J$  = 6.1 Hz, 1H, H11), 5.95 (d,  $J$  = 2.4 Hz, 1H, H1'), 5.76 – 5.70 (m, 2H, H2', H10), 4.99 (dd,  $J$  = 6.4, 2.9 Hz, 1H, H3'), 4.58 (d,  $J$  = 6.1 Hz, 2H, H12), 4.21 – 4.17 (m, 1H, H4'), 3.68 (dd,  $J$  = 11.2, 5.2 Hz, 1H, H5'a), 3.66 – 3.57 (m, 3H, H5'b, H19), 2.22 (td,  $J$  = 7.1, 2.4 Hz, 2H, H21), 2.16 (t,  $J$  = 2.4 Hz, 1H, H23), 1.79 (app. quint,  $J$  = 7.1 Hz, 2H, H20), 1.55 (s, 3H, H7'), 1.36 (s, 3H, H8'), 0.78 (s, 9H, H12'), -0.08 (s, 3H, H9'), -0.09 (s, 3H, H10');  **$^{13}\text{C NMR}$**  (151 MHz,  $\text{CD}_3\text{CN}$ )  $\delta$  = 153.11 (C6), 152.19 (C8), 150.33 (C2), 150.13 (C4), 141.90 (C13), 132.51 (C16), 131.28 (C17), 131.06 (C15), 130.42 (C14), 128.46 (C18), 118.45 (C5)\*, 114.56 (C6'), 89.93 (C1'), 87.75 (C4'), 84.90 (C22), 83.30 (C2'), 82.28 (C3'), 69.91 (C23), 63.99 (C5'), 45.82 (C12), 40.62 (C19), 29.68 (C20), 27.36 (C7'), 26.17 (3C, C12'), 25.59 (C8'), 18.99 (C11'), 16.39 (C21), -5.22 (C9'), -5.42 (C10'); **HRMS** (ESI+)  $m/z$  calculated for  $\text{C}_{31}\text{H}_{43}^{35}\text{Cl}_2\text{N}_6\text{O}_4\text{Si}$  ( $\text{M}+\text{H}$ )<sup>+</sup> 661.2487, found 661.2491; **IR** (thin layer film)  $\nu/\text{cm}^{-1}$  = 3285 (H-C $\equiv$ C).

\*Signal present in  $^1\text{H}$ - $^{13}\text{C}$  HMBC but is under solvent signal in 1D  $^{13}\text{C}$  spectrum.

**9-((3*aR*,4*R*,6*R*,6*aR*)-6-(((*tert*-butyldimethylsilyl)oxy)methyl)-2,2-dimethyltetrahydrofuro[3,4-*d*][1,3]dioxol-4-yl)-*N*8-(3,4-dichlorobenzyl)-*N*6-(pent-4-yn-1-yl)-*N*6,*N*8-bis((2-(trimethylsilyl)ethoxy)methyl)-9*H*-purine-6,8-diamine (160)**

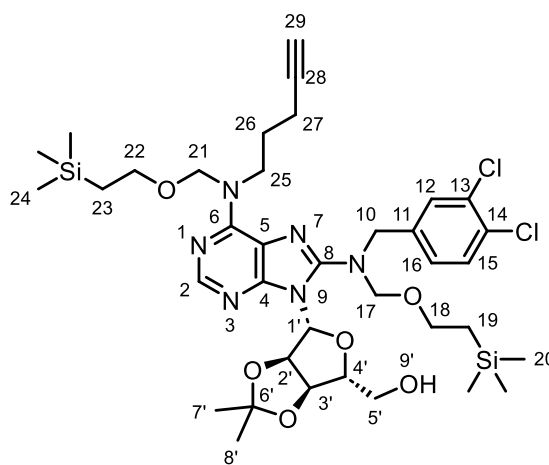


**160** was prepared following general procedure B, with 9-((3*aR*,4*R*,6*R*,6*aR*)-6-(((*tert*-butyldimethylsilyl)oxy)methyl)-2,2-dimethyltetrahydrofuro[3,4-*d*][1,3]dioxol-4-yl)-*N*8-(3,4-dichlorobenzyl)-*N*6-(pent-4-yn-1-yl)-9*H*-purine-6,8-diamine **159** (4.10 g, 6.20 mmol, 1 equiv.), CH<sub>2</sub>Cl<sub>2</sub> (20.7 mL, 0.3 M), 2-(trimethylsilyl)ethoxymethylchloride (3.29 mL, 18.6 mmol, 3 equiv.) and *N,N*-Diisopropylethylamine (3.24 mL, 18.6 mmol, 3 equiv.) for 22 hours. Purification by normal phase column chromatography on silica (EtOAc:cyclohexane 1:99 to 10:90 gradient) yielded **160** (4.07 g, 71%) as a yellow oil. <sup>1</sup>H NMR (600 MHz, CD<sub>3</sub>CN) δ = 8.15 (s, 1H, H2), 7.56 (d, *J* = 1.8 Hz, 1H, H12), 7.43 (d, *J* = 8.2 Hz, 1H, H15), 7.29 (dd, *J* = 8.2, 1.8 Hz, 1H, H16), 6.08 (d, *J* = 1.8 Hz, 1H, H1'), 5.62 (dd, *J* = 6.3, 1.8 Hz, 1H, H2'), 5.45 (s br, 1H, H21a), 5.32 (s br, 1H, H21b), 5.12 (dd, *J* = 6.3, 2.8 Hz, 1H, H3'), 4.81 (d, *J* = 10.4 Hz, 1H, H17a), 4.75 – 4.70 (m, 2H, H10a, H17b), 4.56 (d, *J* = 14.9 Hz, 1H, H10b), 4.18 (app. td, *J* = 6.6, 2.8 Hz, 1H, H4'), 3.92 (s br, 2H, H25), 3.85 (dd, *J* = 10.6, 6.9 Hz, 1H, H5'a), 3.71 (dd, *J* = 10.6, 6.5 Hz, 1H, H5'b), 3.54 – 3.46 (m, 4H, H18, H22), 2.23 (td, *J* = 7.2, 2.6 Hz, 2H, H27), 2.18 (t, *J* = 2.6 Hz, 1H, H29), 1.86 (app. quint, *J* = 7.3 Hz, 2H, H26), 1.54 (s, 3H, H7'), 1.33 (s, 3H, H8'), 0.88 – 0.83 (m, 4H, H19, H23), 0.82 (s, 9H, H12'), -0.06 (s br, 6H, C9', C10'), -0.07 – -0.09 (m, 18H, H20, H24); <sup>13</sup>C NMR (151 MHz, CD<sub>3</sub>CN) δ = 153.68 (C6), 152.69 (C8), 151.75 (C4), 151.17 (C2), 140.25 (C11), 132.60 (C14), 131.36 (C13), 131.29 (C15), 131.26 (C12), 129.29 (C16), 118.30 (C5)\*<sup>1</sup>, 114.26 (C6'), 90.79 (C1'), 88.96 (C4'), 84.85

(C28), 83.72 (C2'), 83.68 (C17), 83.40 (C3'), 69.99 (C29), 66.63 (C18), 65.36 (C22), 64.26 (C5'), 53.38 (C10), 47.62 (C25), 28.31 (C26), 27.47 (C7'), 26.19 (3C, C12'), 25.59 (C8'), 18.91 (C11'), 18.62 (C23), 18.52 (C19), 16.47 (C27), -1.32 (3C, C20), -1.37 (3C, C24), -5.11 (C9'), -5.19 (C10');\*<sup>2</sup> HRMS (ESI+)  $m/z$  calculated for  $C_{43}H_{71}^{35}Cl_2N_6O_6Si_3$  (M+H)<sup>+</sup> 921.4114, found 921.4117; IR (thin layer film)  $\nu/cm^{-1}$  = 3309 (H-C≡C).

\*<sup>1</sup>Signal present in <sup>1</sup>H-<sup>13</sup>C HMBC but is under solvent signal in 1D <sup>13</sup>C spectrum. \*<sup>2</sup>C21 not observed in spectrum.

**((3*aR*,4*R*,6*R*,6*aR*)-6-(8-((3,4-dichlorobenzyl)((2-(trimethylsilyl)ethoxy)methyl)amino)-6-(pent-4-yn-1-yl)((2-(trimethylsilyl)ethoxy)methyl)amino)-9*H*-purin-9-yl)-2,2-dimethyltetrahydrofuro[3,4-*d*][1,3]dioxol-4-yl)methanol (161)**



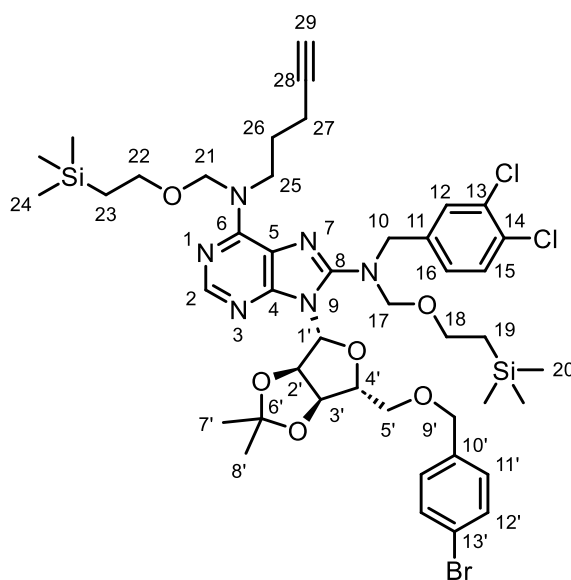
**161**

**161** was prepared following general procedure C, with 9-((3*aR*,4*R*,6*R*,6*aR*)-6-(((*tert*-butyldimethylsilyl)oxy)methyl)-2,2-dimethyltetrahydrofuro[3,4-*d*][1,3]dioxol-4-yl)-*N*8-(3,4-dichlorobenzyl)-*N*6-(pent-4-yn-1-yl)-*N*6,*N*8-bis((2-(trimethylsilyl)ethoxy)methyl)-9*H*-purine-6,8-diamine **160** (4.00 g, 4.34 mmol, 1 equiv.), THF (43.3 mL, 0.1 M) and TBAF (4.77 mL, 1 M in THF, 4.77 mmol, 1.1 equiv.) for 24 hours. Purification by normal phase column chromatography on silica (EtOAc:cyclohexane 5:95 to 50:50 gradient) yielded **161** (3.11 g, 89%) as a pale yellow oil. <sup>1</sup>H NMR (600 MHz, CD<sub>3</sub>CN)  $\delta$  = 8.12 (s, 1H, H2), 7.56 (d,  $J$  = 1.7 Hz, 1H, H12), 7.43 (d,  $J$  = 8.3 Hz, 1H, H15), 7.30 (dd,  $J$  = 8.3, 1.7 Hz, 1H, H16), 6.02 (d,  $J$  = 5.0 Hz, 1H, H1'), 5.70 (app. d,  $J$  = 10.3 Hz, 1H, H9'), 5.56 – 5.19 (m, 3H, H2', H21), 5.06 (app. d,  $J$  = 5.8 Hz, 1H, H3'), 4.80 (d,  $J$  = 10.5 Hz, 1H,

H17a), 4.71 (d,  $J = 10.5$  Hz, 1H, H17b), 4.68 – 4.60 (m, 2H, H10), 4.40 – 4.37 (m, 1H, H4'), 3.93 (app. s br, 2H, H25), 3.77 (app. dt,  $J = 12.5, 2.1$  Hz, 1H, H5'a), 3.70 – 3.65 (m, 1H, H5'b), 3.54 – 3.46 (m, 4H, H18, H22), 2.24 (td,  $J = 7.2, 2.5$  Hz, 2H, H27), 2.19 (t,  $J = 2.5$  Hz, 1H, H29), 1.86 (app. quint,  $J = 7.3$  Hz, 2H, H26), 1.62 (s, 3H, H7'), 1.35 (s, 3H, H8'), 0.88 – 0.82 (m, 4H, H19, H23), -0.07 (s, 9H, H20), -0.08 (s, 9H, H24);  $^{13}\text{C}$  NMR (151 MHz,  $\text{CD}_3\text{CN}$ )  $\delta = 154.02$  (C6), 152.25 (C8), 151.24 (C4), 150.91 (C2), 140.22 (C11), 132.63 (C14), 131.36 (C13), 131.25 (C15), 131.09 (C12), 129.19 (C16), 118.68 (C5), 114.61 (C6'), 92.49 (C1'), 86.54 (C4'), 84.81 (C28), 84.49 (C17), 82.76 (C2'), 82.74 (C3'), 70.04 (C29), 66.96 (C18), 65.46 (C22), 63.82 (C5'), 53.24 (C10), 47.64 (C25), 28.13 (C26), 27.88 (C7'), 25.61 (C8'), 18.59 (C23), 18.43 (C19), 16.47 (C27), -1.35 (3C, C20), -1.44 (3C, C24);\* **HRMS** (ESI+)  $m/z$  calculated for  $\text{C}_{37}\text{H}_{57}^{35}\text{Cl}_2\text{N}_6\text{O}_6\text{Si}_2$  (M+H) $^+$  807.3250, found 807.3273; **IR** (thin layer film)  $\nu/\text{cm}^{-1} = 3309$  (H-C $\equiv$ C);  $[\alpha]_{\text{D}}^{25} = -14^\circ$  ( $c = 0.5$ ,  $\text{CHCl}_3$ ).

\*C21 not observed in spectrum.

**9-((3*aR*,4*R*,6*R*,6*aR*)-6-(((4-bromobenzyl)oxy)methyl)-2,2-dimethyltetrahydrofuro[3,4-*d*][1,3]dioxol-4-yl)-*N*8-(3,4-dichlorobenzyl)-*N*6-(pent-4-yn-1-yl)-*N*6,*N*8-bis((2-(trimethylsilyl)ethoxy)methyl)-9*H*-purine-6,8-diamine (162)**

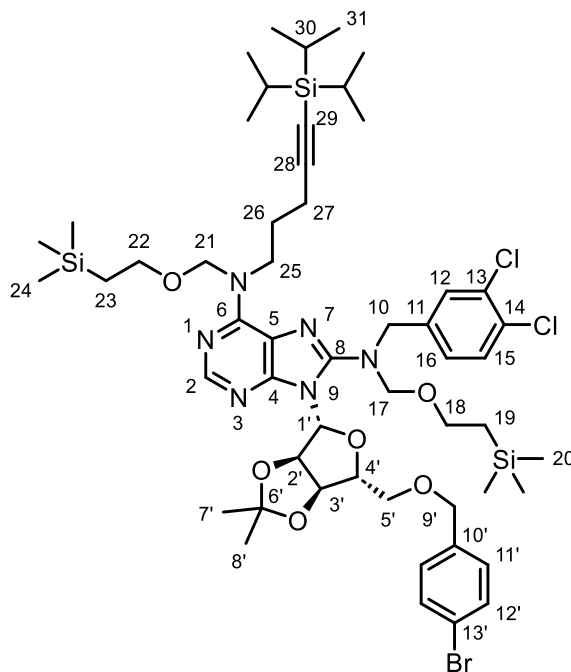


**162**

**162** was prepared following general procedure D, with ((3*aR*,4*R*,6*R*,6*aR*)-6-(8-((3,4-dichlorobenzyl)((2-(trimethylsilyl)ethoxy)methyl)amino)-6-(pent-4-yn-1-yl)((2-(trimethylsilyl)ethoxy)methyl)amino)-9*H*-purin-9-yl)-2,2-dimethyltetrahydrofuro[3,4-*d*][1,3]dioxol-4-yl)methanol **161** (1.55 g, 1.92 mmol, 1 equiv.), THF (3.84 mL, 0.5 M), sodium hydride (92.1 mg, 60% in mineral oil, 2.30 mmol, 1.2 equiv.) and 4-bromobenzyl bromide (959 mg, 3.84 mmol, 2 equiv.). Purification by normal phase column chromatography on silica (EtOAc:cyclohexane 5:95 to 25:75 gradient) yielded **162** (1.69 g, 90%) as a colourless oil. **<sup>1</sup>H NMR** (600 MHz, CD<sub>3</sub>CN)  $\delta$  = 8.04 (s, 1H, H2), 7.55 (d,  $J$  = 2.0 Hz, 1H, H12), 7.42 (d,  $J$  = 8.3 Hz, 1H, H15), 7.39 – 7.35 (m, 2H, H12'), 7.29 (dd,  $J$  = 8.3, 2.0 Hz, 1H, H16), 7.12 – 7.09 (m, 2H, H11'), 6.08 (d,  $J$  = 2.0 Hz, 1H, H1'), 5.58 (dd,  $J$  = 6.3, 2.0 Hz, 1H, H2'), 5.53 – 5.26 (m, 2H, H21), 5.11 (dd,  $J$  = 6.3, 3.2 Hz, 1H, H3'), 4.81 (d,  $J$  = 10.5 Hz, 1H, H17a), 4.75 – 4.70 (m, 2H, H10a, H17b), 4.57 (d,  $J$  = 14.9 Hz, 1H, H10b), 4.44 – 4.37 (m, 2H, H9'), 4.33 (app. td,  $J$  = 6.4, 3.2 Hz, 1H, H4'), 4.06 – 3.77 (m, 2H, H25), 3.68 (dd,  $J$  = 10.2, 5.8, Hz, 1H, H5'a), 3.61 (dd,  $J$  = 10.2, 7.0 Hz, 1H, H5'b), 3.54 – 3.46 (m, 4H, H18, H22), 2.24 (td,  $J$  = 7.1, 2.6 Hz, 2H, H27), 2.18 (t,  $J$  = 2.6 Hz, 1H, H29), 1.88 (app. quint,  $J$  = 7.3 Hz, 2H, H26), 1.55 (s, 3H, H7'), 1.32 (s, 3H, H8'), 0.88 – 0.82 (m, 4H, H19, H23), -0.08 (s, 9H, H20), -0.09 (s, 9H, H24); **<sup>13</sup>C NMR** (151 MHz, CD<sub>3</sub>CN)  $\delta$  = 153.64 (C6), 152.57 (C8), 151.72 (C4), 151.14 (C2), 140.24 (C11), 138.80 (C10'), 132.62 (C14), 132.10 (2C, C12'), 131.39 (C13), 131.28 (2C, C12, C15), 130.30 (2C, C11'), 129.30 (C16), 121.64 (C13'), 118.29 (C5)\*<sup>1</sup>, 114.50 (C6'), 90.62 (C1'), 87.24 (C4'), 84.88 (C28), 83.78 (C17), 83.70 (C2'), 83.41 (C3'), 72.72 (C9'), 70.93 (C5'), 70.02 (C29), 66.67 (C18), 65.36 (C22), 53.44 (C10), 47.71 (C25), 28.31 (C26), 27.48 (C7'), 25.58 (C8'), 18.63 (C23), 18.51 (C19), 16.53 (C27), -1.31 (3C, C24), -1.36 (3C, C20);\*<sup>2</sup> **HRMS** (ESI+)  $m/z$  calculated for C<sub>44</sub>H<sub>62</sub><sup>79</sup>Br<sup>35</sup>Cl<sub>2</sub>N<sub>6</sub>O<sub>6</sub>Si<sub>2</sub> (M+H)<sup>+</sup> 975.2824, found 975.2841; **IR** (thin layer film)  $\nu/\text{cm}^{-1}$  = 3307 (H-C $\equiv$ C).

\*<sup>1</sup>Signal present in <sup>1</sup>H-<sup>13</sup>C HMBC but is under solvent signal in 1D <sup>13</sup>C spectrum. \*<sup>2</sup>C21 not observed in spectrum.

**9-((3*aR*,4*R*,6*R*,6*aR*)-6-(((4-bromobenzyl)oxy)methyl)-2,2-dimethyltetrahydrofuro[3,4-*d*][1,3]dioxol-4-yl)-*N*8-(3,4-dichlorobenzyl)-*N*6-(5-(triisopropylsilyl)pent-4-yn-1-yl)-*N*6,*N*8-bis((2-(trimethylsilyl)ethoxy)methyl)-9*H*-purine-6,8-diamine (**171**)**



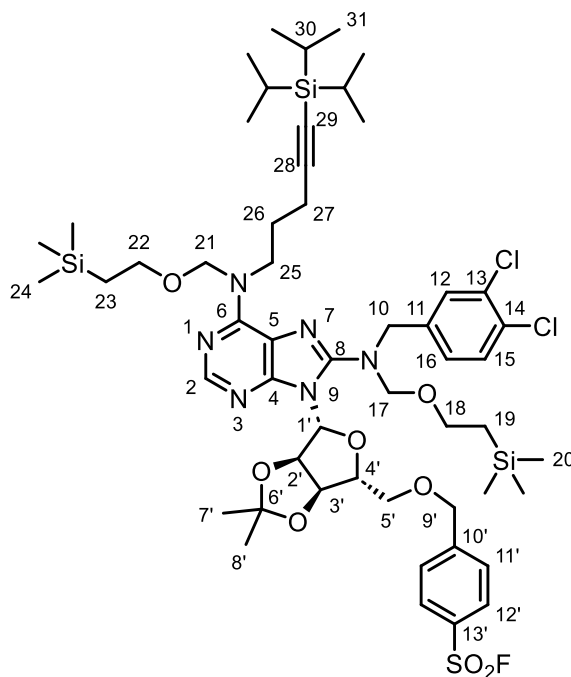
**171**

A glass microwave vial heat-dried under vacuum and equipped with magnetic stirrer was charged with diisopropyl amine (173  $\mu$ L, 1.23 mmol, 1.2 equiv.) and THF (2.05 mL, 0.25 M) under flow of nitrogen. The mixture was cooled to  $-78$   $^{\circ}$ C and *n*-butyllithium (450  $\mu$ L, 2.5 M in hexanes, 1.13 mmol, 1.1 equiv.) was added dropwise, after which the mixture stirred for an hour. A separate microwave vial heat-dried under vacuum and equipped with magnetic stirrer was charged with 9-((3*aR*,4*R*,6*R*,6*aR*)-6-(((4-bromobenzyl)oxy)methyl)-2,2-dimethyltetrahydrofuro[3,4-*d*][1,3]dioxol-4-yl)-*N*8-(3,4-dichlorobenzyl)-*N*6-(pent-4-yn-1-yl)-*N*6,*N*8-bis((2-(trimethylsilyl)ethoxy)methyl)-9*H*-purine-6,8-diamine **162** (1.00 g, 1.02 mmol, 1 equiv.) and THF (2.05 mL) under flow of nitrogen, and the resultant solution was transferred dropwise *via* syringe into the first mixture. After stirring for 1 hour at  $-78$   $^{\circ}$ C, triisopropylsilyl trifluoromethanesulfonate (330  $\mu$ L, 1.23 mmol, 1.2 equiv.) was added and the reaction mixture was stirred for a further 3 hours at  $-78$   $^{\circ}$ C. The reaction mixture was quenched with sat.  $\text{NH}_4\text{Cl}$  solution (40 mL), diluted with EtOAc (40 mL) and the phases were separated. The aqueous phase was extracted with EtOAc (2  $\times$  40 mL) and the resultant combined organic layers were

dried over MgSO<sub>4</sub>, filtered, and concentrated under reduced pressure. The crude product was purified by normal phase column chromatography on silica (EtOAc:cyclohexane 1:99 to 10:90 gradient) to yield **171** (407 mg, 35%) as a colourless oil. **<sup>1</sup>H NMR** (600 MHz, CD<sub>3</sub>CN)  $\delta$  = 8.04 (s, 1H, H2), 7.55 (d,  $J$  = 2.0 Hz, 1H, H12), 7.42 (d,  $J$  = 8.3 Hz, 1H, H15), 7.38 – 7.35 (m, 2H, H12'), 7.29 (dd,  $J$  = 8.3, 2.0 Hz, 1H, H16), 7.11 – 7.08 (m, 2H, H11'), 6.08 (d,  $J$  = 2.0 Hz, 1H, H1'), 5.58 (dd,  $J$  = 6.3, 2.0 Hz, 1H, H2'), 5.55 – 5.22 (m, 2H, H21), 5.11 (dd,  $J$  = 6.3, 3.2 Hz, 1H, H3'), 4.81 (d,  $J$  = 10.4 Hz, 1H, H17a), 4.74 – 4.69 (m, 2H, H10a, H17b), 4.56 (dd,  $J$  = 14.8 Hz, 1H, H10b), 4.44 – 4.37 (m, 2H, H9'), 4.34 – 4.30 (m, 1H, H4'), 4.07 – 3.77 (m, 2H, H25), 3.68 (dd,  $J$  = 10.2, 5.7 Hz, 1H, H5'a), 3.61 (dd,  $J$  = 10.2, 7.1 Hz, 1H, H5'b), 3.52 – 3.46 (m, 4H, H18, H22), 2.32 (t,  $J$  = 7.0 Hz, 2H, H27), 1.90 (app. quint,  $J$  = 7.3 Hz, 2H, H26), 1.56 (s, 3H, H7'), 1.32 (s, 3H, H8'), 1.09 – 1.00 (m, 21H, H30, H31), 0.86 – 0.81 (m, 4H, H19, H23), -0.08 – -0.10 (m, 18H, H20, H24); **<sup>13</sup>C NMR** (151 MHz, CD<sub>3</sub>CN)  $\delta$  = 153.64 (C6), 152.61 (C8), 151.66 (C4), 151.13 (C2), 140.21 (C11), 138.79 (C10'), 132.61 (C14), 132.08 (C2C, C12'), 131.39 (C13), 131.34 (C12), 131.26 (C15), 130.27 (2C, C11'), 129.32 (C16), 121.63 (C13'), 118.34 (C5)\*<sup>1</sup>, 114.46 (C6'), 109.80 (C29), 90.62 (C1'), 87.30 (C4'), 83.74 (C2'), 83.66 (C17), 83.41 (C3'), 81.23 (C28), 72.70 (C9'), 70.91 (C5'), 66.65 (C18), 65.27 (C22), 53.42 (C10), 47.94 (C25), 28.60 (C26), 27.45 (C7'), 25.56 (C8'), 19.02 (6C, C31), 18.68 (C23), 18.49 (C19), 17.93 (C27), 12.07 (3C, C30), -1.32 (3C, C24), -1.37 (3C, C20);\*<sup>2</sup> **HRMS** (ESI+)  $m/z$  calculated for C<sub>53</sub>H<sub>82</sub><sup>79</sup>Br<sup>35</sup>Cl<sub>2</sub>N<sub>6</sub>O<sub>6</sub>Si<sub>3</sub> (M+H)<sup>+</sup> 1131.4159, found 1131.4191;  $[\alpha]_D^{25} = -2^\circ$  (c = 0.5, CHCl<sub>3</sub>).

\*<sup>1</sup>Signal present in <sup>1</sup>H-<sup>13</sup>C HMBC but is under solvent signal in 1D <sup>13</sup>C spectrum. \*<sup>2</sup>C21 not observed in spectrum.

**4-(((3*aR*,4*R*,6*R*,6*aR*)-6-(8-((3,4-dichlorobenzyl)((2-(trimethylsilyl)ethoxy)methyl)amino)-6-((5-(triisopropylsilyl)pent-4-yn-1-yl)((2-(trimethylsilyl)ethoxy)methyl)amino)-9*H*-purin-9-yl)-2,2-dimethyltetrahydrofuro[3,4-*d*][1,3]dioxol-4-yl)methoxy)methyl)benzenesulfonyl fluoride (172)**



172

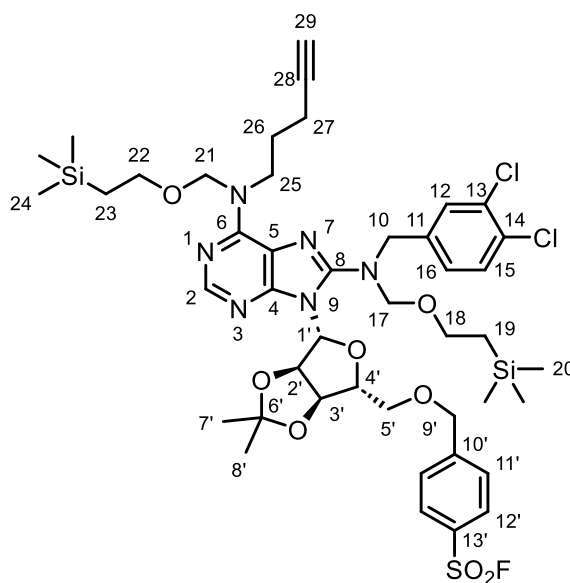
**172** was prepared following general procedure E, with 9-((3*aR*,4*R*,6*R*,6*aR*)-6-(((4-bromobenzyl)oxy)methyl)-2,2-dimethyltetrahydrofuro[3,4-*d*][1,3]dioxol-4-yl)-*N*8-(3,4-dichlorobenzyl)-*N*6-(5-(triisopropylsilyl)pent-4-yn-1-yl)-*N*6,*N*8-bis((2-(trimethylsilyl)ethoxy)methyl)-9*H*-purine-6,8-diamine **171** (582 mg, 0.51 mmol, 1 equiv.), isopropanol (1.90 mL, 0.27 M), DABSO (74.0 mg, 0.31 mmol, 0.6 equiv.), PdCl<sub>2</sub>(AmPhos)<sub>2</sub> (18.2 mg, 0.03 mmol, 5 mol%), triethylamine (0.21 mL, 1.54 mmol, 3 equiv.) and NFSI (243 mg, 0.77 mmol, 1.5 equiv.). Purification by normal phase column chromatography on silica (EtOAc:cyclohexane 1:99 to 20:80 gradient) yielded **172** (194 mg, 33%) as a pale yellow oil. <sup>1</sup>H NMR (600 MHz, CD<sub>3</sub>CN) δ = 8.04 (s, 1H, H2), 7.92 – 7.88 (m, 2H, H12'), 7.55 (d, *J* = 1.8 Hz, 1H, H12), 7.54 – 7.50 (m, 2H, H11'), 7.42 (d, *J* = 8.3 Hz, 1H, H15), 7.29 (dd, *J* = 8.3, 1.8 Hz, 1H, H16), 6.10 (d, *J* = 2.0 Hz, 1H, H1'), 5.60 (dd, *J* = 6.3, 1.9 Hz, 1H, H2'), 5.57 – 5.25 (m, 2H, H21), 5.16 (dd, *J* = 6.3, 3.2 Hz, 1H, H3'), 4.82 (d, *J* = 10.4 Hz, 1H, H17a), 4.76 – 4.69 (m, 2H, H10a, H17b), 4.65 – 4.55 (m, 3H, H9', H10b), 4.39 – 4.35 (m, 1H, H4'), 4.05 – 3.83 (m, 2H, H25), 3.78 (dd, *J* =



10.3, 5.5 Hz, 1H, H5'a), 3.71 (dd,  $J = 10.3, 7.0$  Hz, 1H, H5'b), 3.52 – 3.46 (m, 4H, H18, H22), 2.31 (t,  $J = 7.0$  Hz, 2H, H27), 1.88 (app. quint,  $J = 7.3$  Hz, 2H, H26), 1.56 (s, 3H, H7'), 1.34 (s, 3H, H8'), 1.08 – 0.99 (m, 21H, H30, H31), 0.86 – 0.80 (m, 4H, H19, H23), -0.09 (s, 9H, H24), -0.10 (s, 9H, H20);  $^{13}\text{C}$  NMR (151 MHz,  $\text{CD}_3\text{CN}$ )  $\delta = 153.65$  (C6), 152.62 (C8), 151.72 (C4), 151.16 (C2), 149.01 (C10'), 140.21 (C11), 132.61 (C14), 131.39 (C13), 131.31 (C12), 131.25 (C15), 129.31 (C16), 129.28 (2C, C12'), 129.02 (2C, C11'), 118.35 (C5)\*<sup>1</sup>, 114.56 (C6'), 109.77 (C29), 90.63 (C1'), 87.12 (C4'), 83.74 (C17), 83.71 (C2'), 83.24 (C3'), 81.23 (C28), 72.32 (C9'), 71.51 (C5'), 66.67 (C18), 65.26 (C22), 53.45 (C10), 47.92 (C25), 28.63 (C26), 27.48 (C7'), 25.56 (C8'), 19.00 (6C, C31), 18.66 (C23), 18.47 (C19), 17.89 (C27), 12.06 (3C, C30), -1.35 (3C, C20), -1.41 (3C, C24);\*<sup>2</sup>  $^{19}\text{F}$  NMR (471 MHz,  $\text{CD}_3\text{CN}$ )  $\delta = 65.05$ ; HRMS (ESI+)  $m/z$  calculated for  $\text{C}_{53}\text{H}_{82}^{35}\text{Cl}_2\text{FN}_6\text{O}_8\text{SSi}_3$  (M+H)<sup>+</sup> 1135.4578, found 1135.4591.

\*<sup>1</sup>Signal present in  $^1\text{H}$ - $^{13}\text{C}$  HMBC but is under solvent signal in 1D  $^{13}\text{C}$  spectrum. \*<sup>2</sup>C13' and C21 not observed in spectrum.

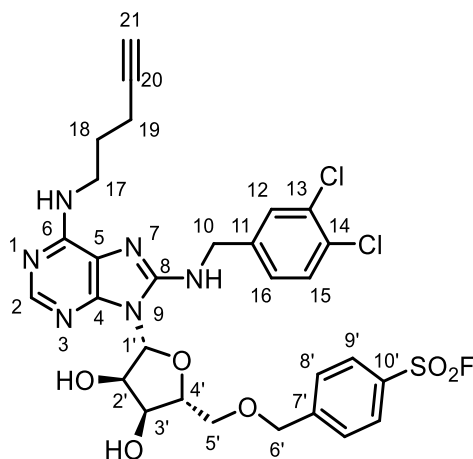
**4-(((3*aR*,4*R*,6*R*,6*aR*)-6-(8-((3,4-dichlorobenzyl)((2-(trimethylsilyl)ethoxy)methyl)amino)-6-(pent-4-yn-1-yl)((2-(trimethylsilyl)ethoxy)methyl)amino)-9*H*-purin-9-yl)-2,2-dimethyltetrahydrofuro[3,4-*d*][1,3]dioxol-4-yl)methoxy)methyl)benzenesulfonyl fluoride (163)**



163

A two-neck round bottom flask equipped with magnetic stirrer was charged with 4-(((3*aR*,4*R*,6*R*,6*aR*)-6-(8-((3,4-dichlorobenzyl)((2-(trimethylsilyl)ethoxy)methyl)amino)-6-((5-(triisopropylsilyl)pent-4-yn-1-yl)((2-(trimethylsilyl)ethoxy)methyl)amino)-9*H*-purin-9-yl)-2,2-dimethyltetrahydrofuro[3,4-*d*][1,3]dioxol-4-yl)methoxy)methyl)benzenesulfonyl fluoride **172** (190 mg, 0.17 mmol, 1 equiv.) and THF (1.67 mL, 0.1 M) under flow of nitrogen. The mixture was cooled to 0 °C and TBAF (0.33 mL, 1 M in THF, 0.33 mmol, 2 equiv.) was added dropwise, after which the mixture was allowed to warm up to room temperature. After stirring at room temperature for 48 hours, the reaction mixture was diluted with water (30 mL) and EtOAc (30 mL) the phases were separated. The aqueous phase was extracted with EtOAc (30 mL) and the resultant combined organic layers were washed with water (30 mL), brine (30 mL), dried over MgSO<sub>4</sub>, filtered, and concentrated under reduced pressure. The crude product was purified by normal phase column chromatography on silica (EtOAc:cyclohexane 1:99 to 30:70 gradient) to yield **163** (6.0 mg, 4%) as a colourless oil. <sup>1</sup>H NMR (600 MHz, CD<sub>2</sub>Cl<sub>2</sub>) δ = 8.11 (s, 1H, H2), 7.93 – 7.89 (m, 2H, H12'), 7.55 – 7.50 (m, 3H, H11', H12), 7.38 (d, *J* = 8.2 Hz, 1H, H15), 7.25 (dd, *J* = 8.2, 2.0 Hz, 1H, H16), 6.10 (d, *J* = 1.9 Hz, 1H, H1'), 5.59 (dd, *J* = 6.4, 1.9 Hz, 1H, H2'), 5.55 – 5.26 (m, 2H, H21), 5.20 (dd, *J* = 6.4, 3.3 Hz, 1H, H3'), 4.77 (d, *J* = 10.1 Hz, 1H, H17a), 4.72 (d, *J* = 10.7 Hz, 1H, H10a), 4.67 (d, *J* = 10.1 Hz, 1H, H17b), 4.65 – 4.53 (m, 3H, H9', H10b), 4.42 – 4.38 (m, 1H, H4'), 4.08 – 3.66 (m, 2H, H25), 3.83 (dd, *J* = 10.3, 5.6 Hz, 1H, H5'a), 3.75 (dd, *J* = 10.3, 6.8 Hz, 1H, H5'b), 3.57 – 3.48 (m, 4H, H18, H22), 2.26 (td, *J* = 7.3, 2.6 Hz, 2H, H27), 2.0 (t, *J* = 2.6 Hz, 1H, H29), 1.91 (app. quint, *J* = 7.3 Hz, 2H, H26), 1.58 (s, 3H, H7'), 1.36 (s, 3H, H8'), 0.93 – 0.87 (m, 4H, H19, H23), -0.04 (s, 9H, H20), -0.05 (s, 9H, H24); <sup>13</sup>C NMR (151 MHz, CD<sub>2</sub>Cl<sub>2</sub>) δ = 153.22 (C6), 151.83 (C8), 151.17 (C4), 150.80 (C2), 147.83 (C10'), 138.77 (C11), 132.65 (C14), 131.91 (d, *J*<sub>C-F</sub> = 24.1 Hz, C13'), 131.50 (C13), 130.85 (C12), 130.73 (C15), 128.81 (2C, C12'), 128.45 (C16), 128.28 (2C, C11'), 117.82 (C5), 114.25 (C6'), 90.15 (C1'), 86.74 (C4'), 84.35 (C28), 83.51 (C2'), 82.93 (C3'), 82.83 (C17), 82.71 (C21), 72.30 (C9'), 71.43 (C5'), 68.81 (C29), 66.40 (C18), 65.16 (C22), 52.92 (C10), 47.31 (C25), 27.89 (C26), 27.39 (C7'), 25.53 (C8'), 18.44 (C23), 18.32 (C19), 16.39 (C27), -1.32 (3C, C20), -1.37 (3C, C24); <sup>19</sup>F NMR (471 MHz, CD<sub>2</sub>Cl<sub>2</sub>) δ = 65.70; HRMS (ESI+) *m/z* calculated for C<sub>44</sub>H<sub>62</sub><sup>35</sup>Cl<sub>2</sub>FN<sub>6</sub>O<sub>8</sub>SSi<sub>2</sub> (M+H)<sup>+</sup> 979.3244, found 979.3248.

**4-(((2*R*,3*S*,4*R*,5*R*)-5-(8-((3,4-dichlorobenzyl)amino)-6-(pent-4-yn-1-ylamino)-9*H*-purin-9-yl)-3,4-dihydroxytetrahydrofuran-2-yl)methoxy)methyl)benzenesulfonyl fluoride (155)**

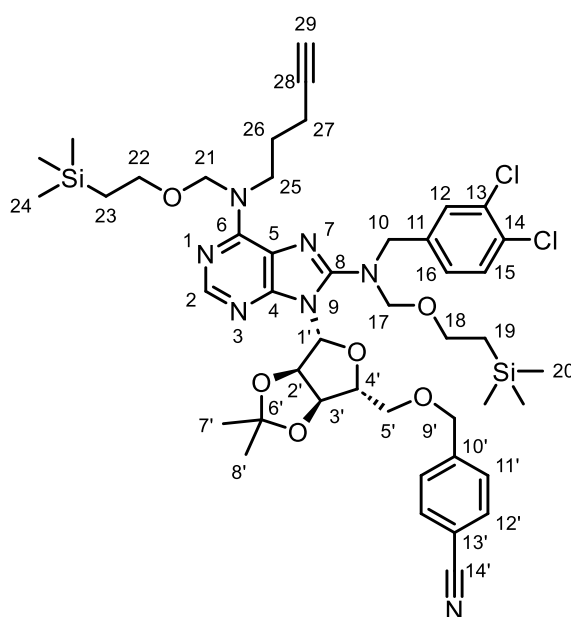


**155**

**155** was prepared following a modification of general procedure F, with 4-(((3*aR*,4*R*,6*R*,6*aR*)-6-(8-((3,4-dichlorobenzyl)((2-(trimethylsilyl)ethoxy)methyl)amino)-6-(pent-4-yn-1-yl)((2-(trimethylsilyl)ethoxy)methyl)amino)-9*H*-purin-9-yl)-2,2-dimethyltetrahydrofuro[3,4-*d*][1,3]dioxol-4-yl)methoxy)methyl)benzenesulfonyl fluoride **163** (6.0 mg, 0.01 mmol, 1 equiv.), and TFA:water 5:2 (v/v) mixture (0.61 mL, 0.01 M) for 2 hours. Purification by reverse phase column chromatography on C18 (acetonitrile:water +0.1% formic acid 20:80 to 80:20 gradient) yielded **155** (2.4 mg, 58%) as a white solid. <sup>1</sup>H NMR (600 MHz, CD<sub>2</sub>Cl<sub>2</sub>) δ = 8.08 (s, 1H, H2), 7.89 – 7.85 (m, 2H, H9'), 7.42 – 7.38 (m, 2H, H8'), 7.34 (d, *J* = 8.3 Hz, 1H, H15), 7.26 (d, *J* = 1.9 Hz, 1H, H12), 7.04 (dd, *J* = 8.3, 1.9 Hz, 1H, H16), 6.02 (d, *J* = 6.2 Hz, 1H, H1'), 4.59 (app. t, *J* = 6.1 Hz, 1H, H2'), 4.52 (d, *J* = 13.5 Hz, 1H, H6'a), 4.46 (d, *J* = 13.5 Hz, 1H, H6'b), 4.40 – 4.35 (m, 2H, H3', H10a), 4.25 – 4.19 (m, 2H, H4', H10b), 3.91 (dd, *J* = 10.8, 2.5 Hz, 1H, H5'a), 3.74 (dd, *J* = 10.8, 2.2 Hz, 1H, H5'b), 3.60 (t, *J* = 6.9 Hz, 2H, H17), 2.28 (td, *J* = 7.2, 2.6 Hz, 2H, H19), 2.01 (t, *J* = 2.6 Hz, 1H, H21), 1.83 (app. quint, *J* = 7.0 Hz, 2H, H18); <sup>13</sup>C NMR (151 MHz, CD<sub>2</sub>Cl<sub>2</sub>) δ = 152.41 (C6), 151.37 (C8), 150.13 (C2), 149.12 (C4), 146.35 (C7'), 139.63 (C11), 132.86 (C14), 132.54 (d, *J*<sub>C-F</sub> = 21.1 Hz, C10'), 131.47 (C13), 130.97 (C15), 129.08 (C9'), 128.84 (2C, C12), 128.29 (2C, C8'), 126.55 (C16), 117.07 (C5), 88.49 (C1'), 84.20 (C4'), 83.94 (C20), 73.01 (C2'), 72.65 (C6'), 70.81 (C3'), 70.53 (C5'), 69.06

(C21), 45.34 (C10), 40.07 (C17), 28.83 (C18), 16.18 (C19);  $^{19}\text{F}$  NMR (471 MHz,  $\text{CD}_2\text{Cl}_2$ )  $\delta = 65.40$ ; HRMS (ESI+)  $m/z$  calculated for  $\text{C}_{29}\text{H}_{30}^{35}\text{Cl}_2\text{FN}_6\text{O}_6\text{S}$  (M+H) $^+$  679.1303, found 679.1311.

**4-(((3*aR*,4*R*,6*R*,6*aR*)-6-(8-((3,4-dichlorobenzyl)((2-(trimethylsilyl)ethoxy)methyl)amino)-6-(pent-4-yn-1-yl)((2-(trimethylsilyl)ethoxy)methyl)amino)-9*H*-purin-9-yl)-2,2-dimethyltetrahydrofuro[3,4-*d*][1,3]dioxol-4-yl)methoxy)methyl)benzotrile (175)**



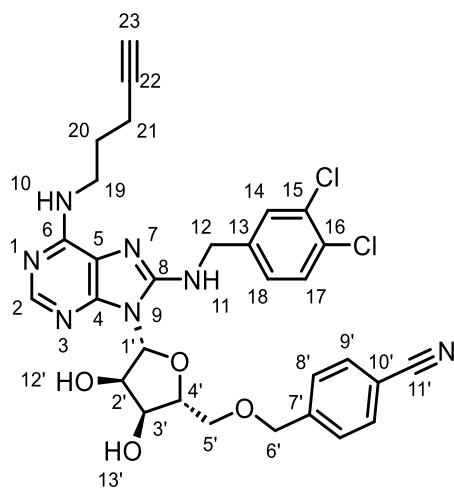
**175**

**175** was prepared following general procedure D, with ((3*aR*,4*R*,6*R*,6*aR*)-6-(8-((3,4-dichlorobenzyl)((2-(trimethylsilyl)ethoxy)methyl)amino)-6-(pent-4-yn-1-yl)((2-(trimethylsilyl)ethoxy)methyl)amino)-9*H*-purin-9-yl)-2,2-dimethyltetrahydrofuro[3,4-*d*][1,3]dioxol-4-yl)methanol **161** (200 mg, 0.25 mmol, 1 equiv.), THF (0.50 mL, 0.5 M), sodium hydride (11.9 mg, 60% in mineral oil, 0.30 mmol, 1.2 equiv.) and 4-cyanobenzyl bromide (97.1 mg, 0.50 mmol, 2 equiv.). Purification by normal phase column chromatography on silica (EtOAc:cyclohexane 1:99 to 25:75 gradient) yielded **175** (171 mg, 75%) as a colourless oil.  $^1\text{H}$  NMR (600 MHz,  $\text{CD}_3\text{CN}$ )  $\delta = 8.02$  (s, 1H, H2), 7.56 (d,  $J = 1.9$  Hz, 1H, H12), 7.55 – 7.52 (m, 2H, H12'), 7.42 (d,  $J = 8.2$  Hz, 1H, H15), 7.33 – 7.28 (m, 3H, H11', H16), 6.10 (d,  $J = 1.8$  Hz, 1H, H1'), 5.59 (dd,  $J = 6.3$  Hz, 1H, H2'), 5.56 – 5.23 (m, 2H, H21), 5.12 (dd,  $J = 6.4, 3.2$  Hz, 1H, H3'), 4.83 (d,  $J = 10.4$  Hz, 1H, H17a), 4.76 – 4.70 (m, 2H, H10a, H17b), 4.60 – 4.53 (m, 2H, H9'a, H10b), 4.48 (d,  $J =$

13.5 Hz, 1H, H9'b), 4.37 – 4.33 (m, 1H, H4'), 4.06 – 3.80 (m, 2H, H25), 3.72 (dd,  $J = 10.5, 5.3$  Hz, 1H, H5'a), 3.66 (dd,  $J = 10.5, 7.2$  Hz, 1H, H5'b), 3.54 – 3.47 (m, 4H, H18, H22), 2.25 (td,  $J = 7.3, 2.5$  Hz, 2H, H27), 2.19 (t,  $J = 2.5$  Hz, 1H, H29), 1.88 (app. quint,  $J = 7.4$  Hz, 2H, H26), 1.55 (s, 3H, H7'), 1.33 (s, 3H, H8'), 0.88 – 0.82 (m, 4H, H19, H23), -0.08 – -0.09 (m, 18H, H20, H24);  $^{13}\text{C NMR}$  (151 MHz,  $\text{CD}_3\text{CN}$ )  $\delta = 153.59$  (C6), 152.53 (C8), 151.66 (C4), 151.08 (C2), 145.19 (C10'), 140.25 (C11), 132.95 (2C, C12'), 132.60 (C13), 131.37 (C14), 131.26 (C15), 131.25 (C12), 129.29 (C16), 128.60 (2C, C11'), 119.66 (C14'), 114.49 (C5), 111.64 (C13'), 90.64 (C1'), 87.25 (C4'), 84.86 (C28), 83.83 (C17), 83.71 (C2'), 83.31 (C3'), 72.56 (C9'), 71.22 (C5'), 70.00 (C29), 66.65 (C18), 65.35 (C22), 53.47 (C10), 47.73 (C25), 28.28 (C26), 27.44 (C7'), 25.54 (C8'), 18.60 (C23), 18.49 (C19), 16.49 (C27), -1.36 (3C, C24), -1.40 (3C, C20);\* **HRMS** (ESI+)  $m/z$  calculated for  $\text{C}_{45}\text{H}_{62}^{35}\text{Cl}_2\text{N}_7\text{O}_6\text{Si}_2$  ( $\text{M}+\text{H}$ ) $^+$  922.3672, found 922.3678; **IR** (thin layer film)  $\nu/\text{cm}^{-1} = 3300$  ( $\text{H}-\text{C}\equiv\text{C}$ ), 2229 ( $\text{C}\equiv\text{N}$ ).

\*C5 and C21 not observed in spectrum.

**4-(((2*R*,3*S*,4*R*,5*R*)-5-(8-((3,4-dichlorobenzyl)amino)-6-(pent-4-yn-1-ylamino)-9*H*-purin-9-yl)-3,4-dihydroxytetrahydrofuran-2-yl)methoxy)methyl)benzonitrile (174)**



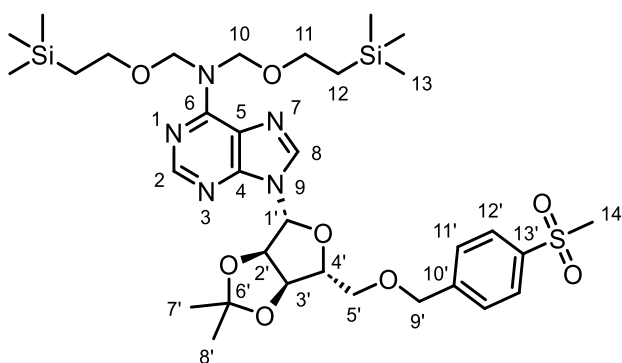
**174**

**174** was prepared following general procedure F, with 4-(((3*aR*,4*R*,6*R*,6*aR*)-6-(8-((3,4-dichlorobenzyl)((2-(trimethylsilyl)ethoxy)methyl)amino)-6-(pent-4-yn-1-yl((2-(trimethylsilyl)ethoxy)methyl)amino)-9*H*-purin-9-yl)-2,2-dimethyltetrahydrofuro[3,4-*d*][1,3]dioxol-4-yl)methoxy)methyl)benzonitrile **175** (165 mg, 0.18 mmol, 1 equiv.), and TFA:water 5:2 (v/v) mixture (1.79 mL, 0.1 M) for 2 hours. Purification by normal phase

column chromatography on silica (100% CH<sub>2</sub>Cl<sub>2</sub> to 15:85 methanol:CH<sub>2</sub>Cl<sub>2</sub> gradient) then reverse phase column chromatography on C18 (methanol:water +0.1% formic acid 20:80 to 90:10 gradient) yielded **174** (50 mg, 45%) as a white solid. **<sup>1</sup>H NMR** (600 MHz, DMSO-d<sub>6</sub>) δ = 7.96 (s, 1H, H2), 7.71 – 7.68 (m, 2H, H9'), 7.52 (d, *J* = 8.3 Hz, 1H, H17), 7.48 (d, *J* = 1.9 Hz, 1H, H14), 7.39 – 7.36 (m, 2H, H8'), 7.26 (dd, *J* = 8.3, 1.9 Hz, 1H, H18), 7.19 (t, *J* = 5.9 Hz, 1H, H11), 6.93 (t, *J* = 5.9 Hz, 1H, H10), 5.86 (d, *J* = 5.6 Hz, 1H, H1'), 5.41 (d, *J* = 5.7 Hz, 1H, H12'), 5.23 (d, *J* = 5.2 Hz, 1H, H13'), 4.96 (app. q, *J* = 5.5 Hz, 1H, H2'), 4.57 – 4.51 (m, 2H, H6'), 4.46 (d, *J* = 5.9 Hz, 2H, H12), 4.35 (app. q, *J* = 4.9 Hz, 1H, H3'), 4.06 – 4.03 (m, 1H, H4'), 3.77 (dd, *J* = 10.9, 3.0 Hz, 1H, H5'a), 3.66 (dd, *J* = 4.5 Hz, 1H, H5'b), 3.54 – 3.44 (m, 2H, H19), 2.74 (t, *J* = 2.6 Hz, 1H, H23), 2.16 (td, *J* = 7.2, 2.6 Hz, 2H, H21), 1.72 (app. quint, *J* = 7.1 Hz, 2H, H20); **<sup>13</sup>C NMR** (151 MHz, DMSO-d<sub>6</sub>) δ = 151.56 (C6), 151.05 (C8), 149.23 (C4), 149.00 (C2), 143.81 (C7'), 141.10 (C13), 132.09 (2C, C9'), 130.78 (C16), 130.33 (C17), 129.20 (C15), 128.91 (C14), 127.64 (C8'), 127.33 (C18), 118.74 (C11'), 117.02 (C5), 110.08 (C10'), 87.04 (C1'), 84.24 (C4'), 82.84 (C22), 71.46 (C6'), 71.22 (C23), 70.54 (C2'), 70.44 (C5'), 70.29 (C3'), 44.31 (C12), 39.32 (C19)\*, 28.49 (C20), 15.45 (C21); **HRMS** (ESI+) *m/z* calculated for C<sub>30</sub>H<sub>30</sub><sup>35</sup>Cl<sub>2</sub>N<sub>7</sub>O<sub>4</sub> (M+H)<sup>+</sup> 622.1731, found 622.1738; **IR** (thin layer film) *v*/cm<sup>-1</sup> = 3328 (H-C≡C), 2227 (C≡N).

\*Signal present in <sup>1</sup>H-<sup>13</sup>C HMBC but is under solvent signal in 1D <sup>13</sup>C spectrum.

**9-((3*aR*,4*R*,6*R*,6*aR*)-2,2-dimethyl-6-(((4-(methylsulfonyl)benzyl)oxy)methyl)tetrahydrofuro[3,4-*d*][1,3]dioxol-4-yl)-*N,N*-bis((2-(trimethylsilyl)ethoxy)methyl)-9*H*-purin-6-amine (178)**

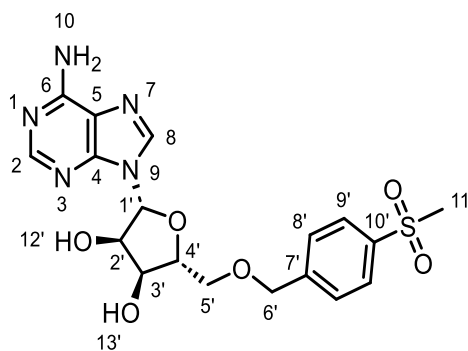


**178**

**178** was prepared following general procedure D, with ((3*aR*,4*R*,6*R*,6*aR*)-6-(6-(bis((2-(trimethylsilyl)ethoxy)methyl)amino)-9*H*-purin-9-yl)-2,2-dimethyltetrahydrofuro[3,4-

*d*][1,3]dioxol-4-yl)methanol **91** (200 mg, 0.35 mmol, 1 equiv.), THF (0.70 mL, 0.5 M), sodium hydride (16.9 mg, 60% in mineral oil, 0.42 mmol, 1.2 equiv.) and 1-(bromomethyl)-4-methanesulfonylbenzene (175 mg, 0.70 mmol, 2 equiv.). Purification by normal phase column chromatography on silica (EtOAc:cyclohexane 10:90 to 50:50 gradient) yielded **178** (210 mg, 86%) as a colourless oil. **<sup>1</sup>H NMR** (600 MHz, CD<sub>3</sub>CN)  $\delta$  = 8.28 (s, 1H, H2), 8.09 (s, 1H, H8), 7.81 – 7.78 (m, 2H, H12'), 7.42 – 7.39 (m, 2H, H11'), 6.15 (d,  $J$  = 2.1 Hz, 1H, H1'), 5.62 – 5.39 (m, 4H, H10), 5.37 (dd,  $J$  = 6.1, 2.1 Hz, 1H, H2'), 5.03 (dd,  $J$  = 6.1, 2.5 Hz, 1H, H3'), 4.56 – 4.47 (m, 3H, H4', H9'), 3.73 (dd,  $J$  = 10.5, 4.0 Hz, 1H, H5'a), 3.66 (dd,  $J$  = 10.5, 5.0 Hz, 1H, H5'b), 3.63 – 3.58 (m, 4H, H11), 3.04 (s, 3H, H14'), 1.57 (s, 3H, H7'), 1.37 (s, 3H, H8'), 0.91 – 0.86 (m, 4H, H12), -0.06 (s, 18H, H13); **<sup>13</sup>C NMR** (151 MHz, CD<sub>3</sub>CN)  $\delta$  = 155.36 (C6), 152.59 (C2), 151.83 (C4), 145.21 (C10'), 140.94 (C13'), 139.93 (C8), 128.90 (2C, C11'), 128.13 (2C, C12'), 121.25 (C5), 114.46 (C6'), 92.25 (C1'), 86.90 (C4'), 85.50 (C2'), 82.93 (C3'), 77.44 (2C, C10), 72.78 (C9'), 71.59 (C5'), 65.78 (2C, C11), 44.53 (C14'), 27.33 (C7'), 25.46 (C8'), 18.59 (2C, C12), -1.40 (6C, C13); **HRMS** (ESI+)  $m/z$  calculated for C<sub>33</sub>H<sub>54</sub>N<sub>5</sub>O<sub>8</sub>SSi<sub>2</sub> (M+H)<sup>+</sup> 736.3226, found 736.3060.

**(2*R*,3*R*,4*S*,5*R*)-2-(6-amino-9*H*-purin-9-yl)-5-(((4-(methylsulfonyl)benzyl)oxy)methyl)tetrahydrofuran-3,4-diol (177)**

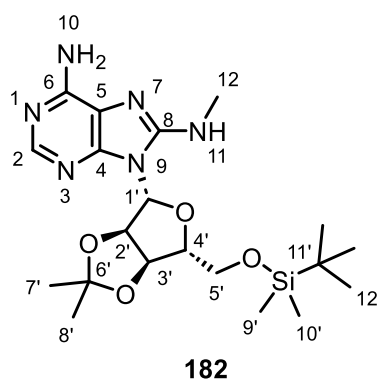


**177**

A glass vial equipped with magnetic stirrer was charged with 9-((3*aR*,4*R*,6*R*,6*aR*)-2,2-dimethyl-6-(((4-(methylsulfonyl)benzyl)oxy)methyl)tetrahydrofuro[3,4-*d*][1,3]dioxol-4-yl)-*N,N*-bis((2-(trimethylsilyl)ethoxy)methyl)-9*H*-purin-6-amine **178** (204 mg, 0.28 mmol, 1 equiv.) and TFA:water 5:2 (v/v) mixture (2.77 mL, 0.1 M). After stirring at room temperature for 1 hour, the reaction mixture was diluted with toluene (30 mL) and the solvent was removed under reduced pressure. The crude residue was redissolved in

CH<sub>2</sub>Cl<sub>2</sub>:THF 1:1 mixture (25 mL), then 7 N ammonia in methanol solution (2.5 mL) and water (2 mL) were added. After stirring at room temperature for 24 hours, the solvent was removed under reduced pressure and the crude product was purified by normal phase column chromatography on silica (100% CH<sub>2</sub>Cl<sub>2</sub> to 15:85 methanol:CH<sub>2</sub>Cl<sub>2</sub> gradient) then reverse phase column chromatography on C18 (methanol:water +0.1% formic acid 40:60 to 80:20 gradient) to yield **177** (12 mg, 10%) as a white solid. <sup>1</sup>H NMR (600 MHz, DMSO-d<sub>6</sub>) δ = 8.27 (s, 1H, H8), 8.13 (s, 1H, H2), 7.90 – 7.87 (m, 2H, H9'), 7.59 – 7.55 (m, 2H, H8'), 7.28 (s br, 2H, H10), 5.91 (d, *J* = 5.1 Hz, 1H, H1'), 5.51 (s br, 1H, H12'), 5.31 (s br, 1H, H13'), 4.65 (s, 2H, H6'), 4.63 (app. t, *J* = 5.1 Hz, 1H, H2'), 4.25 (app. t, *J* = 4.9 Hz, 1H, H3'), 4.11 – 4.06 (m, 1H, H4'), 3.77 (dd, *J* = 10.8, 3.6 Hz, 1H, H5'a), 3.69 (dd, *J* = 10.8, 5.3 Hz, 1H, H5'b), 3.20 (s, 3H, H11'); <sup>13</sup>C NMR (151 MHz, DMSO-d<sub>6</sub>) δ = 156.06 (C6), 152.67 (C2), 149.42 (C4), 144.42 (C7'), 139.78 (C10'), 139.41 (C8), 127.78 (2C, C8'), 127.00 (2C, C9'), 119.06 (C5), 87.54 (C1'), 82.99 (C4'), 73.20 (C2'), 71.41 (C6'), 70.46 (C5'), 70.42 (C3'), 43.57 (C11'); HRMS (ESI+) *m/z* calculated for C<sub>18</sub>H<sub>22</sub>N<sub>5</sub>O<sub>6</sub>S (M+H)<sup>+</sup> 436.1285, found 436.1292;

**9-((3*aR*,4*R*,6*R*,6*aR*)-6-(((*tert*-butyldimethylsilyl)oxy)methyl)-2,2-dimethyltetrahydrofuro[3,4-*d*][1,3]dioxol-4-yl)-*N*8-methyl-9*H*-purine-6,8-diamine (**182**)**

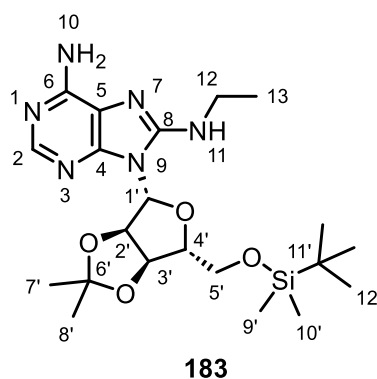


**182** was prepared following a modification of general procedure A, with 8-bromo-9-((3*aR*,4*R*,6*R*,6*aR*)-6-(((*tert*-butyldimethylsilyl)oxy)methyl)-2,2-dimethyltetrahydrofuro[3,4-*d*][1,3]dioxol-4-yl)-9*H*-purin-6-amine **95** (2.00 g, 4.00 mmol, 1 equiv.) and methylamine (13.0 mL, 33 wt% in ethanol, 104 mmol, 26 equiv.). Purification by normal phase column chromatography on silica (100% CH<sub>2</sub>Cl<sub>2</sub> to methanol:CH<sub>2</sub>Cl<sub>2</sub> 10:90 gradient) yielded **182** (1.67 g, 93%) as an off-white foam. <sup>1</sup>H NMR (600 MHz, CDCl<sub>3</sub>) δ = 8.17 (s, 1H, H2), 6.15 (d, *J* = 3.7 Hz, 1H, H1'), 5.71 (s br,



2H, H10), 5.61 (app. s, 1H, H11), 5.22 (dd,  $J = 6.7, 3.7$  Hz, 1H, H2'), 4.90 (dd,  $J = 6.7, 3.7$  Hz, 1H, H3'), 4.21 – 4.18 (m, 1H, H4'), 3.93 (dd,  $J = 11.5, 2.9$  Hz, 1H, H5'a), 3.82 (dd,  $J = 11.5, 2.6$  Hz, 1H, H5'b), 3.07 (d,  $J = 4.83$  Hz, 1H, H12), 1.62 (s, 3H, H7'), 1.37 (s, 3H, H8'), 0.92 (s, 9H, H12'), 0.11 – 0.12 (m, 6H, H9', H10');  $^{13}\text{C NMR}$  (151 MHz,  $\text{CDCl}_3$ )  $\delta = 152.67$  (C8), 151.13 (C6), 149.92 (C4), 149.01 (C2), 116.61 (C5), 115.23 (C6'), 88.71 (C1'), 85.06 (C4'), 82.47 (C2'), 79.61 (C3'), 62.74 (C5'), 30.10 (C12), 27.43 (C7'), 26.15 (3C, C12'), 25.58 (C8'), 18.91 (C11'), -4.95 (C9'), -5.17 (C10'); **HRMS** (ESI+)  $m/z$  calculated for  $\text{C}_{20}\text{H}_{35}\text{N}_6\text{O}_4\text{Si}$  (M+H)<sup>+</sup> 451.2484, found 451.2487.

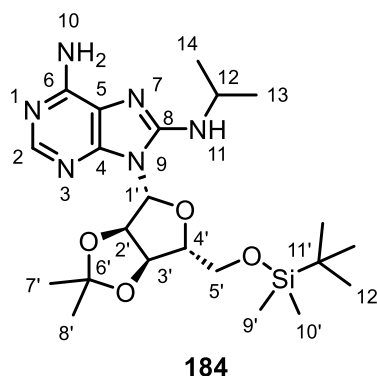
**9-((3*aR*,4*R*,6*R*,6*aR*)-6-(((*tert*-butyldimethylsilyl)oxy)methyl)-2,2-dimethyltetrahydrofuro[3,4-*d*][1,3]dioxol-4-yl)-*N*8-ethyl-9*H*-purine-6,8-diamine (183)**



**183** was prepared following general procedure A, with 8-bromo-9-((3*aR*,4*R*,6*R*,6*aR*)-6-(((*tert*-butyldimethylsilyl)oxy)methyl)-2,2-dimethyltetrahydrofuro[3,4-*d*][1,3]dioxol-4-yl)-9*H*-purin-6-amine **95** (2.00 g, 4.00 mmol, 1 equiv.), ethanol (13.3 mL, 0.3 M) and ethylamine (3.22 mL, 69 wt% in water, 40.0 mmol, 10 equiv.). Purification by normal phase column chromatography on silica (100%  $\text{CH}_2\text{Cl}_2$  to methanol: $\text{CH}_2\text{Cl}_2$  10:90 gradient) yielded **183** (1.70 g, 92%) as a pink foam.  $^1\text{H NMR}$  (600 MHz,  $\text{CDCl}_3$ )  $\delta = 8.15$  (s, 1H, H2), 6.03 (d,  $J = 3.1$  Hz, 1H, H1'), 5.55 (dd,  $J = 6.5, 3.1$  Hz, 1H, H2'), 5.47 (s br, 2H, H10), 5.33 – 5.25 (m, 1H, H11), 4.93 (dd,  $J = 6.5, 3.4$  Hz, 1H, H3'), 4.24 – 4.21 (m, 1H, H4'), 3.80 (dd,  $J = 11.2, 4.2$  Hz, 1H, H5'a), 3.71 (dd,  $J = 11.2, 4.0$  Hz, 1H, H5'b), 3.54 – 3.45 (m, 2H, H12), 1.61 (s, 3H, H7'), 1.38 (s, 3H, H8'), 1.29 (t,  $J = 7.1$  Hz, 3H, H13), 0.87 (s, 9H, H12'), 0.04 – 0.02 (m, 6H, H9', H10');  $^{13}\text{C NMR}$  (151 MHz,  $\text{CDCl}_3$ )  $\delta = 152.05$  (C8), 151.57 (C6), 149.89 (C4), 149.36 (C2), 117.25 (C5), 114.71 (C6'), 89.18 (C1'), 86.09 (C4'), 82.26 (C2'), 80.41 (C3'), 62.83 (C5'), 38.06 (C12), 27.33 (C7'), 26.08

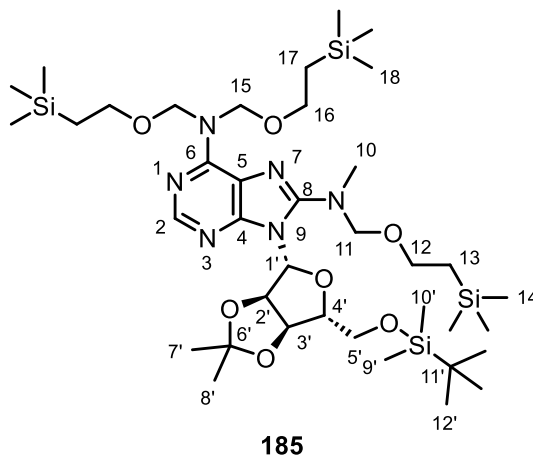
(3C, C12'), 25.55 (C8'), 18.73 (C11'), 15.22 (C13), -5.16 (C9'), -5.30 (C10'); **HRMS** (ESI+)  $m/z$  calculated for  $C_{21}H_{37}N_6O_4Si$  (M+H)<sup>+</sup> 465.2640, found 465.2539.

**9-((3a*R*,4*R*,6*R*,6a*R*)-6-(((*tert*-butyldimethylsilyl)oxy)methyl)-2,2-dimethyltetrahydrofuro[3,4-*d*][1,3]dioxol-4-yl)-*N*8-isopropyl-9*H*-purine-6,8-diamine (**184**)**



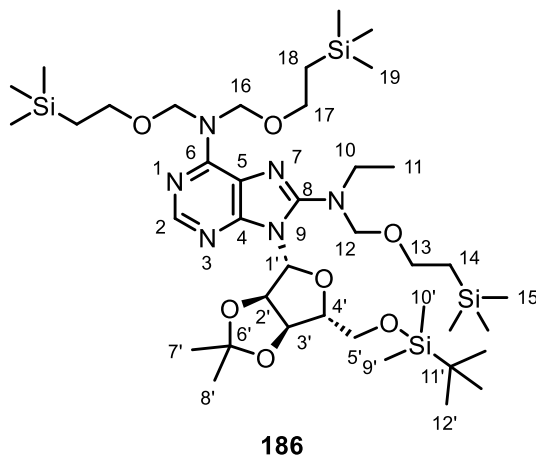
**184** was prepared following general procedure A, with 8-bromo-9-((3a*R*,4*R*,6*R*,6a*R*)-6-(((*tert*-butyldimethylsilyl)oxy)methyl)-2,2-dimethyltetrahydrofuro[3,4-*d*][1,3]dioxol-4-yl)-9*H*-purin-6-amine **95** (2.00 g, 4.00 mmol, 1 equiv.), ethanol (13.3 mL, 0.3 M) and isopropylamine (3.40 mL, 40.0 mmol, 10 equiv.). Purification by normal phase column chromatography on silica (100%  $CH_2Cl_2$  to methanol: $CH_2Cl_2$  10:90 gradient) yielded **184** (1.70 g, 89%) as a pink foam. **<sup>1</sup>H NMR** (600 MHz,  $CDCl_3$ )  $\delta$  = 8.14 (s, 1H, H2), 5.96 (dd,  $J$  = 6.3, 1.8 Hz, 1H, H2'), 5.86 (d,  $J$  = 1.8 Hz, 1H, H1'), 5.51 (s br, 2H, H10), 4.96 (dd,  $J$  = 6.3, 2.7 Hz, 1H, H3'), 4.89 – 4.81 (m, 1H, H11), 4.28 (app. td,  $J$  = 5.6, 2.7 Hz, 1H, H4'), 4.16 – 4.09 (m, 1H, H12), 3.64 (dd,  $J$  = 11.0, 5.6 Hz, 1H, H5'a), 3.58 (dd,  $J$  = 11.0, 5.6 Hz, 1H, H5'b), 1.59 (s, 3H, H7'), 1.41 (s, 3H, H8'), 1.33 – 1.29 (m, 6H, H13, H14), 0.80 (s, 9H, H12'), -0.06 (s, 3H, H9'), -0.07 (s, 3H, H10'); **<sup>13</sup>C NMR** (151 MHz,  $CDCl_3$ )  $\delta$  = 151.57 (C6), 151.55 (C8), 149.61 (C4), 149.08 (C2), 117.33 (C5), 114.05 (C6'), 90.03 (C1'), 87.66 (C4'), 82.21 (C2'), 81.52 (C3'), 63.09 (C5'), 45.22 (C12), 27.19 (C7'), 26.00 (3C, C12'), 25.50 (C8'), 23.16 (C13), 23.14 (C14), 18.53 (C11'), -5.27 (C9'), -5.35 (C10'); **HRMS** (ESI+)  $m/z$  calculated for  $C_{22}H_{39}N_6O_4Si$  (M+H)<sup>+</sup> 479.2797, found 479.2796.

**9-((3*aR*,4*R*,6*R*,6*aR*)-6-(((*tert*-butyldimethylsilyl)oxy)methyl)-2,2-dimethyltetrahydrofuro[3,4-*d*][1,3]dioxol-4-yl)-*N*8-methyl-*N*6,*N*6,*N*8-tris((2-(trimethylsilyl)ethoxy)methyl)-9*H*-purine-6,8-diamine (**185**)**



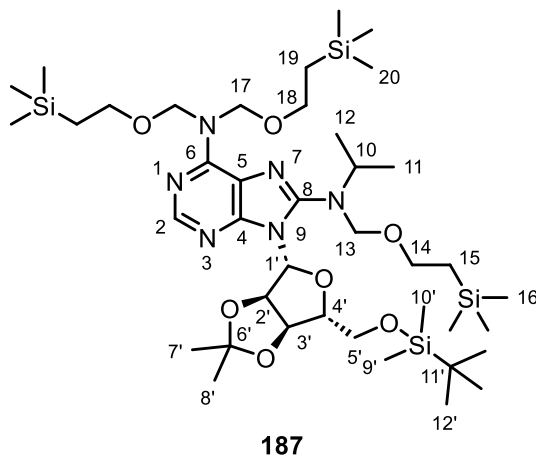
**185** was prepared following general procedure B, with 9-((3*aR*,4*R*,6*R*,6*aR*)-6-(((*tert*-butyldimethylsilyl)oxy)methyl)-2,2-dimethyltetrahydrofuro[3,4-*d*][1,3]dioxol-4-yl)-*N*8-methyl-9*H*-purine-6,8-diamine **182** (1.60 g, 3.55 mmol, 1 equiv.), CH<sub>2</sub>Cl<sub>2</sub> (11.8 mL, 0.3 M), 2-(trimethylsilyl)ethoxymethylchloride (2.83 mL, 16.0 mmol, 4.5 equiv.) and *N,N*-diisopropylethylamine (2.78 mL, 16.0 mmol, 4.5 equiv.) for 18 hours. Purification by normal phase column chromatography on silica (EtOAc:cyclohexane 1:99 to 15:85 gradient) yielded **185** (2.44 g, 82%) as a colourless oil. <sup>1</sup>H NMR (600 MHz, CD<sub>3</sub>CN) δ = 8.21 (s, 1H, H2), 5.99 (app. s, 1H, H1'), 5.59 (app. d, *J* = 6.3 Hz, 1H, H2'), 5.56 – 5.31 (m, 4H, H15), 5.15 (dd, *J* = 6.3, 2.8 Hz, 1H, H3'), 4.80 (d, *J* = 10.3 Hz, 1H, H11a), 4.72 (d, *J* = 10.3 Hz, 1H, H11b), 4.19 (app. td, *J* = 6.7, 2.7 Hz, 1H, H4'), 3.89 (dd, *J* = 10.4, 7.0 Hz, 1H, H5'a), 3.72 (dd, *J* = 10.4, 6.5 Hz, 1H, H5'b), 3.62 – 3.55 (m, 4H, H16), 3.53 – 3.49 (m, 2H, H12), 3.07 (s, 3H, H10), 1.53 (s, 3H, H7'), 1.32 (s, 3H, H8'), 0.92 – 0.86 (m, 6H, H13, H17), 0.84 (s, 9H, H12'), -0.04 – -0.07 (m, 33H, H9', H10' H14, H18); <sup>13</sup>C NMR (151 MHz, CD<sub>3</sub>CN) δ = 154.52 (C8), 153.36 (C6), 152.33 (C4), 150.59 (C2), 118.84 (C5), 114.17 (C6'), 91.12 (C1'), 89.29 (C4'), 84.67 (C11), 84.05 (C2'), 83.57 (C3'), 77.19 (2C, C15), 66.40 (C12), 65.48 (2C, C16), 64.31 (C5'), 38.46 (C10), 27.42 (C7'), 26.24 (3C, C12'), 25.60 (C8'), 18.96 (C11'), 18.66 (2C, C17), 18.62 (C13), -1.28 (6C, C18), -1.30 (3C, C14), -5.05 (C9'), -5.13 (C10'); HRMS (ESI+) *m/z* calculated for C<sub>38</sub>H<sub>77</sub>N<sub>6</sub>O<sub>7</sub>Si<sub>4</sub> (M+H)<sup>+</sup> 841.4925, found 841.4947.

**9-((3*aR*,4*R*,6*R*,6*aR*)-6-(((*tert*-butyldimethylsilyl)oxy)methyl)-2,2-dimethyltetrahydrofuro[3,4-*d*][1,3]dioxol-4-yl)-*N*8-ethyl-*N*6,*N*6,*N*8-tris((2-(trimethylsilyl)ethoxy)methyl)-9*H*-purine-6,8-diamine (**186**)**



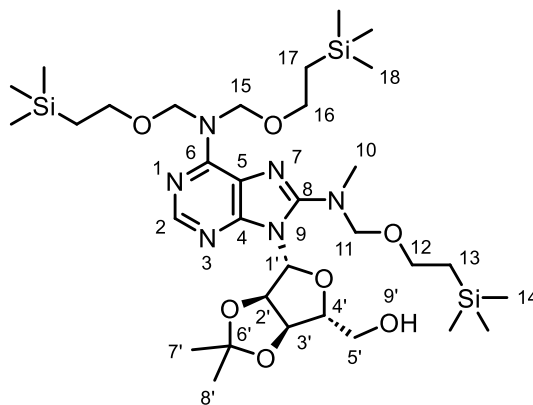
**186** was prepared following general procedure B, with 9-((3*aR*,4*R*,6*R*,6*aR*)-6-(((*tert*-butyldimethylsilyl)oxy)methyl)-2,2-dimethyltetrahydrofuro[3,4-*d*][1,3]dioxol-4-yl)-*N*8-ethyl-9*H*-purine-6,8-diamine **183** (1.70 g, 3.66 mmol, 1 equiv.), CH<sub>2</sub>Cl<sub>2</sub> (12.2 mL, 0.3 M), 2-(trimethylsilyl)ethoxymethylchloride (2.91 mL, 16.5 mmol, 4.5 equiv.) and *N,N*-Diisopropylethylamine (2.87 mL, 16.5 mmol, 4.5 equiv.) for 18 hours. Purification by normal phase column chromatography on silica (EtOAc:cyclohexane 1:99 to 15:85 gradient) yielded **186** (2.74 g, 87%) as a colourless oil. <sup>1</sup>H NMR (600 MHz, CD<sub>3</sub>CN) δ = 8.21 (s, 1H, H2), 6.04 (d, *J* = 1.5 Hz, 1H, H1'), 5.59 (dd, *J* = 6.4, 1.5 Hz, 1H, H2'), 5.57 – 5.30 (m, 4H, H16), 5.14 (dd, *J* = 6.4, 3.0 Hz, 1H, H3'), 4.79 (d, *J* = 10.4 Hz, 1H, H12a), 4.73 (d, *J* = 10.4 Hz, 1H, H12b), 4.18 (app. td, *J* = 6.8, 3.0 Hz, 1H, H4'), 3.87 (dd, *J* = 10.5, 6.8 Hz, 1H, H5'a), 3.72 (dd, *J* = 10.5, 6.8 Hz, 1H, H5'b), 3.65 – 3.56 (m, 5H, H10a, H17), 3.54 – 3.49 (m, 2H, H13), 3.47 – 3.41 (m, 1H, H10b), 1.53 (s, 3H, H7'), 1.32 (s, 3H, H8'), 1.19 (t, *J* = 7.1 Hz, 3H, H11), 0.91 – 0.85 (m, 6H, H14, H18), 0.83 (s, 9H, H12'), -0.05 – -0.07 (m, 33H, H9', H10', H15, H19); <sup>13</sup>C NMR (151 MHz, CD<sub>3</sub>CN) δ = 153.76 (C8), 153.33 (C6), 152.15 (C4), 150.56 (C2), 118.85 (C5), 114.12 (C6'), 90.85 (C1'), 89.27 (C4'), 84.11 (C2'), 83.52 (C3'), 82.79 (C12), 77.16 (2C, C16), 66.11 (C13), 65.47 (2C, C17), 64.36 (C5'), 45.88 (C10), 27.42 (C7'), 26.19 (3C, C12'), 25.57 (C8'), 18.92 (C11'), 18.62 (2C, C18), 18.52 (C14), 13.52 (C11), -1.34 (9C, C15, C19), -5.10 (C9'), -5.18 (C10'); HRMS (ESI+) *m/z* calculated for C<sub>39</sub>H<sub>79</sub>N<sub>6</sub>O<sub>7</sub>Si<sub>4</sub> (M+H)<sup>+</sup> 855.5082, found 855.4919.

**9-((3a*R*,4*R*,6*R*,6a*R*)-6-(((*tert*-butyldimethylsilyl)oxy)methyl)-2,2-dimethyltetrahydrofuro[3,4-*d*][1,3]dioxol-4-yl)-*N*8-isopropyl-*N*6,*N*6,*N*8-tris((2-(trimethylsilyl)ethoxy)methyl)-9*H*-purine-6,8-diamine (**187**)**



**187** was prepared following general procedure B, with 9-((3a*R*,4*R*,6*R*,6a*R*)-6-(((*tert*-butyldimethylsilyl)oxy)methyl)-2,2-dimethyltetrahydrofuro[3,4-*d*][1,3]dioxol-4-yl)-*N*8-isopropyl-9*H*-purine-6,8-diamine **184** (1.80 g, 3.76 mmol, 1 equiv.), CH<sub>2</sub>Cl<sub>2</sub> (12.6 mL, 0.3 M), 2-(trimethylsilyl)ethoxymethylchloride (3.00 mL, 16.9 mmol, 4.5 equiv.) and *N,N*-Diisopropylethylamine (2.95 mL, 16.9 mmol, 4.5 equiv.) for 18 hours. Purification by normal phase column chromatography on silica (EtOAc:cyclohexane 1:99 to 20:80 gradient) yielded **187** (2.93 g, 90%) as an orange oil. <sup>1</sup>H NMR (600 MHz, CD<sub>3</sub>CN) δ = 8.21 (s, 1H, H2), 6.18 (d, *J* = 1.6 Hz, 1H, H1'), 5.57 (dd, *J* = 6.3, 1.6 Hz, 1H, H2'), 5.53 – 5.35 (m, 4H, H17), 5.13 (dd, *J* = 6.3, 3.1 Hz, 1H, H3'), 4.77 (d, *J* = 10.5 Hz, 1H, H13a), 4.70 (d, *J* = 10.5 Hz, 1H, H13b), 4.16 (app. td, *J* = 7.0, 3.2 Hz, 1H, H4'), 3.99 – 3.94 (m, 1H, H10), 3.87 (dd, *J* = 10.8, 6.5 Hz, 1H, H5'a), 3.73 (dd, *J* = 10.8, 7.0 Hz, 1H, H5'b), 3.60 – 3.55 (m, 4H, H18), 3.53 – 3.49 (m, 2H, H14), 1.54 (s, 3H, H7'), 1.32 (s, 3H, H8'), 1.28 (s, 3H, H11), 1.27 (s, 3H, H12), 0.92 – 0.85 (m, 6H, H15, H19), 0.82 (s, 9H, H12'), -0.02 – -0.09 (m, 33H, H9', H10', H16, H20); <sup>13</sup>C NMR (151 MHz, CD<sub>3</sub>CN) δ = 153.62 (C8), 153.42 (C6), 151.88 (C4), 150.69 (C2), 118.81 (C5), 114.15 (C6'), 90.67 (C1'), 89.25 (C4'), 84.26 (C2'), 83.52 (C3'), 79.61 (C13), 77.12 (2C, C17), 65.50 (2C, C18), 65.41 (C14), 64.53 (C5'), 53.01 (C10), 27.53 (C7'), 26.21 (3C, C12'), 25.65 (C8'), 21.26 (C11), 20.83 (C12), 18.93 (C11'), 18.65 (2C, C19), 18.60 (C15), -1.31 (6C, C20), -1.34 (3C, C16), -5.09 (C9'), -5.16 (C10'); HRMS (ESI+) *m/z* calculated for C<sub>40</sub>H<sub>81</sub>N<sub>6</sub>O<sub>7</sub>Si<sub>4</sub> (M+H)<sup>+</sup> 869.5238, found 869.5242.

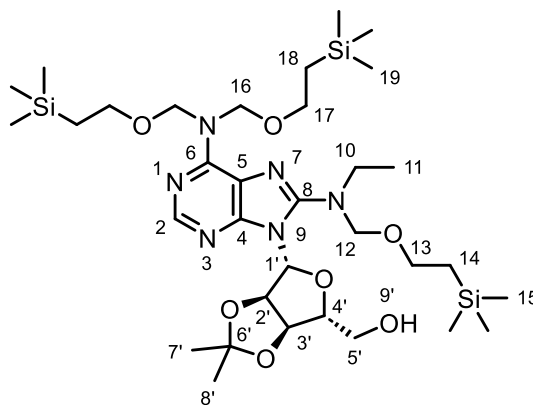
**((3a*R*,4*R*,6*R*,6a*R*)-6-(6-(bis((2-(trimethylsilyl)ethoxy)methyl)amino)-8-(methyl((2-(trimethylsilyl)ethoxy)methyl)amino)-9*H*-purin-9-yl)-2,2-dimethyltetrahydrofuro[3,4-*d*][1,3]dioxol-4-yl)methanol (188)**



**188**

**188** was prepared following general procedure C, with 9-((3a*R*,4*R*,6*R*,6a*R*)-6-(((*tert*-butyldimethylsilyl)oxy)methyl)-2,2-dimethyltetrahydrofuro[3,4-*d*][1,3]dioxol-4-yl)-*N*8-methyl-*N*6,*N*6,*N*8-tris((2-(trimethylsilyl)ethoxy)methyl)-9*H*-purine-6,8-diamine **185** (2.40 g, 2.85 mmol, 1 equiv.), THF (28.5 mL, 0.1 M) and TBAF (3.13 mL, 1 M in THF, 3.13 mmol, 1.1 equiv.) for 48 hours. Purification by normal phase column chromatography on silica (EtOAc:cyclohexane 1:99 to 30:70 gradient) yielded **188** (1.39 g, 67%) as a colourless oil. **<sup>1</sup>H NMR** (600 MHz, acetone-*d*<sub>6</sub>) δ = 8.21 (s, 1H, H2), 6.00 (d, *J* = 4.3 Hz, 1H, H1'), 5.60 – 5.44 (m, 5H, H2', H15), 5.40 (dd, *J* = 8.8, 2.9 Hz, 1H, H9'), 5.13 (dd, *J* = 6.1, 1.5 Hz, 1H, H3'), 4.86 (d, *J* = 10.2 Hz, 1H, H11a), 4.78 (d, *J* = 10.2 Hz, 1H, H11b), 4.37 – 4.34 (m, 1H, H4'), 3.82 – 3.76 (m, 1H, H5'a), 3.72 – 3.63 (m, 5H, H5'b, H16), 3.61 – 3.55 (m, 2H, H12), 3.12 (s, 3H, H10), 1.61 (s, 3H, H7'), 1.38 (s, 3H, H8'), 0.95 – 0.88 (m, 6H, H13, H17), -0.02 (s, 18H, H18), -0.03 (s, 9H, H14); **<sup>13</sup>C NMR** (151 MHz, acetone-*d*<sub>6</sub>) δ = 154.21 (C8), 153.79 (C6), 152.02 (C4), 150.36 (C2), 119.04 (C5), 114.38 (C6'), 92.21 (C1'), 87.14 (C4'), 85.09 (C11), 83.12 (C2'), 82.86 (C3'), 76.48 (2C, C15), 66.46 (C12), 65.38 (2C, C16), 63.69 (C5'), 38.47 (C10), 27.82 (C7'), 25.58 (C8'), 18.63 (2C, C17), 18.46 (C13), -1.18 (9C, C14, C18); **HRMS** (ESI+) *m/z* calculated for C<sub>32</sub>H<sub>63</sub>N<sub>6</sub>O<sub>7</sub>Si<sub>3</sub> (M+H)<sup>+</sup> 727.4061, found 727.4078.

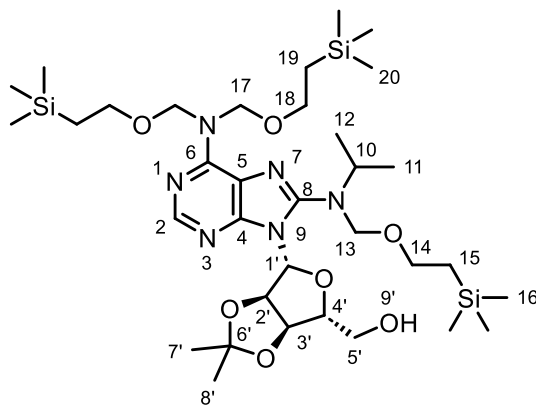
**((3*aR*,4*R*,6*R*,6*aR*)-6-(6-(bis((2-(trimethylsilyl)ethoxy)methyl)amino)-8-(ethyl((2-(trimethylsilyl)ethoxy)methyl)amino)-9*H*-purin-9-yl)-2,2-dimethyltetrahydrofuro[3,4-*d*][1,3]dioxol-4-yl)methanol (189)**



**189**

**189** was prepared following general procedure C, with 9-((3*aR*,4*R*,6*R*,6*aR*)-6-(((*tert*-butyldimethylsilyl)oxy)methyl)-2,2-dimethyltetrahydrofuro[3,4-*d*][1,3]dioxol-4-yl)-*N*8-ethyl-*N*6,*N*6,*N*8-tris((2-(trimethylsilyl)ethoxy)methyl)-9*H*-purine-6,8-diamine **186** (2.73 g, 3.19 mmol, 1 equiv.), THF (31.9 mL, 0.1 M) and TBAF (3.50 mL, 1 M in THF, 3.50 mmol, 1.1 equiv.) for 2 hours. Purification by normal phase column chromatography on silica (EtOAc:cyclohexane 5:95 to 30:70 gradient) yielded **189** (1.52 g, 65%) as a colourless oil. <sup>1</sup>H NMR (600 MHz, CD<sub>3</sub>CN) δ = 8.19 (s, 1H, H<sub>2</sub>), 5.96 (d, *J* = 4.7 Hz, 1H, H<sub>1'</sub>), 5.51 – 5.35 (m, 6H, H<sub>2'</sub>, H<sub>9'</sub>, H<sub>16</sub>), 5.09 (dd, *J* = 6.0, 1.5 Hz, 1H, H<sub>3'</sub>), 4.77 (d, *J* = 10.4 Hz, 1H, H<sub>12a</sub>), 4.71 (d, *J* = 10.4 Hz, 1H, H<sub>12b</sub>), 4.35 – 4.32 (m, 1H, H<sub>4'</sub>), 3.76 (app. dt, *J* = 12.4, 2.5 Hz, 1H, H<sub>5'a</sub>), 3.70 – 3.65 (m, 1H, H<sub>5'b</sub>), 3.62 – 3.58 (m, 4H, H<sub>17</sub>), 3.55 – 3.44 (m, 4H, H<sub>10</sub>, H<sub>13</sub>), 1.60 (s, 3H, H<sub>7'</sub>), 1.35 (s, 3H, H<sub>8'</sub>), 1.18 (t, *J* = 7.0 Hz, 3H, H<sub>11</sub>), 0.91 – 0.82 (m, 6H, H<sub>14</sub>, H<sub>18</sub>), -0.05 (s, 18H, H<sub>19</sub>), -0.06 (s, 9H, H<sub>15</sub>); <sup>13</sup>C NMR (151 MHz, CD<sub>3</sub>CN) δ = 153.74 (C<sub>6</sub>), 153.55 (C<sub>8</sub>), 151.81 (C<sub>4</sub>), 150.41 (C<sub>2</sub>), 119.29 (C<sub>5</sub>), 114.53 (C<sub>6'</sub>), 92.25 (C<sub>1'</sub>), 86.73 (C<sub>4'</sub>), 83.26 (C<sub>12</sub>), 83.08 (C<sub>2'</sub>), 82.74 (C<sub>3'</sub>), 77.18 (2C, C<sub>16</sub>), 66.40 (C<sub>13</sub>), 65.58 (2C, C<sub>17</sub>), 63.76 (C<sub>5'</sub>), 45.90 (C<sub>10</sub>), 27.81 (C<sub>7'</sub>), 25.60 (C<sub>8'</sub>), 18.61 (2C, C<sub>18</sub>), 18.44 (C<sub>14</sub>), 13.42 (C<sub>11</sub>), -1.35 (6C, C<sub>19</sub>), -1.38 (3C, C<sub>15</sub>); HRMS (ESI+) *m/z* calculated for C<sub>33</sub>H<sub>65</sub>N<sub>6</sub>O<sub>7</sub>Si<sub>3</sub> (M+H)<sup>+</sup> 741.4217, found 741.4185; [α]<sub>D</sub><sup>25</sup> = -16 ° (c = 0.5, CHCl<sub>3</sub>).

**((3a*R*,4*R*,6*R*,6a*R*)-6-(6-(bis((2-(trimethylsilyl)ethoxy)methyl)amino)-8-(isopropyl((2-(trimethylsilyl)ethoxy)methyl)amino)-9*H*-purin-9-yl)-2,2-dimethyltetrahydrofuro[3,4-*d*][1,3]dioxol-4-yl)methanol (190)**

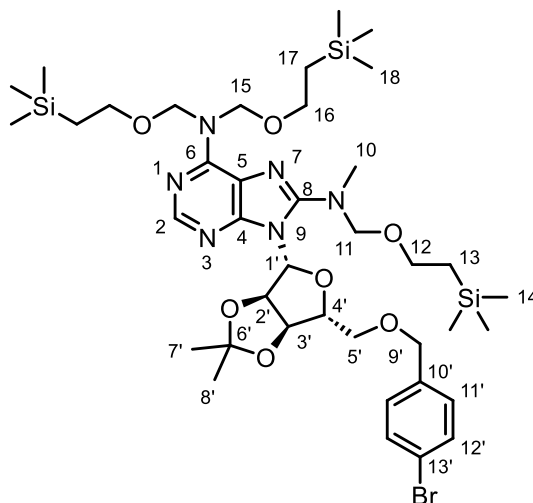


**190**

**190** was prepared following general procedure C, with 9-((3a*R*,4*R*,6*R*,6a*R*)-6-(((*tert*-butyldimethylsilyl)oxy)methyl)-2,2-dimethyltetrahydrofuro[3,4-*d*][1,3]dioxol-4-yl)-*N*8-isopropyl-*N*6,*N*6,*N*8-tris((2-(trimethylsilyl)ethoxy)methyl)-9*H*-purine-6,8-diamine **187** (2.90 g, 3.34 mmol, 1 equiv.), THF (33.4 mL, 0.1 M) and TBAF (3.67 mL, 1 M in THF, 3.67 mmol, 1.1 equiv.) for 2 hours. Purification by normal phase column chromatography on silica (EtOAc:cyclohexane 1:99 to 30:70 gradient) yielded **190** (1.05 g, 42%) as a colourless oil. **<sup>1</sup>H NMR** (600 MHz, CD<sub>3</sub>CN) δ = 8.20 (s, 1H, H2), 6.04 (d, *J* = 4.7 Hz, 1H, H1'), 5.53 – 5.40 (m, 5H, H9', H17), 5.37 – 5.34 (m, 1H, H2'), 5.08 (dd, *J* = 6.0, 1.6 Hz, 1H, H3'), 4.76 (d, *J* = 10.6 Hz, 1H, H13a), 4.72 (d, *J* = 10.6 Hz, 1H, H13b), 4.35 – 4.32 (m, 1H, H4'), 3.86 (sept, *J* = 6.6 Hz, 1H, H10), 3.76 (app. dt, *J* = 12.4, 2.5 Hz, 1H, H5'a), 3.70 – 3.65 (m, 1H, H5'b), 3.62 – 3.58 (m, 4H, H18), 3.53 – 3.49 (m, 2H, H14), 1.60 (s, 3H, H7'), 1.34 (s, 3H, H8'), 1.31 (d, *J* = 6.6 Hz, 3H, H11), 1.27 (d, *J* = 6.6 Hz, 3H, H12), 0.91 – 0.84 (m, 6H, H15, H19), -0.04 – -0.06 (m, 27H, H16, H20); **<sup>13</sup>C NMR** (151 MHz, CD<sub>3</sub>CN) δ = 153.90 (C6), 153.43 (C8), 151.48 (C4), 150.62 (C2), 119.19 (C5), 114.46 (C6'), 92.17 (C1'), 86.69 (C4'), 83.05 (C2'), 82.72 (C3'), 80.06 (C13), 77.17 (2C, C17), 65.68 (C14), 65.60 (2C, C18), 63.81 (C5), 53.35 (C10), 27.93 (C7'), 25.59 (C8'), 21.27 (C11), 20.81 (C12), 18.62 (2C, C19), 18.52 (C15), -1.37 (6C, C20), -1.39 (3C, C16); **HRMS** (ESI+) *m/z* calculated for C<sub>34</sub>H<sub>67</sub>N<sub>6</sub>O<sub>7</sub>Si<sub>3</sub> (M+H)<sup>+</sup> 755.4374, found 755.4384; [α]<sub>D</sub><sup>25</sup> = -18 ° (c = 0.5, CHCl<sub>3</sub>).



**9-((3*aR*,4*R*,6*R*,6*aR*)-6-(((4-bromobenzyl)oxy)methyl)-2,2-dimethyltetrahydrofuro[3,4-*d*][1,3]dioxol-4-yl)-*N*8-methyl-*N*6,*N*6,*N*8-tris((2-(trimethylsilyl)ethoxy)methyl)-9*H*-purine-6,8-diamine (**191**)**

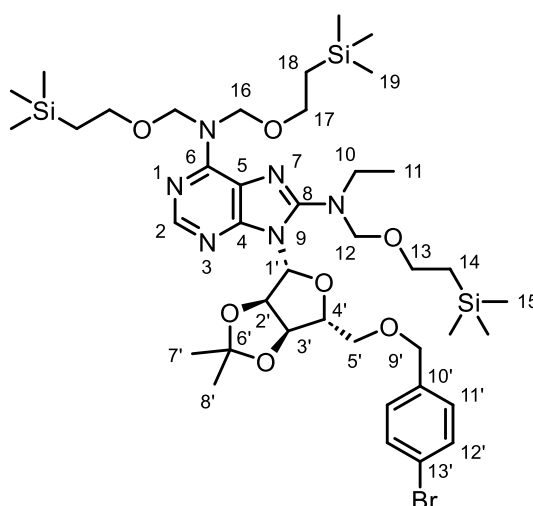


**191**

**191** was prepared following general procedure D, with ((3*aR*,4*R*,6*R*,6*aR*)-6-(6-(bis((2-(trimethylsilyl)ethoxy)methyl)amino)-8-(methyl((2-(trimethylsilyl)ethoxy)methyl)amino)-9*H*-purin-9-yl)-2,2-dimethyltetrahydrofuro[3,4-*d*][1,3]dioxol-4-yl)methanol **188** (1.36 g, 1.87 mmol, 1 equiv.), THF (3.74 mL, 0.5 M), sodium hydride (89.8 mg, 60% in mineral oil, 2.24 mmol, 1.2 equiv.) and 4-bromobenzyl bromide (935 mg, 3.74 mmol, 2 equiv.). Purification by normal phase column chromatography on silica (EtOAc:cyclohexane 1:99 to 25:75 gradient) yielded **191** (1.27 g, 76%) as a colourless oil. <sup>1</sup>H NMR (600 MHz, acetone-*d*<sub>6</sub>) δ = 8.17 (s, 1H, H2), 7.46 – 7.43 (m, 2H, H12'), 7.23 – 7.20 (m, 2H, H11'), 6.07 (d, *J* = 1.8 Hz, 1H, H1'), 5.64 (dd, *J* = 6.3, 1.8 Hz, 1H, H2'), 5.63 – 5.39 (m, 4H, H15), 5.21 (dd, *J* = 6.3, 3.1 Hz, 1H, H3'), 4.89 (d, *J* = 10.2 Hz, 1H, H11a), 4.80 (d, *J* = 10.2 Hz, 1H, H11b), 4.51 – 4.44 (m, 2H, H9'), 4.38 (app. td, *J* = 6.5, 3.1 Hz, 1H, H4'), 3.81 (dd, *J* = 10.2, 6.1 Hz, 1H, H5'a), 3.69 – 3.65 (m, 4H, H5'b, H16), 3.60 – 3.56 (m, 2H, H12), 3.12 (s, 3H, H10), 1.55 (s, 3H, H7'), 1.34 (s, 3H, H8'), 0.95 – 0.88 (m, 6H, H13, H17), -0.03 (s, 18H, H18), -0.04 (s, 9H, H14); <sup>13</sup>C NMR (151 MHz, acetone-*d*<sub>6</sub>) δ = 154.22 (C8), 153.46 (C6), 152.24 (C4), 150.57 (C2), 138.95 (C10'), 132.05 (2C, C12'), 130.25 (2C, C11'), 121.57 (C13'), 118.67 (C5), 114.20 (C6'), 90.91 (C1'), 87.44 (C4'), 84.77 (C11), 83.88 (C2'), 83.63 (C3'), 76.54 (2C, C15), 72.72 (C9'), 71.08 (C5'), 66.30 (C12), 65.31 (2C, C16), 38.37 (C10),

27.50 (C7'), 25.55 (C8'), 18.65 (2C, C17), 18.51 (C13), -1.16 (9C, C14, C18); **HRMS** (ESI+)  $m/z$  calculated for  $C_{39}H_{68}^{79}BrN_6O_7Si_3$  (M+H)<sup>+</sup> 895.3635, found 895.3624.

**9-((3a*R*,4*R*,6*R*,6a*R*)-6-(((4-bromobenzyl)oxy)methyl)-2,2-dimethyltetrahydrofuro[3,4-*d*][1,3]dioxol-4-yl)-*N*8-ethyl-*N*6,*N*8-tris((2-(trimethylsilyl)ethoxy)methyl)-9*H*-purine-6,8-diamine (**192**)**

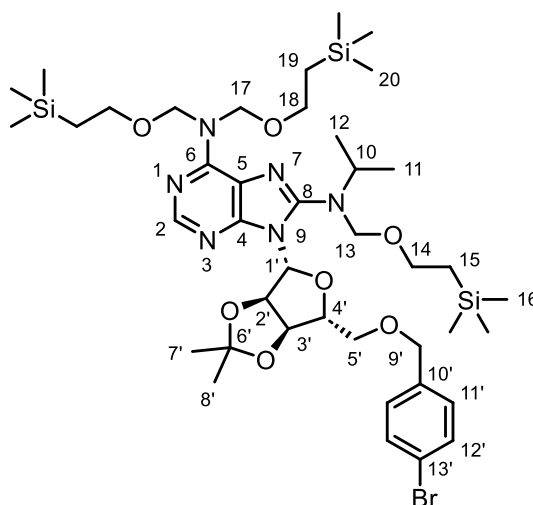


**192**

**192** was prepared following general procedure D, with ((3a*R*,4*R*,6*R*,6a*R*)-6-(6-(bis((2-(trimethylsilyl)ethoxy)methyl)amino)-8-(ethyl((2-(trimethylsilyl)ethoxy)methyl)amino)-9*H*-purin-9-yl)-2,2-dimethyltetrahydrofuro[3,4-*d*][1,3]dioxol-4-yl)methanol **189** (508 mg, 0.69 mmol, 1 equiv.), THF (1.37 mL, 0.5 M), sodium hydride (32.9 mg, 60% in mineral oil, 0.82 mmol, 1.2 equiv.) and 4-bromobenzyl bromide (342 mg, 1.37 mmol, 2 equiv.). Purification by normal phase column chromatography on silica (EtOAc:cyclohexane 1:99 to 20:80 gradient) yielded **192** (546 mg, 88%) as a colourless oil. **<sup>1</sup>H NMR** (600 MHz, CD<sub>3</sub>CN)  $\delta$  = 8.10 (s, 1H, H2), 7.42 – 7.38 (m, 2H, H12'), 7.15 – 7.11 (m, 2H, H11'), 6.05 – 6.02 (m, 1H, H1'), 5.57 – 5.32 (m, 5H, H2', H16), 5.13 (dd,  $J$  = 6.4, 3.0 Hz, 1H, H3'), 4.79 (d,  $J$  = 10.4 Hz, 1H, H12a), 4.72 (d,  $J$  = 10.4 Hz, 1H, H12b), 4.45 – 4.38 (m, 2H, H9'), 4.34 – 4.29 (m, 1H, H4'), 3.71 (dd,  $J$  = 10.1, 5.8 Hz, 1H, H5'a), 3.65 – 3.58 (m, 6H, H5'b, H10a, H17), 3.53 – 3.49 (m, 2H, H13), 3.48 – 3.41 (m, 1H, H10b), 1.54 (s, 3H, H7'), 1.32 (s, 3H, H8'), 1.20 (t,  $J$  = 7.1 Hz, 3H, H11), 0.92 – 0.83 (m, 6H, H14, H18), -0.05 (s, 18H, H19), -0.07 (s, 9H, H15); **<sup>13</sup>C NMR** (151 MHz, CD<sub>3</sub>CN)  $\delta$  = 153.67 (C8), 153.28 (C6), 152.14 (C4), 150.51 (C2), 138.83 (C10'), 132.12 (2C, C12'), 130.35 (2C, C11'), 121.66 (C13'), 118.85 (C5), 114.36

(C6'), 90.67 (C1'), 87.41 (C4'), 84.03 (C2'), 83.53 (C3'), 82.86 (C12), 77.30 (2C, C16), 72.74 (C9'), 71.03 (C5'), 66.14 (C13), 65.49 (2C, C17), 45.94 (C10), 27.41 (C7'), 25.55 (C8'), 18.62 (2C, C18), 18.50 (C14), 13.53 (C11), -1.34 (6C, C19), -1.36 (3C, C15); **HRMS** (ESI+) *m/z* calculated for C<sub>40</sub>H<sub>70</sub><sup>79</sup>BrN<sub>6</sub>O<sub>7</sub>Si<sub>3</sub> (M+H)<sup>+</sup> 909.3792, found 909.3885;  $[\alpha]_D^{25} = -71^\circ$  (*c* = 0.5, CHCl<sub>3</sub>).

**9-((3*aR*,4*R*,6*R*,6*aR*)-6-(((4-bromobenzyl)oxy)methyl)-2,2-dimethyltetrahydrofuro[3,4-*d*][1,3]dioxol-4-yl)-*N*8-isopropyl-*N*6,*N*6,*N*8-tris((2-(trimethylsilyl)ethoxy)methyl)-9*H*-purine-6,8-diamine (**193**)**

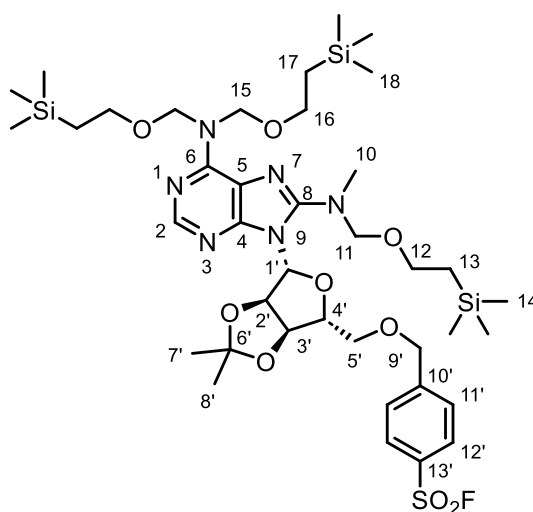


**193**

**193** was prepared following general procedure D, with ((3*aR*,4*R*,6*R*,6*aR*)-6-(6-(bis((2-(trimethylsilyl)ethoxy)methyl)amino)-8-(isopropyl((2-(trimethylsilyl)ethoxy)methyl)amino)-9*H*-purin-9-yl)-2,2-dimethyltetrahydrofuro[3,4-*d*][1,3]dioxol-4-yl)methanol **190** (509 mg, 0.67 mmol, 1 equiv.), THF (1.35 mL, 0.5 M), sodium hydride (32.4 mg, 60% in mineral oil, 0.81 mmol, 1.2 equiv.) and 4-bromobenzyl bromide (337 mg, 1.35 mmol, 2 equiv.). Purification by normal phase column chromatography on silica (EtOAc:cyclohexane 1:99 to 20:80 gradient) yielded **193** (457 mg, 73%) as a colourless oil. **<sup>1</sup>H NMR** (600 MHz, CD<sub>3</sub>CN)  $\delta$  = 8.10 (s, 1H, H2), 7.42 – 7.38 (m, 2H, H12'), 7.14 – 7.11 (m, 2H, H11'), 6.17 (d, *J* = 1.6 Hz, 1H, H1'), 5.54 (dd, *J* = 6.4, 1.6 Hz, 1H, H2'), 5.52 – 5.34 (m, 4H, H17), 5.12 (dd, *J* = 6.4, 3.5 Hz, 1H, H3'), 4.75 (d, *J* = 10.4 Hz, 1H, H13a), 4.69 (d, *J* = 10.3 Hz, 1H, H13b), 4.45 – 4.37 (m, 2H, H9'), 4.31 – 4.27 (m, 1H, H4'), 3.96 (sept, *J* = 6.6 Hz, 1H, H10), 3.71 (dd, *J* = 10.3, 5.7 Hz, 1H, H5'a), 3.64 – 3.57 (m, 5H, H5'b, H18), 3.52 – 3.48 (m, 2H, H14), 1.54 (s, 3H,

H7'), 1.34 – 1.31 (m, 6H, H8', H11), 1.28 (d,  $J = 6.6$  Hz, 3H, H12), 0.91 – 0.85 (m, 6H, H15, H19), -0.05 (s, 9H, H16), -0.06 (s, 18H, H20);  $^{13}\text{C}$  NMR (151 MHz,  $\text{CD}_3\text{CN}$ )  $\delta = 153.53$  (C8), 153.34 (C6), 151.85 (C4), 150.61 (C2), 138.85 (C10'), 132.10 (2C, C12'), 130.35 (2C, C11'), 121.64 (C13'), 118.81 (C5), 114.38 (C6'), 90.48 (C1'), 87.34 (C4'), 84.16 (C2'), 83.53 (C3'), 79.67 (C13), 77.30 (2C, C17), 72.71 (C9'), 71.10 (C5'), 65.50 (2C, C18), 65.40 (C14), 52.99 (C10), 27.50 (C7'), 25.59 (C8'), 21.25 (C11), 20.79 (C12), 18.62 (2C, C19), 18.60 (C15), -1.36 (9C, C16, C20); HRMS (ESI+)  $m/z$  calculated for  $\text{C}_{41}\text{H}_{72}^{79}\text{BrN}_6\text{O}_7\text{Si}_3$  (M+H) $^+$  923.3948, found 923.3968.

**4-(((3*aR*,4*R*,6*R*,6*aR*)-6-(6-(bis((2-(trimethylsilyl)ethoxy)methyl)amino)-8-(methyl((2-(trimethylsilyl)ethoxy)methyl)amino)-9*H*-purin-9-yl)-2,2-dimethyltetrahydrofuro[3,4-*d*][1,3]dioxol-4-yl)methoxy)methyl)benzenesulfonyl fluoride (194)**



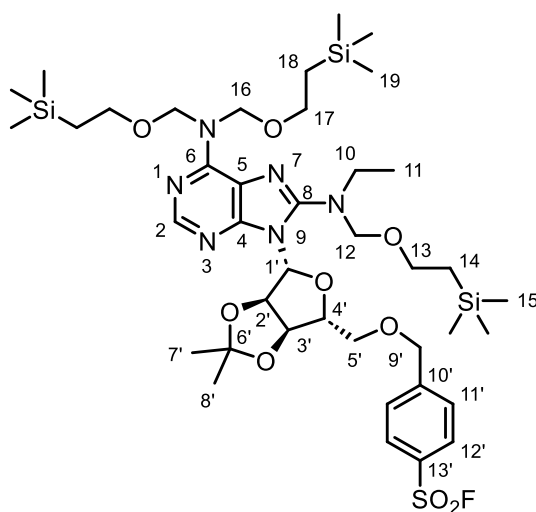
**194**

**194** was prepared following general procedure E, with 9-((3*aR*,4*R*,6*R*,6*aR*)-6-(((4-bromobenzyl)oxy)methyl)-2,2-dimethyltetrahydrofuro[3,4-*d*][1,3]dioxol-4-yl)-*N*8-methyl-*N*6,*N*6,*N*8-tris((2-(trimethylsilyl)ethoxy)methyl)-9*H*-purine-6,8-diamine **191** (1.20 g, 1.34 mmol, 1 equiv.), isopropanol (4.96 mL, 0.27 M), DABSO (193 mg, 0.80 mmol, 0.6 equiv.),  $\text{PdCl}_2(\text{AmPhos})_2$  (47.4 mg, 0.07 mmol, 5 mol%), triethylamine (0.56 mL, 4.02 mmol, 3 equiv.) and NFSI (633 mg, 2.01 mmol, 1.5 equiv.). Purification by normal phase column chromatography on silica (EtOAc:cyclohexane 1:99 to 20:80 gradient) yielded **194** (600 mg, 50%) as a yellow oil.  $^1\text{H}$  NMR (600 MHz, acetone- $d_6$ )  $\delta = 8.16$  (s, 1H, H2), 8.04 – 8.01 (s, 1H, H12'), 7.70 – 7.67 (m, 2H, H11'), 6.09 (d,  $J = 1.8$

Hz, 1H, H1'), 5.66 (dd,  $J = 6.4, 1.8$  Hz, 1H, H2'), 5.61 – 5.40 (m, 4H, H15), 5.26 (dd,  $J = 6.4, 3.3$  Hz, 1H, H3'), 4.90 (d,  $J = 10.2$  Hz, 1H, H11a), 4.80 (d,  $J = 10.2$  Hz, 1H, H11b), 4.74 (d,  $J = 14.0$  Hz, 1H, H9'a), 4.70 (d,  $J = 14.0$  Hz, 1H, H9'b), 4.43 (app. td,  $J = 6.4, 3.3$  Hz, 1H, H4'), 3.91 (dd,  $J = 10.4, 5.9$  Hz, 1H, H5'a), 3.78 (dd,  $J = 10.4, 6.8$  Hz, 1H, H5'b), 3.68 – 3.64 (m, 4H, H16), 3.60 – 3.56 (m, 2H, H12), 3.14 (s, 3H, H10), 1.55 (s, 3H, H7'), 1.35 (s, 3H, H8'), 0.95 – 0.88 (m, 6H, H13, H17), -0.03 (s, 18H, H18), -0.05 (s, 9H, H14);  $^{13}\text{C}$  NMR (151 MHz, acetone- $d_6$ )  $\delta = 154.22$  (C8), 153.47 (C6), 152.26 (C4), 150.59 (C2), 149.12 (C10'), 129.27 (2C, C12'), 129.10 (2C, C11'), 118.69 (C5), 114.31 (C6'), 90.90 (C1'), 87.31 (C4'), 84.80 (C11), 83.90 (C2'), 83.46 (C3'), 76.58 (2C, C15), 72.36 (C9'), 71.65 (C5'), 66.32 (C12), 65.30 (2C, C16), 38.40 (C10), 27.52 (C7'), 25.56 (C8'), 18.63 (2C, C17), 18.51 (C13), -1.18 (9C, C14, C18);\*  $^{19}\text{F}$  NMR (471 MHz, acetone- $d_6$ )  $\delta = 65.14$ ; HRMS (ESI+)  $m/z$  calculated for  $\text{C}_{39}\text{H}_{68}\text{FN}_6\text{O}_9\text{SSi}_3$  (M+H) $^+$  899.4055, found 899.4050.

\*C13' not observed in spectrum.

**4-(((3a*R*,4*R*,6*R*,6a*R*)-6-(6-(bis((2-(trimethylsilyl)ethoxy)methyl)amino)-8-(ethyl((2-(trimethylsilyl)ethoxy)methyl)amino)-9*H*-purin-9-yl)-2,2-dimethyltetrahydrofuro[3,4-*d*][1,3]dioxol-4-yl)methoxy)methyl)benzenesulfonyl fluoride (195)**

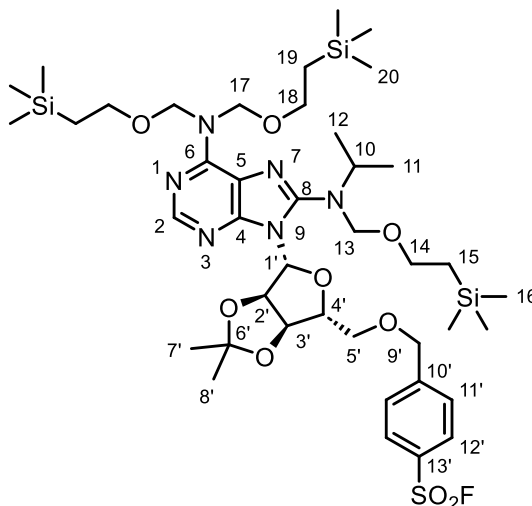


**195**

**195** was prepared following general procedure E, with 9-((3a*R*,4*R*,6*R*,6a*R*)-6-(((4-bromobenzyl)oxy)methyl)-2,2-dimethyltetrahydrofuro[3,4-*d*][1,3]dioxol-4-yl)-*N*8-ethyl-*N*6,*N*6,*N*8-tris((2-(trimethylsilyl)ethoxy)methyl)-9*H*-purine-6,8-diamine **192** (536

mg, 0.59 mmol, 1 equiv.), isopropanol (2.22 mL, 0.27 M), DABSO (84.9 mg, 0.35 mmol, 0.6 equiv.), PdCl<sub>2</sub>(AmPhos)<sub>2</sub> (20.8 mg, 0.03 mmol, 5 mol%), triethylamine (0.25 mL, 1.77 mmol, 3 equiv.) and NFSI (279 mg, 0.88 mmol, 1.5 equiv.). Purification by normal phase column chromatography on silica (EtOAc:cyclohexane 1:99 to 20:80 gradient) yielded **195** (136 mg, 25%) as a pale yellow oil. <sup>1</sup>H NMR (600 MHz, CD<sub>3</sub>CN) δ = 8.11 (s, 1H, H2), 7.95 – 7.92 (m, 2H, H12'), 7.57 – 7.54 (m, 2H, H11'), 6.06 (d, *J* = 1.6 Hz, 1H, H1'), 5.58 (dd, *J* = 6.3, 1.6 Hz, 1H, H2'), 5.54 – 5.30 (m, 4H, H16), 5.17 (dd, *J* = 6.3, 3.4 Hz, 1H, H3'), 4.80 (d, *J* = 10.4 Hz, 1H, H12a), 4.73 (d, *J* = 10.4 Hz, 1H, H12b), 4.65 – 4.57 (m, 2H, H9'), 4.38 – 4.34 (m, 1H, H4'), 3.80 (dd, *J* = 10.4, 5.6 Hz, 1H, H5'a), 3.71 (dd, *J* = 10.4, 7.1 Hz, 1H, H5'b), 3.66 – 3.57 (m, 5H, H10a, H17), 3.53 – 3.48 (m, 2H, H13), 3.48 – 3.41 (m, 1H, H10b), 1.55 (s, 3H, H7'), 1.33 (s, 3H, H8'), 1.20 (t, *J* = 7.2 Hz, 3H, H11), 0.90 – 0.83 (m, 6H, H14, H18), -0.06 (s, 18H, H19), -0.08 (s, 9H, H15); <sup>13</sup>C NMR (151 MHz, CD<sub>3</sub>CN) δ = 153.67 (C8), 153.28 (C6), 152.17 (C4), 150.53 (C2), 149.03 (C10'), 131.90 (d, *J*<sub>C-F</sub> = 24.0 Hz, C13'), 129.34 (2C, C12'), 129.09 (2C, C11'), 118.87 (C5), 114.45 (C6'), 90.68 (C1'), 87.27 (C4'), 84.01 (C2'), 83.37 (C3'), 82.90 (C12), 77.32 (2C, C16), 72.37 (C9'), 71.60 (C5'), 66.15 (C13), 65.48 (2C, C17), 45.98 (C10), 27.43 (C7'), 25.55 (C8'), 18.60 (2C, C18), 18.48 (C14), 13.54 (C11), -1.37 (6C, C19), -1.39 (3C, C15); <sup>19</sup>F NMR (471 MHz, CD<sub>3</sub>CN) δ = 65.49; HRMS (ESI+) *m/z* calculated for C<sub>40</sub>H<sub>70</sub>FN<sub>6</sub>O<sub>9</sub>SSi<sub>3</sub> (M+H)<sup>+</sup> 913.4211, found 913.4222.

**4-(((3*aR*,4*R*,6*R*,6*aR*)-6-(6-(bis((2-(trimethylsilyl)ethoxy)methyl)amino)-8-(isopropyl((2-(trimethylsilyl)ethoxy)methyl)amino)-9*H*-purin-9-yl)-2,2-dimethyltetrahydrofuro[3,4-*d*][1,3]dioxol-4-yl)methoxy)methyl)benzenesulfonyl fluoride (196)**



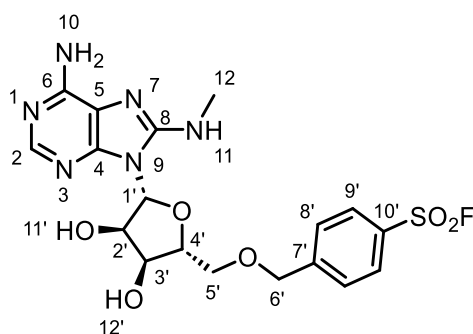
**196**

**196** was prepared following general procedure E, with 9-((3*aR*,4*R*,6*R*,6*aR*)-6-(((4-bromobenzyl)oxy)methyl)-2,2-dimethyltetrahydrofuro[3,4-*d*][1,3]dioxol-4-yl)-*N*8-isopropyl-*N*6,*N*6,*N*8-tris((2-(trimethylsilyl)ethoxy)methyl)-9*H*-purine-6,8-diamine **193** (457 mg, 0.49 mmol, 1 equiv.), isopropanol (1.83 mL, 0.27 M), DABSO (71.3 mg, 0.30 mmol, 0.6 equiv.), PdCl<sub>2</sub>(AmPhos)<sub>2</sub> (17.5 mg, 0.02 mmol, 5 mol%), triethylamine (0.21 mL, 1.48 mmol, 3 equiv.) and NFSI (234 mg, 0.74 mmol, 1.5 equiv.). Purification by normal phase column chromatography on silica (EtOAc:cyclohexane 1:99 to 20:80 gradient) yielded **196** (93 mg, 20%) as a pale yellow oil. <sup>1</sup>H NMR (600 MHz, CD<sub>3</sub>CN) δ = 8.11 (s, 1H, H<sub>2</sub>), 7.95 – 7.92 (m, 2H, H<sub>12'</sub>), 7.57 – 7.53 (m, 2H, H<sub>11'</sub>), 6.20 (d, *J* = 1.6 Hz, 1H, H<sub>1'</sub>), 5.56 (dd, *J* = 6.4, 1.6 Hz, 1H, H<sub>2'</sub>), 5.52 – 5.32 (m, 4H, H<sub>17</sub>), 5.16 (dd, *J* = 6.4, 3.5 Hz, 1H, H<sub>3'</sub>), 4.76 (d, *J* = 10.5 Hz, 1H, H<sub>13a</sub>), 4.70 (d, *J* = 10.5 Hz, 1H, H<sub>13b</sub>), 4.65 (m, 2H, H<sub>9'</sub>), 4.36 – 4.32 (m, 1H, H<sub>4'</sub>), 3.96 (sept, *J* = 6.6 Hz, 1H, H<sub>10</sub>), 3.80 (dd, *J* = 10.5, 5.5 Hz, 1H, H<sub>5'a</sub>), 3.72 (d, *J* = 10.5, 7.1 Hz, 1H, H<sub>5'b</sub>), 3.61 – 3.57 (m, 4H, H<sub>18</sub>), 3.53 – 3.48 (m, 2H, H<sub>14</sub>), 1.55 (s, 3H, H<sub>7'</sub>), 1.34 – 1.31 (m, 6H, H<sub>8'</sub>, H<sub>11</sub>), 1.29 (d, *J* = 6.6 Hz, 3H, H<sub>12</sub>), 0.91 – 0.85 (m, 6H, H<sub>15</sub>, H<sub>19</sub>), -0.05 (s, 9H, H<sub>16</sub>), -0.06 (s, 18H, H<sub>20</sub>); <sup>13</sup>C NMR (151 MHz, CD<sub>3</sub>CN) δ = 153.54 (C<sub>8</sub>), 153.35 (C<sub>6</sub>), 151.89 (C<sub>4</sub>), 150.64 (C<sub>2</sub>), 149.07 (C<sub>10'</sub>), 129.32 (2C, C<sub>12'</sub>), 129.09 (2C, C<sub>11'</sub>), 118.82 (C<sub>5</sub>), 114.48 (C<sub>6'</sub>), 90.48 (C<sub>1'</sub>), 87.18 (C<sub>4'</sub>), 84.14 (C<sub>2'</sub>), 83.36 (C<sub>3'</sub>), 79.71 (C<sub>13</sub>), 77.51 (2C, C<sub>17</sub>),

72.35 (C9'), 71.68 (C5'), 65.49 (2C, C18), 65.40 (C14), 53.02 (C10), 27.52 (C7'), 25.59 (C8'), 21.25 (C11), 20.79 (C12), 18.60 (3C, C15, C19), -1.39 (9C, C16, C20);\* <sup>19</sup>F NMR (471 MHz, CD<sub>3</sub>CN) δ = 65.00; HRMS (ESI+) m/z calculated for C<sub>41</sub>H<sub>72</sub>FN<sub>6</sub>O<sub>9</sub>SSi<sub>3</sub> (M+H)<sup>+</sup> 927.4368, found 927.4386.

\*C13' not observed in spectrum.

**4-(((2*R*,3*S*,4*R*,5*R*)-5-(6-amino-8-(methylamino)-9*H*-purin-9-yl)-3,4-dihydroxytetrahydrofuran-2-yl)methoxy)methyl)benzenesulfonyl fluoride (179)**



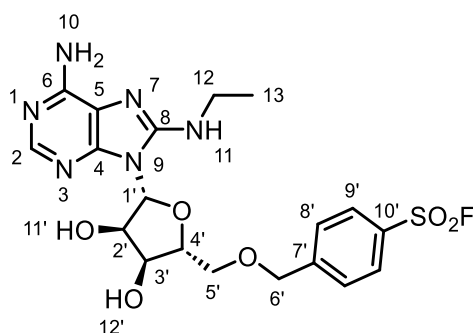
**179**

**179** was prepared following general procedure F, with 4-(((3*aR*,4*R*,6*R*,6*aR*)-6-(6-(bis((2-(trimethylsilyl)ethoxy)methyl)amino)-8-(methyl((2-(trimethylsilyl)ethoxy)methyl)amino)-9*H*-purin-9-yl)-2,2-dimethyltetrahydrofuro[3,4-*d*][1,3]dioxol-4-yl)methoxy)methyl)benzenesulfonyl fluoride **194** (550 mg, 0.61 mmol, 1 equiv.), and TFA:water 5:2 (v/v) mixture (6.12 mL, 0.1 M) for 1 hour. Purification by normal phase column chromatography on silica (100% CH<sub>2</sub>Cl<sub>2</sub> to 15:85 methanol:CH<sub>2</sub>Cl<sub>2</sub> gradient) then reverse phase column chromatography on C18 (acetonitrile:water +0.1% formic acid 5:95 to 50:50 gradient) yielded **179** (112 mg, 39%) as a white solid. <sup>1</sup>H NMR (600 MHz, DMSO-*d*<sub>6</sub>) δ = 8.11 – 8.08 (m, 2H, H9'), 7.89 (s, 1H, H2), 7.69 – 7.66 (m, 2H, H8'), 6.59 (q, *J* = 4.5 Hz, 1H, H11), 6.55 (s br, 2H, H10), 5.77 (d, *J* = 5.4 Hz, 1H, H1'), 5.34 (d, *J* = 5.8 Hz, 1H, H11'), 5.20 (d, *J* = 5.3 Hz, 1H, H12'), 4.91 (app. q, *J* = 5.5 Hz, 1H, H2'), 4.76 – 4.69 (m, 2H, H6'), 4.35 (app. q, *J* = 5.1 Hz, 1H, H3'), 4.04 – 4.01 (m, 1H, H4'), 3.80 (dd, *J* = 10.9, 3.0 Hz, 1H, H5'a), 3.69 (dd, *J* = 10.9, 4.8 Hz, 1H, H5'b), 2.78 (d, *J* = 4.5 Hz, 3H, H12); <sup>13</sup>C NMR (151 MHz, DMSO-*d*<sub>6</sub>) δ = 152.25 (C8), 152.24 (C6), 149.80 (C4), 148.53 (C2), 147.87 (C7'), 130.28 (d, *J*<sub>C-F</sub> = 23.2 Hz, C10'), 128.48 (2C, C9'), 128.47 (2C, C8'), 117.14 (C5), 87.08 (C1'), 82.63 (C4'), 71.19 (C6'), 70.59



(C5'), 70.42 (C2'), 70.19 (C3'), 29.11 (C12);  $^{19}\text{F}$  NMR (471 MHz, DMSO- $d_6$ )  $\delta$  = 66.60; HRMS (ESI+)  $m/z$  calculated for  $\text{C}_{18}\text{H}_{22}\text{FN}_6\text{O}_6\text{S}$  (M+H) $^+$  469.1300, found 469.1307.

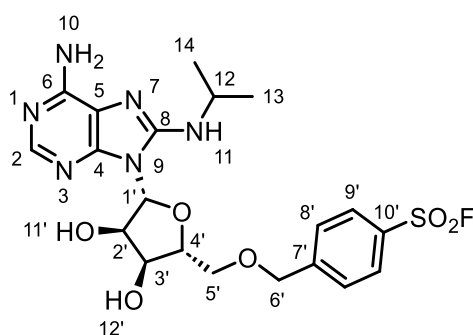
**4-(((2*R*,3*S*,4*R*,5*R*)-5-(6-amino-8-(ethylamino)-9*H*-purin-9-yl)-3,4-dihydroxytetrahydrofuran-2-yl)methoxy)methyl)benzenesulfonyl fluoride (**180**)**



**180**

**180** was prepared following general procedure F, with 4-(((3*aR*,4*R*,6*R*,6*aR*)-6-(6-(bis((2-(trimethylsilyl)ethoxy)methyl)amino)-8-(ethyl((2-(trimethylsilyl)ethoxy)methyl)amino)-9*H*-purin-9-yl)-2,2-dimethyltetrahydrofuro[3,4-*d*][1,3]dioxol-4-yl)methoxy)methyl)benzenesulfonyl fluoride **195** (130 mg, 0.14 mmol, 1 equiv.), and TFA:water 5:2 (v/v) mixture (1.42 mL, 0.1 M) for 1 hour. Purification by normal phase column chromatography on silica (100%  $\text{CH}_2\text{Cl}_2$  to 15:85 methanol: $\text{CH}_2\text{Cl}_2$  gradient) then reverse phase column chromatography on C18 (acetonitrile:water +0.1% formic acid 5:95 to 50:50 gradient) yielded **180** (26 mg, 38%) as a white solid.  $^1\text{H}$  NMR (600 MHz, DMSO- $d_6$ )  $\delta$  = 8.11 – 8.08 (m, 2H, H9'), 7.87 (s, 1H, H2), 7.69 – 7.66 (m, 2H, H8'), 6.58 (t,  $J$  = 5.4 Hz, 1H, H11), 6.47 (s br, 2H, H10), 5.78 (d,  $J$  = 5.3 Hz, 1H, H1'), 5.32 (d,  $J$  = 5.7 Hz, 1H, H11'), 5.19 (d,  $J$  = 5.4 Hz, 1H, H12'), 4.91 (app. q,  $J$  = 5.5 Hz, 1H, H2'), 4.75 – 4.68 (m, 2H, H6'), 4.36 (app. q,  $J$  = 5.2 Hz, 1H, H3'), 4.04 – 4.00 (m, 1H, H4'), 3.81 (dd,  $J$  = 11.0, 3.1 Hz, 1H, H5'a), 3.69 (dd,  $J$  = 11.0, 5.0 Hz, 1H, H5'b), 3.27 (app. quint,  $J$  = 6.6 Hz, 2H, H12), 1.09 (t,  $J$  = 7.2 Hz, 3H, H13);  $^{13}\text{C}$  NMR (151 MHz, DMSO- $d_6$ )  $\delta$  = 152.32 (C6), 151.51 (C8), 149.71 (C4), 148.59 (C2), 147.91 (C7'), 130.26 (d,  $J_{\text{C-F}}$  = 23.3 Hz, C10'), 128.48 (4C, C8', C9'), 117.22 (C5), 87.04 (C1'), 82.54 (C4'), 71.18 (C6'), 70.63 (C5'), 70.48 (C2'), 70.11 (C3'), 36.99 (C12), 14.86 (C13);  $^{19}\text{F}$  NMR (471 MHz, DMSO- $d_6$ )  $\delta$  = 66.59; HRMS (ESI+)  $m/z$  calculated for  $\text{C}_{19}\text{H}_{24}\text{FN}_6\text{O}_6\text{S}$  (M+H) $^+$  483.1457, found 483.1459.

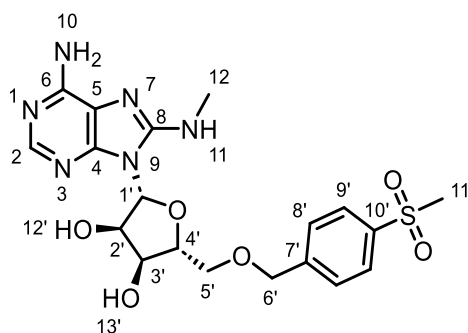
**4-(((2*R*,3*S*,4*R*,5*R*)-5-(6-amino-8-(isopropylamino)-9*H*-purin-9-yl)-3,4-dihydroxytetrahydrofuran-2-yl)methoxy)methyl)benzenesulfonyl fluoride (181)**



**181**

**181** was prepared following general procedure F, with 4-(((3*aR*,4*R*,6*R*,6*aR*)-6-(6-(bis((2-(trimethylsilyl)ethoxy)methyl)amino)-8-(isopropyl((2-(trimethylsilyl)ethoxy)methyl)amino)-9*H*-purin-9-yl)-2,2-dimethyltetrahydrofuro[3,4-*d*][1,3]dioxol-4-yl)methoxy)methyl)benzenesulfonyl fluoride **196** (90 mg, 0.10 mmol, 1 equiv.), and TFA:water 5:2 (v/v) mixture (0.97 mL, 0.1 M) for 2 hours. Purification by normal phase column chromatography on silica (100% CH<sub>2</sub>Cl<sub>2</sub> to 15:85 methanol:CH<sub>2</sub>Cl<sub>2</sub> gradient) then reverse phase column chromatography on C18 (methanol:water +0.1% formic acid 20:80 to 80:20 gradient) yielded **181** (8.0 mg, 17%) as a white solid. <sup>1</sup>H NMR (600 MHz, DMSO-*d*<sub>6</sub>) δ = 8.10 – 8.06 (m, 2H, H9'), 7.85 (s, 1H, H2), 7.67 – 7.64 (m, 2H, H8'), 6.43 (s, 2H, H10), 6.40 (d, *J* = 7.9 Hz, 1H, H11), 5.79 (d, *J* = 4.9 Hz, 1H, H1'), 5.30 (d, *J* = 5.6 Hz, 1H, H11'), 5.17 (d, *J* = 5.5 Hz, 1H, H12'), 4.96 (app. q, *J* = 5.2 Hz, 1H, H2'), 4.73 – 4.66 (m, 2H, H6'), 4.41 – 4.36 (app. q, *J* = 5.4 Hz, 1H, H3'), 4.12 – 4.04 (m, 1H, H12), 4.00 (app. td, *J* = 5.4, 3.2 Hz, 1H, H4'), 3.80 (dd, *J* = 10.9, 3.1 Hz, 1H, H5'a), 3.67 (dd, *J* = 10.9, 5.4 Hz, 1H, H5'b), 1.19 – 1.15 (m, 6H, H13, H14); <sup>13</sup>C NMR (151 MHz, DMSO-*d*<sub>6</sub>) δ = 152.35 (C6), 151.10 (C8), 149.58 (C4), 148.57 (C2), 148.06 (C7'), 130.18 (d, *J*<sub>C-F</sub> = 23.3 Hz, C10'), 128.43 (2C, C9'), 128.39 (2C, C8'), 117.38 (C5), 87.11 (C1'), 82.29 (C4'), 71.08 (C6'), 70.62 (C2'), 70.58 (C5'), 69.94 (C3'), 43.93 (C12), 22.57 (C13), 22.54 (C14); <sup>19</sup>F NMR (471 MHz, DMSO-*d*<sub>6</sub>) δ = 66.61; HRMS (ESI+) *m/z* calculated for C<sub>20</sub>H<sub>26</sub>FN<sub>6</sub>O<sub>6</sub>S (M+H)<sup>+</sup> 497.1613, found 497.1615.

**(2*R*,3*R*,4*S*,5*R*)-2-(6-amino-8-(methylamino)-9*H*-purin-9-yl)-5-(((4-(methylsulfonyl)benzyl)oxy)methyl)tetrahydrofuran-3,4-diol (197)**

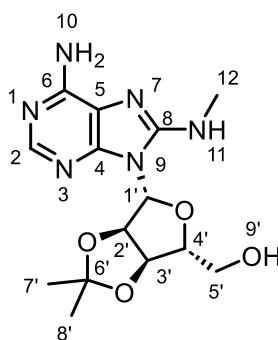


**197**

A two-neck round bottom flask heat-dried under vacuum and equipped with magnetic stirrer was charged with ((3*aR*,4*R*,6*R*,6*aR*)-6-(6-(bis((2-(trimethylsilyl)ethoxy)methyl)amino)-8-(methyl((2-(trimethylsilyl)ethoxy)methyl)amino)-9*H*-purin-9-yl)-2,2-dimethyltetrahydrofuro[3,4-*d*][1,3]dioxol-4-yl)methanol **188** (220 mg, 0.30 mmol, 1 equiv.) and THF (0.61 mL, 0.5 M) under flow of nitrogen. The mixture was cooled to 0 °C and sodium hydride (14.5 mg, 60% in mineral oil, 0.36 mmol, 1.2 equiv.) was added and stirred for 15 minutes. 1-(bromomethyl)-4-methanesulfonylbenzene (151 mg, 0.61 mmol, 2 equiv.) was then added, after which the mixture was allowed to warm up to room temperature. After stirring at room temperature for 18 hours, the reaction mixture was quenched with methanol and the solvent was removed under reduced pressure. The crude mixture was eluted through a silica plug (EtOAc:cyclohexane 20:80), concentrated under reduced pressure and the crude residue was redissolved in TFA:water 5:2 (v/v) mixture (2.8 mL). After stirring at room temperature for 1 hour, the mixture was diluted with toluene (20 mL) and concentrated under reduced pressure. The crude product was purified by normal phase column chromatography on silica (100% CH<sub>2</sub>Cl<sub>2</sub> to methanol:CH<sub>2</sub>Cl<sub>2</sub> 15:85 gradient) then reverse phase column chromatography on C18 (methanol:water +0.1% formic acid 20:80 to 100% methanol gradient) to yield **197** (62 mg, 44%) as a white solid. <sup>1</sup>H NMR (600 MHz, DMSO-*d*<sub>6</sub>) δ = 7.91 – 7.87 (m, 3H, H<sub>2</sub>, H<sub>9</sub>'), 7.58 – 7.54 (m, 2H, H<sub>8</sub>'), 6.55 – 6.50 (m, 3H, H<sub>10</sub>, H<sub>11</sub>), 5.80 (d, *J* = 5.6 Hz, 1H, H<sub>1</sub>'), 5.33 (d, *J* = 5.8 Hz, 1H, H<sub>12</sub>'), 5.19 (d, *J* = 5.1 Hz, 1H, H<sub>13</sub>'), 4.87 (app. q, *J* = 5.5 Hz, 1H, H<sub>2</sub>'), 4.70 – 4.63 (m, 2H, H<sub>6</sub>'), 4.31 (app. q, *J* = 5.0 Hz, 1H, H<sub>3</sub>'), 4.04 – 4.01 (m, 1H, H<sub>4</sub>'), 3.78 (dd, *J* = 10.8, 3.0 Hz, 1H, H<sub>5</sub>'a), 3.67 (dd, *J* = 10.8, 4.5 Hz, 1H, H<sub>5</sub>'b), 3.20 (s, 3H, H<sub>11</sub>'), 2.75

(d,  $J = 4.6$  Hz, 3H, H12);  $^{13}\text{C}$  NMR (151 MHz, DMSO- $d_6$ )  $\delta = 152.32$  (C6), 152.15 (C8), 149.87 (C4), 148.63 (C2), 144.16 (C7'), 139.90 (C10'), 127.90 (C9'), 127.03 (C8'), 117.11 (C5), 86.94 (C1'), 82.75 (C4'), 71.56 (C6'), 70.45 (C5'), 70.37 (C2'), 70.31 (C3'), 43.56 (C11'), 29.06 (C12); HRMS (ESI+)  $m/z$  calculated for  $\text{C}_{19}\text{H}_{25}\text{N}_6\text{O}_6\text{S}$  (M+H) $^+$  465.1551, found 465.1561.

**((3a*R*,4*R*,6*R*,6a*R*)-6-(6-amino-8-(methylamino)-9*H*-purin-9-yl)-2,2-dimethyltetrahydrofuro[3,4-*d*][1,3]dioxol-4-yl)methanol (59)**

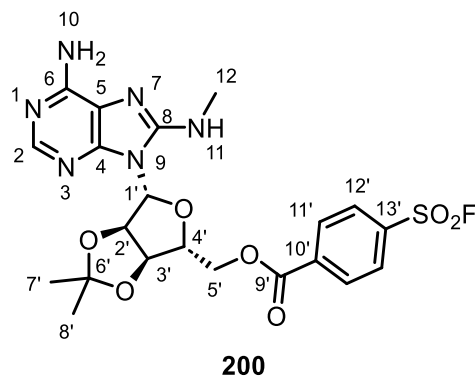


**59**

**59** was prepared following a modification of general procedure A, with ((3a*R*,4*R*,6*R*,6a*R*)-6-(6-amino-8-bromo-9*H*-purin-9-yl)-2,2-dimethyltetrahydrofuro[3,4-*d*][1,3]dioxol-4-yl)methanol **109** (1.15 g, 2.98 mmol, 1 equiv.) and methylamine (9.69 mL, 33 wt% in ethanol, 77.8 mmol, 26 equiv.). Purification by normal phase column chromatography on silica (100%  $\text{CH}_2\text{Cl}_2$  to methanol: $\text{CH}_2\text{Cl}_2$  15:85 gradient) yielded **59** (746 mg, 74%) as an off-white foam.  $^1\text{H}$  NMR (600 MHz, DMSO- $d_6$ )  $\delta = 7.92$  (s, 1H, H2), 6.95 (q,  $J = 4.7$  Hz, 1H, H11), 6.57 (s br, 2H, H10), 6.00 (d,  $J = 3.6$  Hz, 1H, H1'), 5.48 (t,  $J = 4.7$  Hz, 1H, H9'), 5.42 (dd,  $J = 6.3, 3.6$  Hz, 1H, H2'), 4.97 (dd,  $J = 6.3, 2.9$  Hz, 1H, H3'), 4.17 – 4.13 (m, 1H, H4'), 3.61 – 3.51 (m, 2H, H5'), 2.88 (d,  $J = 4.7$  Hz, 3H, H12), 1.54 (s, 3H, H7'), 1.31 (s, 3H, H8');  $^{13}\text{C}$  NMR (151 MHz, DMSO- $d_6$ )  $\delta = 152.56$  (C6), 151.80 (C8), 149.24 (C4), 148.80 (C2), 117.16 (C5), 113.24 (C6'), 87.89 (C1'), 85.28 (C4'), 81.30 (C2'), 81.03 (C3'), 61.27 (C5'), 29.15 (C12), 27.14 (C7'), 25.24 (C8'); HRMS (ESI+)  $m/z$  calculated for  $\text{C}_{14}\text{H}_{21}\text{N}_6\text{O}_4$  (M+H) $^+$  337.1619, found 337.1624.

The spectroscopic and analytical data were in agreement with literature values.<sup>145</sup>

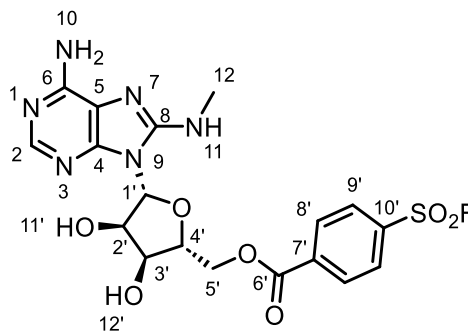
**((3*aR*,4*R*,6*R*,6*aR*)-6-(6-amino-8-(methylamino)-9*H*-purin-9-yl)-2,2-dimethyltetrahydrofuro[3,4-*d*][1,3]dioxol-4-yl)methyl 4-(fluorosulfonyl)benzoate (200)**



A two-neck round bottom flask equipped with magnetic stirrer was charged with ((3*aR*,4*R*,6*R*,6*aR*)-6-(6-amino-8-(methylamino)-9*H*-purin-9-yl)-2,2-dimethyltetrahydrofuro[3,4-*d*][1,3]dioxol-4-yl)methanol **59** (300 mg, 0.89 mmol, 1 equiv.) and DMF (8.92 mL, 0.1 M) under flow of nitrogen. The mixture was cooled to 0 °C, and 4-(fluorosulfonyl)benzoyl chloride (238 mg, 1.07 mmol, 1.2 equiv.) and triethylamine (0.19 mL, 1.34 mmol, 1.5 equiv.) were added in sequence. After stirring at 0 °C for 3 hours, the reaction mixture was quenched with water (30 mL), diluted with EtOAc (25 mL) and the phases were separated. The aqueous phase was extracted with EtOAc (2 x 25 mL) and the resultant combined organic layers were washed with 10% LiCl (w/v) solution (3 x 30 mL), dried over MgSO<sub>4</sub>, filtered, and concentrated under reduced pressure. The crude product was purified by normal phase column chromatography on silica (100% CH<sub>2</sub>Cl<sub>2</sub> to methanol:CH<sub>2</sub>Cl<sub>2</sub> 10:90 gradient) to yield **200** (147 mg, 32%) as a yellow foam. <sup>1</sup>H NMR (600 MHz, DMSO-*d*<sub>6</sub>) δ = 8.29 – 8.26 (m, 2H, H12'), 8.24 – 8.21 (m, 2H, H11'), 7.83 (s, 1H, H2), 7.02 (q, *J* = 4.7 Hz, 1H, H11), 6.55 (s br, 2H, H10), 6.04 (d, *J* = 2.3 Hz, 1H, H1'), 5.78 (dd, *J* = 6.3, 2.3 Hz, 1H, H2'), 5.24 (dd, *J* = 6.3, 3.4 Hz, 1H, H3'), 4.61 – 4.57 (m, 1H, H4'), 4.45 – 4.38 (m, 2H, H5'), 2.87 (d, *J* = 4.7 Hz, 3H, H12), 1.56 (s, 3H, H7'), 1.34 (s, 3H, H8'); <sup>13</sup>C NMR (151 MHz, DMSO-*d*<sub>6</sub>) δ = 163.73 (C9'), 152.54 (C6), 151.91 (C8), 149.20 (C4), 148.74 (C2), 136.13 (C10'), 135.28 (d, *J*<sub>C-F</sub> = 24.3 Hz, C13'), 130.95 (2C, C11'), 128.87 (2C, C12'), 117.42 (C5'), 113.48 (C6'), 87.32 (C1'), 83.18 (C4'), 81.89 (C2'), 81.00 (C3'), 65.06 (C5'), 29.15 (C12), 27.06 (C7'), 25.33 (C8'); <sup>19</sup>F NMR (471 MHz, DMSO-*d*<sub>6</sub>) δ = 65.97; HRMS (ESI+) *m/z* calculated for C<sub>21</sub>H<sub>24</sub>FN<sub>6</sub>O<sub>7</sub>S (M+H)<sup>+</sup> 523.1406, found 523.1412.

The spectroscopic and analytical data were in agreement with literature values.<sup>145</sup>

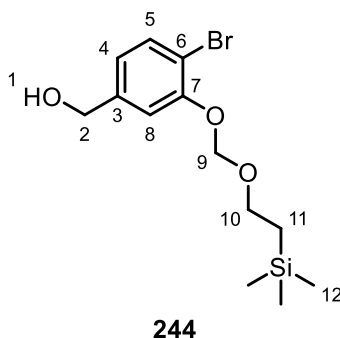
**((2*R*,3*S*,4*R*,5*R*)-5-(6-amino-8-(methylamino)-9*H*-purin-9-yl)-3,4-dihydroxytetrahydrofuran-2-yl)methyl 4-(fluorosulfonyl)benzoate (**199**)**



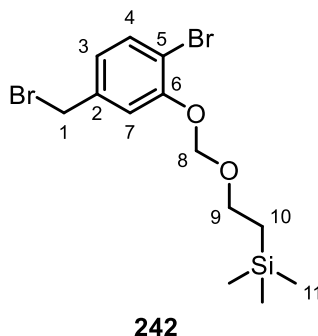
**199**

**199** was prepared following general procedure F, with ((3*aR*,4*R*,6*R*,6*aR*)-6-(6-amino-8-(methylamino)-9*H*-purin-9-yl)-2,2-dimethyltetrahydrofuro[3,4-*d*][1,3]dioxol-4-yl)methyl 4-(fluorosulfonyl)benzoate **200** (140 mg, 0.27 mmol, 1 equiv.), and TFA:water 5:2 (v/v) mixture (2.68 mL, 0.1 M) for 2 hours. Purification by normal phase column chromatography on silica (100% CH<sub>2</sub>Cl<sub>2</sub> to 15:85 methanol:CH<sub>2</sub>Cl<sub>2</sub> gradient) then reverse phase column chromatography on C18 (acetonitrile:water +0.1% formic acid 5:95 to 40:60 gradient) yielded **199** (70 mg, 54%) as an off-white solid. <sup>1</sup>H NMR (600 MHz, DMSO-*d*<sub>6</sub>) δ = 8.24 – 8.21 (m, 2H, H9'), 8.16 – 8.13 (m, 2H, H8'), 7.82 (s, 1H, H2), 6.88 (s br, 1H, H11), 6.54 (s br, 2H, H10), 5.70 (d, *J* = 4.0 Hz, 1H, H1'), 5.42 (d, *J* = 5.2 Hz, 1H, H11'), 5.30 (d, *J* = 5.8 Hz, 1H, H12'), 5.12 (app. q, *J* = 4.6 Hz, 1H, H2'), 4.70 – 4.63 (m, 2H, H3', H5'a), 4.45 (dd, *J* = 12.0 Hz, 5.2 Hz, 1H, H5'b), 4.14 (app. td, *J* = 5.7, 3.4 Hz, 1H, H4'), 2.86 (d, *J* = 4.5 Hz, 3H, H12); <sup>13</sup>C NMR (151 MHz, DMSO-*d*<sub>6</sub>) δ = 163.83 (C6'), 152.51 (C8), 152.23 (C6), 149.47 (C4), 148.41 (C2), 136.23 (C7'), 135.24 (d, *J*<sub>C-F</sub> = 24.1 Hz, C10'), 130.79 (2C, C8'), 128.80 (2C, C9'), 117.39 (C5), 87.67 (C1'), 80.47 (C4'), 70.75 (C2'), 69.60 (C3'), 64.81 (C5'), 29.24 (C12); <sup>19</sup>F NMR (471 MHz, DMSO-*d*<sub>6</sub>) δ = 66.02; HRMS (ESI+) *m/z* calculated for C<sub>18</sub>H<sub>20</sub>FN<sub>6</sub>O<sub>7</sub>S (M+H)<sup>+</sup> 483.1093, found 483.1100.

The spectroscopic and analytical data were in agreement with literature values.<sup>145</sup>

**(4-bromo-3-((2-(trimethylsilyl)ethoxy)methoxy)phenyl)methanol (244)**

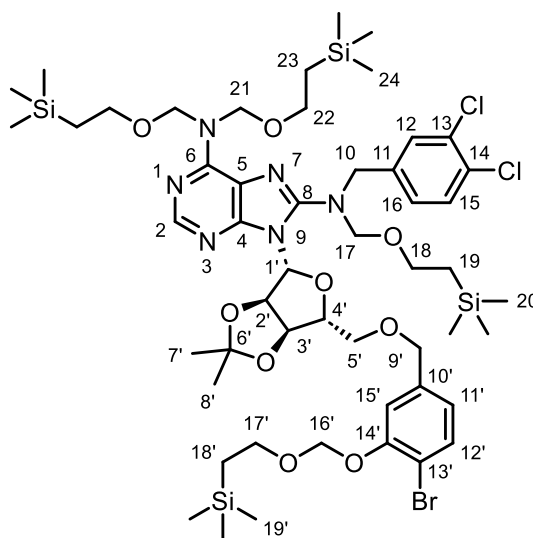
A two-neck round bottom flask heat-dried under vacuum and equipped with magnetic stirrer was charged 2-bromo-5-(hydroxymethyl)phenol **243** (1.30 g, 6.40 mmol, 1 equiv.) and THF (12.8 mL, 0.5 M) under flow of nitrogen. The mixture was cooled to 0 °C and sodium hydride (269 mg, 60% in mineral oil, 6.72 mmol, 1.05 equiv.) was added and stirred for 30 minutes. 2-(trimethylsilyl)ethoxymethylchloride (1.19 mL, 6.72 mmol, 1.05 equiv.) was then added, after which the mixture was allowed to warm up to room temperature. After stirring at room temperature for 22 hours, the reaction mixture was quenched with methanol and the solvent was removed under reduced pressure. The crude product was purified by normal phase column chromatography on silica (EtOAc:cyclohexane 5:95 to 40:60 gradient) to yield **244** (1.44 g, 67%) as a pale yellow oil. **<sup>1</sup>H NMR** (600 MHz, CD<sub>3</sub>CN) δ = 7.50 (d, *J* = 8.1 Hz, 1H, H5), 7.18 – 7.16 (m, 1H, H8), 6.90 – 6.87 (m, 1H, H4), 5.29 (s, 2H, H9), 4.52 (d, *J* = 5.8 Hz, 2H, H2), 3.81 – 3.77 (m, 2H, H10), 3.24 (t, *J* = 5.8 Hz, 1H, H1), 0.95 – 0.91 (m, 2H, H11), -0.01 (s, 9H, H12); **<sup>13</sup>C NMR** (151 MHz, CD<sub>3</sub>CN) δ = 154.57 (C7), 144.38 (C3), 133.82 (C5), 121.96 (C4), 115.37 (C8), 111.31 (C6), 94.26 (C9), 67.30 (C10), 63.95 (C2), 18.49 (C11), -1.46 (3C, C12); **HRMS** (ESI+) *m/z* calculated for C<sub>13</sub>H<sub>21</sub><sup>79</sup>BrNaO<sub>3</sub>Si (M+Na)<sup>+</sup> 355.0336, found 355.0336.

**(2-((2-bromo-5-(bromomethyl)phenoxy)methoxy)ethyl)trimethylsilane (242)**

A two-neck round bottom flask equipped with magnetic stirrer was charged with (4-bromo-3-((2-(trimethylsilyl)ethoxy)methoxy)phenyl)methanol **244** (1.43 g, 4.29 mmol, 1 equiv.) and  $\text{CH}_2\text{Cl}_2$  (0.25 M) under flow of nitrogen. The mixture was cooled to 0 °C and triphenylphosphine (1.69 g, 6.43 mmol, 1.5 equiv.) and NBS (1.15 g, 6.43 mmol 1.5 equiv.) were added in sequence, after which the mixture was allowed to warm up to room temperature. After stirring at room temperature for 3 hours the reaction mixture was quenched with water (40 mL), diluted with EtOAc (30 mL) and the phases were separated. The aqueous phase was extracted with EtOAc (2 × 30 mL) and the resultant combined organic layers were dried over  $\text{MgSO}_4$ , filtered, and concentrated under reduced pressure. The crude product was purified by normal phase column chromatography on silica (EtOAc:cyclohexane 1:99 to 20:80 gradient) to yield **242** (1.23 g, 72%) as a colourless oil.  $^1\text{H NMR}$  (600 MHz,  $\text{CD}_3\text{CN}$ )  $\delta$  = 7.54 (d,  $J$  = 8.1 Hz, 1H, H4), 7.24 (d,  $J$  = 1.8 Hz, 1H, H7), 6.98 (dd,  $J$  = 8.1, 1.8 Hz, 1H, H3), 5.30 (s, 2H, H8), 4.53 (s, 2H, H1), 3.81 – 3.77 (m, 2H, H9), 0.95 – 0.91 (m, 2H, H10), -0.01 (s, 9H, H11);  $^{13}\text{C NMR}$  (151 MHz,  $\text{CD}_3\text{CN}$ )  $\delta$  = 154.71 (C6), 140.20 (C2), 134.42 (C5), 124.53 (C4), 117.80 (C6), 113.20 (C5), 94.28 (C8), 67.42 (C9), 33.70 (C1), 18.46 (C10), -1.43 (3C, C11); **HRMS** (ESI+)  $m/z$  calculated for  $\text{C}_{13}\text{H}_{20}^{79}\text{Br}_2\text{NaO}_2\text{Si}$  ( $\text{M}+\text{Na}$ )<sup>+</sup> 416.9492, found 416.9498.



**9-((3*aR*,4*R*,6*R*,6*aR*)-6-(((4-bromo-3-((2-(trimethylsilyl)ethoxy)methoxy)benzyl)oxy)methyl)-2,2-dimethyltetrahydrofuro[3,4-*d*][1,3]dioxol-4-yl)-*N*8-(3,4-dichlorobenzyl)-*N*6,*N*6,*N*8-tris((2-(trimethylsilyl)ethoxy)methyl)-9*H*-purine-6,8-diamine (**241**)**

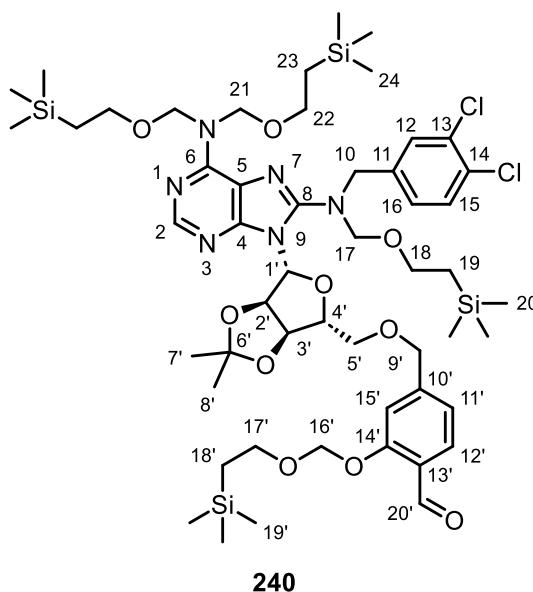


**241**

**241** was prepared following a modification of general procedure D, with ((3*aR*,4*R*,6*R*,6*aR*)-6-(6-(bis((2-(trimethylsilyl)ethoxy)methyl)amino)-8-((3,4-dichlorobenzyl)((2-(trimethylsilyl)ethoxy)methyl)amino)-9*H*-purin-9-yl)-2,2-dimethyltetrahydrofuro[3,4-*d*][1,3]dioxol-4-yl)methanol **125** (362 mg, 0.42 mmol, 1 equiv.), THF (0.83 mL, 0.5 M), sodium hydride (19.9 mg, 60% in mineral oil, 0.50 mmol, 1.2 equiv.) and (2-((2-bromo-5-(bromomethyl)phenoxy)methoxy)ethyl)trimethylsilane **242** (247 mg, 0.62 mmol, 1.5 equiv.) as a solution in THF (0.42 mL). Purification by normal phase column chromatography on silica (EtOAc:cyclohexane 1:99 to 20:80 gradient) yielded **241** (409 mg, 83%) as a colourless oil. <sup>1</sup>H NMR (600 MHz, CD<sub>3</sub>CN) δ = 8.09 (s, 1H, H2), 7.57 (d, *J* = 1.9 Hz, 1H, H12), 7.44 – 7.40 (m, 2H, H12', H15), 7.30 (dd, *J* = 8.2, 1.9 Hz, 1H, H16), 7.09 (d, *J* = 1.8 Hz, 1H, H15'), 6.71 (dd, *J* = 8.1, 1.8 Hz, 1H, H11'), 6.09 (d, *J* = 2.0 Hz, 1H, H1'), 5.58 (dd, *J* = 6.4, 2.0 Hz, 1H, H2'), 5.49 – 5.29 (m, 4H, H21), 5.24 – 5.21 (m, 2H, H16'), 5.13 (dd, *J* = 6.4, 3.2 Hz, 1H, H3'), 4.81 (d, *J* = 10.4 Hz, 1H, H17a), 4.75 (d, *J* = 14.9 Hz, 1H, H10a), 4.72 (d, *J* = 10.4 Hz, 1H, H17b), 4.58 (d, *J* = 14.9 Hz, 1H, H10b), 4.43 – 4.38 (m, 2H, H9'), 4.33 (app. td, *J* = 6.5, 3.2 Hz, 1H, H4'), 3.78 – 3.73 (m, 2H, H17'), 3.70 (dd, *J* = 10.1, 6.1 Hz, 1H, H5'a), 3.60 (dd, *J* = 10.1, 6.7 Hz, 1H, H5'b), 3.57 – 3.53 (m, 4H, H22), 3.51 – 3.46 (m, 2H, H18), 1.55 (s, 3H,

H7'), 1.33 (s, 3H, H8'), 0.92 – 0.88 (m, 2H, H18'), 0.88 – 0.82 (m, 6H, H19, H23), -0.05 (s, 9H, H19'), -0.08 (s, 18H, H24), -0.09 (s, 9H, H20);  $^{13}\text{C}$  NMR (151 MHz,  $\text{CD}_3\text{CN}$ )  $\delta$  = 154.57 (C14'), 153.45 (C6), 153.13 (C8), 152.23 (C4), 150.86 (C2), 140.61 (C10'), 140.10 (C11), 133.82 (C12'), 132.61 (C14), 131.44 (C13), 131.39 (C12), 131.28 (C15), 129.40 (C16), 122.85 (C11'), 118.66 (C5), 116.18 (C15'), 114.52 (C6'), 112.02 (C13'), 94.21 (C16'), 90.72 (C1'), 87.17 (C4'), 83.74 (C2'), 83.53 (C17), 83.49 (C3'), 77.30 (2C, C21), 72.92 (C9'), 70.94 (C5'), 67.31 (C17'), 66.59 (C18), 65.60 (2C, C22), 53.44 (C10), 27.48 (C7'), 25.60 (C8'), 18.61 (2C, C23), 18.49 (C19), 18.47 (C18'), -1.32 (6C, C24), -1.36 (3C, C20), -1.39 (3C, C19'); **HRMS** (ESI+)  $m/z$  calculated for  $\text{C}_{51}\text{H}_{84}^{79}\text{Br}^{35}\text{Cl}_2\text{N}_6\text{O}_9\text{Si}_4$  ( $\text{M}+\text{H}$ ) $^+$  1185.3932, found 1185.3954.

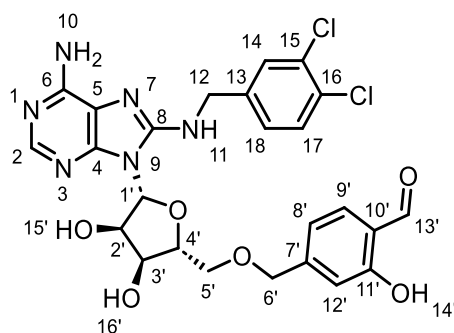
**4-(((3*aR*,4*R*,6*R*,6*aR*)-6-(6-(bis((2-(trimethylsilyl)ethoxy)methyl)amino)-8-((3,4-dichlorobenzyl)((2-(trimethylsilyl)ethoxy)methyl)amino)-9*H*-purin-9-yl)-2,2-dimethyltetrahydrofuro[3,4-*d*][1,3]dioxol-4-yl)methoxy)methyl)-2-((2-(trimethylsilyl)ethoxy)methoxy)benzaldehyde (240)**



A two-neck round bottom flask heat-dried under vacuum and equipped with magnetic stirrer was charged with 9-(((3*aR*,4*R*,6*R*,6*aR*)-6-(((4-bromo-3-((2-(trimethylsilyl)ethoxy)methoxy)benzyl)oxy)methyl)-2,2-dimethyltetrahydrofuro[3,4-*d*][1,3]dioxol-4-yl)-*N*8-(3,4-dichlorobenzyl)-*N*6,*N*6,*N*8-tris((2-(trimethylsilyl)ethoxy)methyl)-9*H*-purine-6,8-diamine **241** (375 mg, 0.32 mmol, 1 equiv.) and THF (1.26 mL, 0.5 M) under flow of nitrogen. The mixture was cooled to -78 °C and *n*-butyllithium (0.15 mL, 2.5 M in hexanes, 0.38 mmol, 1.2 equiv.) was added

and stirred for 10 minutes. DMF (49  $\mu$ L, 0.63 mmol, 2 equiv.) was then added, after which the mixture was allowed to stir at -78  $^{\circ}$ C for 3 hours. The reaction mixture was quenched with methanol and the solvent was removed under reduced pressure, and the crude mixture was purified by normal phase column chromatography on silica (EtOAc:cyclohexane 1:99 to 20:80 gradient) to yield **240** (202 mg, 56%) as a colourless oil.  **$^1$ H NMR** (600 MHz,  $\text{CD}_3\text{CN}$ )  $\delta$  = 10.38 – 10.37, (m, 1H, H20'), 8.07 (s, 1H, H2), 7.63 (d,  $J$  = 7.9 Hz, 1H, H12'), 7.57 (d,  $J$  = 1.9 Hz, 1H, H12), 7.43 (d,  $J$  = 8.3 Hz, 1H, H15), 7.31 (dd,  $J$  = 8.3, 1.9 Hz, 1H, H16), 7.15 (app. s, 1H, H15'), 6.92 (app. d,  $J$  = 7.9 Hz, 1H, H11'), 6.11 (d,  $J$  = 2.0 Hz, 1H, H1'), 5.58 (dd,  $J$  = 6.4, 2.0 Hz, 1H, H2'), 5.50 – 5.29 (m, 4H, H21), 5.28 – 5.24 (m, 2H, H16'), 5.15 (dd,  $J$  = 6.4, 3.3 Hz, 1H, H3'), 4.81 (d,  $J$  = 10.5 Hz, 1H, H17a), 4.77 – 4.71 (m, 2H, H10a, H17b), 4.58 (d,  $J$  = 14.9 Hz, 1H, H10b), 4.53 – 4.46 (m, 2H, H9'), 4.36 (app. td,  $J$  = 6.3, 3.3 Hz, 1H, H4'), 3.80 – 3.71 (m, 3H, H5'a, H17'), 3.65 (dd,  $J$  = 10.1, 6.9 Hz, 1H, H5'b), 3.57 – 3.52 (m, 4H, H22), 3.51 – 3.47 (m, 2H, H18), 1.55 (s, 3H, H7'), 1.33 (s, 3H, H8'), 0.93 – 0.89 (m, 2H, H18'), 0.88 – 0.83 (m, 6H, H19, H23), -0.05 (s, 9H, H19'), -0.07 (s, 18H, H24), -0.08 (s, 9H, H20);  **$^{13}$ C NMR** (151 MHz,  $\text{CD}_3\text{CN}$ )  $\delta$  = 189.91 (C20'), 160.71 (C14'), 153.42 (C6), 153.11 (C8), 152.22 (C4), 150.83 (C2), 148.25 (C10'), 140.11 (C11), 132.62 (C14), 131.45 (C13), 131.38 (C12), 131.28 (C15), 129.39 (C16), 128.62 (C12'), 125.65 (C13'), 121.12 (C11'), 118.66 (C5), 114.85 (C15'), 114.55 (C6'), 93.93 (C16'), 90.74 (C1'), 87.15 (C4'), 83.73 (C2'), 83.56 (C17), 83.42 (C3'), 77.32 (2C, C21), 73.05 (C9'), 71.27 (C5'), 67.51 (C17'), 66.59 (C18), 65.60 (2C, C22), 53.47 (C10), 27.48 (C7'), 25.60 (C8'), 18.61 (2C, C23), 18.55 (C19), 18.48 (C18'), -1.33 (6C, C24), -1.36 (3C, C20), -1.41 (3C, C19'); **HRMS** (ESI+)  $m/z$  calculated for  $\text{C}_{52}\text{H}_{85}^{35}\text{Cl}_2\text{N}_6\text{O}_{10}\text{Si}_4$  (M+H)<sup>+</sup> 1135.4776, found 1135.4788. **IR** (thin layer film)  $\nu/\text{cm}^{-1}$  = 2870 (H–C=O), 1688 (C=O).

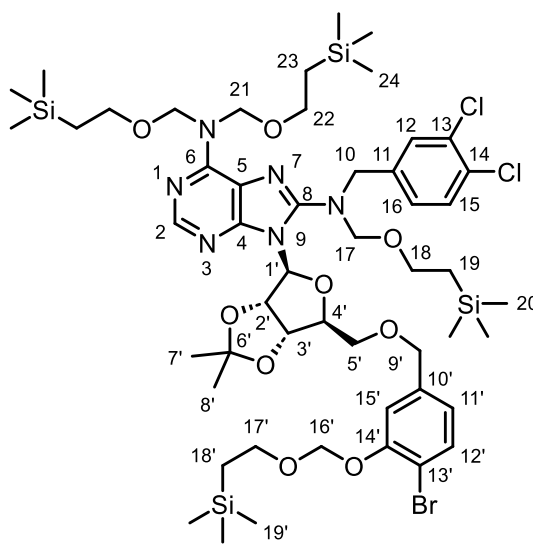
**4-((((2*R*,3*S*,4*R*,5*R*)-5-(6-amino-8-((3,4-dichlorobenzyl)amino)-9*H*-purin-9-yl)-3,4-dihydroxytetrahydrofuran-2-yl)methoxy)methyl)-2-hydroxybenzaldehyde (232)**



**232**

**232** was prepared following general procedure F, with 4-((((3*aR*,4*R*,6*R*,6*aR*)-6-(6-(bis((2-(trimethylsilyl)ethoxy)methyl)amino)-8-((3,4-dichlorobenzyl)((2-(trimethylsilyl)ethoxy)methyl)amino)-9*H*-purin-9-yl)-2,2-dimethyltetrahydrofuro[3,4-*d*][1,3]dioxol-4-yl)methoxy)methyl)-2-((2-(trimethylsilyl)ethoxy)methoxy)benzaldehyde **240** (200 mg, 0.17 mmol, 1 equiv.), and TFA:water 5:2 (v/v) mixture (1.71 mL, 0.1 M) for 1 hour. Purification by normal phase column chromatography on silica (100% CH<sub>2</sub>Cl<sub>2</sub> to 15:85 methanol:CH<sub>2</sub>Cl<sub>2</sub> gradient) then reverse phase column chromatography on C18 (acetonitrile:water +0.1% formic acid 5:95 to 50:50 gradient) yielded **232** (16 mg, 16%) as a pale yellow solid. <sup>1</sup>H NMR (600 MHz, DMSO-*d*<sub>6</sub>) δ = 10.73 (s br, 1H, H14'), 10.16 (s, 1H, H13'), 7.91 (s, 1H, H2), 7.54 (d, *J* = 8.0 Hz, 1H, H9'), 7.51 (d, *J* = 8.2 Hz, 1H, H17), 7.46 (d, *J* = 1.8 Hz, 1H, H14), 7.25 (dd, *J* = 8.2, 1.8 Hz, 1H, H18), 7.12 (t, *J* = 6.1 Hz, 1H, H11), 6.87 (app. s, 1H, H12'), 6.78 (app. d, *J* = 8.0 Hz, 1H, H8'), 6.49 (s br, 2H, H10), 5.88 (d, *J* = 6.1 Hz, 1H, H1'), 5.41 (d, *J* = 6.0 Hz, 1H, H15'), 5.24 (d, *J* = 5.0 Hz, 1H, H16'), 4.91 (app q, *J* = 5.8 Hz, 1H, H2'), 4.49 – 4.43 (m, 4H, H6', H12), 4.31 – 4.27 (m, 1H, H3'), 4.07 – 4.04 (m, 1H, H4'), 3.77 (dd, *J* = 10.7, 3.1 Hz, 1H, H5'a), 3.65 (dd, *J* = 10.7, 4.4 Hz, 1H, H5'b); <sup>13</sup>C NMR (151 MHz, DMSO-*d*<sub>6</sub>) δ = 191.24 (C13'), 160.75 (C11'), 152.55 (C6), 151.08 (C8), 149.97 (C4), 149.05 (C2), 147.03 (C7'), 141.03 (C13), 130.78 (C16), 130.30 (C17), 129.31 (C9'), 129.15 (C15), 128.79 (C14), 127.25 (C18), 121.37 (C10'), 117.88 (C12'), 116.82 (C5), 115.13 (C8'), 86.85 (C1'), 83.01 (C4'), 71.76 (C6'), 70.57 (C5'), 70.47 (C2'), 70.41 (C3'), 44.25 (C12). HRMS (ESI+) *m/z* calculated for C<sub>25</sub>H<sub>25</sub><sup>35</sup>Cl<sub>2</sub>N<sub>6</sub>O<sub>6</sub> (M+H)<sup>+</sup> 575.1207, found 575.1210; IR (thin layer film) ν/cm<sup>-1</sup> = 3344 (ArO–H), 2859 (H–C=O), 1652 (C=O).

**9-((3*aS*,4*S*,6*S*,6*aS*)-6-(((4-bromo-3-((2-(trimethylsilyl)ethoxy)methoxy)methyl)oxy)methyl)-2,2-dimethyltetrahydrofuro[3,4-*d*][1,3]dioxol-4-yl)-*N*8-(3,4-dichlorobenzyl)-*N*6,*N*6,*N*8-tris((2-(trimethylsilyl)ethoxy)methyl)-9*H*-purine-6,8-diamine (*ent*-241)**

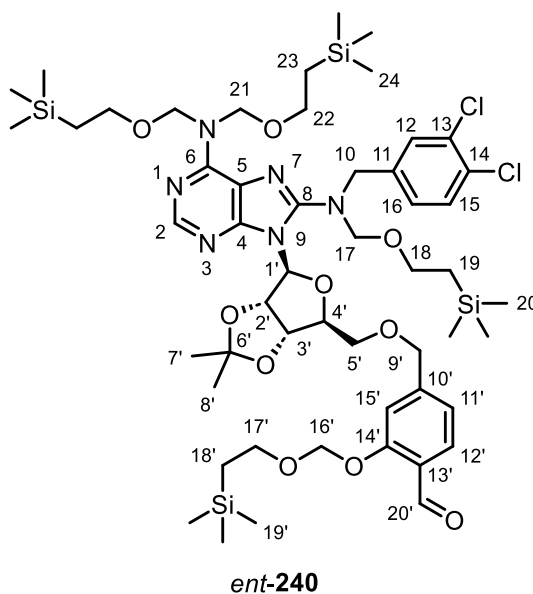


*ent*-241

*ent*-241 was prepared following a modification of general procedure D, with ((3*aS*,4*S*,6*S*,6*aS*)-6-(6-(bis((2-(trimethylsilyl)ethoxy)methyl)amino)-8-((3,4-dichlorobenzyl)((2-(trimethylsilyl)ethoxy)methyl)amino)-9*H*-purin-9-yl)-2,2-dimethyltetrahydrofuro[3,4-*d*][1,3]dioxol-4-yl)methanol *ent*-125 (300 mg, 0.34 mmol, 1 equiv.), THF (0.69 mL, 0.5 M), sodium hydride (16.5 mg, 60% in mineral oil, 0.41 mmol, 1.2 equiv.) and (2-((2-bromo-5-(bromomethyl)phenoxy)methoxy)ethyl)trimethylsilane 242 (204 mg, 0.52 mmol, 1.5 equiv.) as a solution in THF (0.35 mL). Purification by normal phase column chromatography on silica (EtOAc:cyclohexane 1:99 to 20:80 gradient) yielded *ent*-241 (376 mg, 92%) as a colourless oil. <sup>1</sup>H NMR (600 MHz, CD<sub>3</sub>CN) δ = 8.09 (s, 1H, H2), 7.57 (d, *J* = 2.0 Hz, 1H, H12), 7.44 – 7.39 (m, 2H, H12', H15), 7.31 (dd, *J* = 8.3, 2.0 Hz, 1H, H16), 7.09 (d, *J* = 1.8 Hz, 1H, H15'), 6.74 (dd, *J* = 8.1, 1.8 Hz, 1H, H11'), 6.09 (d, *J* = 2.0 Hz, 1H, H1'), 5.58 (dd, *J* = 6.3, 2.0 Hz, 1H, H2'), 5.50 – 5.29 (m, 4H, H21), 5.24 – 5.21 (m, 2H, H16'), 5.13 (dd, *J* = 6.3, 3.2 Hz, 1H, H3'), 4.81 (d, *J* = 10.4 Hz, 1H, H17a), 4.75 (d, *J* = 14.8 Hz, 1H, H10a), 4.72 (d, *J* = 10.4 Hz, 1H, H17b), 5.48 (d, *J* = 14.8 Hz, 1H, H10b), 4.43 – 4.37 (m, 2H, H9'), 4.33 (app. td, *J* = 6.4, 3.2 Hz, 1H, H4'), 3.78 – 3.74 (m, 2H, H17'), 3.70 (dd, *J* = 10.2, 6.1 Hz, 1H, H5'a), 3.60 (dd, *J* = 10.2, 6.7 Hz, 1H, H5'b), 3.58 – 3.54 (m, 4H, H22), 3.51 – 3.47 (m, 2H,

H18), 1.55 (s, 3H, H7'), 1.33 (s, 3H, H8'), 0.92 – 0.88 (m, 2H, H18'), 0.88 – 0.82 (m, 2H, H19, H23), -0.04 (s, 9H, H19'), -0.08 (s, 18H, H24), -0.09 (s, 9H, H20);  $^{13}\text{C}$  NMR (151 MHz,  $\text{CD}_3\text{CN}$ )  $\delta$  = 154.58 (C14'), 153.45 (C6), 153.13 (C8), 152.23 (C4), 150.86 (C2), 140.61 (C10'), 140.10 (C11), 133.82 (C12'), 132.61 (C14), 131.45 (C13), 131.39 (C12), 131.28 (C15), 129.40 (C16), 122.86 (C11'), 118.66 (C5), 116.18 (C15'), 114.52 (C6'), 112.02 (C13'), 94.22 (C16'), 90.72 (C1'), 87.17 (C4'), 83.74 (C2'), 83.53 (C17), 83.49 (C3'), 77.27 (2C, C21), 72.92 (C9'), 70.94 (C5'), 67.31 (C17'), 66.59 (C18), 65.60 (2C, C22), 53.45 (C10), 27.48 (C7'), 25.61 (C8'), 18.62 (2C, C23), 18.50 (C19), 18.48 (C18'), -1.32 (6C, C24), -1.36 (3C, C20), -1.39 (3C, C19'); HRMS (ESI+)  $m/z$  calculated for  $\text{C}_{51}\text{H}_{84}^{79}\text{Br}^{35}\text{Cl}_2\text{N}_6\text{O}_9\text{Si}_4$  (M+H) $^+$  1185.3932, found 1185.3931;

**4-(((3*aS*,4*S*,6*S*,6*aS*)-6-(6-(bis((2-(trimethylsilyl)ethoxy)methyl)amino)-8-((3,4-dichlorobenzyl)((2-(trimethylsilyl)ethoxy)methyl)amino)-9*H*-purin-9-yl)-2,2-dimethyltetrahydrofuro[3,4-*d*][1,3]dioxol-4-yl)methoxy)methyl)-2-((2-(trimethylsilyl)ethoxy)methoxy)benzaldehyde (*ent*-240)**

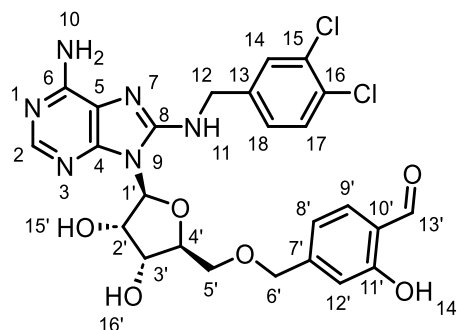


A two-neck round bottom flask heat-dried under vacuum and equipped with magnetic stirrer was charged with 9-((3*aS*,4*S*,6*S*,6*aS*)-6-(((4-bromo-3-((2-(trimethylsilyl)ethoxy)methoxy)benzyl)oxy)methyl)-2,2-dimethyltetrahydrofuro[3,4-*d*][1,3]dioxol-4-yl)-*N*8-(3,4-dichlorobenzyl)-*N*6,*N*6,*N*8-tris((2-(trimethylsilyl)ethoxy)methyl)-9*H*-purine-6,8-diamine *ent*-241 (152 mg, 0.13 mmol, 1 equiv.) and THF (0.51 mL, 0.5 M) under flow of nitrogen. The mixture was cooled to -78 °C and *n*-butyllithium (61  $\mu\text{L}$ , 2.5 M in hexanes, 0.15 mmol, 1.2 equiv.) was added

and stirred for 10 minutes. DMF (20  $\mu$ L, 0.26 mmol, 2 equiv.) was then added, after which the mixture was allowed to stir at -78  $^{\circ}$ C for 2 hours. The reaction mixture was quenched with methanol and the solvent was removed under reduced pressure, and the crude mixture was purified by normal phase column chromatography on silica (EtOAc:cyclohexane 1:99 to 20:80 gradient) to yield *ent*-**240** (63 mg, 43%) as a colourless oil. **<sup>1</sup>H NMR** (600 MHz, CD<sub>2</sub>Cl<sub>2</sub>)  $\delta$  = 10.43 – 10.41 (m, 1H, H20'), 8.18 (s, 1H, H2), 7.72 (d,  $J$  = 8.0 Hz, 1H, H12'), 7.53 (d,  $J$  = 2.0 Hz, 1H, H12), 7.38 (d,  $J$  = 8.3 Hz, 1H, H15), 7.26 (dd,  $J$  = 8.3, 2.0 Hz, 1H, H16), 7.16 (app. s, 1H, H15'), 6.98 (app. d,  $J$  = 8.0 Hz, 1H, H11'), 6.10 (d,  $J$  = 2.0 Hz, 1H, H1'), 5.58 (dd,  $J$  = 6.4, 2.0 Hz, 1H, H2'), 5.53 – 5.33 (m, 4H, H21), 5.32 – 5.29 (m, 2H, H16')\*, 5.19 (dd,  $J$  = 6.4, 3.3 Hz, 1H, H3'), 4.76 – 4.71 (m, 2H, H10a, H17a), 4.67 (d,  $J$  = 10.2 Hz, 1H, H17b), 4.58 (d,  $J$  = 14.8 Hz, 1H, H10b), 4.51 (s, 2H, H9'), 4.39 (app. td,  $J$  = 6.4, 3.3 Hz, 1H, H4'), 3.82 – 3.76 (m, 3H, H5'a, H17'), 3.69 (dd,  $J$  = 10.1, 6.7 Hz, 1H, H5'b), 3.61 – 3.56 (m, 4H, H22), 3.53 – 3.49 (m, 2H, H18), 1.57 (s, 3H, H7'), 1.35 (s, 3H, H8'), 0.97 – 0.93 (m, 2H, H17'), 0.93 – 0.88 (m, 6H, H19, H23), -0.01 (s, 9H, H19'), -0.03 – -0.04 (s, 27H, H20, H24); **<sup>13</sup>C NMR** (151 MHz, CD<sub>2</sub>Cl<sub>2</sub>)  $\delta$  = 189.51 (C20'), 160.36 (C14'), 153.00 (C6), 152.40 (C8), 151.70 (C4), 150.57 (C2), 147.44 (C10'), 138.65 (C11), 132.65 (C14), 131.57 (C13), 130.99 (C12), 130.74 (C15), 128.58 (C16), 128.36 (C12'), 125.12 (C13'), 120.54 (C11'), 118.21 (C5), 114.20 (C6'), 113.96 (C15'), 93.52 (C16'), 90.27 (C1'), 86.74 (C4'), 83.51 (C2'), 83.18 (C3'), 82.48 (C17), 76.80 (2C, C21), 73.07 (C9'), 71.27 (C5'), 67.34 (C17'), 66.33 (C18), 65.40 (2C, C22), 52.88 (C10), 27.39 (C7'), 25.56 (C8'), 18.47 (2C, C23), 18.36 (C19), 18.32 (C18'), -1.30 (6C, C24), -1.34 (C20), -1.38 (C19'); **HRMS** (ESI+)  $m/z$  calculated for C<sub>52</sub>H<sub>85</sub><sup>35</sup>Cl<sub>2</sub>N<sub>6</sub>O<sub>10</sub>Si<sub>4</sub> (M+H)<sup>+</sup> 1135.4776, found 1135.4774.

\*Peak overlaps with solvent signal.

**4-((((2*S*,3*R*,4*S*,5*S*)-5-(6-amino-8-((3,4-dichlorobenzyl)amino)-9*H*-purin-9-yl)-3,4-dihydroxytetrahydrofuran-2-yl)methoxy)methyl)-2-hydroxybenzaldehyde (*ent*-232)**

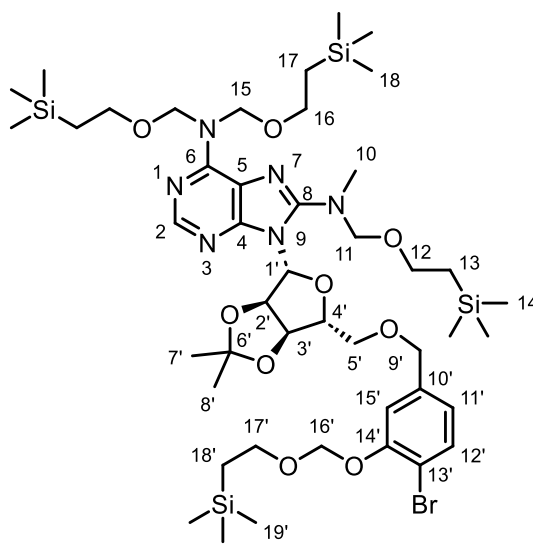


*ent*-232

*ent*-232 was prepared following general procedure F, with 4-((((3*aS*,4*S*,6*S*,6*aS*)-6-(6-(bis((2-(trimethylsilyl)ethoxy)methyl)amino)-8-((3,4-dichlorobenzyl)((2-(trimethylsilyl)ethoxy)methyl)amino)-9*H*-purin-9-yl)-2,2-dimethyltetrahydrofuro[3,4-*d*][1,3]dioxol-4-yl)methoxy)methyl)-2-((2-(trimethylsilyl)ethoxy)methoxy)benzaldehyde *ent*-240 (63.0 mg, 0.05 mmol, 1 equiv.), and TFA:water 5:2 (v/v) mixture (0.54 mL, 0.1 M) for 3 hours. Purification by reverse phase column chromatography on C18 (acetonitrile:water +0.1% formic acid 5:95 to 50:50 gradient) yielded *ent*-232 (14 mg, 45 %) as a pale yellow solid. <sup>1</sup>H NMR (600 MHz, DMSO-*d*<sub>6</sub>) δ = 10.71 (s, 1H, H14'), 10.16 (s, 1H, H13'), 7.91 (s, 1H, H2), 7.54 (d, *J* = 8.0 Hz, 1H, H9'), 7.51 (d, *J* = 8.30 Hz, 1H, H17), 7.46 (d, *J* = 1.8 Hz, 1H, H14), 7.25 (dd, *J* = 8.3, 1.8 Hz, 1H, H18), 7.12 (t, *J* = 6.0 Hz, 1H, H11), 6.87 (app. s, 1H, H12'), 6.78 (app. d, *J* = 8.0 Hz, 1H, H8'), 6.49 (s br, 2H, H10), 5.88 (d, *J* = 6.0 Hz, 1H, H1'), 5.40 (d, *J* = 6.0 Hz, 1H, H15'), 5.24 (d, *J* = 5.1 Hz, 1H, H16'), 4.91 (app. q, *J* = 5.9 Hz, 1H, H2'), 4.49 – 4.43 (m, 4H, H6', H12), 4.31 – 4.27 (m, 1H, H3'), 4.06 (m, 1H, H4'), 3.77 (dd, *J* = 10.8, 3.0 Hz, 1H, H5'a), 3.65 (dd, *J* = 10.8, 4.4 Hz, 1H, H5'b); <sup>13</sup>C NMR (151 MHz, DMSO-*d*<sub>6</sub>) δ = 191.25 (C13'), 160.72 (C11'), 152.54 (C6), 151.08 (C8), 149.96 (C4), 149.03 (C2), 147.04 (C7'), 141.03 (C13), 130.78 (C16), 130.30 (C17), 129.32 (C9'), 129.15 (C15), 128.79 (C14), 127.25 (C18), 121.37 (C10'), 117.89 (C8'), 116.83 (C5), 115.12 (C12'), 86.86 (C1'), 83.00 (C4'), 71.76 (C6'), 70.57 (C5'), 70.46 (C2'), 70.41 (C3'), 44.25 (C12); HRMS (ESI+) *m/z* calculated for C<sub>25</sub>H<sub>25</sub><sup>35</sup>Cl<sub>2</sub>N<sub>6</sub>O<sub>6</sub> (M+H)<sup>+</sup> 575.1207, found 575.1217.



**9-((3*aR*,4*R*,6*R*,6*aR*)-6-(((4-bromo-3-((2-(trimethylsilyl)ethoxy)methoxy)benzyl)oxy)methyl)-2,2-dimethyltetrahydrofuro[3,4-*d*][1,3]dioxol-4-yl)-*N*8-methyl-*N*6,*N*6,*N*8-tris((2-(trimethylsilyl)ethoxy)methyl)-9*H*-purine-6,8-diamine (**247**)**

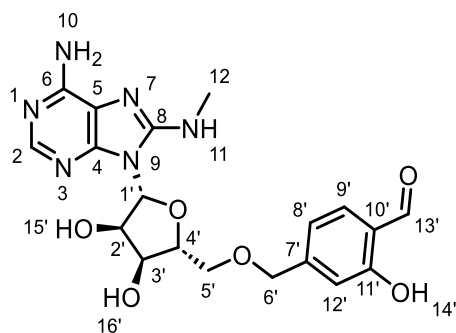


**247**

**247** was prepared following a modification of general procedure D, with ((3*aR*,4*R*,6*R*,6*aR*)-6-(6-(bis((2-(trimethylsilyl)ethoxy)methyl)amino)-8-((3,4-dichlorobenzyl)(methyl)amino)-9*H*-purin-9-yl)-2,2-dimethyltetrahydrofuro[3,4-*d*][1,3]dioxol-4-yl)methanol **188** (300 mg, 0.41 mmol, 1 equiv.), THF (0.83 mL, 0.5 M), sodium hydride (18.9 mg, 60% in mineral oil, 0.50 mmol, 1.2 equiv.) and (2-((2-bromo-5-(bromomethyl)phenoxy)methoxy)ethyl)trimethylsilane **242** (327 mg, 0.83 mmol, 2 equiv.) as a solution in THF (0.41 mL). Purification by normal phase column chromatography on silica (EtOAc:cyclohexane 1:99 to 20:80 gradient) yielded **247** (357 mg, 83%) as a colourless oil. **<sup>1</sup>H NMR** (600 MHz, CD<sub>3</sub>CN) δ = 8.08 (s, 1H, H2), 7.43 (d, *J* = 8.2 Hz, 1H, H12'), 7.09 (app. s, 1H, H15'), 6.76 (app. d, *J* = 8.2, 1H, H11'), 5.99 (app. s, 1H, H1'), 5.55 (app. d, *J* = 6.5 Hz, 1H, H2'), 5.54 – 5.31 (m, 4H, H15), 5.25 – 5.21 (m, 2H, H16'), 5.14 (dd, *J* = 6.5, 3.1 Hz, 1H, H3'), 4.79 (d, *J* = 10.3 Hz, 1H, H11a), 4.71 (d, *J* = 10.3 Hz, 1H, H11b), 4.41 (s, 2H, H9'), 4.34 – 4.30 (m, 1H, H4'), 3.79 – 3.71 (m, 3H, H5'a, H17'), 3.63 – 3.58 (m, 5H, H5'b, H16), 3.52 – 3.48 (m, 2H, H12), 3.07 (s, 3H, H10), 1.54 (s, 3H, H7'), 1.32 (s, 3H, H8'), 0.93 – 0.83 (m, 6H, H13, H17, H18'), -0.04 (s, 9H, H19'), -0.06 (s, 18H, H18), -0.08 (s, 9H, H14); **<sup>13</sup>C NMR** (151 MHz, CD<sub>3</sub>CN) δ = 154.58 (C14'), 154.37 (C8), 153.27 (C6), 152.32 (C4), 150.52 (C2), 140.63 (C10'),

133.83 (C12'), 122.87 (C11'), 118.83 (C5), 116.18 (C15'), 114.43 (C6'), 112.00 (C13'), 94.22 (C16'), 90.90 (C1'), 87.26 (C4'), 84.70 (C11), 83.94 (C2'), 83.57 (C3'), 77.28 (2C, C15), 72.92 (C9'), 70.98 (C5'), 67.31 (C17'), 66.40 (C12), 65.46 (2C, C16), 38.47 (C10), 27.40 (C7'), 25.57 (C8'), 18.62 (2C, C17), 18.49 (C13), 18.46 (C18'), -1.34 (6C, C18), -1.37 (3C, C14), -1.40 (3C, C19'); **HRMS** (ESI+) *m/z* calculated for C<sub>45</sub>H<sub>82</sub><sup>79</sup>BrN<sub>6</sub>O<sub>9</sub>Si<sub>4</sub> (M+H)<sup>+</sup> 1041.4398, found 1041.4417.

**4-(((2*R*,3*S*,4*R*,5*R*)-5-(6-amino-8-(methylamino)-9*H*-purin-9-yl)-3,4-dihydroxytetrahydrofuran-2-yl)methoxy)methyl)-2-hydroxybenzaldehyde (**246**)**



**246**

A two-neck round bottom flask heat-dried under vacuum and equipped with magnetic stirrer was charged with 9-((3*aR*,4*R*,6*R*,6*aR*)-6-(((4-bromo-3-((2-(trimethylsilyl)ethoxy)methoxy)benzyl)oxy)methyl)-2,2-dimethyltetrahydrofuro[3,4-*d*][1,3]dioxol-4-yl)-*N*8-methyl-*N*6,*N*6,*N*8-tris((2-(trimethylsilyl)ethoxy)methyl)-9*H*-purine-6,8-diamine **247** (200 mg, 0.19 mmol, 1 equiv.) and THF (0.61 mL, 0.5 M) under flow of nitrogen. The mixture was cooled to -78 °C and *n*-butyllithium (0.15 mL, 2.5 M in hexanes, 0.38 mmol, 2 equiv.) was added and stirred for 1 hour. DMF (30 μL, 0.38 mmol, 2 equiv.) was then added, after which the mixture was allowed to warm up to room temperature. The reaction mixture was quenched with methanol and the solvent was removed under reduced pressure, and the crude mixture was eluted through a silica plug (EtOAc:cyclohexane 10:90), concentrated under reduced pressure and the crude residue was redissolved in TFA:water 5:2 (v/v) mixture (0.92 mL). After stirring at room temperature for 1 hour, the mixture was diluted with toluene (15 mL) and concentrated under reduced pressure. The crude product was purified by normal phase column chromatography on silica (100% CH<sub>2</sub>Cl<sub>2</sub> to methanol:CH<sub>2</sub>Cl<sub>2</sub> 15:85 gradient) then reverse phase column chromatography on C18 (methanol:water +0.1% formic acid 20:80 to 80:20 gradient) to yield **246** (5.6 mg, 7%) as an orange solid. <sup>1</sup>H NMR (600 MHz,

DMSO- $d_6$ )  $\delta$  = 10.81 (s br, 1H, H14'), 10.22 (s, 1H, H13'), 7.89 (s, 1H, H2), 7.63 (d,  $J$  = 8.0 Hz, 1H, H9'), 6.95 (app. s, 1H, H12'), 6.87 (app. d,  $J$  = 8.0 Hz, 1H, H8'), 6.50 – 6.45 (m, 3H, H10, H11), 5.80 (d,  $J$  = 6.0 Hz, 1H, H1'), 5.33 (d,  $J$  = 5.8 Hz, 1H, H15'), 5.21 (d,  $J$  = 4.7 Hz, 1H, H16'), 4.83 (app. q,  $J$  = 5.5 Hz, 1H, H2'), 4.60 – 4.54 (m, 2H, H6'), 4.27 (app. q,  $J$  = 4.3 Hz, 1H, H3'), 4.04 – 4.01 (m, 1H, H4'), 3.77 (dd,  $J$  = 10.7, 3.0 Hz, 1H, H5'a), 3.64 (dd,  $J$  = 10.7, 4.4 Hz, 1H, H5'b), 2.77 (d,  $J$  = 4.7 Hz, 3H, H12);  $^{13}\text{C}$  NMR (151 MHz, DMSO- $d_6$ )  $\delta$  = 191.24 (C13'), 160.98 (C11'), 152.45 (C6), 152.05 (C8), 149.96 (C4), 148.79 (C2), 147.23 (C7'), 129.29 (C9'), 121.52 (C10'), 117.96 (C8'), 117.08 (C5), 115.31 (C12'), 86.81 (C1'), 82.84 (C4'), 71.85 (C6'), 70.51 (C5'), 70.43 (C2'), 70.28 (C3'), 29.08 (C12); HRMS (ESI+)  $m/z$  calculated for  $\text{C}_{19}\text{H}_{23}\text{N}_6\text{O}_6$  (M+H) $^+$  431.1674, found 431.1666.

## Chapter 7

The standard indole and pyrazole numbering has been used throughout this thesis and experimental section for analogues of indole and pyrazole (Figure 8.2).

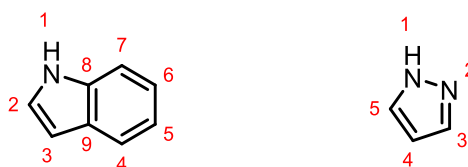


**Figure 8.2** Standard numbering of indole and pyrazole.

### General procedure G — synthesis of aromatic amides

A glass vial equipped with magnetic stirrer was charged with the corresponding aniline (1 equiv.) and  $\text{CH}_2\text{Cl}_2$  (0.5 M). The mixture was cooled to 0 °C and triethylamine (1.1 equiv.) was added, followed by dropwise addition of the corresponding acyl chloride (1 – 1.1 equiv.) after which the mixture was allowed to warm up to room temperature. After stirring at room temperature for 3 – 70 hours, the reaction mixture was diluted with sat.  $\text{NaHCO}_3$  solution (20 mL) and  $\text{CH}_2\text{Cl}_2$  (20 mL) and the phases were separated. The organic phase was washed with sat.  $\text{NaHCO}_3$  solution ( $\times 3$ ), brine ( $\times 3$ ), dried over  $\text{MgSO}_4$ , filtered and concentrated under reduced pressure to yield the desired products.

**General procedure H — *N*-Boc deprotection of anilines**

A glass microwave vial heat-dried under vacuum and equipped with magnetic stirrer was charged with the corresponding *N*-Boc-protected aniline (1 equiv.), CH<sub>2</sub>Cl<sub>2</sub> (0.3 M), and lithium iodide (2.4 equiv.) under flow of nitrogen, after which chlorotrimethylsilane (2.4 equiv.) was added and the mixture was heated to 50 °C. After stirring at 50 °C for 3 hours, the reaction mixture was diluted with CH<sub>2</sub>Cl<sub>2</sub> and water and the phases were separated. The aqueous phase was washed with CH<sub>2</sub>Cl<sub>2</sub> (×3) and then neutralised to pH 8 with sat. NaHCO<sub>3</sub> solution. After washing the aqueous phase with further CH<sub>2</sub>Cl<sub>2</sub> (×4), the resultant combined organic layers were dried over MgSO<sub>4</sub>, filtered and concentrated under reduced pressure to yield the desired products.

**General procedure I — S<sub>N</sub>Ar of 2-chloropyrimidine and anilines**

A glass vial equipped with magnetic stirrer was charged with the corresponding 2-chloropyrimidine (1 equiv.), *tert*-butanol (0.1 M), the corresponding aniline (1 equiv.), and *p*-toluenesulfonic acid monohydrate (1 equiv.) and heated to 100 °C. After stirring at 100 °C for 18 – 72 hours, the solvent was removed under reduced pressure and the crude mixture was purified by flash column chromatography to yield the desired products.

**General procedure J — synthesis of fluorosulfonates from AISF and phenol**

Adapted from a procedure developed by Zhou and coworkers.<sup>280</sup>

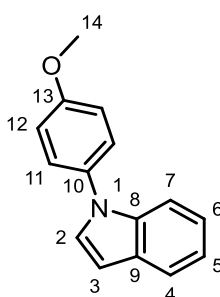
A glass vial equipped with magnetic stirrer was charged with corresponding phenol (1 equiv.), [4-(acetylamino)phenyl]imidodisulfuryl difluoride (1.2 equiv.) and THF:DMSO 5:1 (v/v) mixture (0.1 M). 1,8-Diazabicyclo[5.4.0]undec-7-ene (2.2 equiv.) was then added dropwise. After stirring at room temperature for 1 – 24 hours, the solvent was removed under reduced pressure and the crude mixture was purified by flash column chromatography to yield the desired products.

**General procedure K — palladium catalysed synthesis of sulfonyl fluorides from aryl bromides under microwave irradiation**

Adapted from a procedure developed by Davies and coworkers.<sup>164</sup>

A glass microwave vial equipped with magnetic stirrer was charged with the corresponding aryl bromide (1 equiv.), DABSO (0.6 equiv.), PdCl<sub>2</sub>(AmPhos)<sub>2</sub> (5 mol%), and degassed and backfilled with argon four times. Isopropanol (0.25 – 0.27 M) was added to the mixture, which was then degassed and backfilled with argon four times, after which triethylamine (3 equiv.) was added and the mixture was heated to 110 °C under microwave irradiation. After stirring at 110 °C for 1 hour, the reaction mixture was cooled to room temperature and NFSI (1.5 - 3 equiv.) was added and the reaction mixture was stirred for a further 5 hours. The solvent was removed under reduced pressure, and the crude mixture was purified by flash column chromatography to yield the desired products.

### 1-(4-methoxyphenyl)-1*H*-indole (**274**)



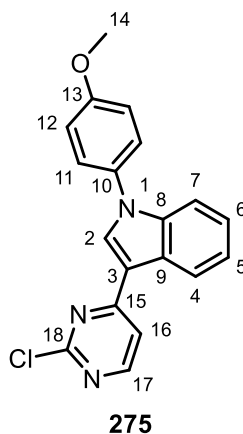
**274**

A two-neck round bottom flask equipped with magnetic stirrer and reflux condenser was charged with indole-2-carboxylic acid **273** (5.00 g, 31.0 mmol, 1 equiv.), NMP (155 mL, 0.2 M), 4-iodoanisole (7.26 g, 31.0 mmol, 1 equiv.), K<sub>3</sub>PO<sub>4</sub> (13.1 g, 62.1 mmol, 2 equiv.), and copper (I) oxide (444 mg, 3.10 mmol, 0.1 equiv.) under flow of nitrogen and heated to 160 °C. After stirring at 160 °C for 5 days, the reaction mixture was diluted with water (500 mL) and EtOAc (400 mL) and the phases were separated. The aqueous phase was extracted with EtOAc (3 × 150 mL) and the resultant combined organic layers were washed with brine (3 × 250 mL), dried over MgSO<sub>4</sub>, filtered, and concentrated under reduced pressure. The crude product was purified by normal phase column chromatography on silica (100% cyclohexane to EtOAc:cyclohexane 5:95 gradient) to yield **274** (6.17 g, 89%) as a white solid. <sup>1</sup>H NMR (500 MHz, CDCl<sub>3</sub>) δ = 7.70 – 7.67 (m, 1H, H4), 7.47 – 7.44 (m, 1H, H7), 7.43 – 7.37 (m, 2H, H11), 7.28 (d, *J* = 3.2 Hz, 1H, H2), 7.22 – 7.18 (m, 1H, H6), 7.17 – 7.13 (m, 1H, H5), 7.06 – 7.01 (m, 2H, H12), 6.66 (dd, *J* = 3.2, 0.9 Hz, 1H, H3), 3.88 (s, 3H, H14); <sup>13</sup>C NMR (126 MHz, CDCl<sub>3</sub>) δ = 158.37 (C13), 136.45 (C8), 132.97 (C10), 129.07 (C9), 128.43 (C2), 126.13 (2C, C11), 122.27 (C6),

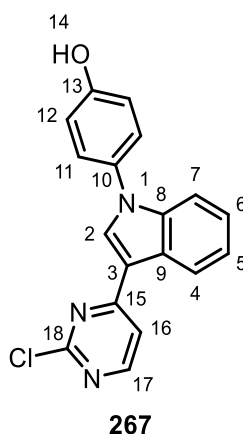
121.14 (C4), 120.20 (C5), 114.86 (2C, C12), 110.50 (C7), 103.01 (C3), 55.75 (C14); **HRMS** (ESI+)  $m/z$  calculated for  $C_{15}H_{14}NO$  (M+H)<sup>+</sup> 224.1070, found 224.1074.

The spectroscopic and analytical data were in agreement with literature values.<sup>296</sup>

### 3-(2-chloropyrimidin-4-yl)-1-(4-methoxyphenyl)-1*H*-indole (275)

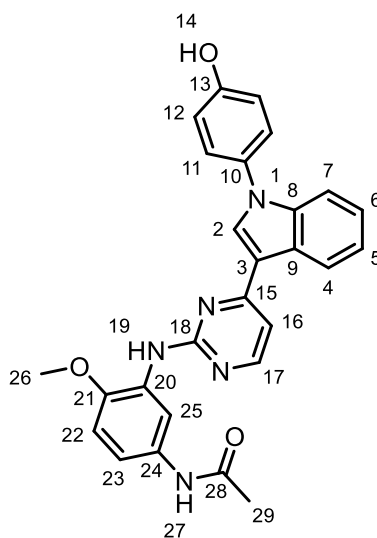


A two-neck round bottom flask heat-dried under vacuum and equipped with magnetic stirrer and reflux condenser was charged with 1-(4-methoxyphenyl)-1*H*-indole **274** (5.87 g, 26.3 mmol, 1 equiv.), anhydrous DME (52.6 mL, 0.5 M), 2,4-dichloropyrimidine (3.92 g, 26.3 mmol, 1 equiv.), iron (III) chloride (4.26 g, 26.3 mmol, 1 equiv.) under flow of nitrogen and heated to 60 °C. After stirring at 60 °C for 20 hours, 1:1  $CH_2Cl_2$ :methanol (100 mL) was added to the crude mixture which was filtered through celite. The filtrate was concentrated under reduced pressure and the crude product was purified by normal phase column chromatography on silica (100%  $CH_2Cl_2$  to 20:80 methanol: $CH_2Cl_2$  gradient) to yield **275** (5.98 g, 68%) as a light brown solid. **<sup>1</sup>H NMR** (500 MHz,  $DMSO-d_6$ )  $\delta$  = 8.75 (s, 1H, H2), 8.59 (d,  $J$  = 5.4 Hz, 1H, H17), 8.58 – 8.55 (m, 1H, H4), 8.01 (d,  $J$  = 5.4 Hz, 1H, H16), 7.62 – 7.56 (m, 2H, H11), 7.48 – 7.44 (m, 1H, H7), 7.37 – 7.30 (m, 2H, H5, H6), 7.20 – 7.16 (m, 2H, H12), 3.86 (s, 3H, H14); **<sup>13</sup>C NMR** (126 MHz,  $DMSO-d_6$ )  $\delta$  = 164.55 (C15), 160.31 (C18), 158.87 (C17), 158.75 (C13), 137.19 (C8), 133.72 (C2), 130.70 (C10), 126.25 (2C, C11), 125.68 (C9), 123.69 (C6), 122.33 (C5), 122.20 (C4), 115.03 (3C, C12, C16), 112.71 (C3), 111.13 (C7), 55.58 (C14); **HRMS** (ESI+)  $m/z$  calculated for  $C_{19}H_{15}^{35}ClN_3O$  (M+H)<sup>+</sup> 336.0898, found 336.0902.

**4-(3-(2-chloropyrimidin-4-yl)-1H-indol-1-yl)phenol (267)**

A two-neck round bottom flask heat-dried under vacuum and equipped with magnetic stirrer was charged with 3-(2-chloropyrimidin-4-yl)-1-(4-methoxyphenyl)-1*H*-indole **275** (5.53 g, 16.5 mmol, 1 equiv.) and anhydrous CH<sub>2</sub>Cl<sub>2</sub> (82.3 mL, 0.2 M) under flow of nitrogen. The mixture was cooled to -78 °C and boron tribromide (35.9 mL, 1 M in CH<sub>2</sub>Cl<sub>2</sub>, 35.9 mmol, 2.2 equiv.) was added slowly after which the mixture was allowed to warm up to room temperature. After stirring at room temperature for 18 hours, the reaction mixture was quenched by pouring over ice, and the resulting precipitate was filtered and purified by normal phase column chromatography on silica (100% CH<sub>2</sub>Cl<sub>2</sub> to 20:80 ethanol:CH<sub>2</sub>Cl<sub>2</sub> gradient) to yield **267** (1.63 g, 31%) as a light brown solid. **<sup>1</sup>H NMR** (500 MHz, DMSO-*d*<sub>6</sub>) δ = 9.90 (s, 1H, H14), 8.72 (s, 1H, H2), 8.58 (d, *J* = 5.5 Hz, 1H, H17), 8.57 – 8.54 (m, 1H, H4), 8.01 (d, *J* = 5.5 Hz, 1H, H16), 7.48 – 7.43 (m, 3H, H7, H11), 7.37 – 7.27 (m, 2H, H5, H6), 7.01 – 6.97 (m, 2H, H12); **<sup>13</sup>C NMR** (126 MHz, DMSO-*d*<sub>6</sub>) δ = 164.59 (C15), 160.29 (C18), 158.82 (C17), 157.19 (C13), 137.30 (C8), 133.78 (C2), 129.22 (C10), 126.32 (2C, C11), 125.60 (C9), 123.58 (C5), 122.24 (C6), 122.14 (C4), 116.21 (2C, C12), 114.98 (C3), 112.47 (C16), 111.18 (C7); **HRMS** (ESI+) *m/z* calculated for C<sub>18</sub>H<sub>13</sub><sup>35</sup>ClN<sub>3</sub>O (M+H)<sup>+</sup> 322.0742, found 322.0754.

***N*-3-((4-(1-(4-hydroxyphenyl)-1*H*-indol-3-yl)pyrimidin-2-yl)amino)-4-methoxyphenyl)acetamide (**277**)**

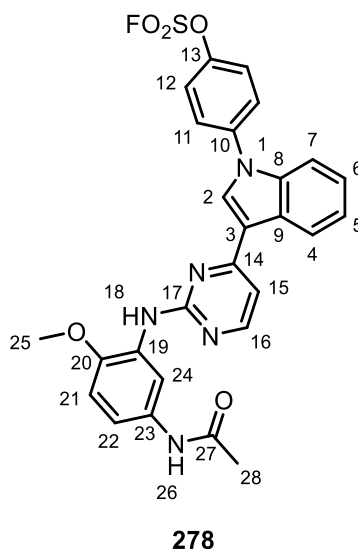


**277**

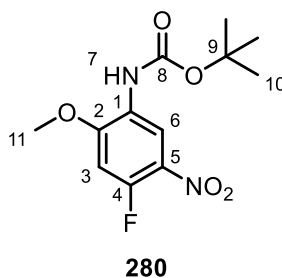
A two-neck round bottom equipped with magnetic stirrer was charged with 4-(3-(2-chloropyrimidin-4-yl)-1*H*-indol-1-yl)phenol **267** (120 mg, 0.37 mmol, 1 equiv.), isobutanol (3.7 mL, 0.1 M), *N*-(3-amino-4-methoxyphenyl)acetamide **276** (67.2 mg, 0.37 mmol, 1 equiv.), and *p*-toluenesulfonic acid monohydrate (70.9 mg, 0.37 mmol, 1 equiv.) under flow of nitrogen and heated to 60 °C. After stirring at 60 °C for 6 days, the solvent was removed under reduced pressure and the crude mixture was purified by normal phase column chromatography on silica (100% CH<sub>2</sub>Cl<sub>2</sub> to 10:90 methanol:CH<sub>2</sub>Cl<sub>2</sub> gradient) then reverse phase column chromatography on C18 (methanol:water +0.1% formic acid 20:80 to 80:20 gradient) to yield **277** (35 mg, 20%) as a pale yellow solid. **<sup>1</sup>H NMR** (600 MHz, DMSO-*d*<sub>6</sub>) δ = 9.84 (s br, 1H, H14) 9.79 (s, 1H, H27), 8.58 (s, 1H, H2), 8.50 – 8.45 (m, 2H, H4, H25), 8.37 (d, *J* = 5.3 Hz, 1H, H17), 8.01 (s, 1H, H19), 7.49 – 7.44 (m, 2H, H11), 7.42 (d, *J* = 8.3 Hz, 1H, H7), 7.38 (d, *J* = 5.3 Hz, 1H, H16), 7.28 – 7.23 (m, 2H, H6, H23), 7.22 – 7.17 (m, 1H, H5), 7.01 – 6.95 (m, 3H, H12, H22), 3.84 (s, 3H, H26), 1.98 (s, 3H, H29); **<sup>13</sup>C NMR** (126 MHz, DMSO-*d*<sub>6</sub>) δ = 167.67 (C28), 161.89 (C15), 159.96 (C18), 157.37 (C17), 156.87 (C13), 145.43 (C21), 137.12 (C8), 132.26 (C24), 132.18 (C2), 129.58 (C10), 128.60 (C20), 126.27 (2C, C11), 125.81 (C9), 122.94 (C6), 122.39 (C4), 121.41 (C5), 116.10 (2C, C12), 114.17 (C3), 113.72 (C23), 113.33 (C25), 110.79 (C7), 110.66 (C22), 107.92 (C16), 55.92 (C26), 23.76 (C29); **HRMS** (ESI+) *m/z* calculated for C<sub>27</sub>H<sub>24</sub>N<sub>5</sub>O<sub>3</sub> (M+H)<sup>+</sup> 466.1874, found 466.1874.



**4-(3-(2-((5-acetamido-2-methoxyphenyl)amino)pyrimidin-4-yl)-1H-indol-1-yl)phenyl sulfurofluoridate (278)**



**278** was prepared following general procedure J, with *N*-(3-((4-(1-(4-hydroxyphenyl)-1H-indol-3-yl)pyrimidin-2-yl)amino)-4-methoxyphenyl)acetamide **277** (21.0 mg, 0.05 mmol, 1 equiv.), THF:DMSO 5:1 (v/v) mixture (0.48 mL, 0.1 M), [4-(acetylamino)phenyl]imidodisulfuryl difluoride (17.0 mg, 0.05 mmol, 1.2 equiv.) and 1,8-Diazabicyclo[5.4.0]undec-7-ene (15  $\mu$ L, 0.10 mmol, 2.2 equiv.) for 1 hour. Purification by reverse phase column chromatography on C18 (methanol:water +0.1% formic acid 20:80 to 80:20 gradient) then normal phase column chromatography on silica (100% CH<sub>2</sub>Cl<sub>2</sub> to methanol:CH<sub>2</sub>Cl<sub>2</sub> 10:90 gradient) yielded **278** (9.0 mg, 38%) as a white solid. <sup>1</sup>H NMR (600 MHz, DMSO-d<sub>6</sub>)  $\delta$  = 9.80 (s, 1H, H26), 8.81 (s, 1H, H2), 8.56 – 8.53 (m, 1H, H24), 8.50 (d, *J* = 8.0 Hz, 1H, H4), 8.42 (d, *J* = 5.3 Hz, 1H, H16), 8.07 (s, 1H, H18), 7.98 – 7.94 (m, 2H, H11), 7.91 – 7.87 (m, 2H, H12), 7.62 (d, *J* = 8.3 Hz, 1H, H7), 7.41 (d, *J* = 5.3 Hz, 1H, H15), 7.35 – 7.31 (m, 1H, H6), 7.28 – 7.24 (m, 1H, H5), 7.21 (dd, *J* = 8.8, 2.4 Hz, 1H, H22), 7.00 (d, *J* = 8.8 Hz, 1H, H21), 3.85 (s, 3H, H25), 1.96 (s, 3H, H28); <sup>13</sup>C NMR (151 MHz, DMSO-d<sub>6</sub>)  $\delta$  = 167.71 (C27), 161.44 (C14), 159.96 (C17), 157.75 (C16), 147.89 (C13), 145.38 (C20), 138.60 (C10), 136.41 (C8), 132.31 (C23), 131.84 (C2), 128.52 (C19), 126.82 (2C, C11), 126.28 (C9), 123.55 (C6), 122.82 (2C, C12), 122.48 (C4), 122.05 (C5), 115.64 (C3), 113.63 (C22), 113.14 (C24), 110.82 (C7), 110.70 (C21), 108.12 (C15), 55.93 (C25), 23.74 (C28); <sup>19</sup>F NMR (471 MHz, DMSO-d<sub>6</sub>)  $\delta$  = 38.74; HRMS (ESI+) *m/z* calculated for C<sub>27</sub>H<sub>23</sub>FN<sub>5</sub>O<sub>5</sub>S (M+H)<sup>+</sup> 548.1398, found 548.1382.

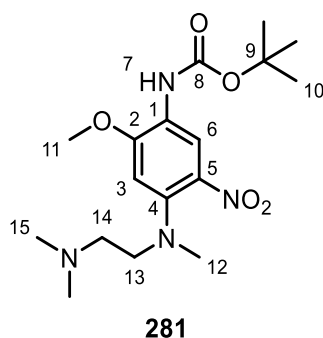
***tert*-butyl(4-fluoro-2-methoxy-5-nitrophenyl)carbamate (280)**

A two-neck round bottom flask equipped with magnetic stirrer was charged with 4-fluoro-2-methoxy-5-nitroaniline **279** (2.00 g, 10.7 mmol, 1 equiv.) and CH<sub>2</sub>Cl<sub>2</sub> (25.0 mL, 0.43 M) under flow of nitrogen. The mixture was cooled to 0 °C and 4-dimethylaminopyridine (131 mg, 1.07 mmol, 0.1 equiv.) was added to the mixture, followed by dropwise addition of di-*tert*-butyl dicarbonate (2.81 g, 12.9 mmol, 1.2 equiv.) as a solution in CH<sub>2</sub>Cl<sub>2</sub> (7.5 mL) after which the mixture was allowed to warm up to room temperature. After stirring at room temperature for 18 hours, the solvent was removed under reduced pressure and the crude mixture was purified by normal phase column chromatography on silica (EtOAc:cyclohexane 5:95 to 20:80 gradient) to yield **280** (1.98 g, 64%) as a pale-yellow solid. <sup>1</sup>H NMR (600 MHz, CDCl<sub>3</sub>) δ = 8.88 (s br, 1H, H6), 6.96 (s br, 1H, H7), 6.71 (d, *J* = 12.0 Hz, 1H, H3), 3.97 (s, 3H, H11), 1.53 (s, 9H, H10); <sup>13</sup>C NMR (151 MHz, CDCl<sub>3</sub>) δ = 152.70 (d, *J*<sub>C-F</sub> = 9.2 Hz, C2), 152.35 (d, *J*<sub>C-F</sub> = 262.1 Hz, C4), 152.30 (C8), 130.20 (C5)\*, 124.82 (d, *J*<sub>C-F</sub> = 3.1 Hz, C1), 114.80 (C6)\*, 99.95 (d, *J*<sub>C-F</sub> = 26.3 Hz, C3), 81.71 (C9), 56.91 (C11), 28.39 (3C, C10); <sup>19</sup>F NMR (471 MHz, DMSO-*d*<sub>6</sub>) δ = -120.28; HRMS (ESI+) *m/z* calculated for C<sub>8</sub>H<sub>8</sub>FN<sub>2</sub>O<sub>5</sub> (M-<sup>t</sup>Bu+H)<sup>+</sup> 231.0412, found 231.0411.

The spectroscopic and analytical data were in agreement with literature values.<sup>297</sup>

\*C5 and C6 observed as broad singlets and so they are reported as singlets due to non-resolvable *J*<sub>C-F</sub>-coupling.

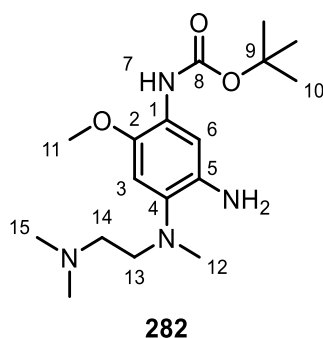
*tert*-butyl (4-((2-(dimethylamino)ethyl)(methyl)amino)-2-methoxy-5-nitrophenyl)carbamate (**281**)



A two-neck round bottom flask equipped with magnetic stirrer was charged with *tert*-butyl(4-fluoro-2-methoxy-5-nitrophenyl)carbamate **280** (1.85 g, 6.46 mmol, 1 equiv.), DMA (21.5 mL, 0.3 M), *N,N*-diisopropylethylamine (1.06 mL, 6.46 mmol, 1 equiv.), and *N,N,N'*-trimethylethylenediamine (1.02 mL, 7.43 mmol, 1.15 equiv.) under flow of nitrogen and heated to 60 °C. After stirring at 60 °C for 2 hours, the reaction mixture was diluted with water (100 mL) and EtOAc (100 mL) and the phases were separated. The aqueous phase was extracted with EtOAc (3 × 50 mL) and the resultant combined organic layers were washed with brine (3 × 100 mL), dried over MgSO<sub>4</sub>, filtered, and concentrated under reduced pressure. The crude product was purified by normal phase column chromatography on silica (100% CH<sub>2</sub>Cl<sub>2</sub> to 10:90 methanol:CH<sub>2</sub>Cl<sub>2</sub> gradient) to yield **281** (2.28 g, 96%) as a red oil. <sup>1</sup>H NMR (600 MHz, CDCl<sub>3</sub>) δ = 8.57 (s, 1H, H6), 6.84 (s, 1H, H7), 6.61 (s, 1H, H3), 3.91 (s, 1H, H11), 3.22 (t, *J* = 7.3 Hz, 2H, H13), 2.83 (s, 3H, H12), 2.55 – 2.51 (t, *J* = 7.3 Hz, 2H, H14), 2.24 (s, 6H, H15), 1.51 (s, 9H, H10); <sup>13</sup>C NMR (151 MHz, CDCl<sub>3</sub>) δ = 152.59 (C8), 151.85 (C2), 143.34 (C4), 134.67 (C5), 121.37 (C1), 116.32 (C6), 102.00 (C3), 80.99 (C9), 57.05 (C14), 56.16 (C11), 54.03 (C13), 45.92 (2C, C15), 41.20 (C12), 28.44 (3C, C10); HRMS (ESI+) *m/z* calculated for C<sub>17</sub>H<sub>29</sub>N<sub>4</sub>O<sub>5</sub> (M+H)<sup>+</sup> 369.2132, found 369.2136.

The spectroscopic and analytical data were in agreement with literature values.<sup>297</sup>

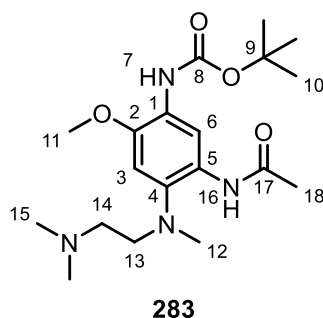
*tert*-butyl (5-amino-4-((2-(dimethylamino)ethyl)(methyl)amino)-2-methoxyphenyl)carbamate (**282**)



A two-neck round bottom flask equipped with magnetic stirrer was charged with *tert*-butyl (4-((2-(dimethylamino)ethyl)(methyl)amino)-2-methoxy-5-nitrophenyl)carbamate **281** (3.52 g, 9.55 mmol, 1 equiv.), methanol (63.7 mL, 0.15 M) and palladium on activated carbon (350 mg, 10 wt.% Pd) under flow of nitrogen. The flask was degassed and backfilled with hydrogen three times, and then stirred at room temperature. After stirring at room temperature for 4 hours, then flask was degassed and backfilled with nitrogen, then the reaction mixture was filtered through celite and concentrated under reduced pressure. The crude product was purified by normal phase column chromatography on silica (methanol:CH<sub>2</sub>Cl<sub>2</sub> + 0.07 N ammonia in methanol 1:99 to 10:90 gradient) to yield **282** (2.44 g, 75%) as a dark brown oil. <sup>1</sup>H NMR (600 MHz, CDCl<sub>3</sub>) δ = 7.53 (s, 1H, H6), 6.95 (s, 1H, H7), 6.63 (s, 1H, H3), 3.77 (s, 3H, H11), 2.94 (t, *J* = 6.9 Hz, 2H, H13), 2.63 (s, 3H, H12), 2.40 (t, *J* = 6.8 Hz, 2H, H14), 2.27 (s, 6H, H15), 1.50 (s, 9H, H10); <sup>13</sup>C NMR (151 MHz, CDCl<sub>3</sub>) δ = 153.00 (C8), 140.58 (C2), 137.03 (C4), 133.13 (C5), 125.31 (C1), 105.95 (C6), 105.03 (C3), 80.21 (C9), 57.84 (C14), 56.74 (C11), 54.89 (C13), 45.95 (2C, C15), 42.80 (C12), 28.52 (C10); HRMS (ESI+) *m/z* calculated for C<sub>17</sub>H<sub>31</sub>N<sub>4</sub>O<sub>3</sub> (M+H)<sup>+</sup> 339.2391, found 339.2388.

The spectroscopic and analytical data were in agreement with literature values.<sup>297</sup>

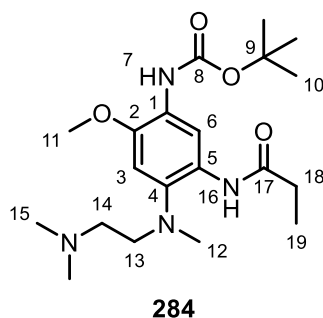
*tert*-butyl (5-acetamido-4-((2-(dimethylamino)ethyl)(methyl)amino)-2-methoxyphenyl)carbamate (**283**)



**283** was prepared following general procedure G, with *tert*-butyl (5-amino-4-((2-(dimethylamino)ethyl)(methyl)amino)-2-methoxyphenyl)carbamate **282** (206 mg, 0.61 mmol, 1 equiv.), CH<sub>2</sub>Cl<sub>2</sub> (1.20 mL, 0.5 M), triethylamine (93 μL, 0.67 mmol, 1.1 equiv.) and acetyl chloride (43 μL, 0.61 mmol, 1 equiv.) for 18 hours to yield **283** (204 mg, 88%) as a brown oil. <sup>1</sup>H NMR (600 MHz, CDCl<sub>3</sub>) δ = 9.88 (s, 1H, H16), 8.89 (s, 1H, H6), 6.87 (s, 1H, H7), 6.69 (s, 1H, H3), 3.81 (s, 3H, H11), 2.86 – 2.81 (m, 2H, H13), 2.66 (s, 3H, H12), 2.29 – 2.22 (m, 8H, H14, H15), 2.11 (s, 3H, H18), 1.52 (s, 9H, H10); <sup>13</sup>C NMR (151 MHz, CDCl<sub>3</sub>) δ = 168.22 (C17), 144.38 (C2), 136.18 (C4), 129.87 (C5), 125.53 (C1), 111.77 (C6), 104.60 (C3), 80.68 (C9), 57.38 (C14), 56.59 (C13), 56.08 (C11), 45.46 (2C, C15), 43.79 (C12), 28.51 (3C, C10), 24.44 (C18);\* HRMS (ESI+) m/z calculated for C<sub>19</sub>H<sub>33</sub>N<sub>4</sub>O<sub>4</sub> (M+H)<sup>+</sup> 381.2496, found 381.2505.

\*C8 not observed in spectrum.

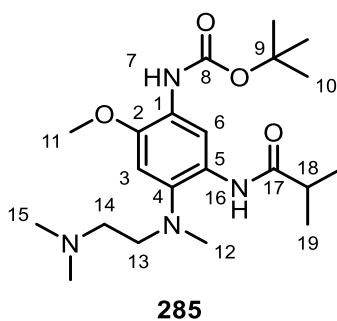
*tert*-butyl (4-((2-(dimethylamino)ethyl)(methyl)amino)-2-methoxy-5-propionamidophenyl)carbamate (**284**)



**284** was prepared following general procedure G, with *tert*-butyl (5-amino-4-((2-(dimethylamino)ethyl)(methyl)amino)-2-methoxyphenyl)carbamate **282** (114 mg, 0.34

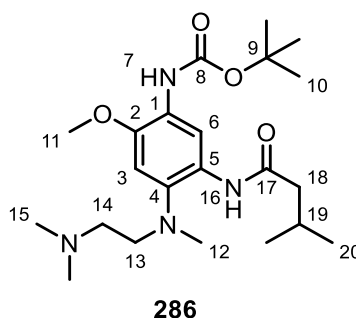
mmol, 1 equiv.), CH<sub>2</sub>Cl<sub>2</sub> (1.20 mL, 0.5 M), triethylamine (52 μL, 0.37 mmol, 1.1 equiv.) and propanoyl chloride (29 μL, 0.34 mmol, 1 equiv.) for 70 hours to yield **284** (103 mg, 78%) as a brown oil. **<sup>1</sup>H NMR** (600 MHz, CDCl<sub>3</sub>) δ = 9.64 (s, 1H, H16), 8.98 (s, 1H, H6), 6.87 (s, 1H, H7), 6.69 (s, 1H, H3), 3.81 (s, 3H, H11), 2.89–2.81 (m, 2H, H13), 2.65 (s, 3H, H12), 2.35 (q, *J* = 7.6 Hz, 2H, H18), 2.29–2.20 (m, 8H, H14, H15), 1.51 (s, 9H, H10), 1.23 (t, *J* = 7.6 Hz, 3H, H19); **<sup>13</sup>C NMR** (151 MHz, CDCl<sub>3</sub>) δ = 172.01 (C17), 152.77 (C8), 144.23 (C2), 135.97 (C4), 129.93 (C5), 125.58 (C1), 111.56 (C6), 104.57 (C3), 80.37 (C9), 57.45 (C14), 56.42 (C13), 56.08 (C11), 45.55 (2C, C15), 43.90 (C12), 30.68 (C18), 28.50 (3C, C10), 10.08 (C19); **HRMS** (ESI+) *m/z* calculated for C<sub>20</sub>H<sub>35</sub>N<sub>4</sub>O<sub>4</sub> (M+H)<sup>+</sup> 395.2653, found 395.2649.

***tert*-butyl (4-((2-(dimethylamino)ethyl)(methyl)amino)-5-isobutyramido-2-methoxyphenyl)carbamate (285)**



**285** was prepared following general procedure G, with *tert*-butyl (5-amino-4-((2-(dimethylamino)ethyl)(methyl)amino)-2-methoxyphenyl)carbamate **282** (199 mg, 0.59 mmol, 1 equiv.), CH<sub>2</sub>Cl<sub>2</sub> (1.18 mL, 0.5 M), triethylamine (90 μL, 0.65 mmol, 1 equiv.) and isobutyryl chloride (62 μL, 0.59 mmol, 1 equiv.) for 3 hours to yield **285** (180 mg, 75%) as a brown oil. **<sup>1</sup>H NMR** (600 MHz, CDCl<sub>3</sub>) δ = 9.42 (s br, 1H, H16), 9.00 (s, 1H, H6), 6.88 (s, 1H, H7), 6.69 (s, 1H, H3), 3.81 (s, 3H, H11), 2.95–2.85 (m, 2H, H13), 2.63 (s, 3H, H12), 2.53 (app. s br, 1H, H18), 2.37–2.15 (m, 8H, H14, H15), 1.51 (s, 9H, H10), 1.23 (d, *J* = 6.9 Hz, 6H, H19); **<sup>13</sup>C NMR** (151 MHz, CDCl<sub>3</sub>) δ = 175.13 (C17), 152.61 (C8), 144.24 (C2), 135.83 (C4), 129.85 (C5), 125.64 (C1), 111.58 (C6), 104.48 (C3), 80.32 (C9), 57.39 (C14), 56.09 (2C, C11, C13), 45.51 (2C, C15), 44.10 (C12), 36.55 (C18), 28.48 (3C, C10), 19.95 (2C, C19); **HRMS** (ESI+) *m/z* calculated for C<sub>21</sub>H<sub>37</sub>N<sub>4</sub>O<sub>4</sub> (M+H)<sup>+</sup> 409.2809, found 409.2770.

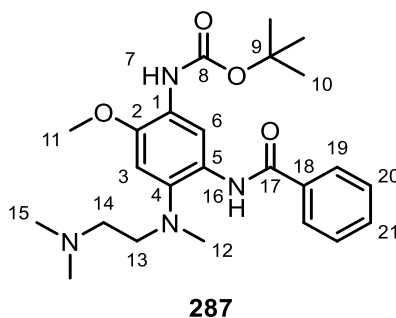
***tert*-butyl (4-((2-(dimethylamino)ethyl)(methyl)amino)-2-methoxy-5-(3-methylbutanamido)phenyl)carbamate (286)**



**286** was prepared following general procedure G, with *tert*-butyl (5-amino-4-((2-(dimethylamino)ethyl)(methyl)amino)-2-methoxyphenyl)carbamate **282** (216 mg, 0.64 mmol, 1 equiv.), CH<sub>2</sub>Cl<sub>2</sub> (1.28 mL, 0.5 M), triethylamine (98 μL, 0.70 mmol, 1.1 equiv.) and isovaleryl chloride (78 μL, 0.64 mmol, 1 equiv.) for 24 hours to yield **286** (220 mg, 82%) as a brown oil. <sup>1</sup>H NMR (600 MHz, CDCl<sub>3</sub>) δ = 9.58 (s br, 1H, H16), 8.92 (s, 1H, H6), 6.87 (s, 1H, H7), 6.68 (s, 1H, H3), 3.81 (s, 3H, H11), 3.03 – 2.81 (m, 2H, H13), 2.64 (s, 3H, H11), 2.47 – 2.11 (m, 11H, H14, H15, H18, H19), 1.51 (s, 9H, H10), 1.02 – 0.99 (m, 6H, H20); <sup>13</sup>C NMR (151 MHz, CDCl<sub>3</sub>) δ = 170.86 (C17), 152.68 (C8), 144.40 (C2), 135.87 (C4), 129.98 (C5), 125.67 (C1), 111.97 (C6), 104.55 (C3), 80.39 (C9), 57.19 (C14), 56.13 (C11), 47.03 (C18), 45.32 (2C, C15), 44.11 (C12), 28.50 (3C, C10), 26.26 (C19), 22.77 (2C, C20);\* HRMS (ESI+) m/z calculated for C<sub>22</sub>H<sub>39</sub>N<sub>4</sub>O<sub>4</sub> (M+H)<sup>+</sup> 423.2966, found 423.2954;

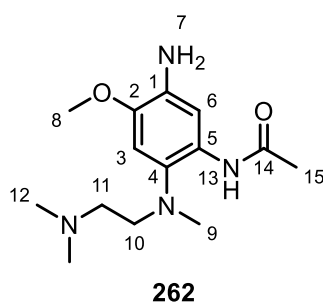
\*C13 not observed in spectrum.

***tert*-butyl (5-benzamido-4-((2-(dimethylamino)ethyl)(methyl)amino)-2-methoxyphenyl)carbamate (287)**



**287** was prepared following general procedure G, with *tert*-butyl (5-amino-4-((2-(dimethylamino)ethyl)(methyl)amino)-2-methoxyphenyl)carbamate **282** (200 mg, 0.59 mmol, 1 equiv.), CH<sub>2</sub>Cl<sub>2</sub> (1.18 mL, 0.5 M), triethylamine (91 μL, 0.65 mmol, 1.1 equiv.) and benzoyl chloride (76 μL, 0.65 mmol, 1.1 equiv.) for 3 hours to yield **287** (175 mg, 67%) as a light brown solid. **<sup>1</sup>H NMR** (600 MHz, CDCl<sub>3</sub>) δ = 10.31 (s br, 1H, H16), 9.19 (s, 1H, H6), 8.00 – 7.96 (m, 2H, H19), 7.51 – 7.47 (m, 1H, H21), 7.47 – 7.42 (m, 2H, H20), 6.94 (s, 1H, H7), 6.76 (s, 1H, H3), 3.84 (s, 3H, H11), 2.95 (app. s br, 2H, H13), 2.70 (s, 3H, H12), 2.24 (app. s br, 2H, H14), 2.07 (s br, 6H, H15), 1.54 (s, 9H, H10); **<sup>13</sup>C NMR** (151 MHz, CDCl<sub>3</sub>) δ = 165.21 (C17), 152.68 (C8), 144.58 (C2), 136.12 (C18), 135.96 (C4), 131.16 (C21), 130.27 (C5), 128.37 (2C, C20), 127.66 (2C, C19), 125.96 (C1), 111.36 (C6), 104.71 (C3), 80.43 (C9), 57.21 (C14), 56.12 (C11), 55.80 (C13), 45.06 (2C, C15), 44.69 (C12), 28.52 (3C, C10); **HRMS** (ESI+) *m/z* calculated for C<sub>24</sub>H<sub>35</sub>N<sub>4</sub>O<sub>4</sub> (M+H)<sup>+</sup> 443.2653, found 443.2641.

***N*-(5-amino-2-((2-(dimethylamino)ethyl)(methyl)amino)-4-methoxyphenyl)acetamide (262)**

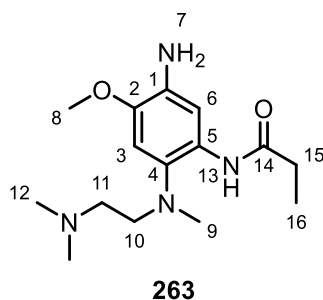


A two-neck round bottom flask heat-dried under vacuum and equipped with magnetic stirrer was charged with *tert*-butyl (5-acetamido-4-((2-(dimethylamino)ethyl)(methyl)amino)-2-methoxyphenyl)carbamate **283** (200 mg, 0.52 mmol, 1 equiv.) and anhydrous CH<sub>2</sub>Cl<sub>2</sub> (1.8 mL, 0.3 M), and iodotrimethylsilane (524 μL, 4.4 mmol, 7 equiv.) under flow of nitrogen and heated to 50 °C. After stirring at 50 °C for 7 days, the reaction mixture was diluted with CH<sub>2</sub>Cl<sub>2</sub> (20 mL) and water (20 mL) and the phases were separated. The aqueous phase was washed with CH<sub>2</sub>Cl<sub>2</sub> (3 × 20 mL) and then neutralised to pH 8 with sat. NaHCO<sub>3</sub>. After washing the aqueous phase with further CH<sub>2</sub>Cl<sub>2</sub> (4 × 20 mL), the resultant combined organic layers were dried over MgSO<sub>4</sub>, filtered and concentrated under reduced pressure to yield **262** (90 mg, 61%) as a brown oil. **<sup>1</sup>H NMR** (600 MHz, CDCl<sub>3</sub>) δ = <sup>1</sup>H NMR (600 MHz, CDCl<sub>3</sub>) δ 9.88 (s, 1H,



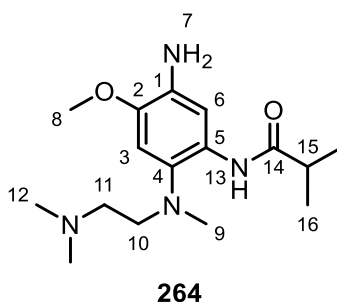
H13), 7.82 (s, 1H, H6), 6.66 (s, 1H, H3), 3.80 (s, 3H, H8), 3.74 (s br, 2H, H7), 2.82 (t,  $J = 5.7$  Hz, 2H, H10), 2.64 (s, 3H, H9), 2.27 – 2.20 (m, 8H, H11, H12), 2.11 (s, 3H, H15);  $^{13}\text{C}$  NMR (151 MHz,  $\text{CDCl}_3$ )  $\delta = 168.35$  (C14), 143.45 (C2), 133.92 (C4), 132.11 (C5), 130.39 (C1), 107.03 (C6), 105.36 (C3), 57.54 (C11), 56.70 (C10), 55.98 (C8), 45.53 (2C, C12), 44.31 (C9), 24.64 (C15); **HRMS** (ESI+)  $m/z$  calculated for  $\text{C}_{14}\text{H}_{25}\text{N}_4\text{O}_2$  ( $\text{M}+\text{H}$ )<sup>+</sup> 281.1972, found 281.1971;

***N*-(5-amino-2-((2-(dimethylamino)ethyl)(methyl)amino)-4-methoxyphenyl)propionamide (263)**



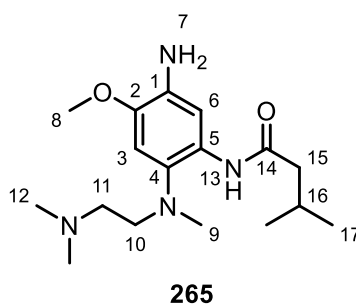
A two-neck round bottom flask heat-dried under vacuum and equipped with magnetic stirrer was charged with *tert*-butyl (4-((2-(dimethylamino)ethyl)(methyl)amino)-2-methoxy-5-propionamidophenyl)carbamate **284** (100 mg, 0.25 mmol, 1 equiv.) and anhydrous  $\text{CH}_2\text{Cl}_2$  (0.84 mL, 0.3 M), and iodotrimethylsilane (87  $\mu\text{L}$ , 0.61 mmol, 2.4 equiv.) under flow of nitrogen and heated to 50  $^\circ\text{C}$ . After stirring at 50  $^\circ\text{C}$  for 2 hours, the reaction mixture was diluted with  $\text{CH}_2\text{Cl}_2$  (10 mL) and water (10 mL) and the phases were separated. The aqueous phase was washed with  $\text{CH}_2\text{Cl}_2$  (3  $\times$  10 mL) and then neutralised to pH 8 with sat.  $\text{NaHCO}_3$ . After washing the aqueous phase with further  $\text{CH}_2\text{Cl}_2$  (4  $\times$  10 mL), the resultant combined organic layers were dried over  $\text{MgSO}_4$ , filtered and concentrated under reduced pressure to yield **263** (55 mg, 74%) as a brown oil.  $^1\text{H}$  NMR (600 MHz,  $\text{CDCl}_3$ )  $\delta = 9.68$  (s, 1H, H13), 7.86 (s, 1H, H6), 6.66 (s, 1H, H3), 3.80 (s, 3H, H8), 3.73 (s, 2H, H7), 2.84 (t,  $J = 5.9$  Hz, 2H, H10), 2.63 (s, 3H, H9), 2.35 (q,  $J = 7.6$  Hz, 2H, H15), 2.26 – 2.20 (m, 8H, H11, H12), 1.23 (t,  $J = 7.6$  Hz, 3H, H16);  $^{13}\text{C}$  NMR (151 MHz,  $\text{CDCl}_3$ )  $\delta = 172.10$  (C14), 143.37 (C2), 133.94 (C4), 132.06 (C5), 130.35 (C1), 107.02 (C6), 105.36 (C3), 57.60 (C11), 56.53 (C10), 55.99 (C8), 45.60 (2C, C12), 44.42 (C9), 30.84 (C15), 10.14 (C16); **HRMS** (ESI+)  $m/z$  calculated for  $\text{C}_{15}\text{H}_{27}\text{N}_4\text{O}_2$  ( $\text{M}+\text{H}$ )<sup>+</sup> 295.2129, found 295.2133;

***N*-(5-amino-2-((2-(dimethylamino)ethyl)(methyl)amino)-4-methoxyphenyl)isobutyramide (264)**



**264** was prepared following general procedure H, with *tert*-butyl (4-((2-(dimethylamino)ethyl)(methyl)amino)-5-isobutyramido-2-methoxyphenyl)carbamate **285** (175 mg, 0.43 mmol, 1 equiv.), CH<sub>2</sub>Cl<sub>2</sub> (1.43 mL, 0.3 M), lithium iodide (138 mg, 1.03 mmol, 2.4 equiv.) and chlorotrimethylsilane (0.13 mL, 1.03 mmol, 2.4 equiv.) to yield **264** (106 mg, 80%) as a brown oil. <sup>1</sup>H NMR (600 MHz, CDCl<sub>3</sub>) δ = 9.48 (s br, 1H, H13), 7.85 (s, 1H, H6), 6.65 (s, 1H, H3), 3.80 (s, 3H, H8), 3.72 (s br, 2H, H7), 2.90 (app. s br, 2H, H10), 2.62 (s, 3H, H9), 2.54 (app. s br, 1H, H15), 2.38 – 2.15 (m, 8H, H11, H12), 1.23 (d, *J* = 6.9 Hz, 6H, H16); <sup>13</sup>C NMR (151 MHz, CDCl<sub>3</sub>) δ = 175.44 (C14), 143.40 (C2), 134.01 (C1), 131.95 (C4), 130.18 (C5), 107.18 (C6), 105.23 (C3), 57.51 (C11), 56.01 (2C, C8, C10), 45.52 (2C, C12), 44.58 (C9), 36.61 (C15), 19.93 (2C, C16); HRMS (ESI+) *m/z* calculated for C<sub>16</sub>H<sub>29</sub>N<sub>4</sub>O<sub>2</sub> (M+H)<sup>+</sup> 309.2285, found 309.228

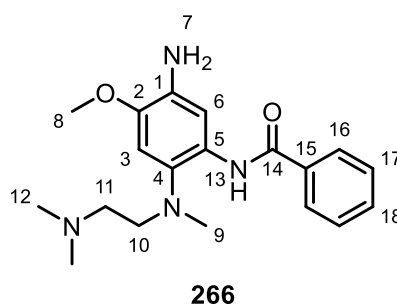
***N*-(5-amino-2-((2-(dimethylamino)ethyl)(methyl)amino)-4-methoxyphenyl)-3-methylbutanamide (265)**



**265** was prepared following general procedure H, with *tert*-butyl (4-((2-(dimethylamino)ethyl)(methyl)amino)-2-methoxy-5-(3-methylbutanamido)phenyl)carbamate **286** (215 mg, 0.51 mmol, 1 equiv.), CH<sub>2</sub>Cl<sub>2</sub> (1.70 mL, 0.3 M), lithium iodide (163 mg, 1.22 mmol, 2.4 equiv.) and chlorotrimethylsilane

(0.16 mL, 1.22 mmol, 2.4 equiv.) to yield **265** (130 mg, 79%) as a brown oil. **<sup>1</sup>H NMR** (600 MHz, CDCl<sub>3</sub>) δ = 9.61 (s br, 1H, H13), 7.82 (s, 1H, H6), 6.65 (s, 1H, H3), 3.79 (s, 3H, H8), 3.73 (s br, 2H, H7), 2.93 – 2.83 (m, 2H, H10), 2.62 (s, 3H, H9), 2.35 – 2.16 (m, 11H, H11, H12, H15, H16), 1.02 – 0.99 (m, 6H, H17); **<sup>13</sup>C NMR** (151 MHz, CDCl<sub>3</sub>) δ = 170.95 (C14), 143.49 (C2), 133.99 (C1), 132.03 (C4), 130.20 (C5), 107.34 (C6), 105.33 (C3), 57.44 (C11), 56.01 (C8, C10), 47.18 (C15), 45.47 (2C, C12), 44.53 (C9), 26.39 (C16), 22.72 (2C, C17); **HRMS** (ESI+) m/z calculated for C<sub>17</sub>H<sub>31</sub>N<sub>4</sub>O<sub>2</sub> (M+H)<sup>+</sup> 323.2442, found 323.2441.

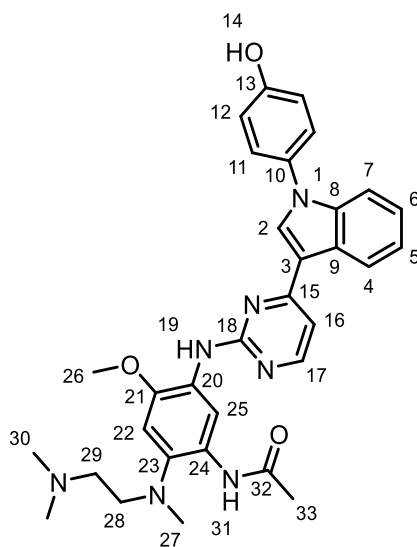
***N*-(5-amino-2-((2-(dimethylamino)ethyl)(methyl)amino)-4-methoxyphenyl)benzamide (266)**



**266** was prepared following general procedure H, with *tert*-butyl (5-benzamido-4-((2-(dimethylamino)ethyl)(methyl)amino)-2-methoxyphenyl)carbamate **287** (174 mg, 0.39 mmol, 1 equiv.), CH<sub>2</sub>Cl<sub>2</sub> (1.31 mL, 0.3 M), lithium iodide (126 mg, 0.94 mmol, 2.4 equiv.) and chlorotrimethylsilane (0.12 mL, 0.94 mmol, 2.4 equiv.) to yield **266** (112 mg, 83%) as a brown solid. **<sup>1</sup>H NMR** (600 MHz, CDCl<sub>3</sub>) δ = 10.39 (s, 1H, H13), 8.05 (s, 1H, H6), 7.99 – 7.95 (m, 2H, H16), 7.53 – 7.49 (m, 1H, H18), 7.48 – 7.44 (m, 2H, H17), 6.73 (s, 1H, H3), 3.83 (s, 3H, H8), 3.81 (s br, 2H, H7), 2.96 (app. s br, 2H, H10), 2.69 (s, 3H, H9), 2.24 (app. s br, 2H, H11), 2.07 (s br, 6H, H12); **<sup>13</sup>C NMR** (151 MHz, CDCl<sub>3</sub>) δ = 165.24 (C14), 143.79 (C2), 136.03 (C15), 134.27 (C1), 131.49 (C4), 131.25 (C18), 130.54 (C5), 128.45 (2C, C17), 127.57 (2C, C16), 106.90 (C6), 105.36 (C3), 57.27 (C11), 56.00 (C8), 45.18 (C9), 45.02 (2C, C12);\* **HRMS** (ESI+) m/z calculated for C<sub>19</sub>H<sub>27</sub>N<sub>4</sub>O<sub>2</sub> (M+H)<sup>+</sup> 343.2129, found 343.2139.

\*C10 not observed in spectrum.

***N*-2-((2-(dimethylamino)ethyl)(methyl)amino)-5-((4-(1-(4-hydroxyphenyl)-1*H*-indol-3-yl)pyrimidin-2-yl)amino)-4-methoxyphenyl)acetamide (**268**)**

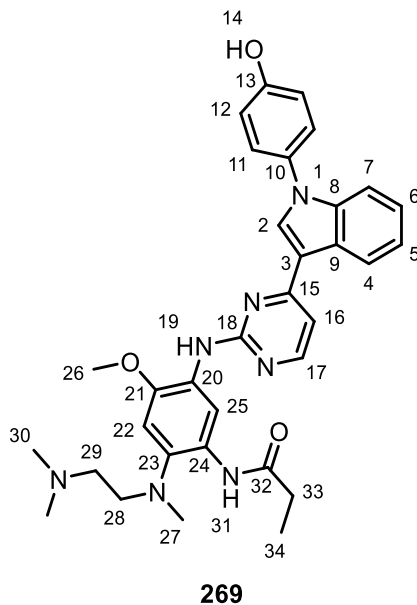


**268**

**268** was prepared following general procedure I, with 4-(3-(2-chloropyrimidin-4-yl)-1*H*-indol-1-yl)phenol **267** (98.7 mg, 0.31 mmol, 1 equiv.), *tert*-butanol (3.07 mL, 0.1 M), *N*-(5-amino-2-((2-(dimethylamino)ethyl)(methyl)amino)-4-methoxyphenyl)acetamide **262** (86.0 mg, 0.31 mmol, 1 equiv.) and *p*-toluenesulfonic acid monohydrate (58.3 mg, 0.31 mmol, 1 equiv.) for 36 hours. Purification by reverse phase column chromatography on C18 (methanol:water +0.1% formic acid 20:80 to 90:10 gradient) then normal phase column chromatography on silica (methanol:CH<sub>2</sub>Cl<sub>2</sub> + 0.07 N ammonia in methanol 1:99 to 15:95 gradient) yielded **268** (97 mg, 56%) as a yellow solid. <sup>1</sup>H NMR (600 MHz, DMSO-*d*<sub>6</sub>) δ = 9.95 – 9.73 (m, 2H, H14, H31), 8.85 (s br, 1H, H19), 8.60 (s, 1H, H2), 8.40 (d, *J* = 7.8 Hz, 1H, H4), 8.33 (d, *J* = 5.3 Hz, 1H, H17), 7.99 (s, 1H, H25), 7.47 – 7.44 (m, 2H, H11), 7.41 (d, *J* = 8.2 Hz, 1H, H7), 7.33 (d, *J* = 5.3 Hz, 1H, H16), 7.26 – 7.22 (m, 1H, H6), 7.21 – 7.16 (m, 1H, H5), 7.00 – 6.95 (m, 3H, H12, H22), 3.83 (s, 3H, H26), 2.93 (app. s br, 2H, H28), 2.70 (s, 3H, H27), 2.40 – 2.20 (m, 8H, H29, H30), 1.99 (s, 3H, H33); <sup>13</sup>C NMR (151 MHz, DMSO-*d*<sub>6</sub>) δ = 167.70 (C32), 161.68 (C15), 160.22 (C18), 157.54 (C17), 156.84 (C13), 146.56 (C21), 137.90 (C23), 137.13 (C8), 132.13 (C2), 128.04 (C10), 126.30 (2C, C11), 125.79 (C9), 125.01 (C20), 122.85 (C6), 122.23 (C4), 121.32 (C5), 116.09 (2C, C12), 114.32 (C3), 110.80 (C7), 107.55 (C16), 105.10 (C25), 55.96 (C26), 42.59 (C27), 23.77 (C33);\* HRMS (ESI+) *m/z* calculated for C<sub>32</sub>H<sub>36</sub>N<sub>7</sub>O<sub>3</sub> (M+H)<sup>+</sup> 566.2874, found 566.2875.

\*C22, C24, C28, C29, and C30 not observed in spectrum.

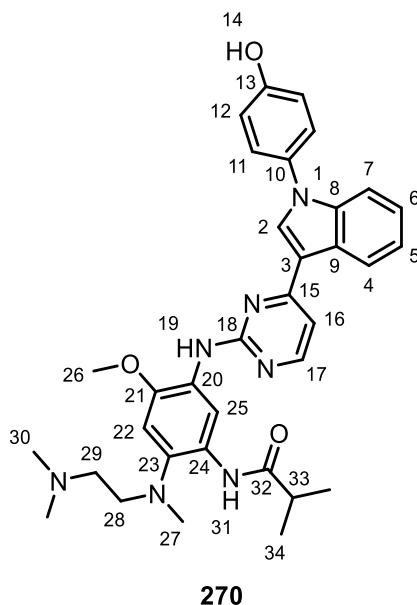
***N*-2-((2-(dimethylamino)ethyl)(methyl)amino)-5-((4-(1-(4-hydroxyphenyl)-1*H*-indol-3-yl)pyrimidin-2-yl)amino)-4-methoxyphenyl)propionamide (**269**)**



**269** was prepared following general procedure I, with 4-(3-(2-chloropyrimidin-4-yl)-1*H*-indol-1-yl)phenol **267** (58.0 mg, 0.18 mmol, 1 equiv.), *tert*-butanol (1.80 mL, 0.1 M), *N*-(5-amino-2-((2-(dimethylamino)ethyl)(methyl)amino)-4-methoxyphenyl)propionamide **263** (53.0 mg, 0.18 mmol, 1 equiv.) and *p*-toluenesulfonic acid monohydrate (34.2 mg, 0.18 mmol, 1 equiv.) for 40 hours. Purification by reverse phase column chromatography on C18 (methanol:water +0.1% formic acid 20:80 to 100% methanol gradient) then normal phase column chromatography on silica (methanol:CH<sub>2</sub>Cl<sub>2</sub> + 0.07 N ammonia in methanol 1:99 to 15:95 gradient) yielded **269** (58 mg, 56%) as a pale yellow solid. <sup>1</sup>H NMR (600 MHz, DMSO-*d*<sub>6</sub>) δ = 9.81 (s, 1H, H14), 9.77 (s, 1H, H31), 8.89 (s, 1H, H25), 8.60 (s, 1H, H2), 8.39 (d, *J* = 8.0 Hz, 1H, H4), 8.33 (d, *J* = 5.3 Hz, 1H, H17), 8.00 (s, 1H, H19), 7.48 – 7.41 (m, 2H, H11), 7.40 (d, *J* = 8.2 Hz, 1H, H7), 7.33 (d, *J* = 5.3 Hz, 1H, H16), 7.25 – 7.21 (m, 1H, H6), 7.20 – 7.14 (m, 1H, H5), 7.00 (s, 1H, H22), 6.99 – 6.94 (m, 2H, H12), 3.83 (s, 3H, H26), 2.89 (t, *J* = 5.8 Hz, 2H, H28), 2.70 (s, 3H, H27), 2.34 – 2.28 (m, 2H, H29), 2.27 – 2.20 (m, 8H, H30, H33), 0.98 (t, *J* = 7.6 Hz, 3H, H41); <sup>13</sup>C NMR (151 MHz, DMSO-*d*<sub>6</sub>) δ = 171.38 (C32), 162.15 (C15), 160.75 (C18), 158.00 (C17), 157.35 (C13), 146.92 (C21), 138.18 (C23), 137.64 (C8), 132.58 (C2), 130.09 (C10), 128.35 (C24), 126.78 (2C, C11), 126.25 (C9), 125.49 (C20), 123.28 (C6), 122.71

(C4), 121.76 (C5), 116.54 (2C, C12), 115.11 (C25), 114.78 (C3), 111.24 (C7), 107.96 (C16), 105.74 (C22), 57.44 (C29), 56.40 (C26), 56.17 (C28), 45.80 (2C, C30), 43.08 (C27), 29.97 (C33), 10.17 (C34); **HRMS** (ESI+)  $m/z$  calculated for  $C_{33}H_{38}N_7O_3$  (M+H)<sup>+</sup> 580.3031, found 580.3036.

***N*-2-((2-(dimethylamino)ethyl)(methyl)amino)-5-((4-(1-(4-hydroxyphenyl)-1*H*-indol-3-yl)pyrimidin-2-yl)amino)-4-methoxyphenylisobutyramide (**270**)**

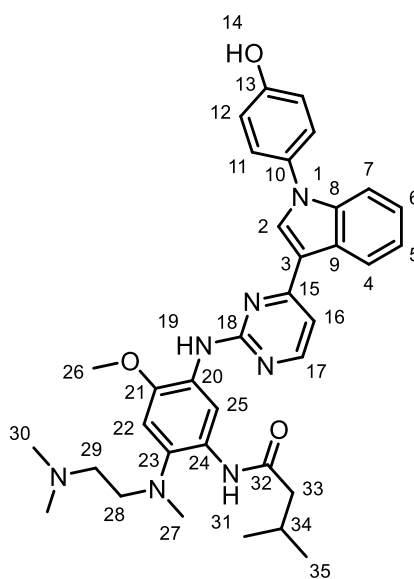


**270** was prepared following general procedure I, with 4-(3-(2-chloropyrimidin-4-yl)-1*H*-indol-1-yl)phenol **267** (50.0 mg, 0.16 mmol, 1 equiv.), *tert*-butanol (1.55 mL, 0.1 M), *N*-(5-amino-2-((2-(dimethylamino)ethyl)(methyl)amino)-4-methoxyphenyl)isobutyramide **264** (47.9 mg, 0.16 mmol, 1 equiv.) and *p*-toluenesulfonic acid monohydrate (29.6 mg, 0.16 mmol, 1 equiv.) for 72 hours. Purification by reverse phase column chromatography on C18 (methanol:water +0.1% formic acid 20:80 to 90:10 gradient) then normal phase column chromatography on silica (methanol:CH<sub>2</sub>Cl<sub>2</sub> + 0.07 N ammonia in methanol 1:99 to 15:95 gradient) yielded **270** (63 mg, 68%) as a yellow solid. <sup>1</sup>H NMR (600 MHz, DMSO-d<sub>6</sub>) δ = 9.82 (s br, 1H, H14), 9.64 (s, 1H, H31), 8.85 (s, 1H, H25), 8.61 (s, 1H, H2), 8.38 (d, *J* = 8.0 Hz, 1H, H4), 8.33 (d, *J* = 5.3 Hz, 1H, H17), 8.01 (s, 1H, H19), 7.45 – 7.41 (m, 2H, H11), 7.38 (d, *J* = 8.2 Hz, 1H, H7), 7.33 (d, *J* = 5.3 Hz, 1H, H16), 7.24 – 7.20 (m, 1H, H6), 7.19 – 7.15 (m, 1H, H5), 7.01 (s, 1H, H22), 6.98 – 6.94 (m, 2H, H12), 3.82 (s, 3H, H26), 2.92 (t, *J* = 5.9 Hz, 2H, H28), 2.69 (s, 3H, H27), 2.51 – 2.46 (m, 1H, H33)\*, 2.29 (t, *J* = 5.9 Hz, 2H, H29), 2.19 (s, 6H, H30), 1.01 (d, *J* = 6.9 Hz, 6H, H34);

$^{13}\text{C}$  NMR (151 MHz, DMSO- $d_6$ )  $\delta$  = 174.05 (C32), 161.71 (C15), 160.31 (C18), 157.51 (C17), 156.93 (C13), 146.55 (C21), 137.71 (C23), 137.22 (C8), 132.08 (C2), 129.59 (C10), 128.00 (C24), 126.37 (2C, C11), 125.76 (C9), 125.11 (C20), 122.77 (C6), 122.23 (C4), 121.31 (C5), 116.11 (2C, C12), 114.85 (C3), 114.29 (C25), 110.75 (C7), 107.49 (C16), 105.42 (C22), 57.02 (C29), 55.93 (C26), 55.45 (C28), 45.41 (2C, C30), 42.81 (C27), 35.17 (C33), 19.49 (2C, C34); **HRMS** (ESI+)  $m/z$  calculated for  $\text{C}_{34}\text{H}_{40}\text{N}_7\text{O}_3$  (M+H) $^+$  594.3187, found 594.3163.

\*Peak overlaps with solvent signal.

***N*-2-((2-(dimethylamino)ethyl)(methyl)amino)-5-((4-(1-(4-hydroxyphenyl)-1*H*-indol-3-yl)pyrimidin-2-yl)amino)-4-methoxyphenyl)-3-methylbutanamide (271)**

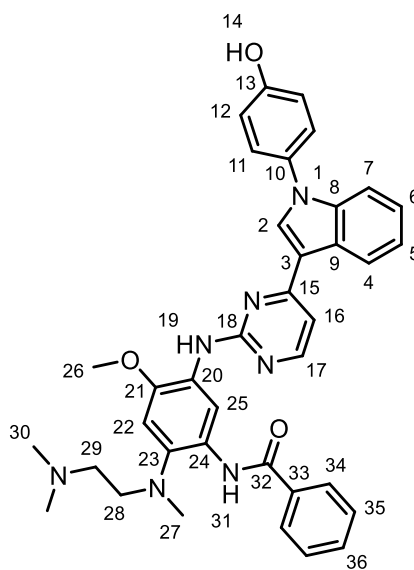


**271**

**271** was prepared following general procedure I, with 4-(3-(2-chloropyrimidin-4-yl)-1*H*-indol-1-yl)phenol **267** (50.0 mg, 0.16 mmol, 1 equiv.), *tert*-butanol (1.55 mL, 0.1 M), *N*-(5-amino-2-((2-(dimethylamino)ethyl)(methyl)amino)-4-methoxyphenyl)-3-methylbutanamide **265** (50.1 mg, 0.16 mmol, 1 equiv.) and *p*-toluenesulfonic acid monohydrate (29.6 mg, 0.16 mmol, 1 equiv.) for 48 hours. Purification by reverse phase column chromatography on C18 (methanol:water +0.1% formic acid 20:80 to 90:10 gradient) then normal phase column chromatography on silica (methanol: $\text{CH}_2\text{Cl}_2$  + 0.07 N ammonia in methanol 1:99 to 15:95 gradient) yielded **271** (59 mg, 62%) as a yellow solid.  $^1\text{H}$  NMR (600 MHz, DMSO- $d_6$ )  $\delta$  = 9.81 (s, 1H, H14), 9.75 (s, 1H, H31), 8.91 (s,

1H, H25), 8.65 (s, 1H, H2), 8.38 – 8.32 (m, 2H, H4, H17), 7.99 (s, 1H, H19), 7.45 (s, 2H, H11), 7.39 (d,  $J = 8.2$  Hz, 1H, H7), 7.33 (d,  $J = 5.3$  Hz, 1H, H16), 7.25 – 7.21 (m, 1H, H6), 7.20 – 7.16 (m, 1H, H5), 7.01 (s, 1H, H22), 6.98 – 6.94 (m, 2H, H12), 3.82 (s, 3H, H26), 2.90 (t,  $J = 5.8$  Hz, 2H, H28), 2.69 (s, 3H, H27), 2.28 (t,  $J = 5.8$  Hz, 2H, H29), 2.21 (s, 6H, H30), 2.08 (d,  $J = 7.3$  Hz, 2H, H33), 1.94 – 1.84 (m, 1H, H34), 0.87 (d,  $J = 6.6$  Hz, 6H, H35);  $^{13}\text{C}$  NMR (151 MHz, DMSO- $d_6$ )  $\delta = 169.57$  (C32), 161.61 (C15), 160.24 (C18), 157.63 (C17), 156.89 (C13), 146.38 (C21), 137.52 (C23), 137.23 (C8), 132.19 (C2), 129.58 (C10), 128.03 (C24), 126.38 (2C, C11), 125.74 (C9), 125.15 (C20), 122.78 (C6), 122.05 (C4), 121.33 (C5), 116.03 (2C, C12), 114.65 (C25), 114.30 (C3), 110.81 (C7), 107.54 (C16), 105.44 (C22), 56.94 (C29), 55.96 (C26), 55.60 (C28), 45.78 (C33), 45.37 (2C, C30), 42.76 (C27), 25.44 (C34), 22.31 (2C, C35); HRMS (ESI+)  $m/z$  calculated for  $\text{C}_{35}\text{H}_{42}\text{N}_7\text{O}_3$  (M+H) $^+$  608.3344, found 608.3347.

***N*-((2-((2-(dimethylamino)ethyl)(methyl)amino)-5-((4-(1-(4-hydroxyphenyl)-1*H*-indol-3-yl)pyrimidin-2-yl)amino)-4-methoxyphenyl)benzamide (272)**



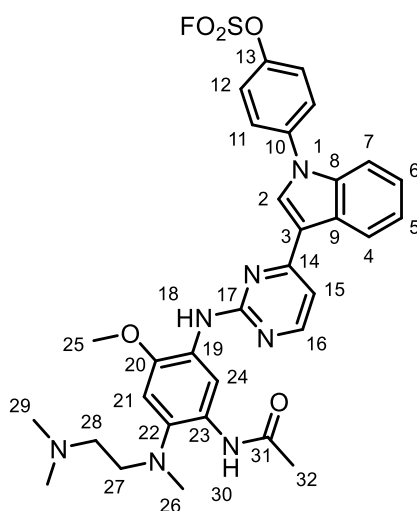
**272**

**272** was prepared following general procedure I, with 4-(3-(2-chloropyrimidin-4-yl)-1*H*-indol-1-yl)phenol **267** (50.0 mg, 0.16 mmol, 1 equiv.), *tert*-butanol (1.55 mL, 0.1 M), *N*-(5-amino-2-((2-(dimethylamino)ethyl)(methyl)amino)-4-methoxyphenyl)benzamide **266** (53.2 mg, 0.16 mmol, 1 equiv.) and *p*-toluenesulfonic acid monohydrate (29.6 mg, 0.16 mmol, 1 equiv.) for 72 hours. Purification by reverse phase column chromatography on C18 (methanol:water +0.1% formic acid 20:80 to 90:10 gradient) then normal phase



column chromatography on silica (methanol:CH<sub>2</sub>Cl<sub>2</sub> + 0.07 N ammonia in methanol 1:99 to 15:95 gradient) yielded **272** (59 mg, 60%) as a yellow solid. <sup>1</sup>H NMR (600 MHz, DMSO-d<sub>6</sub>) δ = 10.54 (s, 1H, H31), 9.84 (s br, 1H, H14), 9.30 (s, 1H, H25), 8.79 (s, 1H, H2), 8.39 (d, *J* = 5.2 Hz, 1H, H17), 8.36 (d, *J* = 7.6 Hz, 1H, H4), 8.02 (s, 1H, H19), 7.74 – 7.69 (m, 2H, H34), 7.60 – 7.56 (m, 1H, H36), 7.53 – 7.48 (m, 2H, H35), 7.46 – 7.42 (m, 2H, H11), 7.40 – 7.36 (m, 2H, H7, H16), 7.22 – 7.15 (m, 2H, H5, H6), 7.13 (s, 1H, H22), 6.93 – 6.89 (m, 2H, H12), 3.88 (s, 3H, H26), 2.97 (t, *J* = 5.8 Hz, 2H, H28), 2.74 (s, 3H, H27), 2.18 (t, *J* = 5.8 Hz, 2H, H29), 1.96 (s, 6H, H30); <sup>13</sup>C NMR (151 MHz, DMSO-d<sub>6</sub>) δ = 163.93 (C32), 161.56 (C15), 160.02 (C18), 157.84 (C17), 156.96 (C13), 146.14 (C21), 137.38 (C8), 136.97 (C23), 135.10 (C33), 132.44 (C2), 131.28 (C36), 129.60 (C10), 128.84 (C24), 128.37 (2C, C35), 127.09 (2C, C34), 126.51 (2C, C11), 125.91 (C20), 125.62 (C9), 122.75 (C6), 121.73 (C4), 121.37 (C5), 116.12 (2C, C12), 114.28 (C3), 112.90 (C25), 110.88 (C7), 107.83 (C16), 105.96 (C22), 56.81 (C29), 56.06 (C26), 55.31 (C28), 44.76 (2C, C30), 43.82 (C27); HRMS (ESI+) *m/z* calculated for C<sub>37</sub>H<sub>38</sub>N<sub>7</sub>O<sub>3</sub> (M+H)<sup>+</sup> 628.3031, found 628.3033.

**4-(3-(2-((5-acetamido-4-((2-(dimethylamino)ethyl)(methyl)amino)-2-methoxyphenyl)amino)pyrimidin-4-yl)-1*H*-indol-1-yl)phenyl sulfurofluoridate (257)**



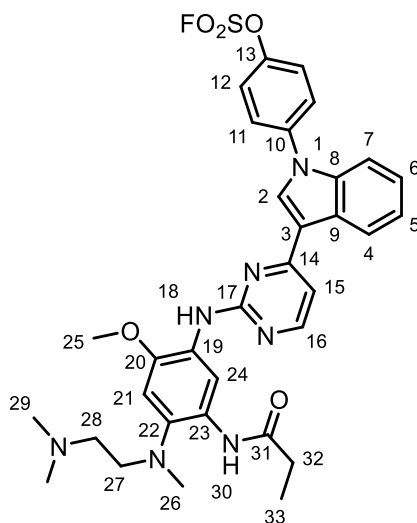
**257**

**257** was prepared following general procedure J, with *N*-(2-((2-(dimethylamino)ethyl)(methyl)amino)-5-((4-(1-(4-hydroxyphenyl)-1*H*-indol-3-yl)pyrimidin-2-yl)amino)-4-methoxyphenyl)acetamide **268** (83.0 mg, 0.15 mmol, 1

equiv.), THF:DMSO 5:1 (v/v) mixture (1.40 mL, 0.1 M), [4-(acetylamino)phenyl]imidodisulfuryl difluoride (55.3 mg, 0.18 mmol, 1.2 equiv.) and 1,8-Diazabicyclo[5.4.0]undec-7-ene (48  $\mu$ L, 0.32 mmol, 2.2 equiv.) for 2 hours. Purification by normal phase column chromatography on silica (100% CH<sub>2</sub>Cl<sub>2</sub> to methanol:CH<sub>2</sub>Cl<sub>2</sub> 10:90 gradient) yielded **257** (67 mg, 70%) as a white solid. **<sup>1</sup>H NMR** (600 MHz, CDCl<sub>3</sub>)  $\delta$  = 9.97 – 9.49 (m, 2H, H24, H30), 9.02 (s, 1H, H2), 8.45 (d,  $J$  = 5.1 Hz, 1H, H16), 8.15 (d,  $J$  = 7.8 Hz, 1H, H4), 7.95 – 7.91 (m, 2H, H11), 7.73 (s, 1H, H18), 7.59 – 7.57 (m, 1H, H7), 7.55 – 7.51 (m, 2H, H12), 7.35 – 7.29 (m, 2H, H5, H6), 7.27 (d,  $J$  = 5.1 Hz, 1H, H15), 6.75 (s, 1H, H21), 3.88 (s, 3H, H25), 2.95 (app. s br, 2H, H27), 2.69 (s, 3H, H26), 2.38 (app. s br, 8H, H28, H29), 2.04 (s br, 3H, H32); **<sup>13</sup>C NMR** (151 MHz, CDCl<sub>3</sub>)  $\delta$  = 161.64 (C14), 159.96 (C17), 158.37 (C16), 148.20 (C13), 144.19 (C20), 139.44 (C10), 137.29 (C8), 134.36 (C22), 132.35 (C2), 129.59 (C23), 127.38 (C19), 127.24 (2C, C11), 126.91 (C9), 123.28 (C5), 122.27 (C6), 122.12 (2C, C12), 120.90 (C4), 117.29 (C3), 111.10 (C7), 110.43 (C24), 108.97 (C15), 104.38 (C21), 57.17 (C27), 56.29 (C25), 45.09 (2C, C29), 44.02 (C26), 24.46 (C32);\* **<sup>19</sup>F NMR** (471 MHz, CDCl<sub>3</sub>)  $\delta$  = 37.25; **HRMS** (ESI+)  $m/z$  calculated for C<sub>32</sub>H<sub>35</sub>FN<sub>7</sub>O<sub>5</sub>S (M+H)<sup>+</sup> 648.2399, found 648.2378.

\*C28 and C31 not observed in spectrum.

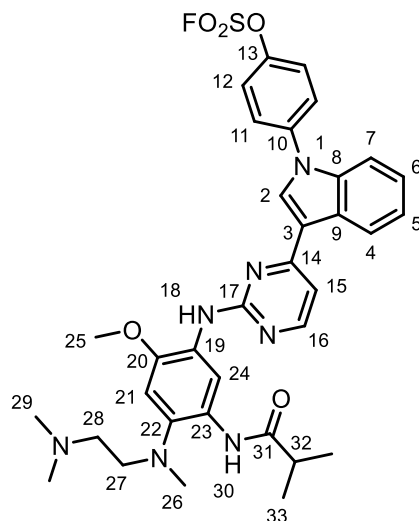
**4-(3-(2-((4-((2-(dimethylamino)ethyl)(methyl)amino)-2-methoxy-5-propionamidophenyl)amino)pyrimidin-4-yl)-1H-indol-1-yl)phenyl sulfurofluoridate (258)**



**258**

**258** was prepared following general procedure J, with *N*-(2-((2-(dimethylamino)ethyl)(methyl)amino)-5-((4-(1-(4-hydroxyphenyl)-1*H*-indol-3-yl)pyrimidin-2-yl)amino)-4-methoxyphenyl)propionamide **269** (35.0 g, 0.06 mmol, 1 equiv.), THF:DMSO 5:1 (v/v) mixture (0.60 mL, 0.1 M), [4-(acetylamino)phenyl]imidodisulfuryl difluoride (22.8 mg, 0.07 mmol, 1.2 equiv.) and 1,8-Diazabicyclo[5.4.0]undec-7-ene (20  $\mu$ L, 0.13 mmol, 2.2 equiv.) for 1 hour. Purification by normal phase column chromatography on amine-functionalised silica (100% CH<sub>2</sub>Cl<sub>2</sub> to methanol:CH<sub>2</sub>Cl<sub>2</sub> 10:90 gradient) yielded **258** (13 mg, 33%) as a white solid. **<sup>1</sup>H NMR** (600 MHz, CD<sub>2</sub>Cl<sub>2</sub>)  $\delta$  = 9.83 (s br, 1H, H30), 9.66 (s, 1H, H24), 8.96 (s, 1H, H2), 8.44 (d, *J* = 5.2 Hz, 1H, H16), 8.24 – 8.19 (m, 1H, H4), 7.92 – 7.87 (m, 2H, H11), 7.68 (s, 1H, H18), 7.61 – 7.53 (m, 3H, H7, H12), 7.36 – 7.30 (m, 2H, H5, H6), 7.29 (d, *J* = 5.2 Hz, 1H, H15), 6.83 (s, 1H, H21), 3.90 (s, 3H, H25), 2.88 (t, *J* = 5.4 Hz, 2H, H27), 2.69 (s, 3H, H26), 2.30 – 2.19 (m, 10H, H28, H29, H32), 1.00 (t, *J* = 7.6 Hz, 3H, H33); **<sup>13</sup>C NMR** (151 MHz, CD<sub>2</sub>Cl<sub>2</sub>)  $\delta$  = 171.87 (C31), 161.74 (C14), 160.40 (C17), 158.67 (C16), 148.66 (C13), 144.28 (C20), 139.72 (C10), 137.75 (C8), 135.24 (C22), 132.44 (C2), 130.15 (C19), 127.57 (2C, C11), 127.18 (C23), 127.02 (C9), 123.54 (C5), 122.50 (3C, C6, C12), 121.25 (C4), 117.24 (C3), 111.34 (C7), 110.27 (C24), 109.06 (C15), 105.19 (C21), 57.82 (C28), 56.82 (C27), 56.47 (C25), 45.68 (2C, C29), 43.82 (C26), 31.05 (C32), 10.17 (C33); **<sup>19</sup>F NMR** (471 MHz, CD<sub>2</sub>Cl<sub>2</sub>)  $\delta$  = 37.22; **HRMS** (ESI+) *m/z* calculated for C<sub>33</sub>H<sub>37</sub>FN<sub>7</sub>O<sub>5</sub>S (M+H)<sup>+</sup> 662.2555, found 662.2551.

**4-(3-(2-((4-((2-(dimethylamino)ethyl)(methyl)amino)-5-isobutyramido-2-methoxyphenyl)amino)pyrimidin-4-yl)-1*H*-indol-1-yl)phenyl sulfurofluoridate (259)**

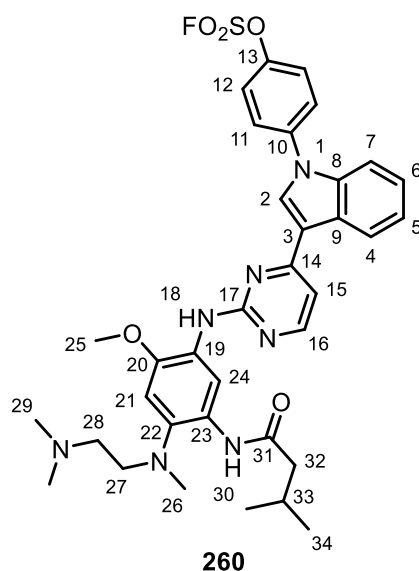


**259**

**259** was prepared following general procedure J, with *N*-(2-((2-(dimethylamino)ethyl)(methyl)amino)-5-((4-(1-(4-hydroxyphenyl)-1*H*-indol-3-yl)pyrimidin-2-yl)amino)-4-methoxyphenyl)isobutyramide **270** (63 mg, 0.11 mmol, 1 equiv.), THF:DMSO 5:1 (v/v) mixture (1.06 mL, 0.1 M), [4-(acetylamino)phenyl]imidodisulfuryl difluoride (40.0, 0.13 mmol, 1.2 equiv.) and 1,8-Diazabicyclo[5.4.0]undec-7-ene (35  $\mu$ L, 0.23 mmol, 2.2 equiv.) for 2 hours. Purification by normal phase column chromatography on amine-functionalised silica (100% CH<sub>2</sub>Cl<sub>2</sub> to methanol:CH<sub>2</sub>Cl<sub>2</sub> 15:85 gradient) yielded **259** (26 mg, 36%) as a white solid. <sup>1</sup>H NMR (500 MHz, CD<sub>2</sub>Cl<sub>2</sub>)  $\delta$  = 9.63 (s br, 1H, H30), 9.61 (s, 1H, H24), 8.95 (s, 1H, H2), 8.44 (d, *J* = 5.2 Hz, 1H, H16), 8.24 – 8.20 (m, 1H, H4), 7.88 – 7.84 (m, 2H, H11), 7.69 (s, 1H, H18), 7.60 – 7.54 (m, 3H, H7, H12), 7.36 – 7.30 (m, 2H, H5, H6), 7.29 (d, *J* = 5.2 Hz, 1H, H15), 6.84 (s, 1H, H21), 3.90 (s, 3H, H25), 2.91 (t, *J* = 6.0 Hz, 2H, H27), 2.67 (s, 3H, H26), 2.43 – 2.35 (m, 1H, H32), 2.25 (t, *J* = 6.0 Hz, 2H, H28), 2.21 (s, 6H, H29), 1.01 (d, *J* = 6.8 Hz, 6H, H33); <sup>13</sup>C NMR (126 MHz, CD<sub>2</sub>Cl<sub>2</sub>)  $\delta$  = 175.01 (C31), 161.81 (C14), 160.44 (C17), 158.63 (C16), 148.74 (C13), 144.29 (C20), 139.77 (C10), 137.90 (C8), 135.24 (C22), 132.27 (C2), 130.18 (C23), 127.75 (2C, C11), 127.25 (C19), 126.99 (C9), 123.55 (C5), 122.67 (2C, C12), 122.48 (C6), 121.26 (C4), 117.26 (C3), 111.30 (C7), 110.24 (C24), 109.16 (C15), 105.24 (C21), 57.91 (C28), 56.49 (C25), 56.44 (C27), 45.74 (2C, C29), 44.05 (C26), 36.86 (C32), 19.75 (2C, C33); <sup>19</sup>F NMR (471 MHz,

CD<sub>2</sub>Cl<sub>2</sub>)  $\delta$  = 37.28; HRMS (ESI+)  $m/z$  calculated for C<sub>34</sub>H<sub>39</sub>FN<sub>7</sub>O<sub>5</sub>S (M+H)<sup>+</sup> 676.2712, found 676.2706.

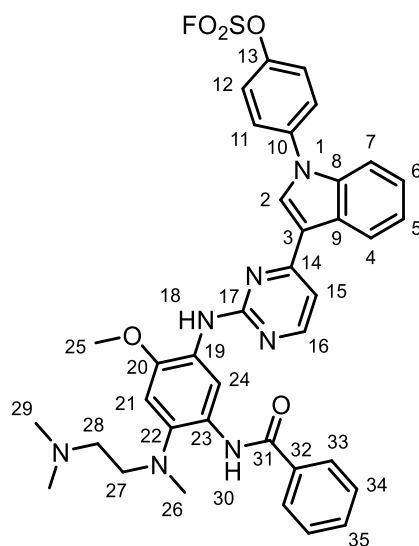
**4-(3-(2-((4-((2-(dimethylamino)ethyl)(methyl)amino)-2-methoxy-5-(3-methylbutanamido)phenyl)amino)pyrimidin-4-yl)-1H-indol-1-yl)phenyl)sulfurofluoridate (260)**



**260** was prepared following general procedure J, with *N*-(2-((2-(dimethylamino)ethyl)(methyl)amino)-5-((4-(1-(4-hydroxyphenyl)-1*H*-indol-3-yl)pyrimidin-2-yl)amino)-4-methoxyphenyl)-3-methylbutanamide **271** (55.0 mg, 0.09 mmol, 1 equiv.), THF:DMSO 5:1 (v/v) mixture (0.90 mL, 0.1 M), [4-(acetylamino)phenyl]imidodisulfuryl difluoride (34.1 mg, 0.11 mmol, 1.2 equiv.) and 1,8-Diazabicyclo[5.4.0]undec-7-ene (30  $\mu$ L, 0.20 mmol, 2.2 equiv.) for 2 hours. Purification by normal phase column chromatography on amine-functionalised silica (100% CH<sub>2</sub>Cl<sub>2</sub> to methanol:CH<sub>2</sub>Cl<sub>2</sub> 15:85 gradient) yielded **260** (34 mg, 54%) as a white solid. <sup>1</sup>H NMR (500 MHz, CD<sub>2</sub>Cl<sub>2</sub>)  $\delta$  = 9.82 (s br, 1H, H30), 9.60 (s, 1H, H24), 8.95 (s, 1H, H2), 8.44 (d,  $J$  = 5.2 Hz, 1H, H16), 8.23 – 8.19 (m, 1H, H4), 7.93 – 7.89 (m, 2H, H11), 7.69 (s, 1H, H18), 7.61 – 7.54 (m, 3H, H7, H12), 7.36 – 7.30 (m, 2H, H5, H6), 7.29 (d,  $J$  = 5.2 Hz, 1H, H15), 6.84 (s, 1H, H21), 3.90 (s, 3H, H25), 2.89 (t,  $J$  = 5.8 Hz, 2H, H27), 2.68 (s, 3H, H26), 2.28 – 2.20 (m, 8H, H28, H29), 2.07 (d,  $J$  = 7.3 Hz, 2H, H32), 1.97 – 1.87 (m, 1H, H33), 0.92 (d,  $J$  = 6.6 Hz, 6H, H34); <sup>13</sup>C NMR (126 MHz, CD<sub>2</sub>Cl<sub>2</sub>)  $\delta$  = 170.50 (C31), 161.76 (C14), 160.43 (C17), 158.66 (C16), 148.64 (C13), 144.41 (C20), 139.69 (C10), 137.74 (C8), 135.29 (C22), 132.33 (C2), 130.20 (C23), 127.58 (2C,

C11), 127.25 (C19), 127.06 (C9), 123.57 (C5), 122.51 (C6), 122.40 (2C, C12), 121.28 (C4), 117.29 (C3), 111.37 (C7), 110.54 (C24), 109.11 (C15), 105.34 (C21), 57.81 (C27), 56.61 (C28), 56.49 (C25), 47.49 (C32), 45.68 (2C, C29), 44.00 (C26), 26.65 (C33), 22.66 (2C, C34);  $^{19}\text{F}$  NMR (471 MHz,  $\text{CD}_2\text{Cl}_2$ )  $\delta = 37.44$ ; HRMS (ESI+)  $m/z$  calculated for  $\text{C}_{35}\text{H}_{41}\text{FN}_7\text{O}_5\text{S}$  ( $\text{M}+\text{H}$ ) $^+$  690.2868, found 690.2869.

**4-(3-(2-((5-benzamido-4-((2-(dimethylamino)ethyl)(methyl)amino)-2-methoxyphenyl)amino)pyrimidin-4-yl)-1H-indol-1-yl)phenyl sulfurofluoridate (261)**

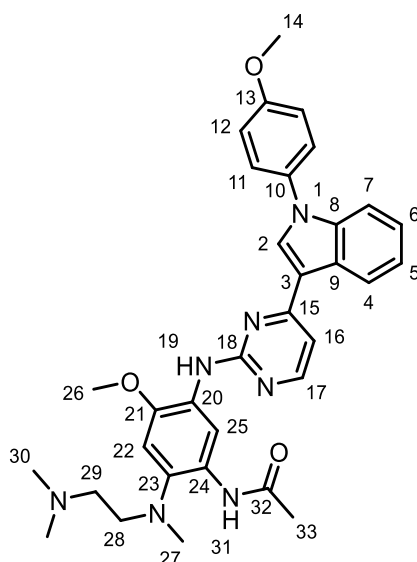


**261**

**261** was prepared following general procedure J, with *N*-(2-((2-(dimethylamino)ethyl)(methyl)amino)-5-((4-(1-(4-hydroxyphenyl)-1H-indol-3-yl)pyrimidin-2-yl)amino)-4-methoxyphenyl)benzamide **272** (52.0 mg, 0.08 mmol, 1 equiv.), THF:DMSO 5:1 (v/v) mixture (0.83 mL, 0.1 M), [4-(acetylamino)phenyl]imidodisulfuryl difluoride (31.2 mg, 0.10 mmol, 1.2 equiv.) and 1,8-Diazabicyclo[5.4.0]undec-7-ene (27  $\mu\text{L}$ , 0.18 mmol, 2.2 equiv.) for 24 hours. Purification by normal phase column chromatography on amine-functionalised silica (100%  $\text{CH}_2\text{Cl}_2$  to methanol: $\text{CH}_2\text{Cl}_2$  15:85 gradient) yielded **261** (8.0 mg, 14%) as a white solid.  $^1\text{H}$  NMR (600 MHz,  $\text{CD}_2\text{Cl}_2$ )  $\delta = 10.58$  (s, 1H, H30), 9.93 (s, 1H, H24), 8.98 (s, 1H, H2), 8.47 (d,  $J = 5.2$  Hz, 1H, H16), 8.20 (d,  $J = 7.9$  Hz, 1H, H4), 7.86 – 7.83 (m, 2H, H11), 7.81 – 7.77 (m, 2H, H33), 7.73 (s, 1H, H18), 7.62 – 7.56 (m, 2H, H7, H35), 7.49 –

7.45 (m, 2H, H34), 7.36 – 7.30 (m, 3H, H5, H6, H15), 7.15 – 7.10 (m, 2H, H12), 6.90 (s, 1H, H21), 3.93 (s, 3H, H25), 2.95 (t,  $J = 5.7$  Hz, 2H, H27), 2.74 (s, 3H, H26), 2.21 (t,  $J = 5.7$  Hz, 2H, H28), 1.97 (s, 6H, H29);  $^{13}\text{C}$  NMR (151 MHz,  $\text{CD}_2\text{Cl}_2$ )  $\delta = 165.51$  (C31), 161.64 (C14), 160.36 (C17), 158.81 (C16), 148.39 (C13), 144.74 (C20), 139.59 (C10), 137.61 (C8), 136.85 (C32), 135.39 (C22), 132.52 (C2), 131.45 (C35), 130.64 (C23), 128.69 (2C, C34), 127.87 (2C, C33), 127.54 (C19), 127.10 (2C, C11), 127.07 (C9), 123.55 (C5), 122.54 (C6), 122.39 (2C, C12), 121.12 (C4), 117.31 (C3), 111.45 (C7), 110.10 (C24), 109.16 (C15), 105.48 (C21), 57.64 (C28), 56.48 (C25), 56.43 (C27), 45.17 (2C, C29), 44.66 (C26);  $^{19}\text{F}$  NMR (471 MHz,  $\text{CD}_2\text{Cl}_2$ )  $\delta = 37.59$ ; HRMS (ESI+)  $m/z$  calculated for  $\text{C}_{37}\text{H}_{37}\text{FN}_7\text{O}_5\text{S}$  (M+H) $^+$  710.2555, found 710.2540.

***N*-((2-((2-(dimethylamino)ethyl)(methyl)amino)-4-methoxy-5-((4-(1-(4-methoxyphenyl)-1*H*-indol-3-yl)pyrimidin-2-yl)amino)phenyl)acetamide (289)**

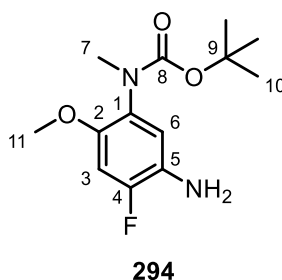


**289**

**289** was prepared following general procedure I, with 3-(2-chloropyrimidin-4-yl)-1-(4-methoxyphenyl)-1*H*-indole **275** (40.0 mg, 0.12 mmol, 1 equiv.), *tert*-butanol (1.19 mL, 0.1 M), *N*-(5-amino-2-((2-(dimethylamino)ethyl)(methyl)amino)-4-methoxyphenyl)acetamide **262** (33.4 mg, 0.12 mmol, 1 equiv.) and *p*-toluenesulfonic acid monohydrate (22.7 mg, 0.12 mmol, 1 equiv.) for 48 hours. Purification by reverse phase column chromatography on C18 (methanol:water +0.1% formic acid 20:80 to 90:10 gradient) then normal phase column chromatography on silica (methanol: $\text{CH}_2\text{Cl}_2$  + 0.07 N ammonia in methanol 1:99 to 20:80 gradient) yielded **289** (39 mg, 56%) as a white

solid. **<sup>1</sup>H NMR** (600 MHz, DMSO-*d*<sub>6</sub>)  $\delta$  = 9.93 (s, 1H, H31), 8.92 (s, 1H, H25), 8.66 (s, 1H, H2), 8.40 (d, *J* = 7.9 Hz, 1H, H4), 8.34 (d, *J* = 5.3 Hz, 1H, H17), 8.01 (s, 1H, H19), 7.62 – 7.58 (m, 2H, H11), 7.44 (d, *J* = 8.3 Hz, 1H, H7), 7.34 (d, *J* = 5.3 Hz, 1H, H16), 7.27 – 7.23 (m, 1H, H6), 7.21 – 7.15 (m, 3H, H5, H12), 7.00 (s, 1H, H22), 3.86 (s, 3H, H14), 3.83 (s, 3H, H26), 2.87 (t, *J* = 5.8 Hz, 2H, H28), 2.71 (s, 3H, H27), 2.30 (t, *J* = 5.8 Hz, 2H, H29), 2.23 (s, 6H, H30), 1.97 (s, 3H, H33); **<sup>13</sup>C NMR** (151 MHz, DMSO-*d*<sub>6</sub>)  $\delta$  = 167.26 (C32), 161.57 (C15), 160.25 (C18), 158.42 (C13), 157.59 (C17), 146.39 (C21), 137.72 (C23), 137.01 (C8), 132.06 (C2), 131.07 (C10), 127.84 (C24), 126.24 (2C, C11), 125.86 (C9), 124.95 (C20), 122.93 (C6), 122.25 (C4), 121.39 (C5), 114.86 (2C, C12), 114.76 (C25), 114.56 (C3), 110.73 (C7), 107.54 (C16), 105.17 (C22), 56.99 (C28), 55.97 (C29), 55.91 (C26), 55.53 (C14), 45.31 (2C, C30), 42.44 (C27), 23.81 (C33); **HRMS** (ESI+) *m/z* calculated for C<sub>33</sub>H<sub>38</sub>N<sub>7</sub>O<sub>3</sub> (M+H)<sup>+</sup> 580.3031, found 580.3014.

***tert*-butyl (5-amino-4-fluoro-2-methoxyphenyl)(methyl)carbamate (294)**



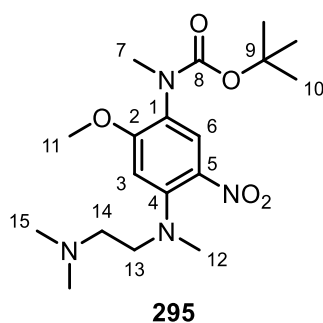
A two-neck round bottom flask heat-dried under vacuum and equipped with magnetic stirrer was charged with *tert*-butyl(4-fluoro-2-methoxy-5-nitrophenyl)carbamate **280** (920 mg, 3.21 mmol, 1 equiv.) and THF (6.43 mL, 0.5 M) under flow of nitrogen. The mixture was cooled to 0 °C and sodium hydride (154 mg, 60% in mineral oil, 3.86 mmol, 1.2 equiv.) was added and stirred for 1 hour. Methyl iodide (0.30 mL, 4.82 mmol, 1.5 equiv.) was then added dropwise, after which the mixture was allowed to warm up to room temperature. After stirring at room temperature for 18 hours, the reaction mixture was quenched with methanol and the solvent was removed under reduced pressure. The crude mixture was purified by normal phase column chromatography on silica (EtOAc:cyclohexane 5:95 to 40:60 gradient) to yield **294** (667 mg, 69%) as a yellow solid. **<sup>1</sup>H NMR** (600 MHz, CDCl<sub>3</sub>)  $\delta$  = 7.97 (s br, 1H, H6), 6.75 (d, *J* = 12.5 Hz, 1H, H3), 3.93 (s, 3H, H11), 3.12 (s, 3H, H7), 1.50 (s br, 9H, H10<sub>minor</sub>), 1.34 (s br, 9H, H10<sub>major</sub>);\* **<sup>13</sup>C NMR** (151 MHz, CDCl<sub>3</sub>)  $\delta$  = 161.05 (C2), 157.09 (d, *J*<sub>C-F</sub> = 265.2 Hz, C4), 155.34



(C8), 154.88 (C5), 129.75 (C1), 129.14 (C6), 101.19 (d,  $J_{C-F} = 25.7$  Hz, C3), 80.70 (C9), 56.78 (C11), 37.10 (C7), 28.33 (3C, C10);  $^{19}\text{F}$  NMR (471 MHz,  $\text{CDCl}_3$ )  $\delta = -112.90$ ; HRMS (ESI+)  $m/z$  calculated for  $\text{C}_8\text{H}_{10}\text{FN}_2\text{O}_3$  (M-Boc+H) $^+$  201.0670, found 201.0664.

\*Rotameric mixture. Resonances for major and minor rotamers are denoted by <sub>major</sub> and <sub>minor</sub> subscripts, respectively.

***tert*-butyl (4-((2-(dimethylamino)ethyl)(methyl)amino)-2-methoxy-5-nitrophenyl)(methyl)carbamate (295)**

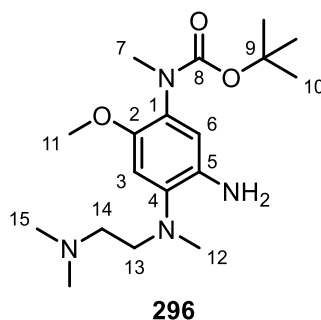


A two-neck round bottom flask equipped with magnetic stirrer was charged with *tert*-butyl (5-amino-4-fluoro-2-methoxyphenyl)(methyl)carbamate **294** (600 mg, 2.00 mmol, 1 equiv.), DMA (6.67 mL, 0.3 M), *N,N*-diisopropylethylamine (0.33 mL, 2.00 mmol, 1 equiv.), and *N,N,N'*-trimethylethylenediamine (0.32 mL, 2.30 mmol, 1.15 equiv.) under flow of nitrogen and heated to 60 °C. After stirring at 60 °C for 2 hours, the reaction mixture was diluted with water (50 mL) and EtOAc (20 mL) and the phases were separated. The aqueous phase was extracted with EtOAc (3 × 20 mL) and the resultant combined organic layers were washed with brine (3 × 50 mL), dried over  $\text{MgSO}_4$ , filtered, and concentrated under reduced pressure. The crude product was purified by normal phase column chromatography on silica (100%  $\text{CH}_2\text{Cl}_2$  to 15:85 methanol: $\text{CH}_2\text{Cl}_2$  gradient) to yield **295** (687 mg, 90%) as a red oil.  $^1\text{H}$  NMR (600 MHz,  $\text{CDCl}_3$ )  $\delta = 7.83$  (s br, 1H,  $\text{H}_{6_{\text{minor}}}$ ), 7.75 (s br, 1H,  $\text{H}_{6_{\text{major}}}$ ), 6.58 (s br, 1H, H3), 3.90 (s, 3H, H11), 3.37 (t,  $J = 7.0$  Hz, 2H, H13), 3.12 (s, 3H, H7), 2.92 (s, 3H, H12), 2.65 (t,  $J = 7.0$  Hz, 2H, H14), 2.32 (s, 6H, H15), 1.53 (s br, 9H,  $\text{H}_{10_{\text{minor}}}$ ), 1.36 (s br, 9H,  $\text{H}_{10_{\text{major}}}$ );\*  $^{13}\text{C}$  NMR (151 MHz,  $\text{CDCl}_3$ )  $\delta = 159.42$  (C2), 155.31 (C8), 147.55 (C4), 132.14 (C5), 128.33 ( $\text{C}_{6_{\text{minor}}}$ ), 127.43 ( $\text{C}_{6_{\text{major}}}$ ), 124.43 (C1), 101.88 ( $\text{C}_{3_{\text{minor}}}$ ), 101.37 ( $\text{C}_{3_{\text{major}}}$ ), 80.39 ( $\text{C}_{9_{\text{minor}}}$ ), 79.87 ( $\text{C}_{9_{\text{major}}}$ ), 56.57 (C14), 56.06 ( $\text{C}_{11_{\text{minor}}}$ ), 55.78 ( $\text{C}_{11_{\text{major}}}$ ), 53.26 (C13), 45.65 (2C, C15),

40.97 (C12<sub>minor</sub>), 40.62 (C12<sub>major</sub>), 37.59 (C7<sub>minor</sub>), 36.87 (C7<sub>major</sub>), 28.25 (3C, C10);\* **HRMS** (ESI+)  $m/z$  calculated for C<sub>18</sub>H<sub>31</sub>N<sub>4</sub>O<sub>5</sub> (M+H)<sup>+</sup> 383.2289, found 383.2263;

\*Rotameric mixture. Resonances for major and minor rotamers are denoted by <sub>major</sub> and <sub>minor</sub> subscripts, respectively.

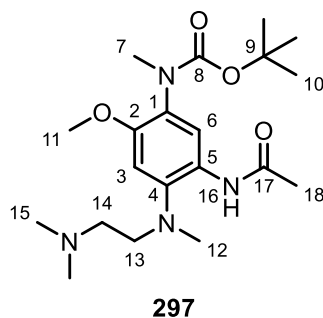
***tert*-butyl (5-amino-4-((2-(dimethylamino)ethyl)(methyl)amino)-2-methoxyphenyl)(methyl)carbamate (296)**



A two-neck round bottom flask equipped with magnetic stirrer was charged with *tert*-butyl 4-((2-(dimethylamino)ethyl)(methyl)amino)-2-methoxy-5-nitrophenylcarbamate **295** (658 mg, 1.72 mmol, 1 equiv.), methanol (11.5 mL, 0.15 M) and palladium on activated carbon (65.0 mg, 10 wt.% Pd) under flow of nitrogen. The flask was degassed and backfilled with hydrogen three times, and then stirred at room temperature. After stirring at room temperature for 2 hours, then flask was degassed and backfilled with nitrogen, then the reaction mixture was filtered through celite and concentrated under reduced pressure. The crude product was purified by normal phase column chromatography on silica (methanol:CH<sub>2</sub>Cl<sub>2</sub> + 0.07 N ammonia in methanol 1:99 to 15:85 gradient) to yield **296** (525 mg, 87%) as a light brown oil. **<sup>1</sup>H NMR** (600 MHz, CDCl<sub>3</sub>)  $\delta$  = 6.71 – 6.44 (m, 2H, H3, H6), 3.73 (s, 3H, H11), 3.09 (s, 3H, H7), 2.97 (t,  $J$  = 6.6 Hz, 2H, H13), 2.67 (s br, 3H, H12), 2.45 (t,  $J$  = 6.6 Hz, 2H, H14), 2.29 (s, 6H, H15), 1.50 (s br, 9H, H10<sub>minor</sub>), 1.34 (s br, 9H, H10<sub>major</sub>);\* **<sup>13</sup>C NMR** (151 MHz, CDCl<sub>3</sub>)  $\delta$  = 155.87 (C8), 147.71 (C2), 138.63 (C4), 136.00 (C5), 129.32 (C1), 116.13 (C6<sub>minor</sub>), 115.54 (C6<sub>major</sub>), 107.08 (C3<sub>minor</sub>), 106.02 (C3<sub>major</sub>), 79.86 (C9<sub>minor</sub>), 79.35 (C9<sub>major</sub>), 57.72 (C14), 56.93 (C11<sub>minor</sub>), 56.52 (C11<sub>major</sub>), 54.45 (C13), 45.98 (2C, C15), 41.96 (C12), 37.69 (C7<sub>minor</sub>), 37.07 (C7<sub>major</sub>), 28.46 (3C, C10);\* **HRMS** (ESI+)  $m/z$  calculated for C<sub>18</sub>H<sub>33</sub>N<sub>4</sub>O<sub>3</sub> (M+H)<sup>+</sup> 353.2547, found 353.2546.

\*Rotameric mixture. Resonances for major and minor rotamers are denoted by <sub>major</sub> and <sub>minor</sub> subscripts, respectively.

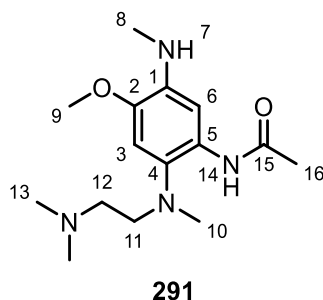
***tert*-butyl (5-acetamido-4-((2-(dimethylamino)ethyl)(methyl)amino)-2-methoxyphenyl)(methyl)carbamate (**297**)**



**297** was prepared following general procedure G, with *tert*-butyl (5-amino-4-((2-(dimethylamino)ethyl)(methyl)amino)-2-methoxyphenyl)(methyl)carbamate **296** (200 mg, 0.57 mmol, 1 equiv.), CH<sub>2</sub>Cl<sub>2</sub> (1.13 mL, 0.5 M), triethylamine (87 μL, 0.62 mmol, 1.1 equiv.) and acetyl chloride (45 μL, 0.57 mmol, 1 equiv.) for 18 hours to yield **297** (167 mg, 75%) as a brown oil. <sup>1</sup>H NMR (600 MHz, CDCl<sub>3</sub>) δ = 9.80 (s br, 1H, H16), 8.24 (s, 1H, H6), 6.71 (s br, 1H, H3), 3.77 (s, 3H, H11), 3.12 (s, 3H, H7), 2.86 (app. s br, 2H, H13), 2.69 (s, 3H, H12), 2.30 (app. s br, 8H, H14, H15), 2.14 (s br, 3H, H18), 1.49 (s br, 9H, H10<sub>minor</sub>), 1.34 (s, 9H, H10<sub>major</sub>);\* <sup>13</sup>C NMR (151 MHz, CDCl<sub>3</sub>) δ = 168.53 (C17), 155.62 (C8), 151.02 (C2), 140.87 (C4), 129.62 (C5), 129.09 (C1), 120.58 (C6), 106.43 (C3<sub>minor</sub>), 105.44 (C3<sub>major</sub>), 79.92 (C9<sub>minor</sub>), 79.47 (C9<sub>major</sub>), 57.36 (C14), 56.27 (C13), 55.84 (C11), 45.73 (2C, C15), 42.89 (C12), 37.67 (C7<sub>minor</sub>), 36.88 (C7<sub>major</sub>), 28.39 (3C, C10), 24.51 (C18);\* HRMS (ESI+) m/z calculated for C<sub>20</sub>H<sub>35</sub>N<sub>4</sub>O<sub>4</sub> (M+H)<sup>+</sup> 395.2653, found 395.2640.

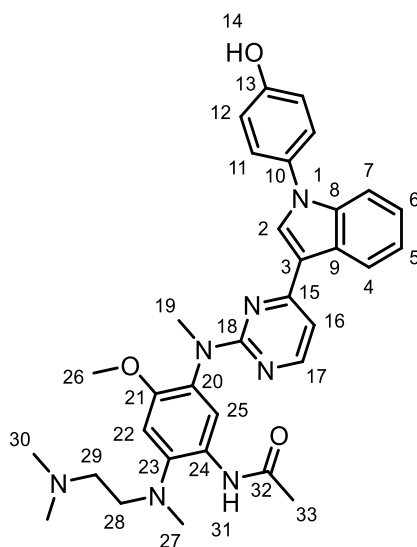
\*Rotameric mixture. Resonances for major and minor rotamers are denoted by <sub>major</sub> and <sub>minor</sub> subscripts, respectively.

***N*-2-((2-(dimethylamino)ethyl)(methyl)amino)-4-methoxy-5-(methylamino)phenylacetamide (**291**)**



**291** was prepared following general procedure H, with *tert*-butyl (5-acetamido-4-((2-(dimethylamino)ethyl)(methyl)amino)-2-methoxyphenyl)(methyl)carbamate **297** (153 mg, 0.39 mmol, 1 equiv.), CH<sub>2</sub>Cl<sub>2</sub> (1.29 mL, 0.3 M), lithium iodide (125 mg, 0.93 mmol, 2.4 equiv.) and chlorotrimethylsilane (0.12 mL, 0.93 mmol, 2.4 equiv.) to yield **291** (94 mg, 82%) as a pink oil. <sup>1</sup>H NMR (600 MHz, CDCl<sub>3</sub>) δ = 9.87 (s br, 1H, H14), 7.72 (s, 1H, H6), 6.63 (s, 1H, H3), 4.12 (s br, 1H, H7), 3.79 (s, 3H, H9), 2.91 – 2.82 (m, 5H, H8, H11), 2.64 (s, 3H, H10), 2.31 – 2.22 (m, 8H, H12, H13), 2.14 (s, 3H, H16); <sup>13</sup>C NMR (151 MHz, CDCl<sub>3</sub>) δ = 168.42 (C15), 143.15 (C2), 137.32 (C4), 130.75 (C5), 129.69 (C1), 104.11 (C3), 101.96 (C6), 57.45 (C12), 56.38 (C11), 55.89 (C9), 45.38 (2C, C13), 44.48 (C10), 30.62 (C8), 24.70 (C16); HRMS (ESI+) *m/z* calculated for C<sub>15</sub>H<sub>27</sub>N<sub>4</sub>O<sub>2</sub> (M+H)<sup>+</sup> 295.2129, found 295.2115.

***N*-2-((2-(dimethylamino)ethyl)(methyl)amino)-5-((4-(1-(4-hydroxyphenyl)-1*H*-indol-3-yl)pyrimidin-2-yl)(methyl)amino)-4-methoxyphenyl)acetamide (**292**)**



**292**

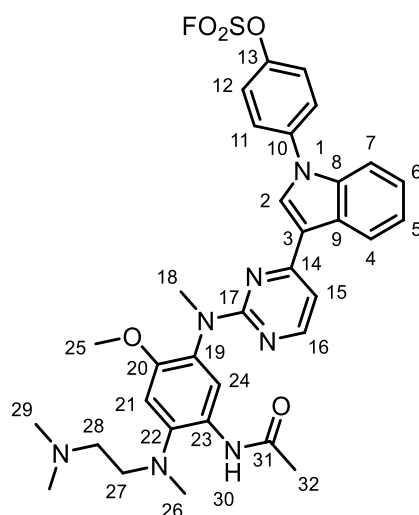
**292** was prepared following general procedure I, with 4-(3-(2-chloropyrimidin-4-yl)-1*H*-indol-1-yl)phenol **267** (92.9 mg, 0.29 mmol, 1 equiv.), *tert*-butanol (2.72 mL, 0.1 M), *N*-2-((2-(dimethylamino)ethyl)(methyl)amino)-4-methoxy-5-(methylamino)phenyl)acetamide **291** (85.0 mg, 0.29 mmol, 1 equiv.) and *p*-toluenesulfonic acid monohydrate (54.9 mg, 0.29 mmol, 1 equiv.) for 48 hours. Purification by reverse phase column chromatography on C18 (methanol:water +0.1% formic acid 20:80 to 100% methanol gradient) then normal phase column chromatography on silica (methanol:CH<sub>2</sub>Cl<sub>2</sub> + 0.07 N ammonia in methanol 1:99 to 20:80 gradient) yielded **292** (45 mg, 27%) as a white solid. <sup>1</sup>H NMR (600 MHz, DMSO-d<sub>6</sub>) δ = 9.89 (s, 1H, H31), 9.81 (s, 1H, H14), 8.67 (s br, 1H, H25<sub>minor</sub>), 8.50 – 8.05 (m, 3H, H2, H4, H17), 7.68 (s br, 1H, H25<sub>major</sub>), 7.49 – 6.71 (m, 9H, H5, H6, H7, H11, H12, H16, H22), 3.68 (s, 3H, H26), 3.40 (s br, 3H, H19), 2.92 (app. s br, 2H, H28), 2.78 (s br, 3H, H27), 2.43 – 2.38 (m, 2H, H29), 2.25 (s, 6H, H30), 2.03 (s, 3H, H33); \*<sup>13</sup>C NMR (151 MHz, DMSO-d<sub>6</sub>) δ = 167.57 (C32), 162.00 (C15), 161.62 (C18), 156.79 (C13), 156.63 (C17), 151.42 (C21), 141.86 (C23), 136.92 (C8), 131.45 (C2), 129.92 (ambiguous), 129.67 (C10), 128.06 (ambiguous), 126.14 (2C, C11), 126.07 (ambiguous), 122.72 (2C, C5, C6), 121.00 (C4), 116.13 (2C, C12), 114.49 (C3), 110.38 (C7), 106.33 (C22), 105.66 (C16), 57.07 (C29), 56.19 (C28), 55.69 (C26), 45.56 (2C, C30), 41.70 (C27), 23.89

(C33);\*<sup>2</sup> **HRMS** (ESI+)  $m/z$  calculated for  $C_{33}H_{38}N_7O_3$  (M+H)<sup>+</sup> 580.3031, found 580.3032.

\*<sup>1</sup>Rotameric mixture, most peaks are highly broad and many overlap. Resonances for major and minor rotamers are denoted by <sub>major</sub> and <sub>minor</sub> subscripts, respectively.

\*<sup>2</sup>Rotameric mixture, three <sup>13</sup>C resonances have ambiguous assignment. Two resonances not observed in spectrum.

**4-(3-(2-((5-acetamido-4-((2-(dimethylamino)ethyl)(methyl)amino)-2-methoxyphenyl)(methyl)amino)pyrimidin-4-yl)-1H-indol-1-yl)phenyl sulfurofluoridate (290)**



**290**

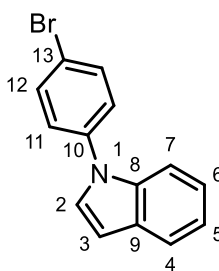
**290** was prepared following general procedure J, with *N*-(2-((2-(dimethylamino)ethyl)(methyl)amino)-5-((4-(1-(4-hydroxyphenyl)-1*H*-indol-3-yl)pyrimidin-2-yl)(methyl)amino)-4-methoxyphenyl)acetamide **292** (40.0 mg, 0.07 mmol, 1 equiv.), THF:DMSO 5:1 (v/v) mixture (0.69 mL, 0.1 M), [4-(acetylamino)phenyl]imidodisulfuryl difluoride (26.0 mg, 0.08 mmol, 1.2 equiv.) and 1,8-Diazabicyclo[5.4.0]undec-7-ene (23  $\mu$ L, 0.15 mmol, 2.2 equiv.) for 3 hours. Purification by normal phase column chromatography on amine-functionalised silica (100%  $CH_2Cl_2$  to methanol: $CH_2Cl_2$  15:85 gradient) yielded **290** (25 mg, 55%) as a white solid. <sup>1</sup>H NMR (500 MHz,  $CD_2Cl_2$ )  $\delta$  = 9.96 (s, 1H, H30), 8.38 (app. s, 1H, H4), 8.27 (app. s br, 1H, H16), 7.96 (s br, 1H, H2), 7.74 – 7.64 (m, 2H, H11), 7.60 – 7.49 (m, 3H, H7, H12), 7.36 – 7.00 (m, 2H, H5, H6), 6.96 – 6.88 (m, 2H, H15, H21), 3.75 (s, 3H, H25),

3.50 (s br, 3H, H18), 2.96 – 2.89 (m, 2H, H27), 2.79 (s, 3H, H26), 2.40 (t,  $J = 5.3$  Hz, 2H, H28), 2.31 (s, 6H, H29), 2.09 (s, 3H, H32);\*<sup>1</sup> <sup>13</sup>C NMR (126 MHz, CD<sub>2</sub>Cl<sub>2</sub>)  $\delta = 168.48$  (C31), 162.95 (C14), 161.67 (C17), 157.62 (C16), 151.97 (C20), 148.62 (C13), 141.69 (C22), 139.78 (C10), 137.38 (C8), 131.54 (C23), 129.99 (C19), 129.62 (C2), 127.46 (ambiguous), 126.83 (2C, C11), 123.84 (C5), 123.49 (ambiguous), 122.92 (2C, C12), 122.27 (C6), 121.32 (C4), 117.83 (C3), 110.65 (C7), 106.82 (C15), 106.12 (C21), 57.93 (C28), 57.51 (C27), 56.38 (C25), 46.08 (2C, C29), 42.52 (C26), 38.18 (C18), 24.48 (C32);\*<sup>2</sup> <sup>19</sup>F NMR (471 MHz, CD<sub>2</sub>Cl<sub>2</sub>)  $\delta = 37.46$ ; HRMS (ESI+)  $m/z$  calculated for C<sub>33</sub>H<sub>37</sub>FN<sub>7</sub>O<sub>5</sub>S (M+H)<sup>+</sup> 662.2555, found 662.2553.

\*<sup>1</sup>H24 not observed in spectrum due to highly broad aromatic region arising from rotameric exchange.

\*<sup>2</sup>Two <sup>13</sup>C resonances have ambiguous assignment.

### 1-(4-bromophenyl)-1H-indole (304)



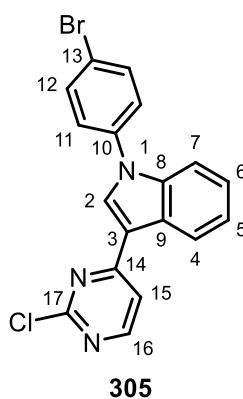
**304**

A two-neck round bottom flask equipped with magnetic stirrer and reflux condenser was charged with indole **303** (1.00 g, 8.54 mmol, 1 equiv.), DMF (85.4 mL, 0.1 M), 1-bromo-4-fluorobenzene **306** (1.88 mL, 17.1 mmol, 2 equiv.) and K<sub>3</sub>PO<sub>4</sub> (9.06 g, 42.7 mmol, 5 equiv.) under flow of nitrogen. The mixture was heated to reflux for 18 hours, after which the reaction mixture was diluted with 10% LiCl (w/v) solution (200 mL) and EtOAc (200 mL) and the phases were separated. The organic layer was washed with 10% LiCl (w/v) solution (2 × 200 mL), dried over MgSO<sub>4</sub>, filtered, and concentrated under reduced pressure. The crude product was purified by reverse phase column chromatography on C18 (methanol:water +0.1% formic acid 40:60 to 100% methanol gradient) then normal phase column chromatography on silica (100% cyclohexane to 5:95 EtOAc:cyclohexane gradient) to yield **304** (1.85 g, 80%) as a light green oil. <sup>1</sup>H NMR (600 MHz, acetone-d<sub>6</sub>)

$\delta = 7.78 - 7.74$  (m, 2H, H12), 7.66 (d,  $J = 7.8$  Hz, 1H, H4), 7.59 – 7.55 (m, 3H, H7, H11), 7.53 (d,  $J = 3.3$  Hz, 1H, H2), 7.24 – 7.20 (m, 1H, H6), 7.16 – 7.12 (m, 1H, H5), 6.71 (app. d,  $J = 3.3$  Hz, 1H, H3);  $^{13}\text{C NMR}$  (151 MHz, acetone- $d_6$ )  $\delta = 139.93$  (C10), 136.49 (C8), 133.66 (2C, C12), 130.65 (C9), 128.74 (C2), 126.76 (2C, C11), 123.39 (C6), 121.99 (C4), 121.39 (C5), 119.92 (C13), 111.10 (C7), 104.95 (C3); **HRMS** (ESI+)  $m/z$  calculated for  $\text{C}_{14}\text{H}_{11}^{79}\text{BrN}$  (M+H) $^+$  272.0069, found 272.0079.

The spectroscopic and analytical data were in agreement with literature values.<sup>287</sup>

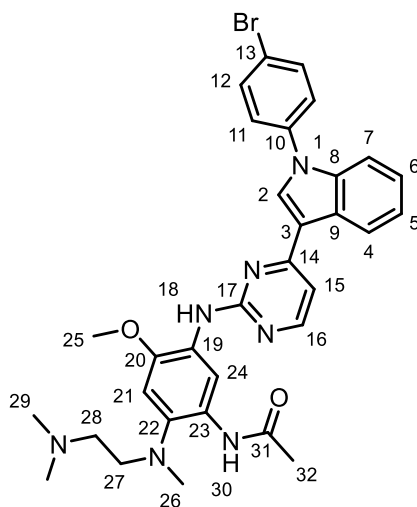
### 1-(4-bromophenyl)-3-(2-chloropyrimidin-4-yl)-1*H*-indole (305)



A two-neck round bottom flask heat-dried under vacuum and equipped with magnetic stirrer and reflux condenser was charged with 1-(4-bromophenyl)-1*H*-indole **304** (1.85 g, 6.80 mmol, 1 equiv.), DME (27.2 mL, 0.25 M), 2,4-dichloropyrimidine (1.01 g, 6.80 mmol, 1 equiv.), iron (III) chloride (1.10 g, 6.80 mmol, 1 equiv.) under flow of nitrogen and heated to 80 °C. After stirring at 80 °C for 72 hours, the solvent was removed under reduced pressure and the crude product was purified by normal phase column chromatography on silica (100%  $\text{CH}_2\text{Cl}_2$  isocratic) to yield **305** (410 mg, 16%) as a yellow solid.  $^1\text{H NMR}$  (600 MHz,  $\text{DMSO}-d_6$ )  $\delta = 8.84$  (s, 1H, H2), 8.63 (d, 1H,  $J = 5.5$  Hz, H16), 8.58 (m, 1H, H4), 8.04 (d,  $J = 5.5$  Hz, 1H, H15), 7.86 – 7.83 (m, 2H, H12), 7.71 – 7.68 (m, 2H, H11), 7.61 – 7.58 (m, 1H, H7), 7.39 – 7.33 (m, 2H, H5, H6);  $^{13}\text{C NMR}$  (151 MHz,  $\text{DMSO}-d_6$ )  $\delta = 164.33$  (C14), 160.29 (C17), 159.06 (C16), 137.14 (C10), 136.53 (C8), 133.25 (C2), 132.85 (2C, C12), 126.65 (2C, C11), 125.97 (C9), 124.00 (C5), 122.65 (C6), 122.28 (C4), 120.44 (C13), 115.24 (C15), 113.54 (C3), 111.16 (C7); **HRMS** (ESI+)  $m/z$  calculated for  $\text{C}_{18}\text{H}_{12}^{79}\text{Br}^{35}\text{ClN}_3$  (M+H) $^+$  383.9898, found 385.9890.



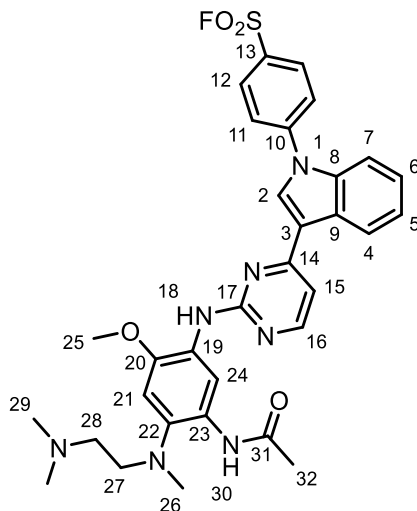
***N*-(5-((4-(1-(4-bromophenyl)-1*H*-indol-3-yl)pyrimidin-2-yl)amino)-2-((2-(dimethylamino)ethyl)(methyl)amino)-4-methoxyphenyl)acetamide (302)**



**302**

**302** was prepared following general procedure I, with 1-(4-bromophenyl)-3-(2-chloropyrimidin-4-yl)-1*H*-indole **305** (200 mg, 0.52 mmol, 1 equiv.), *tert*-butanol (5.20 mL, 0.1 M), *N*-(5-amino-2-((2-(dimethylamino)ethyl)(methyl)amino)-4-methoxyphenyl)acetamide **262** (146 mg, 0.52 mmol, 1 equiv.) and *p*-toluenesulfonic acid monohydrate (98.9 mg, 0.52 mmol, 1 equiv.) for 36 hours. Purification by reverse phase column chromatography on C18 (methanol:water +0.1% formic acid 20:80 to 90:10 gradient) then normal phase column chromatography on silica (methanol:CH<sub>2</sub>Cl<sub>2</sub> + 0.07 N ammonia in methanol 1:99 to 15:95 gradient) yielded **302** (126 mg, 39%) as an off-white foam. <sup>1</sup>H NMR (600 MHz, DMSO-d<sub>6</sub>) δ = 9.93 (s, 1H, H30), 8.93 (s, 1H, H24), 8.75 (s, 1H, H2), 8.41 (d, *J* = 7.7 Hz, 1H, H4), 8.37 (d, *J* = 5.3 Hz, 1H, H16), 8.04 (s, 1H, H18), 7.83 – 7.80 (m, 2H, H12), 7.71 – 7.68 (m, 2H, H11), 7.56 (d, *J* = 8.2 Hz, 1H, H7), 7.36 (d, *J* = 5.3 Hz, 1H, H15), 7.31 – 7.27 (m, 1H, H6), 7.25 – 7.21 (m, 1H, H5), 7.00 (s, 1H, H21), 3.83 (s, 3H, H25), 2.87 (t, *J* = 5.8 Hz, 2H, H27), 2.71 (s, 3H, H26), 2.30 (t, *J* = 5.8 Hz, 2H, H28), 2.23 (s, 6H, H29), 1.98 (s, 3H, H32); <sup>13</sup>C NMR (151 MHz, DMSO-d<sub>6</sub>) δ = 167.28 (C31), 161.30 (C14), 160.25 (C17), 157.79 (C16), 146.36 (C20), 137.71 (C22), 137.48 (C10), 136.38 (C8), 132.65 (2C, C12), 131.57 (C2), 127.87 (C23), 126.70 (2C, C11), 126.21 (C9), 124.92 (C19), 123.30 (C6), 122.33 (C4), 121.78 (C5), 119.88 (C13), 115.51 (C3), 114.60 (C24), 110.81 (C7), 107.70 (C15), 105.21 (C21), 56.99 (C28), 55.98 (C27), 55.92 (C25), 45.32 (2C, C29), 42.44 (C26), 23.81 (C32); HRMS (ESI+) *m/z* calculated for C<sub>32</sub>H<sub>35</sub><sup>79</sup>BrN<sub>7</sub>O<sub>2</sub> (M+H)<sup>+</sup> 628.2030, found 628.2034.

**4-(3-(2-((5-acetamido-4-((2-(dimethylamino)ethyl)(methyl)amino)-2-methoxyphenyl)amino)pyrimidin-4-yl)-1*H*-indol-1-yl)benzenesulfonyl fluoride (298)**

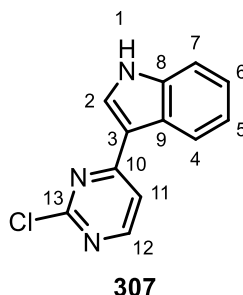


**298**

**298** was prepared following general procedure K, with *N*-(5-((4-(1-(4-bromophenyl)-1*H*-indol-3-yl)pyrimidin-2-yl)amino)-2-((2-(dimethylamino)ethyl)(methyl)amino)-4-methoxyphenyl)acetamide **302** (90.0 mg, 0.14 mmol, 1 equiv.), isopropanol (0.53 mL, 0.27 M), DABSO (20.6 mg, 0.09 mmol, 0.6 equiv.), PdCl<sub>2</sub>(AmPhos)<sub>2</sub> (5.1 mg, 0.01 mmol, 5 mol%), triethylamine (60 μL, 0.43 mmol, 3 equiv.) and NFSI (67.7 mg, 0.21 mmol, 1.5 equiv.). Purification by reverse phase column chromatography on C18 (methanol:water +0.1% formic acid 20:80 to 90:10 gradient) then normal phase column chromatography on amine-functionalised silica (100% CH<sub>2</sub>Cl<sub>2</sub> to methanol:CH<sub>2</sub>Cl<sub>2</sub> 15:85 gradient) yielded **298** (3.2 mg, 4%) as a yellow gel. <sup>1</sup>H NMR (600 MHz, CD<sub>2</sub>Cl<sub>2</sub>) δ = 10.09 (s, 1H, H30), 9.70 (s, 1H, H24), 9.06 (s, 1H, H2), 8.46 (d, *J* = 5.2 Hz, 1H, H16), 8.21 – 8.17 (m, 5H, H4, H11, H12), 7.74 – 7.71 (m, 2H, H7, H18), 7.39 – 7.36 (m, 2H, H5, H6), 7.30 (d, *J* = 5.2 Hz, 1H, H15), 6.84 (s, 1H, H21), 3.90 (s, 3H, H25), 2.89 – 2.84 (m, 2H, H27), 2.70 (s, 3H, H26), 2.31 – 2.23 (m, 8H, H28, H29), 2.03 (s, 3H, H32); <sup>13</sup>C NMR (151 MHz, CD<sub>2</sub>Cl<sub>2</sub>) δ = 168.09 (C31), 161.30 (C14), 160.42 (C17), 158.87 (C16), 145.83 (C10), 144.28 (C20), 137.11 (C8), 135.30 (C22), 131.98 (C2), 130.39 (2C, C12), 130.18 (d, *J*<sub>C-F</sub> = 22.3 Hz, C13), 130.13 (C27), 127.65 (C9), 127.11 (C19), 125.89 (2C, C11), 124.02 (C5), 123.04 (C6), 121.34 (C4), 118.62 (C3), 111.60 (C7), 110.12 (C24), 109.35 (C15), 105.17 (C21), 57.77 (C28), 57.08 (C27), 56.46 (C25), 45.65 (2C, C29),

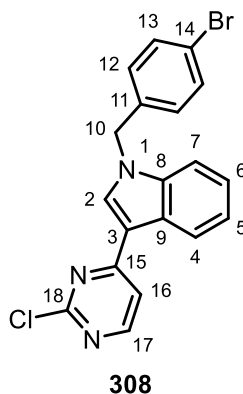
43.64 (C26), 24.56 (C32);  $^{19}\text{F}$  NMR (471 MHz,  $\text{CD}_2\text{Cl}_2$ )  $\delta = 66.16$ ; HRMS (ESI+)  $m/z$  calculated for  $\text{C}_{32}\text{H}_{35}\text{FN}_7\text{O}_4\text{S}$  ( $\text{M}+\text{H}$ ) $^+$  632.2450, found 632.2443.

### 3-(2-chloropyrimidin-4-yl)-1H-indole (307)



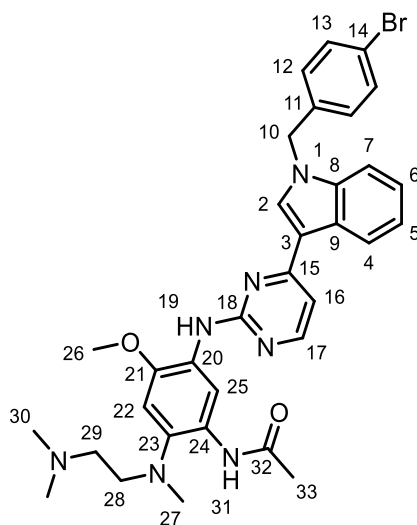
A two-neck round bottom flask heat-dried under vacuum and equipped with magnetic stirrer was charged with indole **303** (4.50 g, 38.4 mmol, 1 equiv.) and DCE (154 mL, 0.25 M) under flow of nitrogen. The mixture was cooled to 0 °C and methylmagnesium bromide (14.1 mL, 3M in diethyl ether, 42.3 mmol, 1.1 equiv.) was added and stirred for 15 minutes. 2,4-dichloropyrimidine (5.84 g, 38.4 mmol, 1 equiv.) was then added, after which the mixture was allowed to warm up to room temperature. After stirring at room temperature for 18 hours, the reaction mixture was quenched with methanol and the solvent was removed under reduced pressure. The crude mixture was purified by normal phase column chromatography on silica (100%  $\text{CH}_2\text{Cl}_2$  to 5:95 methanol: $\text{CH}_2\text{Cl}_2$  gradient) then reverse phase column chromatography on C18 (methanol:water +0.1% formic acid 40:60 to 100% methanol gradient). The resultant solid was washed with methanol (3 x 10 mL) to yield **307** (1.68 g, 19%) as a yellow solid.  $^1\text{H}$  NMR (600 MHz,  $\text{DMSO-d}_6$ )  $\delta = 12.08$  (s, 1H, H1), 8.55 – 8.50 (m, 2H, H2, H12), 8.44 – 8.40 (m, 1H, H4), 7.91 (d,  $J = 5.5$  Hz, 1H, H11), 7.52 – 7.49 (m, 1H, H7), 7.26 – 7.20 (m, 2H, H5, H6);  $^{13}\text{C}$  NMR (151 MHz,  $\text{DMSO-d}_6$ )  $\delta = 165.04$  (C13), 160.28 (C10), 158.57 (C12), 137.25 (C8), 131.09 (C2), 124.89 (C9), 122.72 (C5), 121.57 (C4), 121.38 (C6), 114.54 (C11), 112.37 (C7), 111.85 (C3); HRMS (ESI+)  $m/z$  calculated for  $\text{C}_{12}\text{H}_9^{35}\text{ClN}_3$  ( $\text{M}+\text{H}$ ) $^+$  230.0479, found 230.0478.

The spectroscopic and analytical data were in agreement with literature values.<sup>298</sup>

**1-(4-bromobenzyl)-3-(2-chloropyrimidin-4-yl)-1*H*-indole (308)**

A two-neck round bottom flask heat-dried under vacuum and equipped with magnetic stirrer was charged with 3-(2-chloropyrimidin-4-yl)-1*H*-indole **307** (100 mg, 0.44 mmol, 1 equiv.) and DMF (0.87 mL, 0.5 M) under flow of nitrogen. The mixture was cooled to 0 °C and sodium hydride (39.2 mg, 60% in mineral oil, 0.98 mmol, 2.25 equiv.) was added and stirred for 15 minutes. 4-bromobenzyl bromide (218 mg, 0.87 mmol, 2 equiv.) was then added, after which the mixture was allowed to warm up to room temperature. After stirring at room temperature for 18 hours, the reaction mixture was diluted with water (10 mL) and EtOAc (10 mL) and the phases were separated. The aqueous phase was extracted with EtOAc (2 × 10 mL) and the resultant combined organic layers were washed with 10% LiCl (w/v) solution (3 × 10 mL), dried over MgSO<sub>4</sub>, filtered, and concentrated under reduced pressure. The crude product was purified by normal phase column chromatography on silica (EtOAc:cyclohexane 10:90 to 50:50 gradient) to yield **308** (125 mg, 72%) as a pale yellow solid. <sup>1</sup>H NMR (600 MHz, DMSO-*d*<sub>6</sub>) δ = 8.71 (s, 1H, H2), 8.57 (d, *J* = 5.5 Hz, 1H, H17), 8.44 – 8.40 (m, 1H, H4), 7.87 (d, *J* = 5.5 Hz, 1H, H16), 7.60 – 7.56 (m, 1H, H7), 7.55 – 7.52 (m, 2H, H13), 7.28 – 7.24 (m, 4H, H5, H6, H12), 5.53 (s, 2H, H10); <sup>13</sup>C NMR (151 MHz, DMSO-*d*<sub>6</sub>) δ = 164.35 (C15), 160.29 (C18), 158.98 (C17), 137.02 (C8), 136.54 (C11), 134.09 (C2), 131.63 (2C, C13), 129.47 (2C, C12), 125.50 (C9), 123.03 (C5), 121.90 (C6), 121.76 (C4), 120.88 (C14), 114.66 (C16), 111.61 (C3), 111.28 (C7), 49.06 (C10); HRMS (ESI+) *m/z* calculated for C<sub>19</sub>H<sub>14</sub><sup>79</sup>Br<sup>35</sup>ClN<sub>3</sub> (M+H)<sup>+</sup> 398.0054, found 398.0068.

***N*-5-((4-(1-(4-bromobenzyl)-1*H*-indol-3-yl)pyrimidin-2-yl)amino)-2-((2-(dimethylamino)ethyl)(methyl)amino)-4-methoxyphenyl)acetamide (**309**)**

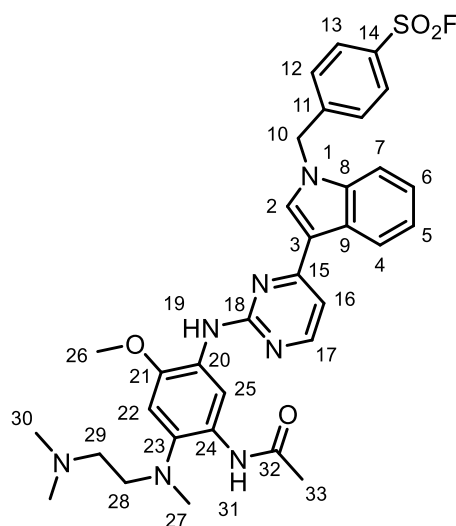


**309**

**309** was prepared following general procedure I, with 1-(4-bromobenzyl)-3-(2-chloropyrimidin-4-yl)-1*H*-indole **308** (100 mg, 0.25 mmol, 1 equiv.), *tert*-butanol (2.51 mL, 0.1 M), *N*-(5-amino-2-((2-(dimethylamino)ethyl)(methyl)amino)-4-methoxyphenyl)acetamide **262** (70.3 mg, 0.25 mmol, 1 equiv.) and *p*-toluenesulfonic acid monohydrate (47.7 mg, 0.25 mmol, 1 equiv.) for 18 hours. Purification by reverse phase column chromatography on C18 (methanol:water +0.1% formic acid 20:80 to 100% methanol gradient) then normal phase column chromatography on silica (methanol:CH<sub>2</sub>Cl<sub>2</sub> + 0.07 N ammonia in methanol 1:99 to 10:90 gradient) yielded **309** (84 mg, 52%) as a pale yellow solid. <sup>1</sup>H NMR (600 MHz, DMSO-*d*<sub>6</sub>) δ = 9.99 (s, 1H, H31), 9.02 (s, 1H, H25), 8.87 (s, 1H, H2), 8.34 (d, *J* = 5.3 Hz, 1H, H17), 8.24 (d, *J* = 7.8 Hz, 1H, H4), 7.90 (s, 1H, H19), 7.54 – 7.50 (m, 3H, H7, H13), 7.30 – 7.26 (m, 2H, H12), 7.24 (d, *J* = 5.3 Hz, 1H, H16), 7.21 – 7.17 (m, 1H, H6), 7.16 – 7.12 (m, 1H, H5), 7.00 (s, 1H, H22), 5.54 (s, 2H, H10), 3.84 (s, 3H, H26), 2.87 (t, *J* = 5.6 Hz, 2H, H28), 2.70 (s, 3H, H27), 2.32 – 2.27 (m, 2H, H29), 2.22 (s, 6H, H30), 2.01 (s, 3H, H33); <sup>13</sup>C NMR (151 MHz, DMSO-*d*<sub>6</sub>) δ = 167.44 (C32), 161.42 (C15), 159.95 (C18), 157.84 (C17), 145.81 (C21), 137.26 (C23), 136.98 (C11), 136.88 (C8), 133.27 (C2), 131.54 (2C, C13), 129.39 (2C, C12), 127.95 (C24), 125.62 (C9), 125.24 (C20), 122.23 (C6), 121.58 (C4), 121.00 (C5), 120.70 (C14), 113.79 (C25), 113.29 (C3), 110.94 (C7), 107.21 (C16), 105.20 (C22), 56.93 (C29), 56.00 (C26), 55.86 (C28), 48.88 (C10), 45.23 (2C, C30), 42.62 (C27), 23.98

(C33); **HRMS** (ESI+)  $m/z$  calculated for  $C_{33}H_{37}^{79}BrN_7O_2$  (M+H)<sup>+</sup> 642.2187, found 642.2197.

**4-((3-(2-((5-acetamido-4-((2-(dimethylamino)ethyl)(methyl)amino)-2-methoxyphenyl)amino)pyrimidin-4-yl)-1H-indol-1-yl)methyl)benzenesulfonyl fluoride (299)**

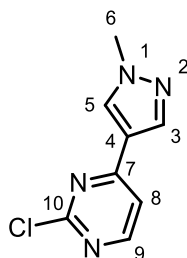


**299**

**299** was prepared following general procedure K, with *N*-(5-((4-(1-(4-bromobenzyl)-1*H*-indol-3-yl)pyrimidin-2-yl)amino)-2-((2-(dimethylamino)ethyl)(methyl)amino)-4-methoxyphenyl)acetamide **309** (40 mg, 0.06 mmol, 1 equiv.), isopropanol (0.23 mL, 0.27 M), DABSO (9.0 mg, 0.04 mmol, 0.6 equiv.), PdCl<sub>2</sub>(AmPhos)<sub>2</sub> (2.2 mg, 3.1 μmol, 5 mol%), triethylamine (26 μL, 0.19 mmol, 3 equiv.) and NFSI (58.9 mg, 0.19 mmol, 3 equiv.). Purification by reverse phase column chromatography on C18 (methanol:water +0.1% formic acid 20:80 to 90:10 gradient) then normal phase column chromatography on amine-functionalised silica (100% CH<sub>2</sub>Cl<sub>2</sub> to methanol:CH<sub>2</sub>Cl<sub>2</sub> 10:90 gradient) yielded **299** (4.5 mg, 11%) as a yellow gel. <sup>1</sup>H NMR (600 MHz, CD<sub>2</sub>Cl<sub>2</sub>) δ = 10.14 (s, 1H, H31), 9.66 (s, 1H, H25), 9.38 (s, 1H, H2), 8.40 (d, *J* = 5.2 Hz, 1H, H17), 8.10 (d, *J* = 8.2 Hz, 1H, H4), 7.95 – 7.92 (m, 2H, H13), 7.72 (s, 1H, H19), 7.58 – 7.55 (m, 2H, H12), 7.29 – 7.22 (m, 4H, H5, H6, H7, H16), 6.84 (s, 1H, H22), 5.74 (s, 2H, H10), 3.91 (s, 3H, H26), 2.87 (t, *J* = 5.6 Hz, 2H, H28), 2.70 (s, 3H, H27), 2.27 – 2.23 (m, 8H, H29, H30), 1.98 (s, 3H, H33); <sup>13</sup>C NMR (151 MHz, CD<sub>2</sub>Cl<sub>2</sub>) δ = 168.09 (C32), 161.77 (C15), 160.12 (C18), 158.80 (C17), 146.72 (C11), 144.34 (C21), 137.76 (C8), 135.32 (C2), 135.12 (C23), 132.29 (d, *J*<sub>C-F</sub> = 24.1 Hz, C14), 130.19 (C24), 129.28 (2C, C13), 128.62 (2C,

C12), 127.59 (C20), 126.58 (C9), 122.70 (C5), 121.80 (C6), 120.90 (C4), 115.06 (C3), 110.84 (C25), 110.04 (C7), 108.25 (C16), 105.25 (C22), 57.70 (C29), 56.93 (C28), 56.46 (C26), 50.24 (C10), 45.52 (2C, C30), 43.91 (C27), 24.69 (C33); **<sup>19</sup>F NMR** (471 MHz, CD<sub>2</sub>Cl<sub>2</sub>)  $\delta$  = 65.50; **HRMS** (ESI+)  $m/z$  calculated for C<sub>33</sub>H<sub>37</sub>FN<sub>7</sub>O<sub>4</sub>S (M+H)<sup>+</sup> 646.2606, found 646.2613.

### 2-chloro-4-(1-methyl-1*H*-pyrazol-4-yl)pyrimidine (**315**)

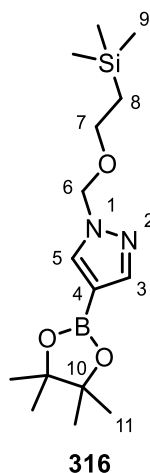


**315**

A two-neck round bottom flask equipped with magnetic stirrer was charged with 2,4-dichloropyrimidine (500 mg, 3.36 mmol, 1 equiv.), acetonitrile:water 1:1 (v/v) mixture (16.8 mL, 0.2 M), 1-methylpyrazole-4-boronic acid pinacol ester **314** (768 mg, 3.69 mmol, 1.1 equiv.), PdCl<sub>2</sub>(dtbpf) (109 mg, 0.17 mmol, 5 mol%), K<sub>2</sub>CO<sub>3</sub> (928 mg, 6.71 mmol, 2 equiv.), and degassed and backfilled with argon four times. The mixture was heated to 80 °C for 18 hours, after which the solvent was removed under reduced pressure and the crude mixture was purified by normal phase column chromatography on silica (EtOAc:cyclohexane 20:80 to 70:30 gradient) to yield **315** (310 mg, 48%) as a white solid. **<sup>1</sup>H NMR** (600 MHz, DMSO-*d*<sub>6</sub>)  $\delta$  = 8.63 (d,  $J$  = 5.3 Hz, 1H, H9), 8.55 (s, 1H, H5), 8.17 (s, 1H, H3), 7.75 (d,  $J$  = 5.3 Hz, 1H, H8), 3.91 (s, 3H, H6); **<sup>13</sup>C NMR** (151 MHz, DMSO-*d*<sub>6</sub>)  $\delta$  = 161.80 (C10), 160.41 (C7), 160.16 (C9), 138.64 (C3), 132.12 (C5), 119.30 (C4), 115.03 (C8), 38.96 (C6); **HRMS** (ESI+)  $m/z$  calculated for C<sub>8</sub>H<sub>8</sub><sup>35</sup>ClN<sub>4</sub> (M+H)<sup>+</sup> 195.0432, found 195.0434.

The spectroscopic and analytical data were in agreement with literature values.<sup>299</sup>

**4-(4,4,5,5-tetramethyl-1,3,2-dioxaborolan-2-yl)-1-((2-(trimethylsilyl)ethoxy)methyl)-1H-pyrazole (316)**

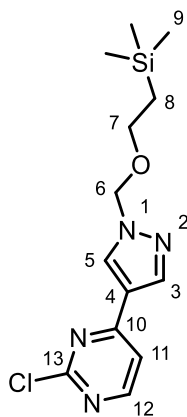


A two-neck round bottom flask equipped with magnetic stirrer was charged with 4-pyrazoleboronic acid pinacol ester **313** (2.16 g, 11.1 mmol, 1 equiv.), NMP (18.5 mL, 0.6 M), K<sub>2</sub>CO<sub>3</sub> (3.07 g, 22.2 mmol, 2 equiv.) and 2-(trimethylsilyl)ethoxymethylchloride (2.16 mL, 12.2 mmol, 1.1 equiv.) under flow of nitrogen. After stirring at room temperature for 20 hours, the reaction mixture was diluted with water (200 mL) and EtOAc (100 mL) and the phases were separated. The aqueous phase was extracted with EtOAc (2 × 100 mL) and the resultant combined organic layers were washed with water (3 × 200 mL), brine (200 mL), dried over MgSO<sub>4</sub>, filtered, and concentrated under reduced pressure. The crude product was purified by normal phase column chromatography on silica (EtOAc:cyclohexane 5:95 to 40:60 gradient) to yield **316** (1.79 g, 50%) as a colourless oil. <sup>1</sup>H NMR (600 MHz, acetone-d<sub>6</sub>) δ = 7.96 (s, 1H, H5), 7.64 (s, 1H, H3), 5.46 (s, 2H, H6), 3.63 – 3.59 (m, 2H, H7), 1.29 (s, 12H, H11), 0.90 – 0.86 (m, 2H, H8), -0.02 (m, 9H, H9); <sup>13</sup>C NMR (151 MHz, acetone-d<sub>6</sub>) δ = 146.01 (C3), 137.93 (C5), 83.87 (2C, C10), 80.35 (C6), 67.05 (C7), 25.13 (4C, C11), 18.25 (C8), -1.32 (3C, C9);\* HRMS (ESI+) m/z calculated for C<sub>15</sub>H<sub>30</sub>BN<sub>2</sub>O<sub>3</sub>Si (M+H)<sup>+</sup> 325.2113, found 325.2111.

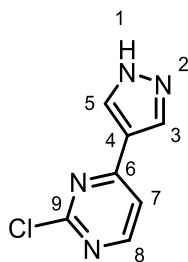
\*C4 not observed in spectrum.

The spectroscopic and analytical data were in agreement with literature values.<sup>300</sup>

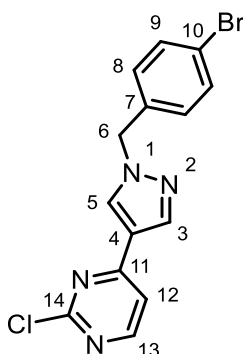


**2-chloro-4-(1-((2-(trimethylsilyl)ethoxy)methyl)-1H-pyrazol-4-yl)pyrimidine (317)****317**

A two-neck round bottom flask equipped with magnetic stirrer was charged with 2,4-dichloropyrimidine (818 mg, 5.49 mmol, 1 equiv.), acetonitrile:water 1:1 (v/v) mixture (27.4 mL, 0.2 M), 4-(4,4,5,5-tetramethyl-1,3,2-dioxaborolan-2-yl)-1-((2-(trimethylsilyl)ethoxy)methyl)-1H-pyrazole **316** (1.78 g, 5.49 mmol, 1.1 equiv.), PdCl<sub>2</sub>(dtbpf) (178 mg, 0.27 mmol, 5 mol%), K<sub>2</sub>CO<sub>3</sub> (1.52 g, 11.0 mmol, 2 equiv.), and degassed and backfilled with argon four times. The mixture was heated to 80 °C for 18 hours, after which the solvent was removed under reduced pressure and the crude mixture was purified by normal phase column chromatography on silica (EtOAc:cyclohexane 5:95 to 30:70 gradient) to yield **317** (1.17 g, 68%) as a pale yellow solid. <sup>1</sup>H NMR (600 MHz, acetone-d<sub>6</sub>) δ = 8.61 – 8.59 (m, 2H, H5, H12), 8.20 (s, 1H, H3), 7.73 (d, *J* = 5.2 Hz, 1H, H11), 5.55 (s, 2H, H6), 3.70 – 3.66 (m, 2H, H7), 0.94 – 0.90 (m, 2H, H8), -0.02 (s, 9H, H9); <sup>13</sup>C NMR (151 MHz, acetone-d<sub>6</sub>) δ = 162.91 (C10), 162.14 (C13), 160.87 (C12), 139.87 (C3), 132.25 (C5), 121.76 (C4), 115.86 (C11), 81.24 (C6), 67.45 (C7), 18.28 (C8), -1.33 (3C, C9); HRMS (ESI+) *m/z* calculated for C<sub>13</sub>H<sub>20</sub><sup>35</sup>ClN<sub>4</sub>OSi (M+H)<sup>+</sup> 311.1089, found 311.1094.

**2-chloro-4-(1*H*-pyrazol-4-yl)pyrimidine (310)****310**

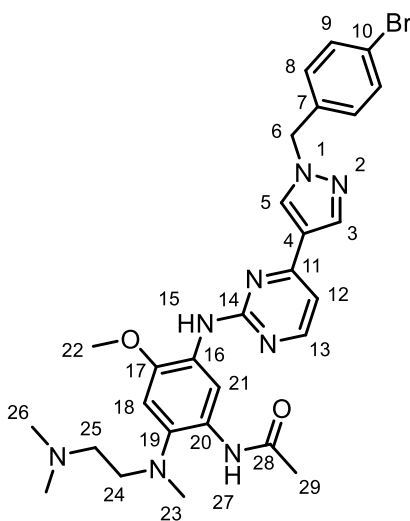
A two-neck round bottom flask equipped with magnetic stirrer was charged with 2-chloro-4-(1-((2-(trimethylsilyl)ethoxy)methyl)-1*H*-pyrazol-4-yl)pyrimidine **317** (500 mg, 1.61 mmol, 1 equiv.) and 1.6 M HCl in dioxane (10.72 mL, 0.15 M) under flow of nitrogen. After stirring at room temperature for 18 hours, the reaction mixture was quenched with sat. NaHCO<sub>3</sub> solution (20 mL) and then concentrated under reduced pressure. The crude mixture was purified by normal phase column chromatography on silica (EtOAc:cyclohexane 20:80 to 100% EtOAc gradient) to yield **310** (248 mg, 85%) as a white solid. <sup>1</sup>H NMR (600 MHz, DMSO-*d*<sub>6</sub>) δ = 13.46 (s, 1H, H1), 8.63 (d, *J* = 5.3 Hz, 1H, H8), 8.60 (s br, 1H, H5), 8.21 (s br, 1H, H3), 7.80 (d, *J* = 5.3 Hz, 1H, H7); <sup>13</sup>C NMR (151 MHz, DMSO-*d*<sub>6</sub>) δ = 162.25 (C6), 160.41 (C9), 160.07 (C8), 138.54 (C3), 130.09 (C5), 118.88 (C4), 115.29 (C7); HRMS (ESI+) *m/z* calculated for C<sub>7</sub>H<sub>6</sub><sup>35</sup>ClN<sub>4</sub> (M+H)<sup>+</sup> 181.0276, found 181.0280;

**4-(1-(4-bromobenzyl)-1*H*-pyrazol-4-yl)-2-chloropyrimidine (311)****311**

A glass microwave vial equipped with magnetic stirrer was charged with 2-chloro-4-(1*H*-pyrazol-4-yl)pyrimidine **310** (220 mg, 1.22 mmol, 1 equiv.) and DMF (2.44 mL, 0.5 M)

under flow of nitrogen.  $\text{K}_2\text{CO}_3$  (337 mg, 2.44 mmol, 2 equiv.) was added and stirred for 30 minutes at room temperature, followed by 4-bromobenzyl bromide (609 mg, 2.44 mmol, 2 equiv.). After stirring at room temperature for 18 hours, the reaction mixture was diluted with toluene (20 mL) and concentrated under reduced pressure. The crude mixture was purified by normal phase column chromatography on silica (EtOAc:cyclohexane 10:90 to 50:50 gradient) to yield **311** (388 mg, 91%) as an off-white solid.  $^1\text{H NMR}$  (600 MHz,  $\text{DMSO-d}_6$ )  $\delta$  = 8.72 (s, 1H, H5), 8.64 (d,  $J$  = 5.3 Hz, 1H, H13), 8.24 (s, 1H, H3), 7.78 (d,  $J$  = 5.3 Hz, 1H, H12), 7.58 – 7.55 (m, 2H, H9), 7.28 – 7.25 (m, 2H, H8), 5.39 (s, 2H, H6);  $^{13}\text{C NMR}$  (151 MHz,  $\text{DMSO-d}_6$ )  $\delta$  = 161.65 (C11), 160.40 (C14), 160.27 (C13), 139.27 (C3), 136.14 (C7), 131.82 (C5), 131.54 (2C, C9), 130.07 (2C, C8), 121.12 (C10), 119.66 (C4), 115.17 (C12), 54.46 (C6); **HRMS** (ESI+)  $m/z$  calculated for  $\text{C}_{14}\text{H}_{11}^{79}\text{Br}^{35}\text{ClN}_4$  (M+H) $^+$  348.9850, found 348.9851.

***N*-(5-((4-(1-(4-bromobenzyl)-1*H*-pyrazol-4-yl)pyrimidin-2-yl)amino)-2-((2-(dimethylamino)ethyl)(methyl)amino)-4-methoxyphenyl)acetamide (312)**

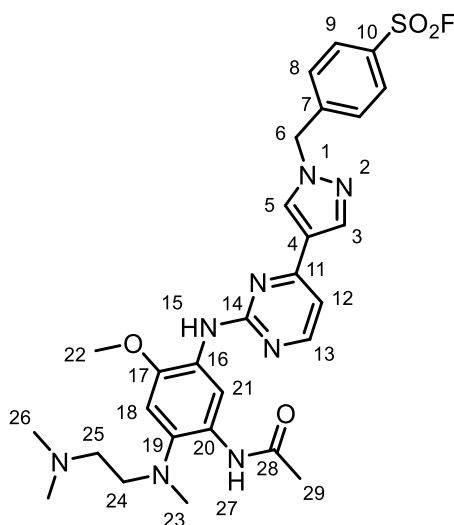


**312**

**312** was prepared following general procedure I, with 4-(1-(4-bromobenzyl)-1*H*-pyrazol-4-yl)-2-chloropyrimidine **311** (350 mg, 1.00 mmol, 1 equiv.), *tert*-butanol (10.0 mL, 0.1 M), *N*-(5-amino-2-((2-(dimethylamino)ethyl)(methyl)amino)-4-methoxyphenyl)acetamide **262** (281 mg, 1.00 mmol, 1 equiv.) and *p*-toluenesulfonic acid monohydrate (190 mg, 1.00 mmol, 1 equiv.) for 48 hours. Purification by reverse phase column chromatography on C18 (methanol:water +0.1% formic acid 20:80 to 90:10 gradient) then normal phase column chromatography on silica (methanol: $\text{CH}_2\text{Cl}_2$  + 0.07 N ammonia in methanol 1:99 to 15:95 gradient) yielded **312** (110 mg, 19%) as an off-

white foam.  $^1\text{H NMR}$  (600 MHz, DMSO- $d_6$ )  $\delta$  = 9.99 (s, 1H, H27), 9.31 (s, 1H, H21), 9.02 (s, 1H, H5), 8.36 (d,  $J$  = 5.2 Hz, 1H, H13), 8.30 (s, 1H, H3), 7.77 (s, 1H, H15), 7.58 – 7.55 (m, 2H, H9), 7.32 – 7.29 (m, 2H, H8), 7.11 (d,  $J$  = 5.2 Hz, 1H, H12), 6.99 (s, 1H, H18), 5.37 (s, 2H, H6), 3.86 (s, 3H, H22), 2.85 (t,  $J$  = 5.7 Hz, 2H, H24), 2.68 (s, 3H, H23), 2.28 – 2.24 (m, 2H, H25), 2.22 (s, 6H, H26), 2.08 (s, 3H, H29);  $^{13}\text{C NMR}$  (151 MHz, DMSO- $d_6$ )  $\delta$  = 167.45 (C28), 159.54 (C14), 158.95 (C11), 158.53 (C13), 144.16 (C17), 138.94 (C3), 136.53 (C4), 136.05 (C19), 131.71 (C5), 131.51 (2C, C9), 129.98 (2C, C8), 128.27 (C20), 125.41 (C16), 121.44 (C4), 121.01 (C10), 111.17 (C21), 107.37 (C12), 105.17 (C18), 56.91 (C25), 56.13 (C22), 55.86 (C24), 54.56 (C6), 45.21 (2C, C26), 42.71 (C23), 24.12 (C29); **HRMS** (ESI+)  $m/z$  calculated for  $\text{C}_{28}\text{H}_{34}^{79}\text{BrN}_8\text{O}_2$  (M+H) $^+$  593.1983, found 593.1982.

**4-((4-(2-((5-acetamido-4-((2-(dimethylamino)ethyl)(methyl)amino)-2-methoxyphenyl)amino)pyrimidin-4-yl)-1H-pyrazol-1-yl)methyl)benzenesulfonyl fluoride (300)**



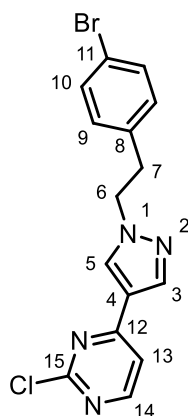
**300**

**300** was prepared following general procedure K, with *N*-(5-((4-(1-(4-bromobenzyl)-1*H*-pyrazol-4-yl)pyrimidin-2-yl)amino)-2-((2-(dimethylamino)ethyl)(methyl)amino)-4-methoxyphenyl)acetamide **312** (104 mg, 0.18 mmol, 1 equiv.), isopropanol (0.70 mL, 0.25 M), DABSO (25.3 mg, 0.11 mmol, 0.6 equiv.),  $\text{PdCl}_2(\text{AmPhos})_2$  (6.2 mg, 0.01 mmol, 5 mol%), triethylamine (73  $\mu\text{L}$ , 0.53 mmol, 3 equiv.) and NFSI (166 mg, 0.53 mmol, 3 equiv.). Purification by reverse phase column chromatography on C18 (methanol:water +0.1% formic acid 20:80 to 90:10 gradient) then normal phase column

chromatography on amine-functionalised silica (100% CH<sub>2</sub>Cl<sub>2</sub> to methanol:CH<sub>2</sub>Cl<sub>2</sub> 10:90 gradient) yielded **300** (15 mg, 14%) as an off-white foam. <sup>1</sup>H NMR (600 MHz, CD<sub>2</sub>Cl<sub>2</sub>) δ = 10.14 (s, 1H, H27), 9.63 (s, 1H, H21), 9.45 (s, 1H, H5), 8.32 (d, *J* = 5.1 Hz, 1H, H13), 8.03 (s, 1H, H3), 8.00 – 7.97 (m, 2H, H9), 7.74 (s, 1H, H15), 7.70 – 7.67 (m, 2H, H8), 6.88 (d, *J* = 5.1 Hz, 1H, H12), 6.83 (s, 1H, H18), 5.54 (s, 2H, H6), 3.89 (s, 3H, H22), 2.87 (t, *J* = 5.5 Hz, 2H, H24), 2.70 (s, 3H, H23), 2.27 – 2.23 (m, 8H, H25, H26), 2.10 (s, 3H, H29); <sup>13</sup>C NMR (151 MHz, CD<sub>2</sub>Cl<sub>2</sub>) δ = 168.14 (C28), 160.36 (C14), 159.60 (C11), 158.87 (C13), 145.89 (C7), 144.20 (C17), 139.12 (C3), 135.20 (C19), 133.54 (C5), 130.20 (C20), 129.54 (2C, C8), 129.23 (2C, C9), 127.34 (C16), 122.96 (C4), 109.84 (C21), 107.41 (C12), 105.24 (C18), 57.73 (C25), 56.96 (C24), 56.45 (C22), 55.74 (C6), 45.58 (2C, C26), 43.84 (C23), 24.86 (C29);\* <sup>19</sup>F NMR (471 MHz, CD<sub>2</sub>Cl<sub>2</sub>) δ = 65.55; HRMS (ESI+) *m/z* calculated for C<sub>28</sub>H<sub>34</sub>FN<sub>8</sub>O<sub>4</sub>S (M+H)<sup>+</sup> 597.2402, found 597.2393.

\*C10 not observed in spectrum.

#### 4-(1-(4-bromophenethyl)-1*H*-pyrazol-4-yl)-2-chloropyrimidine (**318**)

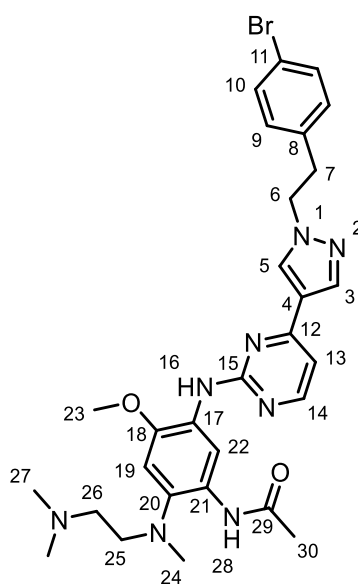


**318**

A glass microwave vial equipped with magnetic stirrer was charged with 2-chloro-4-(1*H*-pyrazol-4-yl)pyrimidine **310** (310 mg, 1.72 mmol, 1 equiv.) and DMF (3.43 mL, 0.5 M) under flow of nitrogen. K<sub>2</sub>CO<sub>3</sub> (475 mg, 3.43 mmol, 2 equiv.) was added and stirred for 30 minutes at room temperature, followed by 4-bromophenethyl bromide (0.52 mL, 3.43 mmol, 2 equiv.). After stirring at room temperature for 18 hours, the reaction mixture was diluted with toluene (30 mL) and concentrated under reduced pressure. The crude mixture was purified by normal phase column chromatography on silica (EtOAc:cyclohexane 10:90 to 50:50 gradient) to yield **318** (436 mg, 70%) as a white solid. <sup>1</sup>H NMR (600

MHz, DMSO- $d_6$ )  $\delta$  = 8.62 (d,  $J$  = 5.3 Hz, 1H, H14), 8.50 (s, 1H, H5), 8.20 (s, 1H, H3), 7.73 (d,  $J$  = 5.3 Hz, 1H, H13), 7.46 – 7.43 (m, 2H, H10), 7.15 – 7.11 (m, 2H, H9), 4.42 (t,  $J$  = 7.2 Hz, 2H, H6), 3.14 (t,  $J$  = 7.2 Hz, 2H, H7);  $^{13}\text{C}$  NMR (151 MHz, DMSO- $d_6$ )  $\delta$  = 161.75 (C12), 160.40 (C15), 160.19 (C14), 138.74 (C3), 137.48 (C8), 131.58 (C5), 131.22 (2C, C10), 130.97 (2C, C9), 119.61 (C11), 119.04 (C4), 115.04 (C13), 52.50 (C6), 34.85 (C7); HRMS (ESI+)  $m/z$  calculated for  $\text{C}_{15}\text{H}_{13}^{79}\text{Br}^{35}\text{ClN}_4$  (M+H) $^+$  363.0007, found 363.0016.

***N***-5-((4-(1-(4-bromophenethyl)-1*H*-pyrazol-4-yl)pyrimidin-2-yl)amino)-2-((2-(dimethylamino)ethyl)(methyl)amino)-4-methoxyphenyl)acetamide (**319**)

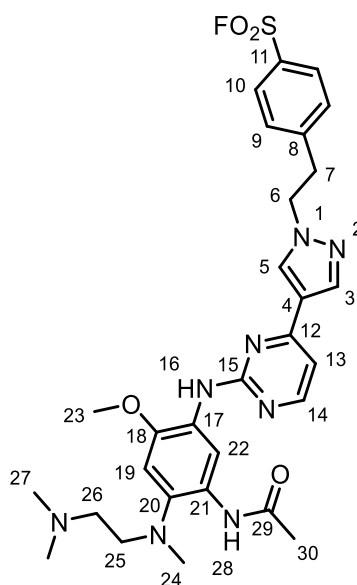


**319**

**319** was prepared following general procedure I, with 4-(1-(4-bromophenethyl)-1*H*-pyrazol-4-yl)-2-chloropyrimidine **318** (423 mg, 1.16 mmol, 1 equiv.), *tert*-butanol (11.0 mL, 0.1 M), *N*-(5-amino-2-((2-(dimethylamino)ethyl)(methyl)amino)-4-methoxyphenyl)acetamide **262** (326 mg, 1.16 mmol, 1 equiv.) and *p*-toluenesulfonic acid monohydrate (221 mg, 1.16 mmol, 1 equiv.) for 18 hours. Purification by reverse phase column chromatography on C18 (methanol:water +0.1% formic acid 20:80 to 90:10 gradient) then normal phase column chromatography on silica (methanol: $\text{CH}_2\text{Cl}_2$  + 0.07 N ammonia in methanol 1:99 to 15:95 gradient) yielded **319** (190 mg, 27%) as an off-white foam.  $^1\text{H}$  NMR (600 MHz, DMSO- $d_6$ )  $\delta$  = 10.01 (s, 1H, H28), 9.31 (s, 1H, H22), 8.84 (s, 1H, H5), 8.35 (d,  $J$  = 5.2 Hz, 1H, H14), 8.25 (s, 1H, H3), 7.75 (s, 1H, H16), 7.47 – 7.43 (s, 2H, H10), 7.19 – 7.15 (m, 2H, H9), 7.07 (d,  $J$  = 5.2 Hz, 1H, H13), 7.00 (s, 1H,

H19), 4.41 (t,  $J = 7.2$  Hz, 2H, H6), 3.87 (s, 3H, H23), 3.21 (t,  $J = 7.2$  Hz, 2H, H7), 2.85 (t,  $J = 5.6$  Hz, 2H, H25), 2.68 (s, 3H, H24), 2.29 – 2.19 (m, 8H, H26, H27), 2.09 (s, 3H, H30);  $^{13}\text{C}$  NMR (151 MHz, DMSO- $d_6$ )  $\delta = 167.41$  (C29), 159.52 (C15), 159.08 (C12), 158.45 (C14), 144.10 (C18), 138.32 (C3), 137.69 (C8), 135.98 (C20), 131.23 (3C, C5, C10), 130.94 (2C, C9), 128.31 (C21), 125.47 (C17), 120.84 (C4), 119.56 (C11), 111.06 (C22), 107.31 (C13), 105.17 (C19), 56.92 (C26), 56.15 (C23), 55.89 (C25), 52.57 (C6), 45.21 (2C, C27), 42.76 (C24), 34.80 (C7), 24.16 (C30); HRMS (ESI+)  $m/z$  calculated for  $\text{C}_{29}\text{H}_{36}^{79}\text{BrN}_8\text{O}_2$  (M+H) $^+$  607.2139, found 607.2144.

**4-(2-(4-(2-((5-acetamido-4-((2-(dimethylamino)ethyl)(methyl)amino)-2-methoxyphenyl)amino)pyrimidin-4-yl)-1H-pyrazol-1-yl)ethyl)benzenesulfonyl fluoride (301)**



**301**

**301** was prepared following general procedure K, with *N*-(5-((4-(1-(4-bromophenethyl)-1H-pyrazol-4-yl)pyrimidin-2-yl)amino)-2-((2-(dimethylamino)ethyl)(methyl)amino)-4-methoxyphenyl)acetamide **319** (185 mg, 0.30 mmol, 1 equiv.), isopropanol (1.13 mL, 0.27 M), DABSO (43.9 mg, 0.18 mmol, 0.6 equiv.), PdCl<sub>2</sub>(AmPhos)<sub>2</sub> (10.8 mg, 0.02 mmol, 5 mol%), triethylamine (0.13 mL, 0.91 mmol, 3 equiv.) and NFSI (288 mg, 0.91 mmol, 3 equiv.). Purification by reverse phase column chromatography on C18 (methanol:water +0.1% formic acid 20:80 to 90:10 gradient) then normal phase column chromatography on amine-functionalised silica (100% CH<sub>2</sub>Cl<sub>2</sub> to methanol:CH<sub>2</sub>Cl<sub>2</sub> 15:85 gradient) yielded **301** (14 mg, 8%) as an off-white solid.  $^1\text{H}$  NMR (600 MHz, acetone-

$d_6$ )  $\delta$  = 10.15 (s, 1H, H28), 9.78 (s, 1H, H22), 9.28 (s, 1H, H5), 8.33 (d,  $J$  = 5.1 Hz, 1H, H14), 8.15 (s, 1H, H3), 8.03 – 8.00 (m, 2H, H10), 7.73 – 7.69 (m, 3H, H9, H16), 7.07 – 7.03 (m, 2H, H13, H19), 4.61 (t,  $J$  = 7.1 Hz, 2H, H6), 3.95 (s, 3H, H23), 3.57 (t,  $J$  = 7.1 Hz, 2H, H7), 2.93 (t,  $J$  = 5.5 Hz, 2H, H25), 2.73 (s, 3H, H24), 2.31 – 2.26 (m, 8H, H26, H27), 2.17 (s, 3H, H30);  $^{13}\text{C}$  NMR (151 MHz, acetone- $d_6$ )  $\delta$  = 168.20 (C29), 160.90 (C15), 160.54 (C12), 159.34 (C14), 149.23 (C8), 144.43 (C18), 138.90 (C3), 135.62 (C20), 133.08 (C5), 131.57 (2C, C9), 130.87 (C21), 129.40 (2C, C10), 127.76 (C17), 122.61 (C4), 110.37 (C22), 107.93 (C13), 105.89 (C19), 58.19 (C26), 57.25 (C25), 56.58 (C23), 53.27 (C6), 45.72 (2C, C27), 43.74 (C24), 36.71 (C7), 24.83 (C30);\*  $^{19}\text{F}$  NMR (471 MHz, acetone- $d_6$ )  $\delta$  = 65.03; HRMS (ESI+)  $m/z$  calculated for  $\text{C}_{29}\text{H}_{36}\text{FN}_8\text{O}_4\text{S}$  (M+H) $^+$  611.2559, found 611.2555;

\*C11 not observed in spectrum.

## 8.2 Biochemical Assays

### 8.2.1 Fluorescence Polarisation

FP procedures were adapted from Pettinger et al.<sup>145</sup>

#### 8.2.1.1 General Experimental

The aqueous buffer contained 50 mM Tris base pH 7.4, 150 mM KCl, 5 mM CaCl<sub>2</sub> and 0.1% (w/w) CHAPS. The assay was conducted using 384 Plus F ProxiPlates (PerkinElmer) with a final assay volume of 10  $\mu\text{L}$ . Plates were centrifuged at 1000 rpm for 1 minute prior to incubation and read using a BMG Labtech PHERAstar FSX microplate reader. Excitation and emission wavelengths used were 485 nm and 520 nm, respectively. Fluorescence polarisation was measured in units of millipolarisation (mP). Data were plotted and analysed using GraphPad Prism 9, graphical data represent the arithmetic mean  $\pm$  curve fitting standard error of the mean for a single representative experiment.

#### 8.2.1.2 $K_a$ Determination

To each well, 5  $\mu\text{L}$  of probe molecule **108** or **148** (20 nM in assay buffer) and increasing concentrations of HSP72-NBD protein (5  $\mu\text{L}$ , two-fold dilution series) were added. Fluorescence polarisation values for tracer control wells (10 nM probe **108** or **148** in assay



buffer only) were subtracted from each data point prior to data analysis.  $K_d$  determination was performed using non-linear regression analysis (GraphPad Prism 9, one site-specific binding model).  $pK_d$  values are quoted as geometric mean  $\pm$  standard error of the mean from 3 independent experiments

### 8.2.1.3 Competitive binding experiments

Compounds (0.2  $\mu$ L at 50  $\times$  screening concentration in DMSO) were dispensed using an ECHO 550 Liquid Handler (Labcyte Inc.). To the corresponding wells was added, 5  $\mu$ L of probe molecule **108** or **148** (20 nM in assay buffer) and 5  $\mu$ L of protein (twice their final concentration in assay buffer) to give a 70 – 85 % bound fraction and incubated in the dark for 2 hours. Tracer controls (10 nM probe molecule **108** or **148** only) and bound tracer controls (10 nM probe in presence of appropriate protein concentration) were included on each assay plate.  $IC_{50}$  determination was performed using non-linear least squares curve fitting (GraphPad Prism 9, log(inhibitor) vs. response – variable slope (four parameters)).  $K_i$  values were calculated using Huang's equation.  $pK_i$  values are quoted as geometric mean  $\pm$  standard error of the mean from 3 independent experiments unless otherwise stated.

### 8.2.1.4 Kinetics Experiments

Compounds (0.2  $\mu$ L at 50  $\times$  screening concentration in DMSO) were dispensed using an ECHO 550 Liquid Handler (Labcyte Inc.). 5  $\mu$ L of probe molecule **108** or **148** (20 nM in assay buffer) and 5  $\mu$ L of protein (twice their final concentration in assay buffer) to give a 70 – 85 % bound fraction were pre-incubated in the dark for two hours and then simultaneously dispensed to the corresponding wells using an INTEGRA VIAFLO electronic multichannel pipette. Tracer controls (10 nM probe molecule **108** or **148** only) and bound tracer controls (10 nM probe in presence of appropriate protein concentration) were included on each assay plate.

## 8.2.2 Mass Spectrometry

### 8.2.2.1 HSP72 Intact Protein Mass Spectrometry

HSP72-NBD (2.3  $\mu$ M) in buffer (50 mM Tris base pH 7.4, 150 mM KCl, 5 mM CaCl<sub>2</sub>) was mixed with compound (20  $\mu$ M from 1 mM DMSO stock) and incubated at 25 °C

prior to analysis. The total reaction volume was 100  $\mu\text{L}$  in a 2ml glass HPLC vial or 200  $\mu\text{L}$  glass HPLC insert vial. 1  $\mu\text{L}$  aliquots were taken from the vial for injection at set time points. 1  $\mu\text{L}$  injections of the sample were made onto a SecurityGuard C8 column cartridge (4 x 3 mm, AJO-4290, Phenomenex). Samples were incubated at 25  $^{\circ}\text{C}$  in a G1367B auto-sampler (Agilent) with G1330B thermostat module prior to injection. Chromatographic separation at 25  $^{\circ}\text{C}$  was carried out using an Agilent 1200 Series HPLC over a 1 minute gradient elution of 95:5 to 5:95 water and acetonitrile (both modified with 0.1% formic acid) at a flow rate of 0.5 mL/min. Sample was loaded onto the column cartridge using a G1312B SL binary pump dispensing a gradient from 95:5 to 5:95 water and acetonitrile (both modified with 0.1% formic acid) at a flow rate of 3 mL/min. Between 0.3 and 0.6 minutes a ten port column selection valve (G1316A column module) was used to reverse eluent flow through the column cartridge. During this stage, a second binary pump (G1312A) was used to elute protein off the cartridge using a gradient from 60:40 to 5:95 water and acetonitrile (both modified with 0.1% formic acid) at a flow rate of 0.5 mL/min. The post column eluent flow was infused into an Agilent 6520 Series qToF mass spectrometer fitted with a dual ESI ionisation source. An initial divert to waste was used to aid desalting. LC eluent and nebulising gas was introduced into the grounded nebuliser with spray direction orthogonal to the capillary axis. The aerosol was dried by heated gas (10 L/min of nitrogen at 350  $^{\circ}\text{C}$ , 50 psi), producing ions by ESI. Ions entered the transfer capillary along which a potential difference of 4 kV was applied. The fragmentor voltage was set at 190 V and skimmer at 65 V. Signal was optimised by AutoTune.m prior to acquisition. Profile mass spectrometry data were acquired in positive ionisation mode over a scan range of  $m/z$  700 – 1500 (scan rate 1.0) with reference mass correction at  $m/z$  922.009798 hexakis(1*H*,1*H*,3*H*-perfluoropropoxy)phosphazene. Raw data were processed using Agilent MassHunter Qualitative Analysis B.07.00 and graphs made using GraphPad Prism 9.

#### **8.2.2.2 EGFR Intact Protein Mass Spectrometry**

Experiments were performed by Marcus Ladds.

EGFR-TKD (50  $\mu\text{L}$ , 500 nM final concentration) in buffer (20 mM Bicine pH 7.5, 100 mM NaCl) was mixed with compound (50  $\mu\text{L}$ , 10  $\mu\text{M}$  final concentration) in a V-shaped Greiner 384 well plate and incubated at 4  $^{\circ}\text{C}$ . 10  $\mu\text{L}$  of formic acid was added at appropriate time points to quench the reaction. At the end of the 24 hour timecourse, each

well was injected onto C4 column and analysed by RapidFireMS. Profile mass spectrometry data were acquired in positive ionisation mode over a scan range of  $m/z$  600 – 2000 with  $m/z$  track filter at  $m/z$  922, 923, 924. Raw data were processed using Agilent MassHunter Qualitative Analysis B.07.00 with a retention time restriction of 0.18 – 0.32 min and graphs made using GraphPad Prism 9.

### 8.2.2.3 Hydrolytic Stability

The respective compound (5  $\mu$ L from 10 mM DMSO stock, 50  $\mu$ L final concentration) and DMSO (15  $\mu$ L) were added to buffer (980  $\mu$ L, 10 mM PBS pH 7.4, 2.7 mM KCl, 137 mM NaCl) incubated at 37 °C prior to analysis. The total reaction volume was 1000  $\mu$ L. Timepoints were collected every hour, up to 24 hours. 1  $\mu$ L standard injections (with needle wash) of the sample were made onto a 30 x 2.1 mm, 2.6 $\mu$ m, Kinetex C18 column (Phenomenex, Torrance, CA, USA). Chromatographic separation at room temperature was carried out using a 1200 Series HPLC (Agilent, Santa Clara, USA) over a 10 minute gradient elution from 95:5 to 5:95 water and methanol (both modified with 0.1% formic acid) at a flow rate of 0.5 mL/min. UV-vis spectra were acquired at 254 nm, 320 nm, 300 nm, 280 nm and 214 nm on a 1200 Series diode array detector. The post column eluent flow was infused into a 6520 Series qToF mass spectrometer (G6520A) fitted with a dual ESI ionisation source. LC eluent and nebulising gas was introduced into the grounded nebuliser with spray direction orthogonal to the capillary axis. The aerosol was dried by heated gas (12 L/min of nitrogen at 350 °C, 60 psi), producing ions by ESI. Ions entered the transfer capillary along which a potential difference of 4 kV was applied. The fragmentor voltage was set at 180 V and skimmer at 65 V. Profile mass spectrometry data was acquired in positive ionisation mode over a scan range of  $m/z$  200-700 (scan rate 1.0). MS data was collected between 1.5 and 6.5 minutes. Between 0 – 1.5 minutes and after 6.5 minutes, eluent was diverted to waste. Raw data was processed using Agilent MassHunter Qualitative Analysis B.07.00. Extracted Ion Chromatograms (EIC) were obtained for each compound with large extraction windows (8Da, from predicted  $[M+H]^+$ ) to ensure isotopic contributions were summed, and peaks integrated to obtain area. Raw data were processed using Agilent MassHunter Qualitative Analysis B.07.00. The processed data was normalised, converted to natural logarithms and then analysed using linear regression (GraphPad Prism 9).  $\ln(\text{AUC})_t = \ln(\text{AUC})_0 - kt$ ,  $t_{1/2} = \ln 2/k$ .  $t_{1/2}$

values are quoted as arithmetic mean  $\pm$  standard error of the mean from 3 independent experiments.

### 8.2.3 EGFR Activity Assay

Experiments performed by Omar Alkhatib using AssayQuant Omnia phosphorylation assay.<sup>285</sup>

Compounds dissolved in DMSO were delivered into a 384-well assay microplate in a 160 nL total volume (1% DMSO) using the Echo 555 acoustic liquid handler (LabCyte) at 16 concentrations with a 1.5-fold dilution starting from 10  $\mu$ M final concentration. WT EGFR-TKD (50 nM final concentration) or TM EGFR-TKD (15 nM final concentration), Sox peptide (10  $\mu$ M final concentration) and ATP (30 – 45  $\mu$ M final concentration) were dispensed into the 384-well assay microplate (Greiner Bio-One 784075) using a Certus Flex liquid dispenser. Reactions were initiated with the enzyme, and the accumulation of the phosphorylated peptide product was monitored using a PHERAstar FSX plate reader (BMG Labtech) equipped with a fluorescence intensity module with excitation at 360 nm and emission at 480 nm. IC<sub>50</sub> determination was performed using non-linear least squares curve fitting (GraphPad Prism 9, log(inhibitor) vs. response – variable slope (four parameters)).

### 8.3 Assay Free Fraction

Experiments were performed by Pharmidex.

#### Conditions

Stock concentration: 10 mM

Solubility: 100% DMSO

Test concentration: 1  $\mu$ M

Final DMSO concentration in assay: 0.5%

#### Control Compounds

Verapamil: Unbound 62.7% $\pm$ 0.6,  $f_{ua}$ =0.627 $\pm$ 0.006

Warfarin: Unbound  $49.6\% \pm 2.0$ ,  $f_{ua} = 0.496 \pm 0.020$

Diclofenac: Unbound:  $14.1\% \pm 0.4$ ,  $f_{ua} = 0.141 \pm 0.004$

Antipyrine: Unbound:  $112\% \pm 4$ ,  $f_{ua} = 1.12 \pm 0.04$

### **Method:**

Cell Culture Medium binding was measured by the Equilibrium Dialysis Method (EDM). 96 well plate blocks were built with two compartments separated by a vertical cylinder of dialysis membrane (molecular weight cut off (MWCO) ~8,000). Cell Culture Medium (DMEM + FBS) was spiked with the compound of interest is placed in the first compartment, in the other was placed just DMEM. The unit was covered and incubated at 37°C on an orbital shaker for 4 hours. After incubation, samples from both Cell Culture Medium (bound) chamber and the buffer (free) chamber were taken and placed into separate microcentrifuge tubes for analysis. The samples were matrix-matched. Acetonitrile containing internal standard was added to all samples. The samples were centrifuged, and the supernatant was analysed by UHPLC-TOF MS for parent compound.

## **8.4 Biology Experimental**

All experiments were performed by Marissa Powers.

### **8.4.1 General Information**

Origin of the human ovarian carcinoma cell lines used in this study, HCT 116, was obtained from ATCC (CCL-247). Prior to use, the cells were analysed by short tandem repeat (STR) profiling. Polymorphic STR loci were amplified using a polymerase chain reaction (PCR) primer set. The PCR product (each locus being labelled with a different fluorophore) was analysed simultaneously with size standards using automated fluorescent detection. The number of repeats at 10 different loci (as recommended by the American Type Culture Collection, ATCC) was used to define the STR profile and this was cross-referenced with online databases to confirm authenticity. Using this method, the HCT 116 cell line showed an acceptable 94% identity with the ATCC reference line (LGC Promochem, UK). The cells were free of mycoplasma contamination as determined by a sensitive biochemical protocol ( MycoAlert PLUS Mycoplasma detection kit, LT07-710, Lonza). Cells were grown in DMEM (D5671, Sigma) supplemented with 10 % FCS

(FBS Good Filtrated Bovine Serum, P40-37500, PAN Biotech), 2 mM glutamine (25030-024, Gibco) and 1% (v/v) non-essential amino acids (11140-050, Gibco) in 5% CO<sub>2</sub>.

#### 8.4.2 HCT116 Western Blot Analysis

Briefly, HCT 116 cells ( $\sim 4 \times 10^5$  cells) were seeded into 25cm<sup>2</sup> flasks and incubated for 24 h prior to the addition of vehicle (DMSO) or compound for 24 h. For experiments using conditioned media (fully supplemented DMEM with pH reduced to 7.4 from 8.4 by preincubating with HCT 116 cells for 96 h), seeding media was removed and replaced with conditioned media prior to the addition of compound or vehicle (DMSO) for 24 h. Cells were collected by trypsinization and lysed using 1 × Cell Lysis Buffer (9803, Cell signalling), supplemented with cOmplete, Mini, EDTA-free Protease Inhibitor tablets (11836153001, Roche) and Halt phosphatase inhibitors (1861281, Thermo Fisher Scientific) and clarified of cellular debris by centrifugation (13,500 rpm, 20 minutes). Protein concentration was determined using the Bicinchoninic acid (BCA) assay (23225, Pierce) and absorbance measured using the Envision multiplate reader (Perkin Elmer, UK).

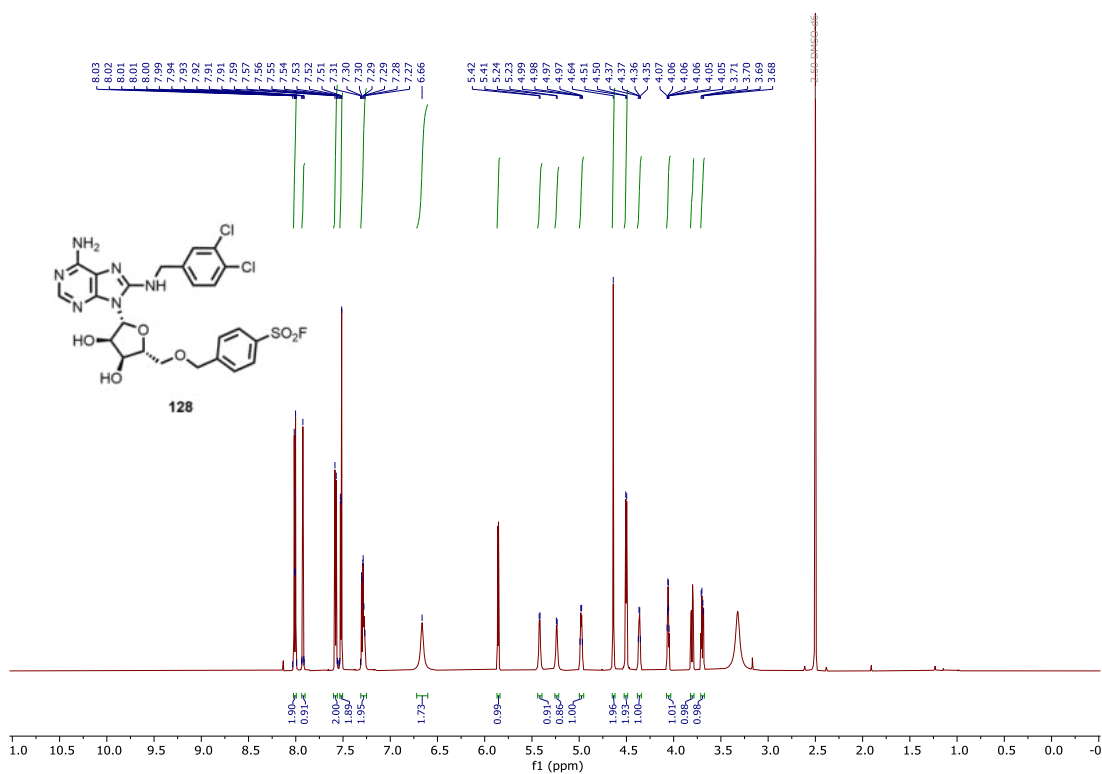
Each lysate was separated by SDS-PAGE using NuPAGE 4-12% Bis-Tris gels (NP0336BOX, Invitrogen, UK), electrotransferred onto nitrocellulose membranes (IB23001, Invitrogen, UK) by rapid dry transfer (iBLOT, Invitrogen), blocked with 1% casein in PBS (1610782, Bio-rad) and probed with specific primary antibody to ERBB2 (ab16901, Abcam), C-RAF (9422, Cell signalling), CDK4 (12790, Cell signalling), HSP72 (ADI SPA-810, Enzo Life Sciences), HSC70 (ab1427-50, Abcam) or Vinculin (13901s, Cell signalling) followed by goat anti-mouse (1705047, BioRad) or anti-rabbit (NA934V, Cytiva) – HRP linked secondary antibody. All primary antibodies were incubated overnight at 4°C in 5% BSA + TBS 0.5% tween, secondary antibodies were incubated for 1 h at room temperature in 1% Casein. Signal detection membranes were incubated with SuperSignal west-pico plus reagent (34575, Pierce) and visualised using a ChemiDoc imager (Bio-Rad).



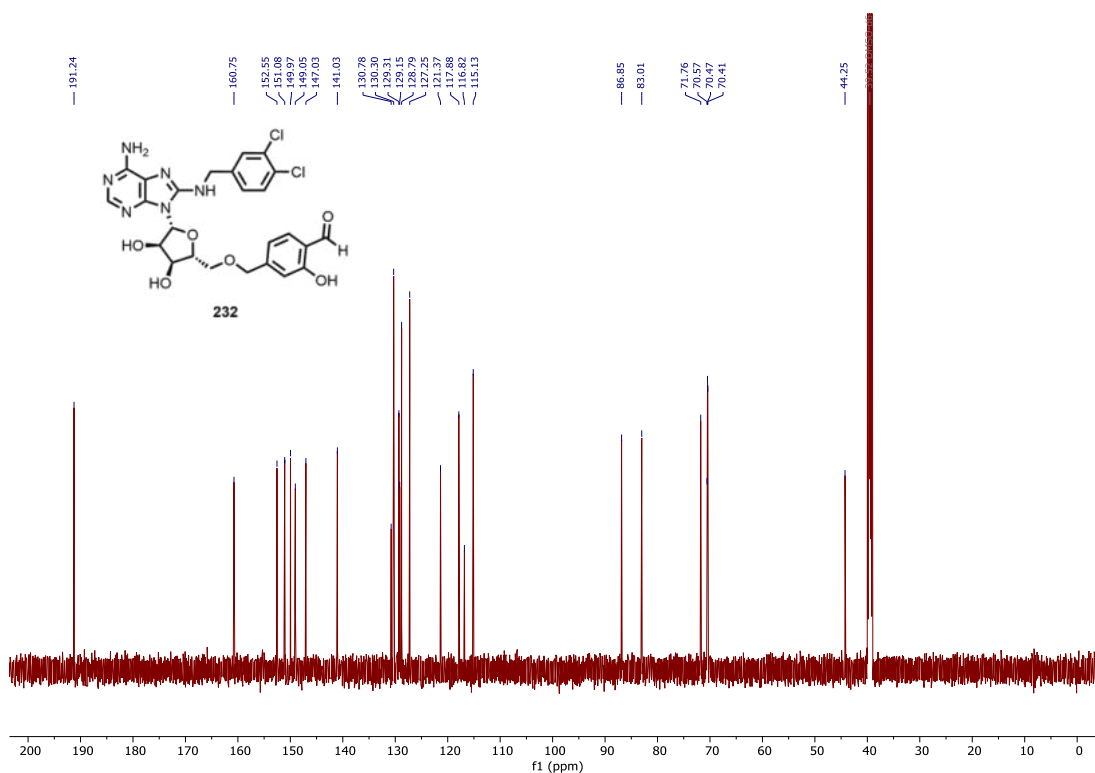
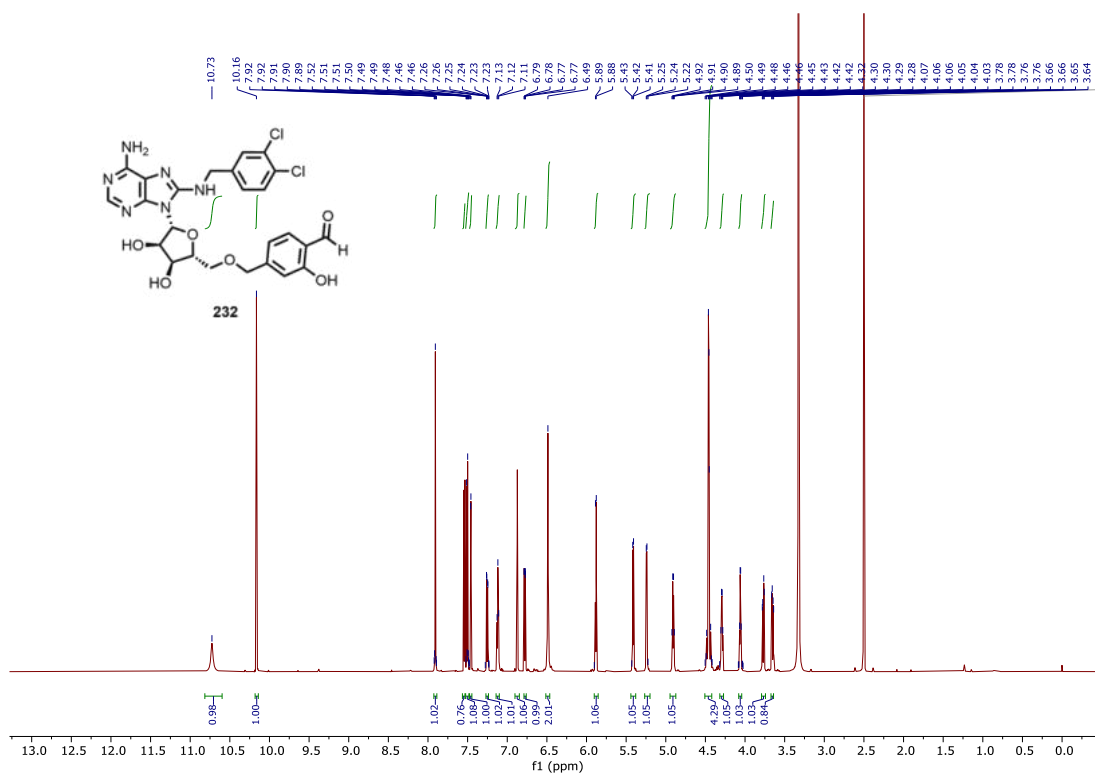
## 9 Appendix

### 9.1 NMR Spectra of Key Compounds

$^1\text{H}$  NMR (DMSO- $d_6$ , 600 MHz) and  $^{13}\text{C}$  NMR (DMSO- $d_6$ , 151 MHz) of compound **128**

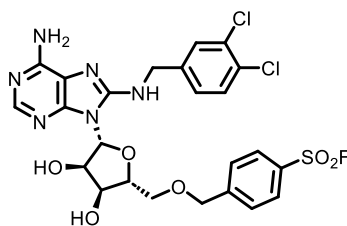




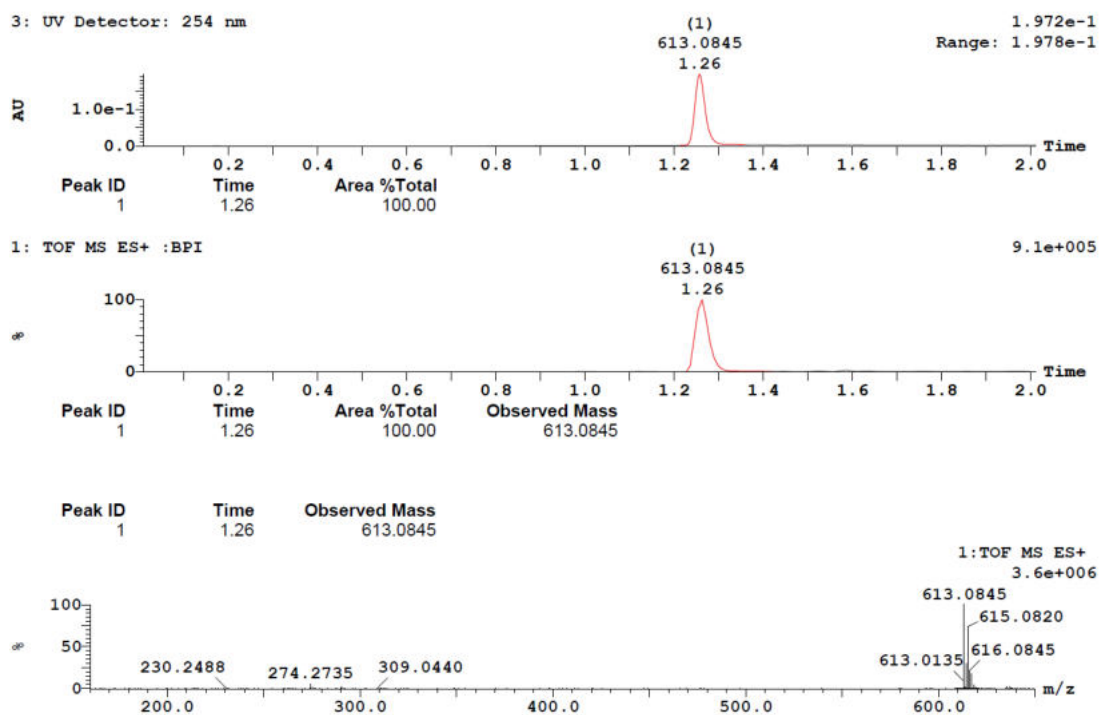
$^1\text{H}$  NMR (DMSO- $d_6$ , 600 MHz) and  $^{13}\text{C}$  NMR (DMSO- $d_6$ , 151 MHz) of compound **232**

## 9.2 HPLC Traces and Mass Spectra of Key Compounds

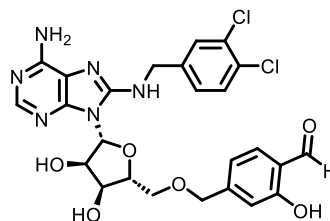
## Compound 128



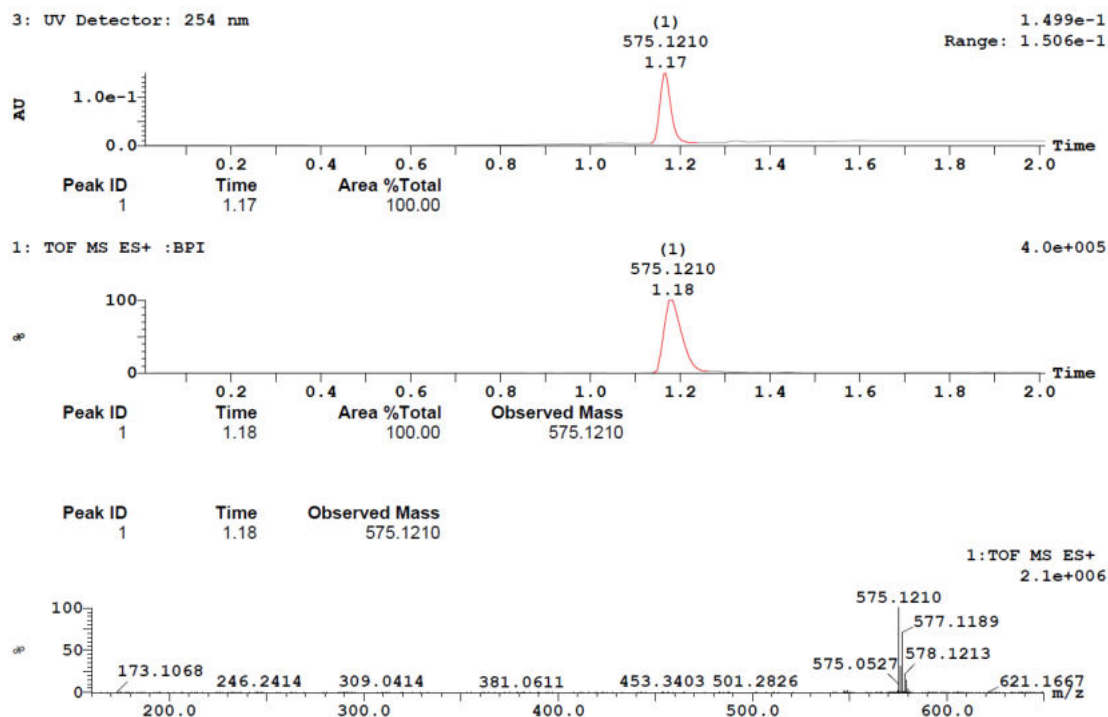
128



## Compound 232



232



### 9.3 Chiral HPLC of Key Compounds

Enantiopure **128**, *ent*-**128**, **232** and *ent*-**232** were screened by Chiral HPLC to assess enantiopurity. Injection of samples and data analysis was performed by Lauren Knightley of the CTU Structural Chemistry department.

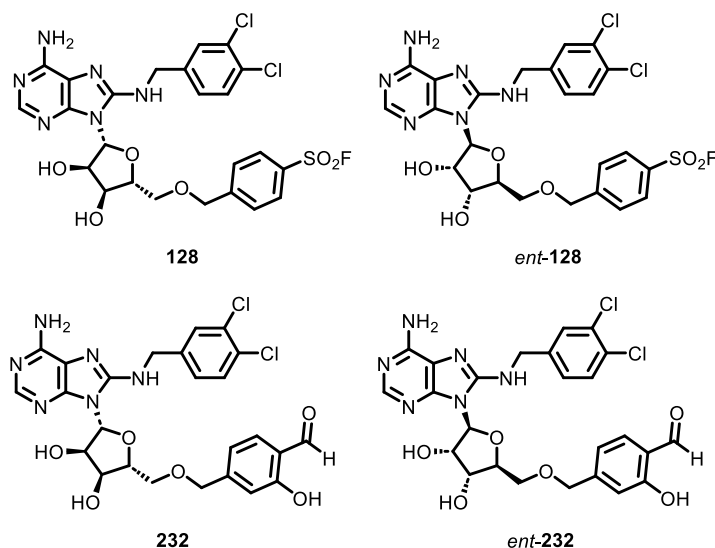


**Figure 9.1** Structures of **128**, *ent*-**128**, **232** and *ent*-**232**.

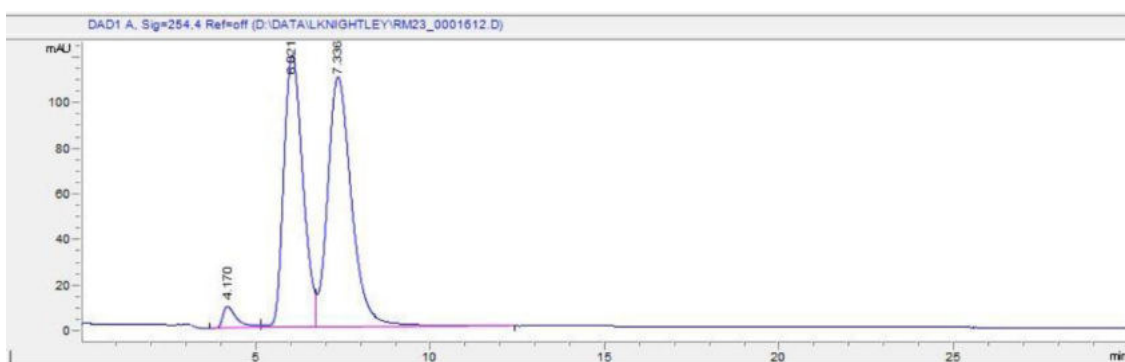
The corresponding racemates *rac*-**128** and *rac*-**232** were prepared by combining equal amounts of compound and its opposite enantiomer. Samples were prepared at a concentration of 10 mM in 100% DMSO.

**Instrumentation:** The samples were screened using 6 different columns using 6 different solvents. The 2 methods, P08 and P09, gave the best separation. For the P08 method, injection volumes of 2  $\mu$ L of the sample solutions (with needle wash) were passed through a Phenomenex Lux 3 $\mu$  Cellulose-2 column (3  $\mu$ m, 250 x 4.6 mm, 100 $\text{\AA}$ , Phenomenex, Torrence, USA). For the P09 method, injection volumes of 2  $\mu$ L of the sample solutions (with needle wash) were passed through a Phenomenex Lux Cellulose-4 column (5  $\mu$ m, 250 x 4.6 mm, 100 $\text{\AA}$ , Phenomenex, Torrence, USA). The solvents were degassed on a 1260 Infinity degasser (Agilent, Santa Clara, USA). Chromatographic separation at room temperature was carried out using a 1200 Series HPLC (Agilent, Santa Clara, USA) over a 45-minute isocratic elution (P08.m) and (P09.m) of 100% MeOH (with no modifier) at a flow rate of 2 mL/min. UV-Vis spectra were acquired at 214nm and 254nm on a 1200 Series diode array detector (Agilent, Santa Clara, USA). Raw data was processed using Agilent Chemstation C.01.05.

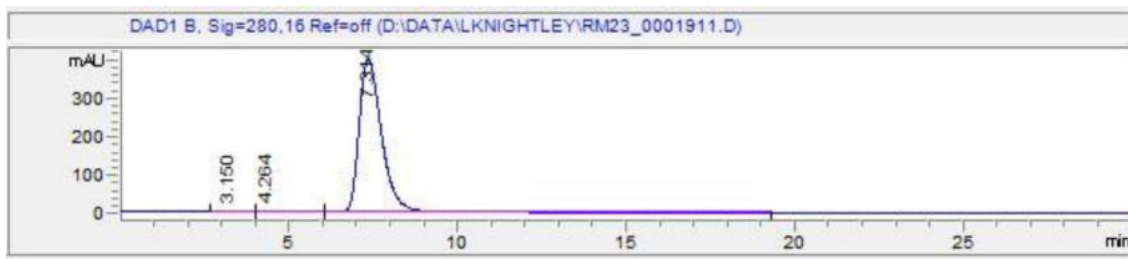
**Results:**

**128** and *ent*-**128** (P08 method used)

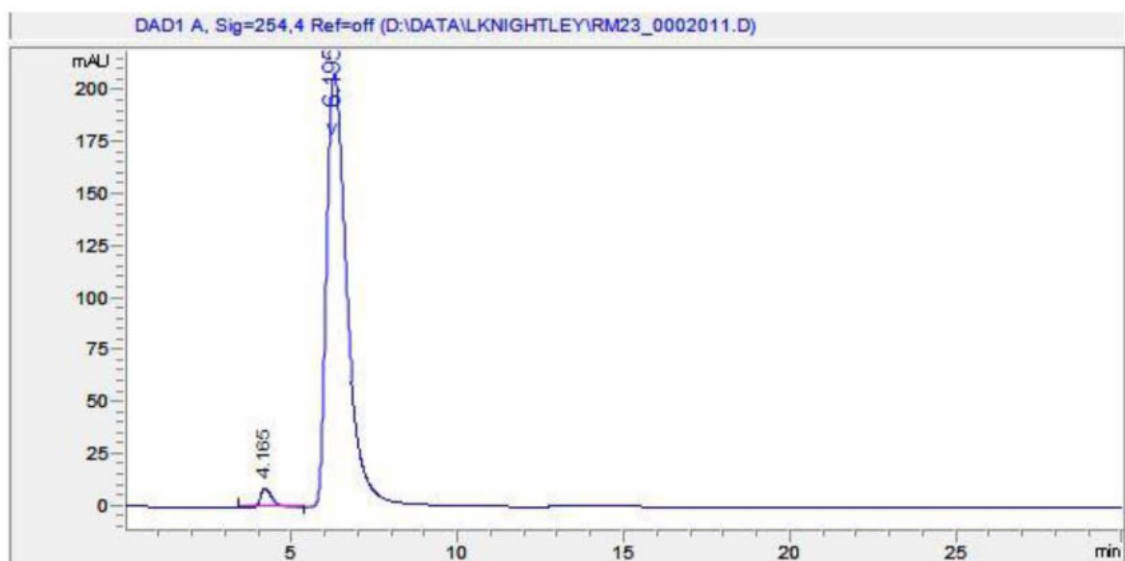
**HPLC trace of *rac*-128:**



HPLC trace of **128**:

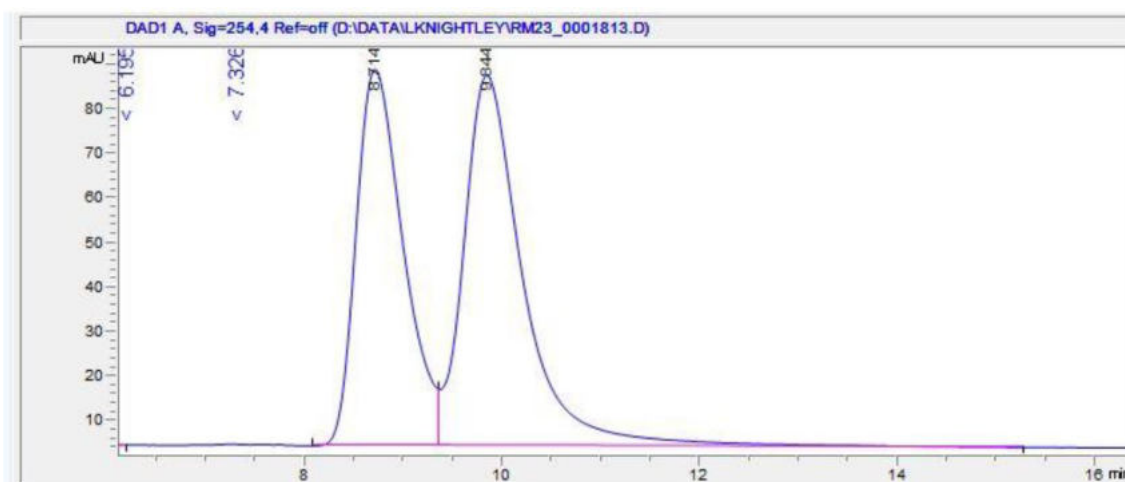


HPLC trace of *ent*-**128**:

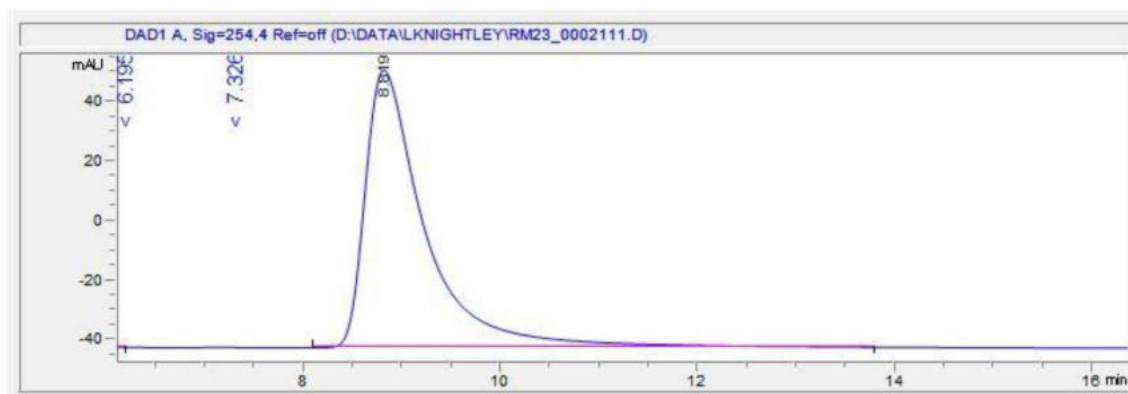


**232** and *ent*-**232** (P09 method used)

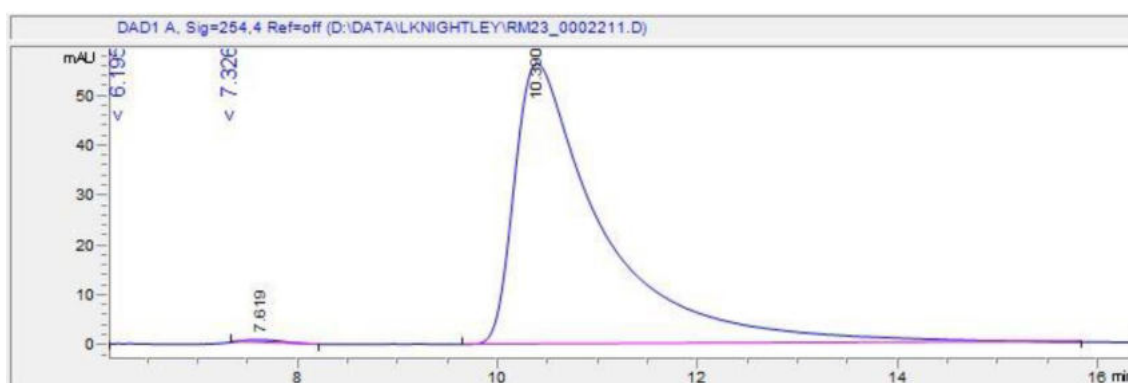
HPLC trace of *rac*-**232**:



HPLC trace of **232**:

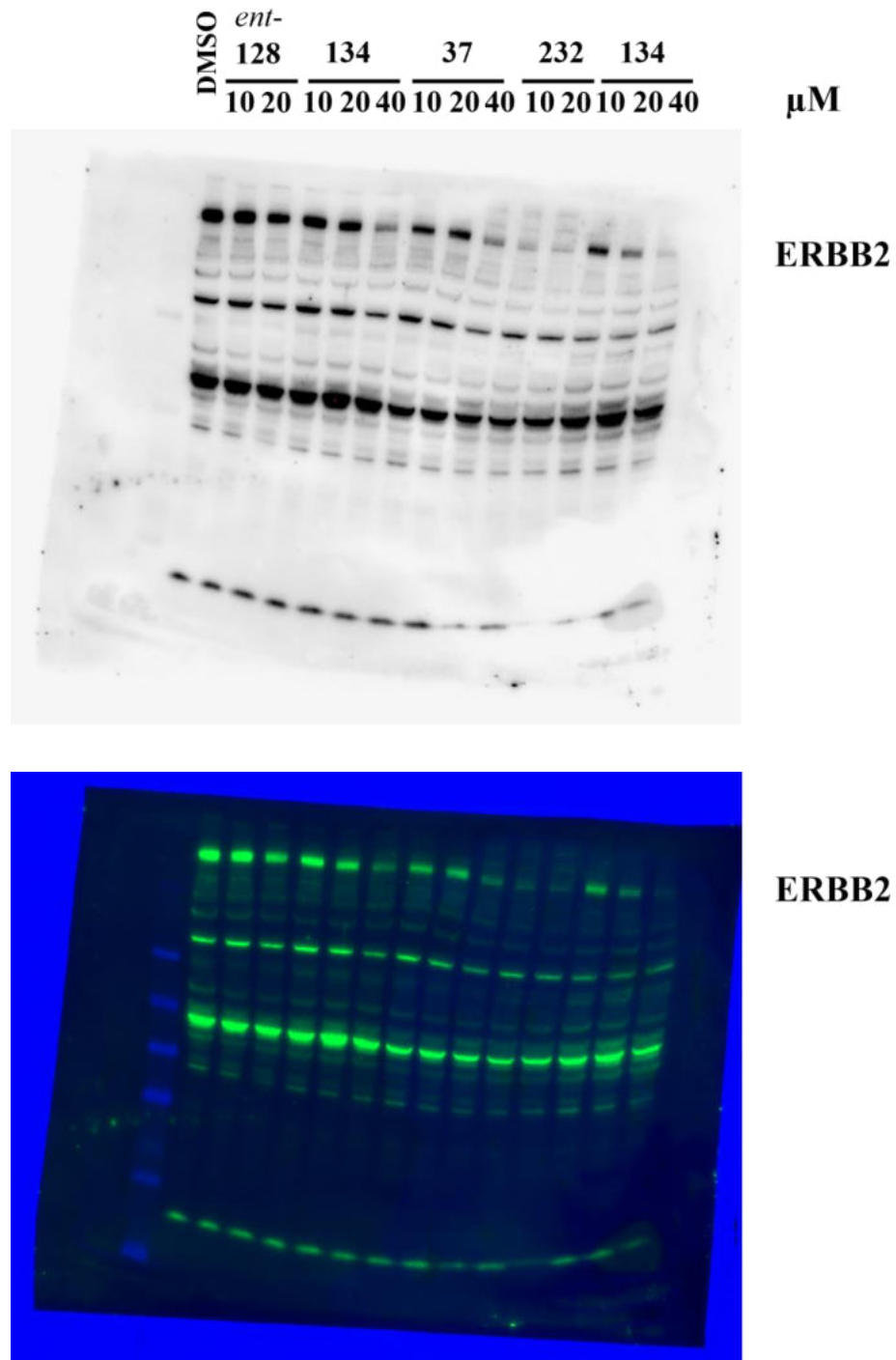


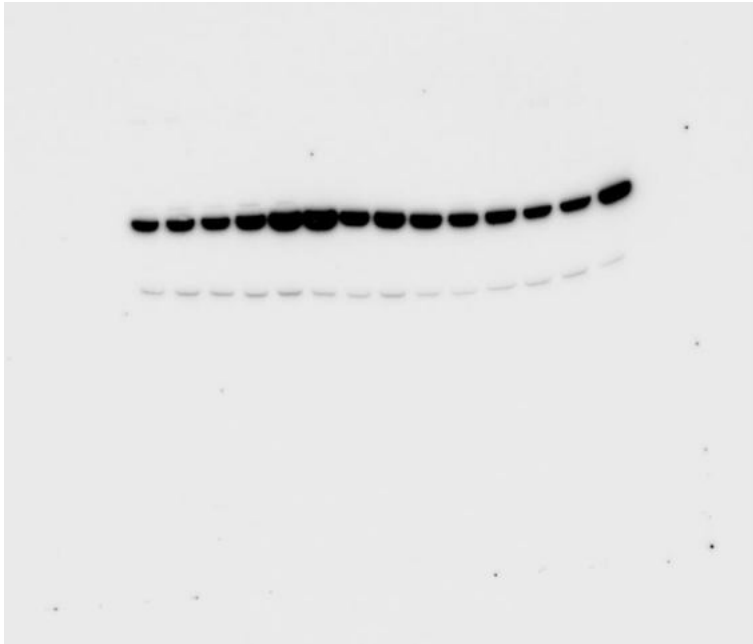
HPLC trace of *ent*-**232**:



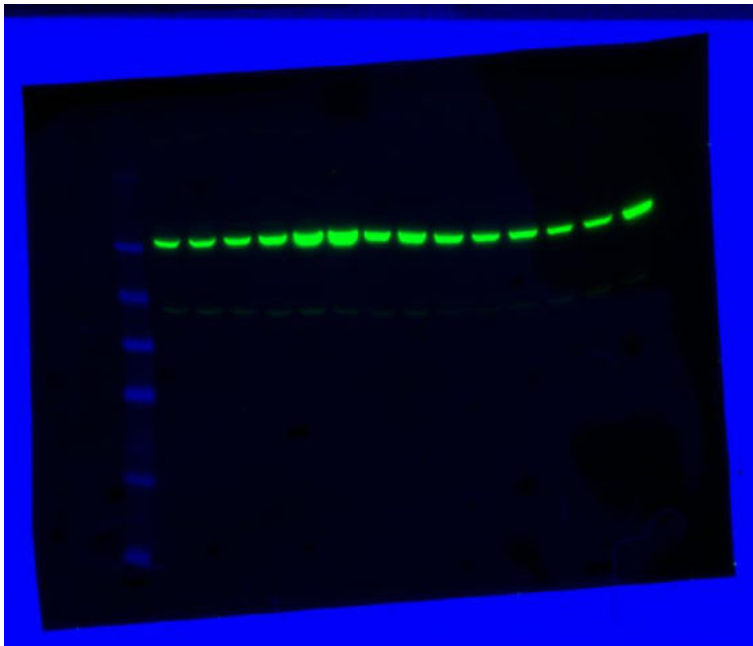
9.4 Western Blot Data

9.4.1 Figure 5.25



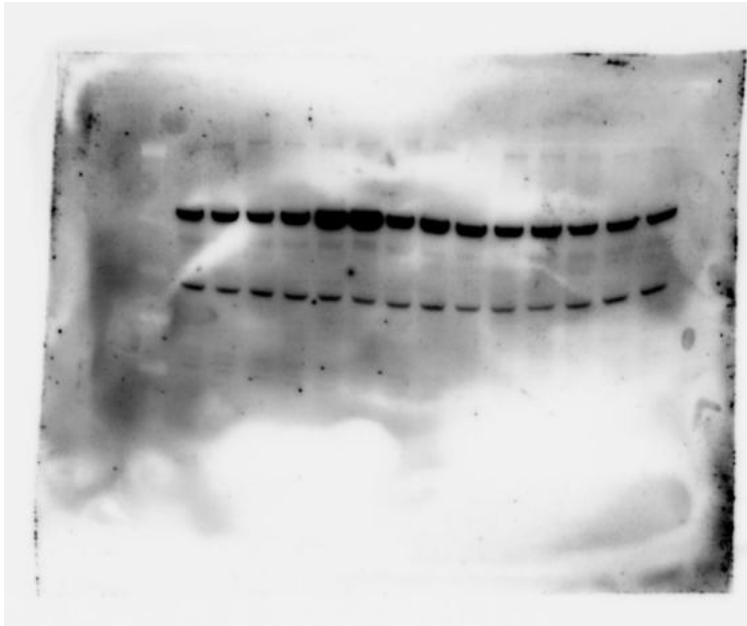


**HSP72**

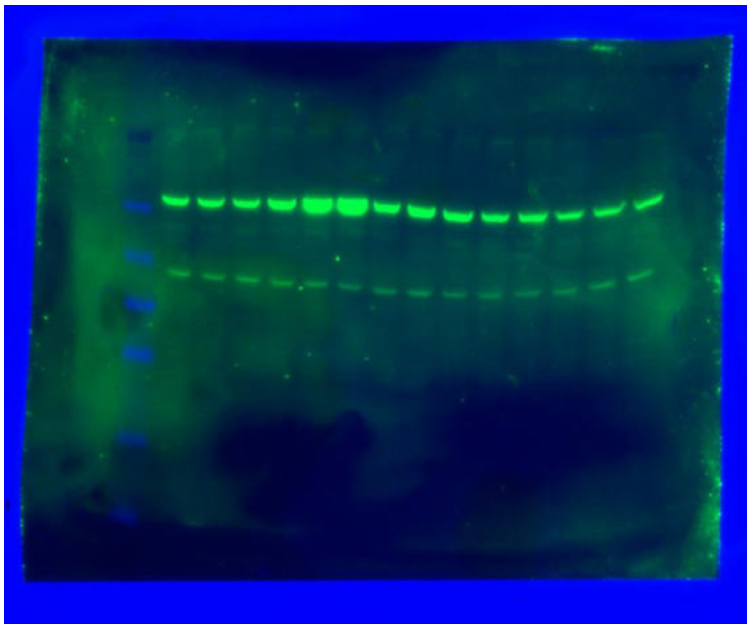


**HSP72**

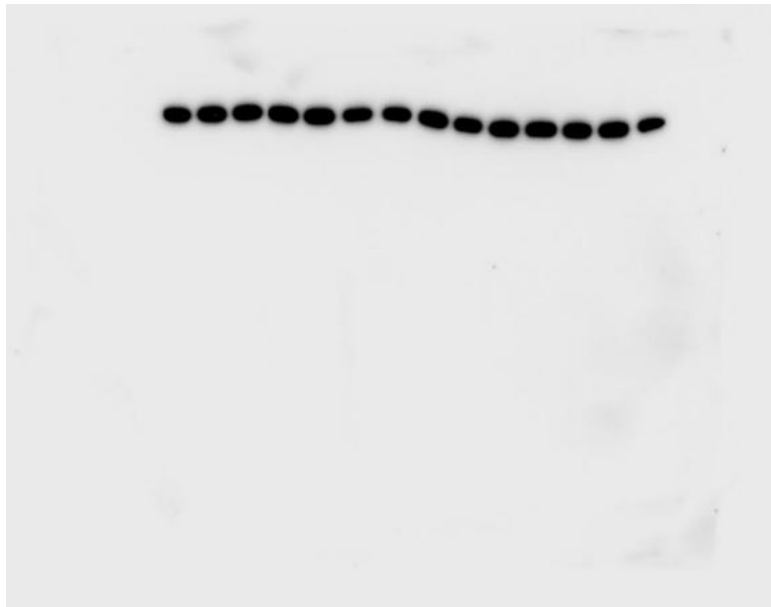




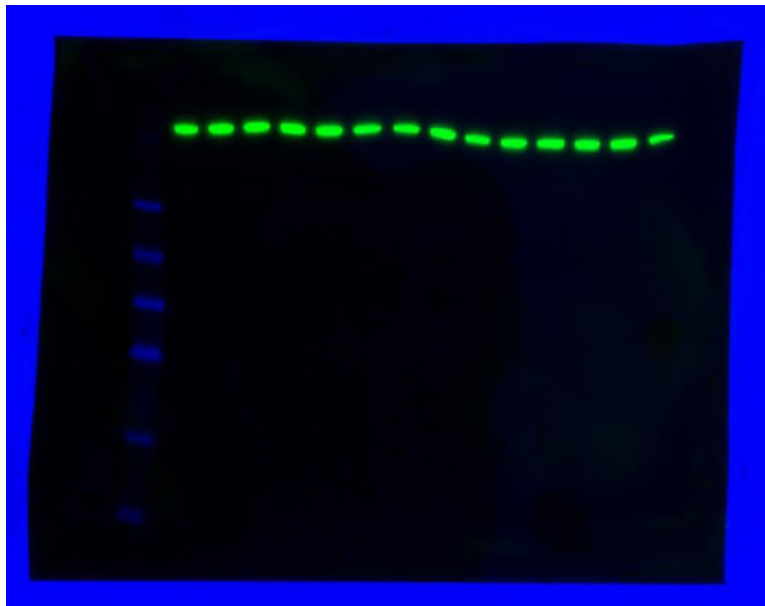
**HSC70**



**HSC70**

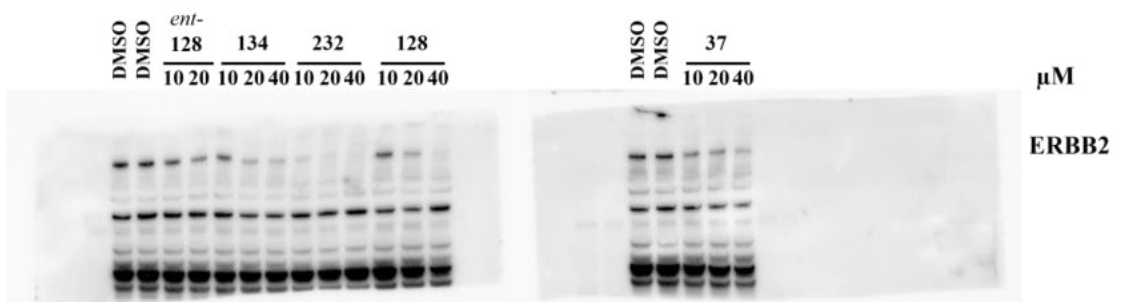


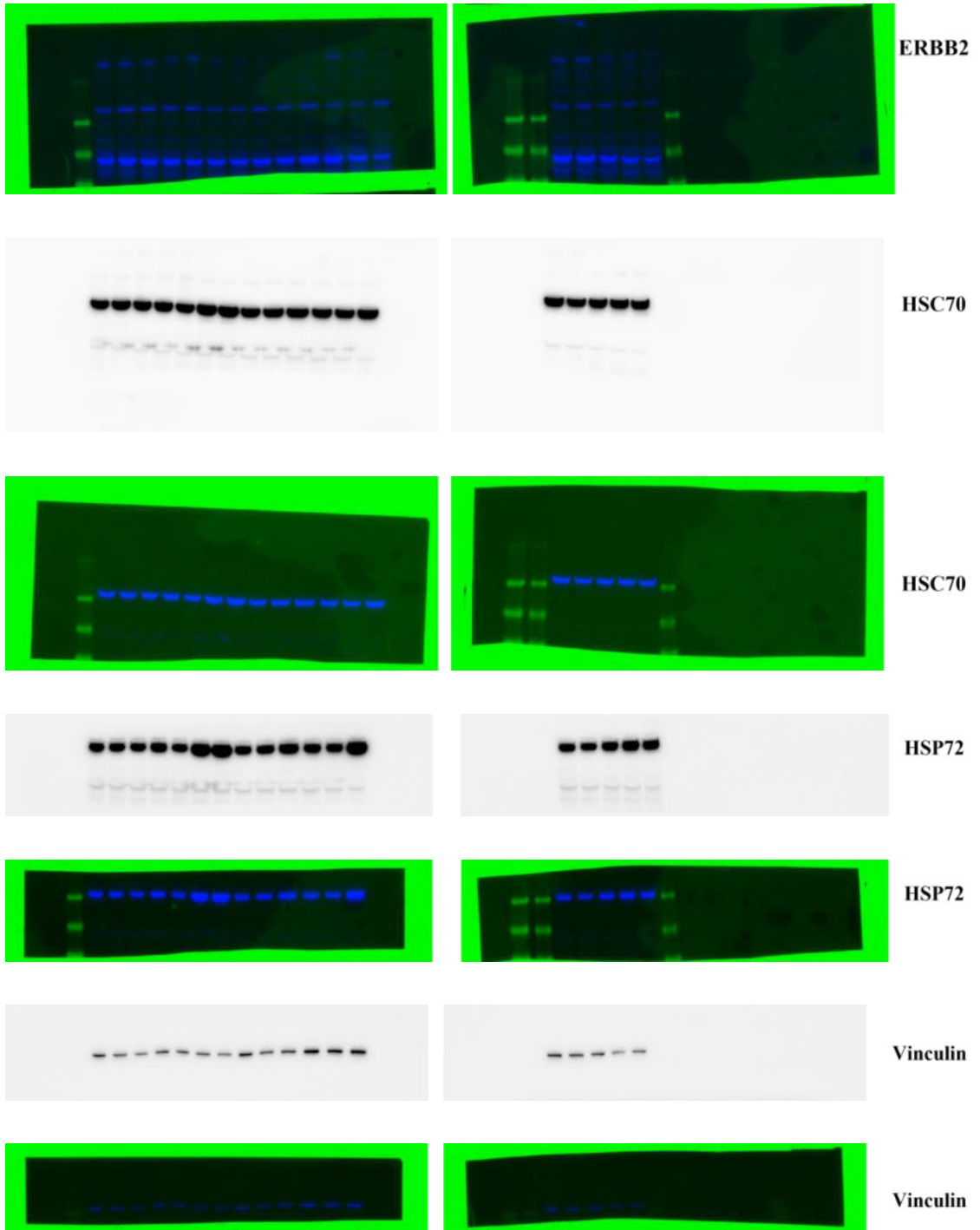
**Vinculin**



**Vinculin**

9.4.2 Figure 6.25

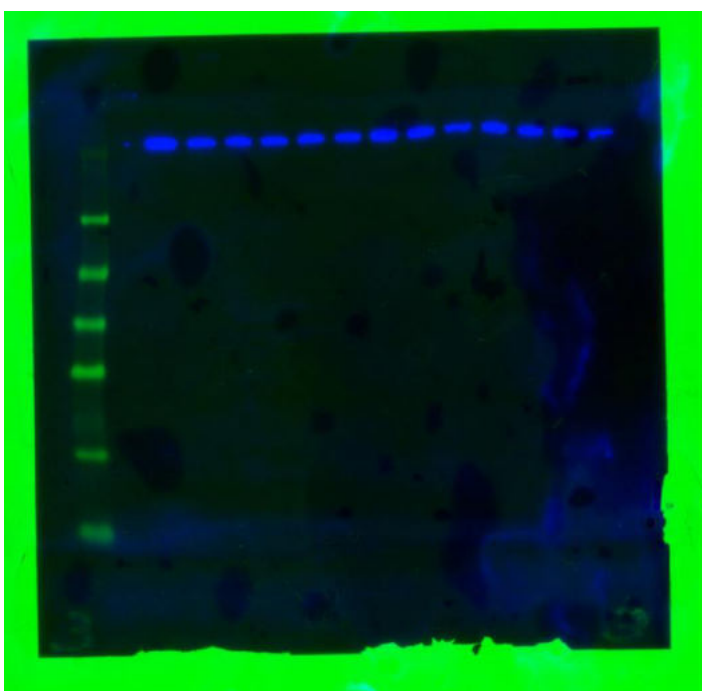








**Vinculin**



**Vinculin**

## 10 References

## 10 References

- (1) Chabner, B. A.; Roberts, T. G. Chemotherapy and the War on Cancer. *Nat. Rev. Cancer* **2005**, *5* (1), 65–72.
- (2) Tilsed, C. M.; Fisher, S. A.; Nowak, A. K.; Lake, R. A.; Lesterhuis, W. J. Cancer Chemotherapy: Insights into Cellular and Tumor Microenvironmental Mechanisms of Action. *Front. Oncol.* **2022**, *12*, 960317.
- (3) Zhong, L.; Li, Y.; Xiong, L.; Wang, W.; Wu, M.; Yuan, T.; Yang, W.; Tian, C.; Miao, Z.; Wang, T.; Yang, S. Small Molecules in Targeted Cancer Therapy: Advances, Challenges, and Future Perspectives. *Signal Transduct. Target. Ther.* **2021**, *6* (1), 1–48.
- (4) Bedard, P. L.; Hyman, D. M.; Davids, M. S.; Siu, L. L. Small Molecules, Big Impact: 20 Years of Targeted Therapy in Oncology. *Lancet* **2020**, *395* (10229), 1078–1088.
- (5) Savage, D. G.; Antman, K. H. Imatinib Mesylate — A New Oral Targeted Therapy. *N. Engl. J. Med.* **2002**, *346* (9), 683–693.
- (6) Pagliarini, R.; Shao, W.; Sellers, W. R. Oncogene Addiction: Pathways of Therapeutic Response, Resistance, and Road Maps toward a Cure. *EMBO Rep.* **2015**, *16* (3), 280–296.
- (7) Nagel, R.; Semenova, E. A.; Berns, A. Drugging the Addict: Non-Oncogene Addiction as a Target for Cancer Therapy. *EMBO Rep.* **2016**, *17* (11), 1516–1531.
- (8) Copeland, R. *Evaluation of Enzyme Inhibitors in Drug Discovery*; John Wiley & Sons, Inc., 2013.
- (9) Bissantz, C.; Kuhn, B.; Stahl, M. A Medicinal Chemist’s Guide to Molecular Interactions. *J. Med. Chem.* **2010**, *53* (14), 5061–5084.
- (10) Robers, M. B.; Friedman-Ohana, R.; Huber, K. V. M.; Huber, K. V. M.; Kilpatrick, L.; Kilpatrick, L.; Vasta, J. D.; Berger, B. T.; Chaudhry, C.; Hill, S.; Hill, S.; Müller, S.; Müller, S.; Knapp, S.; Knapp, S.; Knapp, S.; Knapp, S.; Wood, K. V. Quantifying Target Occupancy of Small Molecules within Living Cells. *Annu. Rev. Biochem.* **2020**, *89*, 557–581.
- (11) Smith, D. A.; Di, L.; Kerns, E. H. The Effect of Plasma Protein Binding on in Vivo Efficacy: Misconceptions in Drug Discovery. *Nat. Rev. Drug Discov.* **2010**, *9* (12), 929–939.
- (12) Morgan, P.; Van Der Graaf, P. H.; Arrowsmith, J.; Feltner, D. E.; Drummond, K. S.; Wegner, C. D.; Street, S. D. A. Can the Flow of Medicines Be Improved? Fundamental Pharmacokinetic and Pharmacological Principles toward Improving Phase II Survival. *Drug Discov. Today* **2012**, *17* (9–10), 419–424.
- (13) Swinney, D. C. Biochemical Mechanisms of Drug Action: What Does It Take for Success? *Nat. Rev. Drug Discov.* **2004**, *3* (9), 801–808.

- (14) Wakefield, A. E.; Kozakov, D.; Vajda, S. Mapping the Binding Sites of Challenging Drug Targets. *Curr. Opin. Struct. Biol.* **2022**, *75*, 102396.
- (15) Singh, J.; Petter, R. C.; Baillie, T. A.; Whitty, A. The Resurgence of Covalent Drugs. *Nat. Rev. Drug Discov.* **2011**, *10* (4), 307–317.
- (16) Bauer, R. A. Covalent Inhibitors in Drug Discovery: From Accidental Discoveries to Avoided Liabilities and Designed Therapies. *Drug Discov. Today* **2015**, *20* (9), 1061–1073.
- (17) Sutanto, F.; Konstantinidou, M.; Dömling, A. Covalent Inhibitors: A Rational Approach to Drug Discovery. *RSC Med. Chem.* **2020**, *11* (8), 876–884.
- (18) Roth, G. J.; Stanford, N.; Majerus, P. W. Acetylation of Prostaglandin Synthase by Aspirin. *Proc. Natl. Acad. Sci.* **1975**, *72* (8), 3073–3076.
- (19) Lecomte, M.; Laneuville, O.; Ji, C.; DeWitt, D. L.; Smith, W. L. Acetylation of Human Prostaglandin Endoperoxide Synthase-2 (Cyclooxygenase-2) by Aspirin. *J. Biol. Chem.* **1994**, *269* (18), 13207–13215.
- (20) Boike, L.; Henning, N. J.; Nomura, D. K. Advances in Covalent Drug Discovery. *Nat. Rev. Drug Discov.* **2022**, *21* (12), 881–898.
- (21) Jollow, D. J.; Mitchell, J. R.; Potter, W. Z.; Davis, D. C.; Gillette, J. R.; Brodie, B. B. Acetaminophen Induced Hepatic Necrosis. II. Role of Covalent Binding in Vivo. *J. Pharmacol. Exp. Ther.* **1973**, *187* (1), 195–202.
- (22) Erve, J. C. L. Chemical Toxicology: Reactive Intermediates and Their Role in Pharmacology and Toxicology. *Expert Opin. Drug Metab. Toxicol.* **2006**, *2* (6), 923–946.
- (23) Ralhan, R.; Kaur, J. Alkylating Agents and Cancer Therapy. *Expert Opin. Ther. Pat.* **2007**, *17* (9), 1061–1075.
- (24) Polavarapu, A.; Stillabower, J. A.; Stubblefield, S. G. W.; Taylor, W. M.; Baik, M. H. The Mechanism of Guanine Alkylation by Nitrogen Mustards: A Computational Study. *J. Org. Chem.* **2012**, *77* (14), 5914–5921.
- (25) Mann, D. J. Aziridinium Ion Ring Formation from Nitrogen Mustards: Mechanistic Insights from Ab Initio Dynamics. *J. Phys. Chem. A* **2010**, *114* (13), 4486–4493.
- (26) Povirk, L. F.; Shuker, D. E. DNA Damage and Mutagenesis Induced by Nitrogen Mustards. *Mutat. Res. Genet. Toxicol.* **1994**, *318* (3), 205–226.
- (27) Drahl, C.; Cravatt, B. F.; Sorensen, E. J.; Cravatt, B. F.; Sorensen, E. J.; Drahl, C. Protein-Reactive Natural Products. *Angew. Chemie Int. Ed.* **2005**, *44* (36), 5788–5809.
- (28) Abeles, R. H.; Maycock, A. L. Suicide Enzyme Inactivators. *Acc. Chem. Res.* **1976**, *9* (9), 313–319.



- (29) Avendaño, C.; Menéndez, J. C. *Medicinal Chemistry of Anticancer Drugs*; Elsevier, 2008.
- (30) Gehrtz, P.; London, N. Electrophilic Natural Products as Drug Discovery Tools. *Trends Pharmacol. Sci.* **2021**, *42* (6), 434–447.
- (31) Huffman, B. J.; Shenvi, R. A. Natural Products in the “Marketplace”: Interfacing Synthesis and Biology. *J. Am. Chem. Soc.* **2019**, *141* (8), 3332–3346.
- (32) Singh, J. The Ascension of Targeted Covalent Inhibitors. *J. Med. Chem.* **2022**, *65* (8), 5886–5901.
- (33) Barf, T.; Kaptein, A. Irreversible Protein Kinase Inhibitors: Balancing the Benefits and Risks. *J. Med. Chem.* **2012**, *55* (14), 6243–6262.
- (34) Soria, J.-C.; Ohe, Y.; Vansteenkiste, J.; Reungwetwattana, T.; Chewaskulyong, B.; Lee, K. H.; Dechaphunkul, A.; Imamura, F.; Nogami, N.; Kurata, T.; Okamoto, I.; Zhou, C.; Cho, B. C.; Cheng, Y.; Cho, E. K.; Voon, P. J.; Planchard, D.; Su, W.-C.; Gray, J. E.; Lee, S.-M.; Hodge, R.; Marotti, M.; Rukazenzov, Y.; Ramalingam, S. S. Osimertinib in Untreated EGFR -Mutated Advanced Non-Small-Cell Lung Cancer. *N. Engl. J. Med.* **2018**, *378* (2), 113–125.
- (35) Nakajima, E. C.; Drezner, N.; Li, X.; Mishra-Kalyani, P. S.; Liu, Y.; Zhao, H.; Bi, Y.; Liu, J.; Rahman, A.; Wearne, E.; Ojofeitimi, I.; Hotaki, L. T.; Spillman, D.; Pazdur, R.; Beaver, J. A.; Singh, H. FDA Approval Summary: Sotorasib for KRAS G12C-Mutated Metastatic NSCLC. *Clin. Cancer Res.* **2022**, *28* (8), 1482–1486.
- (36) Byrd, J. C.; Harrington, B.; O’Brien, S.; Jones, J. A.; Schuh, A.; Devereux, S.; Chaves, J.; Wierda, W. G.; Awan, F. T.; Brown, J. R.; Hillmen, P.; Stephens, D. M.; Ghia, P.; Barrientos, J. C.; Pagel, J. M.; Woyach, J.; Johnson, D.; Huang, J.; Wang, X.; Kaptein, A.; Lannutti, B. J.; Covey, T.; Fardis, M.; McGreivy, J.; Hamdy, A.; Rothbaum, W.; Izumi, R.; Diacovo, T. G.; Johnson, A. J.; Furman, R. R. Acalabrutinib (ACP-196) in Relapsed Chronic Lymphocytic Leukemia. *N. Engl. J. Med.* **2016**, *374* (4), 323–332.
- (37) Strelow, J. M. A Perspective on the Kinetics of Covalent and Irreversible Inhibition. *SLAS Discov.* **2017**, *22* (1), 3–20.
- (38) Maurer, T. S.; Tabrizi-Fard, M. A.; Maurer, T. S. Impact of Mechanism-Based Enzyme Inactivation on Inhibitor Potency: Implications for Rational Drug Discovery. *J. Pharm. Sci.* **2000**, *89* (11), 1404–1414.
- (39) Duffy, M. J.; Crown, J. Drugging “Undruggable” Genes for Cancer Treatment: Are We Making Progress? *Int. J. Cancer* **2021**, *148* (1), 8–17.
- (40) Johnson, D. S.; Weerapana, E.; Cravatt, B. F. Strategies for Discovering and Derisking Covalent, Irreversible Enzyme Inhibitors. *Future Medicinal Chemistry*. Future Science Ltd London, UK June 14, 2010, pp 949–964.
- (41) Lipton, S. A. Paradigm Shift in Neuroprotection by NMDA Receptor Blockade: Memantine and Beyond. *Nat. Rev. Drug Discov.* **2006**, *5* (2), 160–170.

- (42) Kannaiyan, R.; Mahadevan, D. A Comprehensive Review of Protein Kinase Inhibitors for Cancer Therapy. *Expert Rev. Anticancer Ther.* **2018**, *18* (12), 1249.
- (43) Zhang, M.; Liu, Y.; Jang, H.; Nussinov, R. Strategy toward Kinase-Selective Drug Discovery. *J. Chem. Theory Comput.* **2022**, *19*, 10.
- (44) Bosc, N.; Meyer, C.; Bonnet, P. The Use of Novel Selectivity Metrics in Kinase Research. *BMC Bioinformatics* **2017**, *18* (1), 1–12.
- (45) Woyach, J. A.; Furman, R. R.; Liu, T.-M.; Ozer, H. G.; Zapatka, M.; Ruppert, A. S.; Xue, L.; Li, D. H.-H.; Steggerda, S. M.; Versele, M.; Dave, S. S.; Zhang, J.; Yilmaz, A. S.; Jaglowski, S. M.; Blum, K. A.; Lozanski, A.; Lozanski, G.; James, D. F.; Barrientos, J. C.; Lichter, P.; Stilgenbauer, S.; Buggy, J. J.; Chang, B. Y.; Johnson, A. J.; Byrd, J. C. Resistance Mechanisms for the Bruton's Tyrosine Kinase Inhibitor Ibrutinib. *N. Engl. J. Med.* **2014**, *370* (24), 2286–2294.
- (46) Niederst, M. J.; Hu, H.; Mulvey, H. E.; Lockerman, E. L.; Garcia, A. R.; Piotrowska, Z.; Sequist, L. V.; Engelman, J. A. The Allelic Context of the C797S Mutation Acquired upon Treatment with Third-Generation EGFR Inhibitors Impacts Sensitivity to Subsequent Treatment Strategies. *Clin. Cancer Res.* **2015**, *21* (17), 3924–3933.
- (47) Pan, Z.; Scheerens, H.; Li, S. J.; Schultz, B. E.; Sprengeler, P. A.; Burrill, L. C.; Mendonca, R. V.; Sweeney, M. D.; Scott, K. C. K.; Grothaus, P. G.; Jeffery, D. A.; Spoerke, J. M.; Honigberg, L. A.; Young, P. R.; Dalrymple, S. A.; Palmer, J. T. Discovery of Selective Irreversible Inhibitors for Bruton's Tyrosine Kinase. *ChemMedChem* **2007**, *2* (1), 58–61.
- (48) Bender, A. T.; Gardberg, A.; Pereira, A.; Johnson, T.; Wu, Y.; Grenningloh, R.; Head, J.; Morandi, F.; Haselmayer, P.; Liu-Bujalski, L. Ability of Bruton's Tyrosine Kinase Inhibitors to Sequester Y551 and Prevent Phosphorylation Determines Potency for Inhibition of Fc Receptor but Not B-Cell Receptor Signaling. *Mol. Pharmacol.* **2017**, *91* (3), 208–219.
- (49) Goebel, L.; Müller, M. P.; Goody, R. S.; Rauh, D. KRasG12C Inhibitors in Clinical Trials: A Short Historical Perspective. *RSC Med. Chem.* **2020**, *11* (7), 760–770.
- (50) Kwan, A. K.; Piazza, G. A.; Keeton, A. B.; Leite, C. A. The Path to the Clinic: A Comprehensive Review on Direct KRASG12C Inhibitors. *J. Exp. Clin. Cancer Res.* **2022**, *41* (1), 1–23.
- (51) Ostrem, J. M.; Peters, U.; Sos, M. L.; Wells, J. A.; Shokat, K. M. K-Ras(G12C) Inhibitors Allosterically Control GTP Affinity and Effector Interactions. *Nature* **2013**, *503* (7477), 548–551.
- (52) Patricelli, M. P.; Janes, M. R.; Li, L. S.; Hansen, R.; Peters, U.; Kessler, L. V.; Chen, Y.; Kucharski, J. M.; Feng, J.; Ely, T.; Chen, J. H.; Firdaus, S. J.; Babbar, A.; Ren, P.; Liu, Y. Selective Inhibition of Oncogenic KRAS Output with Small Molecules Targeting the Inactive State. *Cancer Discov.* **2016**, *6* (3), 316–329.
- (53) Janes, M. R.; Zhang, J.; Li, L. S.; Hansen, R.; Peters, U.; Guo, X.; Chen, Y.; Babbar, A.; Firdaus, S. J.; Darjanian, L.; Feng, J.; Chen, J. H.; Li, S.; Li, S.; Long,

- Y. O.; Thach, C.; Liu, Y.; Zariéh, A.; Ely, T.; Kucharski, J. M.; Kessler, L. V.; Wu, T.; Yu, K.; Wang, Y.; Yao, Y.; Deng, X.; Zarrinkar, P. P.; Brehmer, D.; Dhanak, D.; Lorenzi, M. V.; Hu-Lowe, D.; Patricelli, M. P.; Ren, P.; Liu, Y. Targeting KRAS Mutant Cancers with a Covalent G12C-Specific Inhibitor. *Cell* **2018**, *172* (3), 578–589.
- (54) Lanman, B. A.; Allen, J. R.; Allen, J. G.; Amegadzie, A. K.; Ashton, K. S.; Booker, S. K.; Chen, J. J.; Chen, N.; Frohn, M. J.; Goodman, G.; Kopecky, D. J.; Liu, L.; Lopez, P.; Low, J. D.; Ma, V.; Minatti, A. E.; Nguyen, T. T.; Nishimura, N.; Pickrell, A. J.; Reed, A. B.; Shin, Y.; Siegmund, A. C.; Tamayo, N. A.; Tegley, C. M.; Walton, M. C.; Wang, H. L.; Wurz, R. P.; Xue, M.; Yang, K. C.; Achanta, P.; Bartberger, M. D.; Canon, J.; Hollis, L. S.; McCarter, J. D.; Mohr, C.; Rex, K.; Saiki, A. Y.; San Miguel, T.; Volak, L. P.; Wang, K. H.; Whittington, D. A.; Zech, S. G.; Lipford, J. R.; Cee, V. J. Discovery of a Covalent Inhibitor of KRASG12C (AMG 510) for the Treatment of Solid Tumors. *J. Med. Chem.* **2020**, *63* (1), 52–65.
- (55) Hansen, R.; Peters, U.; Babbar, A.; Chen, Y.; Feng, J.; Janes, M. R.; Li, L. S.; Ren, P.; Liu, Y.; Zarrinkar, P. P. The Reactivity-Driven Biochemical Mechanism of Covalent KRASG12C Inhibitors. *Nat. Struct. Mol. Biol.* **2018**, *25* (6), 454–462.
- (56) Huynh, M. V.; Parsonage, D.; Forshaw, T. E.; Chirasani, V. R.; Hobbs, G. A.; Wu, H.; Lee, J.; Furdui, C. M.; Poole, L. B.; Campbell, S. L. Oncogenic KRAS G12C: Kinetic and Redox Characterization of Covalent Inhibition. *J. Biol. Chem.* **2022**, *298* (8), 102186.
- (57) Wang, S.; Tian, Y.; Wang, M.; Wang, M.; Sun, G. B.; Sun, X. B. Advanced Activity-Based Protein Profiling Application Strategies for Drug Development. *Front. Pharmacol.* **2018**, *9*.
- (58) Barglow, K. T.; Cravatt, B. F. Activity-Based Protein Profiling for the Functional Annotation of Enzymes. *Nat. Methods* **2007**, *4* (10), 822–827.
- (59) Liu, Y.; Patricelli, M. P.; Cravatt, B. F. Activity-Based Protein Profiling: The Serine Hydrolases. *Proc. Natl. Acad. Sci. U. S. A.* **1999**, *96* (26), 14694–14699.
- (60) Lanning, B. R.; Whitby, L. R.; Dix, M. M.; Douhan, J.; Gilbert, A. M.; Hett, E. C.; Johnson, T. O.; Joslyn, C.; Kath, J. C.; Niessen, S.; Roberts, L. R.; Schnute, M. E.; Wang, C.; Hulce, J. J.; Wei, B.; Whiteley, L. O.; Hayward, M. M.; Cravatt, B. F. A Road Map to Evaluate the Proteome-Wide Selectivity of Covalent Kinase Inhibitors. *Nat. Chem. Biol.* **2014**, *10* (9), 760–767.
- (61) Rostovtsev, V. V.; Green, L. G.; Fokin, V. V.; Sharpless, K. B. A Stepwise Huisgen Cycloaddition Process: Copper(I)-Catalyzed Regioselective “Ligation” of Azides and Terminal Alkynes. *Angew. Chemie - Int. Ed.* **2002**, *41* (14), 2596–2599.
- (62) Lin, A.; Giuliano, C. J.; Palladino, A.; John, K. M.; Abramowicz, C.; Yuan, M. Lou; Sausville, E. L.; Lukow, D. A.; Liu, L.; Chait, A. R.; Galluzzo, Z. C.; Tucker, C.; Sheltzer, J. M. Off-Target Toxicity Is a Common Mechanism of Action of Cancer Drugs Undergoing Clinical Trials. *Sci. Transl. Med.* **2019**, *11* (509).

- (63) Anighoro, A.; Bajorath, J.; Rastelli, G. Polypharmacology: Challenges and Opportunities in Drug Discovery. *J. Med. Chem.* **2014**, *57* (19), 7874–7887.
- (64) Weerapana, E.; Wang, C.; Simon, G. M.; Richter, F.; Khare, S.; Dillon, M. B. D.; Bachovchin, D. A.; Mowen, K.; Baker, D.; Cravatt, B. F. Quantitative Reactivity Profiling Predicts Functional Cysteines in Proteomes. *Nature* **2010**, *468* (7325), 790–797.
- (65) Boja, E. S.; Fales, H. M. Overalkylation of a Protein Digest with Iodoacetamide. *Anal. Chem.* **2001**, *73* (15), 3576–3582.
- (66) Jones, L. H. Design of Next-Generation Covalent Inhibitors: Targeting Residues beyond Cysteine. *Annu. Rep. Med. Chem.* **2021**, *56*, 95–134.
- (67) Roos, G.; Foloppe, N.; Messens, J. Understanding the PKa of Redox Cysteines: The Key Role of Hydrogen Bonding. *Antioxidants Redox Signal.* **2013**, *18* (1), 94–127.
- (68) Harris, T. K.; Turner, G. J. Structural Basis of Perturbed PKa Values of Catalytic Groups in Enzyme Active Sites. *IUBMB Life* **2002**, *53* (2), 85–98.
- (69) Pinitglang, S.; Watts, A. B.; Patel, M.; Reid, J. D.; Noble, M. A.; Gul, S.; Bokth, A.; Naeem, A.; Patel, H.; Thomas, E. W.; Sreedharan, S. K.; Verma, C.; Brocklehurst, K. A Classical Enzyme Active Center Motif Lacks Catalytic Competence until Modulated Electrostatically. *Biochemistry* **1997**, *36* (33), 9968–9982.
- (70) Wang, P. F.; McLeish, M. J.; Kneen, M. M.; Lee, G.; Kenyon, G. L. An Unusually Low PKa for Cys282 in the Active Site of Human Muscle Creatine Kinase. *Biochemistry* **2001**, *40* (39), 11698–11705.
- (71) Kortemme, T.; Creighton, T. E. Ionisation of Cysteine Residues at the Termini of Model  $\alpha$ -Helical Peptides. Relevance to Unusual Thiol PKa Values in Proteins of the Thioredoxin Family. *J. Mol. Biol.* **1995**, *253* (5), 799–812.
- (72) Baillie, T. A. Approaches to Mitigate the Risk of Serious Adverse Reactions in Covalent Drug Design. *Expert Opin. Drug Discov.* **2021**, *16* (3), 275–287.
- (73) Tian, L.; Liu, S.; Wang, S.; Wang, L. Ligand-Binding Specificity and Promiscuity of the Main Lignocellulolytic Enzyme Families as Revealed by Active-Site Architecture Analysis. *Sci. Rep.* **2016**, *6* (1), 1–11.
- (74) Moura, A.; Savageau, M. A.; Alves, R. Relative Amino Acid Composition Signatures of Organisms and Environments. *PLoS One* **2013**, *8* (10), e77319.
- (75) Mukherjee, H.; Grimster, N. P. Beyond Cysteine: Recent Developments in the Area of Targeted Covalent Inhibition. *Curr. Opin. Chem. Biol.* **2018**, *44*, 30–38.
- (76) Platzer, G.; Okon, M.; McIntosh, L. P. PH-Dependent Random Coil <sup>1</sup>H, <sup>13</sup>C, and <sup>15</sup>N Chemical Shifts of the Ionizable Amino Acids: A Guide for Protein PKa Measurements. *J. Biomol. NMR* **2014**, *60* (2–3), 109–129.

- (77) Pahari, S.; Sun, L.; Alexov, E. PKAD: A Database of Experimentally Measured PKa Values of Ionizable Groups in Proteins. *Database* **2019**, *2019* (1).
- (78) Isom, D. G.; Castañed, C. A.; Cannon, B. R.; García-Moreno, B. E. Large Shifts in PKa Values of Lysine Residues Buried inside a Protein. *Proc. Natl. Acad. Sci. U. S. A.* **2011**, *108* (13), 5260–5265.
- (79) LoPachin, R. M.; Geohagen, B. C.; Nordstroem, L. U. Mechanisms of Soft and Hard Electrophile Toxicities. *Toxicology* **2019**, *418*, 62–69.
- (80) Ho, T. L. The Hard Soft Acids Bases (HSAB) Principle and Organic Chemistry. *Chem. Rev.* **1975**, *75* (1), 1–20.
- (81) Dahal, U. P.; Gilbert, A. M.; Obach, R. S.; Flanagan, M. E.; Chen, J. M.; Garcia-Irizarry, C.; Starr, J. T.; Schuff, B.; Uccello, D. P.; Young, J. A. Intrinsic Reactivity Profile of Electrophilic Moieties to Guide Covalent Drug Design:: N - $\alpha$ -Acetyl-L-Lysine as an Amine Nucleophile. *Med. Chem. Commun.* **2016**, *7* (5), 864–872.
- (82) Anscombe, E.; Meschini, E.; Mora-Vidal, R.; Martin, M. P.; Staunton, D.; Geitmann, M.; Danielson, U. H.; Stanley, W. A.; Wang, L. Z.; Reuillon, T.; Golding, B. T.; Cano, C.; Newell, D. R.; Noble, M. E. M.; Wedge, S. R.; Endicott, J. A.; Griffin, R. J. Identification and Characterization of an Irreversible Inhibitor of CDK2. *Chem. Biol.* **2015**, *22* (9), 1159–1164.
- (83) Choi, S.; Connelly, S.; Reixach, N.; Wilson, I. A.; Kelly, J. W. Chemoselective Small Molecules That Covalently Modify One Lysine in a Non-Enzyme Protein in Plasma. *Nat. Chem. Biol.* **2010**, *6* (2), 133–139.
- (84) Dalton, S. E.; Dittus, L.; Thomas, D. A.; Convery, M. A.; Nunes, J.; Bush, J. T.; Evans, J. P.; Werner, T.; Bantscheff, M.; Murphy, J. A.; Campos, S. Selectively Targeting the Kinome-Conserved Lysine of PI3K $\delta$  as a General Approach to Covalent Kinase Inhibition. *J. Am. Chem. Soc.* **2018**, *140* (3), 932–939.
- (85) Hanks, S. K.; Quinn, A. M.; Hunter, T. The Protein Kinase Family: Conserved Features and Deduced Phylogeny of the Catalytic Domains. *Science* **1988**, *241* (4861), 42–52.
- (86) Jones, L. H.; Kelly, J. W. Structure-Based Design and Analysis of SuFEx Chemical Probes. *RSC Med. Chem.* **2020**, *11* (1), 10–17.
- (87) Narayanan, A.; Jones, L. H. Sulfonyl Fluorides as Privileged Warheads in Chemical Biology. *Chem. Sci.* **2015**, *6* (5), 2650–2659.
- (88) Gold, A. M.; Fahrney, D. Sulfonyl Fluorides as Inhibitors of Esterases. II. Formation and Reactions of Phenylmethanesulfonyl  $\alpha$ -Chymotrypsin. *Biochemistry* **1964**, *3* (6), 783–791.
- (89) Pal, P. K.; Wechter, W. J.; Colman, R. F. Affinity Labeling of a Regulatory Site of Bovine Liver Glutamate Dehydrogenase. *Biochemistry* **1975**, *14* (4), 707–715.
- (90) Kamps, M. P.; Taylor, S. S.; Sefton, B. M. Direct Evidence That Oncogenic Tyrosine Kinases and Cyclic AMP-Dependent Protein Kinase Have Homologous

- ATP-Binding Sites. *Nature* **1984**, *310* (5978), 589–592.
- (91) Gushwa, N. N.; Kang, S.; Chen, J.; Taunton, J. Selective Targeting of Distinct Active Site Nucleophiles by Irreversible Src-Family Kinase Inhibitors. *J. Am. Chem. Soc.* **2012**, *134* (50), 20214–20217.
- (92) Grimster, N. P.; Connelly, S.; Baranczak, A.; Dong, J.; Krasnova, L. B.; Sharpless, K. B.; Powers, E. T.; Wilson, I. A.; Kelly, J. W. Aromatic Sulfonyl Fluorides Covalently Kinetically Stabilize Transthyretin to Prevent Amyloidogenesis While Affording a Fluorescent Conjugate. *J. Am. Chem. Soc.* **2013**, *135* (15), 5656–5668.
- (93) Wan, X.; Yang, T.; Cuesta, A.; Pang, X.; Balius, T. E.; Irwin, J. J.; Shoichet, B. K.; Taunton, J. Discovery of Lysine-Targeted EIF4E Inhibitors through Covalent Docking. *J. Am. Chem. Soc.* **2020**, *142* (11), 4960–4964.
- (94) Jones, L. H. Emerging Utility of Fluorosulfate Chemical Probes. *ACS Med. Chem. Lett.* **2018**, *9* (7), 584–586.
- (95) Mortenson, D. E.; Brighty, G. J.; Plate, L.; Bare, G.; Chen, W.; Li, S.; Wang, H.; Cravatt, B. F.; Forli, S.; Powers, E. T.; Sharpless, K. B.; Wilson, I. A.; Kelly, J. W. “Inverse Drug Discovery” Strategy to Identify Proteins That Are Targeted by Latent Electrophiles As Exemplified by Aryl Fluorosulfates. *J. Am. Chem. Soc.* **2018**, *140* (1), 200–210.
- (96) Lodillinsky, C.; Fuhrmann, L.; Irondelle, M.; Pylypenko, O.; Li, X. Y.; Bonsang-Kitzis, H.; Reyal, F.; Vacher, S.; Calmel, C.; De Wever, O.; Bièche, I.; Lacombe, M. L.; Eiján, A. M.; Houdusse, A.; Vincent-Salomon, A.; Weiss, S. J.; Chavrier, P.; Boissan, M. Metastasis-Suppressor NME1 Controls the Invasive Switch of Breast Cancer by Regulating MT1-MMP Surface Clearance. *Oncogene* **2021**, *40* (23), 4019–4032.
- (97) Wang, Y.; Kathryn Leonard, M.; Snyder, D. E.; Fisher, M. L.; Eckert, R. L.; Kaetzel, D. M. NME1 Drives Expansion of Melanoma Cells with Enhanced Tumor Growth and Metastatic Properties. *Mol. Cancer Res.* **2019**, *17* (8), 1665–1674.
- (98) Pettinger, J.; Jones, K.; Cheeseman, M. D. Lysine-Targeting Covalent Inhibitors. *Angew. Chemie Int. Ed.* **2017**, *56* (48), 15200–15209.
- (99) Zhang, G.; Zhang, J.; Gao, Y.; Li, Y.; Li, Y. Strategies for Targeting Undruggable Targets. *Expert Opin. Drug Discov.* **2022**, *17* (1), 55–69.
- (100) Burdon, R. H. Heat Shock and the Heat Shock Proteins. *Biochem. J.* **1986**, *240* (2), 313–324.
- (101) Richter, K.; Haslbeck, M.; Buchner, J. The Heat Shock Response: Life on the Verge of Death. *Mol. Cell* **2010**, *40* (2), 253–266.
- (102) Hartl, F. U.; Bracher, A.; Hayer-Hartl, M. Molecular Chaperones in Protein Folding and Proteostasis. *Nature* **2011**, *475* (7356), 324–332.
- (103) Radons, J. The Human HSP70 Family of Chaperones: Where Do We Stand? *Cell Stress Chaperones* **2016**, *21* (3), 379–404.

- (104) Patury, S.; Miyata, Y.; Gestwicki, J. Pharmacological Targeting of the Hsp70 Chaperone. *Curr. Top. Med. Chem.* **2009**, *9* (15), 1337–1351.
- (105) Hunt, C.; Morimoto, R. I. Conserved Features of Eukaryotic Hsp70 Genes Revealed by Comparison with the Nucleotide Sequence of Human Hsp70. *Proc. Natl. Acad. Sci.* **1985**, *82* (19), 6455–6459.
- (106) Volloch, V. Z.; Sherman, M. Y. Oncogenic Potential of Hsp72. *Oncogene* **1999**, *18* (24), 3648–3651.
- (107) Stricher, F.; Macri, C.; Ruff, M.; Muller, S. HSPA8/HSC70 Chaperone Protein: Structure, Function, and Chemical Targeting. *Autophagy* **2013**, *9* (12), 1937–1954.
- (108) Xia, S.; Duan, W.; Liu, W.; Zhang, X.; Wang, Q. GRP78 in Lung Cancer. *J. Transl. Med.* **2021**, *19* (1), 1–14.
- (109) Wu, P. K.; Hong, S. K.; Chen, W.; Becker, A. E.; Gundry, R. L.; Lin, C. W.; Shao, H.; Gestwicki, J. E.; Park, J. I. Mortalin (HSPA9) Facilitates BRAF-Mutant Tumor Cell Survival by Suppressing ANT3-Mediated Mitochondrial Membrane Permeability. *Sci. Signal.* **2020**, *13* (622), 1478.
- (110) Rosenzweig, R.; Nillegoda, N. B.; Mayer, M. P.; Bukau, B. The Hsp70 Chaperone Network. *Nat. Rev. Mol. Cell Biol.* **2019**, *20* (11), 665–680.
- (111) Kityk, R.; Kopp, J.; Sinning, I.; Mayer, M. P. Structure and Dynamics of the ATP-Bound Open Conformation of Hsp70 Chaperones. *Mol. Cell* **2012**, *48* (6), 863–874.
- (112) Bertelsen, E. B.; Chang, L.; Gestwicki, J. E.; Zuiderweg, E. R. P. Solution Conformation of Wild-Type E. Coli Hsp70 (DnaK) Chaperone Complexed with ADP and Substrate. *Proc. Natl. Acad. Sci. U. S. A.* **2009**, *106* (21), 8471–8476.
- (113) Flaherty, K. M.; DeLuca-Flaherty, C.; McKay, D. B. Three-Dimensional Structure of the ATPase Fragment of a 70K Heat-Shock Cognate Protein. *Nature* **1990**, *346* (6285), 623–628.
- (114) Sriram; Osipiuk, J.; Freeman, B. C.; Morimoto, R. I.; Joachimiak, A. Human Hsp70 Molecular Chaperone Binds Two Calcium Ions within the ATPase Domain. *Structure* **1997**, *5* (3), 403–414.
- (115) Arakawa, A.; Handa, N.; Shirouzu, M.; Yokoyama, S. Biochemical and Structural Studies on the High Affinity of Hsp70 for ADP. *Protein Sci.* **2011**, *20* (8), 1367–1379.
- (116) Thomsen, N. D.; Berger, J. M. Structural Frameworks for Considering Microbial Protein- and Nucleic Acid-Dependent Motor ATPases. *Mol. Microbiol.* **2008**, *69* (5), 1071–1090.
- (117) Rüdiger, S.; Buchberger, A.; Bukau, B. Interaction of Hsp70 Chaperones with Substrates. *Nat. Struct. Biol.* **1997**, *4* (5), 342–349.
- (118) Zhuravleva, A.; Gierasch, L. M. Allosteric Signal Transmission in the Nucleotide-

- Binding Domain of 70-KDa Heat Shock Protein (Hsp70) Molecular Chaperones. *Proc. Natl. Acad. Sci. U. S. A.* **2011**, *108* (17), 6987–6992.
- (119) Kityk, R.; Vogel, M.; Schlecht, R.; Bukau, B.; Mayer, M. P. Pathways of Allosteric Regulation in Hsp70 Chaperones. *Nat. Commun.* **2015**, *6* (1), 1–11.
- (120) Laufen, T.; Mayer, M. P.; Beisel, C.; Klostermeier, D.; Mogk, A.; Reinstein, J.; Bukau, B. Mechanism of Regulation of Hsp70 Chaperones by DnaJ Cochaperones. *Proc. Natl. Acad. Sci.* **1999**, *96* (10), 5452–5457.
- (121) Gässler, C. S.; Wiederkehr, T.; Brehmer, D.; Bukau, B.; Mayer, M. P. Bag-1M Accelerates Nucleotide Release for Human Hsc70 and Hsp70 and Can Act Concentration-Dependent as Positive and Negative Cofactor. *J. Biol. Chem.* **2001**, *276* (35), 32538–32544.
- (122) De Billy, E.; Powers, M. V.; Smith, J. R.; Workman, P. Drugging the Heat Shock Factor 1 Pathway: Exploitation of the Critical Cancer Cell Dependence on the Guardian of the Proteome. *Cell Cycle* **2009**, *8* (23), 3806–3808.
- (123) Sherman, M. Y.; Gabai, V. L. Hsp70 in Cancer: Back to the Future. *Oncogene* **2015**, *34* (32), 4153–4161.
- (124) Luo, J.; Solimini, N. L.; Elledge, S. J. Principles of Cancer Therapy: Oncogene and Non-Oncogene Addiction. *Cell* **2009**, *136* (5), 823–837.
- (125) Neckers, L.; Workman, P. Hsp90 Molecular Chaperone Inhibitors: Are We There Yet? *Clin. Cancer Res.* **2012**, *18* (1), 64–76.
- (126) Hoy, S. M. Pimipib: First Approval. *Drugs* **2022**, *82* (13), 1413–1418.
- (127) Evans, C. G.; Chang, L.; Gestwicki, J. E. Heat Shock Protein 70 (Hsp70) as an Emerging Drug Target. *J. Med. Chem.* **2010**, *53* (12), 4585–4602.
- (128) Prince, T.; Ackerman, A.; Cavanaugh, A.; Schreiter, B.; Juengst, B.; Andolino, C.; Danella, J.; Chernin, M.; Williams, H.; Prince, T.; Ackerman, A.; Cavanaugh, A.; Schreiter, B.; Juengst, B.; Andolino, C.; Danella, J.; Chernin, M.; Williams, H. Dual Targeting of HSP70 Does Not Induce the Heat Shock Response and Synergistically Reduces Cell Viability in Muscle Invasive Bladder Cancer. *Oncotarget* **2018**, *9* (66), 32702–32717.
- (129) Powers, M. V.; Clarke, P. A.; Workman, P. Dual Targeting of HSC70 and HSP72 Inhibits HSP90 Function and Induces Tumor-Specific Apoptosis. *Cancer Cell* **2008**, *14* (3), 250–262.
- (130) Goloudina, A. R.; Demidov, O. N.; Garrido, C. Inhibition of HSP70: A Challenging Anti-Cancer Strategy. *Cancer Lett.* **2012**, *325* (2), 117–124.
- (131) Massey, A. J. ATPases as Drug Targets: Insights from Heat Shock Proteins 70 and 90. *J. Med. Chem.* **2010**, *53* (20), 7280–7286.
- (132) Schlecht, R.; Scholz, S. R.; Dahmen, H.; Wegener, A.; Sirrenberg, C.; Musil, D.; Bomke, J.; Eggenweiler, H. M.; Mayer, M. P.; Bukau, B. Functional Analysis of



- Hsp70 Inhibitors. *PLoS One* **2013**, 8 (11), e78443.
- (133) Evans, L. E.; Cheeseman, M. D.; Yahya, N.; Jones, K. Investigating Apoptozole as a Chemical Probe for HSP70 Inhibition. *PLoS One* **2015**, 10 (10), e0140006.
- (134) Williamson, D. S.; Borgognoni, J.; Clay, A.; Daniels, Z.; Dokurno, P.; Drysdale, M. J.; Foloppe, N.; Francis, G. L.; Graham, C. J.; Howes, R.; Macias, A. T.; Murray, J. B.; Parsons, R.; Shaw, T.; Surgenor, A. E.; Terry, L.; Wang, Y.; Wood, M.; Massey, A. J. Novel Adenosine-Derived Inhibitors of 70 KDa Heat Shock Protein, Discovered through Structure-Based Design. *J. Med. Chem.* **2009**, 52 (6), 1510–1513.
- (135) Massey, A. J.; Williamson, D. S.; Browne, H.; Murray, J. B.; Dokurno, P.; Shaw, T.; Macias, A. T.; Daniels, Z.; Geoffroy, S.; Dopson, M.; Lavan, P.; Matassova, N.; Francis, G. L.; Graham, C. J.; Parsons, R.; Wang, Y.; Padfield, A.; Comer, M.; Drysdale, M. J.; Wood, M. A Novel, Small Molecule Inhibitor of Hsc70/Hsp70 Potentiates Hsp90 Inhibitor Induced Apoptosis in HCT116 Colon Carcinoma Cells. *Cancer Chemother. Pharmacol.* **2010**, 66 (3), 535–545.
- (136) Russell, R.; Jordan, R.; McMacken, R. Kinetic Characterization of the ATPase Cycle of the DnaK Molecular Chaperone. *Biochemistry* **1998**, 37 (2), 596–607.
- (137) Jeung-Hoi, H.; McKay, D. B. ATPase Kinetics of Recombinant Bovine 70 KDa Heat Shock Cognate Protein and Its Amino-Terminal ATPase Domain. *Biochemistry* **1994**, 33 (48), 14625–14635.
- (138) Weikl, T.; Muschler, P.; Richter, K.; Veit, T.; Reinstein, J.; Buchner, J. C-Terminal Regions of Hsp90 Are Important for Trapping the Nucleotide during the ATPase Cycle. *J. Mol. Biol.* **2000**, 303 (4), 583–592.
- (139) Yang, N. J.; Hinner, M. J. Getting across the Cell Membrane: An Overview for Small Molecules, Peptides, and Proteins. *Methods Mol. Biol.* **2015**, 1266, 29–53.
- (140) Chène, P. ATPases as Drug Targets: Learning from Their Structure. *Nat. Rev. Drug Discov.* **2002**, 1 (9), 665–673.
- (141) Shida, M.; Arakawa, A.; Ishii, R.; Kishishita, S.; Takagi, T.; Kukimoto-Niino, M.; Sugano, S.; Tanaka, A.; Shirouzu, M.; Yokoyama, S. Direct Inter-Subdomain Interactions Switch between the Closed and Open Forms of the Hsp70 Nucleotide-Binding Domain in the Nucleotide-Free State. *Acta Crystallogr. Sect. D Biol. Crystallogr.* **2010**, 66 (3), 223–232.
- (142) Cheeseman, M. D.; Westwood, I. M.; Barbeau, O.; Rowlands, M.; Dobson, S.; Jones, A. M.; Jeganathan, F.; Burke, R.; Kadi, N.; Workman, P.; Collins, I.; Van Montfort, R. L. M.; Jones, K. Exploiting Protein Conformational Change to Optimize Adenosine-Derived Inhibitors of HSP70. *J. Med. Chem.* **2016**, 59 (10), 4625–4636.
- (143) Jones, A. M.; Westwood, I. M.; Osborne, J. D.; Matthews, T. P.; Cheeseman, M. D.; Rowlands, M. G.; Jeganathan, F.; Burke, R.; Lee, D.; Kadi, N.; Liu, M.; Richards, M.; McAndrew, C.; Yahya, N.; Dobson, S. E.; Jones, K.; Workman, P.; Collins, I.; Van Montfort, R. L. M. A Fragment-Based Approach Applied to a

- Highly Flexible Target: Insights and Challenges towards the Inhibition of HSP70 Isoforms. *Sci. Rep.* **2016**, *6* (1), 1–13.
- (144) Pettinger, J.; Le Bihan, Y.-V.; Widya, M.; van Montfort, R. L. M.; Jones, K.; Cheeseman, M. D. An Irreversible Inhibitor of HSP72 That Unexpectedly Targets Lysine-56. *Angew. Chemie Int. Ed.* **2017**, *56* (13), 3536–3540.
- (145) Pettinger, J.; Carter, M.; Jones, K.; Cheeseman, M. D. Kinetic Optimization of Lysine-Targeting Covalent Inhibitors of HSP72. *J. Med. Chem.* **2019**, *62* (24), 11383–11398.
- (146) Mons, E.; Roet, S.; Kim, R. Q.; Mulder, M. P. C. A Comprehensive Guide for Assessing Covalent Inhibition in Enzymatic Assays Illustrated with Kinetic Simulations. *Curr. Protoc.* **2022**, *2* (6), e419.
- (147) Mukherjee, H.; Debreczeni, J.; Breed, J.; Tentarelli, S.; Aquila, B.; Dowling, J. E.; Whitty, A.; Grimster, N. P. A Study of the Reactivity of S(VI)–F Containing Warheads with Nucleophilic Amino-Acid Side Chains under Physiological Conditions. *Org. Biomol. Chem.* **2017**, *15* (45), 9685–9695.
- (148) Hansch, C.; Leo, A.; Taft, R. W. A Survey of Hammett Substituent Constants and Resonance and Field Parameters. *Chem. Rev.* **1991**, *91* (2), 165–195.
- (149) Wang, Z. *Comprehensive Organic Name Reactions and Reagents*; John Wiley & Sons, Ltd, 2010.
- (150) Schlosser, M.; Heinz, G. The Carbene/Carbenoid Problem. *Angew. Chemie Int. Ed. English* **1969**, *8* (10), 760–761.
- (151) Gronert, S.; Keeffe, J. R.; More O’Ferrall, R. A. Stabilities of Carbenes: Independent Measures for Singlets and Triplets. *J. Am. Chem. Soc.* **2011**, *133* (10), 3381–3389.
- (152) de Frémont, P.; Marion, N.; Nolan, S. P. Carbenes: Synthesis, Properties, and Organometallic Chemistry. *Coord. Chem. Rev.* **2009**, *253*, 862–892.
- (153) Evans, L. E.; Jones, K.; Cheeseman, M. D. Targeting Secondary Protein Complexes in Drug Discovery: Studying the Druggability and Chemical Biology of the HSP70/BAG1 Complex. *Chem. Commun.* **2017**, *53* (37), 5167–5170.
- (154) Evans, L. E. Small Molecule Probes and Inhibitors of ATPases, The Institute of Cancer Research, University of London, 2014.
- (155) Pettinger, J. Design and Synthesis of Irreversible Inhibitors of HSP72, The Institute of Cancer Research, University of London, 2018.
- (156) MacIas, A. T.; Williamson, D. S.; Allen, N.; Borgognoni, J.; Clay, A.; Daniels, Z.; Dokurno, P.; Drysdale, M. J.; Francis, G. L.; Graham, C. J.; Howes, R.; Matassova, N.; Murray, J. B.; Parsons, R.; Shaw, T.; Surgenor, A. E.; Terry, L.; Wang, Y.; Wood, M.; Massey, A. J. Adenosine-Derived Inhibitors of 78 KDa Glucose Regulated Protein (Grp78) ATPase: Insights into Isoform Selectivity. *J. Med. Chem.* **2011**, *54* (12), 4034–4041.

- (157) Wang, L.; Hashidoko, Y.; Hashimoto, M. Cosolvent-Promoted O-Benzoylation with Silver(I) Oxide: Synthesis of 1'-Benzylated Sucrose Derivatives, Mechanistic Studies, and Scope Investigation. *J. Org. Chem.* **2016**, *81* (11), 4464–4474.
- (158) Schmidt, R. R.; Michel, J. Facile Synthesis of  $\alpha$ - and  $\beta$ -O-Glycosyl Imidates; Preparation of Glycosides and Disaccharides. *Angew. Chemie Int. Ed. English* **1980**, *19* (9), 731–732.
- (159) Kiyoshi, N.; Satoshi, N.; Tsuneo, I.; Akira, H.; Kengo, O.; Yutaka, K.; Hajime, T.; Takatoshi, U.; Masatoshi, G. 2-Aryl-Ethyl Ether Derivatives and Insecticidal and Acaricidal Agents Containing Said Derivatives. US4599362A, 1986.
- (160) Wuts, P. G. M. *Protective Groups in Organic Synthesis*; John Wiley & Sons, Inc., 2014.
- (161) De Ruyscher, D.; Pang, L.; De Graef, S.; Nautiyal, M.; De Borggraeve, W. M.; Rozenski, J.; Strelkov, S. V.; Weeks, S. D.; Van Aerschot, A. Acylated Sulfonamide Adenosines as Potent Inhibitors of the Adenylate-Forming Enzyme Superfamily. *Eur. J. Med. Chem.* **2019**, *174*, 252–264.
- (162) Chandra, T.; Broderick, W. E.; Broderick, J. B. An Efficient Deprotection of N-Trimethylsilylethoxymethyl (SEM) Groups from Dinucleosides and Dinucleotides. *Nucleosides, Nucleotides and Nucleic Acids* **2010**, *29* (2), 132–143.
- (163) Vakalopoulos, A.; Hoffmann, H. M. R. Novel Deprotection of SEM Ethers: A Very Mild and Selective Method Using Magnesium Bromide. *Org. Lett.* **2000**, *2* (10), 1447–1450.
- (164) Davies, A. T.; Curto, J. M.; Bagley, S. W.; Willis, M. C. One-Pot Palladium-Catalyzed Synthesis of Sulfonyl Fluorides from Aryl Bromides. *Chem. Sci.* **2017**, *8* (2), 1233–1237.
- (165) Kan, T.; Hashimoto, M.; Yanagiya, M.; Shirahama, H. Effective Deprotection of 2-(Trimethylsilylethoxy)methylated Alcohols (SEM Ethers). Synthesis of Thyrsiferyl-23 Acetate. *Tetrahedron Lett.* **1988**, *29* (42), 5417–5418.
- (166) Chen, J.; Ding, C. Z.; Dragovich, P.; Fauber, B.; Labadie, S.; Lai, K. W.; Purkey, H. E.; Robarge, K.; Wei, B.; Zhou, A. Piperidine-Dione Derivatives. WO2015140133A1, 2015.
- (167) Ingoglia, B. T.; Wagen, C. C.; Buchwald, S. L. Biaryl Monophosphine Ligands in Palladium-Catalyzed C–N Coupling: An Updated User's Guide. *Tetrahedron* **2019**, *75* (32), 4199–4211.
- (168) Jim-Min, F.; Chen, Y.-L. L.; Lin, J.-H.; Chih-Cheng; Lin, C.-J.; Chern, Y.; Huang, N.-K.; Wang, H.-L.; Tu, B. P. Compounds for Use in Prevention and Treatment of Neurodegenerative Diseases and Pain. WO2015061426A1, 2015.
- (169) Sitta Sittampalam, G.; Coussens, N. P.; Brimacombe, K.; Grossman, A.; Arkin, M.; Auld, D.; Austin, C.; Baell, J.; Bejcek, B.; Chung, T. D.; Dahlin, J. L.; Devanaryan, V.; Foley, T.; Marcie Glicksman Matthew Hall, B. D.; Joseph Hass, B. V.; James Inglese, B.; Philip Iversen Steven D Kahl, B. W.; Madhu Lal-Nag, B.;

- Zhuyin Li, B.; James McGee Owen McManus, B.; Terry Riss, B.; Joseph Trask, B. O.; Jeffrey Weidner Menghang Xia, B. R.; Xin Xu, B.; Minor, L.; Lemmon, V.; Napper, A.; Peltier, J. M.; Nelsen, H.; Gal-Edd, N.; Sittampalam, G. S.; Coussens, N. P.; Brimacombe, K.; Grossman, A.; Arkin, M.; Auld, D.; Austin, C.; Baell, J.; Bejcek, B.; Chung, T. D. Y.; Dahlin, J. L.; Devanaryan, V.; Foley, T. L.; Glicksman, M.; Hall, M. D.; Hass, J. V.; Inglese, J.; Iversen, P. W.; Kahl, S. D.; Lal-Nag, M.; Li, Z.; McGee, J.; McManus, O.; Riss, T.; O. Joseph Trask, J.; Weidner, J. R.; Xia, M.; Xu, X. *Assay Guidance Manual*; Eli Lilly & Company and the National Center for Advancing Translational Sciences, 2004.
- (170) Wisén, S.; Gestwicki, J. E. Identification of Small Molecules That Modify the Protein Folding Activity of Heat Shock Protein 70. *Anal. Biochem.* **2008**, *374* (2), 371–377.
- (171) Chang, L.; Bertelsen, E. B.; Wisén, S.; Larsen, E. M.; Zuiderweg, E. R. P.; Gestwicki, J. E. High-Throughput Screen for Small Molecules That Modulate the ATPase Activity of the Molecular Chaperone DnaK. *Anal. Biochem.* **2008**, *372* (2), 167–176.
- (172) McCarty, J. S.; Buchberger, A.; Reinstein, J.; Bukau, B. The Role of ATP in the Functional Cycle of the DnaK Chaperone System. *J. Mol. Biol.* **1995**, *249* (1), 126–137.
- (173) Laufen, T.; Mayer, M. P.; Beisel, C.; Klostermeier, D.; Mogk, A.; Reinstein, J.; Bukau, B. Mechanism of Regulation of Hsp70 Chaperones by DnaJ Cochaperones. *Proc. Natl. Acad. Sci. U. S. A.* **1999**, *96* (10), 5452–5457.
- (174) Jones, A. M.; Westwood, I. M.; Osborne, J. D.; Matthews, T. P.; Cheeseman, M. D.; Rowlands, M. G.; Jeganathan, F.; Burke, R.; Lee, D.; Kadi, N.; Liu, M.; Richards, M.; McAndrew, C.; Yahya, N.; Dobson, S. E.; Jones, K.; Workman, P.; Collins, I.; Van Montfort, R. L. M. A Fragment-Based Approach Applied to a Highly Flexible Target: Insights and Challenges towards the Inhibition of HSP70 Isoforms. *Sci. Rep.* **2016**, *6* (1), 1–13.
- (175) Bakhtiar, R. Surface Plasmon Resonance Spectroscopy: A Versatile Technique in a Biochemist's Toolbox. *J. Chem. Educ.* **2013**, *90* (2), 203–209.
- (176) Jolley, M. E. Fluorescence Polarization Assays for the Detection of Proteases and Their Inhibitors. *SLAS Discov.* **1996**, *1* (1), 33–38.
- (177) Hall, M. D.; Yasgar, A.; Peryea, T.; Braisted, J. C.; Jadhav, A.; Simeonov, A.; Coussens, N. P. Fluorescence Polarization Assays in High-Throughput Screening and Drug Discovery: A Review. *Methods Appl. Fluoresc.* **2016**, *4* (2), 022001.
- (178) Perrin, F. Polarisation de La Lumière de Fluorescence. Vie Moyenne Des Molécules Dans l'état Excité. *J. Phys. le Radium* **1926**, *7* (12), 390–401.
- (179) Einstein, A. Über Die von Der Molekularkinetischen Theorie Der Wärme Geforderte Bewegung von in Ruhenden Flüssigkeiten Suspendierten Teilchen. *Ann. Phys.* **1905**, *322* (8), 549–560.
- (180) Owicki, J. C. Fluorescence Polarization and Anisotropy in High Throughput

- Screening: Perspectives and Primer. *SLAS Discov.* **2000**, 5 (5), 297–306.
- (181) Jameson, D. M.; Ross, J. A. Fluorescence Polarization/Anisotropy in Diagnostics and Imaging. *Chem. Rev.* **2010**, 110 (5), 2685–2708.
- (182) Burlingham, B. T.; Widlanski, T. S. An Intuitive Look at the Relationship of  $K_i$  and IC50: A More General Use for the Dixon Plot. *J. Chem. Educ.* **2003**, 80 (2), 214–218.
- (183) Yung-Chi, C.; Prusoff, W. H. Relationship between the Inhibition Constant ( $K_i$ ) and the Concentration of Inhibitor Which Causes 50 per Cent Inhibition (I50) of an Enzymatic Reaction. *Biochem. Pharmacol.* **1973**, 22 (23), 3099–3108.
- (184) Huang, X. Fluorescence Polarization Competition Assay: The Range of Resolvable Inhibitor Potency Is Limited by the Affinity of the Fluorescent Ligand. *SLAS Discov.* **2003**, 8 (1), 34–38.
- (185) Zhao, F.; Zhang, J.; Zhang, L.; Hao, Y.; Shi, C.; Xia, G.; Yu, J.; Liu, Y. Discovery and Optimization of a Series of Imidazo[4,5-b]Pyrazine Derivatives as Highly Potent and Exquisitely Selective Inhibitors of the Mesenchymal–Epithelial Transition Factor (c-Met) Protein Kinase. *Bioorg. Med. Chem.* **2016**, 24 (18), 4281–4290.
- (186) Meanwell, N. A. Fluorine and Fluorinated Motifs in the Design and Application of Bioisosteres for Drug Design. *J. Med. Chem.* **2018**, 61 (14), 5822–5880.
- (187) Garrett, E. R.; Mehta, P. J. Solvolysis of Adenine Nucleosides. I. Effects of Sugars and Adenine Substituents on Acid Solvolyses. *J. Am. Chem. Soc.* **1972**, 94 (24), 8532–8541.
- (188) Hett, E. C.; Xu, H.; Geoghegan, K. F.; Gopalsamy, A.; Kyne, R. E.; Menard, C. A.; Narayanan, A.; Parikh, M. D.; Liu, S.; Roberts, L.; Robinson, R. P.; Tones, M. A.; Jones, L. H. Rational Targeting of Active-Site Tyrosine Residues Using Sulfonyl Fluoride Probes. *ACS Chem. Biol.* **2015**, 10 (4), 1094–1098.
- (189) Cravatt, B. F.; Wright, A. T.; Kozarich, J. W. Activity-Based Protein Profiling: From Enzyme Chemistry to Proteomic Chemistry. *Annu. Rev. Biochem.* **2008**, 77, 383–414.
- (190) Speers, A. E.; Cravatt, B. F. Profiling Enzyme Activities In Vivo Using Click Chemistry Methods. *Chem. Biol.* **2004**, 11 (4), 535–546.
- (191) Hao, Y.; Zhou, G.; Wu, W.; Zhang, Y.; Tao, L.; Yao, J.; Xu, W. Synthesis and Antiviral Evaluation of Novel N-6 Substituted Adenosine Analogues. *Tetrahedron Lett.* **2017**, 58 (3), 190–193.
- (192) Garcia, F. J.; Carroll, K. S. Redox-Based Probes as Tools to Monitor Oxidized Protein Tyrosine Phosphatases in Living Cells. *Eur. J. Med. Chem.* **2014**, 88, 28–33.
- (193) Chinchilla, R.; Nájera, C. Chemicals from Alkynes with Palladium Catalysts. *Chem. Rev.* **2014**, 114 (3), 1783–1826.

- (194) Gramlich, P. M. E.; Warncke, S.; Gierlich, J.; Carell, T. Click–Click–Click: Single to Triple Modification of DNA. *Angew. Chemie Int. Ed.* **2008**, *47* (18), 3442–3444.
- (195) Romanov-Michailidis, F.; Ravetz, B. D.; Paley, D. W.; Rovis, T. Ir(III)-Catalyzed Carbocarbation of Alkynes through Undirected Double C-H Bond Activation of Anisoles. *J. Am. Chem. Soc.* **2018**, *140* (16), 5370–5374.
- (196) Fraser, R. R.; Mansour, T. S.; Savard, S. Acidity Measurements on Pyridines in Tetrahydrofuran Using Lithiated Silylamines. *J. Org. Chem.* **1985**, *50* (17), 3232–3234.
- (197) Larson, G. L. Some Aspects of the Chemistry of Alkynylsilanes. *Synthesis (Stuttg.)*. **2018**, *50* (13), 2433–2462.
- (198) Schwartz, P. A.; Kuzmic, P.; Solowiej, J.; Bergqvist, S.; Bolanos, B.; Almaden, C.; Nagata, A.; Ryan, K.; Feng, J.; Dalvie, D.; Kath, J. C.; Xu, M.; Wani, R.; Murray, B. W. Covalent EGFR Inhibitor Analysis Reveals Importance of Reversible Interactions to Potency and Mechanisms of Drug Resistance. *Proc. Natl. Acad. Sci. U. S. A.* **2014**, *111* (1), 173–178.
- (199) MacFaul, P. A.; Morley, A. D.; Crawford, J. J. A Simple in Vitro Assay for Assessing the Reactivity of Nitrile Containing Compounds. *Bioorg. Med. Chem. Lett.* **2009**, *19* (4), 1136–1138.
- (200) Gilbert, K. E.; Vuorinen, A.; Aatkar, A.; Pogány, P.; Pettinger, J.; Grant, E. K.; Kirkpatrick, J. M.; Rittinger, K.; House, D.; Burley, G. A.; Bush, J. T. Profiling Sulfur(VI) Fluorides as Reactive Functionalities for Chemical Biology Tools and Expansion of the Ligandable Proteome. *ACS Chem. Biol.* **2023**, *18* (2), 285–295.
- (201) Arora, M. Cell Culture Media: A Review. *Mater. Methods* **2013**, *3*, 175.
- (202) Freshney, R. I. *Culture of Animal Cells: A Manual of Basic Technique and Specialized Applications: Sixth Edition*; John Wiley & Sons, Inc., 2011.
- (203) Dulbecco's Modified Eagle's Medium - high glucose <https://www.sigmaaldrich.com/GB/en/product/sigma/d5671>.
- (204) Den, R. B.; Lu, B. Heat Shock Protein 90 Inhibition: Rationale and Clinical Potential. *Ther. Adv. Med. Oncol.* **2012**, *4* (4), 211–218.
- (205) Teuscher, K. B.; Zhang, M.; Ji, H. A Versatile Method to Determine the Cellular Bioavailability of Small-Molecule Inhibitors. *J. Med. Chem.* **2017**, *60* (1), 157–169.
- (206) Richardson, P. L.; Marin, V. L.; Koeniger, S. L.; Baranczak, A.; Wilsbacher, J. L.; Kovar, P. J.; Bacon-Trusk, P. E.; Cheng, M.; Hopkins, T. A.; Haman, S. T.; Vasudevan, A. Controlling Cellular Distribution of Drugs with Permeability Modifying Moieties. *Medchemcomm* **2019**, *10* (6), 974–984.
- (207) Fleming, I. *Molecular Orbitals and Organic Chemical Reactions, Student Edition*; John Wiley and Sons, Ltd., 2009.

- (208) Tummino, P. J.; Copeland, R. A. Residence Time of Receptor - Ligand Complexes and Its Effect on Biological Function. *Biochemistry* **2008**, *47* (20), 5481–5492.
- (209) Holdgate, G. A.; Meek, T. D.; Grimley, R. L. Mechanistic Enzymology in Drug Discovery: A Fresh Perspective. *Nat. Rev. Drug Discov.* **2018**, *17* (2), 115–132.
- (210) Takakusa, H.; Masumoto, H.; Yukinaga, H.; Makino, C.; Nakayama, S.; Okazaki, O.; Sudo, K. Covalent Binding and Tissue Distribution/Retention Assessment of Drugs Associated with Idiosyncratic Drug Toxicity. *Drug Metab. Dispos.* **2008**, *36* (9), 1770–1779.
- (211) Faridoo; Ng, R.; Zhang, G.; Li, J. J. An Update on the Discovery and Development of Reversible Covalent Inhibitors. *Med. Chem. Res.* **2023**, *32* (6), 1039–1062.
- (212) *New Comprehensive Biochemistry*; Page, M. I., Ed.; Elsevier, 1984; Vol. 6.
- (213) Bell, R. P.; McDougall, A. O. Hydration Equilibria of Some Aldehydes and Ketones. *Trans. Faraday Soc.* **1960**, *56* (0), 1281–1285.
- (214) Chatterjee, S.; Anslyn, E. V.; Bandyopadhyay, A. Boronic Acid Based Dynamic Click Chemistry: Recent Advances and Emergent Applications. *Chem. Sci.* **2021**, *12* (5), 1585–1599.
- (215) Dunn, H. E.; Gatlin, J. C.; Snyder, H. R. Arylboronic Acids. Imino Derivatives from o-Formylbenzeneboronic Acid. *J. Org. Chem.* **1968**, *33* (12), 4483–4486.
- (216) Cal, P. M. S. D.; Vicente, J. B.; Pires, E.; Coelho, A. V.; Veiros, L. F.; Cordeiro, C.; Gois, P. M. P. Iminoboronates: A New Strategy for Reversible Protein Modification. *J. Am. Chem. Soc.* **2012**, *134* (24), 10299–10305.
- (217) Zhao, Z.-H.; Li, C.-H.; Zuo, J.-L. Dynamic Polymeric Materials Based on Reversible B–O Bonds with Dative Boron–Nitrogen Coordination. *SmartMat* **2023**, *4* (3), e1187.
- (218) Akçay, G.; Belmonte, M. A.; Aquila, B.; Chuaqui, C.; Hird, A. W.; Lamb, M. L.; Rawlins, P. B.; Su, N.; Tentarelli, S.; Grimster, N. P.; Su, Q. Inhibition of Mcl-1 through Covalent Modification of a Noncatalytic Lysine Side Chain. *Nat. Chem. Biol.* **2016**, *12* (11), 931–936.
- (219) Reja, R. M.; Wang, W.; Lyu, Y.; Haeffner, F.; Gao, J. Lysine-Targeting Reversible Covalent Inhibitors with Long Residence Time. *J. Am. Chem. Soc.* **2022**, *144* (3), 1152–1157.
- (220) Metzler, D. E.; Snell, E. E.; Snell, E. E. Some Transamination Reactions Involving Vitamin B6. *J. Am. Chem. Soc.* **1952**, *74* (4), 979–983.
- (221) Metzler, D. E.; Olivard, J.; Snell, E. E. Transamination of Pyridoxamine and Amino Acids with Glyoxylic Acid. *J. Am. Chem. Soc.* **1954**, *76* (3), 644–648.
- (222) French, T. C.; Auld, D. S.; Bruice, T. C. Catalytic Reactions Involving Azomethines. V. Rates and Equilibria of Imine Formation with 3-

- Hydroxypyridine-4-Aldehyde and Amino Acids. *Biochemistry* **1965**, *4* (1), 77–84.
- (223) Metzler, C. M.; Cahill, A.; Metzler, D. E. Equilibria and Absorption Spectra of Schiff Bases. *J. Am. Chem. Soc.* **1980**, *102* (19), 6075–6082.
- (224) Herscovitch, R.; Charette, J. J.; de Hoffmann, E. Physicochemical Properties of Schiff Bases. III. Substituent Effects on the Kinetics of Hydrolysis of N-Salicylidene-2-Aminopropane Derivatives. *J. Am. Chem. Soc.* **1974**, *96* (15), 4954–4958.
- (225) Beddell, C. R.; Goodford, P. J.; Kneen, G.; White, R. D.; Wilkinson, S.; Wootton, R. Substituted Benzaldehydes Designed to Increase the Oxygen Affinity of Human Haemoglobin and Inhibit the Sickling of Sickle Erythrocytes. *Br. J. Pharmacol.* **1984**, *82* (2), 397–407.
- (226) Metcalf, B.; Chuang, C.; Dufu, K.; Patel, M. P.; Silva-Garcia, A.; Johnson, C.; Lu, Q.; Partridge, J. R.; Patskovska, L.; Patskovsky, Y.; Almo, S. C.; Jacobson, M. P.; Hua, L.; Xu, Q.; Gwaltney, S. L.; Yee, C.; Harris, J.; Morgan, B. P.; James, J.; Xu, D.; Hutchaleelaha, A.; Paulvannan, K.; Oksenberg, D.; Li, Z. Discovery of GBT440, an Orally Bioavailable R-State Stabilizer of Sickle Cell Hemoglobin. *ACS Med. Chem. Lett.* **2017**, *8* (3), 321–326.
- (227) Blair, H. A. Voxelotor: First Approval. *Drugs* **2020**, *80* (2), 209–215.
- (228) Oksenberg, D.; Dufu, K.; Patel, M. P.; Chuang, C.; Li, Z.; Xu, Q.; Silva-Garcia, A.; Zhou, C.; Hutchaleelaha, A.; Patskovska, L.; Patskovsky, Y.; Almo, S. C.; Sinha, U.; Metcalf, B. W.; Archer, D. R. GBT440 Increases Haemoglobin Oxygen Affinity, Reduces Sickling and Prolongs RBC Half-Life in a Murine Model of Sickle Cell Disease. *Br. J. Haematol.* **2016**, *175* (1), 141–153.
- (229) Sanches, M.; Duffy, N. M.; Talukdar, M.; Thevakumaran, N.; Chiovitti, D.; Canny, M. D.; Lee, K.; Kurinov, I.; Uehling, D.; Al-Awar, R.; Poda, G.; Prakesch, M.; Wilson, B.; Tam, V.; Schweitzer, C.; Toro, A.; Lucas, J. L.; Vuga, D.; Lehmann, L.; Durocher, D.; Zeng, Q.; Patterson, J. B.; Sicheri, F. Structure and Mechanism of Action of the Hydroxy-Aryl-Aldehyde Class of IRE1 Endoribonuclease Inhibitors. *Nat. Commun.* **2014**, *5* (1), 1–16.
- (230) Sheng, X.; Nenseth, H. Z.; Qu, S.; Kuzu, O. F.; Frahnnow, T.; Simon, L.; Greene, S.; Zeng, Q.; Fazli, L.; Rennie, P. S.; Mills, I. G.; Danielsen, H.; Theis, F.; Patterson, J. B.; Jin, Y.; Saatcioglu, F. IRE1 $\alpha$ -XBP1s Pathway Promotes Prostate Cancer by Activating c-MYC Signaling. *Nat. Commun.* **2019**, *10* (1), 1–12.
- (231) Gabrail, N. Y.; Hamilton, E. P.; Elias, A. D.; Rimawi, M. F.; Li, C.; Corvez, M. M.; Li, W.; Feng, Y.; Wei, J.; Greene, S.; Patterson, J.; Zeng, Q.; Hui, A.-M. A Phase 1/2 Trial of ORIN1001, a First-in-Class IRE1 Inhibitor, in Patients with Advanced Solid Tumors. *J. Clin. Oncol.* **2021**, *39* (15\_suppl), 3080–3080.
- (232) Quach, D.; Tang, G.; Anantharajan, J.; Baburajendran, N.; Poulsen, A.; Wee, J. L. K.; Retna, P.; Li, R.; Liu, B.; Tee, D. H. Y.; Kwek, P. Z.; Joy, J. K.; Yang, W. Q.; Zhang, C. J.; Foo, K.; Keller, T. H.; Yao, S. Q. Strategic Design of Catalytic Lysine-Targeting Reversible Covalent BCR-ABL Inhibitors. *Angew. Chemie Int.*



- Ed.* **2021**, *60* (31), 17131–17137.
- (233) Chen, P.; Sun, J.; Zhu, C.; Tang, G.; Wang, W.; Xu, M.; Xiang, M.; Zhang, C. J.; Zhang, Z. M.; Gao, L.; Yao, S. Q. Cell-Active, Reversible, and Irreversible Covalent Inhibitors That Selectively Target the Catalytic Lysine of BCR-ABL Kinase. *Angew. Chemie - Int. Ed.* **2022**, *61* (26), e202203878.
- (234) Yang, T.; Cuesta, A.; Wan, X.; Craven, G. B.; Hirakawa, B.; Khamphavong, P.; May, J. R.; Kath, J. C.; Lapek, J. D.; Niessen, S.; Burlingame, A. L.; Carelli, J. D.; Taunton, J. Reversible Lysine-Targeted Probes Reveal Residence Time-Based Kinase Selectivity. *Nat. Chem. Biol.* **2022**, *18* (9), 934–941.
- (235) Graham, B. J.; Windsor, I. W.; Gold, B.; Raines, R. T. Boronic Acid with High Oxidative Stability and Utility in Biological Contexts. *Proc. Natl. Acad. Sci. U. S. A.* **2021**, *118* (10), e2013691118.
- (236) Aliyan, H.; Fazaeli, R.; Massah, A. R.; Momeni, A. R.; Naghash, H. J.; Moeinifard, B. Acetalization of Carbonyl Compounds Catalyzed by Bismuth Triflate under Solvent-Free Conditions. *Asian J. Chem.* **2010**, *22* (2), 873–876.
- (237) Invitrogen. *Technical Resource Guide: Fluorescence Polarisation*, 4th ed.; 2006.
- (238) López-Yerena, A.; Perez, M.; Vallverdú-Queralt, A.; Escribano-Ferrer, E. Insights into the Binding of Dietary Phenolic Compounds to Human Serum Albumin and Food-Drug Interactions. *Pharmaceutics* **2020**, *12* (11), 1–18.
- (239) Tan, Y.; Siebert, K. J. Modeling Bovine Serum Albumin Binding of Flavor Compounds (Alcohols, Aldehydes, Esters, and Ketones) as a Function of Molecular Properties. *J. Food Sci.* **2008**, *73* (1), S56–S63.
- (240) Liu, X.; Wright, M.; Hop, C. E. C. A. Rational Use of Plasma Protein and Tissue Binding Data in Drug Design. *J. Med. Chem.* **2014**, *57* (20), 8238–8248.
- (241) Van Rooden, E. J.; Florea, B. I.; Deng, H.; Baggelaar, M. P.; Van Esbroeck, A. C. M.; Zhou, J.; Overkleeft, H. S.; Van Der Stelt, M. Mapping in Vivo Target Interaction Profiles of Covalent Inhibitors Using Chemical Proteomics with Label-Free Quantification. *Nat. Protoc.* **2018**, *13* (4), 752–767.
- (242) Kenny, P. W. Hydrogen-Bond Donors in Drug Design. *J. Med. Chem.* **2022**, *65* (21), 14261–14275.
- (243) Obrzud, M.; Rospenk, M.; Koll, A. Structure of Aggregates of Dialkyl Urea Derivatives in Solutions. *J. Phys. Chem. B* **2010**, *114* (48), 15905–15912.
- (244) Hamid, A. B.; Petreaca, R. C. Secondary Resistant Mutations to Small Molecule Inhibitors in Cancer Cells. *Cancers (Basel)*. **2020**, *12* (4).
- (245) Schlessinger, J. Receptor Tyrosine Kinases: Legacy of the First Two Decades. *Cold Spring Harb. Perspect. Biol.* **2014**, *6* (3), a008912.
- (246) Herbst, R. S. Review of Epidermal Growth Factor Receptor Biology. *Int. J. Radiat. Oncol. Biol. Phys.* **2004**, *59* (No.2 Supplement), 21–26.

- (247) Lemmon, M. A.; Schlessinger, J. Cell Signaling by Receptor-Tyrosine Kinases. *Cell* **2010**, *141* (7), 1117.
- (248) Burgess, A. W.; Cho, H. S.; Eigenbrot, C.; Ferguson, K. M.; Garrett, T. P. J.; Leahy, D. J.; Lemmon, M. A.; Sliwkowski, M. X.; Ward, C. W.; Yokoyama, S. An Open-and-Shut Case? Recent Insights into the Activation of EGF/ErbB Receptors. *Mol. Cell* **2003**, *12* (3), 541–552.
- (249) Tice, D. A.; Biscardi, J. S.; Nickles, A. L.; Parsons, S. J. Mechanism of Biological Synergy between Cellular Src and Epidermal Growth Factor Receptor. *Proc. Natl. Acad. Sci.* **1999**, *96* (4), 1415–1420.
- (250) Lemmon, M. A.; Schlessinger, J.; Ferguson, K. M. The EGFR Family: Not So Prototypical Receptor Tyrosine Kinases. *Cold Spring Harb. Perspect. Biol.* **2014**, *6* (4), a020768.
- (251) Shigematsu, H.; Gazdar, A. F. Somatic Mutations of Epidermal Growth Factor Receptor Signaling Pathway in Lung Cancers. *Int. J. Cancer* **2006**, *118* (2), 257–262.
- (252) Kumari, N.; Kumari, N.; Singh, S.; Haloi, D.; Mishra, S. K.; Krishnani, N.; Nath, A.; Neyaz, Z. Epidermal Growth Factor Receptor Mutation Frequency in Squamous Cell Carcinoma and Its Diagnostic Performance in Cytological Samples: A Molecular and Immunohistochemical Study. *World J. Oncol.* **2019**, *10* (3), 142–150.
- (253) Baselga, J.; Averbuch, S. D. ZD1839 ('Iressa')<sub>1,2</sub> as an Anticancer Agent. *Drugs* **2000**, *60* (Suppl. 1), 33–40.
- (254) Moyer, James D., Elsa G. Barbacci, Kenneth K. Iwata, Lee Arnold, Bruce Boman, Ann Cunningham, Catherine DiOrio, Jonathan Doty, Michael J. Morin, Mikel P. Moyer, Mark Neveu, Vincent A. Pollack, Leslie R. Pustilnik, Margaret M. Reynolds, Don Sloan, April Th, P. M. Induction of Apoptosis and Cell Cycle Arrest by CP-358,774, an Inhibitor of Epidermal Growth Factor Receptor Tyrosine Kinase. *Cancer Res.* **1997**, *57* (21), 4838–4848.
- (255) Yu, H. A.; Arcila, M. E.; Rekhtman, N.; Sima, C. S.; Zakowski, M. F.; Pao, W.; Kris, M. G.; Miller, V. A.; Ladanyi, M.; Riely, G. J. Analysis of Tumor Specimens at the Time of Acquired Resistance to EGFR-TKI Therapy in 155 Patients with EGFR-Mutant Lung Cancers. *Clin. Cancer Res.* **2013**, *19* (8), 2240–2247.
- (256) Yun, C. H.; Mengwasser, K. E.; Toms, A. V.; Woo, M. S.; Greulich, H.; Wong, K. K.; Meyerson, M.; Eck, M. J. The T790M Mutation in EGFR Kinase Causes Drug Resistance by Increasing the Affinity for ATP. *Proc. Natl. Acad. Sci. U. S. A.* **2008**, *105* (6), 2070–2075.
- (257) Zhai, X.; Ward, R. A.; Doig, P.; Argyrou, A. Insight into the Therapeutic Selectivity of the Irreversible EGFR Tyrosine Kinase Inhibitor Osimertinib through Enzyme Kinetic Studies. *Biochemistry* **2020**, *59* (14), 1428–1441.
- (258) Li, D.; Ambrogio, L.; Shimamura, T.; Kubo, S.; Takahashi, M.; Chirieac, L. R.; Padera, R. F.; Shapiro, G. I.; Baum, A.; Himmelsbach, F.; Rettig, W. J.; Meyerson,

- M.; Solca, F.; Greulich, H.; Wong, K. K. BIBW2992, an Irreversible EGFR/HER2 Inhibitor Highly Effective in Preclinical Lung Cancer Models. *Oncogene* **2008**, *27* (34), 4702–4711.
- (259) Yu, H. A.; Pao, W. Targeted Therapies: Afatinib-New Therapy Option for EGFR-Mutant Lung Cancer. *Nat. Rev. Clin. Oncol.* **2013**, *10* (10), 551–552.
- (260) Singh, P. K.; Singh, H.; Silakari, O. Kinases Inhibitors in Lung Cancer: From Benchside to Bedside. *Biochim. Biophys. Acta - Rev. Cancer* **2016**, *1866* (1), 128–140.
- (261) Ou, S. H. I. Second-Generation Irreversible Epidermal Growth Factor Receptor (EGFR) Tyrosine Kinase Inhibitors (TKIs): A Better Mousetrap? A Review of the Clinical Evidence. *Crit. Rev. Oncol. Hematol.* **2012**, *83* (3), 407–421.
- (262) Ellis, P. M.; Shepherd, F. A.; Millward, M.; Perrone, F.; Seymour, L.; Liu, G.; Sun, S.; Cho, B. C.; Morabito, A.; Leighl, N. B.; Stockler, M. R.; Lee, C. W.; Wierzbicki, R.; Cohen, V.; Blais, N.; Sangha, R. S.; Favaretto, A. G.; Kang, J. H.; Tsao, M. S.; Wilson, C. F.; Goldberg, Z.; Ding, K.; Goss, G. D.; Bradbury, P. A. Dacomitinib Compared with Placebo in Pretreated Patients with Advanced or Metastatic Non-Small-Cell Lung Cancer (NCIC CTG BR.26): A Double-Blind, Randomised, Phase 3 Trial. *Lancet Oncol.* **2014**, *15* (12), 1379–1388.
- (263) Lacouture, M. E. Mechanisms of Cutaneous Toxicities to EGFR Inhibitors. *Nat. Rev. Cancer* **2006**, *6* (10), 803–812.
- (264) Finlay, M. R. V.; Anderton, M.; Ashton, S.; Ballard, P.; Bethel, P. A.; Box, M. R.; Bradbury, R. H.; Brown, S. J.; Butterworth, S.; Campbell, A.; Chorley, C.; Colclough, N.; Cross, D. A. E.; Currie, G. S.; Grist, M.; Hassall, L.; Hill, G. B.; James, D.; James, M.; Kemmitt, P.; Klinowska, T.; Lamont, G.; Lamont, S. G.; Martin, N.; McFarland, H. L.; Mellor, M. J.; Orme, J. P.; Perkins, D.; Perkins, P.; Richmond, G.; Smith, P.; Ward, R. A.; Waring, M. J.; Whittaker, D.; Wells, S.; Wrigley, G. L. Discovery of a Potent and Selective EGFR Inhibitor (AZD9291) of Both Sensitizing and T790M Resistance Mutations That Spares the Wild Type Form of the Receptor. *J. Med. Chem.* **2014**, *57* (20), 8249–8267.
- (265) Mok, T. S.; Wu, Y.-L.; Ahn, M.-J.; Garassino, M. C.; Kim, H. R.; Ramalingam, S. S.; Shepherd, F. A.; He, Y.; Akamatsu, H.; Theelen, W. S. M. E.; Lee, C. K.; Sebastian, M.; Templeton, A.; Mann, H.; Marotti, M.; Ghiorghiu, S.; Papadimitrakopoulou, V. A. Osimertinib or Platinum–Pemetrexed in *EGFR* T790M–Positive Lung Cancer. *N. Engl. J. Med.* **2017**, *376* (7), 629–640.
- (266) Jänne, P. A.; Yang, J. C.-H.; Kim, D.-W.; Planchard, D.; Ohe, Y.; Ramalingam, S. S.; Ahn, M.-J.; Kim, S.-W.; Su, W.-C.; Horn, L.; Haggstrom, D.; Felip, E.; Kim, J.-H.; Frewer, P.; Cantarini, M.; Brown, K. H.; Dickinson, P. A.; Ghiorghiu, S.; Ranson, M. AZD9291 in EGFR Inhibitor–Resistant Non–Small-Cell Lung Cancer. *N. Engl. J. Med.* **2015**, *372* (18), 1689–1699.
- (267) Leonetti, A.; Sharma, S.; Minari, R.; Perego, P.; Giovannetti, E.; Tiseo, M. Resistance Mechanisms to Osimertinib in EGFR-Mutated Non-Small Cell Lung Cancer. *Br. J. Cancer* **2019**, *121* (9), 725–737.

- (268) Papadimitrakopoulou, V. A.; Wu, Y.-L.; Han, J.-Y.; Ahn, M.-J.; Ramalingam, S. S.; John, T.; Okamoto, I.; Yang, J. C.-H.; Bulusu, K. C.; Laus, G.; Collins, B.; Barrett, J. C.; Chmielecki, J.; Mok, T. S. K. Analysis of Resistance Mechanisms to Osimertinib in Patients with EGFR T790M Advanced NSCLC from the AURA3 Study. *Ann. Oncol.* **2018**, *29*, viii741.
- (269) Thress, K. S.; Paweletz, C. P.; Felip, E.; Cho, B. C.; Stetson, D.; Dougherty, B.; Lai, Z.; Markovets, A.; Vivancos, A.; Kuang, Y.; Ercan, D.; Matthews, S. E.; Cantarini, M.; Barrett, J. C.; Jänne, P. A.; Oxnard, G. R. Acquired EGFR C797S Mutation Mediates Resistance to AZD9291 in Non-Small Cell Lung Cancer Harboring EGFR T790M. *Nat. Med.* **2015**, *21* (6), 560–562.
- (270) Xu, L.; Xu, B.; Wang, J.; Gao, Y.; He, X.; Xie, T.; Ye, X. Y. Recent Advances of Novel Fourth Generation EGFR Inhibitors in Overcoming C797S Mutation of Lung Cancer Therapy. *Eur. J. Med. Chem.* **2023**, *245*, 114900.
- (271) Carrera, A. C.; Alexandrov, K.; Roberts, T. M. The Conserved Lysine of the Catalytic Domain of Protein Kinases Is Actively Involved in the Phosphotransfer Reaction and Not Required for Anchoring ATP. *Proc. Natl. Acad. Sci.* **1993**, *90* (2), 442–446.
- (272) Fournier, J. C. L.; Evans, J. P.; Zappacosta, F.; Thomas, D. A.; Patel, V. K.; White, G. V.; Campos, S.; Tomkinson, N. C. O. Acetylation of the Catalytic Lysine Inhibits Kinase Activity in PI3K $\delta$ . *ACS Chem. Biol.* **2021**, *16* (9), 1644–1653.
- (273) Liu, R.; Yue, Z.; Tsai, C. C.; Shen, J. Assessing Lysine and Cysteine Reactivities for Designing Targeted Covalent Kinase Inhibitors. *J. Am. Chem. Soc.* **2019**, *141* (16), 6553–6560.
- (274) Zhao, Q.; Ouyang, X.; Wan, X.; Gajiwala, K. S.; Kath, J. C.; Jones, L. H.; Burlingame, A. L.; Taunton, J. Broad-Spectrum Kinase Profiling in Live Cells with Lysine-Targeted Sulfonyl Fluoride Probes. *J. Am. Chem. Soc.* **2017**, *139* (2), 680–685.
- (275) Ferlenghi, F.; Scalvini, L.; Vacondio, F.; Castelli, R.; Bozza, N.; Marseglia, G.; Rivara, S.; Lodola, A.; La Monica, S.; Minari, R.; Petronini, P. G.; Alfieri, R.; Tiseo, M.; Mor, M. A Sulfonyl Fluoride Derivative Inhibits EGFR L858R/T790M/C797S by Covalent Modification of the Catalytic Lysine. *Eur. J. Med. Chem.* **2021**, *225*, 113786.
- (276) Zhang, Y.; Hu, Z. Y.; Li, X. C.; Guo, X. X. Copper-Catalyzed Decarboxylative N-Arylation of Indole-2-Carboxylic Acids. *Synth.* **2019**, *51* (8), 1803–1808.
- (277) Lee, M.; Rucil, T.; Heseck, D.; Oliver, A. G.; Fisher, J. F.; Mobashery, S. Regioselective Control of the SNAr Amination of 5-Substituted-2,4-Dichloropyrimidines Using Tertiary Amine Nucleophiles. *J. Org. Chem.* **2015**, *80* (15), 7757–7763.
- (278) Butterworth, S.; Finlay, M. R. V.; Ward, R. A.; Kadambar, V. K.; Chandrashekar, R. C.; Murugan, A.; Redfearn, H. M. 2 - (2, 4, 5 - Substituted -Anilino) Pyrimidine Derivatives as Egfr Modulators Useful for Treating Cancer. WO2013014448A1,

- 2013.
- (279) 吉民; 李元; 刘海东; 李锐; 蔡进; 胡海燕. Synthetic Method of Anti-Tumor Medicine. CN104817541A, 2015.
- (280) Zhou, H.; Mukherjee, P.; Liu, R.; Evrard, E.; Wang, D.; Humphrey, J. M.; Butler, T. W.; Hoth, L. R.; Sperry, J. B.; Sakata, S. K.; Helal, C. J.; Am Ende, C. W. Introduction of a Crystalline, Shelf-Stable Reagent for the Synthesis of Sulfur(VI) Fluorides. *Org. Lett.* **2018**, *20* (3), 812–815.
- (281) 金云舟; 卜平; 何琦; 兰炯; 周福生; 张亮; 何向宇. Azabicyclo Derivatives, Preparation Methods Thereof, and Pharmaceutical Applications Thereof. CN105524068A, 2016.
- (282) Jung, M. E.; Martinelli, M. J. Iodotrimethylsilane. In *Encyclopedia of Reagents for Organic Synthesis*; 2009.
- (283) Xing, L.; Klug-Mcleod, J.; Rai, B.; Lunney, E. A. Kinase Hinge Binding Scaffolds and Their Hydrogen Bond Patterns. *Bioorg. Med. Chem.* **2015**, *23* (19), 6520–6527.
- (284) Yosaatmadja, Y.; Silva, S.; Dickson, J. M.; Patterson, A. V.; Smaill, J. B.; Flanagan, J. U.; McKeage, M. J.; Squire, C. J. Binding Mode of the Breakthrough Inhibitor AZD9291 to Epidermal Growth Factor Receptor Revealed. *J. Struct. Biol.* **2015**, *192* (3), 539–544.
- (285) AssayQuant <https://www.assayquant.com/> (accessed Jun 29, 2023).
- (286) Jones, L. H. Emerging Utility of Fluorosulfate Chemical Probes. *ACS Med. Chem. Lett.* **2018**, *9* (7), 584.
- (287) Diness, F.; Fairlie, D. P. Catalyst-Free N-Arylation Using Unactivated Fluorobenzenes. *Angew. Chemie Int. Ed.* **2012**, *51* (32), 8012–8016.
- (288) Tsui, H.-C.; Paliwal, S.; Kim, H. M.; Fischmann, T. O.; Kerekes, A. D.; Caplen, M. A.; Mckittrick, B. A.; Esposito, S. J.; Doll, R. J.; Ang, L.; Rainka, M. P. N-Phenyl Imidazole Carboxamide Inhibitors of 3-Phosphoinositide-Dependent Protein Kinase-1. WO2011149874A2, 2011.
- (289) Diez-Martinez, A.; Kim, E. K.; Krishnamurthy, R. Hydrogen-Bonding Complexes of 5-Azauracil and Uracil Derivatives in Organic Medium. *J. Org. Chem.* **2015**, *80* (14), 7066–7075.
- (290) Smit, C.; Blümer, J.; Eerland, M. F.; Albers, M. F.; Müller, M. P.; Goody, R. S.; Itzen, A.; Hedberg, C. Efficient Synthesis and Applications of Peptides Containing Adenylylated Tyrosine Residues. *Angew. Chemie Int. Ed.* **2011**, *50* (39), 9200–9204.
- (291) Sumita, Y.; Shirato, M.; Ueno, Y.; Matsuda, A.; Shuto, S. Nucleosides and Nucleotides. 192. Toward the Total Synthesis of Cyclic ADP-Carbocyclic-Ribose. Formation of the Intramolecular Pyrophosphate Linkage by a Conformation-

- Restriction Strategy in a Syn-Form Using a Halogen Substitution at the 8-Position of The. *Nucleosides, Nucleotides and Nucleic Acids* **2000**, *19* (1–2), 175–187.
- (292) Liu, P.; Hu, Z.; Dubois, B. G.; Moyes, C. R.; Hunter, D. N.; Zhu, C.; Kar, N. F.; Zhu, Y.; Garfinkle, J.; Kang, L.; Chicchi, G.; Ehrhardt, A.; Woods, A.; Seo, T.; Woods, M.; Van Heek, M.; Dingley, K. H.; Pang, J.; Salituro, G. M.; Powell, J.; Terebetski, J. L.; Hornak, V.; Campeau, L. C.; Lamberson, J.; Ujjainwalla, F.; Miller, M.; Stamford, A.; Wood, H. B.; Kowalski, T.; Nargund, R. P.; Edmondson, S. D. Design of Potent and Orally Active GPR119 Agonists for the Treatment of Type II Diabetes. *ACS Med. Chem. Lett.* **2015**, *6* (8), 936–941.
- (293) Carter-O’Connell, I.; Jin, H.; Morgan, R. K.; David, L. L.; Cohen, M. S. Engineering the Substrate Specificity of ADP-Ribosyltransferases for Identifying Direct Protein Targets. *J. Am. Chem. Soc.* **2014**, *136* (14), 5201–5204.
- (294) Chen, K. Q.; Wang, Z. X.; Chen, X. Y. Photochemical Decarboxylative C(Sp<sup>3</sup>)-X Coupling Facilitated by Weak Interaction of N-Heterocyclic Carbene. *Org. Lett.* **2020**, *22* (20), 8059–8064.
- (295) Zelenay, B.; Munton, P.; Tian, X.; Díez-González, S. A Commercially Available and User-Friendly Catalyst for Hydroamination Reactions under Technical Conditions. *European J. Org. Chem.* **2019**, 4725–4730.
- (296) Hong, X.; Tan, Q.; Liu, B.; Xu, B. Isocyanide-Induced Activation of Copper Sulfate: Direct Access to Functionalized Heteroarene Sulfonic Esters. *Angew. Chemie Int. Ed.* **2017**, *56* (14), 3961–3965.
- (297) Hu, J.; Han, Y.; Wang, J.; Liu, Y.; Zhao, Y.; Liu, Y.; Gong, P. Discovery of Selective EGFR Modulator to Inhibit L858R/T790M Double Mutants Bearing a N-9-Diphenyl-9H-Purin-2-Amine Scaffold. *Bioorganic Med. Chem.* **2018**, *26* (8), 1810–1822.
- (298) Ward, R. A.; Anderton, M. J.; Ashton, S.; Bethel, P. A.; Box, M.; Butterworth, S.; Colclough, N.; Chorley, C. G.; Chuaqui, C.; Cross, D. A. E.; Dakin, L. A.; Debreczeni, J. É.; Eberlein, C.; Finlay, M. R. V.; Hill, G. B.; Grist, M.; Klinowska, T. C. M.; Lane, C.; Martin, S.; Orme, J. P.; Smith, P.; Wang, F.; Waring, M. J. Structure- and Reactivity-Based Development of Covalent Inhibitors of the Activating and Gatekeeper Mutant Forms of the Epidermal Growth Factor Receptor (EGFR). *J. Med. Chem.* **2013**, *56* (17), 7025–7048.
- (299) Xin, M.; Zhang, L.; Wen, J.; Shen, H.; Zhao, X.; Jin, Q.; Tang, F. Introduction of Fluorine to Phenyl Group of 4-(2-Pyrimidinylamino)Benzamides Leading to a Series of Potent Hedgehog Signaling Pathway Inhibitors. *Bioorg. Med. Chem. Lett.* **2017**, *27* (15), 3259–3263.
- (300) Ruah, S. S. H.; Miller, M. T.; Bear, B.; McCartney, J.; Grootenhuis, P. D. J. Modulators of ATP-Binding Cassette Transporters. WO2018114786A1, 2007.